



**UNIVERSITÀ DEGLI STUDI DI TORINO**  
Department of Life Sciences and Systems Biology



**Immunotherapeutic approaches for  
ALK-driven Non-Small-Cell Lung  
Cancer (NSCLC)**

Doctoral School in Life and Health Sciences  
PhD Program in Complex Systems for Life Sciences

XXXII Cycle

2016-2019

**Candidate: Inês Mota**

**Tutor: Prof. Roberto Chiarle and Prof. Federico Bussolino**

**Coordinator: Prof. Michele De Bortoli**



UNIVERSITÀ DEGLI STUDI DI TORINO  
Department of Life Sciences and Systems Biology



Immunotherapeutic approaches for  
ALK-driven Non-Small-Cell Lung  
Cancer (NSCLC)

**Doctoral School in Life and Health Sciences**  
**PhD Program in Complex Systems for Life Sciences**

**XXXII Cycle**

**2016-2019**

**Candidate: Inês Mota**

**Tutor: Prof. Roberto Chiarle and Prof. Federico Bussolino**

**Coordinator: Prof. Michele De Bortoli**







A complex network diagram with nodes and connecting lines, serving as a background for the page. The word 'ALKATRAS' is prominently displayed in the center, overlaid on the network.

# ALKATRAS

The European Training Network ALKATRAS is embedded into an established international research program: The European Research Initiative on Anaplastic Lymphoma Kinase (ALK)-related malignancies (ERIA; [www.erialcl.net](http://www.erialcl.net)), which is an existing and functional network of 13 research partners. Eria was instigated to coordinate research into ALK-related malignancies to facilitate the development of less-toxic and more efficacious therapies.

Within the EU-funded ETN ALKATRAS this consortium nurtured a cohort of 15 early stage researchers

The present PhD thesis correspond to Early Stage Researcher (ESR) no. 10 under the title “Novel Therapies for ALK tumors: ALK vaccination and immunotherapy”.



This project has received funding from the European Union’s Horizon 2020 Marie Skłodowska-Curie Innovative Training Networks (ITN-ETN) under grant agreement No.: 675712





*"I am nothing  
I'll never be anything  
I cannot want to be anything  
Apart from this, I have in me all the dreams of the world.  
(...)"*

Álvaro de Campos in The Tobacconist's



To Mom and Grandma,  
Because without you, anything would have been possible...

## Acknowledgments

Usually, the acknowledgments are the last part of a thesis one writes due to the fact that summarizes the miscellaneous feelings felt when such an important stage is finished. However, it was the first chapter I decided to write because since the very beginning I always have been grateful for having this enormous opportunity.

First, I would like to thank Dr. Alberto Órfão who, even before I started my PhD path in ALKATRAS program, has guided me and indirectly forced me to make the best choice.

Second, to Dr. Roberto Chiarle, for giving me the opportunity to work in his laboratories, both in Turin (Italy) and in Boston (USA), and for the scientific guidance during my PhD.

Third, to Enrico Patrucco, who has helped me to come back from hell, who has made me believe in myself again and recover my self-esteem, and has shown me the light at the end of the tunnel. Thank you Enrico, for all guffaws, for all endless conversations and lunches and dinners we have had, for being more than a supervisor, for being my friend.

To Rafael Blasco, probably the most noisy and loudest Spanish I have ever met, and believe me, I have met more than a few! Gracias Rafa, for your support and help during my time in Chiarle's Lab in Boston.

To Professor Michele de Bortoli, coordinator of the PhD program in Turin, who always has been helpful, and to Professor Federico Bussolino for the scientific guidance during my PhD.

To ALKATRAS family; coordinators and PhD students, who have traveled with me during these three intense years.

Since the acknowledgments are the most personalized part of any document, which gives the writer the opportunity to express the deepest feelings and/or thoughts, the reader has to forgive me because, no matter how fluent one is in other languages, there is no better way to express such feelings and thoughts than our native language.

Longe vai o ano de 2009, quando a primeira pequena batalha foi conquistada: licenciei-me. Durante estes dez anos, os sonhos que desde então carregue nos meus ombros foram muitas vezes postos à prova por desencontros e encontros menos bons, vicissitudes que muitas vezes foram quase impossíveis de aceitar e/ou contornar, por portas que teimavam em fechar-se e oportunidades que demoravam a chegar. Estes dez anos ensinaram-me que nenhuma batalha é fácil, que os níveis de resiliência exigidos muitas vezes ultrapassam aquilo que pensávamos ser possível suportar, que haverá quem te queira ajudar e quem de tudo faça para te reduzir a um mero sonhador. Mas estes dez anos ensinaram-me também que todos os sonhos são possíveis de realizar. Não interessa o quão tortuoso e tumultuoso possa ser o caminho, se nunca desistires, se nunca baixares os braços, se sempre acreditares em ti e no teu valor, mesmo que outras pessoas não o façam, se trabalhares dia e noite, mesmo que nunca recebas o devido crédito ou que outras pessoas o tomem de ti, o sonho, um dia, tornar-se-á realidade. E hoje, tendo terminado mais uma batalha, sigo em frente sem medo do que vou encontrar neste nem sempre fácil caminho porque eu sei que o melhor de mim ainda está por chegar.

E por fim, não podia terminar sem fazer referência às pessoas mais importantes da minha vida, mãe e avó, que sempre estiveram do meu lado, que sempre me ajudaram em todos os aspectos, que sempre se orgulharam das pequenas vitórias que fui conquistando ao longo da minha vida e é a vocês, somente a vocês, que dedico este momento.

Inês Mota

*“Your value does not decrease based  
on someone’s inability to see your worth”*

Unknown

## List of publications

- 1) Menotti M, Ambrogio C, Cheong TC, Pighi C, **Mota I**, Cassel SH, Compahno M, et al. **Wiskott-Aldrich syndrome protein (WASP) is a tumor suppressor in T-cell lymphoma.** Nat Med, Jan 2019. **IF: 30.641**
  
- 2) Blasco RB, Patrucco E, **Mota I**, Tai WT, Chiarle R. **Comment on “ALK is a therapeutic target for lethal sepsis”.** Sci. Transl. Med, Dec 2018. **IF: 17.161**
  
- 3) Sharma GG\*, **Mota I\***, Mologni L, Patrucco E, Gambacorti-Passerini C, Chiarle R. **Tumor Resistance against ALK Targeted Therapy – Where it comes from and Where it Goes.** Cancers, Feb 2018. \* equal contribution. **IF: 6.102**

**Introduction:** Around 3-7% of Non-Small Cell Lung Cancer (NSCLC) patients harbor rearrangements in the Anaplastic Lymphoma Kinase (ALK) gene. ALK inhibitors (ALKi) approved by FDA are potent in reducing tumor growth and extending survival of lung cancer patients. However, most of the tumors invariably relapse. In recent years, Immune Checkpoint Inhibitors (ICI) have shown dramatic changes in the treatment of advanced NSCLC. However, their efficacy varies among different immune and molecular profiles. Particularly, the clinical significance of ICI for ALK-driven NSCLC has been controversial. Not only PD-L1 expression but also tumor-infiltrating lymphocytes (TILs) correlate with the efficacy of ICIs and ALK-driven NSCLC display a tumor environment in which PD-L1 is expressed through ALK signaling and TILs are low. Previously, we designed an ALK-DNA-based vaccine directed against the cytoplasmic portion of the human ALK (hALK) and demonstrated the capability of hALK to elicit a strong CD8<sup>+</sup> T-cell response in BALB/c mice that blocks tumor growth. In our preclinical mouse models, triple combination of ALKi, ICIs and vaccination, has shown to be more effective than other treatment combination.

**Methods:** First, we evaluated the synergistic effect of ALKi in combination with ICIs. Lung tumor volume was measured by MRI in EML4-ALK transgenic (Tg) mice which express the hALK and in mice where tumors with the EML4-ALK translocation were induced *in vivo* by CRISPR/Cas9 system (Ad-EA mice; expressing the murine ALK [mALK]). Mice were stratified before treatment based on the total tumor volume and enrolled into 14, 30 or 60 days of ALKi (crizotinib or lorlatinib) with or without ICIs treatment (either anti-PD-1 or anti-PD-L1). Second, we generated a syngeneic hALK-expressing cell line by transducing an immortalized cell line generated from Ad-EA mice with the hEML4-ALK full length. Mice were injected subcutaneously and enrolled into 14 or 30 days of ALKi (lorlatinib) with anti-PD-1 and with or without the ALK vaccine.



**Results:** Tg EML4-ALK mice showed reduced tumor progression when treated with a combination of crizotinib and ICIs as compared to mice treated with crizotinib alone. Ad-EA mice treated with lorlatinib combined with anti-PD-1 showed a significantly slower tumor progression when compared with mice treated with lorlatinib alone in all treatment protocols (14, 30 or 60 days of treatment) (\* $P < 0.05$ , to Mann-Whitney U test), however, this effect was transient and lost during follow-up. The triple combination of lorlatinib, anti-PD-1 and ALK-DNA-based vaccine eradicated cells expressing hALK much more efficiently than the lorlatinib+anti-PD-1 double combination in subcutaneous tumors grown in syngeneic mice. Importantly, disseminated metastases were completely abrogated by triple combination of lorlatinib, anti-PD-1 and DNA-based ALK vaccine compared to lorlatinib+anti-PD-1 double combination (0% vs 83.3%).

**Conclusions:** Mouse models confirmed preliminary observations in ALK-rearranged NSCLC that the addition of ICIs to an ALK inhibitor has limited effect. In this context, the addition of an ALK vaccine strongly potentiates the therapeutic activity of ALK TKIs and prevents metastatic dissemination of ALK<sup>+</sup> lung cancer cells.

**Keywords:** Anaplastic Lymphoma Kinase (ALK); ALK inhibitors (ALKi); ALK DNA-based vaccine; Immunotherapy; Non-Small Cell Lung Cancer (NSCLC); anti-PD-1; anti-PD-L1.

**Introduction:** Several evidences show that Anaplastic Lymphoma Kinase (ALK) is able to generate *per se* an immune response. The presence of anti-ALK antibodies in Anaplastic Large Cell Lymphoma (ALCL) patients' serum, together with the identification of several HLA-A2.1 restricted CD8<sup>+</sup> T-cell epitopes in neuroblastoma and ALCL cell lines, show us the ability of ALK protein to elicit a humoral and cellular immune response. It is also known that PD-L1 expression is upregulated through ALK signaling in NSCLC cell lines. Even though all facts suggest that patients with ALK-driven tumors were suitable for immune checkpoint inhibitors therapy, several clinical trials have shown disappointing results. One aspect that can hamper the activity of immune checkpoint is the low number of cytotoxic T-cells that infiltrate the tumor. In our orthotopic tumor transplantation mouse model we were able to increase the number of CD8<sup>+</sup> T-cell by vaccinating mice with the ALK-specific-CD8<sup>+</sup> T-cell peptide and consecutively, extend substantially the overall survival of the mice.

**Methods:** First, we performed an *in vitro* screening by using splenocytes isolated from mice immunized with the previously used hALK-DNA-based vaccine and pulsed with 21 synthetic long peptides in order to identify the exact CD8<sup>+</sup> T-cell epitope. Once identified the epitope, we have genetically modified a murine cell line that expresses the endogenous mEML4-ALK in order to express the human ALK immunogenic epitope. Once edited, this cell line was able to generate a spontaneous CD8<sup>+</sup> T-cell response in BALB/c background. Sequentially, this cell line was used in an orthotopic tumor transplantation model. Mice were intravenously injected and consecutively enrolled into 15 days of ALKi (lorlatinib) either with anti-PD1, or anti-CTLA-4 or peptide vaccine.

**Results:** We have identified the human ALK-specific-CD8<sup>+</sup> T-cell epitope that generates an immune response in BALB/c mice. By using a genomic edited cell line that expresses the specific identified epitope, we were able to develop an orthotopic tumor transplantation mouse model. Vaccinated mice presented a significantly overall

survival extension. However, in vaccinated mice that relapsed, tumor cells have lost MHC-I expression. In all vaccinated cohorts, brain metastases were not observed.

**Conclusions:** Our orthotopic mouse model has confirmed that by increasing the number of ALK-specific-CD8<sup>+</sup> T-cells through vaccination, mice survival was greatly extended. Also, our data confirmed preliminary observations in preclinical ALK-rearranged NSCLC mouse models that the addition of a strong immune response, completely abrogate brain metastasis.

**Keywords:** Anaplastic Lymphoma Kinase (ALK); ALK-specific-CD8<sup>+</sup> T-cells; peptide-vaccine; Non-Small Cell Lung Cancer (NSCLC); anti-PD-1; anti-CTLA-4.

## Table of contents

Acknowledgments .....	i
List of publications.....	iv
Abstract      Part I.....	v
Abstract      Part II.....	vii
Table of contents .....	ix
List of Figures.....	xiv
Chapter I - Introduction.....	2
A1) Protein Tyrosine Kinases.....	4
A1.1) Receptor Tyrosine Kinase structure, activation and regulation .....	5
A1.2) Mechanisms of receptor tyrosine kinase activation in cancer.....	7
A1.2.1) Activation by gain-of-function mutations .....	7
A1.2.2) Overexpression and genomic amplification.....	9
A1.2.3) Chromosomal rearrangements.....	10
A1.2.4) Constitutive activation by kinase domain duplication.....	12
A1.2.5) Autocrine activation.....	13
A1.2.6) Other mechanisms.....	13
B1) Anaplastic Lymphoma Kinase (ALK).....	14
B1.1) ALK conserved structure, function and signal transducing through species....	14
B1.1.1) <i>Drosophila melanogaster</i> ALK (dALK).....	16
B1.1.2) <i>Caenorhabditis elegans</i> ALK [SCD-2 (suppressor of constitutive dauer-2)] ...	17
B1.1.3) <i>Danio rerio</i> ALK (Zebrafish LTK/ALK).....	17
B1.1.4) Mammalian ALK.....	17
B1.2) Structure of ALK protein kinase domain.....	20
B1.3) ALK in disease; activation and downstream signaling .....	24
B1.3.1) ALK Gain-of-Function Mutations.....	28
B1.3.2) Amplification/overexpression of ALK in cancer .....	30
B1.3.3) Chromosomal rearrangements.....	32
C1) Non-small-cell lung cancer (NSCLC) .....	37
C1.1) Histological classification of NSCLC .....	38

C1.2) Molecular classification of lung adenocarcinomas .....	39
C1.3) The role of ALK in NSCLC .....	41
D1) ALK Inhibitors .....	46
D1.1) Crizotinib .....	47
D1.2) Ceritinib .....	48
D1.3) Alectinib .....	50
D1.4) Brigatinib .....	52
D1.5) Lorlatinib.....	53
E1) ALK inhibitors resistance.....	59
E1.1) ALK TKI resistance mechanism.....	59
E1.1.1) ALK-Dependent Resistance Mechanisms .....	59
E1.1.2) ALK-Independent Resistance Mechanisms .....	68
E1.2) Therapeutic Strategies to Overcome ALK-Related Resistance.....	75
E1.2.2) What comes next?.....	76
F1) From Cancer Immunesurveillance to Cancer Immunoediting .....	80
F1.1) Elimination .....	80
F1.2) Equilibrium.....	81
F1.3) Escape .....	82
F1.4) Cancer cells are immunogenic: antigenic targets of Cancer Immunoediting.....	84
F1.5) Antigenic presentation .....	84
F1.5.1) TCR affinity.....	85
F1.5.2) MHC-class-I and II.....	86
F1.6) Cancer antigenic presentation.....	94
F1.6.1) The role of T-cells in tumor-suppressive mechanisms and tumor outgrowth .....	95
F1.7) CD8 <sup>+</sup> T-cells role in tumor immunity: function and dysfunction.....	102
F1.7.1) Effector CD8 <sup>+</sup> T-cells.....	104
F1.7.2) Trafficking of Effector CD8 <sup>+</sup> T-cells and Memory CD8 <sup>+</sup> T-cells differentiation.....	104
F1.7.3) Immunosuppressive tumor microenvironment and Exhausted CD8 <sup>+</sup> T-cells .....	105
F1.7.4) Immune checkpoints.....	106

F1.8) Cancer Immunotherapy .....	111
F1.8.1) Immune checkpoint inhibitors .....	111
F1.8.2) DNA and peptide vaccines.....	113
G1) ALK immunogenicity .....	115
G1.1) Humoral Immune Response against ALK .....	115
G1.2) Cellular Immune Response against ALK .....	116
G1.2.1) CD8 <sup>+</sup> T-cell response against ALK.....	117
G1.2.2) CD4 <sup>+</sup> T-Cell Response against ALK .....	118
G1.3) ALK immune escape: Therapeutic implications and immunotherapeutic approaches available.....	119
G1.3.1) Crizotinib + Nivolumab (NCT02574078) .....	121
G1.3.2) Ceritinib + Nivolumab (NCT02393625) .....	121
G1.3.3) Lorlatinib + Avelumab (NCT02584634) .....	121
G1.3.4) Alectinib + Atezolizumab (NCT02013219).....	121
Chapter II - Hypothesis .....	124
Part I.....	126
Part II.....	126
Chapter III – Material and Methods .....	128
Part I.....	130
3.1) Cell lines.....	130
3.2) Mice strains.....	130
3.3) ALK inhibitors.....	131
3.4) Antibody dosage for <i>in vivo</i> treatment .....	131
3.5) DNA vaccination.....	131
3.6) hEML4-ALK cloning; retrovirus and lentivirus production and mEML4-ALK KO .....	131
3.7) Histology and Immunohistochemistry.....	133
3.7) Magnetic Resonance Imaging (MRI) .....	133
3.8) Cell Lysis and Immunoblotting .....	133
3.9) Cell viability assay .....	134
3.10) Flow cytometry.....	134
3.11) Statistical Methods .....	135

Part II.....	136
3.12) Cell lines.....	136
3.13) Mice strain .....	136
3.14) DNA vaccination/ Splenocytes isolation .....	136
3.15) Synthetic peptides .....	136
3.16) IFN- $\gamma$ ELISPOT assay .....	137
3.17) CD4 <sup>+</sup> and CD8 <sup>+</sup> T-cell discrimination.....	137
3.18) Algorithms .....	138
3.19) H2-Dd-PGPGRVAKI Dextramer Staining / Flow cytometry.....	138
3.20) Peptide vaccination.....	139
3.21) Genomic editing of mouse ALK.....	139
3.22) DNA and RNA extraction/PCR reaction/ Sanger sequence.....	139
3.23) Animal treatment and tumor transplantation.....	140
3.24) ALK inhibitors .....	140
3.25) Antibody dosage for <i>in vivo</i> treatment .....	140
3.26) Histology.....	141
3.27) Cell lysis and Immunoblotting.....	141
3.28) Cell viability assay .....	141
3.29) <i>ex vivo</i> cell culture.....	142
3.30) Statistical Methods .....	142
Chapter IV - Results.....	144
Part I.....	145
4.1) Combination of immune checkpoint blockade with high doses of ALK inhibitors does not provide significant advantage in Tg EML4-ALK-rearranged NSCLC mice .....	145
4.2) PD-1 blockade in combination with low doses of the potent ALK inhibitor lorlatinib delays tumor relapse in Ad-EA-derived NSCLC mouse models .....	146
4.3) Long-term treatment with the potent ALK inhibitor lorlatinib in combination with anti-PD-1 antibody slightly delays tumor relapse in Ad-EA mouse models....	149
4.4) Murine Alk rearrangement shows poor response to crizotinib but not to lorlatinib.....	151
4.5) Strong human ALK expression results in immunoediting in immunocompetent BALB/c mice .....	153

4.6) Triple combination of lorlatinib, PD-1 blockade and ALK-DNA-based vaccine significantly delays tumor relapse and completely abrogates the development of metastasis in distant organs in graft models.....	156
Part II.....	160
4.7) PGPGRVAKI is a MHC-I-restricted neoantigen in BALB/c background .....	160
4.8) Humanized mouse ALK cell line (Edited-1) generation.....	161
4.9) Tumor localization dictates the intensity of the immune response.....	163
4.10) PGPGRVAKI-peptide vaccine generates less exhausted intratumor CD8 <sup>+</sup> T-cell .....	165
4.11) PGPGRVAKI-peptide vaccine in combination with a potent ALK inhibitor significantly extends mice overall survival and completely abrogates brain metastasis in orthotopic mouse models. ....	166
4.12) Tumors relapse in vaccinated mice due to reversible MHC-I loss.....	168
Chapter V - Discussion .....	202
Part I.....	204
Part II.....	213
Chapter VI - Conclusion.....	224
Part I.....	226
Part II.....	226
Chapter VII - References.....	228



## List of Figures

Figure 1 - Receptor Tyrosine Kinase Families.....	6
Figure 2 - Mechanisms of physiological and oncogenic RTK activation.. ..	8
Figure 3 - Domain structure of human ALK and human LTK.. ..	15
Figure 4 - Ribbon diagram of human ALK. ....	21
Figure 5 - Diagram of the inferred interaction between human ALK catalytic core residues, ATP and a protein substrate.....	23
Figure 6 - ALK downstream pathways and bypass signaling.....	27
Figure 7 - ALK in cancer: an overview. ....	27
Figure 8 - ALK signaling in normal and cancer cells. ....	28
Figure 9 - Some examples of mutations ALK mutations detected in neuroblastoma, ganglioneuroblastoma, glioma, osteosarcoma, PNET, and rhabdomyosarcoma.. ..	29
Figure 10 – Histologic subtypes of lung cancer. ....	39
Figure 11 - Distribution of molecular alterations in lung adenocarcinoma.....	40
Figure 12 - Prevalence of molecular alterations in key oncogenic drivers in lung adenocarcinomas using whole exome sequencing from The Cancer Genome Atlas Project.....	41
Figure 13 - Overview of EML proteins.....	42
Figure 14 - Schematic structural composition of ALK fusion proteins. ....	44
Figure 15 - The acyclic structure of crizotinib and the macrocyclic structure of lorlatinib.....	54
Figure 16 - Comparison of PFS results in selected clinical trials testing TKI sequencing in ALK-driven NSCLC. ....	58
Figure 17 - Crystal structure of ALK in complex with crizotinib (PDB:2XP2). ....	60
Figure 18 - Structural Basis for Resistance to Lorlatinib and Sensitivity to Crizotinib Mediated by ALK C1156Y–L1198F.....	66

Figure 19 - ALK downstream pathways and bypass signaling.....	71
Figure 20 – The optimal sequencing for the treatment sequence with tyrosine-kinase inhibitors.....	74
Figure 21 - Cancer Immunoediting is an extrinsic tumor-suppressor mechanism that engages after cellular transformation has occurred and intrinsic tumor-suppressive mechanisms have failed.....	83
Figure 22 - Structure of MHC-I (left panel) and -II (right panel) molecules.....	87
Figure 23 - Comparison of peptide conformation presented by MHC I and II.....	88
Figure 24 - Schematic representation of the two models of antigens processing.....	93
Figure 25 - Anti-tumor immunity cycle starts with presentation of cancer antigens that are released during the natural process of cell turnover.....	94
Figure 26 - Immune response to cancer.....	103
Figure 27 – CTLA-4 pathway.....	107
Figure 28 - PD-1/PD-L1 pathway.PD-1/PD-L1 pathways.....	110
Figure 29 - Combination of immune checkpoint blockade and high doses of a potent ALK inhibitor does not provide significant advantage in EML4-ALK-rearranged NSCLC Tg mice. ....	172
Figure 30 -Immune checkpoint blockade in combination with low but clinically significant doses of ALK inhibitors (crizotinib and lorlatinib) does not provide any advantage in Tg EML4-ALK mice.. ....	175
Figure 31 - PD-1 blockade in combination with low doses of the potent ALK inhibitor lorlatinib delays tumor relapse in non-small cell lung cancer Ad-EA-derived mouse models.....	178
Figure 32 - Long-term treatment with low doses of the ALK inhibitor lorlatinib in combination with anti-PD-1 antibody slightly delays tumor relapse in non-small cell lung cancer Ad-EA-derived mouse models.....	181
Figure 33 – Murine EML4-ALK <sup>+</sup> lung carcinoma cell lines (TECLA-1 and TECLA-2) generated from primary tumors developed in Ad-EA mice show different sensitivity to ALK TKI.....	184

Figure 34 – Strong human ALK expression results in immunoediting in WT Balb/ mice. .....	187
Figure 35 – Triple combination of lorlatinib, PD-1 blockade and ALK DNA-based vaccine significantly delays tumor relapse in graft models.....	190
Figure 36 – PGPGRVAKI is a MHC-I-restricted neoantigen in BALB/c background...	192
Figure 37 –Humanized mouse ALK cell line (Edited-1) generation. ....	194
Figure 38 – Tumor localization dictated the intensity of the immune response. ....	196
Figure 39 – PGPGRVAKI-peptide vaccine generates less exhausted intratumor CD8 <sup>+</sup> T-cells.....	198
Figure 40 - PGPGRVAKI-peptide vaccine in combination with a potent ALK inhibitor significantly extends mice overall survival and completely abrogates brain metastasis in orthotopic mouse models.....	199
Figure 41 - Tumors relapse in vaccinated mice due to reversible MHC-I loss.....	200

## List of Tables

Table 1 - Important residues in human ALK. ....	24
Table 2 - ALK rearrangements in human malignancies.....	32
Table 3 - Summary of the clinical settings in which the ALK TKIs have been tested. Approval status by EMA and FDA. ....	46
Table 4 - Clinical trials with crizotinib.....	48
Table 5 - Clinical trials with ceritinib.....	49
Table 6 - Clinical trials alectinib.. ....	51
Table 7 - Clinical trials with brigatinib. ....	53
Table 8 - Expansion (EXP) cohort from the phase I/II study of lorlatinib.....	56
Table 9 - Mutational profile of ALK that induce TKI resistance.....	62
Table 10 - Clinical trials of cancer immunotherapy-based combinations in ALK+ NSCLC. ....	122

## Glossary of abbreviations

### A

**ALCL** Anaplastic Large Cell Lymphoma  
**ALK** Anaplastic Lymphoma Kinase  
**ALKi** ALK inhibitors  
**ALL** Acute Lymphoplastic Leukemia  
**AML** Acute Myeloid Leukemia  
**APC** Antigen Presenting Cell

### B

**B7** The B7 family of immune-regulatory ligands  
**BCR** B-cell receptor

### C

**CCL19** C-C Motif Chemokine Ligand 19  
**CCL21** C-C Motif Chemokine Ligand 21  
**CCR7** C-C chemokine receptor type 7  
**CD133** Cluster of differentiation 133  
**CD20** Cluster of differentiation 20  
**CD30** Cluster of differentiation 30  
**CD4** Cluster of differentiation 4  
**CD70** Cluster of differentiation 70  
**CD79a** Cluster of differentiation 79a  
**CD8** Cluster of differentiation 8  
**CD80** Cluster of differentiation 80  
**CIITA** The class II transactivator  
**CLIP** Class II-associated invariant chain peptide  
**CML** Chronic myeloid leukemia  
**CNG** Copy number gain  
**CNS** Central nervous system  
**cTECS** Cortical thymic epithelial cells  
**C-Terminal** Carboxyl-terminus  
**CTL** Cytotoxic T Lymphocytes  
**CTLA-4** Cytotoxic T-lymphocyte-associated protein 4

### D

**dALK** Drosophila ALK  
**DC** Dendritic Cells  
**DNA** Deoxyribonucleic acid  
**DP** Double positive

### E

**ECD** Extracellular Domain  
  
**EGF** Epidermal growth factor  
**EGFR** Epidermal growth factor receptor  
**EMA** European medicines agency  
**EML4** Echinoderm microtubule associated protein-like 4  
**ENU** N-ethyl-N-nitrosourea  
**ER** Endoplasmic reticulum

### F

**FDA** Food and Drug Administration  
**FISH** Fluorescence in situ hybridization  
**FoxP3** Forkhead box P3

### G

**GBM** Glioblastoma

### H

**H2228** NCI-H2228, lung adenocarcinoma cell line (variant 3)  
**H3122** NCI-H3122, lung adenocarcinoma cell line (variant 1)  
**hALK** Human ALK  
**HLA** Human leukocyte antigen

### I

**IFN** Interferon  
**Ig** Immunoglobulin  
**IgG** Immunoglobulin G  
**IL-10** Interleukin - 10  
**IL-12** Interleukin - 12  
**IL-15** Interleukin- 15  
**IMT** Inflammatory myofibroblastic tumor

### J

**JM** juxtamembrane

### K

**kDa** kilodalton  
**KDD** kinase domain duplications

### L

**LAG-3** Lymphocyte-activation gene 3  
**LCMC** Lung Cancer Mutation Consortium  
**LDL** Low-density lipoprotein  
**LDLa** Low-density lipoprotein class A  
  
**LTK** Leukocyte Receptor Tyrosine Kinase

### M

**mALK** mouse ALK  
**MAM** Meprin/A5-protein/PTPmu  
**MCA** Methylcholanthrene  
**MDSC** Myeloid-derived suppressor cells  
**MHC** Major histocompatibility complex  
**MHC-I** Major histocompatibility complex class-I  
**MHC-II** Major histocompatibility complex class-II  
**mTECs** Medullary thymic epithelial cells

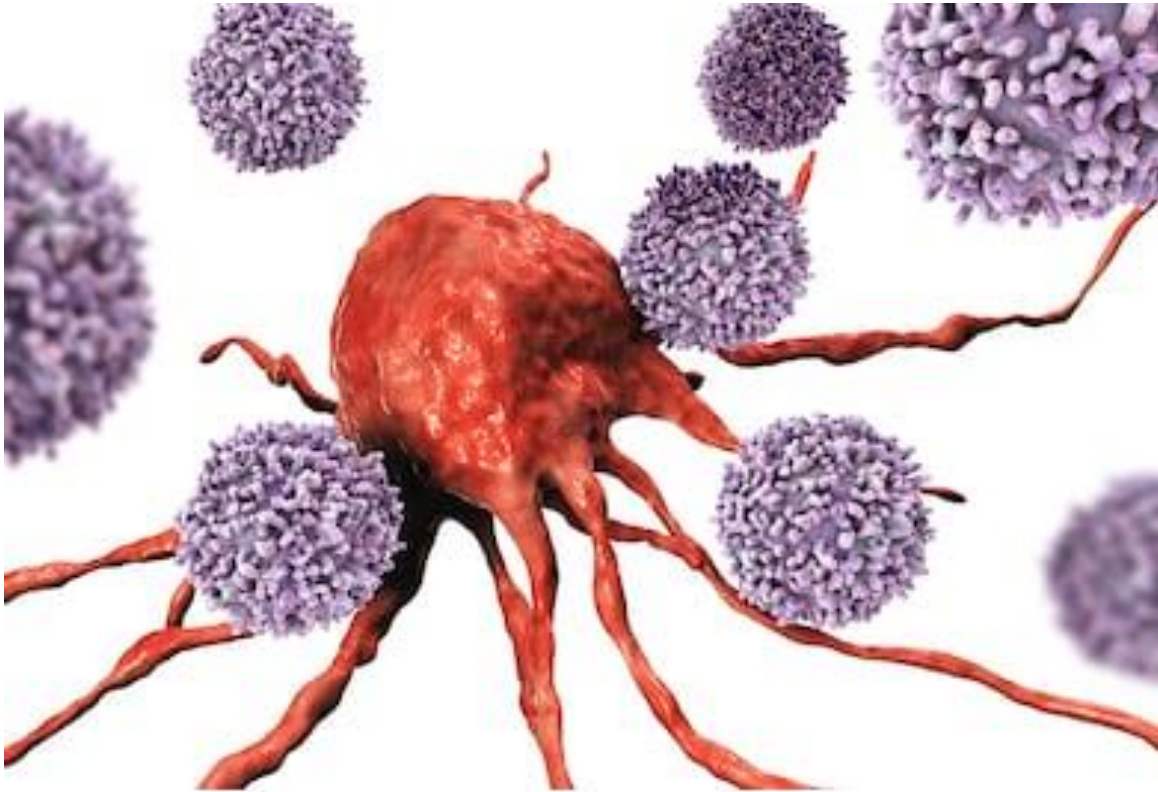
### N

**NSG** Next-generation sequencing  
**NIH 3T3** Fibroblast cell line  
**NK** Natural Killer

<b>NKT</b>	Natural killers T
<b>NPM</b>	Nucleophosmin
<b>NRTKs</b>	Non-receptor tyrosine kinases
<b>NSG</b>	NOD scid gamma mouse
<b>NSCLS</b>	Non-Small-Cell Lung Cancer
<b>P</b>	
<b>PD-1</b>	Programmed cell death protein 1
<b>PDA</b>	pancreatic ductal adenocarcinoma
<b>PD-L1</b>	Programmed death-ligand 1
<b>PD-L2</b>	Programmed death-ligand 2
<b>PTK</b>	Protein tyrosine kinases
<b>PTN</b>	Pleiotrophin
<b>R</b>	
<b>RTK</b>	Receptor Tyrosine Kynase
<b>T</b>	
<b>TAA</b>	Tumor-Associated Antigens
<b>TAP</b>	Transporter 1
<b>TCR</b>	T cell receptor
<b>TF</b>	Transcription factor
<b>TIM-3</b>	T-cell immunoglobulin mucin-3
<b>TKI</b>	Tyrosine kinase inhibitors
<b>TMD</b>	Tranmembrane Domain
<b>TNF</b>	Tumor necrosis factor
<b>TRAIL</b>	TNF-related apoptosis-inducing ligand
<b>Treg</b>	Regulatory T-cells
<b>Tyr</b>	Tyrosine residue
<b>W</b>	
<b>WHO</b>	World Health Organization
<b>WT</b>	Wild-type

---

# Chapter I



*"To be great, be entire: nothing  
yours exaggerate or exclude.  
Be whole in everything. Put all you are  
Into the smallest thing you do.  
So, in every pond the whole moon shines  
Because it blooms up above."*

Ricardo Reis

## **1. Introduction**





### 1) Introduction

Anaplastic Lymphoma Kinase (ALK) is a validated molecular target in several ALK-driven malignancies, particularly in 3-7% of Non-Small-Cell Lung Cancer (NSCLC) patients. The discovery of ALK rearrangements in this small percentage of lung cancer patients has generated considerable interest and effort in developing ALK inhibitors (ALKi). However, the clinical benefit observed in targeting ALK in NSCLC either with first/second- or third-generation of ALKi is almost universally limited by the emergence of drug resistance.

The elucidation of the diverse mechanisms through which resistance to ALKi emerge has led us to a dead end. The more potent the ALKi is, the more difficult it is to overcome the resistance mechanism that arises from it. Thus, possible therapeutic strategies that may overcome the development of resistance are urgently needed for these patients.

In recent years, immunotherapy has given a new hope to cancer patients, more precisely to melanoma and lung cancer diseased. Immunotherapy is based in the principal that the immune system is able to recognize a tumor as a malignant mass but it has lost the ability to fight against it due to the escape mechanisms that cancer cells develop after encounter the immune system.

Now-a-days, several publications attest that ALK expression is able to generate a humoral and cellular immune response. Not only anti-ALK antibodies in serum of patients but also ALK-specific CD8<sup>+</sup> and CD4<sup>+</sup> T-cells responses have been described in patients across ALK malignancies, and vaccination with an ALK-DNA-based vaccine has led to protection against Anaplastic Large Cell Lymphoma (ALCL) and NSCLC in murine models. All together, these data suggest that the ALK-specific immune response is involved in the control of the disease <sup>[1]</sup>.

The scope of this thesis is the development of new immunotherapeutic approaches for ALK-driven NSCLC using murine models.

To fully understand it, in this introductory chapter, the reader will be conducted through the state-of-art of ALK-driven NSCLC. For that, I will start by explaining the importance of Receptor Tyrosine Kinases (RTK) in oncogenesis,

## Chapter I - Introduction

---

followed by what it is known regarding the physiologic role of ALK and its role in cancer. Next, the reader will be elucidated regarding ALK-driven NSCLC patients' features, which treatment lines are available and which problems the clinicians face when there is no other treatment option. Finally, the immunology concepts behind ALK-driven malignancies will be reviewed by stepping back in tumor immunology history and knowledge to understand how we can develop, now-a-days, immunotherapeutic approaches that possibly will overcome ALKi resistance mechanisms.

### A1) Protein Tyrosine Kinases

One of the fundamental mechanisms by which cells in multicellular organisms communicate is the binding of polypeptide ligands to cell surface receptors that carry tyrosine kinase catalytic activity. The enzymes that carry out this mechanism are the protein tyrosine kinases (PTKs). The specific reaction catalyzed by PTKs is the transfer of the  $\gamma$  phosphate of ATP to the hydroxyl group of a tyrosine residue in a protein substrate. Consequently, tyrosine residue phosphorylation is the result of intercellular communication, which modulates enzymatic activity and creates binding sites for the recruitment of downstream signaling proteins [2].

There are two classes of PTKs: (I) the transmembrane receptor PTKs and (II) the non-receptor PTKs. The transmembrane receptor PTKs, or simply known as receptor tyrosine kinases (RTKs), are membrane glycoproteins involved in controlling a wide range of complex biological functions, including cell growth, mobility, differentiation, and metabolism [2, 3]. The human genome encodes 58 RTKs [4] which are further divided into 20 subfamilies, including the receptor for insulin and many growth factors, such as the epidermal growth factor (EGF), fibroblast growth factor (FGF), platelet-derived growth factor (PDGF), vascular endothelial growth factor (VEGF), and nerve growth factor (NGF), among others (figure 1) [2, 5, 6].

Due to the fact that RTKs are critical components of cellular signaling pathways, their catalytic activity is strictly regulated, and the need for such tight regulation is emphasized by the numerous RTKs that have been identified as oncogenes. Given the recent advances of the genomic era and the implementation of next-generation sequencing (NGS) in cancer research and clinical routine practice, mutational landscapes have been established in almost all types of human tumors, revealing the presence of several different types of alterations in genes encoding RTKs, such as ALK, EGFR, HER2/ErbB2, MET, amongst many others [7].

The second class of PTKs is a large family of non-receptor tyrosine kinases (NRTKs) or also known as cytosolic TK, which includes Src, the Janus kinases (Jaks), and Abl, etc. The NRTKs are integral components of the signaling cascades triggered by RTKs and by other cell surface receptors such as G protein-coupled receptors [2]. Even

though NRTKs can also have a key role in oncogenicity, they are not the main subject of this thesis; therefore their role as oncodrivers will not be mentioned.

### A1.1) Receptor Tyrosine Kinase structure, activation and regulation

In general, RTKs exhibit similar structure. They consist of a ligand-binding extracellular hydrophilic domain (which recognizes the polypeptide ligands), followed by a hydrophobic transmembrane helix (also called transmembrane domain [TMD], that makes the embedding possible within the lipid bilayer of the plasma membrane), a juxtamembrane (JM) region and a cytoplasmic portion (that possesses tyrosine kinase catalytic activity) and, finally, a flexible carboxyl-terminal (C-terminal) tail (that is dedicated to signal transduction within the cell). Typically, ligands are soluble and the binding to their receptor is specific, reversible and involves a large number of low-energy bonds (hydrogen, ionic, hydrophobic, and Van der Waals). The vast majority of RTKs exists as a single polypeptide chain and is monomeric in the absence of the ligand.

Briefly, extracellular domains (ECD) vary between subfamilies, with different binding motifs that specify ligand recognition and assembly. Through such diversity, the receptors are able to bind ligands with high specificity, preventing unwanted signal amplification and increasing signal precision. Characteristically, ECDs of RTKs contain globular domains such as immunoglobulin (Ig)-like domains, fibronectin type III-like domains, cysteine-rich domains, and EGF-like domains. The organization of the cytoplasmic portion is simpler and more conserved through receptor families. The JM and the C-terminal tail regions differ in size and tyrosine content among family members, and these differences generate and propagate different intracellular signals [2, 8-10]. Both regions, together with the tyrosine kinase insert, contain tyrosine residues that in normal conditions are autophosphorylated upon ligand binding [2].

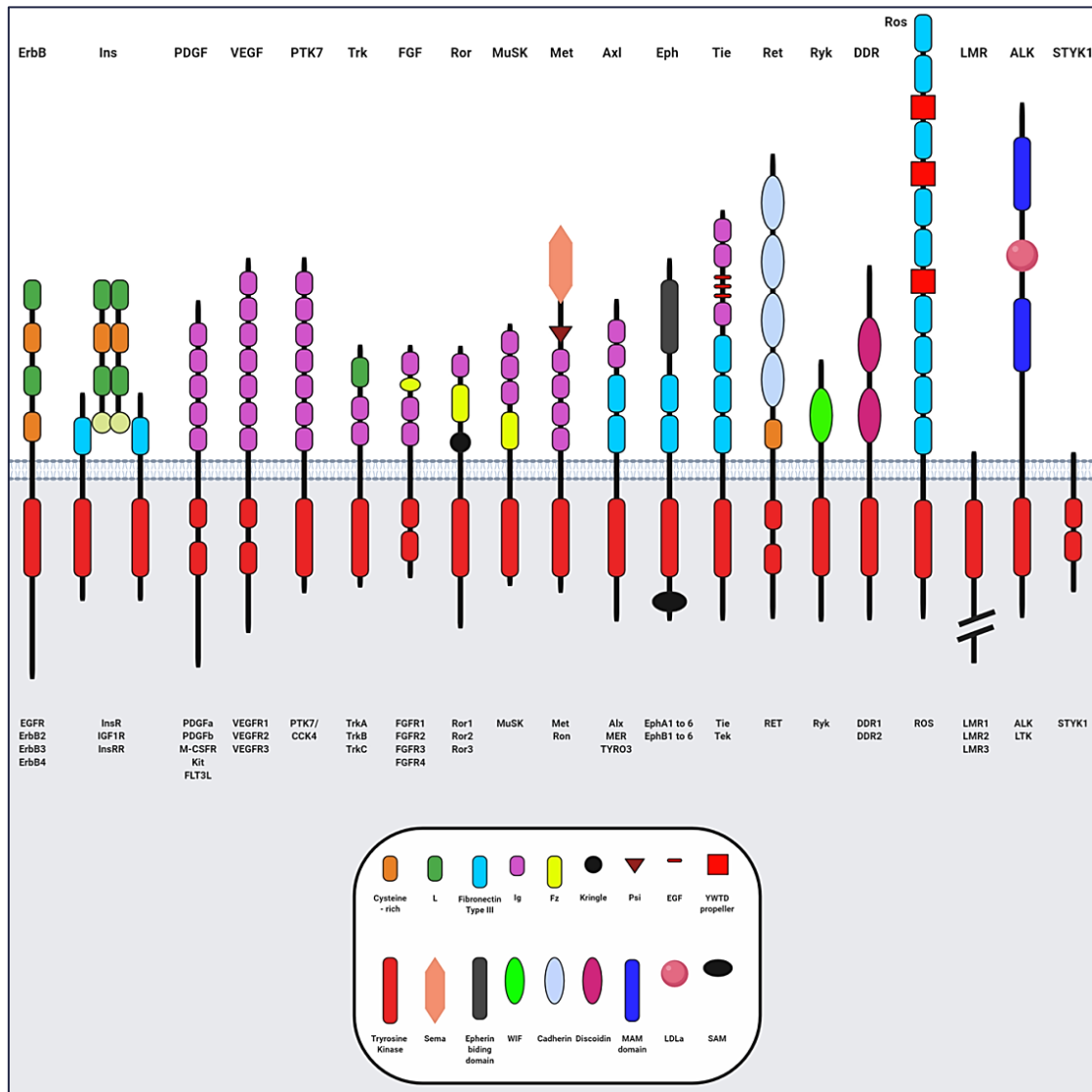


**Figure 1** - Receptor Tyrosine Kinase Families. Human receptor tyrosine kinases are divided into 20 families, shown here schematically with the family members listed beneath each family. Structural domains are marked according to Lemmon MA, et al <sup>[11]</sup>. Created with biorender.com.

Even though each RTK family has their own characteristics, the classical model of RTK activation requires two steps:

- 1) The enhancement of intrinsic catalytic activity and;
- 2) The creation of binding site to recruit downstream signaling proteins.

As a consequence of ligand-binding, the autophosphorylation of tyrosine residues within the kinase domain activation loop, results in stimulation of kinase activity and autophosphorylation of tyrosine residues in the juxtamembrane, in the kinase domain itself, and in the C-terminal region, generating binding sites for modular domains that recognize phosphotyrosine in specific sequence contexts <sup>[11-14]</sup>.

## Chapter I - Introduction

---

Downregulation of RTKs occurs via several processes, including receptor mediated endocytosis <sup>[15]</sup>, ubiquitin-directed proteolysis <sup>[16]</sup>, and the action of NRTKs <sup>[17]</sup>. In the next paragraphs, it will be discussed the known mechanisms of dysregulation of RTK in cancer.

### A1.2) Mechanisms of receptor tyrosine kinase activation in cancer

The RTK activity is tightly balanced under normal physiologic conditions <sup>[18]</sup>, nevertheless, the acquired dysregulation of RTKs results in the disruption of the balance between cell growth/proliferation and cell death <sup>[11, 19]</sup>. This abnormal RTK activation in cancer is mediated by four principal mechanisms: I) gain-of-function mutations, II) genomic amplification, III) chromosomal rearrangements and IV) autocrine activation (figure 2A) <sup>[3, 11]</sup>.

#### A1.2.1) Activation by gain-of-function mutations

It is known that gain-of-function mutations in RTKs lead to abnormal downstream signal transduction, escaping to the normal “checks and balances” that occur in the normal physiological signaling. These mutations that confer a selective growth advantage to the cells are defined as “driver mutations” and their identification and functional characterization have shed light on the understanding of cancer initiation and progression, providing potential opportunities for targeted treatments <sup>[7]</sup>.

These somatic or germline mutations can occur in any domain of RTK and typically cluster in evolutionally conserved residues, such as the DFG motif in the kinase activation loop and around the nucleotide-binding pocket.

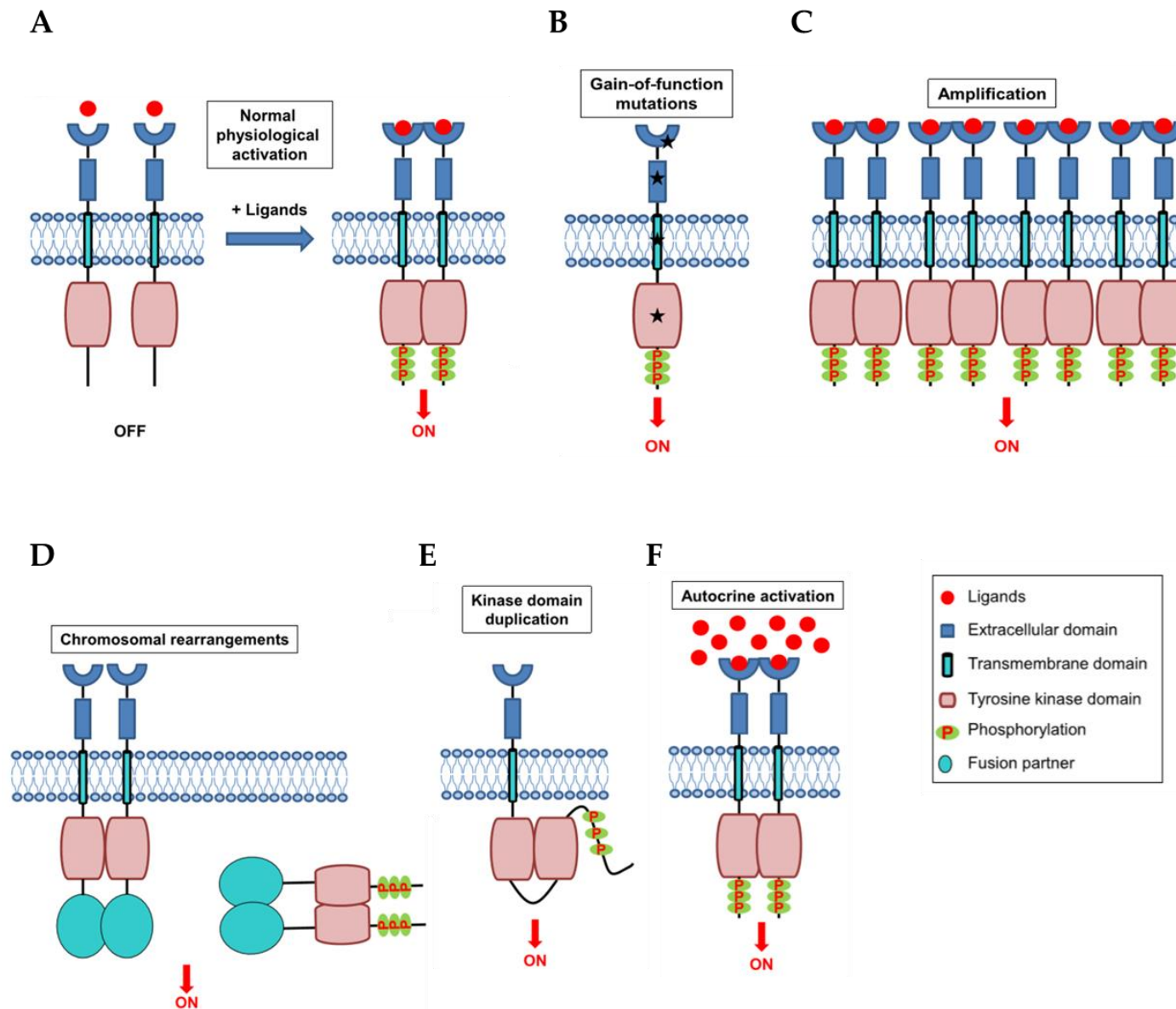


**Figure 2** - Mechanisms of physiological and oncogenic RTK activation. A) Schematic representation of the RTK activation in normal conditions. RTKs are activated through formation of inter-molecular dimerization upon ligand-binding, resulting in kinase activation and phosphorylation of the C-terminal tail. B) Schematic representation of gain-of-function point mutations in all subdomains of an RTK. The point mutations lead to constitutive activation of the RTK, usually in the absence of the ligand. C) Overexpression of RTKs as a result of genomic amplification of the RTK gene, leading to increased local concentration of receptors. D) Chromosomal rearrangements resulting in the formation of a hybrid fusion oncoprotein consisting partly of the RTK and partly of the fusion partner. These proteins can be membrane bound (left side of the figure) or cytoplasmic (right side of the figure) depending on the location of the genomic breakpoint. In either case, the result is an activated kinase domain. E) Duplication of the tyrosine kinase domain that can possibly form an intra-molecular dimer in the absence of ligands, resulting in RTK activation. F) Autocrine activation of RTK signaling. Local increased concentration of ligand activates de RTK, resulting in RTK dimerization and increased kinase activity, and phosphorylation of the C-terminal tail. Figure and legend adapted from Du and Lovly, *Molecular Cancer* (2018) [3].

## Chapter I - Introduction

---

Those conserved residues (D, F, and G) are known for playing key roles in the ATP binding and catalytic activity [20, 21].

One example is the somatic EGFR mutations. The entire EGFR TKD is encoded by exons 18-24 and mutations predominantly cluster among exons 18-21 (which are adjacent to the ATP-binding pocket) [22]. Around 90% are small in-frame deletions within exon 19 or L858R point mutation within exon 21 [23-25]. This mutation constitutively activates the kinase domain and, consequently, the downstream signaling, giving rise to oncogenic properties [22, 26, 27].

Mutations in the TMD of RTKs are also described in the literature. One example is the HER2 G660D and V659E mutations in the TMD of the HER2 receptor in non-small cell lung cancer (NSCLC) [28]. These mutations disturb specific protein-protein and protein-lipid interactions within the HER2 TMD, which are essential for the correct receptor dimerization [29].

Mutations within the JM domains bring auto-inhibitory juxtamembrane interactions and consequently hyperactive the RTKs, such as Kit V560G and PDGFR $\alpha$  V561D mutation in GIST (figure 2B) [30].

### A1.2.2) Overexpression and genomic amplification

Overexpression and genomic amplification leads to increased local concentration of the receptor, which results in elevated RTK signaling, overwhelming the antagonizing regulatory effects [3, 31].

Gene amplification is characterized by the increased number of copies of a define RTK genomic region and might be influenced by common chromosomal fragile sites, defects in the DNA replication, or telomere dysfunction [32]. It can occur as extrachromosomal elements (which tend to result in high level amplification with more than 25 copies), repeated units at a single locus (distributed in a tandem fashion) or distributed throughout the genome (distributed insertions that tend to low level amplification with 5 to 25 copies) [33, 34].

Several RTKs genomic amplification have been reported in lung cancer, such as ALK, EGFR, ERBB2 and MET [32, 35, 36]. Other RTK amplifications include FGFR1 in lung and breast cancer [37, 38], FGFR3 in breast and bladder cancer [39, 40], ERBB4 in breast and



gastric cancer [41, 42], FLT3 in colorectal cancer [43], c-Kit in melanoma and GastroIntestinal Stromal Tumor (GIST) [44, 45], and PDGFR $\alpha$  in Glioblastoma (GBM) [46].

Finally, RTK amplification can also happen either in the context of a wild-type (WT) or a mutated allele. For instance, EGFR amplification was found to occur preferentially on the mutated allele in EGFR-mutant lung cancer [47]. RTK genomic amplification can also act as an avenue for tumor cells to escape target therapies. For example, MET, HER2 and ALK amplification can be detected in ALK-driven lung cancers that became resistant to ALK inhibitors therapy [48].

Although gene amplification is the major mechanism by which RTKs get overexpressed, additional mechanism of overexpression comprise transcriptional/translational enhancement [49, 50]: oncogenic viruses, or the loss of normal regulatory mechanisms such as phosphatases [51] or other negative regulators (figure 2C) [52, 53].

### A1.2.3) Chromosomal rearrangements

The importance of identifying chromosomal rearrangements (figure 2D), which lead to the formation of novel tyrosine kinase fusion oncoproteins, is underscored by the fact that these aberrant fusion proteins are often therapeutically targetable with small-molecules inhibitors [54-56].

The first tyrosine kinase fusion identified was BCR-ALB, characteristically found in patients with Chronic Myeloid Leukemia (CML) and in some patients with Acute Lymphoblastic Leukemia (ALL) [57-59]. This chromosomal rearrangement (the so called “Philadelphia Chromosome”) is the result of the t(9;22)(q34;q11) which fuses the gene encoding the ABL1 tyrosine kinase on chromosome 9 to the BCR gene on chromosome 22, forming the BCR-ABL fusion oncoprotein [59]. With the discovery of fusion oncoproteins, the treatment of patients bearing such chromosomal aberrations was revolutionized and the first tyrosine kinase inhibitor that was developed and approved by the United States (US) Food and Drug Administration (FDA) was imatinib that specifically targets the ABL kinase [60, 61]. Whereas the Philadelphia Chromosome occurs exclusively in leukemia, many others subsequently discovered tyrosine kinase fusions occur in multiple tumor types, both hematologic and solid

## Chapter I - Introduction

---

malignancies. For instance, the t(2;5)(p23;q35) fuses the gene encoding ALK tyrosine kinase on chromosome 2 to the NPM gene on chromosome 5, forming the NPM-ALK fusion oncoprotein [62] and it is found in approximately 50% of the anaplastic large cell lymphoma (ALCL) [48, 63]. Similar ALK tyrosine kinase fusions have been found in other tumor types, particularly ALK rearrangements in 3-7% of NSCLC [64, 65], approximately 50% of all inflammatory myofibroblastic tumors (IMT) [66, 67], as well as small percentages in colon cancer [54, 68, 69], thyroid cancer [54, 70], and several other types of malignancies [48, 54, 62, 71]. Several other tyrosine kinase fusions have been described, such as those that incorporate EGFR [54, 72], HER2 [73], MET [54, 74], PDGFR $\alpha$  [75] PDGFR $\beta$  [54, 67], ROS1 [54, 76, 77], RET [54, 78, 79] that are found in a wide panoply of tumor types, such as sarcoma, melanoma, gliomas, thyroid, lung, colon, breast, head and neck cancer, etc. [54].

Numerous risk factors have been considered to contribute to the chromosomal rearrangements events. Those include exposure to ionizing radiation [80, 81], topoisomerase poisons [82] and oxidative stress [83]. However, the precise molecular mechanisms remain elusive. Notwithstanding the variety of tyrosine kinase fusions described, the resultant structure of the fusion proteins conserves similarity among them. Fusions can occur either in the N-terminal or the C-terminal of the RTK, and in both cases, the TK domain is preserved. In case the genomic breakpoint occurs downstream the exons that encode the full kinase domain (with preservation of the ECD, TMD, and JM domains), the resultant fusion protein functions as a membrane-bound receptor, as it is in the case of the EGFR-RAD51 fusion protein [72]. However, if the genomic breakpoint occurs upstream the exons encoding the full kinase domain but with loss of the ECD, TMD and JMD, then the resulting fusion protein will not be membrane bound. Typically, such fusion proteins are localized in the cytoplasm, as it is in the case of EML4-ALK fusion protein [64].

An additional characteristic of kinase fusions is the occurrence of multiple fusion partners within the same disease [54, 67, 84]. For example, there are up to 10 known ALK fusion partners found in ALCL, including NPM1 (5q35.1), TPM3 (1q21.3), ATIC (2q35), TFG (3q12.2), TRAF1 (9q33.2), CLTC (17q23.1), RNF213 (17q25.3), TPM4 (19p13.1), MYH9 (22q12.3), and MSN (Xq12) [48].

Albeit the variety of the translocation partners, all of them share three features:

- 1) The regulatory unit of the fusion partner is the one dictating the expression of the fusion, which places the tyrosine kinase oncoprotein under the endogenous promoter of the fusion partner [68, 85];
- 2) Most fusion partners contribute with an oligomerization domain that will promote ligand independent constitutive activation of the kinase [54, 86]. It is known that the most common oligomerization domains that were found in the fusion partners are coiled-coil domains. One example is EML4-ALK detected in NSCLC, which homodimerizes due to a coiled-coil domain in EML4 [64]. In case the coiled-coil domain is disrupted, the EML4-ALK fusion protein loses the ability of transforming cells [64];
- 3) The subcellular localization of the fusion protein is determined by the fusion partner [87, 88], and it might have profound effects on the protein interactions that the fusion will encounter, which might affect activation, signaling, function, and degradation of the fusion protein. As a result, tyrosine kinase fusion proteins can regulate similar cell signaling pathways as the “parental” RTK, such as RAS/MAPK, PI3K/AKT, and JAK2/STAT [67, 72], and/or possibly even new pathways, based on their altered cellular localization.

### **A1.2.4) Constitutive activation by kinase domain duplication**

Another known mechanism of constitutive activation of RTK is the intragenic partial duplication, which is a type of chromosomal rearrangement that confers cancer cells the ability to acquire new protein isoforms (figure 2E) [89]. One type of intragenic partial duplication is the kinase domain duplications (KDDs). It is known that these duplications are a method by which species introduce genetic novelty or redundancy, turning them, in this way, more adapted to environmental conditions. One example is the oncogenic EGFR-KDD that has been reported in human cancers such as NSCLC, gliomas, sarcoma and Wilms’ tumor [90, 91]. EGFR-KDDs have also been reported in post-treatment biopsy of patients treated with afatinib, which suggests that KDD can also be involved in the acquired resistance of EGFR TKI [92].

The mechanism of activation of KDD variants involves constitutive intramolecular dimerization; therefore, signaling can be activated in a ligand independent manner <sup>[90]</sup>.

### A1.2.5) Autocrine activation

The constitutive autocrine activation can lead to clonal expansion and tumor formation <sup>[93]</sup>, and this phenomenon has been well characterized (figure 2F) in diverse types of cancers, including TGF $\alpha$ -EGFR <sup>[94]</sup>, HGF-MET <sup>[95, 96]</sup>, and SCF-KIT autocrine loops <sup>[97-99]</sup>. RTK autocrine loop may work synergistically with other autocrine growth pathways and drive tumor development <sup>[97]</sup>. Autocrine pathways could act as a rational target for cancer therapy <sup>[94]</sup>. For example, ligand/receptor autocrine loops renders EGFR-mutant lung cancer cells less sensitive to EGFR TKI inhibition <sup>[100]</sup>.

### A1.2.6) Other mechanisms

There are emerging mechanisms described in the literature that are responsible for the constitutive activation of RTK. One of such is the MicroRNAs that can directly modulate the expression of RKTs and function as both tumor suppressors and oncogenes <sup>[101]</sup>. It has been reported that MicroRNAs inhibitors could have synergist effects when combined with, for instance, monoclonal antibody against EGFR, improving the treatment outcome in GBM <sup>[102]</sup>. Also, MicroRNAs could function as potential prognostic markers and assist in patient stratification <sup>[102]</sup>. Therefore, a better understanding of the involvement of MicroRNAs in RTK signaling may have future implications in cancer detection, therapy and prognosis. Another mechanism that has been described is the alteration in the tumor microenvironment. This mechanism has been notable due to the advances made in the last decade in the recognition of the importance of the tumor microenvironment <sup>[103]</sup>. One example is the RET and GFRA1 that have been shown to be expressed in stromal cells of the bone marrow microenvironment and associate with the development of Acute Myeloid Leukemia (AML) <sup>[104]</sup>. Therefore, RTKs activation in the tumor microenvironment may represent an attractive potential target for drug design.

### B1) Anaplastic Lymphoma Kinase (ALK)

The Anaplastic Lymphoma Kinase (ALK) was originally identified in 1994. ALK acquired transforming capability was described when truncated and fused with nucleophosmin (NPM) as a result of the t(2;5)(p23;q35) chromosomal rearrangement associated with Anaplastic Large Cell Lymphoma (ALCL) [105].

Now-a-days, several point mutation and chromosomal rearrangements, which lead to enhanced ALK activity, have been described in the literature together with their implications in a wide number of cancer types. Most likely, it was EML4 (echinoderm microtubule-associated protein like 4)-ALK fusion protein, reported for the first time back in 2007 by Soda and collaborators in a subset (3-7%) of Non-Small-Cell Lung Cancer (NSCLC) [64], together with the identification of activating point mutations in neuroblastoma that have highlighted ALK as a significant player and target for drug development in cancer [35, 36]. In this subchapter, I will address the physiologic role of ALK across species, and in disease.

#### B1.1) ALK conserved structure, function and signal transducing through species

The characteristics of the full-length ALK were not revealed until 1997 when, for the first time, it was reported by two groups [106, 107] in simultaneous. Based on its overall characteristics, initially ALK was categorized in the insulin receptor superfamily but now-a-days it has its own RTK family together with LTK receptor [8, 11, 106-108].

ALK display classical structural features of RTKs, consisting of an extracellular ligand-binding domain, a transmembrane region followed by an intracellular tyrosine kinase domain (figure 3) [106, 107].

In humans, the ALK gene is located on the chromosomal region 2p23 and encodes a protein of 1620 amino acids, approximately 180 kDa. However, as a result of post-translational modifications such as N-linked glycosylations, ALK full-length protein migrates at approximately 220 kDa on SDS/PAGE [106, 107].

Structurally, the ALK extracellular region contains a unique combination of domains among the RTKs families. It exhibits an N-terminal signal peptide that is followed by two MAM (meprin, A5 protein and receptor protein tyrosine phosphatase

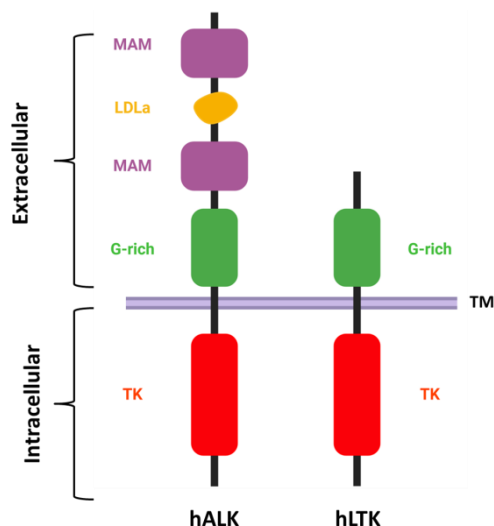


**Figure 3** - Domain structure of human ALK and human LTK. The N-terminal region of human ALK (hALK) comprises two MAM domains (amino acids 264–427 and 480–626), one LDLa domain (amino acids 453–471) and a glycine rich (G-rich) region (amino acids 816–940). A transmembrane (TM) which connects the extracellular region with the tyrosine kinase (TK) domain (amino acids 1116–1383). The closest family member, LTK (hLTK), is illustrated with the corresponding regions. Figure and legend according to R. H. Palmer Biochem. J. (2009) [1]. Created with Biorender.com.

$\mu$ ) domains, an LDLa (low-density lipoprotein class A) motif and a large glycine-rich region that is proximal to the membrane (figure 3) [106, 107, 109, 110]. Even though LDLa mediates the binding between the LDL receptor and LDL [111, 112], suggesting a potential role in ligand binding for this domain of ALK, its function on ALK has an unknown function.

The MAM domains are thought to participate in cell-cell interactions [113], but, as it is with the LDL domains, their function in ALK is still unclear. However, MAM domains importance is emphasized in studies using *Drosophila melanogaster* in which a point mutation altering a highly conserved aspartic acid residue in the MAM domain to arginine renders dALK (*Drosophila* ALK) inactive [114].

The function role of the glycine-rich domain in the extracellular domain of the full-length ALK has also been reported in *Drosophila melanogaster*. Several loss-of-function dALK mutants display point mutations that convert a single glycine residue within the glycine-rich region into an acidic amino acid [114].

ALK receptor structure organization is conserved throughout evolution, having the highest conservation within the kinase domain. Actually, mouse and human ALK show 87% overall homology at the protein level, and more importantly, within the kinase domain they differ at only four amino acids. However, even though both mouse and human ALK are very similar, it should be mention that human ALK contains one extra tyrosine residue, Tyr 1604, which has been implicated in tumor progression [115].

### B1.1.1) *Drosophila melanogaster* ALK (dALK)

Studies performed in *Drosophila melanogaster* have been shown the *in vivo* function of ALK [109]. During embryonic development of *D. melanogaster*, dALK plays an important role in the formation of the visceral musculature of the gut [114]. In the absence of dALK, fruit fly embryos hatch into gut-less larvae and consequently die due to a lack of specification of a particular cell type in the developing gut musculature of *D. melanogaster* embryos [116-118]. The dALK signal transduction pathway in *D. melanogaster* WT is activated through the binding of the Jeb (jelly belly) ligand to a specific set of cells in the embryonic visceral mesoderm (the so called founder cells), that in turn is fused with competent myoblasts to give rise to the visceral musculature of the gut [116-120]. For that reason, loss of dALK results in an absence of founder cells, as well as muscle cell fusion, leading to defective assembly of a functional gut musculature in dALK mutant fruit flies.

The Jeb ligand is a secreted protein of approximately 61 kDa containing a secretory signal and an LDLa domain [121]. Ligand-receptor interaction appears to be mediated fashion the LDLa domain in Jeb, as a Jeb mutant ligand, lacking the LDLa domain is unable to bind dALK [117]. Jeb/dALK signaling pathways leads to ERK activation and further downstream transcription of target molecules such as Duf (dumbfounded)/Kirre (kin of irregular chiasm) [116-118], Org [117], Hand [122], and Dpp (decapentaplegic) [123]. Jeb/dALK pathway is also critical for the development of the *D. melanogaster* embryonic endoderm in an indirect manner since dALK activity in the visceral mesoderm is required for Dpp [TGF $\beta$  (transforming growth factor  $\beta$ )] transcription and subsequent signaling in the adjacent endoderm [123].

Finally, dALK and Jeb play a central role acting as an anterograde signaling pathway mediating neuronal circuit assembly in the fruit fly visual system. In the development of the *D. melanogaster* eye, dALK is expressed in, and required for, the targeting of neurons in the optic lobe, whereas Jeb is primarily produced by photoreceptor axons, functioning to control target selection of R1–R6 axons in the lamina and R8 axons in the medulla. Lack of either proteins results in mistargeting of the R8 axons during later maturation of the optic lobe neuropile [124].

## Chapter I - Introduction

---

### B1.1.2) *Caenorhabditis elegans* ALK [SCD-2 (suppressor of constitutive dauer-2)]

In studies performed in *C. elegans*, ALK has been implicated in neuronal control of entry into dauer and synapse stabilization [125, 126]. *C. elegans* ALK (formally known as SCD-2), was identified as an effector through which the F-box protein Fsn-1 (F-box protein at the synapse-1) stabilizes synapse formation in GABAergic neuromuscular junctions [125]. Finally, epistatic analysis in *C. elegans* suggests that SCD-2 modulates the TGF $\beta$  pathway upstream of Daf3 (abnormal dauer formation 3; Smad)/Daf5 (Sno/Ski) [126]. The SCD-2 ligand has been identified as Hen-1 (hesitation-1) [127], which as it happens in *D. melanogaster*, is a secreted ligand containing an LDLa domain, and the genetically mapped signal transduction pathway employs the adaptor SOC-1 (suppressor of Clr-1) and the MAPK (mitogen activated protein kinase) SMA-5 (small body size-5) [126].

### B1.1.3) *Danio rerio* ALK (Zebrafish LTK/ALK)

The LTK/ALK family in Zebrafish comprises two genes: LTK and ALK, both containing MAM domains [128], contrasting with mouse and human LTK which both lack MAM domains.

Several studies in Zebrafish have demonstrated the *in vivo* role of LTK. During embryogenesis, LTK signaling leads to specification of iridophores from the neural crest lineage and mutants in LTK display defects in pigmentation patterns [128]. Even though LTK in Zebrafish has no reported ligand to date, its expression in the developing neural crest is of particular interest given the human ALK activating mutations in neuroblastoma.

### B1.1.4) Mammalian ALK

In mammals, ALK has been postulated to play an important role in the normal development and function of the nervous system. This hypothesis arises from the extensive expression of ALK mRNA throughout the nervous system during mouse embryogenesis [106, 107, 129]. A similar pattern has been described in a subtype of Dorsal



Root Ganglia (DRG) neurons during DRG development in the rat [130]. However, the expression pattern of ALK diminishes after birth, reaching the minimum level at 3 weeks of age and is maintained at low levels in the adult animal [106].

Studies in human tissues carried out by immunohistochemistry approaches, have revealed the same pattern reported in the mouse ALK, with a weak ALK signal observed in the Central Nervous System (CNS) [131]. However, different sizes of ALK transcripts have also been reported in the testis, small intestine, colon, prostate and brain of adult human material, which suggests that different splicing of ALK may occur [132].

In the early 2000's, Souttou and colleagues have supported the role of ALK in the neuronal development in mammals. They substituted the extracellular region of ALK with the mouse IgG Fc domain, which resulted in the establishment of a constitutively active membrane-bound ALK-IgG Fc hybrid protein that had the capability of inducing the neuronal differentiation of PC12 cells. When the MEK (MAPK/ERK kinase) was inhibited, the hybrid protein signaling was blocked, meaning that neurite outgrowth activity is mediated via the MAPK pathway [133]. Besides, when using antibodies to activate ALK, it has been described that the association of ALK with Shc (Src homology and collagen homology) is required for downstream ERK1/2 activation and neurite extension, further underscoring the hypothesis that neuronal differentiation induced by ALK is mediated via the MAPK pathway [134, 135].

### **B1.1.4.1) Mouse ALK (mALK)**

Morris and his group have developed ALK mutant mice that are viable without any gross alteration [136]. Bilslund et al. [137] and Lasek et al. [138], also reported that ALK deficient mice are viable and fertile without obvious changes. Remarkably, the loss of ALK signaling results in a decrease in newborn neurons and in impaired progenitor generation of myelinated axons [139] and increased number of progenitor cells within the hippocampus [137], also increased performance in hippocampal-associated tasks, as well as increased levels of dopamine within the basal cortex [137]. However, the closest ALK relative, LTK, is expressed in pre-B-cells and adult neurons in the hippocampus and cerebral cortex [140], which gives the idea that LTK might compensate for ALK loss

given the fact that the ALK mutant phenotype is hippocampus related. Also because it is known that LTK is able to promote neuronal differentiation of PC12 cells, which, again, underscores the fact that ALK and LTK may potentially compensate for one another [141]. Nevertheless, mouse LTK appears to be expressed only in the adult life of the mouse and not during development [140], which suggests a clear distinction from ALK that is extensively, but not exclusive, expressed during embryogenesis [106, 107, 129]. Furthermore, whereas LTK and ALK share high similarity within the tyrosine kinase domain, the extracellular region is completely different, with LTK lacking several domains that are found in ALK, such as the MAM and LDLa domains (figure 3).

Up to the present time, there are no reports in the literature with mouse LTK knockout to suggest a role for this RTK *in vivo*, and therefore the question of whether or not LTK may substitute ALK in its absence remains unclear.

### **B1.1.4.2) Human ALK (hALK)**

The hALK is presented in two ways: as a 140 kDa protein, as well as the better known 220 kDa full-length ALK [106]. The 140 kDa ALK is thought to be the result of a cleavage within the extracellular region of full-length ALK, generating an 80 kDa form of unknown function [142]. The 140 kDa ALK protein is phosphorylated in response to activation of ALK [134, 135, 143]. Moreover, the presence of an 85 kDa ALK protein that is phosphorylated in response to activating ALK antibodies has also been observed in NIH 3T3 cells expressing full-length human ALK [135]. It is possible that these shorter forms of ALK are generated after activation of the receptor as part of the down-regulation/degradation processes within the cell. Up on the present time, it is not known the physiological function of these shorter ALK variants.

The specific role of ALK in human development and physiology is still poorly understood because no studies have been performed with this scope; however, as it was mention above, studies performed in other species have predicted the specific role of ALK in humans.

In 1997, Morris and colleagues [62] have reported that ALK mRNA is expressed in adult human brains, small intestine, testis, prostate, and colon but not in normal human lymphoid cells, spleen, thymus, ovary, heart, placenta, lung, liver, skeletal

muscle, kidney, or pancreas. Historically, several proteins have been reported to be the activating ligands of mammalian ALK, such as pleiotrophin (PTN), midkine (MK), osteoblast-specific factor-1 (OSF-1), heparin affinity regulatory peptide (HARP) and heparin-binding neurotrophic factor (HBNF) [144]. However, recent studies have shown that augmentor  $\alpha$  and  $\beta$  (FAM150) are validated ligands of ALK [145-147].

### B1.2) Structure of ALK protein kinase domain

The ALK protein kinase domain has a small amino-terminal lobe and a large carboxyl-terminal lobe that contain several conserved  $\alpha$ -helices and  $\beta$ -strands [148].

The small lobe is dominated by a five-stranded antiparallel  $\beta$ -sheet ( $\beta$  1- $\beta$  5) [149], and it contains an important regulatory C-helix that occurs in active or in quiescent position. Also, contains a conserved glycine-rich (GxGxxG) ATP-phosphate-binding loop (P-loop) which is localized between the  $\beta$  1- and  $\beta$  2-strands (figure 4). This glycine-rich loop, which is the most flexible part of the small lobe, helps to position the  $\beta$ - and  $\gamma$ -phosphates of ATP for catalysis. The  $\beta$  1- and  $\beta$  2- strands harbor the adenine component of ATP. The glycine-rich loop is followed by a conserved valine (V1130) that makes hydrophobic contact with the adenine group of ATP.

The  $\beta$  3-strand typically contains an Ala-Xxx-Lys sequence. This lysine couples the  $\alpha$ - and  $\beta$ -phosphates of ATP to the  $\alpha$ C-helix. A conserved glutamate occurs near the middle of the  $\alpha$ C-helix (E1167) in protein kinases. The presence of a salt-bridge between the  $\beta$  3-lysine and the  $\alpha$ C-glutamate is a pre-requisite for the formation of the activated state and corresponds to the “ $\alpha$ C-in” conformation. The  $\alpha$ C-in conformation is necessary but not sufficient for the expression of full kinase activity. However, the absence of this salt bridge indicates that the kinase is dormant.

The large lobe of ALK protein kinase domain is mostly  $\alpha$ -helical (figure 4) and it has six conserved segments ( $\alpha$ D- $\alpha$ I) [149]. Plus, it contains two short conserved  $\beta$ -strands ( $\beta$  7- $\beta$  8), which contain most of the catalytic residues associates with phosphoryl transfer from ATP to ALK substrates.

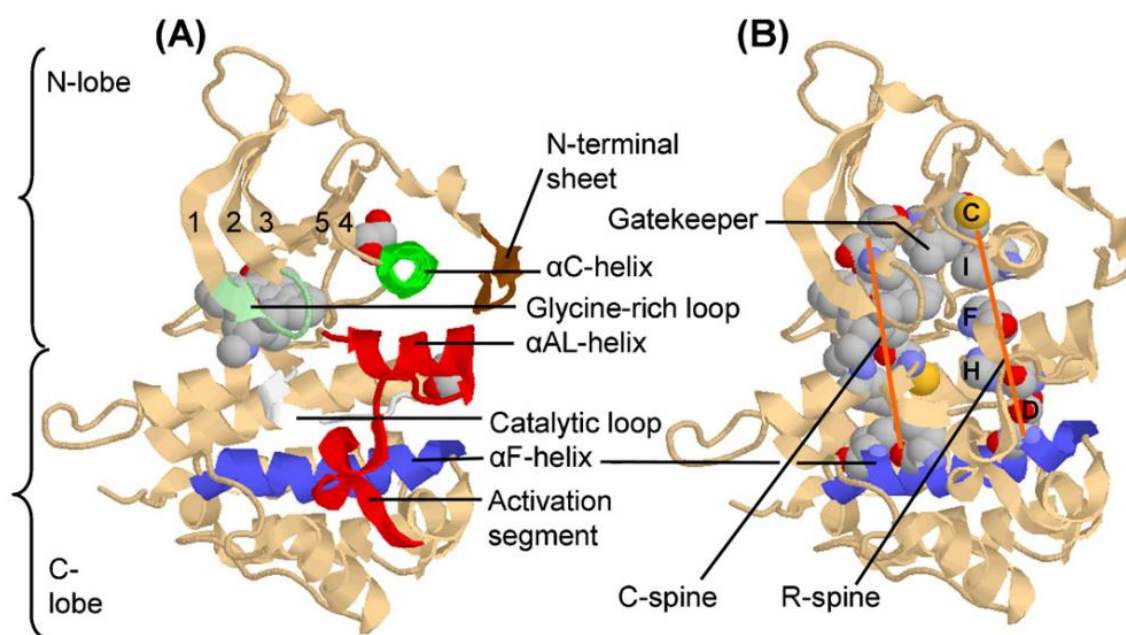


**Figure 4** - Ribbon diagram of human ALK. A) The numbers in the N-lobe label  $\beta$ -strands 1-5. This structure corresponds to a dormant enzyme with the activation segment blocking the peptide binding site. The  $\alpha$ C-helix is viewed from its N-terminus. The  $\alpha$ AL-helix occurs in the activation loop or activation segment. It is shown the space-filling model of staurosporine, which is an inhibitor of many protein kinases, and it is occupying the ATP-binding site beneath the glycine-rich loop, and a glycerol molecule is shown above the  $\alpha$ C-helix and behind the  $\alpha$ AL-helix. B) The orange lines denote the residues (space-filling models) that constitute the catalytic and regulatory spines. Although the regulatory spine of quiescent enzymes may be broken, the structure of unphosphorylated ALK has the DFG-Asp in conformation, which is usually associated with a completed R-spine <sup>[150]</sup>. Although the isoleucine and phenylalanine of the spine are aligned, they do not contact one another as shown in the picture. The ALK gatekeeper (Leu1196) contacts both spines. Figure and legend adapted from Robert Roskoski Jr; Pharmacological research, 2013 <sup>[151]</sup>.

The primary structure of the  $\alpha$ -strands occurs between those of the  $\alpha$ E- and  $\alpha$ F-helices. The quiescent form of ALK tyrosine kinase domain contains an additional helix within the activation loop ( $\alpha$ AL <sup>[152]</sup> or  $\alpha$ EF <sup>[153]</sup>, which immediately follows the  $\beta$  8-strand. Some groups have identified 12 subdomains (I-Via, VIb-XI) with conserved amino-acid residue signatures that constitute the catalytic core of protein kinases <sup>[154]</sup>. Of these, the following three amino-acids, which define a K/D/D (Lys/Asp/Asp) motif, illustrate the catalytic properties of ALK.

An invariant  $\beta$  3-strand lysine (K1150) forms salt bridges with the  $\alpha$  and  $\beta$ -phosphates of ATP (figure 5). The catalytic loops surrounding the actual site of phosphoryl group transfer are different between the protein-serine/threonine and protein-tyrosine kinases. This loop is made up of an YRDLKPEN canonical sequence in

protein serine/threonine kinases and an HRDLAARN sequence in protein-tyrosine kinases.

The AAR sequence in the catalytic loop represents a receptor tyrosine kinase signature, and RAA represents a non-receptor tyrosine kinase. D1249, which is a base occurring within the catalytic loop, plays an important role in catalysis. Zhou and Adams <sup>[155]</sup> suggested that this aspartate places the substrate hydroxyl for an in-line nucleophilic attack.

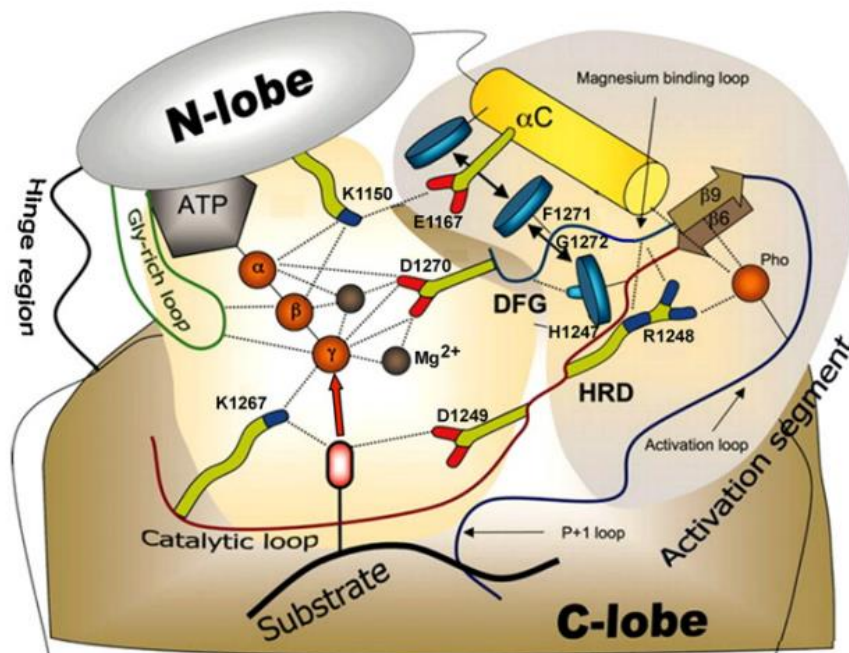
The second aspartate of the K/D/D signature, D1270, is the first residue of the activation segment. The activation segment of almost all tyrosine kinases begins with DFG (Asp-Phe-Gly) and ends with APE (Ala-Pro-Glu). The ALK activation segment begins with DFG but it ends with PPE. Asp1270 binds  $Mg^{2+}$ , which in turn coordinates the  $\alpha$ -  $\beta$  - and  $\gamma$ -phosphates of ATP. The primary structure of the catalytic loop of ALK, which occurs before the  $\beta$  7-strand, contains His1247, Arg1248, and Asp1249 (figure 5). The primary structure of the activation segment occurs after that of the catalytic loop.

The activation segment is the most important regulatory element in protein kinases <sup>[156]</sup>. It influences both substrate binding and catalytic efficiency. The five residues magnesium-positioning loop begins with the DFG of the activation segment. The middle of the activation segment is known as the activation loop. This loop in ALK contains three phosphorylatable tyrosines. It is located close in the three-dimensional sense to the magnesium-binding loop, the amino-terminus of the  $\alpha$ C-helix, and the conserved HRD component of the catalytic loop. The interaction of these three components is hydrophobic in nature, and it is indicated by the double arrows in figure 5.

Negatively charged phosphate in the activation loop of active protein kinases serves as an organizer for the active site and for the P+1 binding site. The phosphorylation site of the peptide/protein substrate is numbered as 0 (zero), the residue immediately after the phosphorylation site is P+1 and the residue immediately before phosphorylation site is P-1. The P+1 binding site of protein kinases helps determine the substrate specificity of these enzymes by selecting amino acid residues

## Chapter I - Introduction

in protein substrates that fit into this site. The P+1 site is generally composed of the last eight



residues of the activation loop.

**Figure 5** - Diagram of the inferred interaction between human ALK catalytic core residues, ATP and a protein substrate. Catalytically important residues that are in contact with ATP and the protein substrate pictured within the light background. Secondary structures and residues that are involved in regulation of catalytic activity are represented within the gray background. Hydrophobic interactions between the HRD motif (the first D of K/D/D), the DFG motif (the second D of K/D/D), and the αC-helix are shown by the double arrows while polar contacts are shown by dashed lines. Pho is the phosphate attached to Tyr1283. Figure and legend adapted from Robert Roskoski Jr; Pharmacological research, 2013 <sup>[151]</sup>.

The most important residues in human ALK are summarized in table 1.

**Table 1** - Important residues in human ALK. Table adapted from Robert Roskoski Jr; Pharmacological research, 2013 <sup>[151]</sup>

Characteristics of Anaplastic Lymphoma Kinase	
Protein kinase domain	116-1393
Glycine-rich loop	1123-1128 GHGAFG
The K of K/D/D, or the $\beta$ 3-lysine	1150
$\alpha$ C-glutamate	1167
Hinge residues	1197-1201
Gatekeeper residue	L1196
Catalytic loop lysine	1267
Activation segment DFG, the second D of K/D/D	1270-1272
Activation segment tyrosine phosphorylation sites	1278, 1282, 1283
End of the activation segment	1297-1299 PPE
No. of residues	1620
UniProtKB ID	Q9UM73

### B1.3) ALK in disease; activation and downstream signaling

As it was mentioned before, the physiologic role of ALK in humans is still unclear. The knowledge that the scientific community has acquired overtime regarding this tyrosine receptor comes, in great part, from ALK-driven tumors.

The constitutive activation of ALK activates many different pathways that are interconnected or overlapping <sup>[157]</sup>. These include the Ras/Raf/MEK/ERK1/2 pathway, the JAK/STAT pathway, the PI3K/Akt pathways, and finally, the PLC- $\gamma$  pathway. Both PLC- $\gamma$  and Ras/ERK1/2 pathways participate in cell proliferation, and the JAK/STAT and PI3K/Akt pathways mediate cell survival (figure 6).

Akt is a protein-serine/ threonine kinase that binds phosphatidylinositol bisphosphate or trisphosphate with high affinity <sup>[158]</sup>. The phosphoinositide-dependent protein kinase 1 (PDK1) and the mammalian target of rapamycin complex 2 (mTORC2) catalyze the phosphorylation of Akt Thr308 and Ser473, respectively and the bisphosphorylated and activated Akt catalyzes the phosphorylation and activation of mTOR (mammalian target of rapamycin).

mTOR is also a protein-serine/threonine kinase that has several substrates and participates in many cellular processes including cell survival. Upon activation of ALK, the tyrosine residues 1139, 1358, 1385, and 1401 in the tyrosine kinase domain and the tyrosine residues 1507, 1585, 1586 and 1604 in the carboxyl-terminal tail became phosphorylated [108]. Some of these residues serve as docking sites for the binding of molecules that participate in ALK-mediated signal transduction.

The protein tyrosine kinase Src interacts with oncogenic ALK and it may participate in some of the phosphorylation reactions within the ALK protein.

Studies in NPM-ALK have reported that pTyr1096 is the binding site for insulin receptor substrate 1 (IRS1); pTyr1507 for Shc and pTyr1604 for PLC- $\gamma$  [108]. Furthermore, Grb2 interacts with the protein tyrosine kinase Src, which binds to pTyr1358, and it also binds to Shc.

IRS1, Shc, PLC- $\gamma$ , Grb2, and Src are upstream the growth-promoting Ras/ERK1/2 pathway [157]. The activation of the ERK1/2 MAP kinase pathway by, in this case NPM-ALK, is intricate. Marzec and colleagues have demonstrated that the depletion of ERK1 or ERK2 separately or together, impairs cell proliferation, whereas ERK1 but not ERK2 depletion increases the apoptotic cell rate in KARPAS-299 ALK-positive cell line [159].

Fujimoto and colleagues have described that the interaction of NPM-ALK with IRS1 and Shc is not required for cellular transformation and oncogenesis due the fact that NPM-ALK mutants that are unable to interact with Shc and IRS1 are still able to transform rat fibroblast NIH 3T3 cells [160]. Thus, IRS1 and Shc do not play an essential role in the activation of ERK1/2 MAP kinase pathway.

JAK/STAT pathway is an important downstream signaling molecule of NPM-ALK [108], and it was demonstrated that NPM-ALK induces the continuous cellular activation of STAT3. STAT3 is activated upon its phosphorylation on a tyrosine residue that is catalyzed by a receptor or by a member of the activated JAK protein tyrosine kinase enzyme family.

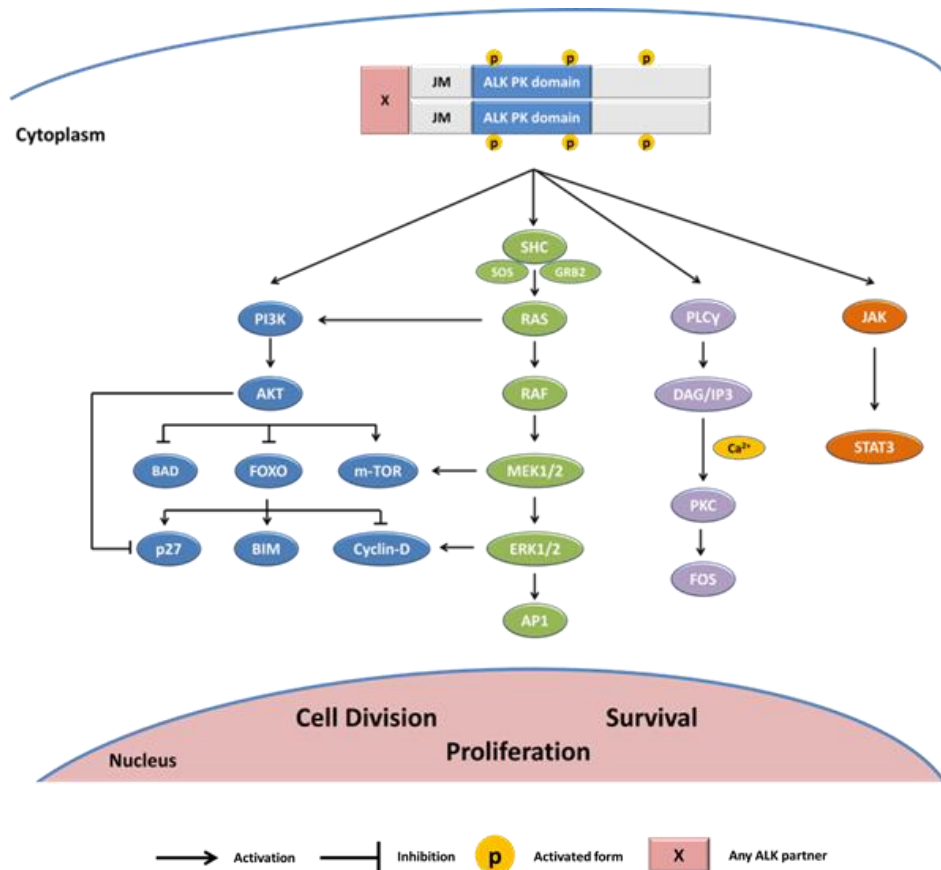
Galkin et al. have reported that the ALK inhibitor TAE-684 reduces STAT3 phosphorylation in KARPAS-299 and SU-DHL-1 ALK-positive ALCL cell lines [161]. Another group has shown that STAT3 is phosphorylated and activated in KARPAS-299



cells, and they demonstrated by immunoprecipitation that NPM-ALK and STAT3 form a complex.

However, the nature of the binding site was not determined. Therefore, STAT3 is activated by ALK either directly or indirectly through JAK [157]. Finally, the PLC- $\gamma$  pathway is downstream NPM-ALK and participates in the activation of Ras/ERK1/2 MAP kinase pathway. Following its activation, PLC- $\gamma$  catalyzes the hydrolysis of phosphatidylinositol bisphosphate to form inositol trisphosphate and diacylglycerol [157].

Inositol trisphosphate increases the release of  $\text{Ca}^{2+}$  from the endoplasmic reticulum and diacylglycerol activates the protein-serine /threonine kinase C (PKC). One of the downstream effectors of PKC is the Raf/MEK/ERK1/2 pathway leading to cell



proliferation in a process that bypasses Ras [151].

**Figure 6** - ALK downstream pathways and bypass signaling. A) ALK mediates signaling via the P13K/AKT, RAS/MAPK, PLC- $\gamma$  and JAK/STAT. Figure and legend adapted from Sharma et al, *Cancers*, 2018 [48].

As mentioned before, ALK has been associated with a large variety of tumors.

Figure 7 schematically summarizes the different categories of ALK-driven cancers.

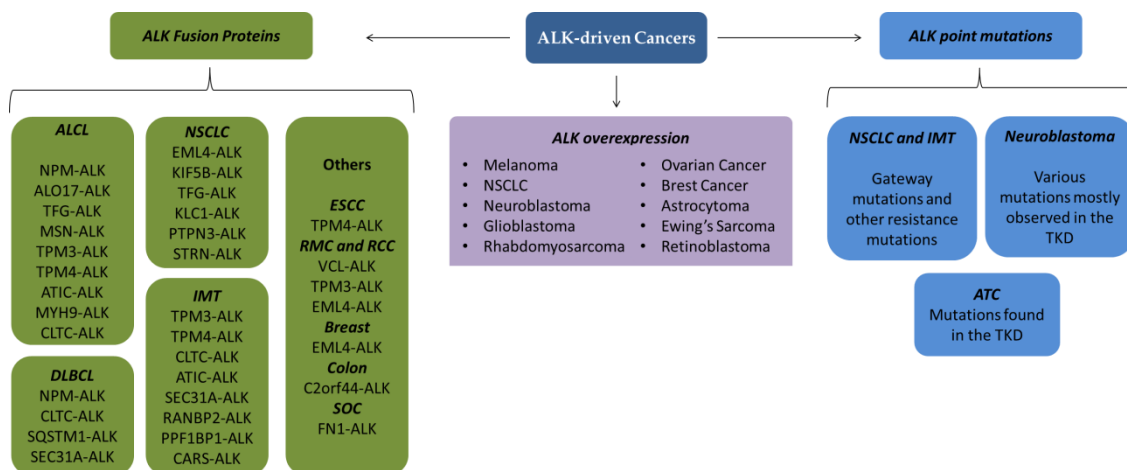


**Figure 7** - ALK in cancer: an overview. Schematic summary of the different categories of ALK-positive cancer. Shown in green, some of the ALK fusion proteins that have been described in numerous cancers, ALCL, IMT, Diffuse Large B cell Lymphoma (DLBCL), NSCLC, Renal Medulla Carcinoma (RMC), Renal Cell Carcinoma (RCC), breast cancer, colon carcinoma, Serous Ovarian Carcinoma (SOC) and Esophageal Squamous Cell Carcinoma (ESCC). ALK overexpression has been reported in various cancer types and cell lines (violet). ALK mutations comprise a third category (blue), and include both primary tumor-associated mutations and secondary mutations that are observed in crizotinib-resistant patients. Secondary mutations in the context of ALK fusions have been described in NSCLC, IMT and Anaplastic Thyroid Cancer (ATC).

ALK point mutations have been found mainly in neuroblastoma, as well as in NSCLC and ATC; most of the mutations are situated within the kinase domain of ALK. Figure and legend adapted from Hallberg B et al, *Nat Rev Cancer*, 2013 [144].

ALK overexpression can be due to different genetic mechanisms, like gain-of-function mutations, amplification and most known, chromosomal rearrangements (figure 8).

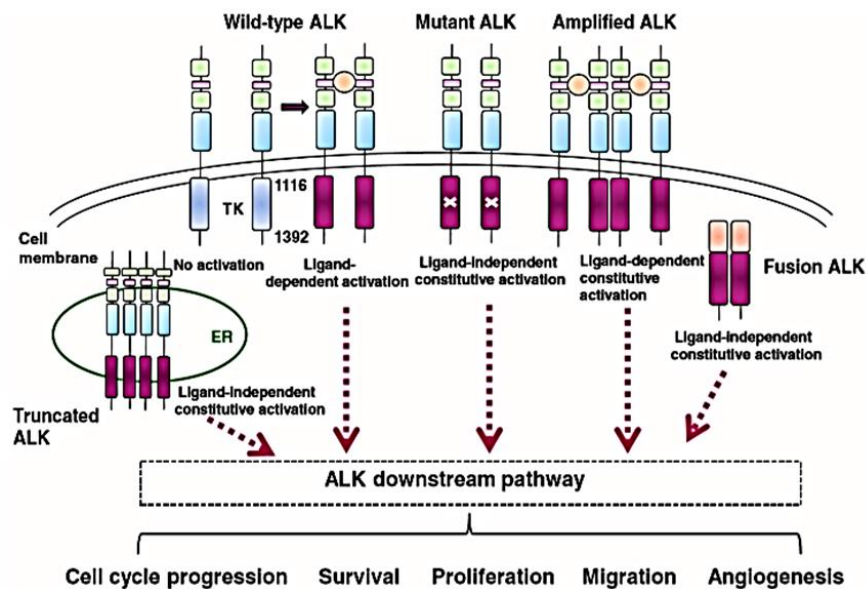


**Figure 8** - ALK signaling in normal and cancer cells. WT ALK activation through ligand binding is shown (ligand pictured in orange); ALK mutations result in ligand-independent constitutive activation of the downstream ALK pathway; whereas ALK amplification results in ligand-dependent constitutive activation

of ALK signaling. In expressed ALK fusion proteins, ligand-independent dimerization with the oligomerization domains of the partner genes leads to the constitutive activation of the ALK pathway. Finally, an aberrant form of ALK that lacks exons 2 and 3 was amplified, leading to the high-level expression of an N-terminal truncated kinase. This short form of ALK is mainly located at endoplasmic reticulum (ER) and aberrantly activates the STAT3 pathway from ER. Figure adapted from Takita J, *Cancer Sci*, 2017 [162].

### B1.3.1) ALK Gain-of-Function Mutations

Gain-of-function mutations in the full-length ALK were first described in sporadic and familial neuroblastomas, which are common childhood solid tumors [163-166]. Subsequently, activating ALK mutations were reported in adult cases of anaplastic thyroid cancer [167], pediatric cases with rhabdomyosarcoma, primitive neuroectodermal tumor (PNET) and osteosarcoma. Most of these mutations are located in the kinase domain and can be classified into three groups: 1) ligand-independent mutations (F1174I, F1174S, F1174L, and R1275Q); 2) ligand-dependent mutations (D1091N, T1151M, and A1234T), and 3) a kinase-dead mutation (I1250T) (figure 9).

## Chapter I - Introduction

ALK mutations are also acquired in ALK fusion genes as a result of resistance to ALK inhibitors in cases of NSCLC as well as ALCL [168, 169].

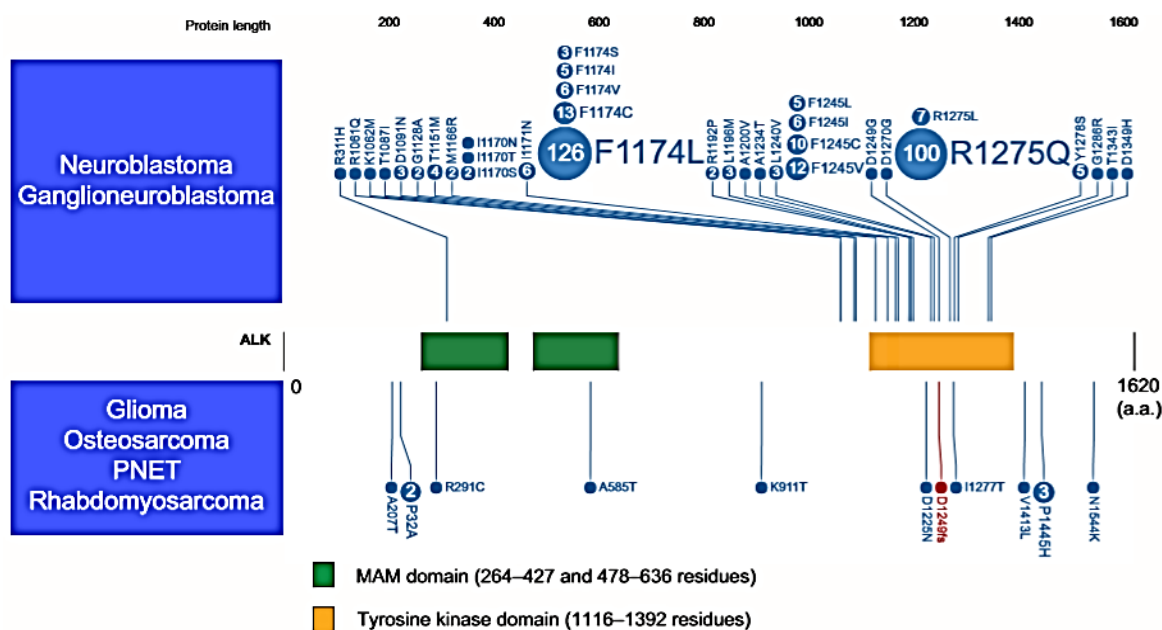


**Figure 9** - Some examples of mutations ALK mutations detected in neuroblastoma, ganglioneuroblastoma, glioma, osteosarcoma, PNET, and rhabdomyosarcoma. COSMIC frequencies of ALK mutations from published reports with functional and/or with therapeutic significance are shown. A missense mutation is indicated by a blue circle, and a frameshift mutation is indicated by a red circle. The numbers in the circles are the reported mutation numbers. a.a., amino acids. Figure and legend adapted from Takita J, Cancer Sci, 2017 [162].

### B1.3.1.1) Neuroblastoma

Neuroblastoma is the most common pediatric extracranial solid tumor and accounts for 15% of all pediatric oncology deaths [170]. This disease is derived from neural crest cells of the sympathetic adrenal lineage and therefore can arise throughout the sympathetic nervous system [171, 172]. It has a broad spectrum of clinical behaviors, ranging from localized disease with spontaneous regression with little or no therapy, to aggressive clinical course difficult to cure with current regimes and death from progressive disease [171, 172]. The best characterized genetic alteration associated with a poor prognosis is the amplification of the N-MYC oncogene [171]; also, deletions of part of chromosome arms 1p and 11q, gain of parts of 17q and triploidies were also found to correlate with poor prognosis [173, 174]. Several groups have reported ALK to be a major oncogene target in sporadic and familial neuroblastoma cases [163-166]. In familial cases,

germline ALK mutations were observed in 50% of the cases, whereas approximately 10% of sporadic cases showed ALK oncogenic mutations. Greater than 90% of all ALK mutations occur within the kinase domain (but not exclusive), being the F1174, R1275, and F1245 positions three mutations hot spots. The R1275 mutation is more frequent in familial cases compared to the F1174 mutation, which is a common mutation in sporadic cases<sup>[175]</sup>.

According to RTK homology models, F1174 is located at the end of the  $\alpha$ C-helix1, whereas the other two common mutations are located in the two  $\beta$  sheets: before the catalytic loop ( $\beta$  6) (F1245) and within the activation loop ( $\beta$  9) (R1275). The R1192P mutation, which has been reported only in familial cases, is found in the  $\beta$  4-strand of the kinase domain <sup>[152]</sup>. Expression of the F1174L and K1062M mutant proteins in NIH 3T3 cells induces neoplastic transformation <sup>[163]</sup>. In accordance with these findings, molecules located downstream ALK (Akt, STAT3, and ERK) were found to be activated in cells expressing ALK mutant forms <sup>[163-166]</sup>. Interestingly, RNAi-mediated ALK knockdown resulted in a reduced cell proliferation in cell lines harboring the F1175L mutation, but these effects were less clear in wild-type ALK-expression neuroblastoma cell lines <sup>[163, 164]</sup>.

Finally, ALK mutations were found to be highly correlated with N-MYC amplification: approximately 50% of ALK mutations co-exist with N-MYC amplifications <sup>[163, 176]</sup>. And their synergy is highlighted in transgenic and knock-in ALK mutation models <sup>[177, 178]</sup>.

### **B1.3.2) Amplification/overexpression of ALK in cancer**

ALK amplification, copy number gain, and rare structural variants ALK gene amplification can occur in a variety of cancers, and are also recognized as a therapeutic target. It has been reported ALK overexpression in thyroid carcinoma, NSCLC, breast cancer, melanoma, neuroblastoma, glioblastoma, astrocytoma, retinoblastoma, Ewing sarcoma and rhabdomyosarcoma, leiomyosarcoma and malignant peripheral nerve sheath tumors, and fibrous histiocytoma <sup>[179, 180]</sup>. However, the significance of ALK overexpression in many of these types of cancers is uncharacterized at the molecular level.

In neuroblastoma, high grade amplification of ALK has been found in cell lines and primary tissues, and the subsequent overexpression of ALK protein correlates with tumorigenesis [157]. In this case, the constitutive activation of ALK results in the phosphorylation of downstream molecules, including Shc and MAPK pathway-related proteins [181] and, as it is in point mutations, strongly correlates with N-MYC amplification [178]. In addition, recurrent copy number gain of chromosome 2p23.2 involving the ALK locus has been reported in neuroblastoma with a frequency of 35–40% [163, 178]. High ALK expression has been shown to be tightly associated with ALK amplification/mutation, as well as copy number gain of the ALK locus, suggesting the upregulation of ALK expression by increasing DNA dose [178].

Amplification or copy number gain of the ALK locus, as reported in a subset of rhabdomyosarcoma cases, is also intriguing from a therapeutic perspective. Rhabdomyosarcoma is the most common soft-tissue sarcoma in children and can be divided into two histological subtypes, embryonal (ERMS) and alveolar (ARMS). Alveolar rhabdomyosarcoma shows an aggressive phenotype, whereas embryonal has a more favorable prognosis [182].

In the case of glioblastoma, PTN has been reported to induce ALK phosphorylation and subsequent downstream PKB/Akt activation. Consequentially, glioblastoma cell lines that are depleted of ALK signaling grow at a reduced rate when compared to the parental cell line [183]. When treated targeting ALK and PTN, U87 glioblastoma cell line tumor growth is impaired in an *in vivo* xenograft model [184].

In breast cancer, the role of overexpression of ALK has not been established. First, ALK is strongly expressed in several different subtypes of human breast cancer in a pattern that is not consistent with normal tissue [185]. Second, PTN, the historically ligand associated with ALK, is extensively expressed in breast cancer [186, 187], and expression of a truncated form of PTN in a human breast cancer cell line impairs tumor formation in nude mice [188]. Finally, the PTN receptor, RPTP $\beta$ / $\zeta$ , is strongly expressed in different subtypes of human breast cancer. Taken together with the hypothesis that ALK is indirectly activated via PTN/RPTP $\beta$ / $\zeta$  signaling, it is possible that ALK has oncogenic potential in breast cancer development [188].

### B1.3.3) Chromosomal rearrangements

Since the initial discovery of ALK in form of NPM-ALK fusion protein in patients with ALCL [62, 189], various chromosomal rearrangements have been reported at the ALK locus on chromosome 2q23.2, leading to the generation of fusion genes that encode the entire intracellular domain of ALK at the 3'-end fused to several 5'-end partner genes. With the enormous advance of genome-wide studies, it has been revealed the presence of nearly 30 different ALK fusion partner in multiple type of cancer (table 2). Even though a large number of different N-terminal partners have been identified, they all share common oncogenic features, and the subsequent expression of fusion proteins is regulated by the promoter of the N-terminal partner, which is generally expressed in normal tissues and can lead to the ectopic expression of ALK [190]. The presence of oligomerization domains in the N-terminal of the partner genes is essential for the oncogenic potential of the fusion protein.

ALK fusion proteins have also been identified in IMT [191], NSCLC [64, 192], DLBL [193] and Squamous Cell Carcinoma (SCC) of the esophagus [194].

**Table 2** - ALK rearrangements in human malignancies. Table and legend adapted from Sharma et al, Cancers, 2018 [48].

Cancer Type	ALK Fusion Partner (Chromosomal Localization)	Frequency %
ALCL	NPM1 (5q35.1)	~55% (in adults)
	TPM3 (1q21.3)	
	ATIC (2q35)	
	TFG (3q12.2)	
	TRAF1 (9q33.2)	
	CLTC (17q23.1)	
	RNF213 (17q25.3)	
	TPM4 (19p13.1)	
	MYH9 (22q12.3)	
	MSN (Xq12)	
	Additional rare rearrangements	
Breast cancer	EML4 (2p21)	N.D.
Colorectal cancer	EML4 (2p21)	<1%
	WDCP (2p23.3)	
	CLTC (17q23.1)	
DLBCL	RANBP2 (2q13)	<1%
	EML4 (2p21)	
	SEC31A (4q21.22)	
	SQSTM1 (5q35)	
	NPM1 (5q35.1)	

<b>Esophageal cancer</b>	TPM4 (19p13.1)	N.D.
	TPM3 (1q21.3)	
	RANBP2 (2q13)	
	ATIC (2q35)	
<b>IMT</b>	SEC31A (4q21.22)	Up to 50%
	CARS (11p15.4)	
	PPFIBP1 (12p11)	
	CLTC (17q23.1)	
	TPM4 (19p13.1)	
	EML4 (2p21)	
	TPR (1q31.1)	
	CRIM1 (2p22.2)	
	STRN (2p22.1)	
<b>NSCLC</b>	TFG (3q12.2)	3-7%
	HIP1 (7q11.23)	
	PTPN3 (9q31)	
	KIF5B (10p11.22)	
	KLC1 (14q32.3)	
	CLTC (17q23.1)	
<b>Ovarian cancer</b>	FN1 (2q35)	N.D.
	VCL (10q22.2)	
<b>RCC</b>	TPM3 (1q21.2)	<1%
	EML4 (2p21)	
	STRN (2p22.2)	
<b>RMC</b>	VCL (10q22.2)	N.D.

### B1.3.3.1 Anaplastic Large Cell Lymphoma (ALCL)

ALK has been extensively studied in the context of ALCL, a disease first described in 1985 [195]. ALCL is a T-cell non-Hodgkin's lymphoma, and is characterized by the expression of CD30. It is mostly observed in young adults and children, accounting for 3% of adult non-Hodgkin's lymphoma and 10-30% of all non-Hodgkin's lymphoma in children [196, 197]. Moreover, ALK-driven patients have a significantly higher 5-year survival rate as compared with ALK-negative patients [198-202].

Currently, there is no FDA or European Medicines Agency (EMA) approved treatment for ALK-positive ALCL aimed at directly targeting ALK. Thus, combinatorial chemotherapy treatment is still applied for treatment of ALCL patients as a first approach [200, 202, 203].



The most frequent ALK fusion protein found in ALCL is NPM-ALK. The kinase domain of ALK is fused to NPM, creating the constitutively expressed fusion protein NPM-ALK [62]. NPM is a multifunctional protein which serves as a molecular chaperone involved in the shuttling of pre-ribosome subunits from the nucleus to the cytoplasm during ribosome biogenesis; in addition, it plays a role in DNA repair, transcriptional and genomic instability [204].

In NPM-ALK fusion protein, the oligomerization is mediated via NPM juxtaposes two tyrosine kinase domains, resulting in autophosphorylation and activation of ALK kinase activity [160, 205]. NPM-ALK fusion protein is present both in the cytoplasm and the nucleus and its location seems not to be critical for NPM-ALK-mediated transformation. Besides the dimerization ability of NPM, the kinase activity of the fusion protein is an absolute requirement for transforming activity, since mutation in the ATP-binding site (K219R) renders NPM-ALK kinase dead and eliminates transformation [205]. After NPM-ALK, numerous other fusion partners have been reported in ALCL, namely ALO17 [206], TFG [207, 208], MSN [209], TPM2 and 3 [210-212], ATIC [213-215], MYH9 [216] and CLTL [217].

As it happens in other diseases, in which several ALK fusions have been described, the fusion partners of ALK share several common characteristics, specifically: 1) the transcription of the fusion protein is driven via the promoter of the ALK partner protein; 2) the localization of the fusion protein is determined by the ALK partner proteins and; 3) oligomerization via the ALK partner protein induces autophosphorylation and thereby activation of the ALK kinase domain.

The TPM3 and TFG fusion partners contain dimeric  $\alpha$ -coiled-coil structures that are hypothesized to mediate the dimerization of TPM3-ALK [210] and TFG-ALK [207], respectively. Due the fact that ATIC exists as a homodimer [218], this property is assumed to be responsible for the activation of ATIC-ALK [213-215]. Regarding MSN, MYH9 and CLTC, the means of dimerization seems to be more complex [209, 217].

### **B1.3.3.2) ALK-positive Diffuse Large B-Cell Lymphoma (DLBCL)**

Among DLBCL there is an ALK-positive subpopulation which shows some features of plasmablastic morphology. ALK-positive DLBCL usually expresses markers

such as epithelial membrane antigen, CD138 and cytoplasmic Ig, together with ALK expression. Additionally, ALK-positive DLBCL lacks the expression of some B-cell markers (CD20, CD79a), and is typically negative for CD30 expression [219, 220]. ALK-positive DLBCL has been reported in all age groups and displays an overall predominance in males (male/female ratio 5:1). Also, it is correlated with an aggressive clinical outcome as well as a poor response to treatment [220-224].

The most frequent chromosomal rearrangement involving ALK that has been found in DLBCL is the t(2;17)(p23;q23) which generates CLTC-ALK fusion protein, although a few cases of NPM-ALK fusions have also been described [225, 226]. As previously discussed, NPM-ALK translocation induces activation of STAT3 [227, 228], and this also seems to be true in CLTC-ALK-driven DLBCL, but not in ALK-negative DLBCL [221].

### **B1.3.3.3) Inflammatory myofibroblastic tumors (IMT)**

IMT is a benign malignancy of mesenchymal origin with a prominent inflammatory component that consists of plasma cells and lymphocytes [229]. When it was described for the first time in the literature, IMT was considered a post-inflammatory condition rather than a malignant process [230]. It can be manifested in any age, even though affects mostly young people and in almost any anatomical site, although this type of benign tumors are most common in tissues such as the lung, abdomen and retroperitoneum [229, 231].

Back in 1999, Griffin and colleagues [191] have reported an association between the 2p33 chromosomal rearrangement and expression of ALK with IMTs. This was the first indication that IMTs, or a subpopulation of IMTs, had neoplastic origin rather than reactive [191]. After that, several studies have confirmed the presence of different ALK-fusion proteins in IMTs, all of them containing the kinase domain of ALK together with one of a variety of partner proteins that are responsible for dimerization of the ALK kinase domain and consequentially its activation. Some of these different ALK fusion proteins are: TMP3-ALK and TMP4-ALK [232], ATIC-ALK [233], CLTC-ALK [234, 235], CARS (cysteinyI-tRNA synthetase)-ALK [206, 236], RANBP2 (Ran-binding protein 2)-ALK [237] and SEC31L1 (SEC31 homologue A)-ALK [238]. Actually, 35-60% of all IMTs appear

to harbor ALK rearrangements [232, 239, 240]. Even though the prognosis appears to be better, and low risk of distant metastasis, around 50% of the ALK-positive cases re-occur [66].

Armstrong and colleagues have reported that TPM3-ALK fusion protein is present in 50% of the ALK-driven IMTs and its downstream signaling involves STAT3 [190]. Still little is known about this disease and what is the functional relevance and consequences of ALK signaling.

### **B1.3.3.4) Non-Small-Cell Lung Cancer (NSCLC)**

Lung cancer is the most common cause of cancer death worldwide and in 2007, when a novel gene fusion between ALK and EML4 was reported in NSCLC [238, 241], the scientific community put a tremendous effort in the development of a series of ALK TKI in different companies. About 3-7% of NSCLC patients harbor the EML4-ALK fusion protein. Since its first report [64], several EML4-ALK fusion variants have been described, among them eight different breakpoints in different exons of the EML4 gene (exons 2,6,13,14,15,17, 18 and 20 [242] but all of them containing the same portion of ALK gene [exon 20-29] which encodes the entire intracellular segment of ALK). The downstream signaling includes the Ras/ERK1/2 Akt and JAK/STAT pathways [243].

Many other studies have identified several additional ALK fusion proteins (table 2) which occur less frequently than EML4-ALK.

ALK-driven lung cancers are mostly adenocarcinomas, and unfortunately, only a small proportion of patients are diagnosed before the spread of the tumor from its original site. Even though the proportion of NSCLC with ALK rearrangements is low, the number of total cases is large. Thus, the total number of cases of NSCLC amenable to treatment with ALK inhibitors is greater than that for all other known ALK-related cancers combined.

### C1) Non-small-cell lung cancer (NSCLC)

Lung cancer is the second most frequently diagnosed malignancy in the world and it is the leading cause of cancer-related death in both men and women in the United States. About 13% of all new diagnosed cancers are lung cancers. The American Cancer Society (ACS) estimates about 228,150 new cases (116,440 in men and 111,710 in women) and about 142,670 deaths from lung cancer (76,650 in men and 66,020 in women) in the United States in 2019 <sup>[244]</sup>.

Most frequently is detected at advanced stages, usually with clinical and symptomatic evidence of metastatic disease <sup>[245]</sup>, constituting a diminished survival rate, ranging from a 5-year survival rate to 97% for stage IA1 tumors (<1 cm in diameter and no lymph node involvement) to 10% for patients with stage IV (metastatic disease) <sup>[246]</sup>.

According to World Health Organization (WHO), lung cancer is divided into two major categories based on its biology, prognosis and therapy: NSCLC and Small-Cell Lung Cancer (SCLC). NSCLC accounts for more than 80%, and SCLC accounts for less than 20% of all lung cancer cases <sup>[247]</sup>. Both lung cancer subtypes have distinct histology, biologic features and, of course, treatment strategies. However, for the purpose of this thesis, the focus will be given to NSCLC subtype <sup>[248, 249]</sup>.

As it is known even outside the scientific community, tobacco exposure is the main risk factor of lung cancer <sup>[250, 251]</sup>. Smoke contains approximately 70 carcinogens including the polycyclic aromatic hydrocarbons, and N-nitrosamines. All these compounds cause DNA damage which results in the onset of oncogenic mutations leading to lung carcinogenesis <sup>[252]</sup>. Moreover, second-hand smoking is also an important factor that is related with lung carcinogenesis, and it is responsible for 7.330 deaths from lung cancer each year in the United States <sup>[253, 254]</sup>. However, lung cancer is not restricted to patients with smoking history. Non-smokers, defined as individuals who have smoked less than 100 cigarettes in a lifetime, are also at risk of lung cancer. Worldwide, approximately 25% of lung cancers occur in non-smokers, and the incidence of this disease in never smokers is particularly high among Asian population <sup>[255-257]</sup>. These epidemiological differences between smoking status, geographic

localization and race are also correlated with significant differences in the molecular profile of NSCLC patients, particularly in the adenocarcinoma histology. Several environmental factors have been linked to the development of lung adenocarcinoma in never smoker's population. For instance, residential radon gas exposure is the leading cause of lung cancer in never smokers and second cause after smoking, which accounts for 21.000 deaths annually in the US [258, 259]. Also, exposure to asbestos, air pollution and, in lesser extent, germline mutations that result in hereditary lung cancer predisposition syndromes [260-262], have also been associated to risk factors that lead to NSCLC. However, it is still unclear why the prevalence of lung cancer in non-smoking patients around the world, and especially in Asia, is increasing lately.

### C1.1) Histological classification of NSCLC

The evolution of pathology and molecular biology has shed light into the different subtypes of NSCLC in the last decades [263]. NSCLC accounts for about 80% of all lung cancers, and several histological subtypes of lung cancer can be found within NSCLC; lung adenocarcinoma, squamous cell carcinoma, large cell neuroendocrine carcinoma, and sarcomatoid carcinomas, amongst others [247]. This sub-classification is supported, beside histology features, by the distinct molecular profiles of these tumors [55, 264]. Regarding prevalence, lung adenocarcinoma is the most frequent histological subtype in smokers and non-smokers patients, whereas lung squamous cell carcinoma is the second most common histologic subtype of NSCLC, however rare in patients with no history of tobacco exposure.

The histological classification was the first step towards a better distinction of the intrinsic molecular, phenotypical and prognostic features of NSCLC, and had become the first approach to develop “personalized” treatment strategies based on the tumor characteristics. However, the development of molecular biology techniques applied to the study of cancer genomics has revealed the complexity of genomic and epigenetic differences between these histologic subtypes. The discovery of potent oncogenic drivers in lung adenocarcinoma has given rise to the era of targeted therapies for lung cancer [265].

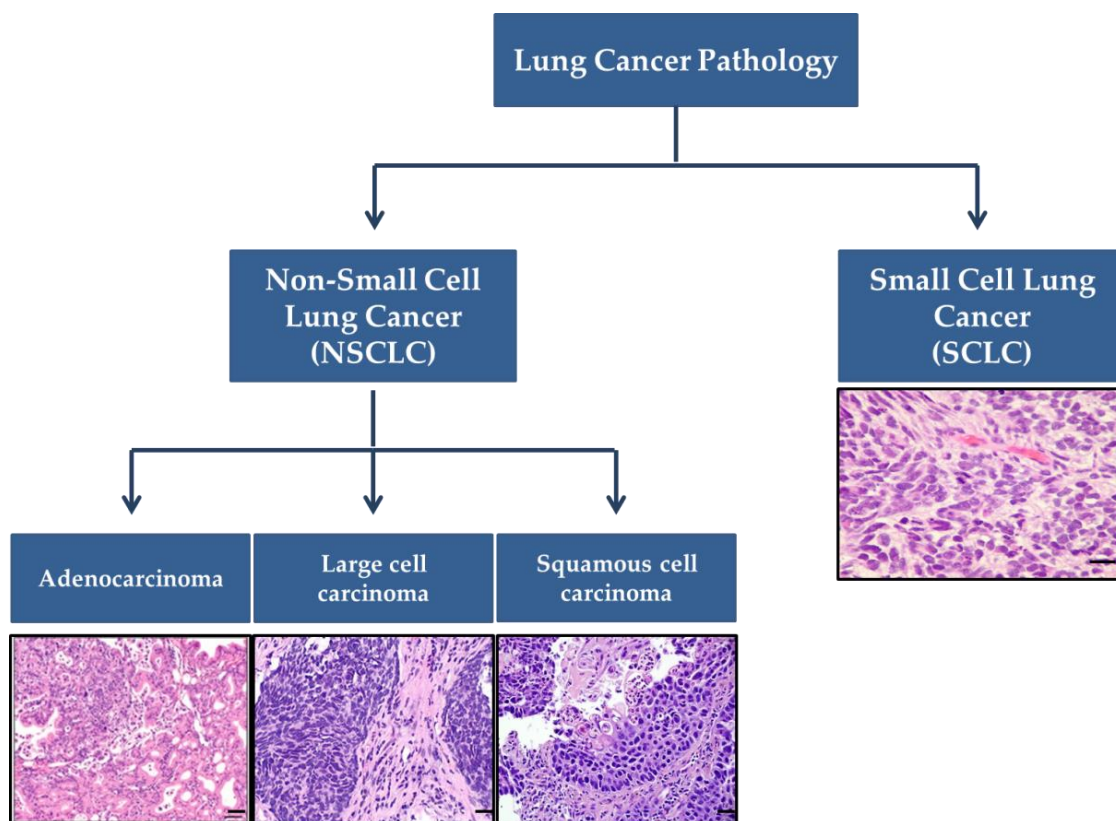


**Figure 10** – Histologic subtypes of lung cancer. (40x magnification, 100µm). Adapted from Travis, 2015 [247].

### C1.2) Molecular classification of lung adenocarcinomas

Lung adenocarcinomas are classified in molecular subtypes, according to the presence of well-identified and characterized molecular alterations that drive cancer initiation and progression [55]. This genomic classification relies on the detection of point mutations, copy number alterations, insertions and deletions (indel), and rearrangements in key oncogenes. Most of these oncogenic drivers are RTK and NRTK. In the majority of the cases, several tyrosine kinase inhibitors (TKI) have been successfully developed to target these alterations. The most relevant oncodrivers and the molecular alterations leading to classification of genomic subtypes of lung adenocarcinoma are the following: KRAS mutations, EGFR mutations and indels, ALK and ROS1 fusions, MET exon 14 skipping mutations and amplifications, BRAF mutations, RET fusions and NTRK fusions [266]. The distribution of these alterations varies across geographical regions, race, sex, and methods used to study tumor genomics. In 2016, the French Cooperative Thoracic Intergroup (IFCT) has

characterized the prevalence of the oncogenic alterations in advanced lung adenocarcinoma [267]. This extensive characterization has analyzed a total of 18.679 samples from 17.664 patients, and mostly were adenocarcinoma histology (76%). In the adenocarcinoma subtype, the prevalence of KRAS mutations was 32%, EGFR mutations 12%, BRAF mutations 2%, HER2 exon 20 insertions 2% and the prevalence of ALK rearrangement was 5%. 1619 patients were never smokers and the proportion of EGFR mutations reached 44% and ALK rearrangements 14%. KRAS mutation in non-smokers is present in only 9% (figure 11).

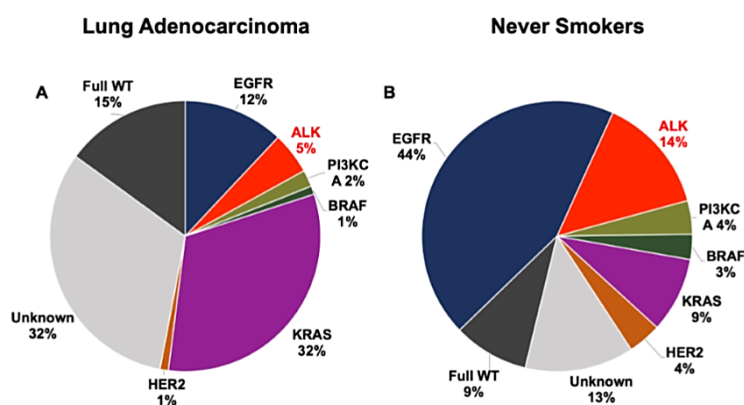


**Figure 11** - Distribution of molecular alterations in lung adenocarcinoma. A) Charts of the overall genomic view from patients with diagnosis of lung adenocarcinomas and B) in never-smokers. Figure and legend adapted from Barlesi F et al. *Lancet Oncology* 2016 [267].

Also, the Lung Cancer Mutation Consortium (LCMC), pioneered in the molecular characterization of lung adenocarcinomas in 14 academic institutions in the US, has analyzed 1.102 eligible patients and had found KRAS mutations in 25% of the tumors, EGFR mutation in 17%, ALK rearrangements in 8%, HER2 exon 20 insertions in 3%, and BRAF mutations in 2% of cases [268].

Recently, the development of high-throughput NGS platforms, has allowed an expansion within testing for multiple genes by targeted sequencing using customized gene panels that require small quantities of tumor DNA [269]. Furthermore, whole-exome and RNA sequencing have provide a more comprehensive view of the molecular landscape alterations in coding regions and gene expression.

The Cancer Genome Atlas (TCGA) program is currently ongoing and has characterized over 20.000 tumor samples from 33 different types of cancer using whole-exome and RNA sequencing. In the first report on lung adenocarcinoma, mainly from early stage resected specimens, the driver alterations detected were, without any surprise, KRAS in 32.2% of samples with driver alterations, EGFR mutations in 11.3%,

BRAF mutations in 7%, ALK rearrangements 1.3%, ROS1 fusions 1.7%, RET fusions in 0.9%, and MET exon 14 alterations in 4.3% (figure 12). Worth mentioning that the differences in the prevalence in ALK rearrangements in the set, in which most of the samples were from stage I/II resected tumors, can suggest that the prevalence of molecular alterations might also be stage-dependent.

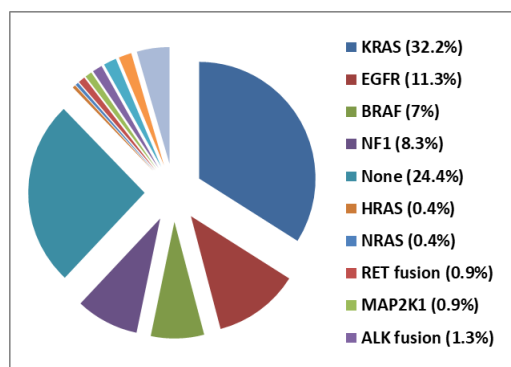


**Figure 12** - Prevalence of molecular alterations in key oncogenic drivers in lung adenocarcinomas using whole exome sequencing from The Cancer Genome Atlas Project. Figure and legend adapted from TCGA, Nature 2014, <sup>(68)</sup>.

As mentioned before, the prevalence of oncodrivers varies according to the geographic distribution. Across Asia Pacific, the prevalence of EGFR mutations is significantly higher than in western countries, reaching an impressive 49% of cases of lung adenocarcinoma, and inversely, the prevalence of KRAS mutations is low in Asia compared to western countries <sup>[270]</sup>. However, the prevalence of ALK rearrangements in Asia population is similar to the observed in Europe and/or United States (4.2%) <sup>[270, 271]</sup>. Presently, there are no scientific explanations for these differences that are observed among western and Asian populations; however, the role of radon exposure and air pollution is being studied <sup>[272, 273]</sup>.

For the purpose of this thesis, only ALK rearrangements will be approached.

### C1.3) The role of ALK in NSCLC

ALK rearrangements occur in about 3-7% of lung adenocarcinomas. As mentioned before, the activation of ALK is due to the complex formation of fused proteins between the translocation partner and ALK gene, and this is the sole mechanism of ALK oncogenicity in lung cancer. In 2007, Soda and colleagues have published the first report that characterized the EML4-ALK rearrangement in lung cancer <sup>[64]</sup>. They identified a 3.926 bp cDNA, coding for a 1.059 amino-acid protein with an amino-terminal sequence identical to EML4 and a C-terminal sequence identical to ALK. This fusion protein EML4-ALK (variant 1) was the product of a disrupted EML4



in the exon 13 with ALK in exon 20, including the full ALK kinase domain in the 3' extreme.

Echinoderm microtubule like proteins (EML) are a family of proteins that have an active role in the microtubule regulation. In humans, there are six different subtypes of expressed EML proteins [274]. EML4 is a member of the EML family and is composed of an amino-terminal coiled-coil domain and a C-terminal domain that contains a hydrophobic EML protein (HELP) domain. The coiled-coil region of EML4 protein is necessary for oligomerization and the C-terminal region also contains a tandem atypical  $\beta$ -propeller in EML protein (TAPE) domain that participates in the hydrophobic core of this protein. Also, the hydrophobic core of EML4-ALK mediated the binding to tubulin in human cells (figure 13).

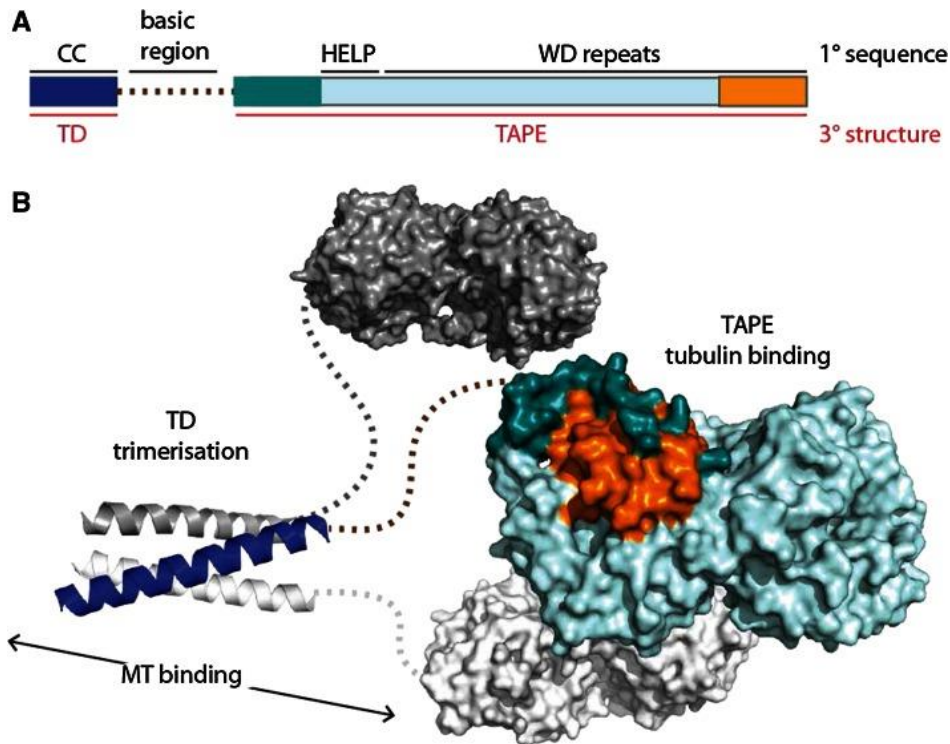


**Figure 13** - Overview of EML proteins. A) Domain structure of human EML4 with structural features labelled. Primary sequence features are labelled in black: CC, coiled-coil; basic region; HELP, Hydrophobic motif found in EML proteins; WD repeats, Trp-Asp repeats. Tertiary structure features are labelled in red text: TD, trimerisation domain; TAPE, tandem atypical propeller domain found in EML proteins. The TAPE domain N-terminal region is colored teal and the C-terminal region is colored orange. B) Hypothetical model of the overall trimeric architecture of the EML4 protein. Crystal structures of the EML4 TD and EML1 TAPE domain are connected with dotted lines to show the basic region that is predicted to be unstructured. One protomer of the trimer is colored using the scheme in 1a – this shows how the N- and C-terminal regions of the TAPE domain (teal and orange, respectively) come together to close the fold of this domain. Figure and legend adapted from Bayliss et al, Cell Mol Life Sci, 2016 [275].

EML4-ALK fusion protein forms homodimers through the coiled-coil domain of EML4, inducing trans-phosphorylation of the kinase domain and activation of oncogenic downstream pathway signaling. Both EML4 and ALK are oriented in opposite directions within the short arm of chromosome 2 in humans (and chromosome 17 in mice) and EML4-ALK fusion is produced by paracentric inversions [*inv*(2)(p21p23) in humans] in this locus. However, different breakpoints in the EML4 gene give rise to a spectrum of EML4-ALK fusion variants [275]. At least 15 different EML4-ALK variants have been identified, and the most common EML4 break points occur in intron 13 (variant 1) in 43% of cases, intron 20 (variant 2) in 5% and intron 6 (variant 3) in 40% (figure 14A) [276]. The EML4-ALK variant 3 was identified in 2008 by Choi and colleagues. This variant comprises two isoforms: variant 3a and variant 3b, which are the result of alternative splicing. Worth mentioning is the fact that the EML4-ALK variants 3a/b and 5a/b (figure 14A) are the only variants that lack the EML4 TAPE domain. This domain confers instability, which can explain the higher sensitivity of these variants to ALK inhibitors [277]. For that reason, shorter variants that do not contain the TAPE domain are more stable. Nevertheless, all variants of EML4-ALK confer transforming properties *in vitro*, and phosphorylated EML4-ALK is successfully inhibited with ALK inhibitors [278]. Furthermore, the variant type also determines the sub-cellular localization of the fusion protein. For instance, the variant 1 is detected in the cell cytoplasm while the variant 3 is located in the microtubules and in the nucleus [279]. Even though clinical studies have not shown a significant impact of the different variant types in the response to ALK inhibitors in ALK-driven lung cancer patients, this subject is still scope of study [276, 280]. However, regarding resistance to TKI, there is an initial evidence showing associations between the type of variants and specific mechanisms of resistance [276].

After 2007, multiple fusion partners have been described, including KIF5B, KLC1, PTPN3, STRN, SLC2A, CMTR1, VIT, GCC2, CUX1, BCL11A and KLC1. Nonetheless, EML4-ALK rearrangements are the most common fusions in patients with ALK-driven lung adenocarcinoma (figure 14B) [281].

Interestingly, most of the ALK-driven lung cancers are lung adenocarcinomas. Rarely ALK is rearranged in squamous cell carcinomas and large cell carcinomas

however have been reported in non-smoker patients [282]. Adenocarcinomas with ALK rearrangements may present signet cell features under pathology revision, and is associated with poor prognostic [283].

ALK-driven lung cancer can be diagnosed in pathologic specimens of lung cancers in different ways, for instance, by immunohistochemistry (IHC) using the FDA approved ALK D5F3 CST antibody, fluorescence in situ hybridization (FISH) using the Vysis ALK Break Apart FISH probe kit (FDA approved) and NGS (figure 15) [284].

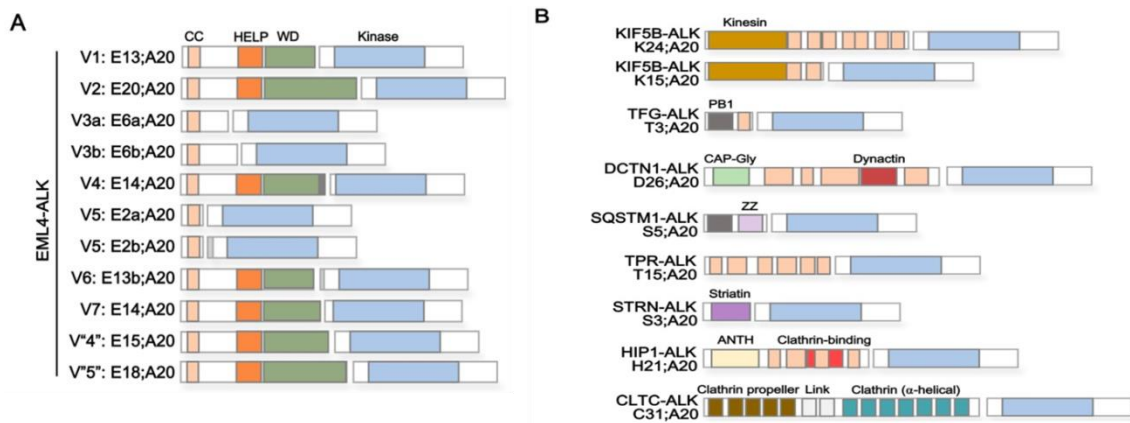


**Figure 14** - Schematic structural composition of ALK fusion proteins. A) EML4-ALK fusion proteins. The breakpoint in ALK gene is always at exon 20 (intron 19); the breakpoint in EML4 gene can be in different introns (for instance, exon 2, 6, 13, 14, 15, 18 and 20), which results in variable EML4-ALK fusion proteins. Variant 1 (E13; A20) and variant 2 (E20; A20) contain exons 1 to 13 and 1 to 20 of EML4, respectively, that are fused to exon 20 of ALK gene. In these two variants, the EML4 portion includes its C-terminal coiled-coil domain, the HELP domain and parts of the WD repeat domain of EML4. The variant 3a/b (E6a/b;A20) is shorter, consisting of exons 1 to 6 of EML4, with exon 6b being 188bp downstream of exon 6a, fused to exon 20 of ALK. Variant 4 (E14;A20) contains exons 1 to 14 of EML4, the insertion of four amino-acids of unknown origin, and fusion to exon 20 of ALK, that lacks in its N-terminal 49bp. The variant 5 (E2a/b;A20) contains the first two exons of EML4 fused to exon 20 of ALK (E2a;A20) or to 117 bp upstream of exon 20 of ALK (E2b;A20). Variant 6 (E13b;A20) contains exons 1 to 13 of the EML4 gene fused to exon 20 of ALK with and insertion of 19 amino acids derived from upstream intron 19. Variant 7 (E14;A20), is very similar to variant 4, but exon 20 of ALK lacks the first four amino-acids. Variant “4” (E15; A20) is characterized as a fusion product of EML4 at exon 15 and ALK at exon 20. Variant “5” (E18;A20) contains exon 1 to 18 of EML4 fused to exon 20 of ALK. B) Other X-ALK fusion proteins, in which the X represents any fusion partner including, among others that are not pictured, KIF5B-ALK (K24;A20 and K15;A20), TFG-ALK (T3;A20), DCTN1-ALK (D26;A20), SQSTM1-ALK (S5;A20), TPR-ALK (T15;A20), STRN-ALK (S3;A20), HIP1-ALK (H21;A20); and CTLC-ALK (C31;A20). Protein domains are indicated by color and include: coiled-coil (CC, light orange), HELP (dark orange), WD repeats (dark green), ALK kinase domains (blue), kinesin (ocher), PB1 (dark grey), CAP-Gly (light green), dynactn (dark red), zinc finger (ZZ, light violet), striatin (dark violet), ANTH (light yellow), clathrin-binding (light red), clathrin propeller (olive green), clathrin link (light grey), and clathrin (petrol) domains. Figure and legend adapted from Wu et al, *Cancers*, 2017 [285].

Regarding the epidemiology of ALK-driven lung cancers, it tends to occur at younger age and can be detected in about 13% of patients with less than 50 years old

## Chapter I - Introduction

---

who have lung adenocarcinoma [286-288]. It was been reported a strong association between this molecular subtype and light history (<10 pack/year) or never smokers and its prevalence is higher in women.

Usually, the diagnose is done at advanced stages and ALK<sup>+</sup> tumor cells have a high tropism for the central nervous system (CNS), which represents a frequency of 20% of brain metastasis at the time of diagnosis. However, the incidence of brain metastasis increases during the course of treatment with ALK tyrosine kinase inhibitors (TKI) rising up to 60%, which conveys significant morbidity and mortality [289, 290].

For this reason, effective and highly CNS penetrant TKI have been developed to achieve both intracranial and extracranial disease control. Now-a-days, there are five effective ALK TKI available for the treatment of these patients, with proven efficacy and conferring prolonged disease control and survival. In the next subchapter, each one of the ALK inhibitors will be refer with more detail.

### D1) ALK Inhibitors

Currently, there are five ALK TKIs available for treatment of ALK-driven NSCLC patients: the first-generation ALK inhibitors crizotinib, second-generation ALK inhibitors ceritinib, alectinib and brigatinib and the third and last-generation ALK TKI lorlatinib (table 3). After the creation of ALK inhibitors, the ALK-rearranged patients' survival and life quality increased substantially, and greatly, this has been achieved by the sequential use of first-, second-, and third-generation ALK inhibitors.

**Table 3** - Summary of the clinical settings in which the ALK TKIs have been tested. Approval status by EMA and FDA.

Drug	Generation	Clinical Setting	Approval
Crizotinib	First	First Line	EMA/FDA
Ceritinib	Second	First Line	EMA/FDA
		Second after crizotinib	
Alectinib	Second	First Line	EMA/FDA
		Second after crizotinib	
Brigatinib	Second	First Line	No EMA/FDA
		Second after crizotinib	
Lorlatinib	Third	After two lines of ALK TKIs including crizotinib or 2 <sup>nd</sup> line after a second-generation ALK TKI	EMA/FDA

The original approach for ALK-driven lung cancer patients' treatment consists of providing first-line treatment with crizotinib and switching to second- or third-generation ALK inhibitors after progression. Patients who have received crizotinib as first line achieve responses around 74% of cases, with median progression-free survival (PFS) of 10.9 months (figure 16) <sup>[291]</sup>. Second-generation ALK TKIs can overcome most of the on-target resistant mutations developed with crizotinib (see next subchapter). Treatment with ceritinib, alectinib or brigatinib as second or further lines after disease progression with crizotinib originates response rates ranging from 37% to 73% of patients and median progression-free survival durations between 5.4 and 12.9 months <sup>[292]</sup>. Regarding the third-generation ALK inhibitor, lorlatinib, it was then developed to overcome resistance mechanisms to first- and second-generation ALK TKIs, in

particular the highly resistant mutation G1202R [292]. Recent reports from phase I/II studies in lorlatinib, have shown that in patients treated with >2 previous lines of ALK TKI, lorlatinib elicited responses in 39% of patients and the median PFS duration in this groups was 6.9 months [293].

In the past years, we have seen the placement of more and more potent and selective second-generation ALK inhibitors in the first line setting. This has been supported by improved PFS observed with ceritinib, alectinib and brigatinib in the first line [280, 294-296].

### D1.1) Crizotinib

Crizotinib (PF-2341066, Pfizer), first-generation ALK inhibitor, is an oral available ATP-competitive inhibitor of ALK, MET and ROS1 [297]. The first preclinical studies have shown that crizotinib is a potent ALK inhibitor in KARPAS-299 and SU-DHL-1 ALCL cells (IC50: 24 nM). ALK-driven cells when treated with crizotinib enter in G1-S-phase cell cycle arrestment and are induced to apoptosis [298]. Other earlier *in vitro* studies have reported crizotinib inhibitory properties in NSCLC cell lines, such as H3122 (which harbor the EML4-ALK variant 1 rearrangement) that has been extensively used to characterize ALK inhibitors [299].

Four clinical trials were conducted and had shown the efficacy of crizotinib in the treatment of patients with ALK<sup>+</sup> lung cancer (table 4). The most relevant study was the PROFILE 1014, a phase III trial that compared the efficacy of crizotinib with chemotherapy as first line setting [291, 300]. Treatment with crizotinib has resulted in an increased response rate (74% vs 45%), in a prolonged the PFS (10.9 months vs 7 months), and in an impressive survival rates in patients, having reached 4-years survival in 56.6% patients [291, 300].

Contrary of what was said initially, crizotinib does penetrate the blood brain barrier and can confer higher intracranial disease control when compared with chemotherapy (DCR 85% vs 45%) [301]. However, in patients with baseline treated brain metastasis, approximately 43% of patients experienced intracranial disease progression and 22% of patients without baseline brain metastasis have developed CNS progression. This, of course, has highlighted the need for the development of enhanced

brain penetrating ALK inhibitors to confer better CNS disease control. However, the above described evidences have accelerated the approval in 2011 of crizotinib for the treatment of patients with advanced ALK-driven NSCLC as a first or subsequent line of treatment (subsequent to chemotherapy).

**Table 4** - Clinical trials with crizotinib. ORR, overall response rate; DOR, duration of response; TTR, time to treatment response; PFS, progression free survival; OS, overall survival. Adapted from Recondo et al [292].

Trial (references)	Trial design (phase, primary end point, and treatment arms)	Median follow-up (months)	Outcomes *ORR; * median PFD and * median OS
PROFILE 1001 [302, 303]	I ORR, DOR, TTR, PFS, 6-12 mo OS, safety profile Crizotinib (n= 149)	16.3	* 60.8% *9.7 mo * 1-year OS 74.8%
PROFILE 1005 [304]	II ORR Crizotinib (n=1069)	NA	*54% *8.4 mo *21.8 mo
PROFILE 1007 [305]	III PFS Crizotinib (n=173) vs pemetrexed or docetaxel (n=174)	12.2 mo (crizotinib) and 12.1 mo (chemotherapy)	*65% vs 20% *7.7 mo vs 3.0 mo (HR 0.49; $P<0.001$ ) *20.3 mo vs 22.3 mo (HR 1.02, $P=0.54$ )
PROFILE 1014 [291, 300]	III PFS Crizotinib (n=172) vs platinum + pemetrexed (n=171)	46 mo	*74% vs 45% *10.9 mo vs 7.0 mo (HR 0.45, $P<0.001$ ) *NR (45.8 mo-NR) vs 47.5 mo (32.2 mo – NR; HR 0-76; $P<0.048$ )

### D1.2) Ceritinib

Ceritinib (LDK375, Zykadia, Novartis) is a second-generation ATP-competitive ALK inhibitor. It can also inhibit the Insulin Growth Factor Receptor (IGFR) [306]. It was designed to overcome the most frequent point mutations that led to crizotinib resistance in patients at disease progression, like L1196M gatekeeper mutations [307].

## Chapter I - Introduction

This compound was the first second-generation ALK inhibitor tested in the context of resistance to crizotinib and has shown responses rates in about 40% of patients with median PFS durations of 6 months (table 5) [308-311].

As first-line setting, ceritinib was superior to chemotherapy, producing higher response rates (72.5% vs 26.7%) and PFS (16.6 months vs 8.1 months) [295]. Thus, ceritinib is an upfront treatment option for ALK-driven lung cancer patients. However, given the fact that other very potent and better tolerated second-generation ALK inhibitors have been developed, the current role of ceritinib in the second- or first-line treatment seems to be declining.

**Table 5** - Clinical trials with ceritinib. ORR, overall response rate; DOR, duration of response; TTR, time to treatment response; PFS, progression free survival; OS, overall survival. Adapted from Recondo et al. [292].

Trial (references)	Trial design (phase, primary end point, and treatment arms)	Median follow-up (months)	Outcomes *ORR; * median PFD and * median OS
ASCEND-1 [308, 309]	I MTD Ceritinib (n=246) First line (33%) or second line after crizotinib (66%)	11.1 mo	*72% or 56% * 18.4 mo or 6.9 mo *NR or 16.7 mo
ASCEND-2 [310]	II ORR Ceritinib (n=140) Second line after crizotinib	11.3 mo	*38.6% *5.7 mo * 14.9 mo
ASCEND-3 [312]	III ORR Ceritinib (n=124) First line	8.3 mo	*63.7% * 11.1 mo * NA
ASCEND-4 [295]	III PFS Ceritinib (n=189) vs platinum + pemetrexed (n=187) First line	19.7 mo	*72.5% vs 26.7% *16.6 mo vs 8.1 mo (HR 0.55; P<0.00001) *NE (29.3 mo-NE) vs 26.2 mo (22.8 mo-NR); HR 0.73; P=0.056
ASCEND-5 [311]	III PFS	16.5 mo	*39.1% vs 6.9% * 4 mo vs 1.6 mo (HR 0.49;



Ceritinib (n=115) vs pemetrexed or docetaxel (n=116) Second line after crizotinib	P<0.0001) * 18.1 mo vs 20.1 mo (HR 1.00; P=0.5)
--	---

### D1.3) Alectinib

Alectinib (CH5424802; Chugai-Roche) is a benzo[b]carbazole derivative that was developed to be highly potent, with an IC<sub>50</sub> of 1.9 nM in cell-free assays and confers high levels of ALK inhibition in EML4-ALK positive cell lines *in vitro* and *in vivo* [169]. Initially, alectinib was developed as a second line regimen for patients who had been treated with crizotinib (table 6). The phase III study ALUR, has compared alectinib to single agent docetaxel or pemetrexed in patients who had previously progressed on treatment with crizotinib, and similarly to ceritinib, higher responses rates than chemotherapy were achieved (37.5% vs 2.9%) as well as and prolonged PFS (9.6 vs 1.4 months) [313]. Based on these results, alectinib was approved for the treatment of patients who had had disease progression after treatment with the first-generation ALK inhibitor crizotinib.

Contrarily to what happen with crizotinib and ceritinib, alectinib is not a substrate of the P-glycoprotein (P-gp), also known as multidrug resistance protein 1 (MDR1) or ATP-binding cassette sub-family B member 1 (ABCB1) [314]. P-gp is a key efflux transporter present in the capillary endothelial cells of the blood brain barrier, and by this mean, it can reduce the bioavailability of drug in different body compartments, like the brain. Thus, alectinib is a highly penetrant drug and it can achieve high concentrations in the CNS [315]. Phase II studies have revealed that in patients with measurable brain metastasis, the intracranial ORR with alectinib was 64%, with a median intracranial duration of response of 10.8 months [316].

In Japan, a phase III trial J-ALEX, and the international ALEX trial, have compared the efficacy of first-line alectinib treatment to crizotinib treatment [317, 318]. Achieving a median duration of PFS of 34.8 months, alectinib has been associated with a significant PFS benefit as well as a more favorable toxicity profile than crizotinib. Also, the intracranial responses rates were superior with alectinib (81% vs 50%,

## Chapter I - Introduction

compared with crizotinib) and lower incidence of brain metastases. Based on ALEX and J-ALEX trials, alectinib has become the standard choice for the first line treatment of patients with ALK-driven NSCLC worldwide.

**Table 6** - Clinical trials alectinib. ORR, overall response rate; DOR, duration of response; TTR, time to treatment response; PFS, progression free survival; OS, overall survival. Adapted from Recondo et al [292].

Trial (references)	Trial design (phase, primary end point, and treatment arms)	Median follow-up (months)	Outcomes *ORR; * median PFD and * median OS
AF-001 JO [317, 318]	I/II DLT and MTD (phase I) or ORR (phase II) Alectinib (n=46) First line	36 mo	*93.5% *NR; 3-year PF; 62% *NE; 3-year OS; 78%
AF-002 JG [319]	I/II Recommended phase II dose Alectinib (n=47) Second line after crizotinib	4.2 mo	*55% *NA * NA
NP28761/ NP28673 [320]	III ORR (n=225; n=189 evaluable for response) Second line after crizotinib	92.3 weeks	*51.3% *8.3 mo *29.1 mo
ALUR [313]	III PFS Alectinib (n=72) vs docetaxel or pemetrexed (n=35) Second line after crizotinib	6.5 mo	*37.5% vs 2.9% *9.6 mo vs 1.4 mo (HR 0.15; P<0.001) *12.6 mo (9.7 mo-NR) vs NR (NR-NR; HR 0.89)
AF-001 JP [317, 318]	I/II DLT and MTD (phase I) or ORR (phase II) Alectinib (n=46) First line	36 mo	*93.5% *NR; 3-year PFS: 62% *NE; 3-year OS: 78%

	III		*92% vs 79%
J-ALEX [321]	IRC-assessed PFS Alectini (n=103; 300mg BID) vs crizotinib (n= 104)	12 mo (alectinib) and 12.2 mo (crizotinib)	*NR (95% CI 20.3 mo-NE vs 10.2 mo; HR 0.34; P<0.0001) *NA (immature data)
ALEX [280, 294]	Investigator – assessed PFS Alectinib (n=152; 600mg BID) vs crizotinib (n=151)	22.8 (alectinib) and 27.8 (crizotinib)	* 82.9% vs 75.5% *34.8 mo vs 10.9 mo (HR 0.43) * 1-year OS 84.3% vs 82.5% (HR 0.76; P=0.24)

### D1.4) Brigatinib

Brigatinib (AP26113; Ariad) is, as ceritinib and alectinib, a second-generation ALK inhibitor. It was originally developed as an ALK inhibitor that could potentially overcome the point mutation G1202R (known mechanism of resistance to first- and second-generation ALK inhibitor, see next subchapter).

The *in vitro* results were very enthusiastic; brigatinib inhibited the kinase activity of WT EML4-ALK with an IC<sub>50</sub> of 0.6nM and its inhibition activity in acquired resistance mutations was impressive: C1156Y (0.6 nM), F1174L (1.4 nM), L1196M (1.7 nM), and G1202R (4.9 nM). However, and unfortunately, the *in vitro* activity for the G1202R mutation was not replicated *in vivo* or in patients. Worth mentioning is the fact that brigatinib has a modest activity against EGFR mutants, namely the T790M mutation [322]. The pre-clinical models have also revealed the high CNS penetration, as it was proven by the significant tumor reductions in orthotopic mouse brain tumor models.

Regarding the clinical setting, three clinical trials have supported the efficacy of brigatinib as a second line after crizotinib relapse (table 7). Phase II study ALTA trial showed that treatment with brigatinib resulted in 56% response rate with a median PFS of 15.6 months. Brigatinib was compared to crizotinib in the first line setting in a phase III randomized study, (ALTA1L trial) resulting in improved responses rates (71% vs 60%) and disease control [296]. Like it was observed with alectinib in the first line, brigatinib conferred higher intracranial response rates (78% vs 29%) and lower incidence of brain metastasis during treatment, when compared with crizotinib.

## Chapter I - Introduction

Consequently, brigatinib was approved as a second line treatment option for patients who were previously treated with crizotinib.

**Table 7** - Clinical trials with brigatinib. ORR, overall response rate; DOR, duration of response; TTR, time to treatment response; PFS, progression free survival; OS, overall survival. Adapted from Recondo et al [292].

Trial (references)	Trial design (phase, primary end point, and treatment arms)	Median follow-up (months)	Outcomes *ORR, *median PFS and *median OS
NCT01449461 [323, 324]	Recommended phase II dose (phase I) or ORR (phase II) Brigatinib (n=79) First line (10%, n=8), second line after crizotinib (85%, n=68), or third line after crizotinib and ceritinib (5%, n=3)	>31 mo	First-line brigatinib (n=8) *100% *34.2 mo *NR (2-year OS 100%) Brigatinib after crizotinib (n=71) *73% *13.2 mo *30.1 mo (2-year OS 61%)
ALTA [325]	II ORR Brigatinib 90 mg daily (n=112) vs brigatinib 180 mg with a 7-day lead in of 90 mg/d (n=110) Second line after crizotinib	19.6 mo (90 mg daily) 24.3 mo (standard dose)	*46% vs 56% *9.2 mo vs 15.6 mo *29.5 mo (18.2 mo-NR) vs 34.1 mo (27.7mo-NR)
ALTA1L [296]	III PFS First line: Brigatinib 180 mg with a 7-day lead in of 90 mg/d (n=137) or crizotinib 250 mg BID (n=138)	11.0 mo in the brigatinib group and 9.3 months in the crizotinib group	*71% vs 60% *12-month PFS: 67% (95% CI, 56 to 75) vs 43% (95% CI, 32 to 53) *12-month OS: 85% (95% CI, 76 to 91) vs 86% (95% CI, 77 to 91)

### D1.5) Lorlatinib

Lorlatinib (PF-06463922, Pfizer) is the most potent, sole third-generation ALK inhibitor, the last to receive FDA approval and is currently available in the clinical setting for the treatment of ALK-driven NSCLC patients. Besides ALK, lorlatinib is a

potent reversible and ATP-competitive ROS1 inhibitor and it was developed to inhibit ALK in the presence of all known single resistant mutations within the kinase domain [326]. Its inhibition capacity is clearly shown by the impressive IC<sub>50</sub> of <0.07 nM. Also, its unique macrocyclic structure confers different conformational binding properties, which remains unaffected by amino-acidic changes that can occur due to single known secondary resistance mutations (figure 15) [327]. Plus, its lipophilic properties and low susceptibility to P-glycoprotein efflux confer high levels of CNS penetration and intracranial activity.

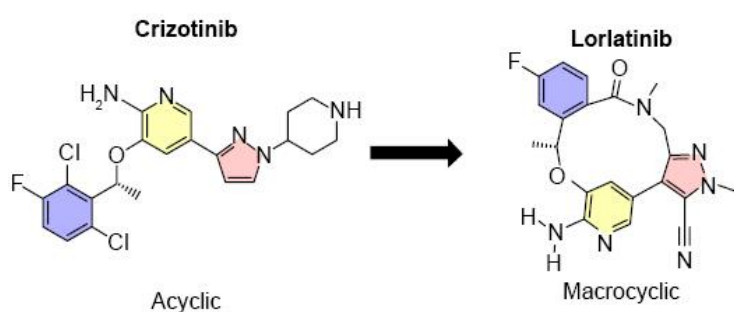


**Figure 15** - The acyclic structure of crizotinib and the macrocyclic structure of lorlatinib. Adapted from Akamine et al, *OncoTargets and therapy*, 2018 [328]

Preclinical studies have shown that lorlatinib has elevated potency in ALK suppression and cell death in Ba/F3 cells expressing WT ALK, non-mutant rearranged and a wide spectrum of mutant forms that can occur with first- and second-generation ALK inhibitors, namely L1196M, I1171T, L1152R, 1151Tins, C1156Y, G1269A, F1174L, S1206Y and G1202R [326]. In addition, lorlatinib has shown significant activity in G1202R mutant expressed in H3122 cells *in vivo*. The IC<sub>50</sub> of lorlatinib in Ba/F3 cells expressing this mutant form is about 50 nM and the IC<sub>50</sub> values for all other single resistant mutations range from this value to 4.6 nM.

Moreover, lorlatinib has achieved important and impressive tumor responses in brain orthotopic mice models and prolonged survival of mice bearing patient-derived tumors [326]. Also, in these models, the lorlatinib pharmacokinetic was analyzed showing that the free fraction of lorlatinib in brain in reference to plasma was 4-fold higher than crizotinib.

Lorlatinib is orally bioavailable and the established dose for humans is 100 mg daily based on the safety and the estimated plasma concentration needed to target the

## Chapter I - Introduction

---

G1202R mutation. The maximum time in plasma is between 1-2 hours and its half-life extends from 19 to 28.8 hours [329].

The phase I trial has enrolled 41 ALK-driven lung cancer patients heavily pretreated, among which 72% had brain metastasis at the time of enrollment, 12 of whom had not received radiation therapy. The response rate was 57% among patients treated with one previous line of ALK TKI, and 42% among patients treated with two or more lines of ALK TKIs. In patients with measurable and non-measurable brain metastasis, a partial or complete response was observed in 31% of the cases, of whom 50% had been previously treated with two or more ALK inhibitors lines. This efficacy in the treatment of brain metastasis is relevant in the context of elevated levels of CNS progression with first- and second-generation ALK TKIs.

The multicohort phase II study of lorlatinib included patients with treatment naïve disease (EXP1, n=30), patients who had received crizotinib without a second-generation ALK TKI (EXP2, n=27) or with previous chemotherapy (EXP3A, n=32), patients previously treated with one non-crizotinib ALK TKI with or without chemotherapy (EXP3B, n=28), and finally, patients who had previously received two (EXP4, n=66) or three (EXP5, n=46) lines of ALK TKI. About 60% of the patients previously treated with an ALK TKI had baseline brain metastasis. The response, PFS and CNS activity for all cohorts are summarized in table 8. In patients crizotinib only pre-treated, the ORR was 69% and the median PFS has reached almost one year, and intracranial responses were observed in 87% of cases. In patients treated with second-generation ALK inhibitors alone or treated with two or three ALK TKIs, responses rates ranged between 32-39% with median PFS duration of 5.5 months and 6.9 months, respectively. An increased intracranial activity was observed in heavily pretreated patients, with approximately 55% of intracranial responses and median duration of response reaching 14.5 months (95% CI, 6.9-14.5). Plus, this multicohort phase II study also provided a hint on the activity of this drug in treatment naïve patients, with 90% response rates and long PFS durations. Also, lorlatinib was highly active in patients with detectable mutant forms that occur in earlier generation of ALK inhibitors but also active in patients with undetectable kinase domain mutations. In patients previously treated with crizotinib, there were no differences in response rates among

patients with detectable ALK resistance mutation compared to patients without detectable resistance mutation (ORR: 73% vs 75%) and median PFS was similar between groups (HR, 1.03 [95% CI, 0.39 to 2.69]) [330]. In contrary, the response rate of lorlatinib in patients with detectable ALK resistance mutation was 62% compared to 32% for patients with undetectable ALK resistance mutation in plasma, after progression to second generation ALK TKI. Median PFS was significantly longer in patients with detectable ALK mutant forms in tissue (11 vs 5.3 months), as it was the median duration of response (24.4 vs 4.3 months), reflecting that patients with undetectable on-target resistance to previous ALK TKI have less benefit with lorlatinib than patients whose tumors had developed on-target resistance mechanisms. More importantly, lorlatinib was highly effective in patients with detectable G1202R mutation, with response rates of 57% and median duration of PFS of 8.2 months [330].

Finally, based on the clinical efficacy and safety, lorlatinib has received approval from FDA in November 2018 and EMA in May 2019 for the treatment of patients who have experienced disease progression with first- and second-generation ALK TKIs, or to first line treatment with alectinib or ceritinib.

In accordance with this new paradigm, in which we can observe a shift in the treatment of ALK-driven patients, moving second-generation to the first line setting, and due to the fact that in preclinical models, first line treatment with lorlatinib was highly efficacious, there is already an ongoing phase III study which compares first line treatment with lorlatinib to crizotinib (CROWN trial, NCT03052608).

**Table 8** - Expansion (EXP) cohort from the phase I/II study of lorlatinib. ORR, overall response rate; PFS, progression free survival; IC, intracranial Adapted from Solomo BJ, et al [293].

Cohort	Previous ALK TKI	N	ORR	Median PFS months (95% CI)	IC ORR
EXP 1	None	30	90%	NR (11.4-NR)	66.7%
EXP 2	Crizotinib no chemotherapy	27	69.5%	NR (12.5 - NR)	87%
EXP 3A	Crizotinib no chemotherapy	32			

## Chapter I - Introduction

EXP 3B	Second-generation ALK TKI +/- chemotherapy	28	32.1%	5.5 (2.7-9.0)	55.6%
EXP 4	Two lines of ALK TKI	66	38.7%	6.9 (5.4 – 9.5)	53.1%
EXP 5	Three lines ALK TKI	46			



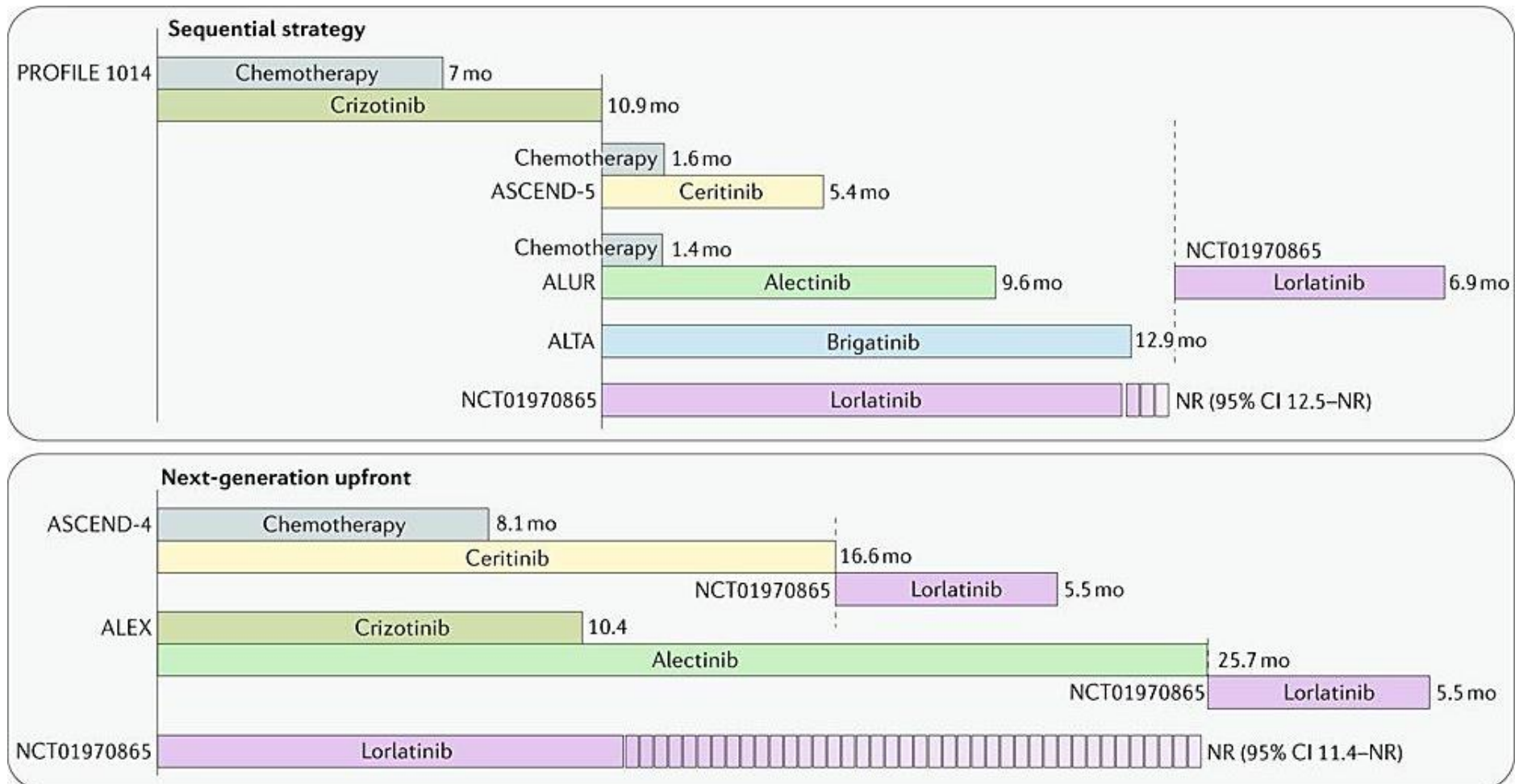


**Figure 16** - Comparison of PFS results in selected clinical trials testing TKI sequencing in ALK-driven NSCLC. Summary of PFS durations in different trials of frontline ALK inhibitors in NSCLC patients. Adapted from Recondo et al, Nat Rev Clin Oncol, 2018 [292].

### E1) ALK inhibitors resistance

#### E1.1) ALK TKI resistance mechanism

Resistance to targeted therapies can be either primary or acquired. Primary resistance to a targeted therapy implies an intrinsic lack of response to the treatment from the beginning while acquired resistance denotes disease progression after an initial response (partial or complete) to the therapy [331]. Though mechanisms of intrinsic resistance are poorly understood, acquired resistance mechanisms broadly fall under two categories: ALK-dependent or ALK-independent mechanisms of resistance.

##### E1.1.1) ALK-Dependent Resistance Mechanisms

###### E1.1.1.1) Secondary mutations in the ALK tyrosine kinase domain

In general, secondary mutations within the target kinase cause drug resistance by re-activation of the kinase and its downstream signaling pathways despite the presence of the TKI. These resistance mutations often occur around the surface lining the drug binding site, although a number of mutations have been described far from the active site. Depending on their location, mutations can directly hamper TKI binding to the target kinase, alter the conformation of the kinase, and/or modify the ATP-binding affinity of the kinase.

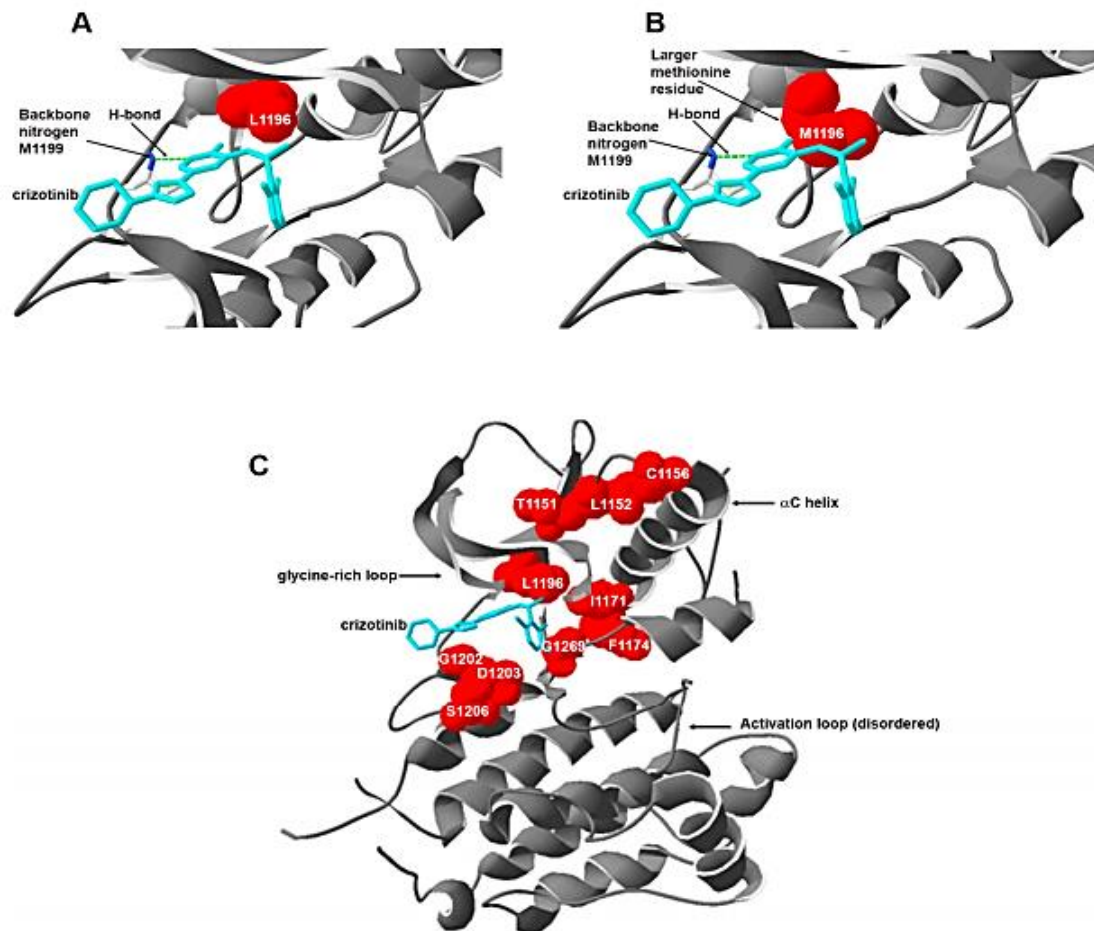
- *Resistance against Crizotinib*

Despite the remarkable responses that have been observed in patients with ALK rearrangements, resistance to crizotinib eventually develops and rather quickly, making durable response unachievable.

One of the important mechanisms of acquired resistance to crizotinib is the selection of point mutations within the drug target that alter drug sensitivity (table 9).

The first case of resistance against crizotinib in EML4-ALK<sup>+</sup> NSCLC patient was reported in 2010 [168]. The tumor resumed growth after an initial partial response over a

period of 5 months. Deep sequencing analysis of the patient sample revealed a L1196M



mutation and a C1156Y substitution at a relatively high frequency.

**Figure 17** - Crystal structure of ALK in complex with crizotinib (PDB:2XP2). A) Close view of crizotinib bound in the active site of WT ALK. The gatekeeper residue L1196 is shown as red surface. Crizotinib is shown as cyan sticks. The green dashed line indicates the hydrogen bonding to the backbone nitrogen of M1199 (indicated in sticks). Secondary structures are represented as grey ribbon. B) The native L1196 from panel A mutated in silico to M1196, to show steric clash with crizotinib. C) Overall architecture of ALK bound to crizotinib. Key residues associated with resistance to crizotinib are shown as red surface and labeled. Some important regulatory regions of the kinase are indicated by arrows. Figure and legend adapted from Sharma et al, *Cancers*, 2018 [48].

The L1196 residue is a conserved gatekeeper residue located close to the ATP pocket and crizotinib binding site. In this secondary mutation, a smaller residue (leucine) is replaced by a larger residue (methionine) (figure 17A/B). In contrast to a larger residue, a smaller one does not block the access of the inhibitor to the adjacent hydrophobic pocket [332]. Methionine substitution, in addition, has been reported to increase the enzyme activity by strengthening the hydrophobic R-spine which then promotes the formation of the active protein conformation [333]. L1196M mutant EML4-

ALK protein was found to have higher phosphorylation levels <sup>[334]</sup> conferring drug resistance by increasing the protein kinase activity. On the other hand, the C1156Y mutation creates a displacement of crizotinib along with some conformational changes in the binding site of the drug that eventually decreases crizotinib affinity and leads to drug resistance <sup>[335]</sup>. Interestingly, a different gatekeeper mutation (L1196Q) was identified in crizotinib-resistant ALCL cells *in vitro* <sup>[336]</sup>. The same group described an I1171N mutant that was resistant to all tested inhibitors; this mutation was later identified in an ALCL patient progressing on crizotinib <sup>[337]</sup>.

Sasaki and colleagues have described another case of crizotinib resistance in an IMT patient <sup>[338]</sup>. These investigators found the F1174L mutation in the RANBP2-ALK kinase domain in the relapsed tumor lesions. Also, the F1174L mutation had earlier been detected in neuroblastoma <sup>[163]</sup>. The 1174 residue is found at the C-terminal end of the  $\alpha$ C-helix and has been shown to reduce ALK sensitivity to crizotinib by increasing ATP binding affinity in neuroblastoma cell lines and in *in vivo* models <sup>[339]</sup>. Another mutant variant at the same position, F1174V, was also found in an ALK<sup>+</sup> NSCLC patient resistant to crizotinib <sup>[340]</sup>.

Secondary mutation L1152R with an EGFR and c-Met hyperactivation was reported in a cell line established from the NSCLC patient who relapsed after 3 months of crizotinib treatment <sup>[341]</sup>. The L1152R mutation affected crizotinib-mediated inhibition of downstream AKT and ERK phosphorylation in the resistant cells. As the L1152R mutation does not seem to be in direct contact with the ATP-binding pocket <sup>[153]</sup>, how L1152R mediates ALK inhibitor resistance is still unclear.

A number of other secondary mutations such as S1206Y, G1202R, 1151Tins, G1269A were also found in crizotinib-refractory NSCLC patients (figure 17C) <sup>[342, 343]</sup>. Both, G1202R and S1206Y, are located at the solvent front of the TKD and presumably interfere with inhibitor binding due to steric hindrance and conformational changes of the kinase, while the insertion of a threonine residue at 1151 position is speculated to lead to a change in the affinity of ALK for ATP <sup>[153]</sup>. The Gly1269 residue is situated at the end of the ATP-binding pocket of ALK and its substitution with the larger Ala residue leads to a decrease in the binding of crizotinib to ALK due to steric hindrance <sup>[343]</sup>.

**Table 9** - Mutational profile of ALK that induce TKI resistance

TKI	Sensitive Mutants	Resistant Mutants	Disease	Evidence ( <i>in vitro/in vivo/clinical</i> )	Reference
<b>Crizotinib</b>	L1198F	I1151Tins	NSCLC	Clinical	
		L1152R	NSCLC	Clinical	[342]
		C1156Y	NSCLC	Clinical	[341]
		I1171T/N	NSCLC	Clinical	[168]
		F1174L	IMT	Clinical	[344]
		L1196M	NSCLC	Clinical	[341]
		L1196Q	NSCLC	Clinical	[168]
		L1198P	EML4-ALK BaF3 cells	<i>in vitro</i>	[345, 346]
		G1202R	NSCLC	Clinical	[342]
		D1203N	NSCLC	Clinical	[342, 343, 345, 347]
		S1206Y	NSCLC	Clinical	
<b>Ceritinib</b>	G1269A, I1171T, S1206Y, L1196M	G1269A	NSCLC, IMT	Clinical	
		R1275Q	Neuroblastoma	<i>in vitro</i>	[176]
		L1152P/R	NSCLC	<i>in vitro</i>	[307]
		D1203	NSCLC	Clinical	[348]
		G1202R	NSCLC	Clinical	[307]
		F1174C/V	NSCLC	Clinical	[307]
		L1198F	NSCLC	<i>in vitro</i>	[314]
<b>Alectinib</b>	G1269A, S1206Y, L1152R, F1174L, 1151Tins	C1156Y/T	NSCLC	<i>in vitro</i>	[307]
		I1171T	NSCLC	Clinical	[349]
		V1180L	NSCLC	<i>in vitro</i>	[340]
		G1202R	NSCLC	Clinical	
<b>Brigatinib</b>	G1269A, S1206Y, L1152R, F1174C, 1151Tins,	F1174V+L1198F	ALCL	<i>in vitro</i>	[350]
		G1202R	NSCLC	Clinical	[351]
		S1206C/F	NSCLC	Clinical	
		I1171T,			
		D1203N, E1210K, F1245C			
<b>Lorlatinib</b>	L1196M, G1202R, G1269A	L1198F			[352]
		I1171N + L1198F	NSCLC	Clinical	[353]
		I1171N+D1203N			[354]
		G1202R+G1269A			

## Chapter I - Introduction

G1202R+L1196M

L1196M+D1202N

F1174L+G1202R

C1156Y+G1269A

- *Resistance to Second-Generation ALK TKIs (ceritinib, alectinib, brigatinib)*

Even though the second-generation of ALK inhibitors is proven to be more potent and highly selective with tolerable adverse events, the biggest setback still stays in the form of acquired resistance against them. For instance, while ceritinib was able to overcome some of the secondary ALK resistance mutations that arise after crizotinib, G1202R, F1174C/V mutations were reported to be selected by ceritinib treatment. Structural analysis revealed that G1202R substitution causes a significant loss in ceritinib binding due to steric hindrance [307]. Other secondary mutations such as C1156Y, I1152T, and L1152R, G1123S have also been documented to be associated with resistance against ceritinib [344, 355].

On the other hand, alectinib was shown to be effective against crizotinib or ceritinib resistant mutations, but it was described that alectinib leads to the acquisition of I1171T and V1180L resistant mutations *in vitro* and in a patient upon alectinib treatment. Interestingly, these two mutations can be overcome with ceritinib treatment, which supports the idea of using two different inhibitors/combinatorial therapy. Again, the G1202R emerged as a highly intractable mutant [356]. Indeed, this mutation was reported to be resistant to all clinically available inhibitors before the third-generation had been developed [357].

Point mutations L1122V, F1174V+L1198F, S1206C, and L1198F were shown to confer resistance against brigatinib in ALCL cell lines. Except for the S1206C mutation, most of the brigatinib resistance could be overcome by switching back to crizotinib or other ALK TKIs [350].

Given the structural differences among the available ALK TKIs, it is perhaps not surprising that each ALK TKI appears to be associated with a specific profile of secondary ALK resistance mutations (table 9). One such example of this compound mutation phenomenon include detection of C1156Y and I1171N double mutation after progression on crizotinib, ceritinib, and alectinib sequential treatment and also the

presence of E1210K with D1203N mutations after sequential crizotinib and brigatinib treatment [358]. Given the number of different ALK TKIs that are being approved and their implementation in clinic for sequential TKI treatment, we are bound to see an increase in the number and variety of compound mutations (table 9).

- *Preclinical and clinical evidences on resistance mechanism to third-generation ALK inhibitor, lorlatinib*

Unlike first- and second-generation ALK TKI, mechanisms of resistance to third-generation (lorlatinib) still need to be intensively explored.

The first report was derived from the molecular study of a patient's tumor at the time of lorlatinib progression in the context of the phase I study performed by Alice Shaw and her colleagues [359]. The patient had been treated with crizotinib in the first setting and upon progression a resistant ALK C1156Y mutation was detected. This mutation conferred resistance to crizotinib and ceritinib. The patient was treated sequentially with ceritinib and a HSP90 inhibitor without any benefit and fourth line chemotherapy with a total duration of response of 6 months. Then, the patient has received lorlatinib and achieved a partial response that lasted for 8 months. When the disease progressed, a liver biopsy was performed and NGS analysis of the tumor sample had revealed two ALK mutations: the previously detected crizotinib resistant C1156Y and a new L1198F mutation. These two mutations were present in the same allele (compound mutation), and clonal analysis using whole-exome sequencing data has showed that the cancer cells containing the compound mutation resistant to lorlatinib were sub-clones derived from tumor cells that had acquired the C1156Y mutation with crizotinib.

Using crystallography modeling, the substitution of a leucine for a phenylalanine in position 1198 leads to a steric clash with lorlatinib, which affects the binding (figure 18). The binding affinity (ALK L1198F and L1198F+C1156Y mutant) was lower with lorlatinib and most second-generation ALK inhibitors. However, the L1198F mutation did not clash with crizotinib, and in fact, improved crizotinib binding and affinity for ALK. The patient was then treated with crizotinib, experiencing a significant response and proving that this compound mutation re-sensitized this patient to crizotinib. The increased affinity for crizotinib binding, induced by the

presence of the phenylalanine counteracted the negative effect of C1156Y. The induction of resistance to lorlatinib and the re-sensitization to crizotinib by the sequential acquisition of the C1156Y and the L1198F mutation was also demonstrated *in vitro* in Ba/F3 models.

Compound mutations acquired sequentially with first- and second- generation ALK TKI had also been reported to drive resistance to brigatinib, like the D1203N + E1210K, but these compound mutations remain sensitive to lorlatinib inhibition <sup>[358]</sup>. These initial observations suggested that compound mutations had differential activity on resistance to ALK TKI. Also, the same group has further explored the role of compound mutations in lorlatinib resistance by performing an N-ethyl-N-nitrosourea (ENU) mutagenesis screen in Ba/F3 cells expressing non-mutant EML4-ALK rearrangements and EML4-ALK rearrangement with known single resistance mutation to first- or second-generation ALK inhibitors. After exposure to ENU, Ba/F3 cells were treated with crizotinib and lorlatinib. In Ba/F3 cells harboring non-mutant form of EML4-ALK, there were no resistant clones to lorlatinib, but as it was expected, multiple clones have emerged with crizotinib. This suggested that no single ALK mutation conferred resistance to lorlatinib at physiological doses that are achieved in patients. These findings were then proved *in vivo* by injecting H3122 cells in immune-compromised mice and treated with lorlatinib. After tumor regrowth, none of the resistance cancer cells harbored a single ALK mutation <sup>[353]</sup>.

To check the effect of the sequential acquisition of resistance mutations, Ba/F3 harboring the most common resistance mutations to first- and second-generation ALK inhibitors (C1156Y, F1174C, L1196M, G1202R, and G1269A) underwent ENU mutagenesis screen with lorlatinib. Multiple compound mutations were then identified in lorlatinib resistant clones (G1202R+L1196M, G1202R+L1198F and L1196M+L1198F compound mutations). However, the compound mutations containing the L1198F mutation were sensitive to crizotinib <sup>[353]</sup>.

In patients, the following compound mutations were identified as lorlatinib resistant forms: I1171N + L1198F, I1171N + D1203N, G1202R + G1269A, G1202R + L1196M, including the “triple mutants” G1202R + L1204V + G1269A and E1210K + D1203N + G1269A. This study has then demonstrated that the consecutive acquisition



of kinase domain mutations after sequential exposure to first- and second-generation ALK TKI and lorlatinib (third-generation) can induce conformational changes in the kinase domain that hamper lorlatinib binding and can also result in increased kinase ATP affinity in about 35% of cases [353].

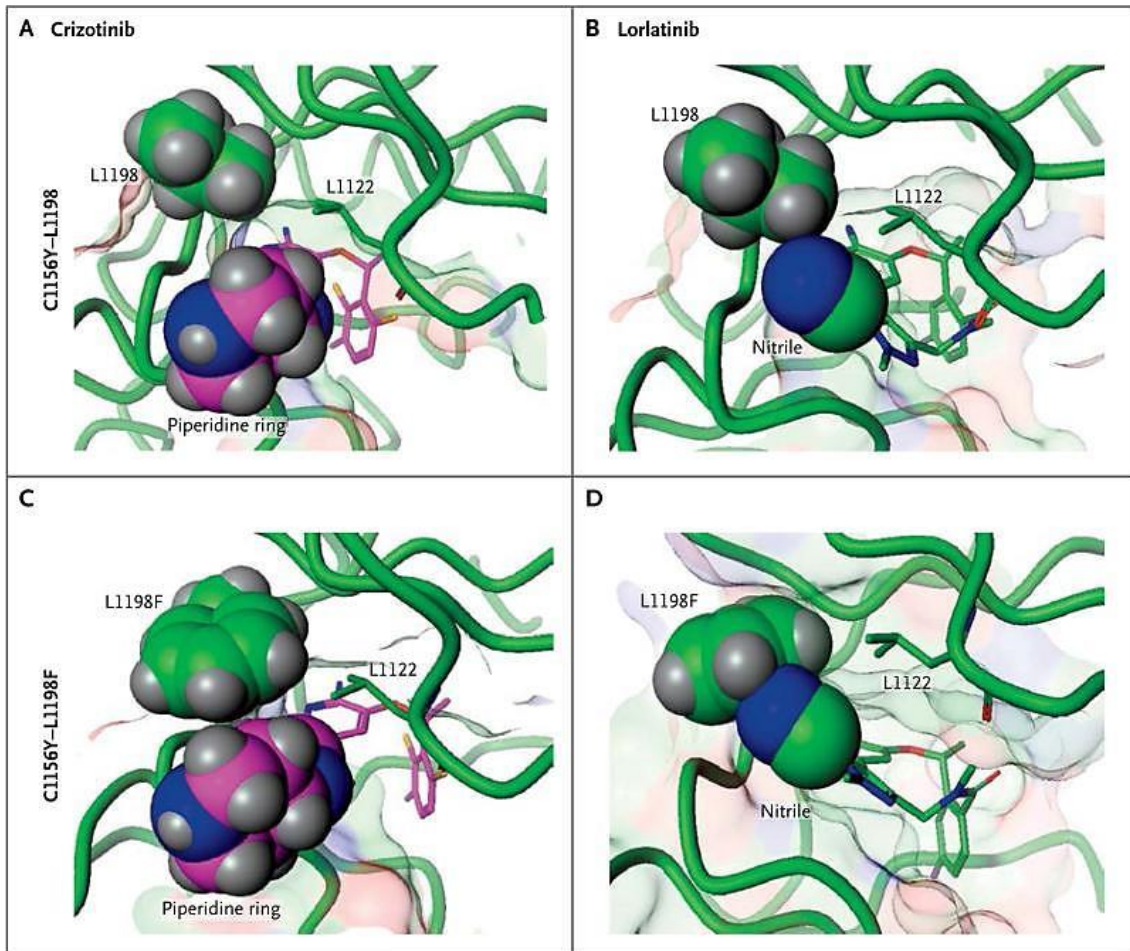


**Figure 18** - Structural Basis for Resistance to Lorlatinib and Sensitivity to Crizotinib Mediated by ALK C1156Y-L1198F. Non-phosphorylated WT ALK and mutant (C1156Y, L1198F, C1156Y-L1198F) kinase domains were co-crystallized with crizotinib or lorlatinib. A) Co-crystal structures of crizotinib bound to the single ALK C1156Y mutant. B) Lorlatinib bound to the single ALK C1156Y mutant. C) Crizotinib bound to the ALK C1156Y-L1198F double mutant. D) Modeling of lorlatinib bound to the double ALK C1156Y-L1198F mutant, highlighting the steric clash between the phenylalanine residue and lorlatinib. L1122 is a g-loop leucine residue that creates a binding pocket with L1198F just above the piperidine and nitrile groups. Figure and legend adapted from Alice Shaw et al, NEJM, 2016 [359].

In another study, Okada and colleagues have also performed ENU mutagenesis screen on G1202R and I1171N mutant EML4-ALK Ba/F3 cells and have shown similar findings [360]. In total, the group has identified 13 ALK compound mutations involving G1202R and I1171N, including the new compound mutation that caused lorlatinib

resistance but remained targetable with alectinib (L1256F). The G1202R + G1269A compound mutation was also identified by this group in a patient derived cell line resistant to lorlatinib. Even though most compound mutations will cause resistance to all available ALK inhibitors, in few selected cases, resistance can be overcome with an earlier generation ALK TKI.

These studies apparently suggest that sequential administration of ALK TKIs is more likely to develop third-generation resistance in form of compound mutations.

### E.1.1.1.2) Amplification of ALK

Another ALK-dependent resistance mechanism is the amplification of ALK gene which occurs less frequently than secondary mutations.

Katayama and colleagues have reported high-level of WT EML4-ALK gene amplification in 1 of the 15 patients that had progressed on crizotinib [342]. It was not found any additional secondary mutations. Also, Doebele and colleagues have documented an increase in the copy number of rearranged ALK gene per cells in 2 out of 13 patients' samples from post-crizotinib treatment [343]. However, copy number gain (CNG) in rearranged ALK gene was accompanied by the resistant mutation G1269A in 1 of these 2 samples.

Genomic amplification of the ALK locus has also been described to mediate ALK TKI resistance in ALLC cell lines [350, 361]. Ceccon and colleagues have observed that brigatinib resistant ALCL cells had overexpressed NPM-ALK due to the ALK amplification [350]. Interestingly, the resistant cells were addicted to the TKI for their growth and proliferation [362], because as soon as the drug was removed, the drug addicted cells experienced an apoptotic death. Most likely, cell death was mediated by the activation of the DNA damage response pathway due to an unbalanced NPM-ALK signaling [362].

Nevertheless, and based on the present clinical evidences, it is difficult to say under which circumstances and/or factors, amplification of ALK gene is sufficient enough to render tumor cells resistant.

### E1.1.2) ALK-Independent Resistance Mechanisms

#### E1.1.2.1) Activation of Bypass Signaling Pathways

Another important category is the ALK-independent resistance mechanism as bypass signaling pathways through genetic alterations, autocrine signaling, or dysregulation of feedback signaling, which leads to the survival and growth of tumor cells even when the target driven gene is inhibited by the TKI (figure 19).

In first- and second-generation ALK inhibitors, several bypass mechanisms have been extensively reported in the literature. One example is the EGFR activation [341, 342, 363]. Studies conducted in ALK-rearranged lung cancer cell lines have shown an increment of EGFR phosphorylation in crizotinib-resistant cell lines which did not present secondary ALK mutations or upregulations of ALK, when compared with the parental crizotinib-sensitive cells. This has led to a persistent activation of the downstream ERK and AKT signaling. However, those cells did not present EGFR mutation or amplification, telling that EGFR activity may result from receptor or ligand up-regulation [341, 363].

Gene expression profiling of crizotinib-resistant vs crizotinib-naïve NSCLC tumor samples using RNA sequencing followed by single-sample gene set enrichment analysis (ssGSEA) has identified EGFR and HER2 (member of the HER receptor family) signatures as two of the most enriched gene expression marks in resistant tumors [364].

Doebele and colleagues have reported mutation in KRAS gene in two out of the eleven NSCLC patients who relapsed on crizotinib [343]. One patient had a KRAS<sup>G12C</sup> mutation which was detected in both, pre- and post-crizotinib biopsy samples.

The second patient had a G12V substitution in KRAS gene only in the post-crizotinib biopsy sample. Interestingly, when the author introduced the G12V substitution in H3122 cells to evaluate its effects on resistance, they did not see a significant difference in the IC50 values between parental and mutant cells [343]. Additionally, re-activation of MAPK signaling pathway due to CNG of WT KRAS gene

or reduced levels of MAPL phosphatase DUSP6 was also reported to impart resistance against ALK TKI in mouse models [365].

However, using an upfront dual ALK and MEK-inhibitor therapy, the authors were able to suppress the development of resistance *in vitro*. In addition, c-KIT gene amplification in the presence of stem cell factor (SCF) has also been reported to impart some degree of resistance against crizotinib in patient samples [342]. However, a combination of crizotinib and imatinib (c-KIT/ABL inhibitor) treatment was able to overcome the resistance in c-KIT overexpressing crizotinib resistant H3122 cells [342].

Laimer and colleagues [366] have shown that, in a mouse model of NPM-ALK<sup>+</sup> lymphoma, the activator protein 1 family member JUN and JUNB promote lymphoma development and tumor dissemination via transcriptional regulation of PDGFR $\beta$ . When PDGFR $\beta$  is inhibited therapeutically, the survival of NPM-ALK transgenic mice is prolonged. Also, its inhibition leads to an increased efficacy of an ALK-specific inhibitor in transplanted NPM-ALK tumors. Remarkably, a patient with refractory late-stage ALK<sup>+</sup> ALCL treated with PDGFR $\alpha$ /PDGFR $\beta$  inhibitors had a rapid and complete remission [367]. Also, in ALK-driven lung adenocarcinoma cell lines and mouse xenograft models, the RAS-MEK pathway was found to be the critical downstream effector of EML4-ALK. In a recent study using NGS analysis in a patient-derived ALK<sup>+</sup> lung cancer cell line after ceritinib treatment, a MAP2K1-K57N activating mutations was found as the primary genetic alteration which has led to MEK activation.

More importantly, a separate study verified that ALK/MEK dual blockade may be effective not only in overcoming but also in delaying ALK TKI resistance [365, 368]. Other examples of bypass mechanisms clinically implicated in ALK TKI resistance mechanism include PIK3CA mutations (one out of 27 samples [3.7%], post-alectinib; one case post-ceritinib) [358, 368]. IGF1R activation (four out of five samples [80%], post-crizotinib) [369], and SRC activation [368]. Also for the third-generation ALK inhibitors, lorlatinib, ALK-independent mechanisms of resistance have been already reported. For instance, the off-target mechanisms of resistance in ALK rearranged NSCLC cell lines have also been characterized *in vitro* by exposing H3122 and H2228 ALK<sup>+</sup> NSCLC cell lines to increasing lorlatinib concentrations. The resulting lorlatinib resistant cell

lines showed over-activation of EGFR as a bypass mechanism to ALK inhibition *in vitro* [370]. This over-activation of EGFR has been previously seen in H3122 cell lines resistant to crizotinib, which suggests that EGFR activation might be a recurring mechanism of resistance in this cell line [341].

Another example, neuroblastoma cell lines with full length ALK carrying the R1275Q point mutations were exposed to lorlatinib and resistant clones harboring a truncated mutation in NF1 have emerged. However, combined treatment with trametinib and lorlatinib overcame resistance in this *in vitro* model.

From the largest reported series of patients with lorlatinib resistance, 65% of tumor samples did not present any compound mutation that could explain resistance to lorlatinib. This fact suggests that bypass mechanisms or histologic transformation could cause resistance in a significant proportion of patients [353].

Reported cases of neuroendocrine transformation at the time of resistance to lorlatinib with a concomitant L1196M mutation, has demonstrated that histologic transformation, like it happens in EGFR mutant lung cancer, can occur independently of acquired resistance mutations. Also suggests that relying only on liquid biopsies without tissue analysis can lead to underdiagnoses of histological transformation.

More recently, Gonzalo Recondo and colleagues have analyzed five ALK-driven lung cancer patients resistant to lorlatinib. Tumor biopsies were analyzed by high-throughput NGS and patients-derived models were developed by this group to better characterize the acquired resistance mechanism.

Recondo et al have described several biological mechanisms that led to lorlatinib resistance, such as Epithelial Mesenchymal Transition (EMT), which mediated resistance in two patients-derived cell lines; three new ALK kinase domain compound mutations (L1196M+D1202N; F1174L+G1202R; C1156Y+G1269A); and a novel bypass mechanism of resistance caused by NF2 loss of function mutations. The two patients-derived cell lines that experienced EMT were susceptible to dual SRC and ALK inhibition; the ALK compound mutations had different susceptibility to ALK inhibition by lorlatinib and finally, the novel bypass mechanism described by this group is sensitive to treatment with mTOR inhibitors [354].

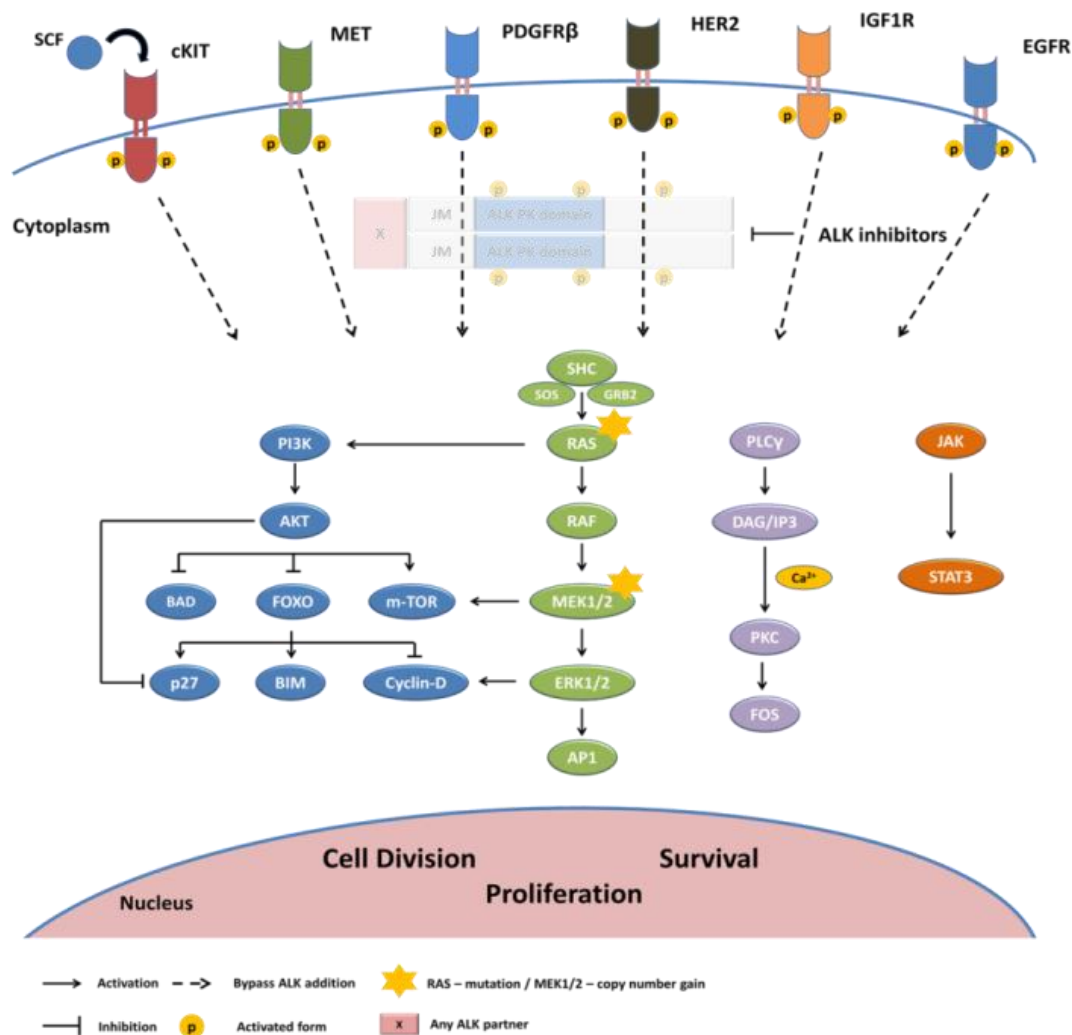


**Figure 19** - ALK downstream pathways and bypass signaling. ALK-independent resistance mechanisms. Activation of bypass signaling pathways when ALK is inhibited with TKIs: EGFR activation, without EGFR mutations or amplifications; HER2 activation; c-KIT gene amplification in the presence of Stem Cell (SCF); MET activation bypassing ALK inhibitors without anti-MET activity; regulation via transcriptional of PDGFR $\beta$  and IGF1R activation. Mutations in KRAS and copy number gain of WT KRAS; JM, Juxtamembrane. Figure and legend adapted from Sharma et al, *Cancers*, 2018 <sup>[48]</sup>.

### E1.1.2.2) Histologic Transformation

One of the less understood mechanisms of resistance is the shift of the histologic phenotype that tumors can experience upon exposure to TKIs in lung cancer; namely 1) epithelial-mesenchymal transition (EMT), 2) small-cell lung cancer (SCLC) transformation, and 3) squamous cell carcinoma (SCC) transformation from originally lung adenocarcinoma tumors.

- *Epithelial-Mesenchymal Transition*

Epithelial-Mesenchymal Transition (EMT) is a dynamic and usually reversible process that consists in the transient acquisition of mesenchymal features from epithelial cells <sup>[371]</sup>.

Briefly, cells can shift from an epithelial to a partial or even full mesenchymal state and backwards. In normal and physiological conditions, this process is important during embryogenesis and in wound healing in adulthood. However, in cancer, this phenomenon favors cell migration and metastasis. It can also be induced by treatment exposure and trigger resistance to chemotherapy and TKI therapy.

To better understand this phenomenon, it is necessary to mention that normal epithelial cells usually display apico-basal polarity and are in contact with each other by lateral cell-cell junctions, such as adherent and tight junctions by multiple proteins including cadherin molecules like E-cadherin. What is known is that the expression of E-cadherin in epithelial cells is repressed by various transcription factors (TF), such as SNAIL, SLUG, ZEB1, TWIST1/2, while N-cadherin, vimentin and fibronectin expression is induced. Tumor cells lose the apico-basal polarity and polygonal shape and induce the degradation of the basal cell membrane, resulting in the acquisition of mesenchymal phenotype, shifting their polarity and acquiring higher capacity to invade and metastasize. The TF involved in this biologic process are activated through several signaling pathways, such as TGF $\beta$ , WNT, NOTCH, SRC, AXL and MET <sup>[372-377]</sup>. The TGF $\beta$  pathway is frequently involved in EMT. The binding of TGF $\beta$  ligand to its receptor triggers the downstream phosphorylation of SMAD proteins that form SMAD complexes and induce the transcription of EMT related genes that finally inhibit the expression of E-cadherin and induce the differentiation to mesenchymal phenotype. Finally, SRC is also a key determinant of EMT by localizing to the peripheral cell-substrate adhesions, regulating its disassembly through phosphorylation of focal adhesion kinase (FAK) and promoting the degradation of cell-adhesion components <sup>[378]</sup>. Also, it can suppress the function of E-cadherin <sup>[375]</sup>.

Depending on the mechanism of induction of EMT, resistance to TKIs can be potentially reversed *in vitro* by combining the TKI targeting the primary oncogenic driver and a second drug targeting the EMT pathway activation. Nevertheless, this has not translated into clinical development, and there is an unmet need to design effective

strategies to diagnose and target EMT as a resistance mechanism to targeted therapies in lung cancer.

EMT was reported in about 40% of tissue samples from twelve ceritinib resistant tumors with IHC staining showing loss of E-cadherin and gain of vimentin expression <sup>[358]</sup>. It was also reported that EMT has mediated resistance to crizotinib in H3122 cells <sup>[379]</sup>.

- *Small-Cell Lung Cancer and Squamous Cell Carcinoma transformation*

Histological transformation from NSCLC (most commonly lung adenocarcinoma) to the high grade neuroendocrine SCLC phenotype has been extensively reported as a mechanism of resistance to TKIs in lung cancer <sup>[380-382]</sup>, and also in ALK-driven lung cancer, even though it seems to be a rare event. Only single cases of SCLC transformation in the context of treatment with crizotinib, ceritinib, alectinib and lorlatinib have been reported <sup>[383-386]</sup>.

Transformation from lung adenocarcinoma to SCC histology has also been recently reported as a mechanism of resistance to ALK inhibitor alectinib in a single case <sup>[383]</sup>. The biological bases of resistance to ALK inhibitors in this context are still unknown.



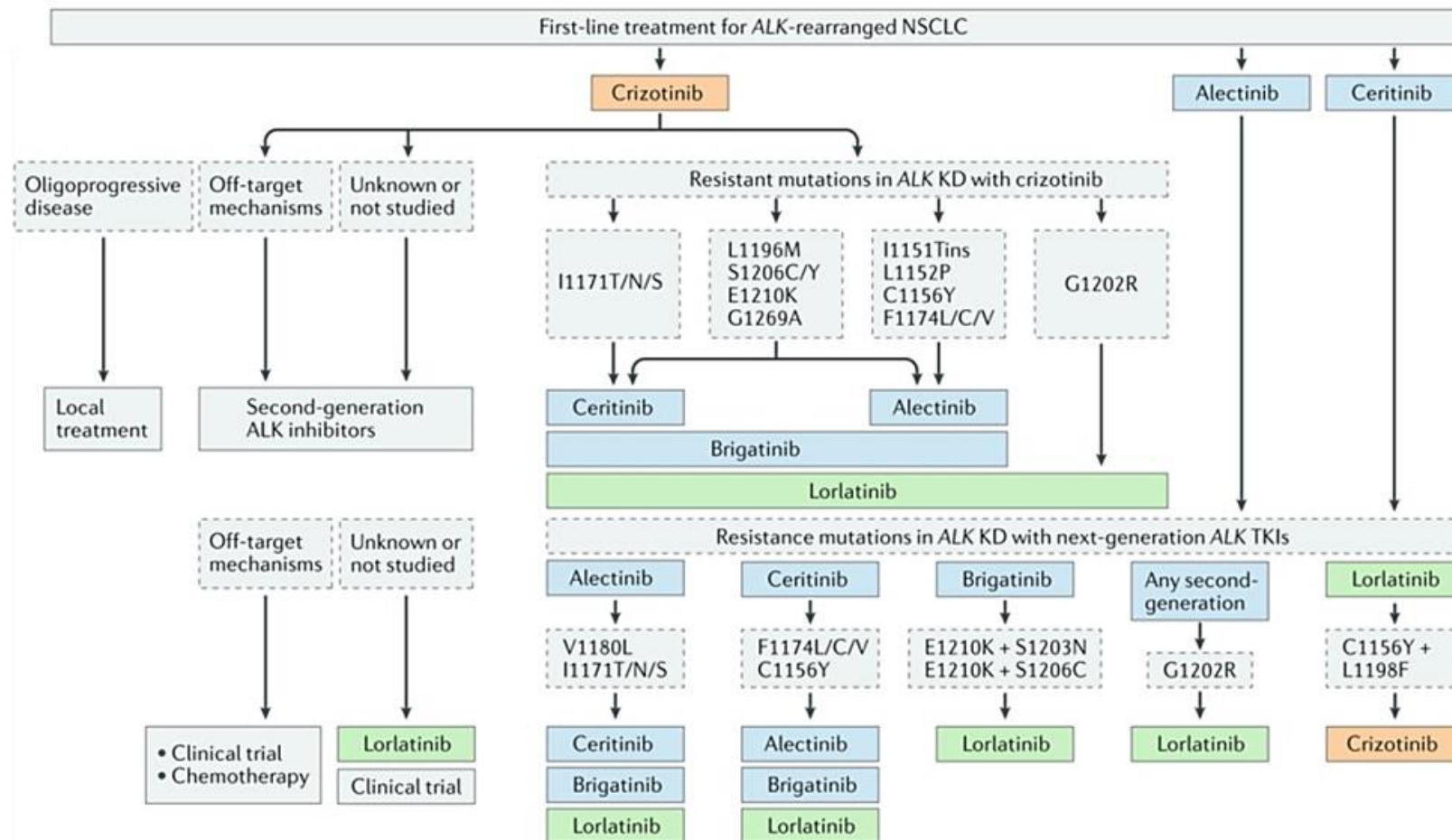


**Figure 20** – The optimal sequencing for the treatment sequence with TKIs (either first- or next-generation), based on the type of acquired mechanisms of resistance in patients with NSCLC harboring ALK rearrangements. In first-line treatment with crizotinib, secondary kinase domain mutations can select for specific second generation ALK TKIs based on the differential sensitivity to these compounds. This is repeatedly the case in the second line setting, were for the exception of the G1202R mutation, other secondary kinase domain mutations could be overcome by switching to another second generation TKI. In the presence of the G1202R, the sole effective ALK directed treatment is lorlatinib. Off target mechanism in resistance to crizotinib can be overcome with second generation TKI. If resistance mutations are not identified at progression with a second generation TKI, lorlatinib is still an option, but in the presence of a known bypass mechanisms, a potential benefit could be obtained with clinical trials of combination therapies. KD: kinase domain. Figure and legend adapted from Recondo et al. Nat Rev Clin Oncol, 2018 [292].

### E1.2) Therapeutic Strategies to Overcome ALK-Related Resistance

#### E1.2.1) ALK TKIs Combined with Other Inhibitors Targeting Different Kinases

The majority of studies performed on ALK TKI resistance have focused on the development of next-generation ALK inhibitors, which can overcome at least some of the resistant mutants. Around 30% of crizotinib resistance in ALK-driven NSCLC is related to secondary ALK mutations and/or amplifications, which maintain their sensitivity to next-generation ALK inhibitors. However, approximately 40% of the resistant cases to second-generation inhibitors are no longer ALK-dependent. The activation of bypass signaling has emerged as other potential strategy to combat ALK TKI resistance. Combination strategies that target both ALK and a second kinase might be needed to overcome the different bypass pathways that mediate ALK resistance.

MEK reactivation is a key example of resistance mechanism involving other TKIs. Crystal and colleagues have shown that MEK inhibitor selumetinib was a potent hit when combined with ceritinib in a patient-derived ALK-rearranged lung cancer cell line post-ceritinib harboring MAP2K1<sup>K57N</sup> activation mutation of MEK [368]. Confirming these results, an independent study led by Hrustanovic and colleagues, demonstrated that the dual blockade of ALK/MEK may be effective not only in overcoming but also in delaying ALK TKI resistance [365]. These findings suggest that combining therapies such as ALK and MEK inhibitors might be a potential therapeutic strategy to overcome bypass resistant mechanisms.

Clinical trials are testing the efficacy of ALK TKI in combination with other target agents. Alectinib combined with bevacizumab (angiogenesis agent targeting vascular endothelial growth factor–VEGF) is being tested in patients with ALK-rearranged NSCLC with at least one target lesion in CNS (NCT02521051) and combinations of ceritinib with either LEE011 (CDK4/6 inhibitor) or everolimus (mTOR inhibitor) are in early-phase testing in NSCLC (NCT02292550 and NCT02321501, respectively). Other potential combinations include ALK TKI with EGFR inhibitor, c-KIT inhibitor and SRC inhibitor. The selection of the appropriate combination should

be individualized based on the resistance mechanism identified. However, toxicities due to combination of drugs may be the major concern/limitation.

MET activation is a very well-known bypass signaling pathway in EGFR-mutant NSCLC but in ALK-rearranged NSCLC does not cause resistance to the first-generation TKI crizotinib, which is also a potent MET inhibitor [381, 387]. However, some of the next-generation ALK TKIs do not have activity against MET and indeed, it has been reported as a bypass signaling mechanism in a patient who has failed second-generation ALK inhibitors. As expected, this patient subsequently responded to crizotinib [388]. Similarly, the fact that each ALK TKI is associated with a unique spectrum of ALK resistance mutations, suggests that combinations of ALK TKIs could also be beneficial and enable more durable responses than those achieved in monotherapies.

### **E1.2.2) What comes next?**

ALK inhibitors resistance has prompted the development of more and better inhibitors that would overcome all ALK-dependent resistance. However, what really took the scientific community by surprise was the fact that, even with the most potent ALK inhibitor (third-generation lorlatinib), cancer cells invariably develop resistance, leading to cancer proliferation and disease progression. It seems that the stronger the ALK inhibitor is, the stronger and more complicate the mechanism of resistance tends to be. Besides the emergence of compound mutations causing resistance to lorlatinib, the spectrum of biologic mechanisms that drives resistance is enormous and sometimes, the same patient can harbor more than one mechanism of resistance. This represents a significant barrier to the successful treatment of ALK-positive patients. Therefore, the development of strategies to overcome/prevent/delay resistance is a priority. With the current knowledge of the complex and heterogeneous mechanisms process behind ALK resistance, multiple next-generation ALK inhibitors and combinatorial treatment approaches can be envisioned. These potential new therapeutic strategies have the promise to improve the treatment of an increasing portion of patients ALK-positive cancers. One such therapeutic strategy is immunotherapy.

Immunotherapy aims to establish or enhance an effective immune response against tumor cells and this could be accomplished in different strategies, including tumor vaccination, adoptive transfer of immune cells, and modification of the immune system to boost an already established immune response [389]. With the discovery of inhibitory pathways in immune cells, the so-called immune checkpoints, and the development of antibody-based blockades against these checkpoint molecules, such as Cytotoxic T Lymphocyte-Associated protein 4 (CTLA-4) and Programmed Cell Death Protein (PD-1)/PD-1 Ligand 1 (PD-L1), cancer immunotherapy entered in a new era [390].

NSCLC patients with high PD-L1 expression have been experiencing good responses to immune checkpoint inhibitors (ICI) against PD-1 with an objective response rate of up to 20% [391-393]. In general, patients with squamous NSCLC respond to ICI better than patients with non-squamous-NSCLC, and amongst the latter, a better response is observed in patients with heavy smoking history than those with light- or non-smoking recorder [394]. The differences between smoker and non-smoker NSCLC patient cohorts that might be linked to their ICI response may include the following:

1. Smokers usually harbor higher mutational burden and thus have a higher number of expressed neo-antigens than non-smokers;
2. The tumor microenvironment (TME) in smokers is characterized by an increased frequency of active tumor-infiltrating CD8<sup>+</sup> T-cells as well as increased levels of anti-tumor cytokines such as IFN- $\gamma$  and granzyme, while the TME in non-smokers shows elevated immunosuppressive features such as a high number of FOXP3<sup>+</sup> regulatory T cells, the accumulation of M2-like macrophages and less activated effector CD8<sup>+</sup> T cells [395].

As it was mentioned before, ALK-rearranged NSCLC patients are non- or light-smokers which may represent a lower number of non-synonymous mutations than other subtypes of NSCLC [396]. Clinical trials, where the effect of ICI in these patients was evaluated, have shown minimal responses [391, 393]. Experimental evidences have demonstrated that ALK-driven NSCLC patients harbor an immunosuppressive TME and T-cell exhausted state [397]. Therefore, the strategy seems to be the conversion of the

TME in ALK-driven NSCLC to such extent that an effective immune response against the tumor will be possible. So, how can we convert an immune-unresponsive TME into a responsive TME?

Tumor associated antigens (TAA) / neo-antigens-based cancer vaccination can activate T-cells and promote tumor-associated infiltrating effector lymphocytes into the TME [398]. TAA and tumor neo-antigens are the products of all genetic alterations accumulated in the cancer genome during tumorigenesis. TAA are co-expressed by normal and tumor cells, however, in tumor cells its expression usually is stronger due to gain-of-function mutations, overexpression of a given gene, etc. The neo-antigens are superior to other TAA due to:

1. Neo-antigens are presented only in tumor cells;
2. Neo-antigens are not subject to central tolerance in the thymus;
3. Neo-antigens produce strong immunogenicity, with persistent cytotoxic T-cell activation.

These antigens can arise not only from missense mutations but also fusion proteins [399] or any altered open reading frame that encodes a novel protein sequence that is not encoded in the normal genome.

As it was mentioned before, ALK expression is restricted to a subset of cells in the nervous system. ALK expression in lung cancer and other malignancies is due to point mutations in the kinase domains, amplification or chromosomal translocations that lead to the formation of ALK fusion proteins, which are overexpressed and constitutively activated in cancer cells. The high level of ALK expression in ALK-driven malignancies, the ALK-addicted status of cancer cells in line with the fact that normal ALK expression is expressed at such low levels, makes it an ideal tumor-specific target for immunotherapy.

In the literature is possible to find evidences that ALK generates *per se* an immune response. For instance, the presence of anti-NPM-ALK antibodies in ALCL patients has been reported [400]. Another example, two HLA-A2.1 restricted CD8<sup>+</sup> T-cell epitopes, p280–289 (SLAMLDLLHV) and p375–389 (GVLLWEIFSL) from the ALK kinase domain, were identified and confirmed to be immunogenic in HLA-matched ALCL and neuroblastoma cell lines [401]. In principle, these peptides could be used for

## Chapter I - Introduction

---

vaccination in ALK-driven tumors. In fact, Chiarle et al <sup>[402]</sup> have shown that ALK-DNA-based vaccination with plasmids encoding portions of the cytoplasmic domain of ALK protects mice from local and systemic lymphoma growth. Chiarle has reported that the protection is potent and durable by eliciting an ALK-specific IFN- $\gamma$  response and CD8<sup>+</sup> T cell-mediated cytotoxicity. The efficacy of ALK-DNA-based vaccination was also observed in lung cancer graft models with EML4-ALK<sup>+</sup> cell lines as well as in a EML4-ALK and TFG-ALK transgenic lung cancer mouse model <sup>[397]</sup>. However, in animals with high tumor burden, the anti-tumor effect of an ALK-DNA-based vaccine is diminished. This may correlate with an exhausted phenotype of CD8<sup>+</sup> T-cells and PD-L1 expression. Thus, the combination of an ALK vaccine and ALK inhibitors, as expected, increased the anti-tumor efficacy <sup>[397]</sup> due to an increase of ALK antigens exposure and possible TME changes (e.g., more tumor-infiltrating lymphocytes).

PD-L1 expression is increased in ALK<sup>+</sup> lung cancer cells through downstream pathway signaling, in particular ERK and AKT activation but not JAK/STAT3/5 signaling <sup>[403]</sup>. Given a higher objective response rate of anti-PD-1 and anti-CTLA-4 in PD-L1 positive lung cancer, it is reasonable to consider adding anti-PD-1 and/or anti-PD-L1 antibodies to the treatment of ALK<sup>+</sup> lung cancer, particularly if in combination with an ALK vaccine. These findings indicate that ALK represents a compelling tumor antigen for vaccination-based therapies. Thus, neo-antigen-based vaccines could provide an alternative therapeutic option to treat refractory ALK<sup>+</sup> cancers such as lung cancer. To fully understand the concepts behind this statement, in the next subchapter the reader will be guided through the evolution of the immunotherapy concept.

### F1) From Cancer Immunesurveillance to Cancer Immunoediting

Now-a-days, it is established and accepted within the scientific community that the immune system plays an important and major role in host-protecting and tumor sculpting on developing tumors. However, this concept took a long way until it got accepted. In the last two decades, several groups have unequivocally documented that immunity can, in fact, facilitate cellular transformation, prevent or control tumor outgrowth and shape the immunogenicity of tumors. These apparently paradoxical functions of the immune system are separable based on their temporal occurrence during tumor formation, the nature of the transforming event, the particular components of immunity involved in each process, and in the nature of the tumor specific antigens expressed in the transformed cell <sup>[404]</sup>.

Several studies have revealed that an intact immune system can prevent/control and shape/promote cancer by a process called “Cancer Immunoediting” <sup>[405, 406]</sup>. The evolution of this concept from the older (and perhaps more controversial) “Cancer Immunosurveillance” hypothesis has helped to interpret the predictive and prognostic significance of immune infiltrated into tumors. The immunesurveillance theory was originally proposed more than 50 years ago by Burnet and Thomas, whom claimed that the immune system acts as a sentinel in recognizing and eliminating nascent transformed cells <sup>[407]</sup>. However, extensive work over the past two decades has revealed that this surveillance function of the immune system was only a part of the story and encouraged the scientific community to re-define and extend the concept into one called “cancer immunoediting”, which can describe the many facets of immune system-tumor interactions more accurately <sup>[405, 406]</sup>. This new dynamic proves that the immune system not only protects against cancer development but also shapes the characteristics of the emerging tumors. Cancer immunoediting hypothesis is composed of three phases: 1) Elimination, 2) Equilibrium and 3) Escape <sup>[404]</sup>.

#### F1.1) Elimination

Elimination, the first phase of cancer immunoediting, represents a modernized and expanded view of the Cancer Immunosurveillance hypothesis, where the

molecules and cells of innate and adaptive immunity work together to recognize and destroy a developing tumor [408].

The key components involved in the Elimination phase include cells of both innate immunity (natural killers [NK], macrophages and dendritic cells [DC]) and adaptive immunity (NKT, CD4<sup>+</sup> and CD8<sup>+</sup> T-cells) [409, 410]. Similarly, host effector molecules such as tumor necrosis factor-alpha (TNF- $\alpha$ ), Fas/FasL, granzyme, perforin, TNF-related apoptosis-inducing ligand (TRAIL), as well as recognition molecules such as NKG2D in protective antitumor immunity have been shown to play critical roles in the Elimination phase [404, 411, 412]. Both type I interferons (IFN- $\alpha/\beta$ ) and IFN- $\gamma$  are required for the development of protective antitumor immune responses but play distinct roles in this Elimination phase. Whereas IFN- $\gamma$  targets both tumor and hematopoietic cells, IFN- $\alpha/\beta$  acts primarily on host cells [413]. Specifically, in mice, type I IFNs enhance the cross-presentation activity of tumor antigens by CD8 $\alpha^+$ /CD103<sup>+</sup> DCs while IFN- $\gamma$  promotes the induction of CD4<sup>+</sup> T helper I (Th1) cells and CD8<sup>+</sup> cytotoxic T lymphocytes (CTL), and is critical for enhancing MHC-class-I (MHC-I) expression on tumor cells [413, 414]. If all cancer cells are eliminated, then the Elimination phase represents the full extent of the Cancer Immunoediting process (figure 21).

### F1.2) Equilibrium

However, if some cancer cells survive, then the process can progress to the second phase – the Equilibrium phase, a period in which immunity is able to control the net outgrowth of cancer cells and thereby keep them clinically unapparent without completely eliminating them [408].

Evidences for the Equilibrium phase came from observations of cancer transfer following organ transplantation. A particularly well-documented event was the case of two patients who received kidney transplant from the same cadaver donor. Both subsequently developed malignant melanoma [415]. The origins of the cancer were then traced back to the donor who had been diagnosed with melanoma and was successfully treated 16 years before death, and presumed to be cancer free. However, by transfer of a kidney from this donor into naïve recipients who were then immunosuppressed to protect against graft rejection, it was presumed that tumor cells



held in equilibrium by the donor's immune system were then released from their dormant state and began to grow in a progressive manner. This clinical scenario was then recapitulated, back in 2007, in a defined preclinical model which provided the first experimental evidence of the postulated Equilibrium phase <sup>[416]</sup>. In this study, 80% of mice that were treated with low doses of MCA (chemical tumor-inducer) remained free of clinically apparent cancers for more than 200 days. However, when these mice were treated on day 200 with a cocktail of monoclonal antibodies that depleted CD4<sup>+</sup> and CD8<sup>+</sup> T-cells and blocked IFN- $\gamma$ , they showed a rapid appearance of sarcomas at the original site of MCA injection. Subsequent studies have shown that adaptive immunity was the driver of the Equilibrium phase due to the fact that antibodies that inhibited the adaptive immunity released the dormant tumor cells from their equilibrium state while antibodies that inhibit innate immunity did not <sup>[408]</sup>. Interestingly, dormant tumor cells were found in lesions that contained actively proliferating lymphocytes. Tumor cells held in equilibrium retained their highly immunogenic phenotype and thus remained unedited. In contrast, the rare dormant cancer cells that spontaneously progressed to actively growing tumors displayed reduced immunogenicity and thus had undergone editing. Thus, the Equilibrium phase can represent an end stage of Cancer Immunoediting where cancer cells remain in a durable state of immunity-induced dormancy throughout the remaining lifespan of the host without progressing to clinically apparent cancer (figure 21) <sup>[408]</sup>.

### F1.3) Escape

An immune-suppressive TME is developed when immunoediting results in a reduction of tumor immunogenicity such that the immune system can no longer control tumor cell growth. The immune-suppressive TME results in the outgrowth of tumor cells that eventually became clinically apparent tumors. This phenomenon pictures the third phase of Cancer Immunoediting – Escape <sup>[408]</sup>.

Immune escape can occur through many different mechanisms involving both changes in the tumor cells and/or in the tumor microenvironment. Tumors may avoid immune recognition through loss of NKG2D ligands, down-regulation of MHC-I,  $\beta$ -2 microglobulin and calreticulin, reduced expression of costimulatory molecules, and/or

## Chapter I - Introduction

antigen loss [417, 418]. Tumor cells also upregulated proteins that allow increased resistance to apoptosis and promoting of survival (such as STAT3 or the anti-apoptotic molecules BCL-2) [419]. The development of an immune-suppressive TME is due to the recruitment of suppressive cells such as Myeloid-Derived Suppressor Cells (MDSC) and regulatory T-cells (Tregs), secretion of immune-suppressive cytokines such as IL-10 and TGF $\beta$  or expression of immune checkpoints of the B7 family such as PD-1/PD-L1, CTLA-4, Lymphocyte-Activation Gene 3 (LAG-3), T-cell Immunoglobulin and Mucin domains 3 (TIM-3) by either tumor cells, immune cells, or both (figure 21) [408].

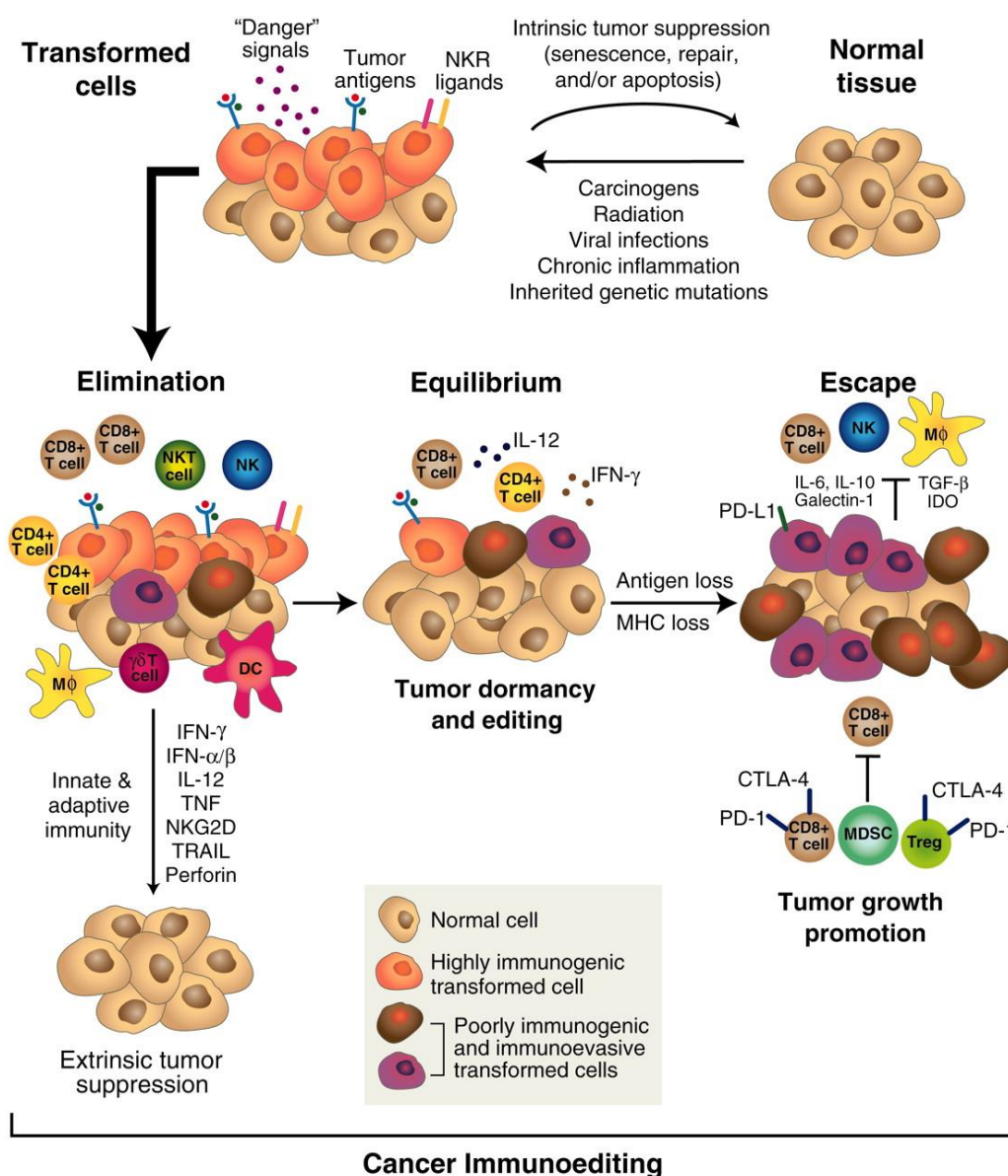


**Figure 21** - Cancer Immunoediting is an extrinsic tumor-suppressor mechanism that engages after cellular transformation has occurred and intrinsic tumor-suppressive mechanisms have failed. Cancer Immunoediting consists of three phases: Elimination, Equilibrium, and Escape. Figure and legend adapted from Ward et al, Adv Immunol, 2016 [408].

### F1.4) Cancer cells are immunogenic: antigenic targets of Cancer Immunoediting

The principal of Cancer Immunoediting is that the recognition of tumor antigens by T-cells drives the immunological sculpting of cancers. Tumor antigens can be divided into three major categories; 1) tumor-associated antigens (TAA); 2) cancer-germline/cancer testis antigens (CTA); and 3) tumor-specific antigens (TSAs) or neoantigens [408, 420, 421].

TAA are comprised of proteins encoded in the normal genome that may represent either normal differentiation antigens or aberrantly expressed normal proteins that are also expressed by normal cells [408]. Overexpressed normal proteins that possess growth/survival-promoting functions represent TAA that directly participate in oncogenesis [422, 423]. CTA is the second category of tumor antigens which are normally expressed in germ cells (testis and ovary) and trophoblast tissues as well as in cancer cells. Due the fact that their expression is relatively restricted to certain tissues, these antigens have represented attractive targets for immunotherapy [408]. The third antigen category, TSA or neoantigens, includes genes that are exclusively expressed in tumor cells and may represent either oncogenic viral proteins or abnormal proteins that arise as a consequence of somatic mutations or posttranslational modifications. Spontaneous arising mutations, from exposure to carcinogens and/or from the genomic instability that is characteristic of neoplastic cells, can produce mutations (missense mutations), alterations in the reading frame, extending the coding sequence beyond the normal stop codon (nonstop mutations), DNA insertions or deletions (Indel), or by chromosomal translocations [421]. In contrast to TAA, TSA are almost exclusively unique to an individual.

### F1.5) Antigenic presentation

Antigenic recognition is made by T-cells that are constantly searching for non-self-antigens. T-cells are derived from hematopoietic stem cells that are found in the bone marrow. The progenitors of these cells migrate to and colonize the thymus.

The thymus selects newly produced T-cells to generate a functionally competent and self-tolerant T-cell pool. After migrating into the microenvironment of the thymic-cortex, T-cell progenitors are induced to develop into T-cell antigen receptor (TCR)-expressing CD4<sup>+</sup>CD8<sup>+</sup> double-positive (DP) thymocytes. The V(D)J rearrangement of TCR $\alpha$  and TCR $\beta$  genomic loci in early T-cells allows the formation of a great diversity in the pre-selected repertoire of TCR recognition specificities in newly generated cortical DP thymocytes, which are individually selected for their fate according to their TCR recognition specificities.

DP thymocytes that express TCRs interacting at low affinity with self-peptide-associated with MHC-I or MHC-class-II (MHC-II) molecules displayed in the thymic cortex, are rescued from cell death to survive and differentiate into CD4<sup>+</sup>CD8<sup>-</sup> or CD4<sup>-</sup>CD8<sup>+</sup> single-positive (SP) thymocytes, a process called positive selection in the thymus [424-426]. Positively selected thymocytes start to express the chemokine receptor CCR7 and migrate to the thymic medulla, where a subpopulation of medullary thymic epithelial cells (mTECs) produces CCR7 ligands (CCL19/CCL21) [427, 428], which attracts the newly positively selected thymocytes. There, a distinct subpopulation of mTECs produces a wide range of self-molecules, including 'tissue-specific' self-proteins (i.e. proteins that are otherwise only found in specific peripheral tissues) and displays the vast majority of self-antigens, in cooperation with dendritic cells (DCs) [429-431]. Medullary thymocytes that express TCRs with high affinity for self-peptide-MHC (self-pMHC) complexes displayed in the medullary microenvironment are either deleted by apoptosis or destined to become regulatory T-cells (Treg) [426, 432, 433]. Negative selection in the thymus conventionally refers to the process of self-antigen-mediated deletion of developing thymocytes through apoptosis, including deletion of the high-affinity self-reactive thymocytes in the medulla. Thus, the TCR affinity threshold in the thymocyte selection has great importance in this process.

### F1.5.1) TCR affinity

The affinity between TCRs and their peptide-MHC ligands determines the fate of developing thymocytes. Early studies have shown that differences in ligand concentration and ligating TCR valency (valency is reported to be the measure of the

combining power of an element with other atom) as well as differences among agonist and antagonist peptide ligands affect life-or-death determination in immature thymocytes [434-437]. The findings that agonist peptide ligation promotes differentiation into unconventional T-cell lineages, including Treg, pointed to the view that the quality of TCR signals triggered in developing thymocytes not only determines life-or-death selection in generating a conventional T-cell pool but also contributes to determining a way to direct cells towards Treg subpopulation [438, 439].

It is now understood that the affinity between TCRs expressed by developing thymocytes and self-pMHC complexes displayed in the thymus is the major parameter that determines the fate of newly generated T cells. The TCR–ligand affinity determines positive or negative selection as well as lineage direction to become functionally distinct cells (e.g. conventional CD4<sup>+</sup> helper and CD8<sup>+</sup> killer T cells). A low-affinity interaction between TCR and pMHC promotes thymocyte maturation to give rise to functionally competent T-cells (i.e. positive selection), whereas a high affinity interaction causes the deletion of self-reactive T-cells (i.e. negative selection) or the generation of Tregs [424, 440].

The narrow TCR–pMHC affinity range sets the threshold for life or death in developing thymocytes, contributing to the enrichment of functionally potent and self-protective T-cells while excluding potentially harmful self-reactive T-cells from the mature T-cell pool [441, 442].

### F1.5.2) MHC-class-I and II

Antigenic peptides are recognized by T-cells receptors but only in the context of MHC-I or -II molecules that display the antigens on the cell surface.

Endogenously synthesized antigens in the cytosol of all cells are presented to CD8<sup>+</sup> T-cells as peptides bound to MHC-I molecules, and antigens ingested into endocytic (exogenously) compartments of macrophages, dendritic cells or B-cells are presented to CD4<sup>+</sup> T-cells as peptides bound to MHC- II molecules. However, the exogenous pathway also presents antigens in the context of MHC- I to CD8<sup>+</sup> T-cells.

Briefly, MHC-I and -II molecules have two Ig-domains topped by two parallel  $\alpha$ -helixes resting on a platform of  $\beta$ -pleated sheets.

## Chapter I - Introduction

This structure generated a peptide-binding groove between the  $\alpha$ -helices (figure 22) <sup>[443, 444]</sup>.

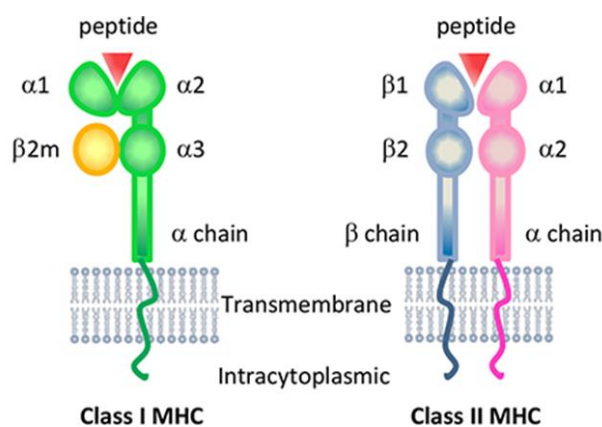


**Figure 22** - Structure of MHC-I (left panel) and -II (right panel) molecules. Created with Biorender.com.

The extreme polymorphism (>10,000 different of MHC-I have been identified so far) turns MHC-I and -II molecules unique in the proteome, and this has interesting consequences. Polymorphic residues on the top  $\alpha$ -helices interact with the T-cell receptors and are the basis for the specificity of TCRs for both an antigen peptide plus a particular allelic form of an MHC molecule (a phenomenon called MHC restriction).

Polymorphic residues in the MHC peptide binding groove change the nature and location of so-called pockets. These variable pockets are filled by complementary variable amino-acid side chains of peptides (so-called anchor residues), meaning that different fragments from a defined antigen are presented by different polymorphic MHC molecules <sup>[445, 446]</sup>.

Also, next to the anchor residues, the other amino-acids of the peptide fill a free space and can be (almost) any of the 20 amino-acids <sup>[447, 448]</sup>. Due the fact that these molecules have pockets with specificity for only a few side chains and the remaining 6-10 amino-acids can vary between all possibilities, each kind of MHC molecules can present a very large repertoire of peptides (figure 23).

Moreover, by having 3 to 6 different MHC-I as well as 3 to 12 different MHC-II molecules (the exact number depends on how many different MHC alleles were inherited from one's parents and how the MHC-II subunits paired), cells can present a large fraction of the universe of peptides, although not all sequences.

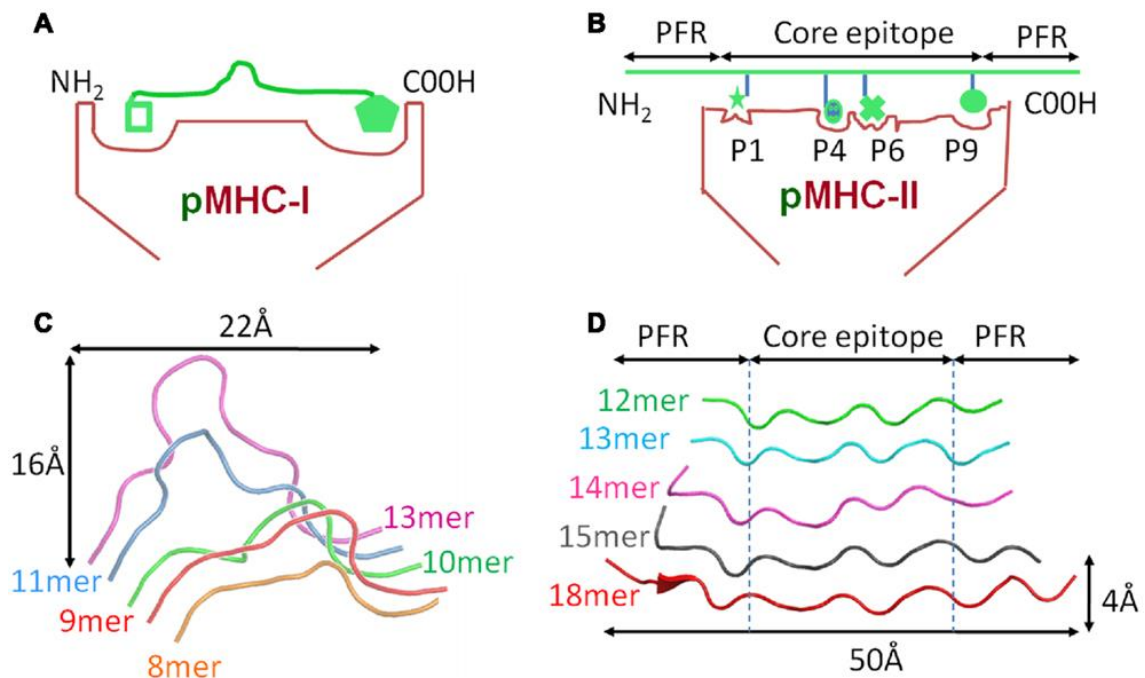


**Figure 23** - Comparison of peptide conformation presented by MHC I and II. (A) pMHC I and (B) pMHC II binding grooves; it is shown the key anchor sites in the floor of each groove that determine which peptide can be associated and the conformation it can assume. (C) The structural database of pMHC I complexes shows that peptides presented by MHC I molecules (represented as ribbon cartoons) generally assume a central bulged conformation. As peptide length increases, the “closed” nature of the pMHC I binding groove forces the central residues of the peptide up out of the groove to accommodate the extra residues. (D) In contrast, the pMHC II binding is “open” enabling longer peptide to extend out of the groove to form peptide flanking regions. Thus, peptides presented by MHC II molecules (represented as ribbon cartoons) generally assume a much flatter conformation in the MHC II binding groove, irrespective of the length of the peptide presented. Figure and legend adapted from Christopher J. Holland, *Front. Immunol.* 2013 <sup>[449]</sup>.

In theory, MHC-I molecules can present a peptidome of around  $6 \times 20^{(6-7)}$  different peptides, and MHC-II can display up to  $12 \times 20^{(10)}$  peptides. However, such a large array of peptides cannot all be presented at the same time due to the fact that there are only around 200,000 MHC-I and 20,000 MHC-II molecules on some subsets of antigen presenting cells <sup>[450]</sup>.

Additionally, since some peptides are presented in high number (coming from highly expressed proteins), the real number of different peptides presented by one cell is likely less than 10,000. Worthy mentioning is the fact that when a specific pathogen alters a critical anchor residue in one of its antigenic epitopes, it may prevent presentation of this specific antigen in one individual but not in another person with different MHC molecules that will simply select different peptides from the same

pathogen <sup>[451]</sup>. Therefore, it seems reasonable that MHC polymorphisms are good for the survival of the species and not necessarily the individual.

### F1.5.2.1) MHC-I and CD8<sup>+</sup> T-Cells

As mentioned above, MHC-I molecules present peptides from proteins that are synthesized by cells. In healthy cells, all proteins presented in a MHC-I manner are autologous and therefore, CD8<sup>+</sup> T-cells are tolerant to them. However, when cells are expressing mutant sequences, as it is in cancer, microbial genes or polymorphic genes, these “non-self” antigenic peptides are included in the presented peptidome, which allows CD8<sup>+</sup> T-cells to detect and eliminate the abnormal cells.

Briefly, normal and pathogenic/neoplastic proteins are degraded by the proteasome into small peptide fragments <sup>[452-454]</sup>, which are further trimmed to a large extent and destroyed by cytosolic peptidases <sup>[455]</sup>. However, some survive by escaping into the endoplasmic reticulum (ER) through a peptide transporter called Transporter Associated with antigen Processing (TAP) that is embedded in the ER membrane <sup>[452]</sup>.

Within the ER, TAP forms the center of a peptide loading complex (that includes a chaperone called tapasin, empty MHC-I molecules waiting for peptides and two other common chaperons, calreticulin and protein disulfide isomerase ERp57 <sup>[456]</sup>) and translocates the peptides that are considered for binding by MHC-I molecules.

Tapasin holds empty MHC-I molecules in a peptide-receptive state and promotes MHC-I binding of peptides with a slow-off rate, consequently helping to shape the repertoire of presented peptides <sup>[457]</sup>. Therefore, MHC-I molecules test the binding of many peptides and subsequently release most of these until a proper (slow-off rate) peptide is bound <sup>[458]</sup>. Usually, these are peptides of a very specific length of 8-10 amino acids with appropriate anchor residues.

Peptides that are too long can be trimmed by an ER resident aminopeptidase, ERAP1 <sup>[459, 460]</sup> before consideration by MHC-I molecules that are either in the peptide-loading complex or associating with another tapasin look-alike chaperone in the ER called TAPBPR. Like tapasin, TAPBPR also shapes the peptide repertoire on MHC-I molecules <sup>[461, 462]</sup>. Interestingly, binding of peptides longer than 8–9 residues, but not shorter ones, triggers a conformational change in ERAP1 that activates its hydrolysis



[463-465]. Through this mechanism, ERAP1 trims most peptides only down to 8–9 residues, corresponding to the size needed for optimal binding to MHC-I molecules.

In the end, the peptides that are available to be presented are the ones that have been cleaved to the right size and have somehow escaped further hydrolysis to a size that is too small to stably bind to MHC-I molecules. Peptides that are unable to bind an MHC-I molecule are ultimately translocated back into the cytosol for degradation [466]. Whether there are mechanisms that help to protect some of these peptides from destruction or release from the ER during the time before they bind MHC-I molecules, is not entirely clear.

Peptides form the third subunit of MHC-I molecules as they are required to stabilize these complexes when the MHC-I molecules are not bound to chaperones in the ER [467]. Also, they allow the MHC-I molecules to be released from the ER for transport to the cell surface for presentation to CD8<sup>+</sup> T-cells [468, 469].

This system of low off-rate peptide selection, exporting only peptide-loaded MHC-I complexes may help prevent healthy cells from easily replacing their bound endogenous peptides for exogenous antigenic peptides, an event that would lead to the presentation of peptides that does not reflect the status of a given cell and possible execution by CD8<sup>+</sup> T-cells (figure 24). However, the described mechanism is much more complex if it is taken in consideration the diversity of the MHC-I family. Indeed, the different loci expressed (in human, HLA-A, -B and -C) and the many polymorphic allelic forms behave differently with respect to expression, peptide binding and stability [470, 471]. Also, peptides derived from abnormal cells may be produced in greater amounts during high protein synthesis conditions (such as neoplastic transformation) and their degradation would quickly generate peptides after initial translation of the antigen and this may allow rapid detection of unhealthy cells [472, 473]. Furthermore, also the cleavage of these antigens can be done by different proteasomes. The development of the immune system coincided with the evolution of alternate forms of active site subunits of the proteasome, leading to the assembly of an immunoproteasome. A set of these subunits ( $\beta 1i$ ,  $\beta 2i$ ,  $\beta 5i$ ) [474] is constitutively expressed in dendritic cells and lymphocytes and can be induced in all other cells by interferons [475, 476]. When these subunits are expressed, they preferentially incorporate into newly assembling particles

to form immunoproteasomes, which generate a distinct set of peptides during protein degradation [477]. This shift from constitutive to immunoproteasome in cells often enhances the generation of peptides presented by MHC-I molecules, including many unique ones [478].

Generation of new peptides will be at the cost of other peptide fragments that are cleaved to make the new fragment [479]. Another set of alternate active site subunits of the proteasome ( $\beta 1i$ ,  $\beta 2i$ ,  $\beta 5t$ ) are expressed uniquely in cortical thymic epithelial cells (cTECs), where they incorporate into thymoproteasome particles [480]. Among the peptides generated by thymoproteasomes, certain are unique and these play a critical role in the auditioning of developing CD8<sup>+</sup> T-cells during positive selection and also in allowing many of these cells to avoid subsequent negative selection [478]. Proteasomes but also the cytosolic and ER associated peptidases are variable in content and numbers. From proteolytic activities only an estimated 0.02% of the peptides generated by the proteasome survive for presentation to the immune system [481]. Moreover, cells may also alter signaling in response to transformation of infection, which results in an altered phosphoproteosome [482], acetylome, glycome [483] or many other small post-translational modifications [484-486]. TAP allows peptides with these small modifications to enter in the ER and some of these can bind to MHC-I molecules for presentation to CD8<sup>+</sup> T-cells. These modified peptides are in fact not genetically-encoded but neo-epitopes to which the immune system may not be tolerant [487, 488], and consequently be able to eliminate cells that express them.

Through these various mechanisms, the repertoires of MHC-I presented peptides is expanded beyond the genetically-encoded sequences and add an additional option for the detection of abnormal cells, but also provides risks for auto-immune reactions.

### F1.5.2.2) MHC-CLASS-II and CD4<sup>+</sup> T-cells

MHC-II molecules are expressed on immune cells such as B-cells, monocytes, macrophages, DC and on epithelial cells following inflammatory signals.

MCH-II molecules on DCs present antigens to naïve CD4<sup>+</sup> T-cells to activate them, and later participate in the interaction of B-cells and macrophages with these

specific CD4<sup>+</sup> effector T-cells <sup>[489]</sup>. The structure of MHC-II resembles that of MHC-I and both are polymorphic proteins <sup>[489, 490]</sup>. However, the nature of the peptides presented by MHC-II is different and so does the underlying biology of MHC-II antigens presentation.

MHC-II presents peptide fragments that are larger than those that are presented by MHC-I, due the fact that the peptide-binding groove of MHC-II is open and so allows the peptides to extend out of their site (figure 22) <sup>[491]</sup>. These peptides are derived from extracellular proteins and from self-proteins that are degraded in the endosomal pathway <sup>[492]</sup>. During their assembly in the ER, MHC-II molecules associate with the invariant chain Ii that acts as a pseudo-peptide by filling the MHC-II peptide-binding groove and in addition targets MHC-II molecules into the endosomal pathway through its cytosolic dileucine motif <sup>[452, 493]</sup>. In a compartment named MIIC <sup>[494]</sup>, MHC-II molecules meet the antigen fragments that are generated by resident proteases. For the binding to occur, the invariant chain has to be degraded by the same mix of proteases, especially cathepsin L and S <sup>[489]</sup>. This leaves an invariant chain fragment (namely CLIP) inaccessible for proteases, that remains in the peptide-binding groove of MHC-II molecules <sup>[495]</sup>. Then, this CLIP fragment has to be exchanged for higher affinity peptides with the help of a MHC-II-like chaperone called DM (in human, HLA-DM) <sup>[496]</sup>. The structure of this chaperone in association with MHC-II reveals that DM locally opens the groove to release low-affinity peptides such as CLIP. After DM is released from MHC-II, it locks the proper peptide fragments in the MHC-II peptide-binding groove <sup>[497]</sup>. Finally, MHC-II molecules move to the plasma membrane either via vesicular transport or in the form of tubules <sup>[498-500]</sup>. Since the targeting information in the invariant chain has been removed after its degradation in MIIC, MHC-II molecules can stably reside on the plasma membrane (figure 24).

Similar to MHC-I molecules, there are also different MHC-II loci in most species (in humans three named HLA-DR, HLA-DQ and HLA-DP). Also, MHC-II molecules are polymorphic (>3,000 alleles known) <sup>[489]</sup> and their polymorphic amino-acids similarly cluster in and around the peptide-binding groove, shaping the peptide-binding pockets. As a consequence, different MHC-II alleles bind different peptides according to their different anchor residues <sup>[501]</sup>.

## Chapter I - Introduction

There are some variations involving the transport and surface half-life of MHC-II molecules [502]. For instance, the MHC-II transport from MIIC to the plasma membrane is not constitutive but controlled in DCs, monocytes and B-cells. The activation of DCs promotes MHC-II transport to the cell membrane and strongly enhances the half-life of these molecules [503, 504]. As a result, the activated DCs have high numbers (around 2 million per cell) of MHC-II molecules on the cell surface that continue to present antigens for long peptides. Another control mechanism is the fact that in human monocytes, IL-10 increases the expression of an ubiquitin ligase membrane associated RING-CH1 (MARCH-1) that ubiquitinates the tail of cells surface MHC-II molecules, which initiates their rapid internalization and destruction [504].

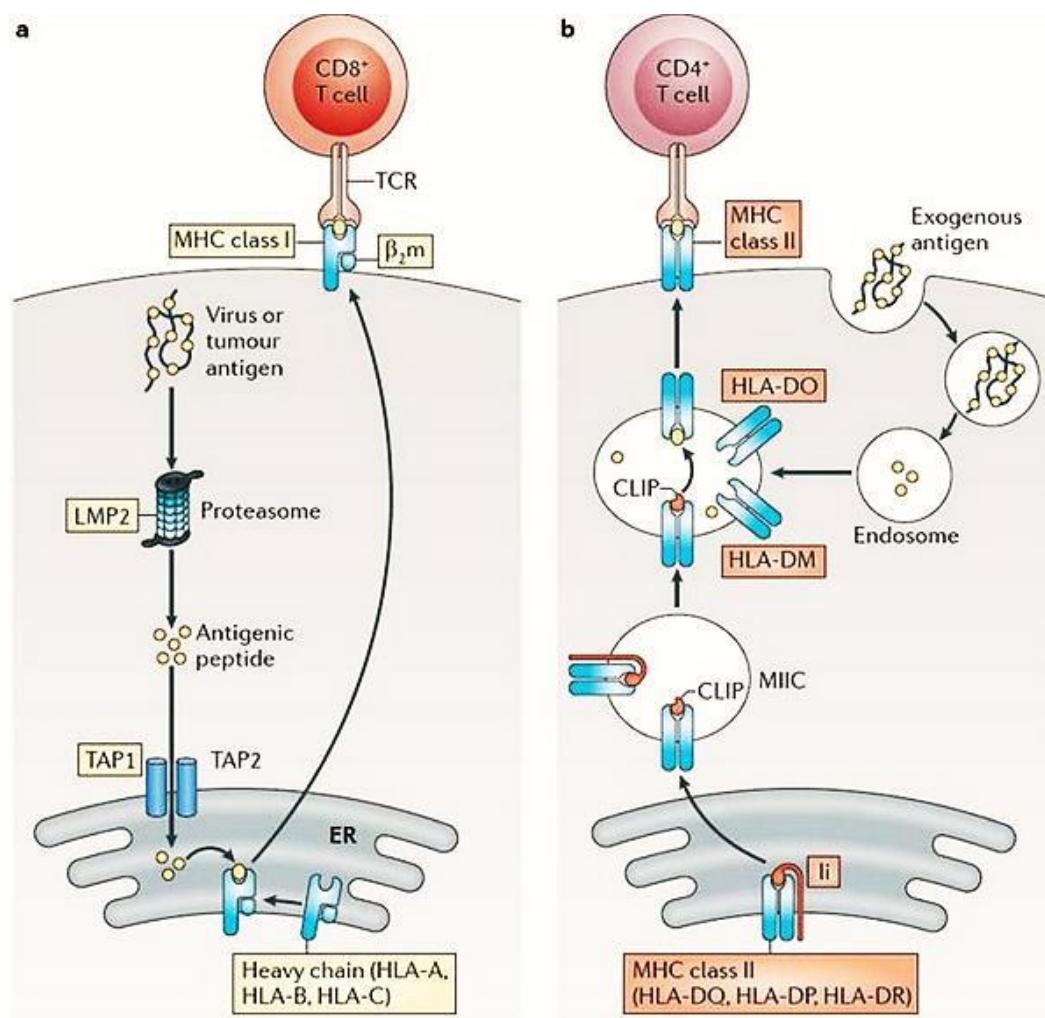


**Figure 24** - Schematic representation of the two models of antigen processing. The left panel shows the endogenous pathway, which presents the peptide products from a target cell to a CD8<sup>+</sup> T-cell in the context of MHC-I. The right panel represents the exogenous pathway, which present the peptide products from an APC to CD4<sup>+</sup> T-cell in the context for MHC-II. Figure source: nature.com

## F1.6) Cancer antigenic presentation

Cancer antigens are presented to T-cells either at tumor sites or in draining lymph nodes by DC. Cancer antigens, soluble and cell-bearing are transported to lymph nodes via lymphatic vessels. The soluble antigens are captured by the lymph-node-resident DCs, whilst tissue-resident DCs capture at tumor sites. DC population can either present antigens locally or migrate through lymphatic vessels to present in the lymph nodes [505]. DCs display the protein antigens in both MHC-I and -II context, allowing the selection of rare antigen-specific T-cells ( $CD8^+$ ,  $CD4^+$ , and NK T-cells). DCs are extremely efficient in their ability to induce antigen-specific T-cell responses, justifying the “professional APCs” designation [506]. Once in contact with the specific antigen,  $CD8^+$  T-cells differentiate into cytotoxic T-cells (CTLs) in lymphoid organs through co-stimulation signals (CD80, CD70, and 4-1BB, as well DC-derived cytokines such as IL-12, type I interferon, and IL-15) [507]. The priming of new T-cell repertoires during tumorigenesis may be critical for the success of therapeutic agents that aim to unleash antigen-specific CTL activities. Also, naïve  $CD4^+$  T-cells can give rise to helper cells with distinct cytokines profiles or to  $FoxP3^+$  Tregs that diminish the CTL activity and avoid autoimmune responses (figure 25) [508].

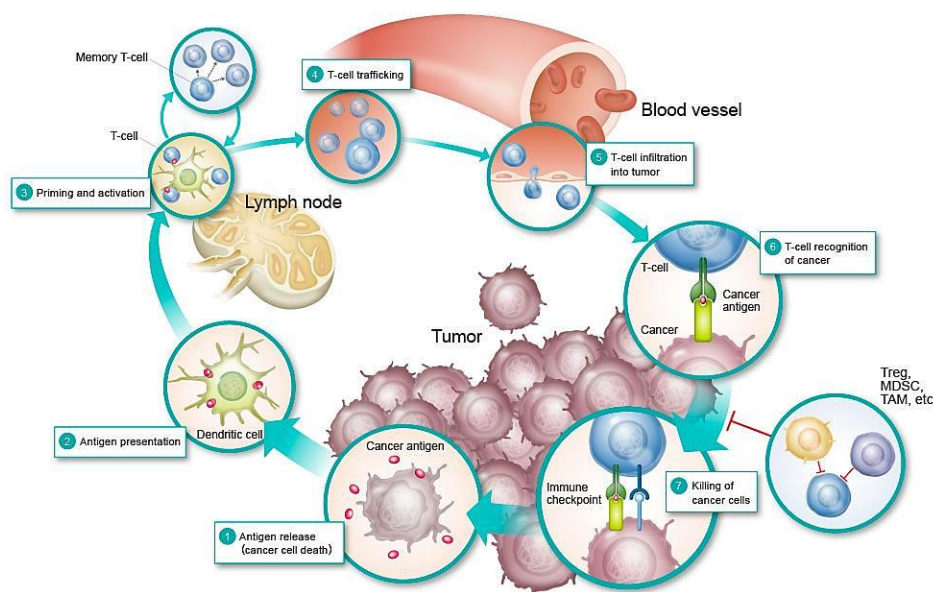


**Figure 25** - Anti-tumor immunity cycle starts with presentation of cancer antigens that are released during the natural process of cell turnover. The antigens are sensed and captured either by tissue-resident DCs or by DCs in draining lymph nodes. Dcs initiate an immune response by presenting those antigens in the

form of pMHC complexes, to naïve T-cells in the lymphoid tissues. Figure and legend adapted from Chen DS, *Immunity*, 2013 [509].

### **F1.6.1) The role of T-cells in tumor-suppressive mechanisms and tumor outgrowth**

It is known that the intrinsic tumor-suppressive mechanisms of healthy cells are active before the immune system becomes involved in tumor surveillance [510]. It is also known that the aberrant activation of oncogenes in normal cells is able to induce a p53-dependent state of stable cell-cycle arrest that is called cellular senescence. Cells that are in senescent stage exhibit a secretory phenotype called SASP (senescence-associated secretory phenotype) [511] that is characterized by the secretion of several cytokines that mediate the attraction of immune cells, which, ultimately lead to clearance of senescent cells in a process called senescence surveillance [512]. This process is restricted to the pre-malignant state and requires macrophages and CD4<sup>+</sup> T-cells. Surprisingly, it has been shown that CD8<sup>+</sup> T-cells are not required in this mechanism as long as the pre-malignant cells can be identified by SASP. However, in case the senescence state is no longer maintained due to the accumulation of additional genetic alterations, cells become finally malignant and lose SASP, thereby no longer recognized by senescence surveillance. It is at this point that CD8<sup>+</sup> T-cells start to play a crucial role in mediating tumor growth control [513], and this control mechanism minimizes the risk of CD8<sup>+</sup> T-cells to drive autoimmunity, since they are only induced in the last stage of tumor development. Additionally, the reactivation of cellular senescence in tumor by Th1-cytokines derived from CD4<sup>+</sup> T-cells has been identified as an additional mechanism of controlling tumor growth [514].

The tumor outgrowth is mainly controlled by CD4<sup>+</sup> and CD8<sup>+</sup> T-cells [405] during the three phases of cancer immunoeediting I have discussed in the previous subchapter. However, an incomplete elimination process promotes the generation of tumor cell variants with decreased immunogenicity, which leads to an expansion of a clinically manifest tumor. This low immunogenicity has considerable impact on the induction and expansion of T-cell immune responses that can determine accessibility to immunotherapies [394, 515-517].

Another important mechanism that affects tumor-suppressive T-cell responses is the induction of a dysfunctional state, anergy or even apoptosis of these cells [518]. Under certain conditions, suppression of CTLs can be established upon direct cell-to-cell contact with their corresponding target cell. Tumors are able to suppress T-cell once they migrate into tumor margin or infiltrate the TME. Highly dynamic cell signaling networks, cross-talks, and adaptations within components of the TME during tumor progression, often confer resistance to tumor immunity and negatively influence therapeutic regimens by numerous mechanisms, such as T-cell exhaustion [519]. In addition, the low immunogenicity is not always a result of immunoselection, but may also derive from a lack of suitable target structures for T-cell recognition. As tumor-directed CD4<sup>+</sup> and CD8<sup>+</sup> T-cells belong to the adaptive arm of the immune system, they can only develop in dependence on their corresponding antigens. This makes TSAs to be a very decisive molecular determinant for tumor growth control and the fundamental source of all T-cell responses against cancer.

### **F1.6.1.1) Tumor-specific antigens of CD8<sup>+</sup> and CD4<sup>+</sup> T-cells**

As mentioned before, MCH is a highly variable genomic region that encodes a large number of different loci comprising genes with many allelic variants [520]. Whereas all nucleated cells express MHC-I that binds endogenous peptides, MHC-II presents peptides of exogenous origin and is predominantly expressed by APCs [452]. However, under abnormal conditions, some cells also express MHC-II and tumor cells can fall in this category [521-524]. Moreover, MHC-II expression can also vary depending on the location of the tumor cells: expression levels can be high in primary tumor lesions but absent in distant metastases [525]. Abundant expression of MHC-II can also lead to potent tumor-specific CD4<sup>+</sup> T-cell responses that dampen cytotoxic CD8<sup>+</sup> T-cell responses in a TNF-related manner [526]. However, most tumor cells do not express MHC-II at all [527].

Several preclinical studies have investigated the role of CD4<sup>+</sup> T-cell responses in MHC-II positive tumors and determine that MHC-II expression on tumor cells crucially affects tumor immunity. In a murine model of pancreatic ductal adenocarcinoma (PDA), two different cell lines were transduced with the MHC-II

transactivator (CIITA) and injected into syngeneic mice <sup>[528]</sup>. CIITA-positive PDA tumors were rejected, long-lasting memory responses were established, and recruitment of T-cells to the tumor area was evident. In another study, it has been shown in humans that the magnitude of CD4<sup>+</sup> T-cells in microsatellite-unstable (MSI-H) colon carcinomas is significantly higher in HLA-II-negative tumors harboring mutations in HLA-II-regulatory genes such as RFX5, CIITA, and RFXAP <sup>[529]</sup>. This study suggests that lacking HLA-II expression on MSI-H colon carcinoma cells favored tumor progression in an environment of dense CD4<sup>+</sup> T-cell infiltration. Taken together, these studies indicate that expression of MHC-II on tumor cells and corresponding CD4<sup>+</sup> T-cell responses behave differently in a variety of tumor entities.

Besides the presence or absence of MHC-II on the tumor cell surface, it is worthy mention that the frequency of tumor-specific MHC-II epitopes is usually much higher than MHC-I epitopes <sup>[530, 531]</sup>, because of the stringent sequence requirements and the defined length of peptides binding MHC, which can explain the different effects CD4<sup>+</sup> T-cells play in the tumor immunogenicity.

MHC-I is essential for CTL-mediated tumor elimination and therefore frequently downregulated in tumors. However, a complete loss is a rare event, probably due to other counter regulations of the immune system such as recognition of MHC-I depleted cells by NK cells <sup>[532]</sup>. Usually, MHC-I binding peptides are tumor-derived peptides that can significantly shape the tumor immunity and their recognition by CD8<sup>+</sup> T-cell is very important for the development of new immunotherapeutic approaches. For that reason, *in silico* approaches of cancer neoantigen prediction have been extensively used based on genomic sequencing data to generate putative peptide:MHC binders, such as NetMHC <sup>[501, 533]</sup>. Using such prediction algorithms, the identification of high affinity neoepitopes that are able to elicit a strong CD8<sup>+</sup> T-cell response, has been very successful in several studies <sup>[394, 534-537]</sup>.

The binding affinities between antigenic peptides and MHC-I together with the binding affinity of peptide:MHC-I complex to the corresponding TCR are critical determinants for CD8<sup>+</sup> T-cell reactivity and ultimately for tumor rejection <sup>[538]</sup>. However, there are several caveats to focus on single high affinity binding epitopes.



First of all, neoepitope patterns are more or less unique among cancer patients with very little overlap. Immunotherapies such as DC-vaccination targeting a specific neoepitope are therefore at best limited to a small number of patients. Even if more common neoepitopes bind to MHC-I with high affinity it is likely that such epitopes have undergone high selection pressure during immunoediting. Consistently, potent CD8<sup>+</sup> T-cell responses against a particular epitope can also promote the occurrence of antigen-loss variants by epigenetic gene silencing of protein expression [539].

A study performed by Zhong et al. suggests that binding affinities above a certain threshold do not necessarily improve efficacy [540]. Additionally, neoepitope-directed CD8<sup>+</sup> T-cell responses of lower affinity have also been shown to play a role in immunotherapeutic applications when regarding polyvalent responses [541, 542]. These responses would probably be best suited to prevent the generation of escape variants by the tumor.

Taken together, occurrence of tumor-specific CD4<sup>+</sup> and CD8<sup>+</sup> T-cells in tumor tissue is regarded as a good prognostic factor [543, 544], but tumor immunogenicity is not a general characteristic of tumor development [545].

### **F1.6.2) The interplay of CD4<sup>+</sup> and CD8<sup>+</sup> T-cells in controlling tumor growth**

CD8<sup>+</sup> T-cell responses are usually considered of supreme importance for the control of tumor growth due to their potent cytotoxicity effect and by the observation that tumors can prevent elimination by downregulation of MHC-I expression [546, 547]. On the other hand, the role of CD4<sup>+</sup> T-cell in cancer immunity is much less understood. However, it has now become increasingly clear that tumor-specific CD4<sup>+</sup> T-cells display a complex biology and their roles are far beyond the mere task of providing helper signals to CD8<sup>+</sup> T-cells [548].

Naïve CD4<sup>+</sup> T-cells are able to differentiate into multiple effector subsets that can mediate various functions. The predominant helper cell subtypes are Th1 and Th2. Th1 commitment depends on local IL-12 secretion, while Th2 cells arise in dependence on IL-4 and in the absence of IL-12. Even though Th2 cells have been reported to exert antitumor effects [549, 550], Th1 cells are considered the most important helper cell type for cancer immunity, being involved in the killing of tumor cells by secretion of

## Chapter I - Introduction

---

cytokines that activate death receptors on the tumor cell surface and in the induction of epitope spreading <sup>[550, 551]</sup>. Th1 cells are also able to activate DC cytotoxic functions that eliminate tumor cells in an IFN- $\gamma$ -dependent manner and provide a source of tumor-associated antigens derived from the killed tumor cells <sup>[552]</sup>.

In cellular immunity, the mutual relationship between antigen-experienced CD4<sup>+</sup> and CD8<sup>+</sup> T-cells is required for both populations to trigger antitumor immunity. On other words, the crosstalk of these T lymphocytes is part of the cancer cycle <sup>[509, 553]</sup>. This cycle describes the sequence of events that leads to the generation of tumor-directed T-cells responses induced by DCs that have captured TSAs, migrate to the lymph nodes and presented their antigens to T-cells. Upon presentation, tumor-specific T-cells clonally expand and subsequently migrate to the TME. There, malignant cells are successfully eliminated by these tumor-antigen-experienced T-cells. Any interruption or defect within a single step of this crucial cycle can lead to failure of the whole process.

Pioneering *in vitro* studies that addressed CD4<sup>+</sup> and CD8<sup>+</sup> T-cells interplay emphasized the importance of both population for tumor immunity <sup>[554]</sup>. The use of TCR transgenic mice with specific TCRs for both MHC-I and -II specific peptides of malignant mesothelioma has shown a great enhanced T-cell response and tumor rejection when CD4<sup>+</sup> T-cells and a suboptimal number of CD8<sup>+</sup> lymphocytes were co-transferred; whereas adoptive transfer of CD8<sup>+</sup> T-cells alone was not sufficient to induce tumor remissions <sup>[555]</sup>. Consistently, in another study performed by Church and colleagues, it was demonstrated that tumor-specific CD4<sup>+</sup> T-cells help to maintain functionality of tumor-specific CD8<sup>+</sup> T-cells <sup>[556]</sup>. This group observed that CD8<sup>+</sup> T-cells expressed lower levels of PD-1 suggesting that the presence of CD4<sup>+</sup> T-cells partially inhibits CD8<sup>+</sup> T-cell exhaustion (T-cell exhaustion will be further addressed). It has also been shown that the presence of tumor-specific CD4<sup>+</sup> T-cells enhanced recruitment, proliferation, and effector function of CD8<sup>+</sup> T-cells by IFN- $\gamma$ -dependent manner and production of chemokines as IL-2 <sup>[557]</sup>. Another study has shown that the cooperation of CD4<sup>+</sup> T-cells enabled further improvement of the functionality of CD8<sup>+</sup> T-cells with high affinity TCRs <sup>[558]</sup>, but controversially, Wong and colleagues reported that CD4<sup>+</sup> T-cells render the TME permissive for infiltration by low avidity CD8<sup>+</sup> T-cells <sup>[559]</sup>. This

might be explained by the fact that CD4<sup>+</sup> T-cells are able to lower the threshold of tumor immune recognition for CD8<sup>+</sup> T-cell epitopes by inducing epitope spreading to antigens that do not trigger tumor remission without CD4<sup>+</sup> T-cells. In an interesting study performed by Surman and colleagues <sup>[560]</sup> it is suggested that lowering the threshold for immune recognition was only achieved by CD4<sup>+</sup> T-cells that enhanced the ability of APCs to trigger CTLs to a model antigen. The interaction between CD4<sup>+</sup> T-cells and APCs revealed CD40-CD40L crosstalk to trigger effective CTLs in a CCL5-dependent manner <sup>[561]</sup>. This group also showed that CCR5<sup>+</sup>-DCs were attracted to the tumor site and were then licensed by CD4<sup>+</sup> T-cells prior to the generation of CD8<sup>+</sup> T-cells. This CD4-mediated CD40-dependent licensing of DCs as a precondition for functional CTLs has also been shown *in vitro* for human cancers <sup>[562]</sup>. Another study demonstrating the importance of CD4<sup>+</sup> T-cells in a murine model showed that CD8<sup>+</sup> T-cell tolerance to the self-antigen MDM-2 could be overcome by adoptive transfer of TCR-modified CD4<sup>+</sup> T-cells <sup>[563]</sup>. TCR-engineered CD8<sup>+</sup> T-cells displayed an exhausted phenotype lacking cytotoxic function, and engineered CD4<sup>+</sup> T-cells allowed for T-cell help that facilitated a partial reversal of tolerance with the same MDM-2-specific TCR. Similar results of converting tolerized CD8<sup>+</sup> T-cells were observed in a rodent TCR transgenic model with weakly immunogenic tumors <sup>[564]</sup>. Finally, the group of Hans Schreiber <sup>[565]</sup> has demonstrated that co-expression of MHC-I and -II antigens is required for bystander elimination of cancer cells. However, an inoculation of a mixture of tumor cells with separated antigens for either MHC-I or II led, in sharp contrast to double MHC-I and II positive cancer cells, to progressive growth of mosaic tumors. The required expression of both MHC-I and -II antigens by the same cell clearly demonstrated a local cooperation of CD4<sup>+</sup> and CD8<sup>+</sup> T-cells during the effector phase. These results also highlight that the orchestration of immune responses by CD4<sup>+</sup> T-cells is not only limited to local tumors, is also able to differentiate between individual sub-clones within the tumor tissue that are class II-positive or -negative.

However, the majority of these experiments here described have used transgenic T-cells with high affinity model antigens that do not match with the nature of most human tumors. In humans, the individual mutanome gives rise to neoantigens of various affinities and is itself subject to a high plasticity of *de novo* generation and

elimination of neoantigens <sup>[566]</sup>. Theoretically, the generation of high affinity T-cell epitopes during advanced tumor stages by a subset of cells merely slows down the tumor progression due the fact that only a fraction of the whole tumor mass bearing the mutation would induce potent responses and be eliminated. However, neopitopes that arise in early stage of tumor development should be present in most, if not all, tumor cells. Nonetheless, the interplay of CD4<sup>+</sup> T-cells and CD8<sup>+</sup> T-cells is not always beneficial in terms of tumor control growth. Regulatory T-cells were initially defined as CD4<sup>+</sup> T-cells with high expression of CD25. The FoxP2 gene, a member of the Forkhead/winged-helix family of transcriptional regulators, was then discovered as a master regulator in developing Treg cells <sup>[567]</sup>. The forced expression of FoxP3 in naïve T-cells results in an immune suppressive function. CD4<sup>+</sup>CD25<sup>-</sup> naïve T-cells that are transfected with FoxP3 can convert to CD4<sup>+</sup>CD25<sup>+</sup> Treg-like cells that produce inhibitory cytokines and express typical Treg-cell molecules, such as CD25, CTLA-4 and TNF receptor-related protein (GITR) <sup>[568]</sup>. Thus, FoxP3 is a lineage-specific marker and a master regulatory gene in the generation, maintenance, and immune suppressive functions of Treg cells.

Regulatory T-cells are classified into natural/thymic and peripheral induced Treg cells based on where they develop <sup>[569]</sup>. FoxP3<sup>+</sup> natural Treg cells are generated in the thymus as the functionally mature T-cell subpopulation specialized for immune suppression (natural/thymic Treg cells). Some Treg cells are converted from conventional T-cells following *in vitro* TCR stimulation with TGFβ or retinoic acid (peripherally induced Treg cells) <sup>[570, 571]</sup>. Because human T-cells transiently express Foxp3 in conventional T-cells following TCR stimulation, FoxP3<sup>+</sup> T-cells in humans are heterogeneous in function and phenotype. CD25<sup>+</sup>CD4<sup>+</sup> Treg cells express low levels of CD127 (the α-chain of the IL-7 receptor); thus, CD4<sup>+</sup>CD25<sup>+</sup>CD127<sup>lo</sup> T cells are considered to be Treg cells with suppressive activity <sup>[572]</sup>. Regulatory T-cells suppress abnormal/excessive immune responses to self- and non-self-antigens to maintain immune homeostasis. In tumor immunity, Treg cells are involved in tumor development and progression by inhibiting antitumor immunity. There are several Treg cell immune suppressive mechanisms: inhibition of costimulatory signals by CD80 and CD86 expressed by dendritic cells through CTLA-4; IL-2 consumption by

high-affinity IL-2 receptor with high CD25 (IL-2 receptor  $\alpha$ -chain) expression; secretion of inhibitory cytokines, metabolic modulation of tryptophan and adenosine, and direct killing of effector T cells. Infiltration of Treg cells into the TME occurs in multiple murine and human tumors. These cells are chemoattracted to the TME by chemokine gradients such as CCR4-CCL17/22, CCR8-CCL1, CCR10-CCL28, and CXCR3-CCL9/10/11. Once in the TME, they are then activated and inhibit antitumor immune responses. A high infiltration by Treg cells is associated with poor survival in various types of cancer. Therefore, strategies to deplete Treg cells and control of Treg cell functions to increase antitumor immune responses are urgently required in the cancer immunotherapy field. Various molecules that are highly expressed by Treg cells, such as immune checkpoint molecules, chemokine receptors, and metabolites, have been targeted by antibodies or small molecules, but additional strategies are needed to fine-tune and optimize for augmenting antitumor effects restricted in the TME while avoiding systemic autoimmunity <sup>[573]</sup>.

CD4<sup>+</sup> T-cells and CD8<sup>+</sup> T-cells interplay is an intricate balance of positive and negative signals that even now-a-day is difficult to picture. However, CD4<sup>+</sup> and CD8<sup>+</sup> T-cells responses frequently fail to maintain proper function during tumor remission. Therapeutic intervention to sustain and promote T-cell immune reactions directed to the tumor is therefore a major aim in clinical oncology.

Figure 26 schematically represents a briefly overview of the immune response against cancer.

### **F1.7) CD8<sup>+</sup> T-cells role in tumor immunity: function and dysfunction**

It is well known that CD8<sup>+</sup> T-cells play a central role in cancer immunity due to their capacity to kill malignant cells upon recognition of specific antigenic peptides.

The anti-tumor function of CD8<sup>+</sup> T-cells is highly dependent on two crucial factors: 1) CD8<sup>+</sup> T-cell differentiation, and 2) infiltration of CD8<sup>+</sup> T-cells into the tumor site which occurs by trafficking or transporting CD8<sup>+</sup> T-cells into the TME <sup>[574]</sup>.

Researchers have linked elevated levels of cytotoxic CD8<sup>+</sup> T-cells in the TME with positive anti-tumor effects in several types of tumors, such as breast <sup>[575]</sup>, colorectal, glioblastoma <sup>[576]</sup>, and cervical cancers <sup>[577]</sup>. Thus one can positively link

## Chapter I - Introduction

elevated cytotoxic CD8<sup>+</sup> T cells in the TME with a good prognosis in various types of cancer.

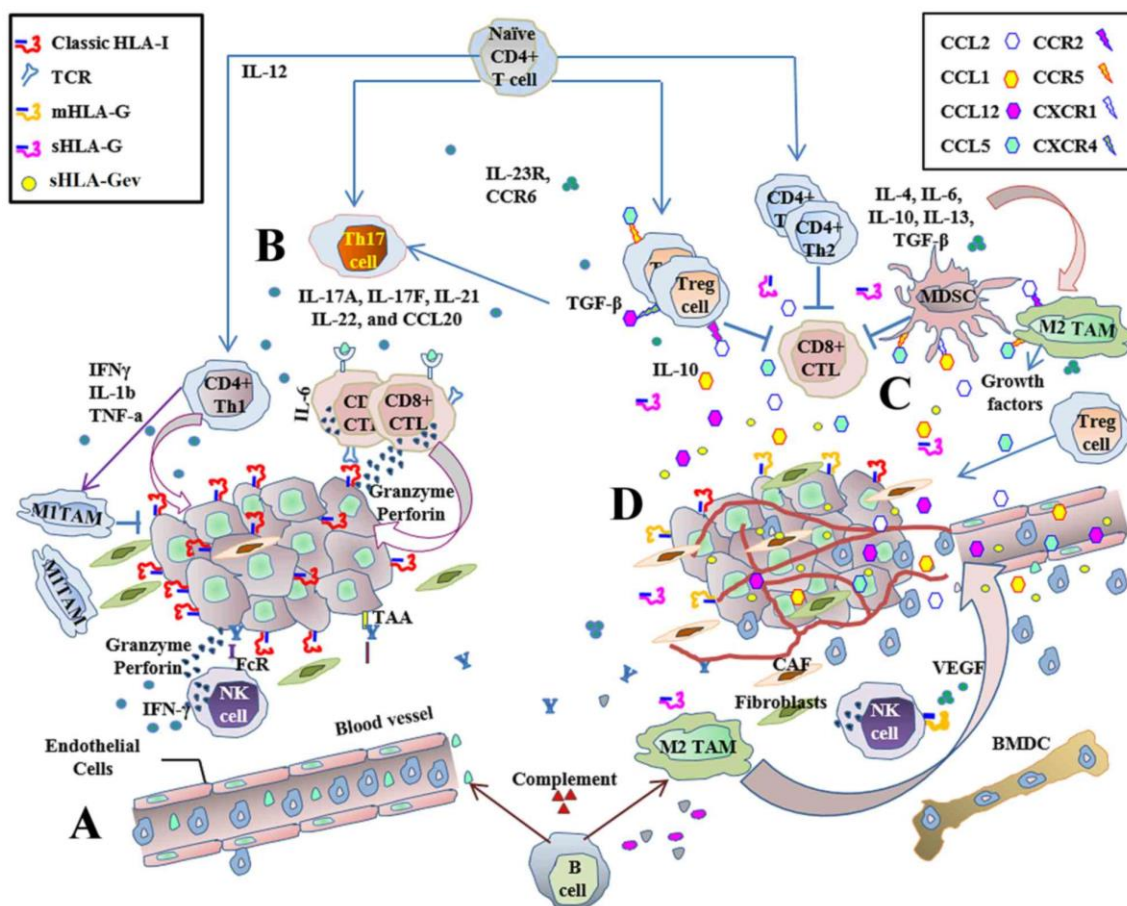


**Figure 26 - Immune response to cancer.** A) The main antitumor immune effectors are NK and CD8<sup>+</sup> T-cells, which are capable of responding directly against the tumor with cytotoxicity or by secreting cytokines. Inflammatory cells infiltrate the TME and exert antitumor immune responses; B) Cytotoxic CD8<sup>+</sup> T-cells are the main adaptive immune effectors. CD4<sup>+</sup> T-cells help to improve the antitumor response through the secretion of Th1 cytokines. CTLs-mediated antitumor responses are effective but ultimately insufficient to prevent disease progression; C) When inflammatory responses become chronic, regulatory cell populations generate a tolerant pro-tumor immune response via cytokine secretion and the production of growth factors. Tumor-promoting activity favors angiogenesis, invasion and metastasis, and is capable of suppressing adaptive immunity; D) Aberrant expression of classical and non-classical HLA-I contributes to the establishment of an immunosuppressive TME, promoting tumor growth by controlling immune stimulation and suppression signals. BMDC, bone marrow-derived cells; CAF, cancer-associated. Figure and legend adapted from Josefa A. Rodríguez, *Cancer letters*, 2017 [578].

The activation of CD8<sup>+</sup> T-cells is a 3-step process that follows T-cell priming and includes 1) the interaction between TCR and the antigenic peptide-MHC-I complex, 2) the delivery of a costimulatory or coinhibitory signals from DCs, and lastly 3) the stimulation from extracellular cytokines [579-582].

### F1.7.1) Effector CD8<sup>+</sup> T-cells

Naïve CD8<sup>+</sup> T-cells differentiate into Effector T-cells (T<sub>EFF</sub>) upon TCR engagement with antigen and costimulation by APCs. In antitumor responses, robust CD8<sup>+</sup> T-cells priming occurs primarily in tumor-draining lymph nodes, however, activation and differentiation of effector CD8<sup>+</sup> T-cells can also occur directly in the tumor by tissue-resident, cross-presenting APCs as well as tumor cells themselves [583-586].

T<sub>EFFs</sub> are identified based on the expression of surface markers such as CD25, CD69, CD95 and CD137 [587, 588], and when terminally differentiated are dependent on IL-2 and highly cytotoxic, expressing high levels of IFN- $\gamma$ , TNF $\alpha$ , perforin, and granzymes following activation [589, 590]. Tumor-antigen-specific T<sub>EFFs</sub> that efficiently invade primary tumor lesions are termed TILs and likely represent the majority of TIL population in well-controlled tumors, being responsible for positive clinical responses [591-594]. In acute immune responses, T<sub>EFFs</sub> are short-lived and undergo apoptosis upon elimination of the antigen [595]. However, tumor load or prime-boost cancer vaccines can chronically stimulate CD8<sup>+</sup> T-cells, leading to phenotypic changes and functional impairment.

The switch from a highly active CD8<sup>+</sup> TIL population to chronically stimulated CD8<sup>+</sup> T-cells favor the tumor over the host immune response and can ultimately lead to immune escape [596]. These dysfunctional CD8<sup>+</sup> T-cell fates that are induced by uncontrolled tumor load will be further discussed in this chapter.

### F1.7.2) Trafficking of Effector CD8<sup>+</sup> T-cells and Memory CD8<sup>+</sup> T-cells differentiation

In order for CD8<sup>+</sup> T-cells to be successfully trafficked into the tumor site, certain chemokine receptors on the T-cells should interact with the corresponding chemokines that are secreted by tumor cells and other cells in the TME [597].

Some molecules, such as CXCR3, are expressed on activated CD8<sup>+</sup> T-cells in breast and colorectal cancers and additionally in melanoma. CXCR3 attracts CXCL9, CXCL10, and CXCL11 chemokines which are highly secreted by tumor cells in a variety of solid tumors [598-601]. Conversely, certain tumors may express low levels of

CXCL9, CXCL10, and CXCL11 which in turn results in decreased infiltration of CD8<sup>+</sup> T cells into the TME.

Once in the microenvironment, in several types of acute infectious challenges, T<sub>EFFs</sub> undergo into a rapid, apoptosis-induced contractile phase following antigen clearance. After acute infection resolution, a small subset of antigen-experienced CD8<sup>+</sup> T-cells remains as memory CD8<sup>+</sup> T-cells [602-605]. However, this adaptive “memory” implies the absence of antigen, a condition that is not often met in an antitumor immune response. I will continue to refer to these cells as memory CD8<sup>+</sup> T-cells, even though their characterization might be more appropriate as “persistent” CD8<sup>+</sup> T-cells in the context of the antitumor immune response.

Memory CD8<sup>+</sup> T-cells can be broadly subdivided into two subsets, central memory (T<sub>CM</sub>) and effector memory (T<sub>EM</sub>), distinguished by the relative expression of two homing molecules: CD62L and CCR7 [606-608].

T<sub>EM</sub> have a phenotype more similar to that of effector cells, characterized by a loss of CCR7 expression and intermediate to negative CD62L expression. These cells exhibit rapid effector function, ready to differentiate into T<sub>EFF</sub> that secrete high amounts of IFN $\gamma$  and are highly cytotoxic [609]. In contrast, T<sub>CM</sub> are less differentiated, acquiring effector functions less rapidly, have increased proliferative potential and greater self-renewal capability and can produce high amounts of IL-2. Upon secondary antigen challenge, both subsets give rise to progeny that differentiate into T<sub>EFF</sub> [610-612]. Subsets of tumor-specific T<sub>EM</sub> and T<sub>CM</sub> have been identified in breast and colorectal cancer patients [613-615]. Similarly, studies in both mice and humans have demonstrated that memory CD8<sup>+</sup> T-cells develop *in vivo* following adoptive transfer, maintain effector capabilities, and mediate tumor regression [616, 617].

### **F1.7.3) Immunosuppressive tumor microenvironment and Exhausted CD8<sup>+</sup> T-cells**

Cells and factors of the TME have an immunosuppressive effect on tumor infiltrated CD8<sup>+</sup> T-cells. Immune cells express checkpoint proteins, which bind to corresponding ligands presented on tumor cells, leading to the activation of a



coinhibitory checkpoint pathways and inhibiting CD8<sup>+</sup> T-cell function and tumor cellular death [592]. From this inhibition a new cell type arises: Exhausted T-cells (T<sub>EX</sub>).

T<sub>EX</sub> are defined as a persistent T-cell population with low IL-2 and IFN- $\gamma$  production, reduced cytotoxic activity, reduced proliferative potential, and eventual deletion of the population of antigen-specific T cells. It is believed that chronic antigen exposure drives CD8<sup>+</sup> T-cells to an exhausted fate [579, 618, 619]. A number of inhibitory receptors are upregulated on T<sub>EX</sub>, indicating a role for these receptors in the attenuation of T cell function. In healthy individuals, inhibitory receptors on CD8<sup>+</sup> T cells promote self-tolerance and prevent autoimmunity by competing for costimulatory receptor ligands, attenuating positive TCR signaling, and/or inducing immunosuppressive genes.

In the context of an antitumor immune response, elevated expression of multiple inhibitory receptors promotes CD8<sup>+</sup> T-cell exhaustion and immune evasion.

Some of these receptors include PD-1, CTLA-4, TIM-3, LAG-3, CD160, BTLA, TIGIT, and 2B4 [618, 620, 621]. However, for the scope of this thesis, only PD-1/PD-L1 and CTLA-4 pathways will be mentioned.

### F1.7.4) Immune checkpoints

#### F1.7.4.1) CTLA-4 pathway

As it was mentioned before, T-cell activation is a process that requires more than one stimulatory signal. TCR binding to MHC provides specificity to T-cell activation; however, further costimulatory signals are required. Binding of B7-1 (CD80) or B7-2 (CD86) molecules on the APC with CD28 molecules on the T-cell leads to signaling within the T-cell. Sufficient levels of CD28:B7-1/2 binding lead to proliferation of T-cells, increased T-cell survival and differentiation through the production of growth cytokines such as IL-2, increased metabolism, and upregulation of cell survival genes.

CTLA-4 is a CD28 homolog with much higher binding affinity of the B7 molecules [622, 623]. However, differently from CD28, the binding of CTLA-4 to B7 molecules, does not provide a stimulatory signal. Consequently, this competitive

binding can prevent the co-stimulatory signal normally provided by CD28:B7 binding

[622, 624, 625].

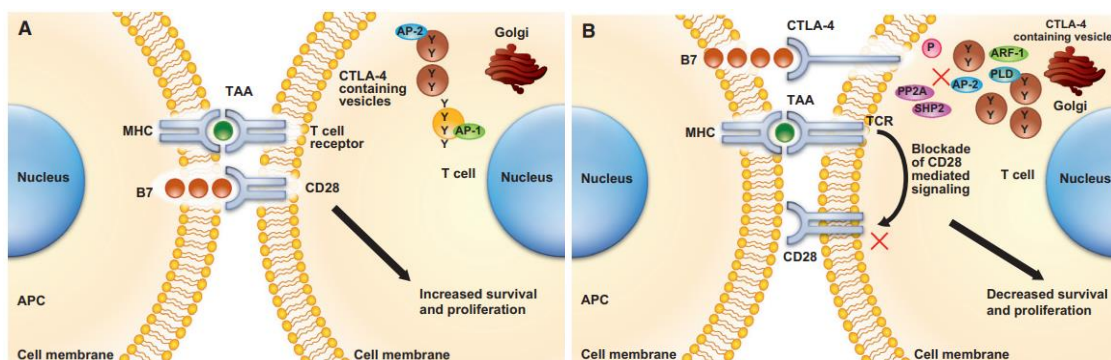


**Figure 27 – CTLA-4 pathway.** A) T-cell activation. T-cell priming in response to a specific antigenic epitope requires coordination of multiple signals. The initial signal is created when a full-length peptide is processed and presented on the surface of an APC. The resulting fragments, or tumor-associated antigens (TAA), are bound to MHC molecules present on the surface of the APC. This MHC/TAA complex then allows for detection and binding of the TAA by the TCR. A second costimulatory signal, however, is necessary to complete T-cell activation and expansion. The binding of CD28 on the T-cell with B7 on the APC creates this second signal, which leads to activation of the PI3K/AKT pathway, upregulation of the anti-apoptotic proteins BCL-2 and BCL-XL, and an increase in the nuclear transcription factor NF- $\kappa$ B. This collectively leads to increased cellular proliferation, cytokine production, and prolonged survival. Initially, regulatory proteins like CTLA-4 are primarily inactive and remain complexed with AP-2 within the intracellular compartment. B) Upregulation of CTLA-4 and maintenance of immune tolerance. TCR activation induces upregulation of CTLA-4 via a number of mechanisms. ARF-1 and PLD bind to enhance the exocytosis of CTLA-4-containing vesicles as they exit the Golgi apparatus. Phosphorylation of the cytoplasmic tail of CTLA-4 prevents binding of AP-2, which normally functions to promote receptor internalization, resulting in an increase in CTLA-4 surface expression. CTLA-4 is then capable of directly competing with CD28 for binding of B7. CTLA-4 may also exert a direct negative effect on CD28 signaling, mediated by the binding of the phosphatases PP2A and SHP-2. Additional regulatory molecules, including PD-1, are also important in limiting T-cell activation and may also inhibit TCR-mediated signaling via blockade of specific downstream effectors. The resultant decrease in pro-survival signaling serves to limit T-cell activation and expansion. Figure and legend adapted from Edward Cha, *Cancer Medicine*, 2013 [626].

The relative amount of CD28:B7 binding vs CTLA-4:B7 binding determines whether a T-cell will undergo into activation or anergy [627]. Moreover, there are evidences that suggest that CTLA-4 binding to B7 molecules may actually produce inhibitory signals that counteract the stimulatory signals from CD28:B7 and TCR:pMHC binding [628, 629]. The mechanisms proposed in the literature for such inhibition include the direct inhibition at the TCR immune synapse, inhibition of CD28 or its signaling pathway, or the increased mobility of T-cells leading to decrease ability to interact with DCs [624, 629, 630].

However, CTLA-4 expression itself is subject of regulation, particularly by localization within the cell. In resting naïve T-cells, CTLA-4 is located primarily in the intracellular compartment <sup>[631]</sup>. The stimulatory signals resulting from both TCR:pMHC and CD28:B7 binding induce the upregulation of CTLA-4 on the cell surface by exocytosis of CTLA-4 containing vesicles. This process operates in a graded feedback loop in which a stronger TCR:pMHC binding elicits more CTLA-4 translocation to the cell surface (negative signal, preventing the full activation of T-cells through inhibition of IL-2 production and cell cycle progression) and weaker TCR:pMHC binding results in less CTLA-4 is translocated to the cell surface (positive signal, which gives rise to full activation of the T-cells) <sup>[632]</sup>.

Moreover, CTLA-4 is also involved in other aspects of the immune control, as it is in the case of Tregs. Unlike effector T-cells, Tregs constitutively express CTLA-4. And this is thought to be important for their suppressive functions <sup>[633, 634]</sup>. One of the mechanisms whereby the Tregs are thought to control effector T-cells is the downregulation of B7 ligands on APCs, leading to reduced CD28 costimulation (figure 27) <sup>[635, 636]</sup>.

### **F1.7.4.2) PD-1/PD-L1 pathway**

PD-1 is a member of the B7/CD28 family of costimulatory receptors. It regulates T-cell activation through the binding to its ligands PD-L1 and PD-L2. As it is with CTLA-4, PD-1 binding inhibits T-cell proliferation, IFN- $\gamma$ , TNF- $\alpha$  and IL-2 production, reducing T-cell survival <sup>[637]</sup>. If a T-cell experiences coincident TCR and PD-1 binding, PD-1 generates signals that prevent phosphorylation of key TCR signaling, which ends in early exhausted T-cells that have experienced high levels of stimulation or reduced CD4<sup>+</sup> T-cell help <sup>[618]</sup>. This exhaustion state, that is known to occur during chronic infection and cancer, is characterized by T-cell dysfunction that ultimately results in suboptimal control of infections and tumors. Both CTLA-4 and PD-1 binding have similar negative effects on T-cell activity, however, the timing of downregulation, the responsible signaling mechanisms, and the anatomic location of immune inhibition by these two immune checkpoints are different.

Unlike CTLA-4 (which is confined to T-cells), PD-1 is broadly expressed on activated T-cell, B-cells, and myeloid cells [637, 638]. CTLA-4 functions during the priming phase of T-cell activation, whilst PD-1 functions during the effector phase, which is predominantly within peripheral tissues [637]. Also, the distribution of PD-1 ligands differs from the ligands of CTLA-4. The B7 ligands for CTLA-4 are expressed by professional APCs, but PD-L1 and PD-L2 are more widely expressed [625, 638-640]. PD-L1 is expressed on leukocytes, on non-hematopoietic cells, and in non-lymphoid tissues, and can be induced on parenchymal cells by INF- $\gamma$  or tumorigenic signaling pathways [641]. One mechanism of tumor evasion that has been extensively described in the literature recently is the fact that PD-L1 expression is also found in many different tumor types, which can be associated with an increased amount of tumor-infiltrating lymphocytes [642-644]. PD-L2 is primarily expressed on DCs and monocytes, but can be induced in a wide variety of other immune cells and non-immune cells, depending on the microenvironment [645]. Curiously, PD-1 has a higher binding affinity for PD-L2 than for PD-L1 and this difference may be responsible for differential contributions of these ligands to immune responses [646]. Since PD-1 ligands are expressed in peripheral tissues, PD-1:PD-L1 and PD-1:PD-L2 interactions are thought to maintain tolerance within locally infiltrated tissues [638].

Expectedly, the plurality of ligands for PD-1 leads to variation in biological effects, depending upon which ligand is bound. One model showed opposing roles of PD-L1 and PD-L2 signaling in activation of natural killer T cells [647]. Inhibition of the PD-L2 binding leads to enhanced T<sub>H</sub>2 activity [648], whereas PD-L1 binding to CD80 has been shown to inhibit T-cell responses [649]. These different biological effects are likely to contribute to differences in activity and toxicity between antibodies directed at PD-1 (preventing binding to both ligands) as opposed to those directed at PD-L1, and therefore have potential therapeutic implications. Although Tregs express PD-1 as well as CTLA-4, the function of PD-1 expression on these cells remains unclear. PD-L1 has shown to contribute to the conversion of naive CD4<sup>+</sup> T cells into Treg cells and to inhibit T-cell responses by promoting the induction and maintenance of Tregs [650]. Consistent with these findings, PD-1 blockade can reverse Treg-mediated suppression of effector T cells *in vitro* [651].

The binding of PD-1 with its ligands decreases the magnitude of the immune response in T cells that are already engaged in an effector T-cell response [618]. This results in a more restricted spectrum of T-cell activation compared with CTLA-4 blockade, which may explain the apparently lower incidence of immune-mediated adverse events (AEs) associated with PD-1 compared with a CTLA-4 blockade [652].

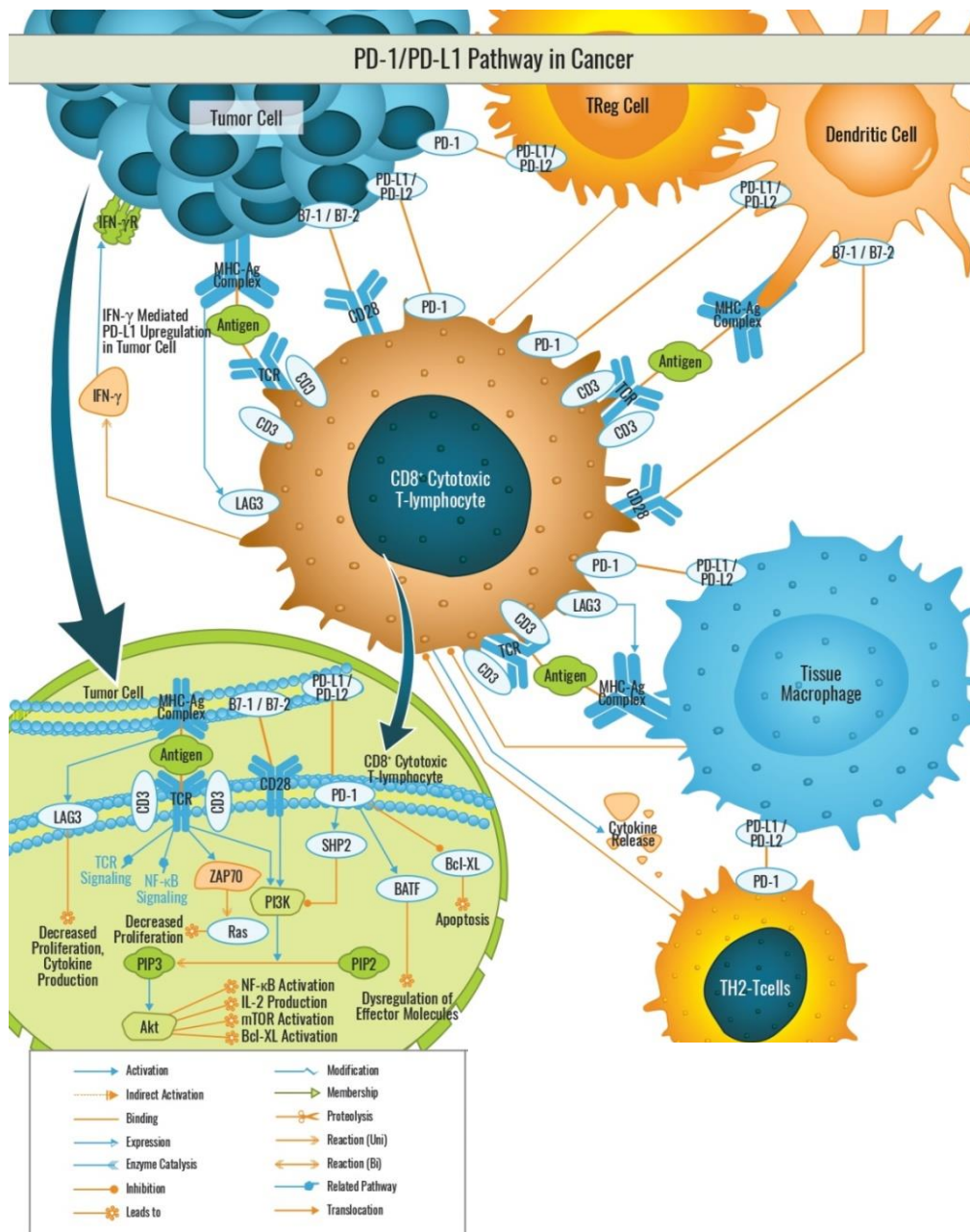


**Figure 28** - PD-1/PD-L1 pathways. PD-1 is a receptor of the CD28 family and it has two ligands: PD-L1 (also named B7-H1; CD274) and PD-L2 (B7-DC; CD273), that are both co-inhibitory. PD-1 is inducibly expressed by T cells and B cells after activation as well as natural killer T (NKT) cells, NK cells, activated monocytes and some subsets of DCs. PD-1 is upregulated after TCR or BCR engagement on naïve lymphocytes and persistent antigen stimulation maintains high PD-1 expression. The common  $\gamma$ -chain

cytokines (IL-2, IL-7, IL-15 and IL-21), TLRs and interferons also can potentiate PD-1 expression on T-cells. NFATc1 together with AP-1 and NF- $\kappa$ B constitute the most critical transcription factors activated upon antigen recognition by T-cells. PD-1 transduces an inhibitory signal when it is bound by its ligands in the presence of TCR or BCR activation. Phosphorylation of the ITSM motif of PD-1 leads to the recruitment of SH2-domain containing tyrosine phosphatase 2 (SHP-2), and possibly SHP-1, to the cytoplasmic domain of PD-1, which then down-regulates CD28-mediated PI3K activity and consequently, leads to less activation of Akt. PD-1 ligation also inhibits the phosphorylation of other signaling molecules including CD3, ZAP70 and PCK. The PD-1/PD-L1 interaction inhibits T lymphocyte proliferation, survival and effector functions (cytotoxicity, cytokine release), induces apoptosis of tumor-specific T-cells, promotes the differentiation of CD4<sup>+</sup> T-cells into Foxp3<sup>+</sup> Tregs, as well as the resistance of tumor cells to CTL attack. PD-L1 is expressed on resting T-cells, B-cells, DC, macrophage, vascular endothelial cells and pancreatic islet cells. PD-L2 expression is seen on macrophages and DCs alone and is far less prevalent than PD-L1 across tumor types. PD-L1 is also expressed in various types of cancers, especially in NSCLC, melanoma, renal cell carcinoma, gastric cancer, hepatocellular as well as cutaneous and various leukemias, multiple myeloma and so on. Figure and legend adapted from <https://www.abeomics.com>.

### F1.8) Cancer Immunotherapy

Over the last few years, cancer immunotherapy evolved into a very promising new frontier for fighting some types of cancers and has become an established pillar of cancer treatment, improving the prognosis of many patients with a broad variety of both hematological and solid malignancies. The two main drivers behind this success are the checkpoint inhibitors and the chimeric antigen receptor (CAR)-T-cells. However, other immunotherapeutic approaches have also been recognized with potent antitumor activity, such as cancer vaccines. Even though cancer immunotherapy has a broad spectrum of methods, we will only focus on checkpoint inhibitors and cancer vaccines.

#### F1.8.1) Immune checkpoint inhibitors

The development of immune checkpoint inhibitors was a revolutionary milestone in the field of immuno-oncology. As described before, tumor cells evade immunosurveillance and progress through different mechanisms, including activation of immune checkpoint pathways that suppress antitumor immune responses. Immune checkpoint inhibitors reinvigorate antitumor immune responses by interrupting coinhibitory signaling pathways and promoting immune-mediated elimination of tumor cells.

Ipilimumab, which targets CTLA-4, was the first approved immune checkpoint inhibitor for treating patients with advanced melanoma [625-629]. This antibody prevents

T-cell inhibition and promotes the activation and proliferation of effector T cells. Following the approval of ipilimumab, other antibodies that target immune checkpoints were examined. Currently, hundreds of phase I and II clinical trials and phase III/IV clinical trials are being carried out across the globe to evaluate the efficacy of multiple ICIs as monotherapy or in combination.

Pembrolizumab and nivolumab, both targeting PD-1, showed promising results in melanoma and NSCLC patients, with an objective response rate of 40–45% [634-638]. Additionally, urothelial bladder cancer patients treated with PD-1/PD-L1 inhibitors showed an increase in overall response rate, between 13 and 24% [653]. In triple-negative breast cancer patients, the response to PD-1 inhibitors was relatively moderate (19%) [620]. In contrast, in relapsed or refractory Hodgkin's lymphoma, nivolumab showed an objective response rate of 87% with 17% complete response [654]. Pembrolizumab and nivolumab are currently under phase IV clinical trials for treating various malignancies.

Despite the success of anti-CTLA-4 and anti-PD-1/PD-L1 therapies, only a fraction of patients benefit from checkpoint inhibitors. Antitumor immunity, regulated through complex factors in the TME, could create variable immune responses. The TME is segregated into three major types based on the infiltration of immune cells: 1) immune desert; 2) immune excluded and; 3) immune inflamed [650]. These phenotypes have their own mechanisms for preventing immune responses from eradicating tumor cells [650]. Immune deserts are characterized by the absence of T-cells in the TME and the lack of suitable T-cell priming or activation. The immune excluded phenotype exhibits the presence of multiple chemokines, vascular factors or mediators and stromal-based inhibition; however, accumulated T-cells are unable to infiltrate the TME. And finally, immune inflamed tumors demonstrate infiltration of multiple immune cell subtypes [650].

Accumulating evidences suggest that only a fraction of cancer patients benefit from checkpoint inhibitors, and severe immune-related adverse events are seen in some patients undergoing checkpoint inhibitors therapy [651]. These severe immune-related adverse events are due to the inhibition of immune checkpoints that reinforce the normal physiological barriers against autoimmunity, leading to various local and

systemic autoimmune responses. Therefore, the development of predictive biomarkers is critical for differentiating responders and non-responders to avoid any adverse effects.

Predictive biomarkers could determine the outcome of therapy in a patient before the initiation of a proposed therapy. These biomarkers should indicate whether a patient would benefit from a particular checkpoint monotherapy or if there is a need for combination therapy.

### F1.8.2) DNA and peptide vaccines

The discovery of TAA has led to the development of therapeutic cancer vaccines, based on either synthetic peptides, “naked” DNA, DC, or recombinant viruses, that attempt to elicit a stronger antitumor immune response, and particularly tumor antigen-specific CTL response [656-660].

DNA vaccines have generated widespread global interest for a variety of applications due to the fact that are able to generated both humoral and cellular response. The DNA plasmid used consisted in basic element elements: eukaryotic promoter, a gene of interest and a polyadenylation. However, the use of DNA vaccines has become controversial since many advert events have been described. There is the possibility that the patient develops auto-immunity overtime due to the fact that the antigen presentation is chronic and also, the DNA plasmid can integrated the host genome [629].

On the other hand, peptide vaccines have many advantages, including inexpensive, convenient acquisition of clinical-grade peptides, easy administration, higher specificity, potency due to their higher compatibility with targeted proteins, ability to penetrate the cell membrane and improved safety with few side effects [656-660]. Mechanisms underlying priming of anticancer immune responses by peptide-based vaccines, and enhance their efficacy, is dependent, at least in part, on the size of the peptides. While short peptides (8–11 aa) bind directly to HLA-I molecules and mount MHC-I-restricted antigen-specific CD8+ T-cell immunity [656-664], long synthetic peptides (25–50 aa) must be taken up, processed, and presented by APC to elicit a T-cell response. Vaccination with long peptides usually results in broader immunity than



with short peptides, along with induction of both cytotoxic CD8<sup>+</sup> T-cells and CD4<sup>+</sup> helper T-cells when conjugated with efficient adjuvants [656-660].

Recent technological advances in identifying mutation-derived tumor antigens have enabled the development of patient-specific therapeutic vaccines, including peptides, proteins, DC, tumor cells, and viral vectors, that target individual cancer mutations [655]. Over the past few years, examples of TSA-based personalized cancer immunotherapies have begun to emerge.

The antigen presentation prompt by DNA and peptide vaccines is similar to the cancer antigen presentation discussed in previous subchapters.

### G1) ALK immunogenicity

Some specific characteristics make ALK a potentially relevant tumor antigen. First, ALK is not expressed by normal somatic cells except in low amounts and in specific regions of the central nervous system. Therefore, activated anti-ALK-specific CTLs are unlikely to react against normal cells due to the low amount of ALK expression in normal physiologic conditions. Second, ALK is required for the transformation and maintenance of neoplastic cells and thus, the immune escape of tumor cells lacking ALK expression is unlikely, and finally, ALK-positive tumors, either point mutation, amplification or chromosomal translocation-driven, have in common the cytoplasmic portion of ALK, meaning that an ALK personalized immune approach could cover several types of tumors.

Many pieces of evidence support that ALK is spontaneously recognized as a tumor antigen in human patients, which represents a strong potential for the development of a clinical ALK-directed immunotherapy.

The first clinical observation providing the first hint that ALK generates an immune response in patients came from the fact that 60% of children and adolescents with ALK-positive ALCL present B-symptoms <sup>[655, 656]</sup>. Another very peculiar observation in ALK-driven ALCL is the fact that a small percentage of patients experience spontaneous remission of the lymphoma before treatment, being tumor free for weeks or even months, and ultimately relapse.

Likewise, very late relapses of ALK-positive ALCL, between five and up to 20 years from initial diagnosis, have also been observed, which could be explained by a weakening immunological control, especially because in some of these patients the relapse occurred during a time of immunosuppression such as pregnancy or autoimmune disease treatment <sup>[657]</sup>.

#### G1.1) Humoral Immune Response against ALK

Karen Pulford and colleagues have described in 2000 the humoral immune response against ALK in patients with ALCL, by using an indirect immunocytochemical approach. The authors detected circulating antibodies against

ALK in the plasma of eleven ALK<sup>+</sup> ALCL patients but not in healthy controls [400], and in different time points after diagnosis, the presence of anti-ALK antibodies was confirmed in subsequent analysis by the same group [658]. Another study, led by Mussolin, also described anti-ALK antibodies in the serum of 25 out of 28 pediatric ALK-driven ALCL patients [659]. Even though statistically not significant, in this study also was reported that patients with higher ALK antibody titers prior to and after therapy had a trend toward a reduced relapse risk.

These findings were confirmed by a pre-treatment analysis of anti-ALK antibodies in 95 ALK-positive pediatric ALCL patients enrolled in clinical studies with comparable short-pulse chemotherapies [660]. When categorizing patients' anti-ALK antibody titers into low ( $\leq 1/750$ ), intermediate ( $1/750$  to  $< 1/60,750$ ) and high ( $\geq 1/60,750$ ) titers, a significant correlation with clinical and biological risk factors was demonstrated. The anti-ALK antibody titers inversely correlated with the risk of relapse, which indicates that ALK antibody titer may be useful as a prognostic parameter for risk stratification or as a surrogate marker for the measurement of the strength of patients' ALK-specific immune response.

Not surprising, the presence of anti-ALK antibodies was also observed in ALCL patients harboring different ALK fusion partners, in ALK-positive DLBCL, and in ALK-driven NSCLC [661, 662]. More recently, the epitopes within the intracytoplasmic domain of ALK recognized by anti-ALK antibodies were described in nine ALK-driven NSCLC patients by our group [662]. However, ALK fusion proteins are expressed exclusively intracellularly, and therefore, ALK antibodies might not have a direct anti-tumor activity but rather represent a surrogate marker for the ALK-specific T-cell response. This observation is supported by the fact that ALK-DNA-based vaccination of B-cell-deficient BALB/c mice showed protection against tumor growth and a cytotoxic T-cell response after challenge with ALK-positive lymphoma cells [402].

### G1.2) Cellular Immune Response against ALK

ALK is spontaneously recognized as tumor antigen in ALK-driven tumors. Several studies have demonstrated the presence and persistence of not only an

antibody response to ALK but also an ALK-specific CD8<sup>+</sup> and CD4<sup>+</sup> T-cells in ALK-positive patients.

### G1.2.1) CD8<sup>+</sup> T-cell response against ALK

Cytotoxic T-cell response against ALK was first demonstrated by Passoni and colleagues. In a reverse immunological approach, two HLA-A\*02:01-binding ALK-derived predicted peptides were tested for their capacity to initiate a specific CTL immune response *in vivo* in HLA-A\*02:01 transgenic mice. Also, *in vitro*, functional ALK-specific CD8<sup>+</sup> HLA-A\*02-positive T-cell precursors were detected within the peripheral T-cell repertoire in healthy donors. The generated donor-derived ALK-specific CTLs induced an antigen-specific HLA-A\*02:01 restricted response with significant IFN- $\gamma$  release. These cells were able to effectively kill HLA-matched ALCL and neuroblastoma cell lines endogenously expressing ALK [401].

Another study performed in ALCL patients, has also reported CTL response against ALK. Ait-Tahar performed an ELISPOT analysis to detect ALK-specific CD8<sup>+</sup> T-cells activity against two ALK-derived HLA-A\*02:01-restricted peptides after short-time culture of mononuclear cells of seven ALK-positive ALCL patients, two ALK-negative ALCL patients, and six healthy controls, and a significant IFN- $\gamma$  response was detected in the patients with ALK-positive ALCL but not in the controls [658].

More interesting is the fact that the responsive patients were in clinical remission at the time of CD8<sup>+</sup> T-cell response analysis, indicating the presence of long-lived memory T-cells with possible protective immunity.

The natural frequency and functional phenotype of circulating ALK-specific CD8<sup>+</sup> T-cell precursors in the peripheral blood of healthy donors and ALK-positive ALCL patients was assessed by tetrameric MHC/peptide analysis, IFN- $\gamma$  ELISPOT assay, and *in vitro* lysis of ALK-positive target cells. Even though high frequencies of ALK-specific CD8<sup>+</sup> T-cells were found in both patients and health donors, the immunological phenotype of ALK-specific CD8<sup>+</sup> T-cells revealed effector and memory cells only in patients, while in healthy donors the phenotype was clearly naïve. Finally, the memory phenotype was evaluated by ALK-specific CD8<sup>+</sup> T-cells *in vitro* stimulation with peptide p280-89. Isolated patients ALK-specific CD8<sup>+</sup> T-cells released IFN- $\gamma$  and

GM-CSF and successfully killed the ALK-positive ALCL cell lines, demonstrating their functional activity <sup>[663]</sup>.

Another proof of the ALK-specific CD8<sup>+</sup> T-cells comes from our laboratory. Chiarle et al have examined the *in vivo* potential and clinical relevance of ALK DNA-based vaccine in ALK<sup>+</sup> ALCL-bearing mice. Mice were vaccinated and subsequently challenged with ALK<sup>+</sup> lymphoma cells. The immunization led to a long-lasting local and systemic ALK<sup>+</sup> lymphoma protection in ALK-vaccinated mice, and has elicited ALK-specific IFN- $\gamma$  responses and CD8<sup>+</sup> T-cell-mediated cytotoxicity. Also in the therapeutic setting, ALK-DNA-based vaccine has demonstrated its potential. ALK-driven ALCL-bearing mice were vaccinated and a significant protection against tumor growth was observed, even though only in limited tumor burden <sup>[402]</sup>.

In 2015, our group also has demonstrated that the same ALK DNA-based vaccine used in lymphoma, was able to elicit a strong ALK-specific CTL immune response that inhibited primary tumor growth in grafted and primary mouse models of ALK-positive NSCLC <sup>[397]</sup>.

Another group has also provided strong evidences. They examined NPM-ALK-specific CD8<sup>+</sup> T-cell responses in NPM-ALK-positive ALCL patients in remission after chemotherapy <sup>[664]</sup>. To circumvent HLA-preselection and to ensure endogenous NPM-ALK peptide processing, they used autologous dendritic cells as antigen presenting cells transfected *in vitro* with transcribed NPM-ALK mRNA to stimulate donor-derived CD8<sup>+</sup> T-cells. The stimulated CD8<sup>+</sup> T-cells were then analyzed in an IFN- $\gamma$  ELISPOT assay. Three out of five ALCL patients, but none of the healthy donors, had HLA-C-restricted CD8<sup>+</sup> T-cell responses to NPM-ALK. One patient exhibited a CD8<sup>+</sup> T-cell response after short-time stimulation, indicating a reactivation of persisting ALK-specific memory cells. Taken together, the *in vitro* and *in vivo* data reveal the existence of ALK-specific CD8<sup>+</sup> T-cell responses in ALK-driven tumors.

### G1.2.2) CD4<sup>+</sup> T-Cell Response against ALK

The presence of IgG antibodies and CD8<sup>+</sup> memory T-Cell against ALK in patients has suggested the involvement of CD4<sup>+</sup> T-cells in the ALK immunogenic landscape <sup>[665, 666]</sup>.

Another study performed by Ait-Tahar and colleagues has provided the first evidence of ALK-specific CD4<sup>+</sup> T-Cells in ALK-positive ALCL patients, by using an IFN- $\gamma$  ELISPOT assay, the authors showed that two *in silico* selected DRB1-restricted ALK-derived peptides were immunogenic in ALK-positive ALCL patients but not in ALK-negative ALCL patients or healthy controls. Mononuclear cells from all ALK-positive ALCL patients exhibited a significant IFN- $\gamma$  response to the peptides, which could be intensified following repeated stimulation. The CD4<sup>+</sup> T-cell-mediated and DRB1-restricted nature of the anti-ALK response was demonstrated by CD4<sup>+</sup> T-Cell depletion and the addition of anti-HLA-DR antibodies, which abrogated the IFN- $\gamma$  release to both peptides. Peptide-specific CD4<sup>+</sup> T-cell lines raised from one patient recognized and lysed ALK-positive tumor cell lines in an MHC-II restricted manner [667]. The majority of ALK-positive ALCL patients were in clinical remission and exhibited an antibody response to ALK at the time of analysis. Therefore, the presence of a significant CD4<sup>+</sup>-mediated IFN- $\gamma$  response suggests the existence of effector/memory CD4<sup>+</sup> Th1 subsets in ALK-positive ALCL patients.

These findings might play an important role in protective tumor immunity as well as in the maintenance of the CTL memory response and the production of antibodies against ALK.

### **G1.3) ALK immune escape: Therapeutic implications and immunotherapeutic approaches available**

Even though all the above described findings clearly suggested that ALK itself is able to generate a humoral and cellular immune response, during carcinogenesis ALK-driven cancer cells acquire complex immune escape mechanisms which overcome the immune system pressure, turning the tumors clinically apparent.

Some mechanisms have been already described; studies have shown that ALK-positive ALCL cell lines secrete TGF- $\beta$ , IL-10 and expression of FoxP3 [668]. In addition, it was shown that IL-10 decreases the expression of MHC-II molecules on monocytes or dendritic cells [669-671]. However, whether IL-10 secreted by ALK-positive tumor cells affects MHC class II expression in ALCL patients has not been shown directly.

Interestingly, *in vitro* studies have demonstrated that in ALCL tumor cells, ALK regulates PD-L1 overexpression through STAT3 [672]. Also in ALK<sup>+</sup> NSCLC, it was described that tumor cells upregulated PD-L1 expression by activating PI3K-AKT and MEK-ERK signaling pathways through ALK activation. Likewise, it has been demonstrated that patients with ALK-rearranged NSCLC have higher frequency of tumor PD-L1 overexpression when compared with EGFR or KRAS-mutated disease [673, 674]. This overexpression of PD-L1, regulated by ALK activation, could be one requisite to make these patients suitable for immune checkpoint inhibitors therapy.

In recent years, immune checkpoint inhibitors have shown dramatic changes in the treatment of advanced NSCLC, largely extending patients' survival [391, 393]. However, their efficacy varies among different immune and molecular profiles. Particularly, the clinical significance of immune checkpoint inhibitors for ALK-driven NSCLC has been controversial. Not only PD-L1 expression but also tumor-infiltrating lymphocytes correlate with the efficacy of immune checkpoint inhibitors and ALK-driven NSCLC display a tumor environment in which PD-L1 is expressed through ALK signaling and TILs are low. ALK-rearrangements are supposed to confer a survival advantage to the respective cells and it is usually isolated, explaining the low tumor mutation burden observed in these tumors [675], which leads to less inflamed tumor microenvironments with death of tumor-infiltrating CD8<sup>+</sup> T-cells. Also, ALK rearrangements are usually found in non-smokers. It is clearly established that tobacco exposure is associated with higher tumor mutation burdens and correlates with higher responsiveness to immune checkpoint blockade, while non-smokers will likely respond less due to the non-inflamed microenvironment [393, 676-678]. However, pre-clinical studies have shown that ALK targeted inhibition promoted T-cell interaction with monocytes and tumor cells, enhancing the T-cell proliferation as well as cytokine production, and increased T-cell tumor infiltration [679, 680] which has provided the biological rationale for combination strategies.

Therefore, several clinical trials are investigating the efficacy and safety of an ALK TKI combined with immunotherapy in ALK<sup>+</sup> NSCLC namely, anti-PD-1 (pembrolizumab, nivolumab) with ALK inhibition (crizotinib, ceritinib), anti-CTLA-4

(ipilimumab) with ALK inhibition (crizotinib) or anti-PD-L1 (durvalumab, avelumab, atezolizumab) with ALK inhibition (crizotinib, alectinib, lorlatinib, ensartinib).

### G1.3.1) Crizotinib + Nivolumab (NCT02574078)

The CheckMate 370 phase I/II study (ClinicalTrials.gov Identifier: NCT02574078) investigated activity and tolerability of crizotinib plus nivolumab in untreated *ALK*-rearranged advanced NSCLC patients. Recruitment was stopped due to the occurrence of severe hepatic toxicities in 5 of the first 13 patients, 2 of these 5 patients died <sup>[681]</sup>. Efficacy was reduced with the combination treatment as the ORR was only ~38% compared to ~65% reported with crizotinib monotherapy <sup>[305]</sup>.

### G1.3.2) Ceritinib + Nivolumab (NCT02393625)

Likewise, combination of ceritinib and nivolumab in a phase I study (ClinicalTrials.gov Identifier: NCT02393625) in a cohort of *ALK*-positive NSCLC patients was associated with high rate of adverse effects (83%), which led to protocol adjustments in order to address the observed hepatic toxicities <sup>[682]</sup>.

### G1.3.3) Lorlatinib + Avelumab (NCT02584634)

The JAVELIN Lung 101 (ClinicalTrials.gov Identifier: NCT02584634) is a phase Ib/II dose finding trial evaluating lorlatinib plus avelumab in 28 patients with advanced/metastatic *ALK*-negative/*WT* (*ALK*-) or *ALK*-rearranged NSCLC <sup>[683]</sup>.

This combination showed a manageable safety profile along with great antitumor activity (ORR: 46.4%, PR in 12 patients; complete response in 1 patient), in a heavily pre-treated population (on average two prior *ALK* inhibitors) with *ALK*-rearranged NSCLC, ensuring further development in clinical trials.

### G1.3.4) Alectinib + Atezolizumab (NCT02013219)

Finally, the phase Ib study (ClinicalTrials.gov Identifier: NCT02013219) is testing alectinib plus atezolizumab in treatment-naïve patients with *ALK*+ NSCLC regardless of PD-L1 status, including patients with untreated asymptomatic brain



metastases. Patients received alectinib 600 mg PO BID for 7 days (safety evaluation), followed by alectinib 600 mg PO BID with atezolizumab 1200 mg IV every 3 weeks (expansion stage) until progression or unacceptable toxicity. Patients showed a grade  $\geq 3$  treatment-related adverse effects rate of 52.4% [684], a rate higher than expected for alectinib alone [685]. However, no DLT and grade 4–5 AEs were reported. Early efficacy data at a median follow up of 13 months were promising with ORR of 85% and median progression-free survival of 21.7 months [684].

**Table 10** - Clinical trials of cancer immunotherapy-based combinations in ALK+ NSCLC.

Combination	ALK inhibitor	Checkpoint inhibitor	ClinicalTrials.gov Identifier	Phase	Time frame*	Recruitment status*	Ref
anti PD-1 + ALK inhibitor	Crizotinib	Pembrolizumab	NCT02511184	I	2015-2017	Terminated†	[686]
	Crizotinib	Nivolumab	NCT02574078	I/II	2015-2019	Completed	[681]
	Ceritinib	Nivolumab	NCT02393625	I	2015-2020	Recruiting	[682]
anti CTLA-4 + ALK inhibitor	Crizotinib	Nivolumab	NCT01998126	I	2013-2018	Completed	*
	Crizotinib	Ipilimumab	NCT01998126	I	2013-2018	Completed	*
anti PD-L1 + ALK inhibitor	Ensartinib	Durvalumab	NCT02898116	I/II	2017	Completed	*
	Lorlatinib	Avelumab	NCT02584634	II	2015-2020	Active	[683]
	Alectinib	Atezolizumab	NCT02013219	Ib	2014-2019	Active	[684]

\* as stated on the ClinicalTrials.gov webpage.

†Decision based on the low enrollment mainly due to high efficacy drugs available in 1st line ALK-positive NSCLC, not due to safety concerns

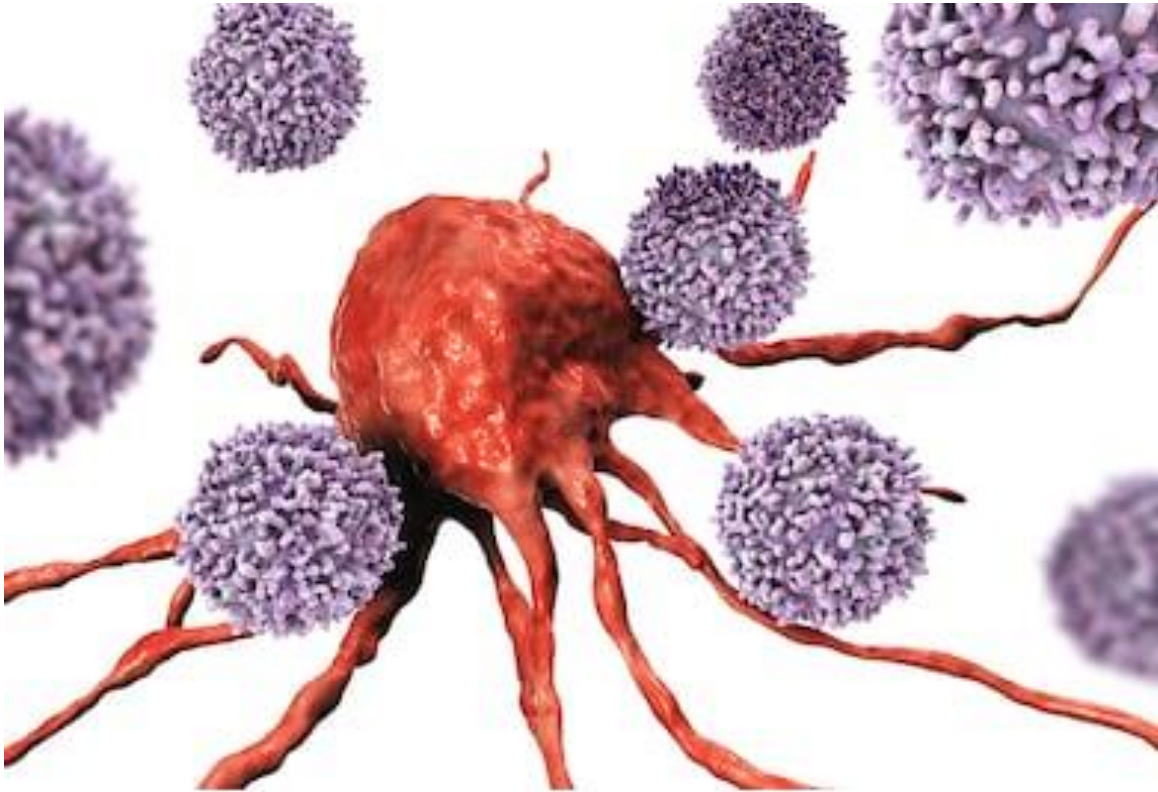
The poor results achieved with immune checkpoint inhibitors so far, have been largely disappointed. It is well known that ALK-driven tumor cells express PD-L1 through ALK signaling. However, it is also known that ALK-driven tumors present a low number of TILs, turning them into a cold tumor.

A possible alternative therapeutic approach would be increasing the number of ALK-specific-CD8<sup>+</sup> T-cells in the TME and sequentially treated with immune checkpoint inhibitors.



---

## Chapter II



*“Lack of focus is the major cause of failure;  
Those who do not set aims never reach goals (...)”*

*Reinaldo Ribeiro*

## **2. Hypothesis**



### 2. Hypothesis

#### Part I

In the Part I of my work, our hypothesis was that the combination of the novel and potent ALK inhibitor lorlatinib with anti-PD-1/PD-L1 antibodies and/or ALK-DNA-based vaccine could have synergistic effects in the treatment of ALK-rearranged NSCLC preclinical models.

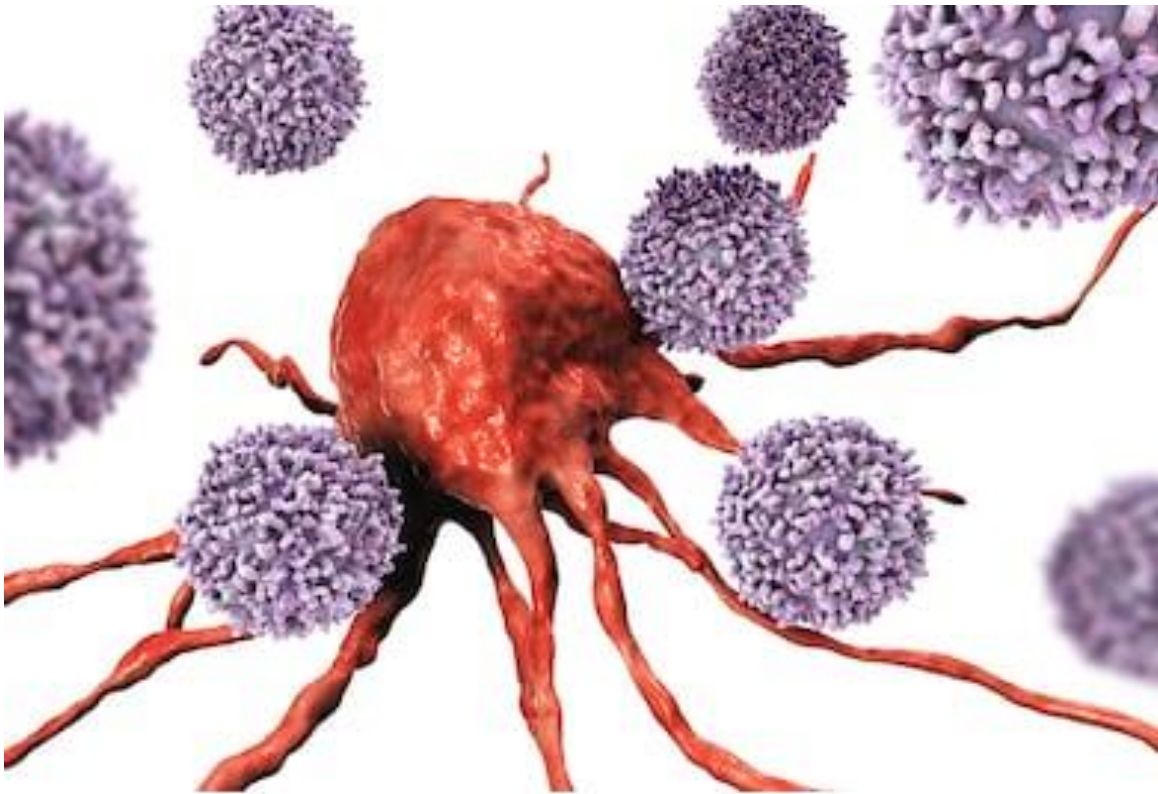
#### Part II

In the Part II of my work, our hypotheses were that human ALK (hALK) is immunogenic in BALB/c background due to the presence of ALK neoantigens, and the therapeutic immune response to a weak neoantigen (weak MHC-I binder) is only efficient when the spontaneous immune response is unleashed by a tumor vaccine.



---

## Chapter III



*“The repetition makes the technique,  
and the practice the perfection”*

Unknown

## **3. *Material and Methods***





### 3) Material and Methods

#### Part I

#### 3.1) Cell lines

Human ALK-rearranged NSCLC cell line (H3122 – variant 1; E13;A20) was obtained from the ATCC collection and passed for fewer than 6 months after receipt and resuscitation. This cell line was further internally tested for the presence of EML4-ALK rearrangement.

The murine cell lines (TECLA-1 and TECLA-2) were originated from Ad-EA mouse model [687]. Primary cultures were established using the Lung Dissociation Kit (Miltenyi Biotec, Germany) according to the manufacturer's instructions; first cultured in 3D culture and finally in 2D culture. These cell lines were further internally tested for the presence of murine EML4-ALK (mEML4-ALK) rearrangement, and passaged for less than 6 months after primary culture.

KP is cloned cell line established *in vitro* from lung carcinoma that arose spontaneously in a K-ras<sup>LA1</sup>/p53<sup>R172HΔg</sup> mouse [688].

HEK-293FT packaging cells were used for retrovirus and lentivirus production and obtained from ATCC collection.

All cell lines were maintained in DMEM (Lonza, Switzerland) with 10% fetal bovine serum (FBS) (Gibco, USA), 2% penicillin, streptomycin 5mg/mL (Gibco, USA), and 1% glutamine (Gibco, USA), and were grown at 37°C in humidified atmosphere with 5% CO<sub>2</sub>.

#### 3.2) Mice strains

Mice strains used in this study include Tg SP-C-EML4-ALK expressing the human EML4-ALK [397] (henceforth referred as Tg EML4-ALK mice), BALB/c TP53 KO (Charles River, Italy), WT BALB/c and C57BL/6 (Charles River, Italy) infected with Adenovirus carrying the CRISPR/Cas9 system as previously described [687].

Mice were handled and treated in accordance with the European Community guidelines.

### 3.3) ALK inhibitors

Crizotinib and lorlatinib were kindly provided by Pfizer (Pfizer, USA). Alectinib, ceritinib, and brigatinib were purchased from Selleckchem (Selleckchem, USA).

For *in vivo* treatment, crizotinib and lorlatinib were administrated via oral gavage either every day or twice a day. Crizotinib was administrated in a short-term treatment (15 days) and lorlatinib either in a short-term or long-term treatment. (Crizotinib: 100mg/Kg or 40mg/Kg; Lorlatinib 10mg/Kg or 2mg/Kg; vehicle solution: 0.5% Methylcellulose, 0.05% Tween-80).

### 3.4) Antibody dosage for *in vivo* treatment

For immune checkpoints blockade, anti-PD-1 (clone RMP1-14), anti-PD-L1 (clone 10F.9G2) and control anti-hamster polyclonal IgG were purchased from BioXcell (USA). Mice received either 200 $\mu$ g or 300 $\mu$ g of anti-hamster IgG, anti-PD-1 or anti-PD-L1 intraperitoneal (i.p.) injections every 3 days or every week for a total of 5 injections.

### 3.5) DNA vaccination

For DNA vaccination, 50 $\mu$ g of pDEST or pDEST-ALK plasmids were diluted in 20 $\mu$ L 0.9% NaCl with 6mg/mL polyglutamate and injected at day 1 and day 20 into both tibial muscles of anesthetized BALB/c mice. Electric pulses were applied through two electrodes placed on the skin; two square-wave 25-ms, 375V/cm pulses were generated by a T820 electroporator (BTX).

### 3.6) hEML4-ALK cloning; retrovirus and lentivirus production and mEML4-ALK KO

hEML4-ALK was amplified from a human NSCLC cell line and cloned into a retrovirus backbone vector (pBABE\_puro; Plasmid #1764; addgene) using restriction enzyme method according to the cloning information provided by the manufacture, as previously described <sup>[397]</sup>.

For retrovirus (or lentivirus) production,  $5 \times 10^6$  HEK-293FT cells were seeded in 10 cm dishes the day before transfection. Transfection was performed using Xfect transfection reagent kit (Takara, Japan), according to manufacturer's instructions.

For each dish, 15 $\mu$ g of pBABE\_puro plasmid containing the hEML4-ALK construct (pBABE\_puro\_hEML4-ALK) and 5 $\mu$ g of pCL-ECO Retrovirus Packaging Vector (mouse and rat cells only) (Novus Biologicals, USA) were re-suspended in 600 $\mu$ L of reaction buffer and 9 $\mu$ L of Xfect polymer was added in the mixture. Then, the mixture was incubated for 10 minutes at room temperature (RT) before being added to the culture dish containing the HEK-293FT cells. After 4 hours incubation at 37°C and 5% CO<sub>2</sub>, the medium was removed and replaced with 10mL of fresh DMEM-complete medium. After 36 hours, the medium was collected and centrifuged at 2,000g at 4°C for 5 min to pellet possible death cells in suspension. The supernatant was filtered through a 0.45 $\mu$ m low protein-binding membrane (VWR Sterile HV/PVDF).

The pBABE\_puro\_hEML4-ALK virus was used to transduce the human EML4-ALK into the murine TECLA-1 cell line.  $3 \times 10^6$  TECLA-1 cells were seeded 24 hours before infection in a 10 cm dish. In the day of infection, 10mL of non-concentrated virus was added to TECLA-1 dishes (around 65% confluency) for 24 hours, being replaced by fresh DMEM-complete medium. Posteriorly, TECLA-1 cell line was selected with puromycin (100ng/mL) for 4 days. hEML4-ALK expression was confirmed by western blot by using the human specific antibody ALK D5F3 (Cell Signaling Technology, USA) (henceforth, TECLA-1 transduced with hEML4-ALK is referred as hTECLA-1).

After transduction of the hEML4-ALK, the mouse EML4-ALK was knocked out by using CRISPR/Cas9 system. A sgRNA directly against the exon 20 of mALK was designed using deskgene tool ([www.deskgen.com](http://www.deskgen.com)) (ALK exon 20 sgRNA: ATCTGTCTGCAGTGTACCGT; PAM CGG; cut site: chr17 [+71,897,986 : -71,897,986]; GC% : 50; activity score: 57; off-target score: 93) and cloned into lentiCRISPRv2 puro (Plasmid #98290; addgene) using restriction enzyme method according to the cloning information provided by the manufacture. Lentivirus production, hTECLA-1 infection and puromycin selection were performed as described above. After selection, single cell clones were obtained through sequential dilutions. Once the single cell clones were

expanded, the mEML4-ALK KO was confirmed by western blot by using the mouse specific antibody ALK SP8 (Abcam, UK).

### 3.7) Histology and Immunohistochemistry

Hematoxylin and Eosin (H&E) and Immunohistochemistry staining's were performed in formalin-fixed paraffin-embedded subcutaneous tumors and lung sections of WT, Tg EML4-ALK, Ad-EA and graft mice models, and executed as previously described [397]. Immunohistochemistry stainings of the hALK protein were performed using the anti-ALK D5F3 rabbit monoclonal antibody (Cell Signaling Technology, USA).

### 3.7) Magnetic Resonance Imaging (MRI)

Anatomical T<sub>2</sub>-weighted coronal images were acquired with a respiratory-triggered multislice fast spin echo sequence (TR=4 s, TE=4.5 ms, RF=16, FOV=30 mm<sup>2</sup>, Matrix=256x256, slices=16-20, slice thickness=1mm, 2 averages, providing an in-plane spatial resolution of 117μm). Animals were anesthetized through i.p. injection containing a combination of Rompun® (5mg/Kg; Bayer, Germany) and Zoletil 100® (20mg/Kg; Laboratories Virbac, France); and breathing was monitored during acquisition of the MR images with a respiratory sensor (SA Instruments, Inc). Tumor volume and number of tumor masses were calculated by manual segmentation (slice by slice contouring) with ITK-SNAP software ([www.itksnap.org](http://www.itksnap.org)).

### 3.8) Cell Lysis and Immunoblotting

Cells (5x10<sup>5</sup>) were seeded in 6-well plates in DMEM complete medium. The following day, cells were treated either with crizotinib or lorlatinib using an increasing concentration scheme from 1nM to 1μM. After 6 hours of *in vitro* treatment, cells were collected and total cellular protein was extracted using GST-FISH buffer (10mM MgCl<sub>2</sub>, 150mM NaCl, 1% NP40, 2% Glycerol, 1mM EDTA, 25mM HEPES pH 7.5), mixed with 1 mM phenylmethylsulfonyl fluoride (PMSF), 10 mM NaF, 1 mM Na<sub>3</sub>VO<sub>4</sub>, and protease inhibitors (Roche, Germany).

Total cell lysates were cleared by centrifugation (12,000g) at 4°C in a microcentrifuge for 10 minutes and quantified using the Bio-Rad protein assay method (Bio-Rad, USA). Protein samples were normalized based on protein concentration, denatured by addition of Laemmli buffer and boiled for 5 minutes at 96°C. Fifty micrograms (50µg) of protein were run on sodium dodecyl sulfate–polyacrylamide gel electrophoresis (SDS-PAGE) under reducing conditions and transferred to nitrocellulose membrane (GE Healthcare, USA). Subsequently, membranes were incubated with specific antibodies, detected with peroxidase-conjugated secondary antibodies (GE Healthcare, USA) and enhanced using chemiluminescent reagent (Amersham). The following primary antibodies were used: anti-ALK D5F3 (Cell Signaling Technology, USA); anti-ALK SP8 16670 (Abcam, UK) and anti-Actin (Sigma, USA).

### 3.9) Cell viability assay

Cell viability was measured on TECLA-1 and TECLA-2 after incubation with ALK inhibitors, using CellTiter-Glo (Promega, USA) according to manufacturer's instruction. Briefly, cells were seeded into white walled 96-well plates (3wells/sample) in DMEM-complete medium and incubated using a ten-point dose titration scheme from 1nM to 1µM of ALK inhibitors (crizotinib, lorlatinib, alectinib, ceritinib, brigatinib). After 72h, CellTiter-Glo reagent was added to each well and luminescence output data were taken by GloMax-Multi Detection System (Promega, USA). The correspondent IC<sub>50</sub> value for each AKL inhibitor was calculated with GraphPad Prism 5 software (GraphPad Prism, USA).

### 3.10) Flow cytometry

PD-L1 cell surface expression in TECLA-1 and TECLA-2 cell lines was evaluated by flow cytometry. Briefly, cells were seeded in 6-well plates (5x10<sup>5</sup>cells) in DMEM-complete medium and the day after were detached using cold PBS 1X. Resuspended cells were washed in FACS buffer (PBS containing 1% of FBS and 2nM of EDTA) and consequently stained with anti-PD-L1-PE (clone 10F.9G2; BioLegend, USA) for 20 minutes at 4C in the dark. Next, cells were washed twice with FACS buffer and events

were acquired using a FACSCalibur flow cytometer (BS Bioscience, USA). Data analysis was performed with FlowJo™ software version 7 (FlowJo LLC, EUA).

### 3.11) Statistical Methods

Kaplan-Meier analyses for survival curves were performed with GraphPad Prism 5 software (USA). Paired data were compared with the Student's t-test and Mann-Whitney U test. *P* values of <0.05 were considered to be significant. Unless otherwise noted, data are presented as means ± SEM.

Tumor volume was calculated as follows:

$$\textit{Tumor volume} = (\textit{Length} * \textit{Width}^2)1/2$$

Quantification of volume changes compared with baseline tumor volume (change from baseline) was calculated as follow:

$$\textit{Change from baseline} = ((\textit{after value}-\textit{before value})/\textit{before value})100$$

### 3.12) Cell lines

The murine cell lines (TECLA-1 – originated before; and Edited-1) were maintained in DMEM (Lonza, Switzerland) with 10% fetal bovine serum (FBS), 2% penicillin, streptomycin 5mg/mL (Gibco, USA) and 1% glutamine (Gibco, USA) and were grown at 37°C in humidified atmosphere with 5% CO<sub>2</sub>.

### 3.13) Mice strain

The mice strain used in this study was Wild-Type (WT) BALB/c (Charles River) at 8 weeks of age. Mice were handled and treated in accordance with the Animal Resources Children's Hospital (ARCH) guidelines (Boston Children's Hospital – Harvard Medical School, Boston, US).

### 3.14) DNA vaccination/ Splenocytes isolation

As performed before, 50µg of pDEST (control) or pDEST-ALK plasmids were diluted in 20µL 0.9% NaCl with 6mg/mL polyglutamate and injected at day 1 and day 20 into both tibial muscles of anesthetized BALB/c mice. Electric pulses were applied through two electrodes placed on the skin; two square-wave 25-ms, 375V/cm pulses were generated by a T820 electroporator (BTX). Seven days after the second vaccination, mice from both groups (ALK unvaccinated [control] and ALK vaccinated) were sacrificed and the spleens were harvested. Operating in sterile conditions, spleens were mechanically disaggregated in RPMI medium until a single cell suspension was obtained.

### 3.15) Synthetic peptides

A set of 21 synthetic long peptides, each one 36 amino acids in length, covering the entire cytoplasmic portion of ALK encoded in pDEST-ALK DNA vaccine were purchased from Genscript (NJ, USA).

### 3.16) IFN- $\gamma$ ELISPOT assay

The interferon- $\gamma$  release enzyme-linked immune absorbent spot (ELISPOT) assay was performed using a commercial kit (Mouse IFN- $\gamma$  ELISPOT, Mabtech, Stockholm, Sweden) according to the manufacturer's instructions.

Briefly, the ELISPOT plate was prepared in sterile conditions and washed with sterile PBS (200 $\mu$ L/well) for 5 times. Consecutively, the plate was conditioned with fresh DMEM medium (200 $\mu$ L/well) contained 10% of the same fetal bovine serum used for the splenocytes suspension, and incubated for 30 minutes at room temperature. After incubation, the medium was discarded and  $2.5 \times 10^5$  splenocytes were plated in each well together with the appropriate stimuli. The plate was incubated over/night at 37°C in humidified conditions with 5% CO<sub>2</sub>.

The day after, cells were discarded and the plate was washed 5 times with PBS. Biotinylated detection anti-IFN- $\gamma$  mAb (1  $\mu$ g/ml) was added into the wells, followed by 2 hours of incubation at room temperature. Successively, and after another wash step, the plate was then incubated for a further 1 hour at room temperature with diluted streptavidin-ALP (1: 1000) in PBS-0.5% FCS at 100  $\mu$ l per well. Finally, the plate was washed again for 5 times with PBS, followed by the addition of substrate solution BCIP/NBT-plus. Tap water was used to stop the reaction when distinct spots appeared. All plates were evaluated by a computer-assisted ELISPOT reader (Cell Technology Inc., Jessup, MD, USA).

### 3.17) CD4<sup>+</sup> and CD8<sup>+</sup> T-cell discrimination

After identification of the responsive peptides, splenocytes from pDEST-ALK vaccinated mice were placed in U-botton 96 well plate (100 $\mu$ L per well in T-cell media [RPMI with 10% FBS, P/S, glutamine, HEPES]).

Splenocytes were then pulsed with the 5 identified long peptides with a final concentration of 10 $\mu$ g/mL overnight. The day after, cells were incubated for 4 hours at 37°C with brefeldin A (E-Biosciences, USA), (that works as a golgi-plug) which allowed cytokine accumulation within the cells. Sequentially, cells were washed with very cold FACS buffer and incubated with Fc block for 10 minutes at room temperature. After



membrane proteins staining (PE-CD4: clone RM4-4, Biolegend, USA; and FITC-CD8: clone G42-8, BD Pharmingen™, USA) was performed, cells were fixed with BD Cytotfix/Cytoperm fixation solution and incubated for 10 minutes at 4°C. Sequentially, intracellular staining was performed (APC-IFN- $\gamma$ : XMG1.2, Biolegend, USA). After two washes with BD Perm Wash solution, cells were ready to be acquired.

### 3.18) Algorithms

Peptide-MHC-I binding affinity analysis was performed *in silico* by using prediction algorithms. In this study, three different peptide-MHC-I binding prediction algorithms were used.

- 1) netMHCpan 4.0 (<http://www.cbs.dtu.dk/services/NetMHCpan/>);
- 2) ANN 4.0 ([http://tools.iedb.org/auto\\_bench/mhci/server/3](http://tools.iedb.org/auto_bench/mhci/server/3));
- 3) SMM ([http://www.cbs.dtu.dk/courses/27625.algo/exercises/ex\\_SMM/SMM.php](http://www.cbs.dtu.dk/courses/27625.algo/exercises/ex_SMM/SMM.php)).

### 3.19) H2-Dd-PGPGRVAKI Dextramer Staining / Flow cytometry

Allophycocyanin (APC)-conjugates H2-Dd-PGPGRVAKI Dextramer reagents were obtained from Immudex (Immudex, Denmark).

Briefly,  $1 \times 10^6$  cells (either from total splenocytes or total lung disaggregation) were stained with Zombie Aqua (Biolegend, USA) viability marker for 30 minutes at room temperature. After this initial step, cells were treated with 50nM of dasatinib at room temperature for 30 minutes and were not washed prior to staining with dextramer. Dextramer staining was performed together with mouse Fc block for 20 minutes at room temperature protected from light. Without prior washing, cells were finally stained with mouse FITC-CD8 conjugated (clone G42-8, BD Pharmingen™, USA) antibody for 10 minutes at 4°C. After washing step, cells were ready to be acquired. When referred, also PD-1 (clone RMP1-30; BV421-PD-1, BD Pharmingen™, USA) expression was evaluated together with dextramer staining, being added together with FITC-CD8.

H2-Dd MHC-I expression was measured on relapsed tumors after treatment. Tumor lungs were isolated and cultured *ex vivo* until an appropriate number of cells was reached. Briefly, cells seeded in DMEM complete medium were detached by using

cold PBS 1x. Resuspended cells were then stained with APC-anti-H-2Dd (clone 34-1-2S; ThermoFisher) for 20 minutes, washed and resuspended again in PBS.

All cells were acquired in a BD Celesta flow cytometer (BD Bioscience, USA) and analyzed by using the FlowJo software (FlowJo LCC, USA).

### 3.20) Peptide vaccination

PGPGRVAKI short peptide (ALK-peptide 7) was purchased from Genscript (NJ, USA). Peptide vaccine was prepared by mixing the PGPGRVAKI short ALK-peptide 7 (10 $\mu$ g) with CDN adjuvant (25 $\mu$ g), according to manufacturer instructions. Mice were vaccinated subcutaneously with 100 $\mu$ L of peptide vaccine.

### 3.21) Genomic editing of mouse ALK

We have designed one CRISPR shRNA targeting the region of interest. Then we designed crRNA that in 5' end contained a large template of the sequence we wanted to edit. The 3' end of the crRNA was complementary with a commercial available tracrRNA. To avoid CAS9 off-targets, we have used CAS9 protein that has a life-time of only 4 hours. TECLA-1 was electroporated with the mixture solution, collected, washed and plated in fresh medium. Once recovered from electroporation, we performed single cell clones by consecutive dilutions. Single cell clones were then analyzed through DNA and RNA sequencing.

(crRNA: TATGAAATTAAGAACCCTGTTTTCTTCCCAGGGATATTGCTGCTAGAACTGTCTGTTGACCTGCCAGGTCCGGGAAGAGTAGCAAAGATTGGAGACTTTGGGATGGCCCGAGATATCTA; shRNA: CTGCCAGGTCCGGGAAGAG).

### 3.22) DNA and RNA extraction/PCR reaction/ Sanger sequence

DNA and RNA samples were extracted as previously described [397]. PCR reactions were established to detect the genomic DNA or cDNA of peptide 7. PCR products were purified by using the QIAquick pCR Purification Kit (QIAGEN, USA) and the amplicons were sent to Sanger Sequencing through GeneScript Company (USA). Sanger sequencing were analyzed by SnapGen software (SnapGen, USA).

(Primers: gDNA, For: TATGAAGGCCAGGTGTCTGGAATGC; Rev: GACAAACTCCAGAACTTCCTGGTTGC)

(Primers: cDNA, For: ACCTCGACCATCATGACCGACT; Rev: ACACCTGGCCTTCATACACCTC)

### 3.23) Animal treatment and tumor transplantation

The designs of the animal studies and procedures were approved by ARCH committee.

1x10<sup>6</sup> Edited-1 and TECLA-1 cells were injected subcutaneously into WT BALB/c mice and treated with immune checkpoint inhibitors (anti-PD-1; anti-CTLA-4 or combo) at day 3, 6, and 9 through ip. injection. A cohort was kept for survival and the second cohort was sacrificed at day 15 after tumor transplantation to perform anti-ALK immune response evaluation.

1x10<sup>6</sup> Edited-1 cells were injected intravenously into WT BALB/c mice and vaccinated with 10ng of synthetic ALK-7-peptide at day 1, 14, and 21 to elicit an anti-ALK immune response. In parallel, mice were treated with lorlatinib (2mg/Kg daily) through oral gavage and/or immune checkpoint inhibitors (anti-PD-1; anti-CTLA-4 or combo) at day 3, 6, and 9 through ip. injection. For this particular experiment, mice were kept for survival.

### 3.24) ALK inhibitors

Crizotinib and lorlatinib were kindly provided by Pfizer (Pfizer, USA). Alectinib, ceritinib, and brigatinib were purchased from Selleckchem (Selleckchem, USA).

For *in vivo* treatment, lorlatinib was administrated via oral gavage daily for 15 days. (Lorlatinib 2mg/Kg; vehicle solution: 0.5% Methylcellulose, 0.05% Tween-80).

### 3.25) Antibody dosage for *in vivo* treatment

For immune checkpoints blockade, anti-PD-1 (clone RMP1-14) and anti-CLTLA-4 (clone 9D9) were purchased from BioXcell (BioXcell, USA). Mice received 200µg per injection (ip. injection) at day 3, 6, and 9 after tumor cells injections (either SC. or IV.).

### 3.26) Histology

Hematoxylin and Eosin (H&E) stainings were performed in formalin-fixed paraffin-embedded lung and brain sections of WT BALB/c mice and executed as previously described [397].

### 3.27) Cell lysis and Immunoblotting

TECLA-1 and Edited-1 cells ( $5 \times 10^5$ ) were seeded in 6-well plates in DMEM complete medium. The following day, cells were treated with lorlatinib using a ten-point dose titration scheme from 1nM to  $1 \mu\text{M}$ . After 6 hours of *in vitro* treatment, cells were collected and total cellular protein was extracted with GST-FISH buffer (10mM  $\text{MgCl}_2$ , 150mM NaCl, 1% NP40, 2% Glycerol, 1mM EDTA, 25mM HEPES pH 7.5), added with 1 mM phenylmethylsulfonyl fluoride (PMSF), 10 mM NaF, 1 mM  $\text{Na}_3\text{VO}_4$ , and protease inhibitors (Roche, Germany).

Total cell lysate were cleared by centrifugation (12,000g) at  $4^\circ \text{C}$  in a microcentrifuge for 10 minutes and quantified using the Bio-Rad protein assay method (Bio-Rad, USA). Protein samples were normalized based on protein concentration, denaturated by addition of Laemmli buffer and boiled for 5 minutes at  $96^\circ \text{C}$ . Fifty micrograms ( $50 \mu\text{g}$ ) of protein were run on sodium dodecyl sulfate–polyacrylamide gel electrophoresis (SDS-PAGE) under reducing conditions and transferred to nitrocellulose (GE Healthcare, USA). Membranes were incubated with specific antibodies, detected with peroxidase-conjugated secondary antibodies (GE Healthcare, USA) and enhanced using chemiluminescent reagent (Amersham). The following primary antibodies were used: anti-pALK (Y1586) (Cell Signaling Technology, USA); anti-ALK SP8 16670 (Abcam, UK) and anti-Actin (Sigma, USA).

### 3.28) Cell viability assay

Cell viability assay was performed in immortalized cell lines (TECLA-1 and Edited-1) by using CellTiter-Glo (Promega, USA) according to manufacturer's instruction. Briefly, cells were seeded into white walled 96-well plates (3wells/sample) in DMEM and incubated using a ten-point dose titration scheme from 1nM to  $1 \mu\text{M}$  of

ALK inhibitors (crizotinib, lorlatinib, alectinib, ceritinib, brigatinib). After 72h, CellTiter-Glo reagent was added to each well and luminescence output data were taken by GloMax-Multi Detection System (Promega, USA). The correspondent IC50 value for each ALK inhibitor was calculated with GraphPad Prism 5 software (GraphPad, USA).

### 3.29) *ex vivo* cell culture

Three (3) lung lobes were mechanically disaggregated until a single cell suspension was obtained. Consecutively, cells were plated in 6-well plates in DMEM complete medium. After 15 days in culture and at least 3 passages, cell lines were established.

### 3.30) Statistical Methods

Kaplan-Meier analyses for survival curves were performed with GraphPad Prism 5 software (GraphPad, USA). Paired data were compared with the Student's t-test and Mann-Whitney U test *P* values of <0.05 were considered to be significant. Unless otherwise noted, data are presented as means ± SEM.

Tumor volume was calculated as follows:

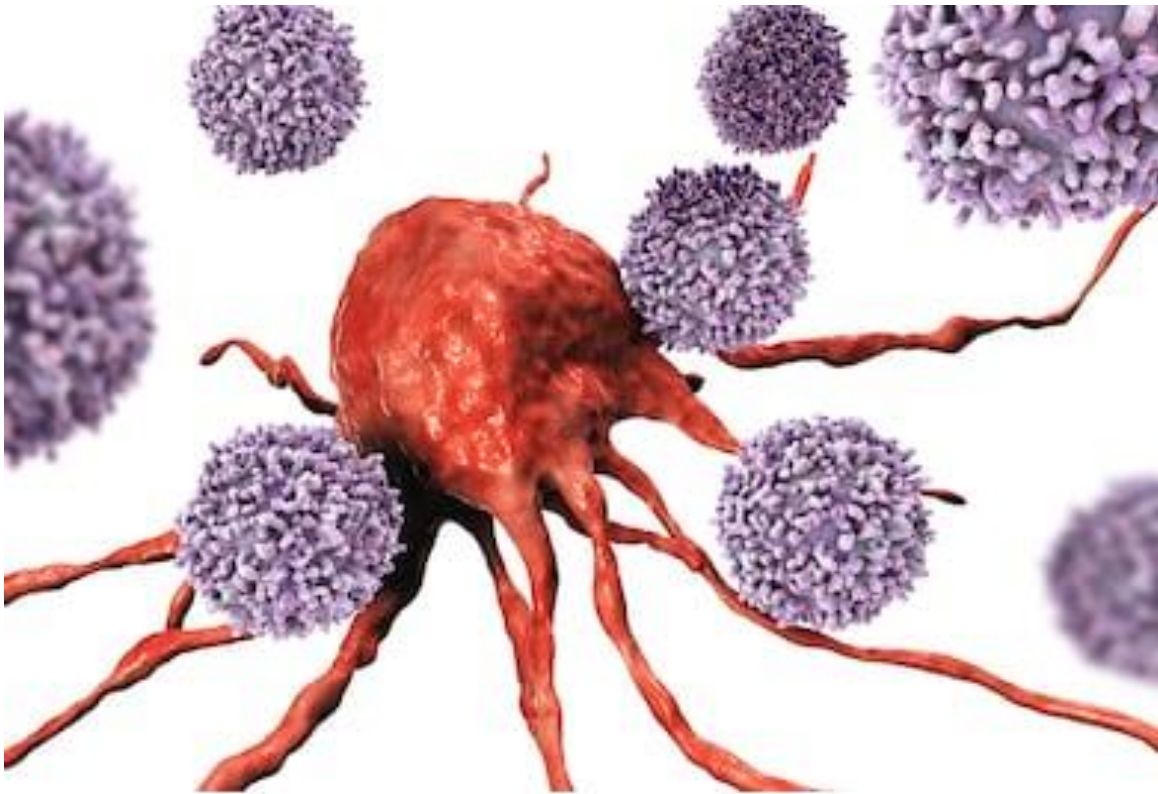
$$\textit{Tumor volume} = (\textit{Length} * \textit{Width}^2)1/2$$

Or through the software ImageJ (ImageJ, USA).



---

## Chapter IV



*“Your questions are false if you  
already know the answer”*

José Saramago,  
Noble prize in Literature 1998

## **4. Results**

## 4) Results

### Part I

#### 4.1) Combination of immune checkpoint blockade with high doses of ALK inhibitors does not provide significant advantage in Tg EML4-ALK-rearranged NSCLC mice

In our previous published work, we have proved the efficacy of the ALK-DNA-based vaccine against the cytoplasmic portion of the human ALK in eliciting a strong CD8<sup>+</sup> T-cell response that extends overall survival in BALB/c mice bearing ALK-driven tumors. With these results, we have proved the immunogenicity of human ALK in BALB/c background [397, 402]. The fact that ALK protein elicits indeed an immune response, we have hypothesized that the blockade of the immune checkpoint could have synergistic effects when combined with ALK inhibitors.

In order to test the efficacy of both crizotinib (first-generation ALK inhibitors) and lorlatinib (third-generation ALK inhibitors) administrated as single agents or in combination with immune checkpoint therapy (either anti-PD-1 or anti-PD-L1), we used a transgenic mouse model of ALK-driven lung tumors (Tg EML4-ALK mice), in which the human rearrangement EML4-ALK (variant 1, E13;A20) is expressed under the human lung-specific surfactant protein-C (SP-C) promoter as previously described [397].

Few weeks after birth, mice rapidly developed multifocal and well-differentiated ALK<sup>+</sup> tumors. In order to obtain a pairwise comparison of mice between all experimental groups (supplementary table of figure 29), mice were screened by MRI when 12-16 weeks old and stratified before treatment based on the total tumor volume.

Mice were treated with high doses of crizotinib (100mg/Kg once a day) or lorlatinib (10mg/Kg twice a day) and two different protocols of immune checkpoint therapy were performed: either anti-PD-1/PD-L1 antibodies were administrated simultaneously with the ALK inhibitor or after TKI treatment as describe in figure 29A. Immune checkpoint monotherapy was also performed as controls.



Follow-up MRIs were performed at the end of the TKI treatment and at 4 and 8 weeks after treatment suspension (figure 29 B1/B2). Also, after treatment, mice were monitored for survival. Change between baseline and post-treatment tumor volume was calculated in percentage.

Regarding the immune checkpoint monotherapy, tumors treated only with anti-PD-1 or anti-PD-L1 antibodies were stabilized at the end of the treatment (PD-1 vs Ctrl Rat IgG,  $*P<0.05$ ; PD-L1 vs Ctrl Rat IgG,  $*P<0.05$  according to Mann-Whitney U test) and showed a slower growth rate during follow-up when compared with tumor growth in control mice (figure 29 C/D/E). However, the monotherapy with anti-PD-L1 antibody was more efficient controlling tumor growth than anti-PD-1 antibody (PD-L1 vs Ctrl Rat IgG,  $*P<0.05$  at 4 and 8 weeks-follow-up according to Mann-Whitney U test) (figure 29 D/E).

Mice treated with high doses of TKIs (both crizotinib or lorlatinib) alone achieved almost complete tumor regression ( $\approx 100\%$ ) at the end of treatment followed by a longer lasting lung tumor regression when treated with high doses of lorlatinib (compare crizotinib alone from figure 29 F/G/H with lorlatinib alone from figure 29I/J/K).

The combination of anti-PD-1 or anti-PD-L1 antibodies administrated either at the same time with lorlatinib or at the end of lorlatinib treatment, did not show any statistically significant advantage over single TKI treatment neither at the end of the treatment nor at 4 or 8 weeks follow-up (figure 29 I/J/K). However, our data suggested that the anti-tumor effect of crizotinib may be potentiated by adding immunotherapy checkpoint inhibitors (figure 29 F/G/H) crizotinib vs crizotinib + PD-1 or + PD-L1), even though it is not statistically significant.

None of the treatment protocols showed any benefit in terms of overall survival as it is pictured in the Kaplan-Meier curves (figure 29 M/N/L).

#### **4.2) PD-1 blockade in combination with low doses of the potent ALK inhibitor lorlatinib delays tumor relapse in Ad-EA-derived NSCLC mouse models**

Next, we evaluated the synergistic effect between low, but still clinically relevant, doses of crizotinib and lorlatinib either with anti-PD-1 or anti-PD-L1 antibodies.

For this purpose, we used two mouse models: Tg EML4-ALK mice, as in previous experiments, and Adeno CRISPR/Cas9 Eml4-Alk infected mice (henceforth referred as Ad-EA mice) which models the most common EML4-ALK variant in human NSCLC (variant 1, E13; A20).

CRISPR/Cas9 system was used to induce concomitant double-strand DNA (dsDNA) breaks at intron 13 of Eml4 and intron 19 of Alk by using single-guide RNA molecules (sgRNA) targeting both Eml4 and Alk mouse loci, respectively. The adenovirus carrying this system was inoculated through intratracheal administration as previously described <sup>[687]</sup>. After inoculation, Eml4-Alk rearranged lung tumors typically developed within 2-3 months. We have infected two mouse strains (BALB/c and C57BL/6) in order to verify the efficacy of the combined treatment on different strains. After approximately 10 weeks from inoculation, mice were submitted to tumor volume evaluation by MRI as in previous experiments, and stratified before treatment, based on the total tumor volume.

Mice from both models (Tg EML4-ALK and Ad-EA mice) were treated according to the experimental protocol schematically described in figure 30A and figure 31A, respectively (supplementary table of figure 30 and supplementary table of figure 31). Follow-up MRIs were then performed at the end of treatment and at 4 and 8 weeks after treatment suspension (figure 30 B1/B2 and figure 31 B1/B2). As in previous experiments, mice were monitored for survival. Change between baseline and post-treatment tumor volume was calculated in percentage.

In this particular experiment, also the concentration of the administrated antibodies was reduced (200µg/mouse). However, at this concentration was not possible to reproduce the previous results obtained in Tg-EML4-ALK mice when treated with immune checkpoint inhibitors as monotherapy.

Anti-PD-1 monotherapy seems to have an effect that is maintained until 8 weeks follow-up (even though not statistically significant when compared with untreated control mice). But, anti-PD-L1 seems to have, paradoxically, the reverse

effect of what was observed before. This effect is not statistically significant, most likely because of the low number of mice (n=3).

However, and as expected, Tg-EML4-ALK treated with lower doses of crizotinib (40mg/Kg twice a day) had significant tumor regression compared to the control group (figure 30 F and 30 C, respectively), although less effective when compared to higher doses (100mg/Kg daily) (compare figure 29 F to figure 30 F). At 4 weeks follow-up (figure 30 G), mice treated with crizotinib in combination either with anti-PD-1 or anti-PD-L1 showed larger tumor volume when compared with mice treated with crizotinib alone, however, at 8 weeks follow-up this scenario is reversed (figure 30 H) suggesting that immune checkpoint inhibitors may have a delayed effect when combined with crizotinib. Nevertheless, mice treated with low doses of the more potent TKI lorlatinib, showed a complete tumor regression at the end of the treatment (figure 30 I). However, the addition of immune checkpoint inhibitors did not provide any advantage at any time point when combined with lorlatinib (figure 30 I/J/K). As it was observed in previous experiments, none combination has extended mice survival (figure 30 L/M/N).

In Ad-EA mouse model, we observed that lung tumors developed equally in both mouse strains (BALB/c and C57BL/6) and no significant differences between the two strains in the course of the experiments were observed (data not shown). Due to their similarity, both strains were grouped and analyzed as a whole group.

Immune checkpoint monotherapy (figure 31 C/D/E) did not show any efficacy on Ad-EA mice, which has suggested us that the Eml4-Alk-rearranged tumors induced by CRISPR/Cas9 were less immunogenic than lung tumors in Tg EML4-ALK mouse model (figure 30 I/J/K).

Surprisingly, Ad-EA mice did not respond to crizotinib treatment (40mg/Kg twice a day) as Tg EML4-ALK mice (compared figure 30 F/G/H with figure 31 F/G/H), reaching a medium change from baseline of 10% at the end of treatment (under treatment, tumors increased 10% of their initial volume). In this context, the combination of low doses of a weaker TKI with immune checkpoint blockade (both anti-PD-1 and anti-PD-L1) did not show any additional benefit neither at the end of treatment nor during follow-up (4 and 8 weeks after treatment suspension).

However, when treated with lorlatinib, Ad-EA mice showed almost complete tumor regression at the end of the treatment (figure 31 I) as it was observed in Tg EML4-ALK mouse model (figure 30 I).

The combination of lorlatinib+anti-PD-L1 did not provide synergistic effect in any analyzed time point (figure 31 I/J/K), suggesting that ALK<sup>+</sup> lung tumors driven by the mouse Eml4-Alk fusion protein might have either a lower expression of PD-L1 when compared to Tg mice tumors or express other inhibitory molecules (such as PD-L2).

Extraordinarily, at 4 weeks after treatment suspension, Ad-EA mice treated with lorlatinib+anti-PD-1 showed a significantly slower relapse rate when compared with tumors treated with lorlatinib alone (figure 31 J) (lorlatinib+anti-PD-1 vs lorlatinib, \* $P < 0.05$  at 4 weeks follow-up according to Mann-Whitney U test). However, the advantage provided by the addition of anti-PD-1 to lorlatinib was lost at 8 weeks follow-up (figure 31 K). Nevertheless, this transient effect was not reflected in the overall survival of the mice (figure 31 L/M/N).

### **4.3) Long-term treatment with the potent ALK inhibitor lorlatinib in combination with anti-PD-1 antibody slightly delays tumor relapse in Ad-EA mouse models**

Having the best result obtained so far in mind (lorlatinib+anti-PD-1), and assuming that Ad-EA mice are putatively curable, we next aimed the total tumor eradication and complete cure of the mice by administering lorlatinib in combination with anti-PD-1 in two (2) long-term treatment protocols (one [1] and two [2] months of TKI treatment).

After approximately 10 weeks from intratracheal Adenovirus infection, mice were submitted to tumor volume evaluation by MRI and divided into two (2) major cohorts (one [1] and two [2] months). Each cohort was then subdivided into three (3) different groups according to PD-1 administration protocol (supplementary table of figure 32). Mice were treated with lorlatinib alone or in combination with anti-PD-1 administered either every three (3) days up to fifteen (15) days or once a week up to

one (1) month, in a total of five (5) injections each, as it is represented schematically in figure 32 A. Follow-up MRIs were performed at the end of the treatment and at 4 and 8 weeks after treatment suspension, as in previous experiments. After treatment, mice were monitored for survival. Change between baseline and post-treatment tumor volume was calculated in percentage.

In both long-term treatment protocols (lorlatinib 1 month and lorlatinib 2 months), CRISPR/Cas9-induced tumors showed almost complete regression at the end of treatment when treated with lorlatinib alone, as it was expected (figure 32 B/E). Also, either at 4 or 8 weeks after treatment suspension, relapse rate was similar in both long-term protocols; not showing any evident advantage provided by the 2 months treatment protocol vs the 1 month long-term treatment (figure 32 C/D and F/G).

The addition of PD-1 antibody (both 15 day and 1 month) has no clear effect at the end of the treatment time point. However, both long-term lorlatinib treatments in combination with 1 month administration of anti-PD-1 showed a significantly slower relapse rate at 4 weeks follow-up when compared with tumor treated with lorlatinib alone at the same time point (lorlatinib [1 month] + anti-PD-1 [1 month] vs lorlatinib [1 month],  $*P < 0.05$  at 4 weeks follow-up according to Mann-Whitney U test; lorlatinib [2 month] + anti-PD-1 [1 month] vs lorlatinib [2 months],  $*P < 0.05$  at 4 weeks follow-up according to Mann-Whitney U test) (figure 32 C/F). Nonetheless, this advantage was lost at 8 weeks of follow-up, as it was observed previously in the short-time treatment (compared figure 31 J/K with figure 32 C/D and F/G). Remarkably, the 1 month anti-PD-1 protocol showed advantage in a long-term follow-up when compared with 15 days anti-PD-1 protocol (lorlatinib [1 month] + anti-PD-1 [1 month] vs lorlatinib [1 month] + anti-PD-1 [15 days],  $*P < 0.05$  at 8 weeks follow-up according to Mann-Whitney U test) (figure 32 D). This suggests that a longer immune checkpoint blockade could be beneficial in long-term follow-up. However, the same was not observed in the 2 month long-term treatment (figure 32 G), which raises the question regarding the negative effect of 2 months long-term lorlatinib treatment in the immune system.

Although with a longer TKI treatment protocol, total tumor eradication was not achieved and once suspended, mice from both cohorts treated with lorlatinib alone had similar overall survival, suggesting that prolonged TKI treatment is not beneficial in

terms of survival. However, even though not statistically significant, it can be appreciated the slight extension of overall survival in mice treated with the combination lorlatinib + anti-PD-1 (figure 32 H/I).

#### 4.4) Murine Alk rearrangement shows poor response to crizotinib but not to lorlatinib

The poor response to crizotinib, but not to lorlatinib, in CRISPR/Cas9-induced Eml4-Alk tumors, encouraged us to further investigate this feature.

As mentioned before, tumors in Tg EML4-ALK mice are driven by the human EML4-ALK fusion protein; in contrast, CRISPR/Cas9-induced Eml4-Alk tumors are promoted by an *in vivo* direct inversion of the endogenous mouse loci, and therefore are driven by the murine Eml4-Alk rearrangement. It is known that the domains' organization of ALK is conserved throughout evolution, and the highest conservation is found in the kinase domain. In fact, mouse and human ALK show 87% overall homology at the protein level, and within the kinase domain they differ only in four (4) amino acids; however, it should be noted that the human ALK contains an extra tyrosine residue, Tyr 1604, that is absent in the mouse Alk <sup>[108]</sup>.

These molecular differences can be pointed as a possible reason for the low response of Ad-EA mice to crizotinib when compared to Tg EML4-ALK mice.

In order to address this point, we generated two immortalized murine Eml4-Alk<sup>+</sup> lung adenocarcinoma cell lines (henceforth referred as TECLA-1 and TECLA-2) from primary tumors developed in BALB/c TP53 KO mice infected intratracheally with Adeno-CRISPR/Cas9 Eml4-Alk virus. The resulting two immortalized cell lines harbored the Eml4-Alk inversion, expressed the Eml4-Alk fusion protein and, when injected into syngeneic BALB/c mice, formed tumors that displayed histopathological and molecular features typically found in ALK-driven human NSCLC (figure 33 A/B/C).

The sensitivity of TECLA-1 cell line to crizotinib and lorlatinib was analyzed. TECLA-1 cells were treated *in vitro* either with crizotinib or lorlatinib using an increasing concentration scheme (from 0 to 1000nM) for 6 hours. Protein lysates were collected and Alk phosphorylation levels were analyzed. Even though Alk

dephosphorylation *in vitro* was observed at low concentrations of lorlatinib (1nM), indicating a good response to this potent ALK inhibitor as it was observed *in vivo* in Ad-mice, TECLA-1 cell line showed a poor response to crizotinib even at high concentrations (300nM), usually enough to completely dephosphorylate the human ALK (figure 33 D).

Next, we evaluated PD-L1 expression in TECLA-1 and TECLA-2 cell lines by flow cytometry. Not surprisingly, both cell lines presented positivity for PD-L1 in a small sub-population (figure 33 E).

Then, in order to understand whether the resistance observed was crizotinib-related, we have analyzed the immortalized cell line response to different ALK inhibitors. TECLA-1 cells were then treated with other FDA-approved ALK inhibitors, such as ceritinib, alectinib, brigatinib, as well as crizotinib and lorlatinib, using a ten-point dose titration scheme for 72 hours. Thereafter, cell viability was measured by CellTiter-Glo. As expected, TECLA-1 showed low sensitivity to crizotinib but also to ceritinib, being necessary a higher concentration of both inhibitors (close to 1 $\mu$ M) to achieve  $\geq 50\%$  of non-viable cells (figure 33 F). However, alectinib and brigatinib showed a better efficacy (when compared to crizotinib and ceritinib), showing  $\geq 50\%$  of non-viable cells at concentrations close to 100nM. Lorlatinib, as expected, was the most effective showing  $\geq 50\%$  of non-viable cells at concentrations lower than 1nM (figure 33 F).

To confirm these results,  $1 \times 10^6$  TECLA-1 cells were injected subcutaneously into syngeneic BALB/c mice. When tumors reached 5mm of diameter, mice were treated either with crizotinib (n=4) or lorlatinib (n=4) (100mg/Kg once a day and 10mg/Kg twice a day, respectively) or used as untreated controls (n=4). The treatment protocol was performed for 10 days and tumor volume was measured every 3 days since the injection time point until tumors have reached 15mm of diameter length (humane endpoint), according to figure 33 G. Mice treated with crizotinib presented modestly slower tumor growth when compared to controls; however, during the treatment course tumor shrinkage was never achieved (figure 33 H). Yet, mice treated with lorlatinib have shown complete tumor regression after 10 days of treatment (figure 33 I), confirming once more the high sensitivity to this ALK inhibitor. Follow-up after

treatment suspension was not performed, which has hindered the analysis of eventual relapse after lorlatinib administration.

Even though the poor response to crizotinib is an interesting feature that should be further investigated, these immortalized murine Alk<sup>+</sup> NSCLC cell lines represent an important tool for ALK-driven NSCLC studies by reducing considerably the *in vivo* experiments time course and providing an excellent model that mimics the human condition in a syngeneic and immunocompetent BALB/c background.

#### **4.5) Strong human ALK expression results in immunoediting in immunocompetent BALB/c mice**

With the new syngeneic mouse model, next we aimed, once again, the total tumor eradication and complete cure of the mice by using the combination of lorlatinib and anti-PD-1.

For that, we injected subcutaneously  $1 \times 10^6$  cells of TECLA-1 or TECLA-2 cell lines into syngeneic BALB/c mice in order to generate subcutaneous (sc) tumors. Tumors were measured every 3 days and when reached 5mm in diameter, mice were enrolled into a short-term (15 days) treatment as it is described in figure 34 A (supplementary table of figure 34). After treatment, mice were monitored for tumor relapse. Change between baseline and post-treatment tumor volume was calculated in percentage.

As expected, both cell lines developed sc. tumors in all injected mice.

Paradoxically, TECLA-1-derived tumors, when treated with PD-1 antibody alone, showed a higher tumor rate compared to untreated controls ( $*P < 0.05$  at the end of treatment according to Mann-Whitney U test) (figure 34 C). However, the same was not observed in TECLA-2-induced tumors in which PD-1 blockade showed a similar tumor growth rate when compared to untreated controls tumors (figure 34 E).

As it was predicted by the previous *in vitro* and *in vivo* experiments, mice bearing tumors induced either by TECLA-1 or TECLA-2 cell lines, and treated with lorlatinib (alone or in combination with anti-PD-1) reached complete tumor remission



at the end of the treatment protocol (change from baseline  $\approx$ -100% - no palpable tumor).

After the end of treatment, mice were kept in order to evaluate the relapse rate in each treatment arm. Tumors were measured every 3 days until tumor diameter reached 15 mm (humane endpoint).

Surprisingly, mice bearing TECLA-1-induced tumors enrolled in the TKI arms have reached the humane point in only 2 weeks after treatment suspension (figure 34 D) in contrast with mice bearing TECLA-2-induced tumors that presented a long lasting relapse rate (humane endpoint was reached 4 weeks after treatment suspension), suggesting that TECLA-2 has a slower tumor growth rate when compared to TECLA-1 (figure 34 F).

Although it can be appreciate in both cell lines the slight difference between lorlatinib alone and lorlatinib+anti-PD-1 in terms of relapse, statistically, the addition of PD-1 antibody to lorlatinib did not provide any advantage in controlling tumor regrowth (figure 34 D/F).

The poor response to PD-1 antibody led us to hypothesize that the endogenous mouse Eml4-Alk fusion protein expressed in TECLA-1 and TECLA-2-derived tumors could be less immunogenic than the human EML4-ALK rearrangement expressed since early development stage in Tg EML4-ALK mice. This hypothesis came not only due to the fact that TECLA-1 and TECLA-2-derived tumors express low levels of PD-L1 (data not shown), suggesting a weak interaction with the mouse immune system, but also because the human ALK protein can act as a neoepitope in BALB/c mice that were never challenge with human ALK peptides. Therefore, we decided to insert the hEML4-ALK gene into TECLA-1 cells in order to obtain a more immunogenic cell line in BALB/c <sup>[397, 402]</sup> (henceforth referred as hTECLA-1). Four (4) different viral infections were performed and after several passages in culture, hALK protein expression was evaluated by western blot (figure 34 I-left panel). The hTECLA-1 cell line with the highest expression of hALK was then injected subcutaneously into syngeneic BALB/c mice. Subcutaneous tumor growth was monitored every 3 days and mice were enrolled in the same treatment protocol as before (figure 34 A).

Remarkably, in this case, monotherapy with anti-PD-1 showed similar tumor growth as untreated controls (figure 34 G), different from what was observed in TECLA-1 “WT” (compare figure 34 G with figure 34 C). Also, in the presence of an hALK antigen, TECLA-1 cell line presented a long lasting relapse rate after treatment suspension, when compared with TECLA-1 expressing the endogenous mouse Eml4-Alk only, suggesting that the presence of a stronger antigen *per se* is enough to better control the tumor relapse (figure 34 H).

Finally, the combination of lorlatinib+anti-PD-1 provided a clear advantage in controlling tumor regrowth when compared with lorlatinib alone (lorlatinib vs lorlatinib+PD-1, at 3 and 4 weeks after treatment suspension,  $*P<0.05$ , according to Mann-Whitney U test), suggesting that PD-1 blockage could be beneficial to ALK<sup>+</sup> NSCLC when ALK is strongly expressed. However, the major aim was not achieved due to the fact that the complete eradication of the tumors did not occur.

To better understand the tumor escape mechanism, at the humane endpoint (15mm of diameter), tumors were collected and total proteins were extracted in order to measure the hALK expression by western blot. Surprisingly, we verified that all tumors treated with lorlatinib (alone or in combination with anti-PD-1) had lost hALK expression (figure 34 I-right panel), suggesting that tumors carrying overexpression of hALK are more susceptible to immunoediting. The immune pressure might have “forced” hTECLA-1-derived tumors to lose hALK expression. The regrowth of the tumors was supported by mEML4-ALK.

To confirm this hypothesis, and discard possible technical issues (it is known that some cell lines do not bear overexpression of certain proteins, losing them gradually after viral infection throughout *in vitro* passages), we injected subcutaneously hTECLA-1 into immunocompromised NSG and BALB/c mice simultaneously, according to figure 34 B. Tumor growth with or without immune pressure was evaluated and compared. Once reached the humane endpoint, mice were sacrificed, tumors were collected and total proteins extracted to assess the possible loss of hALK after *in vivo* passage in both immune backgrounds (NSG and BALB/c mice).

Not surprisingly, hTECLA-1 has grown faster in NSG mice than BALB/c mice (figure 34 J). Nevertheless, when analyzed regarding hALK protein content, we verified that tumors grown in immunocompromised NSG mice have kept the hEML4-ALK expression, discarding any technical issue. The same was not observed in immunocompetent BALB/c mice. hTECLA-1-induced tumors grown in a immunocompetent environment have practically lost completely hALK expression, suggesting a strong immunoediting provided by the presence of a strong antigen (figure 34 K).

#### **4.6) Triple combination of lorlatinib, PD-1 blockade and ALK-DNA-based vaccine significantly delays tumor relapse and completely abrogates the development of metastasis in distant organs in graft models.**

The previous experiments have shown us that the regrown hTECLA-1-induced tumors had lost the hEML4-ALK protein expression in an immunocompetent context, and their regrowth was supported by the endogenous mouse Eml4-Alk expression.

Having confirmed the strong immunogenicity of human ALK protein in BALB/c background, we next hypothesized that PD-1 blockade would not be beneficial to the spontaneous immune response generated by the tumor itself and that would rather add an advantage when the CD8<sup>+</sup> T-cell response is strongly elicited by an ALK-DNA-based vaccine.

Based on our previous published work <sup>[397, 402]</sup>, we decided to evaluate the synergistic effect a novel triple combination: ALK-DNA-based+lorlatinib+anti-PD-1. The ALK-DNA-based vaccine is a DNA vector that encodes the cytoplasmic portion of the human ALK protein, turning it a possible therapeutic approach for virtually all ALK-driven malignancies.

To reach this aim, and in order to eliminate a possible tumor escape mechanism, we decided to knock out the endogenous mouse Eml4-Alk and maintain the human EML4-ALK as an oncodriver.

For that, we have used CRISPR/Cas9 system to introduce a sgRNA in hTECLA-1 cell line to disrupt the mouse Alk DNA sequence and consequently eliminate the endogenous mouse Alk protein expression. Next, we have performed several dilutions to obtain a pure single cell clone. The resultant cell line (henceforth hTECLA-1 mAlk KO) was assessed for hEML4-ALK expression and mEml4-Alk knock out (data not shown).

hTECLA-1 mAlk KO cells were injected subcutaneously into syngeneic BALB/c and two (2) cohorts were established. The first (n=10), mice were vaccinated the day after injection and boosted 10 days after. The second group (n=11) was not vaccinated. Both groups were enrolled into 15 days of treatment protocol in which the combination lorlatinib (2mg/Kg twice a day) + anti-PD-1 (200µg/mouse every 3 days in a total of 5 injections) was administered when tumors reached 5mm of diameter. Tumor volume was measured every 3 days during the experiment timeline. Change between baseline and post treatment tumor volume was calculated in percentage.

Remarkably, the triple combination (ALK-DNA-based vaccine+lorlatinib+PD-1) showed great reduction of the tumor relapse after treatment suspension when compared to the double combination (lorlatinib+PD-1) (lorlatinib+PD-1 vs ALK-DNA-Vax+ lorlatinib+PD-1, \* $P < 0.0001$ , according to Mann-Whitney U test) (figure 35 A).

When the humane endpoint was reached, mice were sacrificed, subcutaneous tumors were collected and hALK expression was assessed by immunohistochemistry (figure 35 B/C/D/E).

Previous experiments with TECLA-1 cell line have shown its enormous metastatic ability. Upon subcutaneous injection, TECLA-1 cell line metastasizes in distant organs such as lungs (maybe due to the tropism of these cells to their original environment), liver, brain, kidney, spleen and lymph nodes (data not shown). For this reason, apart from the subcutaneous tumors, we also collected the lungs (first distant organ where TECLA-1 cells metastasize; data not shown) and analyzed the hALK expression by immunohistochemistry.

Remarkably, in the double combination group (lorlatinib+anti-PD-1), in 7 out of 9 mice, more than 80% of the subcutaneous tumor mass was hALK positive (figure 35 B), and 5 out of 6 mice presented lung metastasis positive for hALK (figure 35 C).

However, in the triple combination, only 3 out of 8 mice were positive for ALK in less than 20% of the subcutaneous tumor mass (figure 35 D), and surprisingly, none have developed lung metastasis (% of lung metastasis: double combination vs triple combination; 83.3% vs 0%) (figure 35 E).



#### 4.7) PGPGRVAKI is a MHC-I-restricted neoantigen in BALB/c background

We have previously proved the capacity of human ALK to elicit a CD8<sup>+</sup> T-cell response in BALB/c mice [397, 402]. However, it remained unclear which ALK-specific peptides are presented on the surface of ALK-driven NSCLC cells by the MHC-I and recognized by CD8<sup>+</sup> ALK-specific T-cells in BALB/c.

In order to determine the ALK-specific T-cell epitopes, we performed an *in vitro* screening by using isolated splenocytes from mice immunized with the pDEST-ALK DNA vaccine that encodes the entire cytoplasmic portion of human ALK. First, a set of 21 synthetic long peptides (SLP) were produced; each one 36 amino acids in length, covering the cytoplasmic portion of human ALK (hALK<sub>1058-1620</sub>). Since MHC-I typically present peptides between 8-11 amino acids; each synthetic long peptide overlapped 15 amino acids with the previous and following peptide to ensure that every possible T-cell epitope was represented (figure 36 A). After, the 21 SLP were incubated with splenocytes from mice immunized with the pDEST-ALK DNA vaccine or alternatively, from a non-ALK vaccinated (pDEST empty vector) in an IFN $\gamma$ -ELISPOT assay (figure 36 B).

Remarkably, SLP7 (hALK<sub>1250-1285</sub>) induced a 6.27 fold increase in the number of IFN $\gamma$ -spots in the ALK-vaccinated group compared to the non-ALK vaccinated group (203 $\pm$ 21.6 vs 32.3 $\pm$ 6.6) (figure 36 C). Regarding the other 20 SLPs, we observed weaker responses in four (4) SLPs: SLP2 (hALK<sub>1130-1165</sub>), SLP3 (hALK<sub>1154-1189</sub>), SLP20 (hALK<sub>1562-1597</sub>) and SLP21 (hALK<sub>1585-1620</sub>) (2.63, 2.87, 1.91 and 4.13 respectively fold increase in the number of IFN $\gamma$ -spots in the ALK-vaccinated group vs. the non-ALK-vaccinated) (figure 36 C).

In order to identify which peptide(s) was/were able to generate a CD8<sup>+</sup> T-cell response, we have vaccinated WT BALB/c mice with the identified five (5) SLPs, harvested the spleens and pulse *in vitro* the splenocytes suspension with those five (5) peptides individually. After, we have performed INF- $\gamma$  intracytoplasmic staining

together with CD4 and CD8 membrane staining. Extraordinarily, only peptide 7 (SLP7) was able to elicit a CD8<sup>+</sup> T-cells response (figure 36 D). The other four (4) SLPs (SLP2, SLP3, SLP20 and SLP21) elicited a CD4<sup>+</sup> T-cell response (data not shown).

As it was mentioned before, MHC-I typically present peptides between 8-11 amino acids. In order to identify the 8-11 amino acids peptide within the SLP7, we have performed an *in silico* analysis through three MHC-I epitope-binding algorithms. By using this approach, we predicted the 9mer PGPGRVAKI (hALK<sub>1260-1268</sub>) to weakly bind H-2Dd (figure 36 E). No peptides were predicted to bind H-2Kd and H-2Ld (data not shown). These findings were then validated; the PGPGRVAKI short peptide was synthesized and used to challenge splenocytes of SLP7-vaccinated mice. The splenocytes of previous mice challenged with SLP7 recognize and reacted against the short peptide in an IFN $\gamma$ -ELISPOT assay (figure 36 F). To further confirm these results, we have used dextramer molecules that contained the H2-Dd-PGPGRVAKI-MHC-I complex conjugated with APC (figure 35 G) and analyzed splenocytes from naïve mice (figure 36 H right panel) and PGPGRVAKI-vaccinated mice (figure 36 H left panel). 21.6% of total CD8<sup>+</sup> splenocytes from PGPGRVAKI-vaccinated mice were PGPGRVAK-specific. These results confirmed that the short peptide 7 is the core of CD8<sup>+</sup> T-cell epitope.

#### 4.8) Humanized mouse ALK cell line (Edited-1) generation

Once identified the specific human ALK epitope that elicits a strong CD8<sup>+</sup> T-cell response in BALB/c mice, we decided to have a close look at the mouse Alk. Mouse and human ALK have a great homology. Actually, within the tyrosine kinase domain, they differ only in four (4) amino acids. Most interesting, two (2) of these four (4) amino acids are located within the identified peptide 7 (figure 37 A). In order to understand if these amino acid changes were enough to hamper the mouse peptide 7 to bind to MHC-I, we performed another *in silico* analysis by using the three (3) peptide-MHC-I binding algorithms we have used before. As it is with the human ALK peptide 7, mouse peptide 7 is predicted to bind to H-2-Dd allele; however it has a much higher predicted IC50 value than the corresponded human ALK peptide 7. This means that, to generate a CD8<sup>+</sup> T-cell response in BALB/c, the mouse Alk protein needs



to be in much higher concentration in the cells. This IC<sub>50</sub> result was consistent in all three (3) algorithms used (netMHCpan 4.0 mouse IC<sub>50</sub> 17725.3nM vs human IC<sub>50</sub> 3030.9nM; ANN 4.0 mouse IC<sub>50</sub> 5705.4 vs human IC<sub>50</sub> 602.96; SMM mouse IC<sub>50</sub> 2229.87 vs human IC<sub>50</sub>556.26) (figure 37 B).

In order to develop a syngeneic mouse model where we could study the immune value of ALK, we decided to use the previously generated TECLA-1 cell line (that carries the endogenous expression of mouse Elm4-Alk) and edit the genomic DNA correspondent to peptide 7 and replace the two (2) mouse amino acids by the two (2) human amino acids. We have generated one (1) CRISP breakpoint close to the region of interest. We also have designed a crRNA that in 5' end contained a large template of the sequence we wanted to edit. The 3' end of the crRNA was complementary with a commercial available tracrRNA. Once matched, the tracrRNA stabilizes the crRNA. To avoid CAS9 off-targets, we have used CAS9 protein that has a life-time of only 4 hours. TECLA-1 was electroporated with the mixture solution, collected, washed and plated in fresh medium. Once recovered from electroporation, we performed single cell clones by consecutive dilutions (figure 37 C). Single cell clones were then analyzed through DNA and RNA sequencing (figure 37 D). We obtained one (1) single cell clone that was successfully edited (henceforth Edited-1).

The sensitivity of Edited-1 to lorlatinib was analyzed and compared to TECLA-1 sensitivity. ALK dephosphorylation was observed at low concentrations of lorlatinib (1nM), indicating a good response to this potent ALK inhibitor, as it was observed with TECLA-1 (figure 37 E). In order to compare different responses to different ALK inhibitors, and understand whether the genomic editing had caused off-targets that could affect the sensitivity of Edited-1 to ALK inhibitors, Edited-1 and TECLA-1 cells were treated with crizotinib, ceritinib, alectinib, brigatinib and lorlatinib at increasing concentrations for 72 hours. Thereafter, cell viability was measured by CellTiter-Glo. As expected, Edited-1 presented very similar IC<sub>50</sub> values to TECLA-1 (figure 37 F).

Once confirmed that Edited-1 responds to ALK inhibitors as TECLA-1, we next decided to evaluate the potential ability of Edited-1 to elicit a CD8<sup>+</sup> T-cell response. The edited peptide 7 (humanized mouse ALK) should be able to generate an immune response in BALB/c background. We injected subcutaneously 1x10<sup>6</sup> cells (both Edited-1

and TECLA-1, independently) into WT BALB/c. Mice were sacrificed at day 15 after tumor transplantation (figure 37G) and we isolated the splenocytes in order to analyze the spontaneous immune response by performing an IFN- $\gamma$  ELISPOT assay and H-2-Dd-PGPGRVAKI-dextramer staining. Surprisingly, Edited-1 was able to generate a strong immune response measurable by IFN- $\gamma$  ELISPOT assay, even though weaker than PGPGRVAKI-peptide vaccine. As expected, TECLA-1 did not elicit any IFN- $\gamma$ -induced response when pulsed with the peptide 7 (figure 37 H). In the dextramer staining, we were able to identify 1.8% of the total CD8<sup>+</sup> as H-2-Dd-PGPGRVAKI-dextramer<sup>+</sup>. Once again, TECLA-1 cell line did not present any positivity for dextramer staining (figure 37 I). These results suggest that Edited-1 carries a neoepitope that elicits a CD8<sup>+</sup> T-cell response in BALB/c background.

#### 4.9) Tumor localization dictates the intensity of the immune response

After generating a syngeneic cell line that carries an ALK-neoepitope, we questioned whether the spontaneous immune response could be potentiated by immune checkpoint blockade. For that, we performed a classical *in vivo* experiment in which  $1 \times 10^6$  TECLA-1 and Edited-1 cells were injected subcutaneously into WT BALB/c mice. Mice were treated with anti-PD-1, anti-CTLA-4, or combination of both (anti-PD-1+anti-CTLA-4) at day 3, 6, and 9, according to figure 38 A. All mice injected with TECLA-1 were kept for survival analysis. A cohort of mice injected with Edited-1 was kept for survival purposes and a second cohort was sacrificed at day 15 after tumor transplantation for immune response analysis.

Mice injected subcutaneously with TECLA-1 did not respond to any treatment protocol. The tumor volume (measured every 3 days) of the treated groups (anti-PD-1, anti-CTLA-4 or combination of both [anti-PD-1+anti-CTLA-4]) practically overlap with the tumor volume of the untreated group (control) (figure 38 B). Another way to interpret these results is by analyzing the Kaplan Meier survival curves (figure 38 C). In this case, the death event is considered when the subcutaneous tumor reaches 1.5cm and the mouse has to be sacrificed due to ethical practices. As expected, all mice injected subcutaneously with TECLA-1 have died around the same time (day 20 after tumor transplantation) independently of the treatment performed.

However, mice injected subcutaneously with Edited-1 have behaved differently. In the untreated group (control), all mice have developed subcutaneous tumors even though in the presence of a neoantigen (figure 38 D, first panel). However, when compared with TECLA-1 untreated group, Edited-1 subcutaneous tumors have a slower tumor growth rate (compare figure 38 B with first panel of figure 38 D). Surprisingly, when treated with anti-PD-1, only a mild effect was observed around day 10, however, after this initial mild response, all tumors escaped and grew (figure 38 B, second panel). Remarkably, when treated with anti-CTLA-4, only one (1) mouse developed subcutaneous tumor. All the other mice reached a tumor volume pick around day 10 and by day 30 after tumor transplantation were tumor-free (figure 38 D third panel). Finally, in the group treated with the combination (anti-PD-1+anti-CTLA-4), a larger number of mice (4 mice) have developed subcutaneous tumor after treatment when compared to anti-CTLA-4 treatment group. All the other mice, as it was observed in the anti-CTLA-4 treatment group, have reached a tumor volume pick around day 10 and by day 40 after tumor transplantation were tumor-free (figure 38 D, fourth panel). When analyzing the Kaplan Meier survival curves, we observed that all mice from untreated and anti-PD1 treated groups have died between day 30 and 50 after tumor transplantation (around 10 to 20 days after TECLA-1 untreated/treated groups). However, 80% and 55% of the mice treated with anti-CTLA-4 or immune checkpoint inhibitors combination, respectively, were tumor-free, and consequently survived (figure 38 E).

One cohort of Edited-1 injected mice was sacrificed at day 15 after tumor transplantation and the immune response was evaluated in the four (4) different groups. Unexpectedly, IFN- $\gamma$  ELISPOT assay did not show statistically significant differences between the four (4) groups (figure 38 F) at day 15 after tumor transplantation. Dextramer staining showed that the combination (anti-PD-1+anti-CTLA-4) group had a higher number of CD8<sup>+</sup>/Dextramer<sup>+</sup> T-cells (Combo vs Ctrl, \* $P < 0.05$ , at 15 days after tumor transplantation, according to U-test) (figure 38 G). Both IFN- $\gamma$  ELISPOT assay and dextramer staining were performed in isolated splenocytes.

Enthusiastic about these results, we then decided to perform orthotopic tumor transplantation in order to reproduce the results obtained in the skin (subcutaneous

tumors). WT BALB/c mice were injected intravenously with  $1 \times 10^6$  cells. At day 6 after tumor transplantation, tumor cells niched in the lung forming lung tumor foci (data not shown). Mice were treated as previously (figure 38 A). One cohort was kept for survival analysis and the second cohort was sacrificed at day 15 after tumor transplantation. Unpredictably, all mice from all treatment protocol groups have died due to respiratory failure around day 20 and 25 after tumor transplantation and by day 30 the experiment was finished. Immune checkpoint inhibitors (alone or in combination) did not add any advantage in terms of survival. As it was observed in the skin model, the IFN- $\gamma$  ELISPOT assay results were not astonishing. However, the combination (anti-PD-1+anti-CTLA-4) showed a modest higher number of IFN- $\gamma$ -induced spots (Combo vs Ctrl,  $*P < 0.05$ , at 15 days after tumor transplantation, according to U-test) (figure 38 I). The dextramer staining has showed that mice treated with anti-CTLA-4 had a slight increase of CD8<sup>+</sup>/dextramer<sup>+</sup> T-cells (anti-CTLA-4 vs Ctrl,  $*P < 0.05$ , at 15 days after tumor transplantation, according to U-test) (figure 38 J).

These results suggest that different organs establish different immune responses that might be a consequence of a more or less immunosuppressive microenvironment.

#### **4.10) PGPGRVAKI-peptide vaccine generates less exhausted intratumor CD8<sup>+</sup> T-cell**

After understanding that the lung microenvironment might be more immunosuppressive than the skin microenvironment, we then questioned whether the peptide vaccine was able to turn the lung microenvironment into a more immune responsive environment. For that, we have again performed the orthotopic tumor transplantation experiment in WT BALB/c mice by injecting  $1 \times 10^6$  Edited-1 cells intravenously. Mice were subdivided into four (4) groups (untreated [control], anti-PD-1, anti-CTLA-4, and PGPGRVAKI-peptide vaccine) according to (figure 39 A). One cohort was kept for survival analysis and a second cohort was sacrificed at day 15 after tumor transplantation in order to analyze the tumor immune infiltrate. Not surprisingly, peptide vaccine has slightly extended the mice survival for 10 days, when

compared with the remaining groups (figure 39 B). In the second cohort, mice were sacrificed at day 15 and 3 lung lobes were harvested and mechanically disaggregated until a cell suspension was obtained. On total lung cells we performed a H-2-Dd-PGPGRVAKI-dextramer staining and gated on CD8<sup>+</sup>/Dextramer<sup>+</sup>/PD-1<sup>+</sup>. Intratumor dextramer staining did not add any additional information. Surprisingly, peptide vaccine was not able to increase the number of ALK-specific-CD8<sup>+</sup> T-cells intratumor (figure 39 C). However, when the PD-1 expression was assessed in intratumor dextramer<sup>+</sup> cells, we observed that ALK-specific-CD8<sup>+</sup> T-cells that infiltrate the lung tumors were less exhausted compared with the other groups. Surprisingly, also anti-CTLA-4 treatment generated less exhausted ALK-specific-CD8<sup>+</sup> T-cells (Ctrl vs peptide-vaccine, \**P*<0.001 at 15 days after tumor transplantation, according to U-test; PD-1 vs CTLA-4, \**P*<0.001 at 15 days after tumor transplantation, according to U-test; PD-1 vs peptide-vaccine, \**P*<0.001 at 15 days after tumor transplantation, according to U-test; CTLA-4 vs peptide-vaccine, \**P*<0.001 at 15 days after tumor transplantation, according to U-test) (figure 39 D). The remaining lung lobes were analyzed by histology (figure 39 E). Macroscopically, the tumor burden seems to be smaller in the CTLA-4 and peptide-vaccine treated groups. We then decided to measure the tumor volume by ImageJ analysis and we verified that indeed, CTLA-4 and peptide-vaccine had a significantly smaller tumor burden at day 15 after tumor transplantation (Ctrl vs peptide-vaccine, \**P*<0.001 at 15 days after tumor transplantation, according to U-test; Ctrl vs CTLA-4, \**P*<0.01 at 15 days after tumor transplantation, according to U-test, PD-1 vs peptide-vaccine, \**P*<0.001 at 15 days after tumor transplantation, according to U-test; PD-1 vs CTLA-4, \**P*<0.05 at 15 days after tumor transplantation, according to U-test; CTLA-4 vs peptide-vaccine, \**P*<0.05 at 15 days after tumor transplantation, according to U-test) (figure 39 F).

#### **4.11) PGPGRVAKI-peptide vaccine in combination with a potent ALK inhibitor significantly extends mice overall survival and completely abrogates brain metastasis in orthotopic mouse models.**

After, we questioned the therapeutic value of the PGPGRVAKI-peptide vaccine. Mice were injected with 1x10<sup>6</sup> Edited-1 cells intravenously and divided into several

therapeutic groups according to figure 40 A. All mice were kept for survival analysis after treatment suspension. Remarkably, all vaccinated groups (independently the combination with immune checkpoint inhibitors) have a significantly extended overall mice survival. Untreated mice (control) presented a median survival of 19 days (showing how aggressive the tumor is). Not surprisingly, lorlatinib alone and lorlatinib+PD-1 groups have shown the same median survival (37 days), indicating that the overall survival is extended only during lorlatinib treatment and PD-1 does not add any significant effect to the combination. However, when mice were treated with lorlatinib in combination with CTLA-4 inhibitor, the median survival was 42 days and 10% of the mice have survived more than 100 days after tumor transplantation. Both lorlatinib + peptide vaccine and lorlatinib + peptide vaccine+PD-1 groups have reached an approx. median survival of 60 days (23 days more than lorlatinib alone) and about ≈25% of the mice from each group have survived more than 100 days after tumor transplantation. Surprisingly, the lorlatinib + peptide vaccine+CTLA-4 inhibitor median survival was not reached until the end of the experiment and 80% of the mice have survived longer than 100 days after tumor transplantation (figure 40 B), suggesting that CTLA-4 inhibitor potentiates the immune response elicited by the peptide-vaccine.

Despite the incredible results obtained with the therapeutic experiment, where for the very first time in ALK-driven NSCLC history, we can affirmed that a great percentage of mice were cured, we observed that control, lorlatinib alone, lorlatinib + PD-1 and lorlatinib + CTLA-4 treated mice experienced changes in their behavior during the experiment. Around day 15/16 after tumor transplantation in control mice, and day 30/35 after tumor transplantation in lorlatinib alone, lorlatinib + PD-1 and lorlatinib + CTLA-4, mice started to present motor disability, and in some cases even hemiparesis. They also presented an aggressive behavior accompanied by drastic involuntary movements. This phenotype made us wondering whether mice had developed brain metastasis. To analyze this hypothesis, upon death event, brains were collected and analyzed by histology. Several sections were done in order to cover the maximum brain area.

Shockingly, almost all mice from the non-vaccinated groups presented brain metastases whilst in the vaccinated groups, none have developed brain lesions (figure 40 C). This outstanding result is a clear message of hope for all ALK-driven NSCLC patients. (Brain metastasis incidence was not assessed in lorlatinib + peptide vaccine + CTLA-4 due to the reduced number of samples [80% of the mice survived]). In figure 40 D, we can appreciate the histology of two brain lesions in non-vaccinated mice.

#### 4.12) Tumors relapse in vaccinated mice due to reversible MHC-I loss

Finally, we were wondering why still a great percentage of vaccinated mice did not respond to the treatment. Due the fact that Edited-1 tumor cells do not have a marker that allows us to easily identify them by flow cytometry, we have developed several *ex vivo* cell lines in order to eliminate all the other microenvironment components. Upon death event, 3 lung lobes were collected, mechanically disaggregated and cultured in an *ex vivo* manner. After 15 days in culture, cells were collected and Edited-1 *ex vivo* cell lines were analyzed. First, to ensure that the non-response was not due to the fact that cells either lost ALK expression or lost the edited peptide, we performed western blot analysis to measure protein expression, and re-sequenced the humanized mouse peptide. All *ex vivo* cell lines (derived from all therapeutic groups) presented a normal ALK protein expression and had not lost the edited peptide (data not shown). Then, we evaluated by flow cytometry the expression of H-2-Dd (where the PGPGRVAKI peptide is predicted to be expressed) on the surface of the *ex vivo* cell lines. Surprisingly, the vaccinated groups presented a significantly reduced H-2-Dd expression, when compared with the non-vaccinated groups (Ctrl vs lorlatinib + peptide vaccine, \* $P < 0.001$  according to U-test; Ctrl vs lorlatinib + peptide vaccine + PD-1, \* $P < 0.001$  according to U-test; lorlatinib alone vs lorlatinib + peptide vaccine, \* $P < 0.001$  according to U-test; lorlatinib alone vs lorlatinib + peptide vaccine + PD-1, \* $P < 0.001$  according to U-test; lorlatinib + PD-1 vs lorlatinib + peptide vaccine, \* $P < 0.001$  according to U-test; lorlatinib + PD-1 vs lorlatinib + peptide vaccine + PD-1, \* $P < 0.001$  according to U-test; lorlatinib + CTLA-4 vs lorlatinib + peptide vaccine, \* $P < 0.001$  according to U-test; lorlatinib + CTLA-4 vs lorlatinib + peptide vaccine + PD-1, \* $P < 0.001$  according to U-test) (figure 41 A).

Finally, we asked whether the MCH-I loss was an irreversible event. For that, representative *ex vivo* cell lines were incubated with high concentrations (10ng) of recombinant mouse IFN- $\gamma$  for 24 hours. After incubation time, H-2-Dd expression was again measured by flow cytometry and compared with non-stimulated cells. Remarkably, all representative *ex vivo* cell lines upregulated H-2-Dd expression upon IFN- $\gamma$  stimulation, indicating that IFN- $\gamma$  pathway was not affected (figure 41 B).

Why these relapsed tumors downregulated MHC-I expression is still an open question, however the fact that is a reversible downregulation leaves an open door for further immunotherapy combinations.



*Figures Part I*



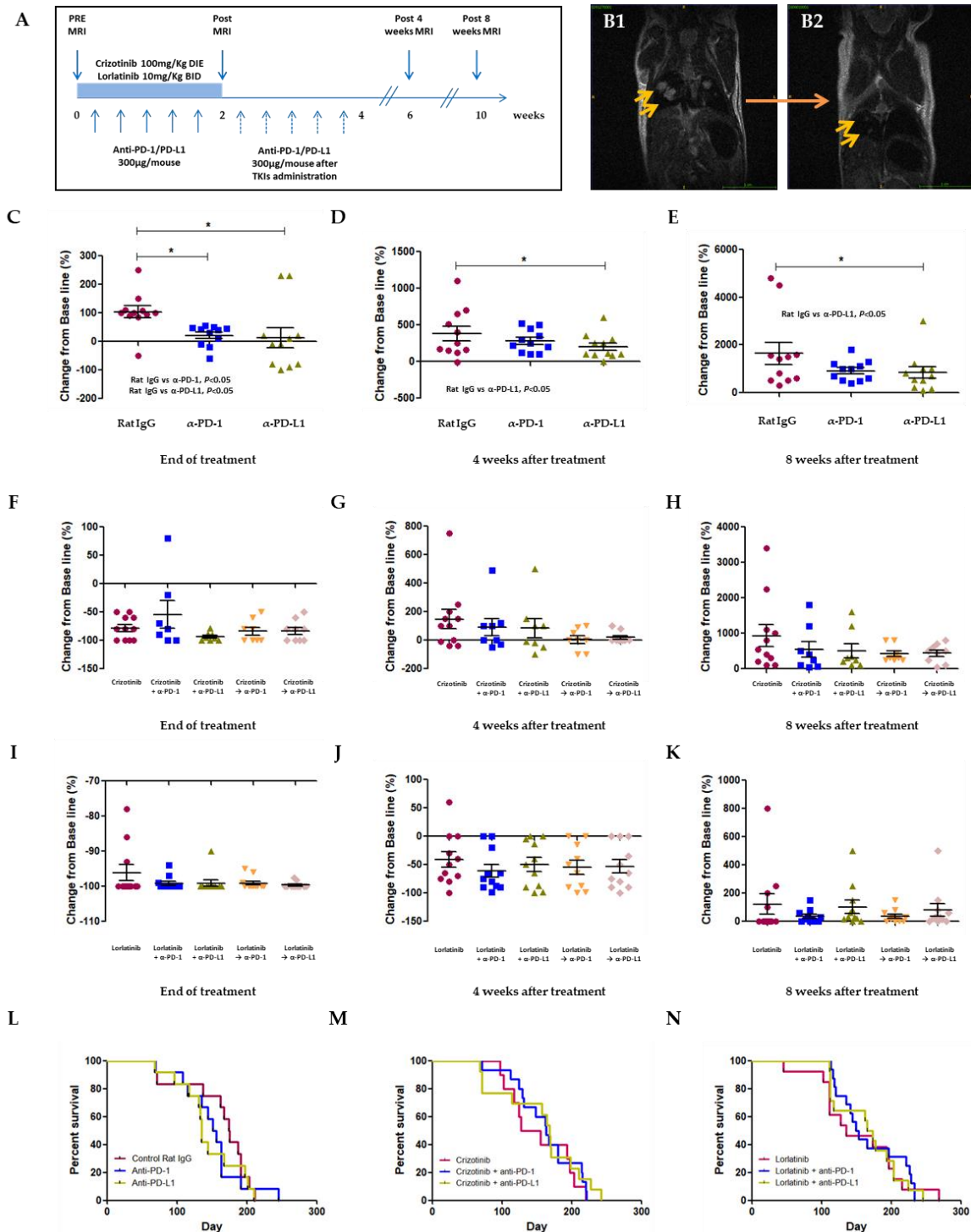


**Figure 29 - Combination of immune checkpoint blockade with high doses of ALK inhibitors does not provide significant advantage in Tg EML4-ALK-rearranged NSCLC mice.** A) Schematic representation of treatment protocol – mice were enrolled into 15 days of treatment according to different groups. Crizotinib was administrated once a day and lorlatinib twice a day by oral gavage whereas control Rat IgG, Anti-PD-1 and Anti-PD-L1 were given five (5) times every three (3) days (synchronized or after ALK TKI administration) by intraperitoneal injection (ip.). MRI screening was performed before treatment for mice stratification based on total tumor volume. Follow-up MRIs were performed at the end of the TKI

treatment and at 4 and 8 weeks after treatment suspension to evaluate tumor growth. Mice were monitored for survival. B1/B2) Representative MRI of a Tg EML4-ALK mouse at (B1) crizotinib pre-treatment and at (B2) 4 weeks after treatment suspension; small light orange arrows indicate tumor masses and it can be appreciated the effect of crizotinib alone; from B1 to B2 tumors have reduced their size. C/D/E) Quantification of volume changes compared with baseline tumor volume in mice treated with immune checkpoint inhibitors monotherapy at (C) the end of treatment: anti-PD-1 and anti-PD-L1 antibodies stabilized tumor relapse at the end of treatment (PD-1 vs Ctrl Rat IgG,  $*P<0.05$ ; PD-L1 vs Ctrl Rat IgG,  $*P<0.05$ , end of treatment, according to Mann-Whitney U test); at (D) 4 weeks after treatment suspension: in the anti-PD-L1 antibodies group, tumors relapsed slightly slower when compared with controls (PD-L1 vs Ctrl Rat IgG,  $*P<0.05$ , at 4 weeks after treatment, according to Mann-Whitney U test); at (E) 8 weeks after treatment: the same result is shown at 8 weeks after treatment (PD-L1 vs Ctrl Rat IgG,  $*P<0.05$ , at 8 weeks after treatment, according to Mann-Whitney U test). F/G/H) Quantification of volume changes compared with baseline tumor volume at (F) end of treatment and (G) 4 and (H) 8 weeks follow-up of crizotinib treatment alone or in combination with immune checkpoint inhibitors either synchronized or sequential; no significant values were found. I/J/K) Quantification of volume changes compared with baseline tumor volume at (I) the end of the treatment and (J) 4 and (K) 8 weeks follow-up of lorlatinib treatment alone or in combination with immune checkpoint inhibitors either synchronized or sequential; no significant values were found. L/M/N) Kaplan-Meier curves of overall survival of (L) immune checkpoint monotherapy; (M) crizotinib alone or in combination with immune checkpoint inhibitors (mice from both simultaneous and sequential arms were put together for the survival curves); and (N) lorlatinib alone or in combination with immune checkpoint inhibitors (mice from both simultaneous and sequential arms were put together for the survival curves). In Kaplan-Meier graphs, day zero (0) corresponds to the last day of treatment. BID (*bis in die*) – twice a day; DIE – once a day; + Simultaneous administration; → Sequential administration.

Supplementary table of figure 29 – Treatment protocol and number of Tg EML4-ALK mice used in this experiment

Groups		No. of Tg EML4-ALK mice
Immune checkpoint inhibitors (monotherapy)	Anti-Rat IgG	11
	Anti-PD-1	11
	Anti-PD-L1	11
Crizotinib (100mg/Kg once a day)	+ Anti-Rat IgG	11
	+ Anti-PD-1	8
	+ Anti-PD-L1	8
	→ Anti-PD-1	8
	→ Anti-PD-L1	8
Lorlatinib (10mg/Kg twice a day)	+ Anti-Rat IgG	11
	+ Anti-PD-1	11
	+ Anti-PD-L1	11
	→ Anti-PD-1	11
	→ Anti-PD-L1	11
<b>Total</b>		<b>131</b>

+ Simultaneous administration

→ Sequential administration

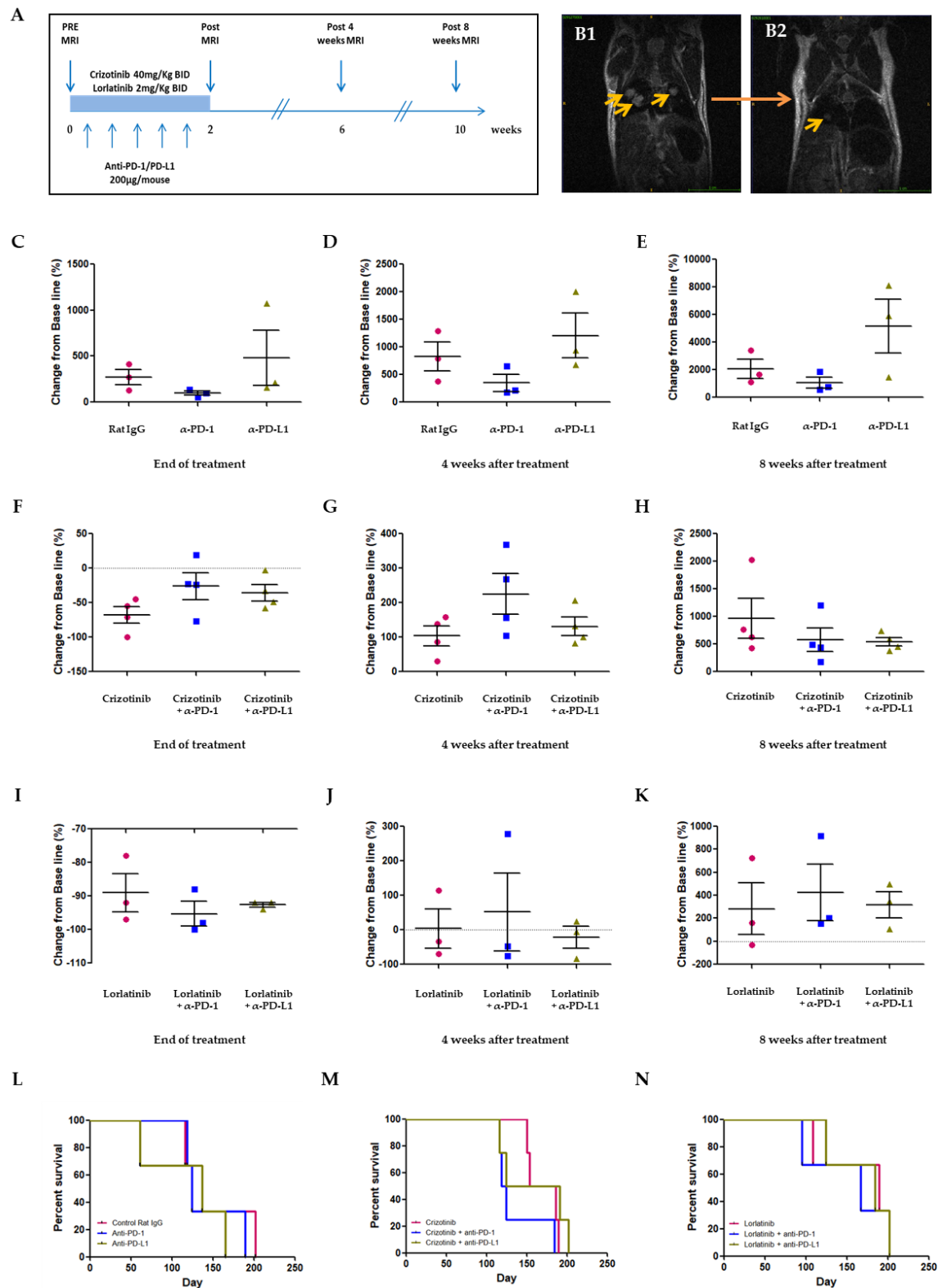


**Figure 30 -Immune checkpoint blockade in combination with low but clinically significant doses of ALK inhibitors (crizotinib and lorlatinib) does not provide any advantage in Tg EML4-ALK mice.** A) Schematic representation of treatment protocol – mice were enrolled into 15 days of treatment according to different groups. Both ALK TKIs (crizotinib – 40mg/Kg and lorlatinib – 2mg/Kg) were administered twice a day by oral gavage whereas control Rat IgG, anti-PD-1 and anti-PD-L1 were given five (5) times every

three (3) days simultaneously with ALK TKI administration (also the concentration of antibodies was reduced in this experiment; 200µg each injection) through i.p. injection. MRI screening was performed before treatment for mice stratification based on total tumor volume. Follow-up MRIs were performed at the end of the TKI treatment and at 4 and 8 weeks after treatment suspension to evaluate tumor growth. Mice were monitored for survival. B1/B2) Representative MRI of a Tg EML4-ALK mouse at (B1) lorlatinib pre-treatment time point and (B2) 4 weeks after treatment suspension; small light orange arrows indicate tumor masses, and it can be appreciated the effect of lorlatinib alone, from B1 to B2 tumors have reduced their size. C/D/E) Quantification of volume changes compared with baseline tumor volume in mice treated with immune checkpoint inhibitors as monotherapy at (C) the end of treatment, (D) 4 and (E) 8 weeks after treatment suspension. F/G/H) Quantification of volume changes compared with baseline tumor volume at (F) end of treatment and (G) 4 and (H) 8 weeks follow-up of crizotinib treatment alone or in combination either with anti-PD-1 or anti-PD-L1. I/J/K) Quantification of volume changes compared with baseline tumor volume at (I) the end of the treatment, at (J) 4 and (K) 8 weeks follow-up of lorlatinib treatment alone or in combination either with anti-PD-1 or anti-PD-L1. L/M/N) Kaplan-Meier curves of overall survival of (L) immune checkpoint monotherapy; (M) crizotinib alone or in combination with immune checkpoint inhibitors; and (N) lorlatinib alone or in combination with immune checkpoint inhibitors. In Kaplan-Meier graphs, day zero (0) corresponds to the last day of treatment. BID (*bis in die*) – twice a day; + Simultaneous administration.

Supplementary table of figure 30 - Treatment protocol and number of Tg EML4-ALK mice used in this experiment

Groups		No. of Tg EML4-ALK mice
Immune checkpoint inhibitors (monotherapy)	Anti-RAT IgG	3
	Anti-PD-1	3
	Anti-PD-L1	3
Crizotinib (40mg/Kg twice a day)	+ Anti-RAT IgG	4
	+ Anti-PD-1	4
	+ Anti-PD-L1	4
Lorlatinib (2mg/Kg twice a day)	+ Anti-RAT IgG	3
	+ Anti-PD-1	3
	+ Anti-PD-L1	3
<b>Total</b>		<b>30</b>

+ Simultaneous administration



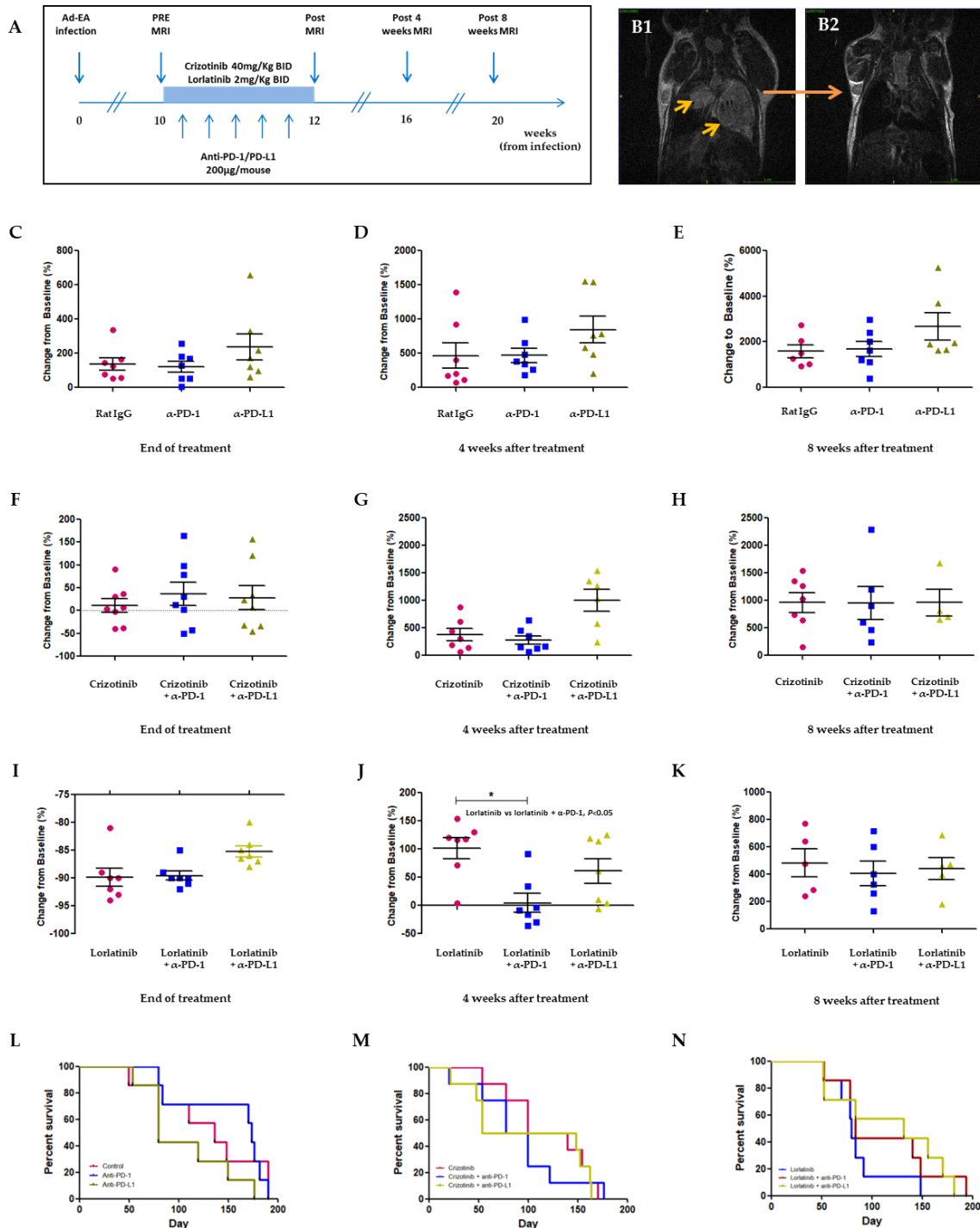


**Figure 31 – PD-1 blockade in combination with low doses of the potent ALK inhibitor lorlatinib delays tumor relapse in Ad-EA-derived NSCLC mouse model.** A) Schematic representation of treatment protocol – mice were infected with Adeno-CRISPR/Cas9 Eml4-Alk virus at week zero (0) and enrolled into 15 days of treatment according to different groups within 10 weeks after injection. Both ALK TKIs (crizotinib - 40mg/Kg, and lorlatinib - 2mg/Kg) were administrated twice a day by oral gavage whereas control Rat IgG, anti-PD-1 and anti-PD-L1 (200µg each) were given five (5) times every three (3) days simultaneously with ALK TKI administration through ip. injection. MRI screening was performed before treatment for mice stratification based on total tumor volume. Follow-up MRIs were performed at the end

of treatment and at 4 and 8 weeks after treatment suspension to evaluate tumor growth. Mice were monitored for survival. B1/B2) Representative MRI of an Ad-EA mouse at (B1) lorlatinib+anti-PD-1 pre-treatment time point and (B2) 4 weeks after treatment suspension; small light orange arrows indicate tumor masses, and from B1 to B2 it can be appreciated that the effect of lorlatinib+anti-PD-1 is extended until week 4 of the follow-up. C/D/E) Quantification of volume changes compared with baseline tumor volume in mice treated with immune checkpoint inhibitors monotherapy at (C) the end of treatment; at (D) 4 weeks after treatment suspension; and at (E) 8 weeks after treatment. F/G/H) Quantification of volume changes compared with baseline tumor volume at (F) end of treatment and at (G) 4 and (H) 8 weeks follow-up of crizotinib treatment alone or in combination either with anti-PD-1 or anti-PD-L1. I/J/K) Quantification of volume changes compared with baseline tumor volume at (I) the end of treatment and at (J) 4 and (K) 8 weeks follow-up of lorlatinib treatment alone or in combination either with anti-PD-1 or anti-PD-L1. At 4 weeks after treatment, the combination lorlatinib+anti-PD-1 has a slight, but statistically significant, synergistic effect (lorlatinib+PD-1 vs lorlatinib,  $*P<0.05$  at 4 weeks-follow-up according to Mann-Whitney U test). However, the effect observed is transient and it is lost at 8 weeks of follow-up. L/M/N) Kaplan-Meier curves of overall survival of (L) immune checkpoint monotherapy; (M) crizotinib alone or in combination with immune checkpoint inhibitors; and (N) lorlatinib alone or in combination with immune checkpoint inhibitors. In Kaplan-Meier graphs, day zero (0) corresponds to the last day of treatment. BID (*bis in die*) – twice a day; + Simultaneous administration.

Supplementary table of figure 31 –Treatment protocol and number of Ad-EA mice used in this experiment

Groups		No. of Ad-EA mice
Immune checkpoint inhibitors (monotherapy)	Anti-Rat IgG	4 BALB/c & 3 C57BL/6
	Anti-PD-1	4 BALB/c & 3 C57BL/6
	Anti-PD-L1	4 BALB/c & 3 C57BL/6
Crizotinib (40mg/Kg twice a day)	+ Anti-Rat IgG	4 BALB/c & 4 C57BL/6
	+ Anti-PD-1	4 BALB/c & 4 C57BL/6
	+ Anti-PD-L1	4 BALB/c & 4 C57BL/6
Lorlatinib (2mg/Kg twice a day)	+ Anti-Rat IgG	4 BALB/c & 3 C57BL/6
	+ Anti-PD-1	4 BALB/c & 3 C57BL/6
	+ Anti-PD-L1	4 BALB/c & 3 C57BL/6
<b>Total</b>		<b>66 (36 BALB/c &amp; 30 C57BL/6)</b>

+ Simultaneous administration

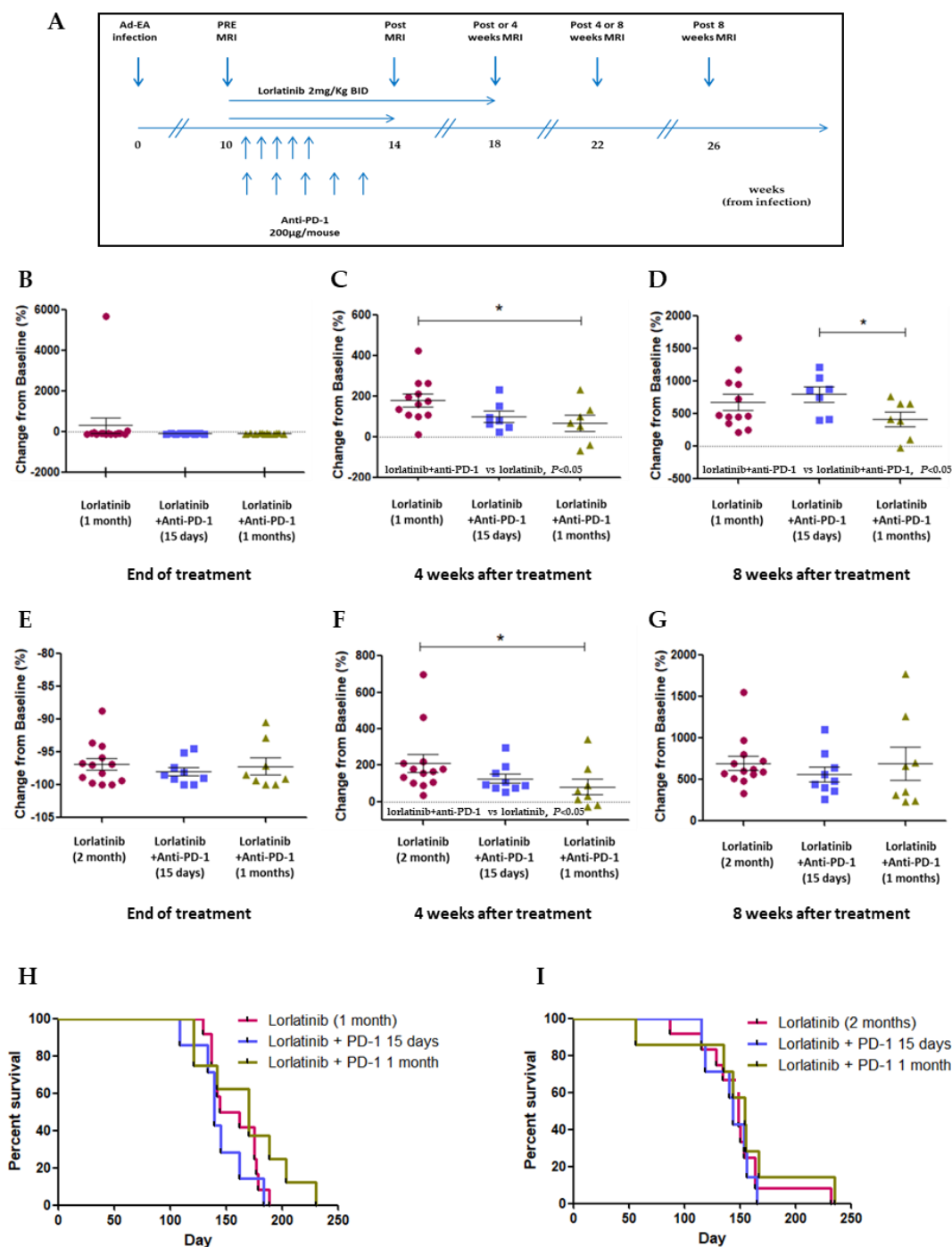


**Figure 32 - Long-term treatment with the potent ALK inhibitor lorlatinib in combination with anti-PD-1 antibody slightly delays tumor relapse in Ad-EA mouse models.** A) Schematic representation of treatments protocols – mice were infected with Adeno-CRISPR/Cas9 Eml4-Alk virus at week zero (0) and tumor volume was evaluated by MRI at week 10 after infection. Mice were enrolled into two different long-term treatment arms. First cohort of mice received lorlatinib for 1 month and the second arm for 2 months. Each cohort was subsequently subdivided into 3 different groups according with PD-1 administration protocol. Mice were treated with lorlatinib alone or in combination with PD-1 antibody either for 15 days or 1 month (total of 5 i.p. injections each). Lorlatinib was administrated twice a day by

oral gavage. B/C/D) Quantification of volume changes compared with baseline tumor volume in long-term lorlatinib treatment (1 month) alone or in combination with PD-1 administered either for 15 days or 1 month, at (B) the end of the treatment, (C) 4 weeks after treatment suspension, and at (D) 8 weeks follow-up (D); (lorlatinib [1 month] + PD-1 [1 month] vs lorlatinib [1 month],  $*P < 0.05$  at 4 weeks-follow-up according to Mann-Whitney U test; lorlatinib [1 month] + PD-1 [15 days] vs lorlatinib [1 month] + PD-1 [1 month]  $*P < 0.05$  at 8 weeks-follow-up according to Mann-Whitney U test). E/F/G) Quantification of volume changes compared with baseline tumor volume in long-term lorlatinib treatment (2 months) alone or in combination with anti-PD-1 administered either for 15 days or 1 month, at (E) the end of the treatment, (F) 4 weeks after treatment suspension, and at (G) 8 weeks follow-up; (lorlatinib [2 months] + PD-1 [1 month] vs lorlatinib [2 months],  $*P < 0.05$  at 4 weeks-follow-up according to Mann-Whitney U test). H/I) Kaplan-Meier curves of overall survival of both long-term treatment protocols with (H) lorlatinib - 1 month, and (I) 2 months. Even though is not statistically significant, it can be appreciated a slight increase in the overall survival. In Kaplan-Meier graphs, day zero (0) corresponds to the last day of treatment. BID (*bis in die*) – twice a day; + Simultaneous administration.

Supplementary table of figure 32 – Treatment protocol and number of Ad-EA mice used in this experiment

Groups		No. of Ad-EA mice (BALB/c)
Lorlatinib (2mg/Kg twice a day) (1 month)	+ Anti-Rat IgG	13
	+ Anti-PD-1 (15 days)	7
	+ Anti-PD-1 (1 month)	7
Lorlatinib (2mg/Kg twice a day) (2 months)	+ Anti-Rat IgG	13
	+ Anti-PD-1 (15 days)	9
	+ Anti-PD-1 (1 month)	8
<b>Total</b>		<b>57</b>

+ Simultaneous administration

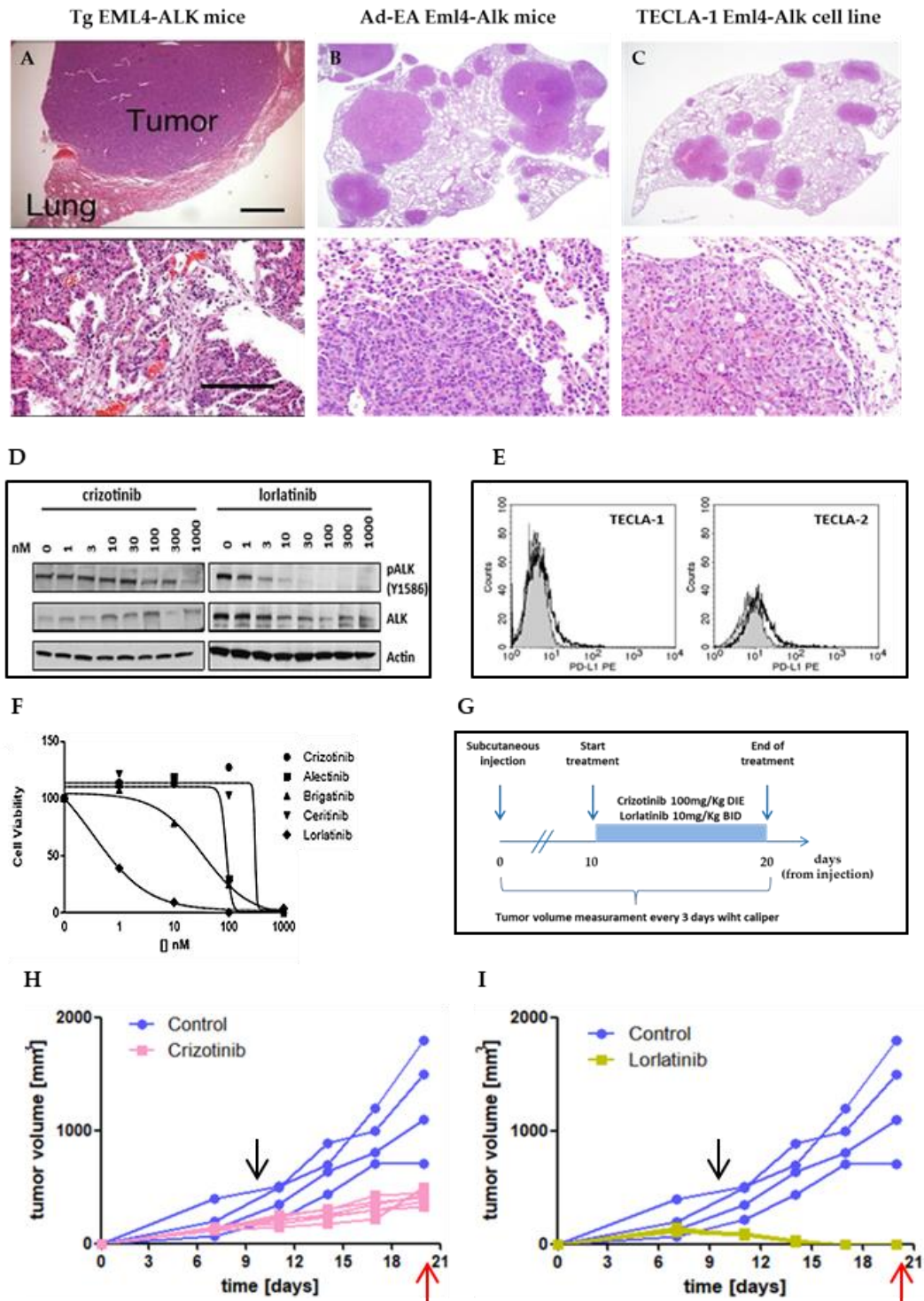


**Figure 33 – Murine Alk rearrangement shows poor response to crizotinib but not lorlatinib.** A/B/C) Hematoxylin & Eosin histological sections of lung tumors from (A; upper and lower panel) Tg EML4-ALK mouse model; (B; upper and lower panel) tumors generated in Ad-EA mice model; and (C; upper and lower panel) from lung tumors of a WT BALB/c mouse injected in the tail vein with TECLA-1 cell line (Upper panel: 2x magnification; lower panel: 40x magnification). The lung tumors that are generated in these three mouse models share the same adenocarcinoma morphology. D) TECLA-1 cells were treated with crizotinib and lorlatinib at the indicated concentrations for 6h. Total cell lysates were blotted with the

indicated antibodies. E) PD-L1 expression was evaluated by flow cytometry in both cell lines. Grey histogram corresponds to isotype control staining and bold black line represents the cell lines stained with anti-PD-L1-PE; F) TECLA-1 cells were treated with the indicated doses of crizotinib, alectinib, ceritinib, brigatinib and lorlatinib for 72h. Cell viability was assessed by CellTiter-Glo; G) TECLA-1 cells were injected subcutaneously into syngeneic BALB/c mice and treated according to the schematic representation of the treatment protocol. H/I Tumors were treated when 5 mm of length with crizotinib and lorlatinib for 10 days and measured every 3 days until tumors reached 15mm of length or the end of the experiment; (H) mice treated with crizotinib never achieved complete tumor regression in contrast (I) mice treated with lorlatinib. Black arrows indicate the starting time point of the treatment; red arrows illustrate the ending time point of the treatment protocol. BID (*bis in die*) – twice a day; DIE – once a day; + Simultaneous administration.



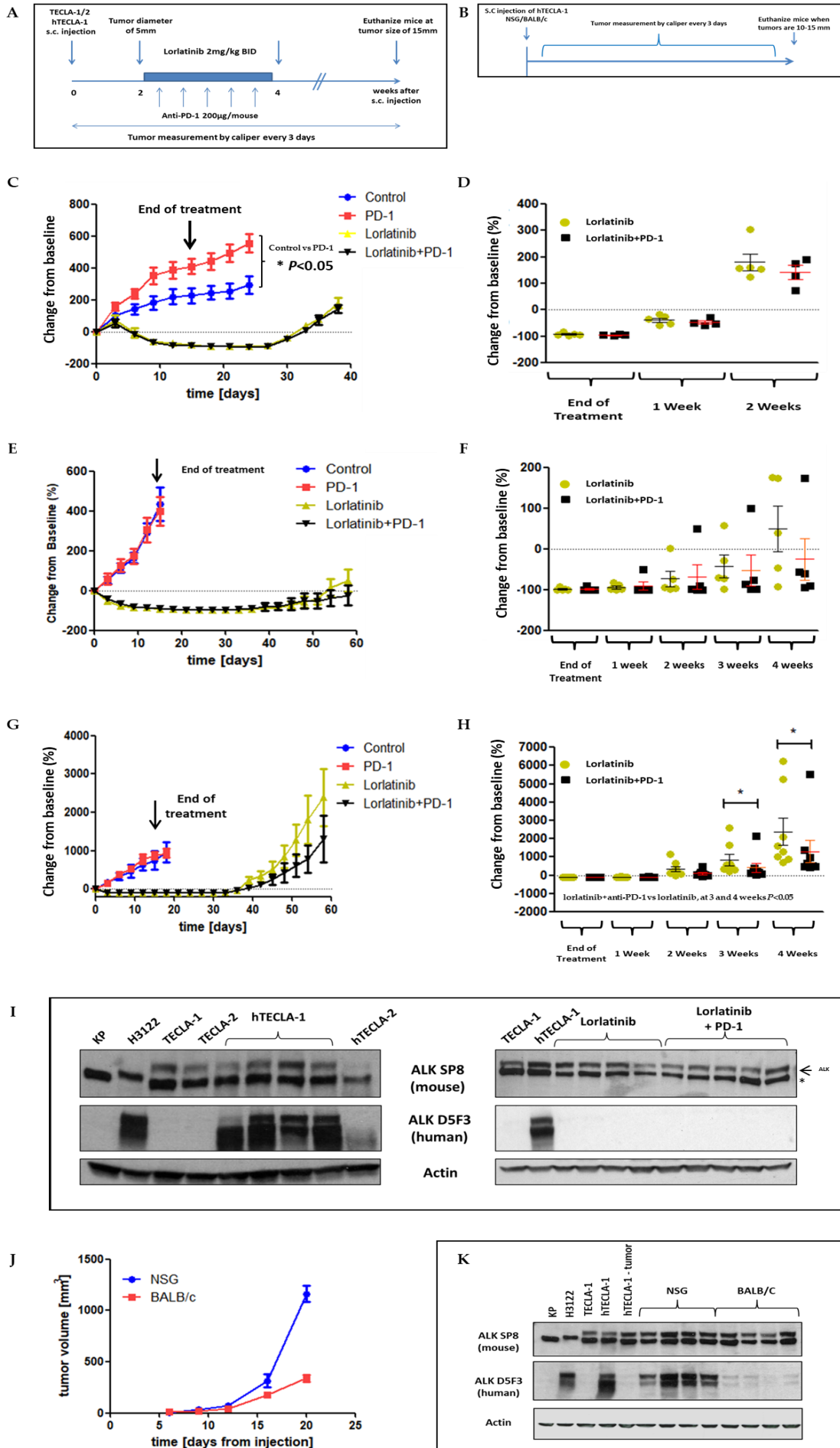


**Figure 34 – Strong human ALK expression results in immunoediting in immunocompetent BALB/c mice.** A) Schematic representation of treatment protocol – mice were injected either with TECLA-1, TECLA-2 or hTECLA-1 cell lines and when tumors reached 5mm of diameter were enrolled into 15 days of treatment according to different groups. Lorlatinib (2mg/Kg) was administrated twice a day by oral gavage whereas anti-PD-1 (200 µg each injection) was given five (5) times every three (3) days simultaneously with ALK TKI administration. Mice were then follow-up after treatment suspension and sacrificed when tumor reached 1.5cm of diameter. B) Schematic representation of the NSG vs BALB/c experiment chronology. hTECLA-1 cells were injected in both NSG and BALB/c mice, and when tumors reached 15mm of diameter, mice were sacrificed. C/D) The charts represent TECLA-1 cell line experiment. C) Overall quantification of volume changes compared with baseline tumor volume during and after treatment (anti-PD-1 vs untreated controls,  $*P<0.05$ , according to Mann-Whitney U test). D) Quantification of volume changes compared with baseline tumor volume of lorlatinib and lorlatinib+anti-PD-1 arms at the end of treatment and during follow-up. E/F) The charts represent TECLA-2 cell line experiment. E) Overall quantification of volume changes compared with baseline tumor volume during and after treatment suspension. F) Quantification of volume changes compared with baseline tumor volume of lorlatinib and lorlatinib+PD-1 arms at the end of treatment and during follow-up. G/H) The charts represent hTECLA-1 cell line experiment. G) Overall quantification of volume changes compared with baseline tumor volume during and after treatment. H) Quantification of volume changes compared with baseline tumor volume of lorlatinib and lorlatinib+PD-1 arms at the end of the treatment and during follow-up (lorlatinib vs lorlatinib+anti-PD-1 at 3 weeks,  $*P<0.05$ , according to Mann-Whitney U test; and lorlatinib vs lorlatinib+anti-PD-1 at 4 weeks of follow-up,  $*P<0.05$ , according to Mann-Whitney U test). I) Immunoblot analyzing the expression of human ALK and mouse ALK. On the left panel, the human and mouse ALK expression is evaluated in several cell lines. From left to right: KP (ALK negative NSCLC mouse cell line), negative control for mouse Alk; H3122 (human ALK<sup>+</sup> NSCLC cell line), positive control for hALK; TECLA-1 and TECLA-2; four (4) different viral infections of hTECLA-1; hTECLA-2 (TECLA-2 was also subjected to overexpression of hEML4-ALK, however the viral infection rate was very low). On the right panel, the expression of human and mouse ALK is analyzed in subcutaneous tumors after treatment with lorlatinib and lorlatinib+PD1. TECLA-1 and hTECLA-1 cell lines were used as negative and positive controls for hALK, respectively. Tumors treated either with lorlatinib alone or lorlatinib in combination with anti-PD-1 did not show hALK expression, only mouse ALK. J) Quantification of the tumor volume of hTECLA-1 subcutaneous tumors overtime in NSG (blue line) and BALB/c (red line). K) Immunoblot analyzing human and mouse ALK protein expression from tumors grown both in NSG and BALB/c mice. After *in vivo* passage, tumors were collected from both NSG and BALB/c and human ALK protein expression was analyzed by western blot. Tumors that have grown in immunocompromised mice (NSG) kept the expression of hALK protein. On the other hand, tumors grown in immunocompetent mice (BALB/c) lost considerably the expression of human ALK. Cell lines were used as controls; KP (mouse NSCLC cell line ALK negative); H3122 (human ALK-driven NSCLC cell line); TECLA-1; hTECLA-1; hTECLA-1 tumor (one negative sample from the previous experiment was used as an internal control);

NSG (4 tumors collected from NSG mice show human ALK expression); BALB/c (4 tumor collected from BALB/c mice show much less human ALK expression when compared with tumors grown in NSG mice). ALK SP8 (mouse): antibody that recognizes specifically mouse ALK; ALK D5F3 (human): FDA-approved antibody for the diagnosis of ALK<sup>+</sup> NSCLC that recognizes specifically the human ALK; Actin: antibody that recognizes actin protein was used as loading control; \* Unspecific band; BID (*bis in die*) – twice a day; + simultaneous administration.

Supplementary table of figure 34 – Treatment protocol and number of mice used in this experiment

Cell line	Groups	No. of mice
<b>TECLA-1</b> (1x10 <sup>6</sup> cells injected in each mouse)	Untreated control	5
	Anti-PD-1	5
	Lorlatinib	5
	Lorlatinib+Anti-PD-1	5
<b>TECLA-2</b> (1x10 <sup>6</sup> cells injected in each mouse)	Untreated control	5
	Anti-PD-1	5
	Lorlatinib	5
	Lorlatinib+Anti-PD-1	5
<b>hTECLA-1</b> (1x10 <sup>6</sup> cells injected in each mouse)	Untreated control	5
	Anti-PD-1	8
	Lorlatinib	8
	Lorlatinib+Anti-PD-1	8
<b>Total</b>		<b>69</b>

+ Simultaneous administration

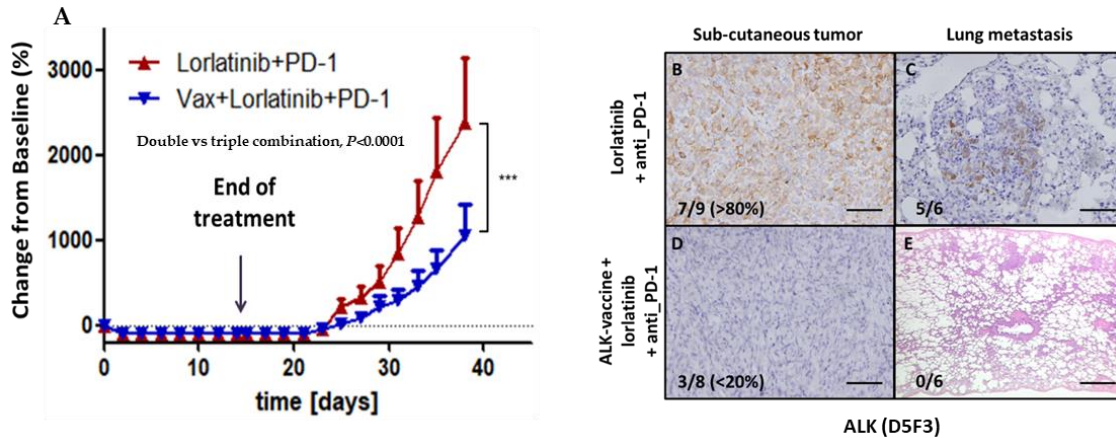


**Figure 35 – Triple combination of lorlatinib, PD-1 blockade and ALK-DNA-based vaccine significantly delays tumor relapse and completely abrogates the development of metastasis in distant organs in graft models.** A) Overall quantification of tumor volume changes compared with baseline tumor volume of double and triple combination (lorlatinib+anti-PD-1 and ALK DNA-based vaccine+lorlatinib+anti-PD-1, respectively); The combination of ALK DNA-based vaccine+lorlatinib+anti-PD-1 showed a great reduction of the tumor relapse after treatment suspension when compared to the double combination (lorlatinib+anti-PD-1) (lorlatinib+PD-1 vs ALK-DNA-Vax+ lorlatinib+PD-1,  $*P<0.0001$ , according to Mann-Whitney U test). B/C/D/E) Immunohistochemistry analysis of hALK expression in subcutaneous tumors and paired lungs. B/D) Immunohistochemistry of subcutaneous tumors treated with (B) lorlatinib+PD-1 and with (D) ALK DNA-based vaccine+lorlatinib+PD-1. In the double combination group (lorlatinib+PD-1), in 7 out of 9 mice, more than 80% of the subcutaneous tumor mass was hALK positive and in the triple combination 3 out of 8 mice were positive for hALK in less than 20% of the subcutaneous tumor mass. D/E) Immunohistochemistry analysis of hALK in paired lungs. In (D) the double combination, 5 out of 6 mice presented lung metastases that were positive for hALK and in (E) the triple combination no lung metastasis were detected (% lung metastasis: double combination vs triple combination; 83.3% vs 0%). ALK (D5F3): FDA-approved antibody for the diagnosis of ALK<sup>+</sup> NSCLC that recognizes specifically the human ALK; + Simultaneous administration.

*Figures Part II*

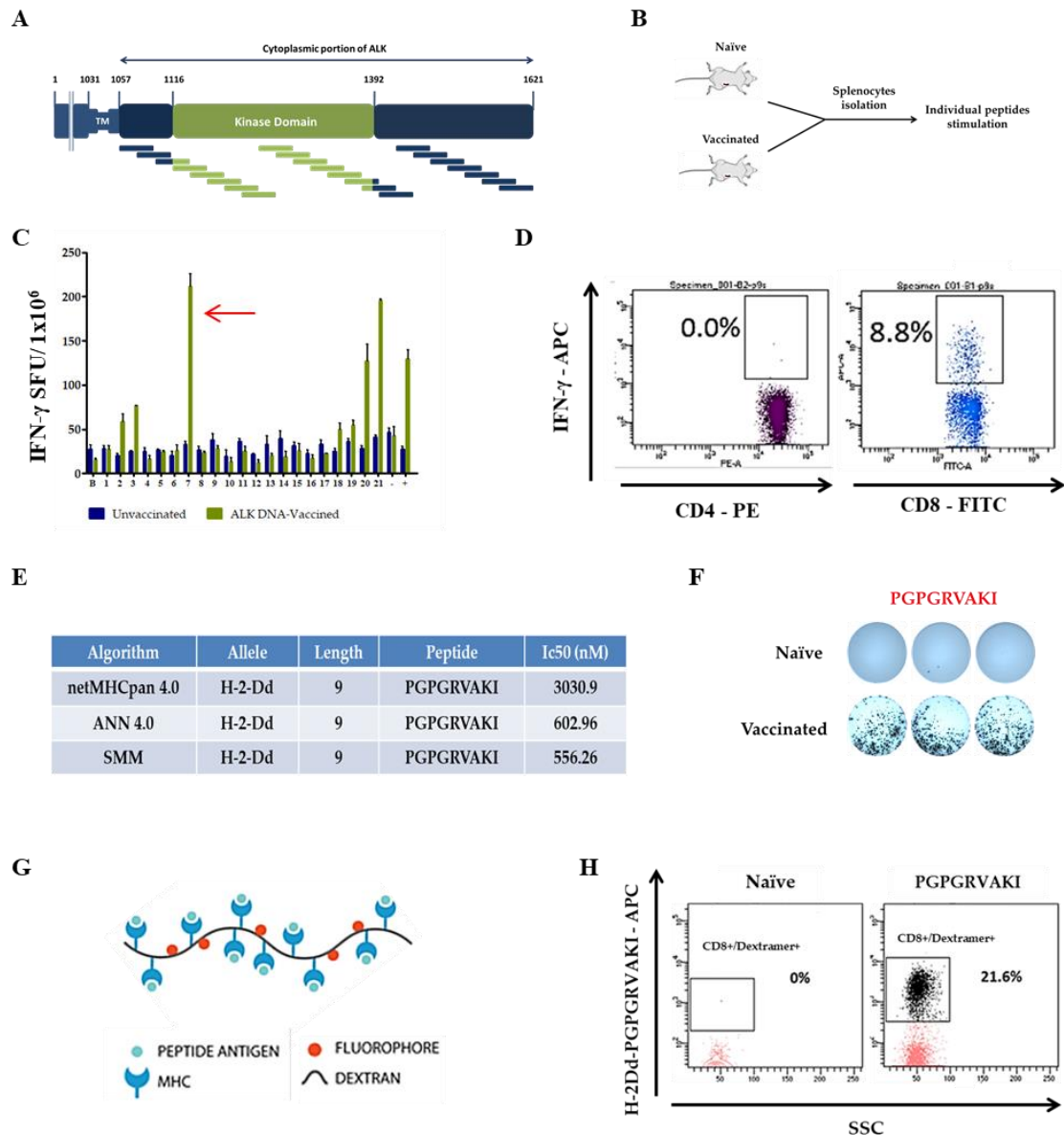


**Figure 36 – PGPGRVAKI is a MHC-I-restricted neoantigen in BALB/c background.** A) Schematic representation of the synthetic long peptide (SLP) screening method. A set of 21 long peptides were synthesized; each one 36 amino acids in length, covering the entire cytoplasmic portion of human ALK (hALK<sub>1058-1620</sub>). To ensure that every possible T-cell epitope was represented, each peptide overlapped 15 amino acids with the previous and following peptide. B) Schematic representation of the peptide *in vivo* screening. Splenocytes from ALK-vaccinated and non-ALK-vaccinated were collected and pulsed *in vitro* with the 21 synthetic long peptides individually and analyzed through an IFN- $\gamma$  ELISPOT assay. C) SLP7 presented 6.27 fold increase in the number of IFN- $\gamma$  number of spots compared to non-ALK-vaccinated mice. D) CD4 and CD8 discrimination. Dot blots represent splenocytes from an independent experiment where mice were vaccinated with SLP7, the splenocytes were isolated and pulsed *in vitro* with SLP7. After, *in vitro* stimulation, intracytoplasmic staining of IFN- $\gamma$  as well as CD4 and CD8 membrane staining were performed. The IFN- $\gamma$  staining in the CD8<sup>+</sup> compartment is representative of the CD8<sup>+</sup> T-cell activity against SLP7. E) Table summarizes the *in silico* analysis performed using three MHC-I-binding algorithms.

It was possible to predict that the 9mer PGPRVAKI peptide is the core of CD8<sup>+</sup> T-cell epitope, presented in H-2-Dd allele. F) IFN- $\gamma$  ELISPOT assay confirming that PGPRVAKI short peptide is able to elicit a T-cell response. G) Illustration of dextramer molecule. H) H-2-Dd-PGPRVAKI Dextramer staining performed in naïve and PGPRVAKI vaccinated mice. 21.6% of total CD8<sup>+</sup> splenocytes of PGPRVAKI-vaccinated mice recognize the short peptide.



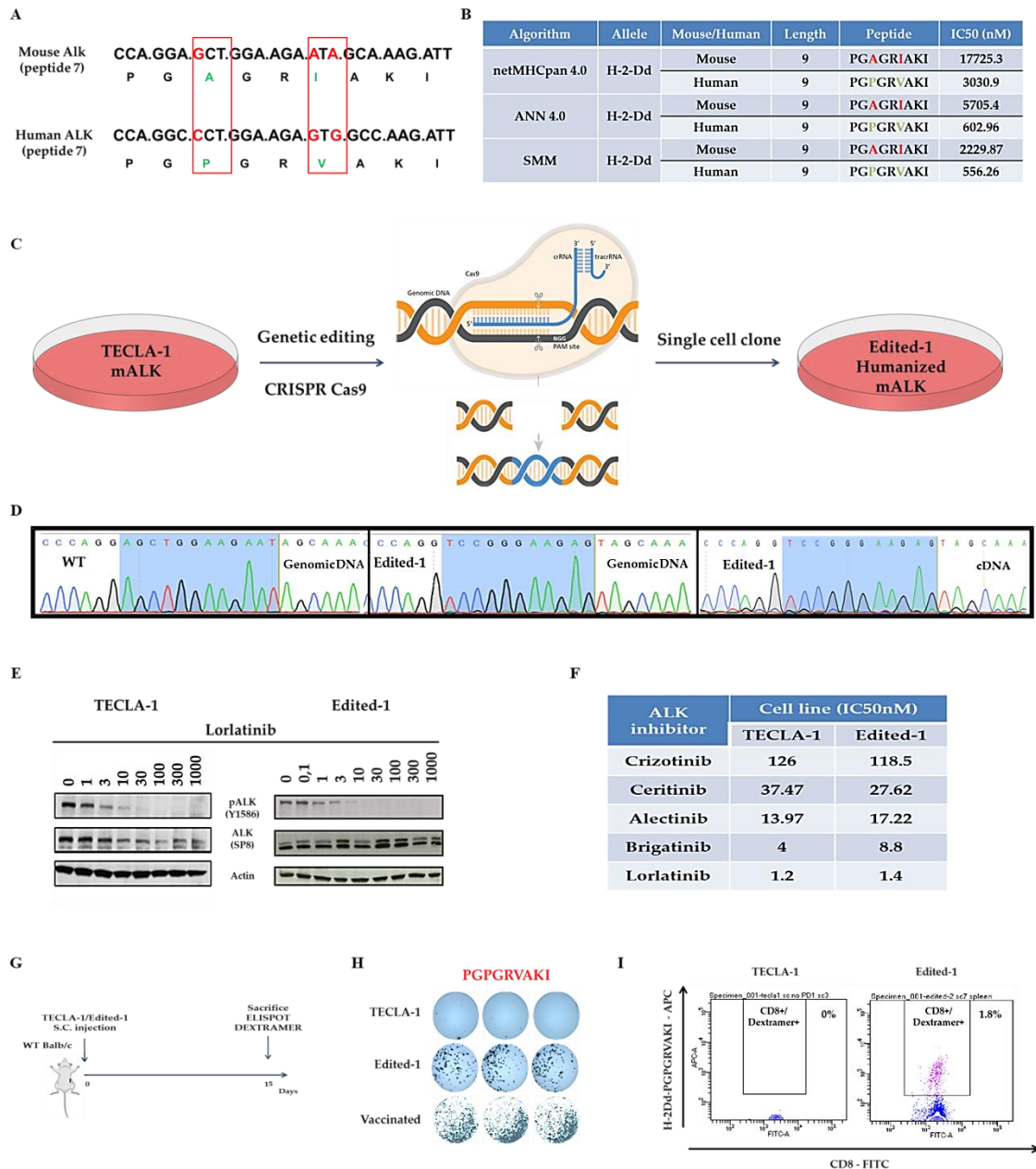


**Figure 37 –Humanized mouse ALK cell line (Edited-1) generation.** A) Mouse peptide 7 and human peptide 7 comparison. They differ in only two (2) amino acids in position 3 and 5 of the short 9mer ALK peptide 7. Genomic differences highlighted in red and amino acids highlighted in green. B) Table summarizes the *in silico* analyses performed using three MHC-I-binding algorithms. Both mouse and human ALK peptide 7 were compared. As human ALK peptide 7, mouse peptide 7 is predicted to bind H-2-Dd; however, the IC50 values are much higher compared to human ALK peptide 7. This IC50 result was consistent in all three (3) algorithms used (netMHCpan 4.0 mouse IC50 17725.3nM vs human IC50 3030.9nM; ANN 4.0 mouse IC50 5705.4 vs human IC50 602.96; SMM mouse IC50 2229.87 vs human IC50 556.26). C) Schematic representation of humanized mouse ALK cell line generation. TECLA-1 cell line, previously generated (carrying the endogenous mouse Eml4-Alk) was genetically modified in order to express the human peptide 7. Only the two (2) codons that generate the two (2) different amino acids were

edited. We have generated one (1) CRISPR breakpoint close to the region of interest. We also designed a crRNA crRNA that in 5' end contained a large template of the sequence we wanted to edit. The 3' end of the crRNA was complementary with a commercial available tracrRNA. Once matched, the tracrRNA stabilizes the crRNA. To avoid CAS9 off-targets, we have used CAS9 protein that has a life-time of only 4 hours. TECLA-1 was electroporated with the mixture solution, collected, washed and plated in fresh medium. Once recovered from electroporation, we performed single cell clones by consecutive dilutions. D) Chromatogram of the genomic DNA of TECLA-1 (left panel) and Edited-1 (central panel). The genomic sequence in Edited-1 contains the required changes. Chromatogram of the complementary DNA (cDNA) of Edited-1 shows that the RNA resultant from the edited genomic DNA carries the information that will be translated as a humanized mouse ALK protein. E) TECLA-1 and Edited-1 cells were treated with lorlatinib at the indicated concentrations for 6h. Total cell lysates were blotted with the indicated antibodies. F) TECLA-1 and Edited-1 cells were treated with increasing doses of crizotinib, ceritinib, alectinib, brigatinib and lorlatinib (1nM to 1µM) for 72h. Cell viability was assessed by CellTiter-Glo and the IC50 values were calculated. The table shows the different IC50 values to different ALK inhibitors from both TECLA-1 and Edited-1 cell lines. G) Schematic representation of the *in vivo* validation of Edited-1. Mice were injected with  $1 \times 10^6$  cells (both TECLA-1 and Edited-1, independently) into WT BALB/c mice. Mice were sacrificed at day 15 after tumor transplantation. H) IFN- $\gamma$ -ELISPOT assay picture which shows that, contrary to TECLA-1, Edited-1 generates a spontaneous IFN- $\gamma$ -induced response, even though weaker than the PGPGRVAKI-vaccine. I) Dot blots represent H-2-Dd-PGPGRVAKIdextramer staining in splenocytes of mice injected with TECLA-1 (left panel) and mice injected with Edited-1 (right panel).

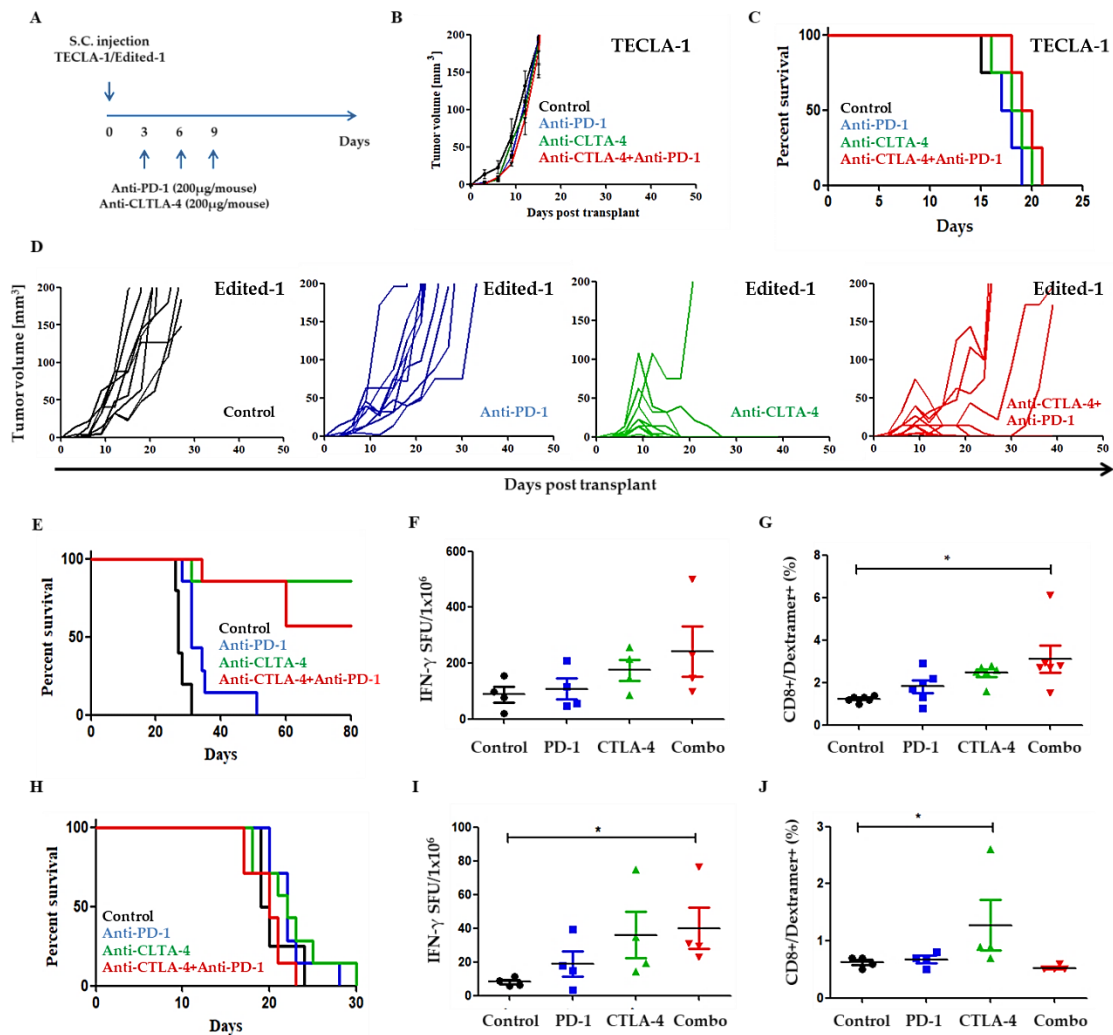


**Figure 38 – Tumor localization dictates the intensity of the immune response.** A) Schematic representation of the *in vivo* treatment. Mice were injected subcutaneously either with TECLA-1 or Edited-1 cell lines and treated with anti-PD-1, anti-CTLA-4 or combination (anti-PD-1+anti-CTLA-4) at day 3, 6 and 9. B) Graphic representation of the tumor volume (mm<sup>3</sup>) of TECLA-1 injected mice. C) Kaplan-Meier curves of overall survival of TECLA-1 injected mice groups. D) Graphic representation of the tumor volume (mm<sup>3</sup>) of Edited-1 injected mice. Each individual mouse is represented. First panel represents the tumor growth of untreated group (control), second panel represents the anti-PD-1 treated group, third panel represents the anti-CTLA-4 treated group and fourth group represents the combo (anti-PD-1+anti-CTLA-4) treated group. E) Kaplan-Meier curves of overall survival of Edited-1 injected mice treated groups. F) Graphical representation of IFN- $\gamma$  ELISPOT assay performed in isolated splenocytes from the four (4) treatment protocol applied in Edited-1 subcutaneously injected mice. G) Graphical representation of H-2-Dd-PGPRVAKI-dextramer staining performed in isolated splenocytes from the four (4) treatment protocol applied in Edited-1 subcutaneously injected mice (combo vs Ctrl, \* $P < 0.05$ , at 15 days after tumor transplantation, according to U-test). H) Kaplan-Meier curves of overall survival of orthotopic tumor transplantation. I) Graphical representation of IFN- $\gamma$  ELISPOT assay performed in isolated splenocytes from the four (4) treatment protocol applied in Edited-1 intravenously injected mice (combo vs Ctrl,

\* $P < 0.05$ , at 15 days after tumor transplantation, according to U-test). J) Graphical representation of H-2-Dd-PGPGRVAKI-dextramer staining performed in isolates splenocytes from the four (4) treatment protocol applied in Edited-1 intravenously injected mice (CTLA-4 vs Ctrl, \* $P < 0.05$ , at 15 days after tumor transplantation, according to U-test).

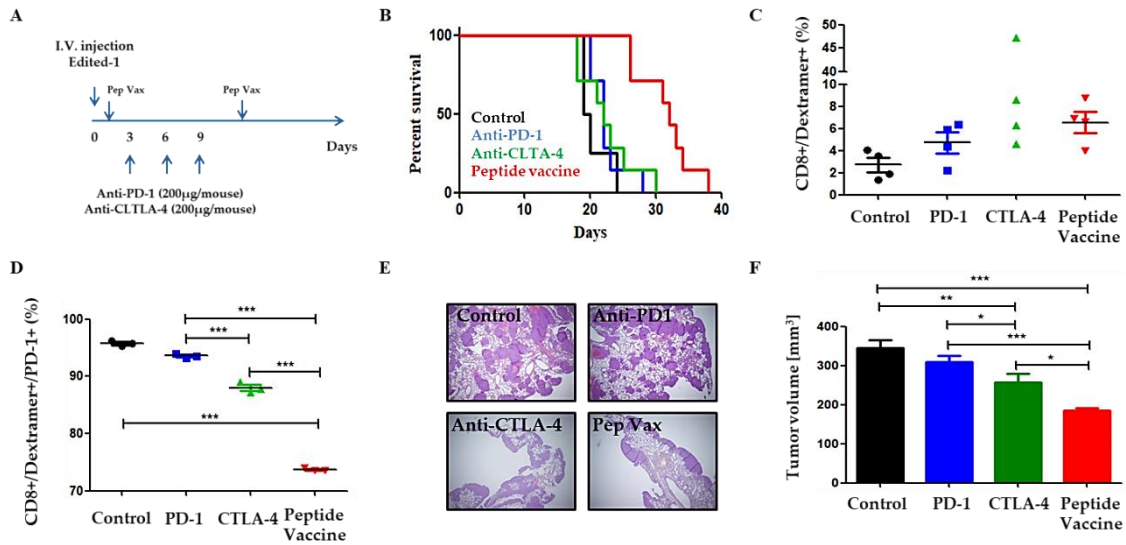


**Figure 39 – PGPRVAKI-peptide vaccine generates less exhausted intratumor CD8<sup>+</sup> T-cells.** A) Schematic representation of the *in vivo* treatment. WT BALB/c mice were injected intravenously with  $1 \times 10^6$  Edited-1 cells and subdivided into four (4) groups (untreated [control], anti-PD-1, anti-CTLA-4 and peptide-vaccine treated groups). Mice were treated with anti-PD-1 or CTLA-4 at day 3, 6, and 9 after tumor transplantation. Peptide-vaccination was performed at day 1 and 11 after tumor transplantation. B) Kaplan-Meier curves of overall survival of Edited-1 intravenously injected mice. Peptide-vaccine has roughly prolonged mice survival for 10 days when compared with the other groups. C) Graphical representation of H-2Dd-PGPRVAKI-dextramer staining performed in total lung cells harvested from the four (4) treatment protocols applied in Edited-1 intravenously injected mice. D) Graphical representation of the percentage of CD8<sup>+</sup>/Dextramer<sup>+</sup>/PD-1<sup>+</sup> in the tumor microenvironment (Ctrl vs peptide-vaccine,  $P < 0.001$  at 15 days after tumor transplantation, according to U-test; PD-1 vs CTLA-4,  $P < 0.001$  at 15 days after tumor transplantation, according to U-test; PD-1 vs peptide-vaccine,  $*P < 0.001$  at 15 days after tumor transplantation, according to U-test; CTLA-4 vs peptide-vaccine,  $*P < 0.001$  at 15 days after tumor transplantation, according to U-test). E) Histology of harvested lungs at day 15 after tumor transplantation. Upper panel on the left represents the control group; upper panel on the right represents the PD-1 treated group; the lower panel on the left represents CTLA-4 treated group; and finally, the lower panel on the left represents the peptide-vaccine treated group. It can be appreciated that both CTLA-4 and peptide-vaccine have a smaller tumor burden. Tumors seem to localize in the periphery of the lobes. F) Graphical representation of the tumor volume calculated by ImageJ (Ctrl vs peptide-vaccine,  $*P < 0.001$  at 15 days after tumor transplantation, according to U-test; Ctrl vs CTLA-4,  $*P < 0.01$  at 15 days after tumor transplantation, according to U-test, PD-1 vs peptide-vaccine,  $*P < 0.001$  at 15 days after tumor transplantation, according to U-test; PD-1 vs CTLA-4,  $*P < 0.05$  at 15 days after tumor transplantation, according to U-test; CTLA-4 vs peptide-vaccine,  $*P < 0.05$  at 15 days after tumor transplantation, according to U-test).

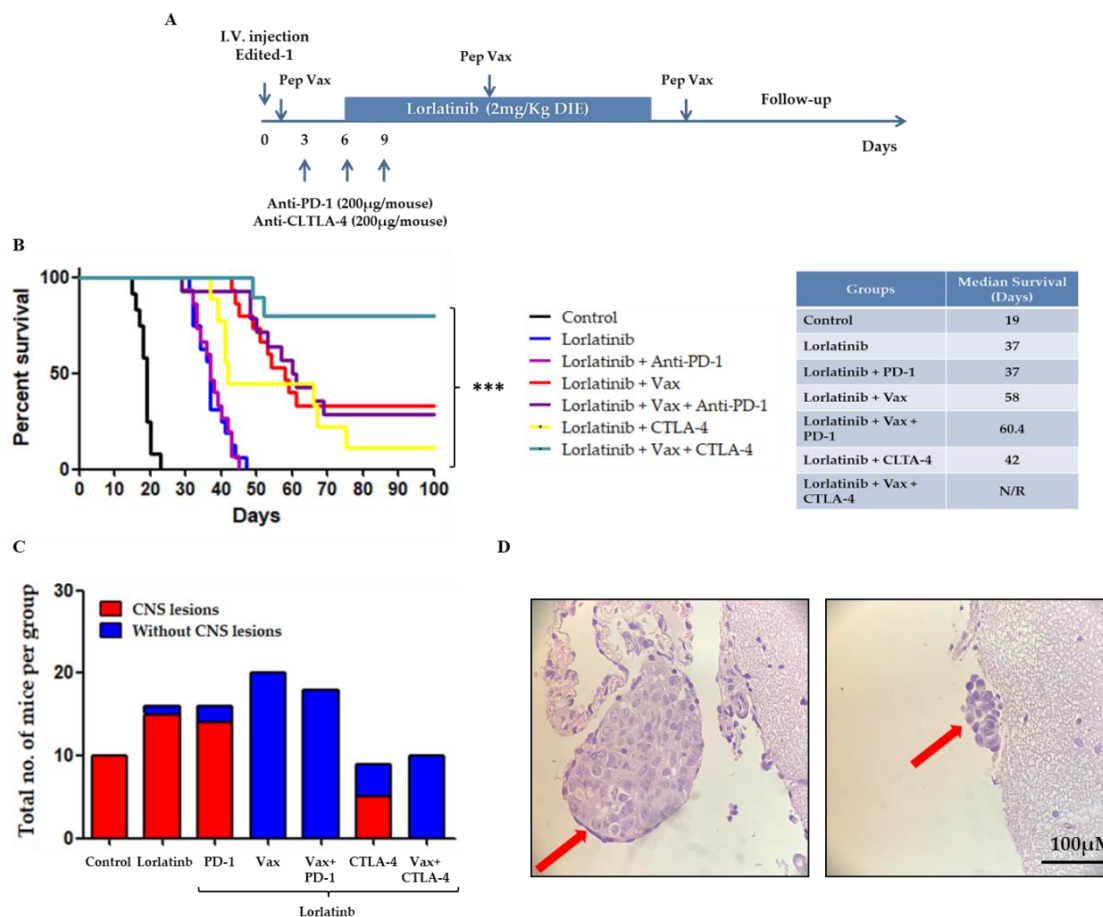


**Figure 40 - PGPGRVAKI-peptide vaccine in combination with a potent ALK inhibitor significantly extends mice overall survival and completely abrogates brain metastasis in orthotopic mouse models.**

A) Schematic representation of the therapeutic experiment protocol. Mice were injected with  $1 \times 10^6$  Edited-1 cells intravenously and divided into several groups (Untreated [control], lorlatinib alone, lorlatinib + PD-1, lorlatinib + peptide vaccine, lorlatinib + peptide vaccine + PD-1, lorlatinib + peptide vaccine + CTLA-4). Mice were vaccinated at day 1, 11 and 21 after tumor transplantation and treated with immune checkpoint inhibitors at day 3, 6, and 9 after tumor transplantation. Lorlatinib (2mg/Kg daily) was administrated from day 6 to day 19 after tumor transplantation by oral gavage. B) Kaplan-Meier curves of overall survival of therapeutic protocols. Vaccinated mice survival was significantly extended. Table presents the median survival (days) for each treatment group; N/R: Not Reached. C) Graphical representation of the total number of mice per group, with (red) and without (blue) brain lesions (i.e, control group, 10 animals were used and 10 animals developed brain metastasis [no blue color]). D) Representative histology of two (2) brain lesions from non-vaccinated mice.

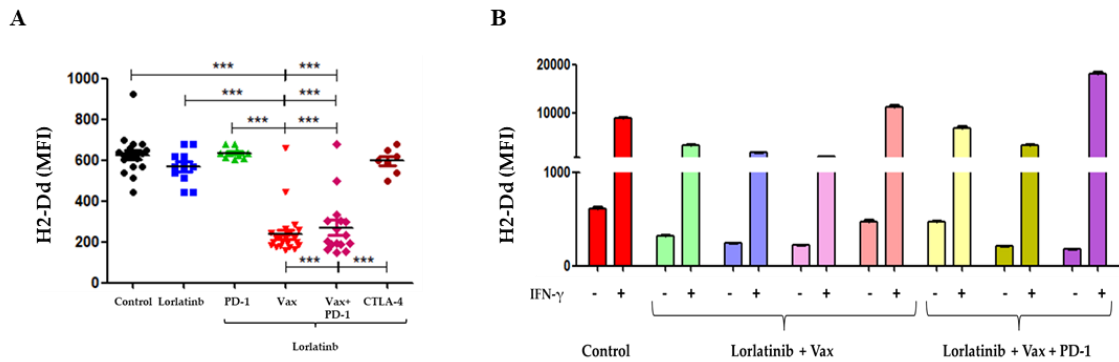


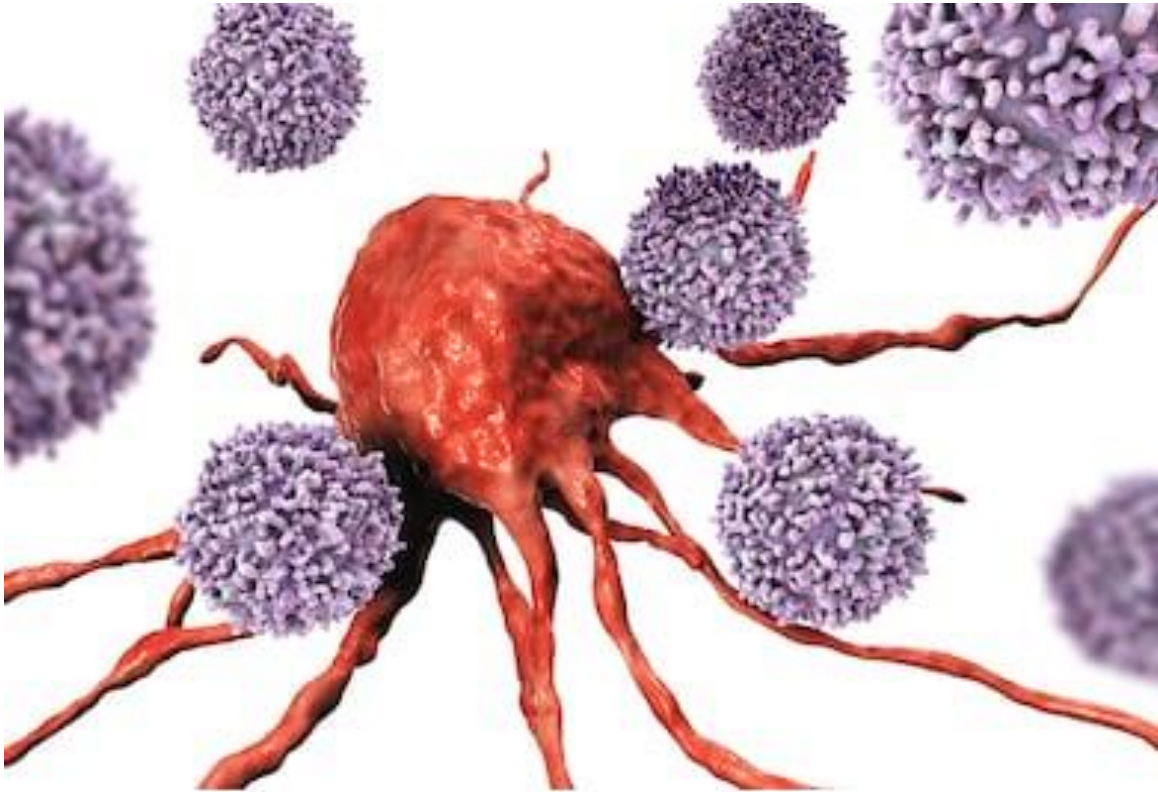
**Figure 41 - Tumors relapse in vaccinated mice due to reversible MHC-I loss.** A) Graphical representation of H2-Dd mean fluorescence intensity (MFI) in relapsed tumors (Ctrl vs lorlatinib + peptide vaccine,  $P < 0.001$  according to U-test; Ctrl vs lorlatinib + peptide vaccine + PD-1,  $*P < 0.001$  according to U-test; lorlatinib alone vs lorlatinib + peptide vaccine,  $*P < 0.001$  according to U-test; lorlatinib alone vs lorlatinib + peptide vaccine + PD-1,  $*P < 0.001$  according to U-test; lorlatinib + PD-1 vs lorlatinib + peptide vaccine,  $*P < 0.001$  according to U-test; lorlatinib + PD-1 vs lorlatinib + peptide vaccine + PD-1,  $*P < 0.001$  according to U-test; lorlatinib + CTLA-4 vs lorlatinib + peptide vaccine,  $*P < 0.001$  according to U-test; lorlatinib + CTLA-4 vs lorlatinib + peptide vaccine + PD-1,  $*P < 0.001$  according to U-test). B) Graphical representation of H2-Dd MFI upon *in vitro* stimulation of representative *ex vivo* cell lines with recombinant mouse IFN- $\gamma$ .





---

## Chapter V



*“Knowledge without transformation  
is not wisdom”*

Paulo Coelho

## **5. Discussion**



## 5) Discussion

### Part I

Lung cancer is the leading cause of cancer-related deaths worldwide. The American Cancer Society (ACS) has estimated about 228,150 new cases in the United States in 2019 [244]. Back in 2007, it was reported for the first time that 3-7% of NSCLC patients harbor the EML4-ALK fusion protein [64]. This fusion protein results in the constitutive activation of the tyrosine kinase domain of ALK protein, leading to the activation of downstream pathways that are related to cell proliferation, cell differentiation, and anti-apoptotic mechanisms [144, 157, 169].

The discovery of the gene fusion between ALK and EML4 (and latter other translocation partners of ALK were reported) led the scientific community to put a tremendous effort in the development of a series of ALK inhibitors. However, despite the remarkable initial effect of ALK inhibitors, their effect resulted to be transient and virtually all patients relapse due to resistant mechanisms that can be ALK dependent or independent, leading to cancer proliferation and disease progression [130].

Taken by surprise, the scientific community is now-a-days prompted to develop new strategies to overcome/prevent/delay resistance, and finally find the cure for these young patients.

One such therapeutic strategy is immunotherapy. By enhancing an effective immune response against tumor cells (that can include tumor vaccination, adoptive transfer of immune cells, and modifications of the immune system that unleash the already established immune response) [389], immunotherapy has been given tremendous results in the past few years in several types of cancer.

With the discovery of inhibitory pathways in immune cells, the so-called immune checkpoint inhibitors, NSCLC patients with high PD-L1 expression have been experiencing good responses to antibodies against PD-1/PD-L1 with an objective response rate of up to 20% [391, 393]. In general, patients with heavy smoking history have

better response than light or never smokers [394]. Several studies have correlated this therapeutic success with the high tumor burden characteristic of heavy smokers.

However, the therapeutic effect of immune checkpoint inhibitors in ALK-driven NSCLC is still unclear. Several *in vitro* studies have demonstrated that ALK regulates PD-L1 overexpression through STAT3 [672] in ALCL, and through activation of PI3K-AKT and MEK-ERK signaling pathways in NSCLC. Also, it has been demonstrated that ALK-driven NSCLC patients have higher frequency of tumor PD-L1 overexpression when compared with EGFR or KRAS-mutated disease [673, 674]. This overexpression of PD-L1, regulated by ALK activation, could be one requisite to make these patients suitable for immune checkpoint inhibitors therapy. Several clinical trials, that evaluate the effect of immune checkpoint inhibitors in ALK-driven NSCLC patients, are ongoing and the results are, however, controversial (NCT02574078; NCT02393625; NCT02584634, and NCT02013219). Actually, some clinical trials have been stopped even before the end of Phase I due to toxic effects generated by the combination of ALK inhibitors and immune checkpoint antibodies.

In this work, we described the therapeutic effect of ALK inhibitors, in particular lorlatinib, in mouse models of ALK-driven NSCLC, in combination with immunotherapy.

We have used three ALK-driven lung adenocarcinoma mouse models; a transgenic mouse model that expresses the hEML4-ALK fusion protein, CRISPR/Cas9-induced Alk-driven NSCLC mouse model, which expresses the mouse Eml4-Alk, and a graft mouse model where immortalized mouse cell lines harboring the mEml4-Alk, both m/hEML4-ALK or only hEML4-ALK were injected in syngeneic BALB/c.

In Tg hEML4-ALK mouse model, immune checkpoint blockade monotherapy has showed a slight, but statistically significant, efficacy in controlling the tumor relapse overtime, especially anti-PD-L1, suggesting the presence of an immunogenic antigen. However, when combined with a high dose of lorlatinib, immune checkpoint blockade does not show any effect in delaying tumor regrowth after treatment suspension. Nevertheless, when we used high doses of crizotinib, a less potent ALK TKI, immune checkpoint inhibitors have a modest, although not statistically significant, effect in delaying tumor relapse. This could be explained by the fact that

lorlatinib is a very potent ALK inhibitor. Using this specific high concentration, lorlatinib effect appears to be long-lasting and dominant and it is not improved by concomitant immunotherapy. Another aspect that we can hypothesize, is the fact that high concentrations of lorlatinib can hamper specific CD4<sup>+</sup>/CD8<sup>+</sup> T-cells that might be in the tumor microenvironment. The direct off-targets of lorlatinib are already described (LTK, FER and FES <sup>[327]</sup>), however, it remains to be clarified the effect of lorlatinib in the immune system.

In the crizotinib treated groups (where we could see a slight but not statistically significant effect), the administration timing of immune checkpoint inhibitors (either simultaneously or after ALK inhibitor administration) seems that does not affect the outcome of the treatment. We could have hypothesized that after ALKi treatment, tumors would have been smaller or inexistent, and the already mounted and putatively exhausted CD8<sup>+</sup> T-cell response would easily eliminated the residual tumor cells and/or avoid the formation of new tumor foci, once its activation status would have been restored by the immune checkpoint inhibitors. However, we faced a technical limitation. This mouse model is a transgenic model that expresses the human EML4-ALK fusion protein in the lung epithelium. Tumor formation is continuously ongoing during the lifespan of the mice, and therefore, newly formed tumors can mask possible results of the less potent ALK inhibitor crizotinib in combination with immune checkpoint inhibitors in a long-term follow-up. It will be very difficult if not impossible to evaluate long-term responses using this model.

However, we have observed that Tg EML4-ALK mice treated with low, but still clinically significant doses of crizotinib and simultaneous administration of immune checkpoint inhibitors have a smaller response rate at the end of the treatment and at 4 weeks follow-up, when compared with crizotinib alone. Nevertheless, this outcome is reverted in a longer observation period. At 8 weeks follow-up, we clearly see a shift in change from baseline, showing a slight, even though not statistically significant, advantage added by the administration of immune checkpoint inhibitors. It has been described in some ALK-negative NSCLC patients, who were subjected to immune checkpoint therapy, a phenomenon called pseudoprogression. This phenomenon is characterized by an increased tumor volume after immune checkpoint therapy that

overtime results in a better outcome. This tumor volume increase is due to the proliferation of re-activated T-cells in the tumor microenvironment [689]. We can argue that when Tg hEML4-ALK mice are treated with low doses of crizotinib in combination with immune checkpoint inhibitors, there is a local T-cell response and proliferation that by image, seems to be tumor progression but overtime turns out to present a better outcome. However, more studies are needed to testify this hypothesis.

Groups treated with low doses of lorlatinib alone or in combination either with anti-PD-1 or anti-PD-L1 are not conclusive, most likely because of the reduced number of mice.

By comparing high with low doses of ALK inhibitors we have observed that low doses of ALK inhibitors in combination with immune checkpoint antibodies seem to have stronger synergistic effects. For that reason, the next experiments were performed using low, but still clinically relevant, doses of crizotinib and lorlatinib.

With the complete tumor eradication in mind, something that was never achieved before, next we have used another mouse model. Immunocompetent BALB/c and C57BL/6 were infected intratracheally with adenovirus containing an Eml4 sgRNA and Alk sgRNA and Cas9 protein. Ten to twelve weeks upon adenovirus infection, mice have developed lung tumors bearing the mEml4-Alk fusion gene.

Unlikely Tg hEML4-ALK mice, Ad-EA mice are in principal curable once complete elimination of tumor cells is achieved. Only infected and correctly rearranged cells will give rise to neoplastic Alk-driven cells, and the non-tumor counterpart of the tumor microenvironment is preserved in this model. Also, the intratumoral heterogeneity originated in this model [687] should be taken in account as different treatment grades of response may occur as in humans. In this way, this mouse model seems to better recapitulate the human physiologic condition.

Differently from what was seen in Tg hEML4-ALK mouse model, in Ad-EA mice, anti-PD-1 or anti-PD-L1 treatment alone did not show any efficacy in blocking tumor regrowth. This has suggested us that CRISPR/Cas9 induced Eml4-Alk tumors could be less immunogenic than lung tumor in Tg hEML4-ALK mice.

Surprisingly, Ad-EA mice treated with crizotinib, showed a markedly insensitivity to this TKI. When compared with Tg hEML4-ALK, crizotinib is less

effective in controlling tumor growth and neither anti-PD-1 nor anti-PD-L1 brought any additional benefit at the end of the treatment or during follow-up. This observation might be explained by the fact that human and mouse ALK kinase domains are highly similar but not identical. In particular, human and mouse ALK differ in 2 amino acids in the predicted crizotinib binding site [108, 151]. These two amino-acids could confer a different tertiary structure to the mAlk protein, and therefore hamper the crizotinib binding. However, crystallography studies of the mouse Alk tyrosine kinase domain are necessary to confirm this hypothesis. Due the fact that Ad-EA mice have poorly responded to crizotinib, the possible synergistic effect with immune checkpoint inhibitors could not be assessed.

However, when Ad-EA mice were treated with low doses of lorlatinib alone, we observed almost complete tumor shrinkage, proving the efficacy of lorlatinib overcoming resistance to first- (and second-) generation of ALK inhibitors.

Surprisingly, we observed a clear advantage when lorlatinib was combined with anti-PD-1, but not with anti-PD-L1, at 4 weeks after treatment suspension. The right drug effect (more potent than crizotinib), dosage (lower concentration might not hamper the existent T-cell response), and a more appropriate mouse model (in principal curable and closer to the human physiologic condition) may have reunited the right conditions for the synergistic effect of lorlatinib and PD-1 antibodies. Nevertheless, this effect was lost at 8 weeks follow-up, likely because when treatment was suspended, possible residual tumor cells rapidly relapsed, which suggested that a long-term treatment protocol of lorlatinib could be beneficial.

The different responses between combinations of lorlatinib+anti-PD-1 and lorlatinib+anti-PD-L1, could be explained by the low expression of PD-L1 by tumor cells (data not shown), or the different potency of the antibodies. But can also be explained by the fact that PD-1 has another less described ligand, PD-L2, which as PD-L1 is expressed not only in tumor cells, but also APCs, macrophages and monocytes. It plays a crucial role in modulation of T-cell response, proliferation and might play a role in tumor immune escape. However, unlike PD-L1, PD-L2 is usually less expressed in the tumor microenvironment but it has higher affinity for PD-1. This can explain the fact that we have obtained better results when anti-PD-1 antibodies were used;

blocking only PD-L1 could not be enough since PD-L2 has similar functions; however, blocking PD-1 avoids its activation by both ligands [690].

Based on these results, we then aimed to complete eradicate tumor cells that remain after 15 of treatment by extending lorlatinib administration. Ad-EA mice were enrolled into two long-treatment protocols (one month of lorlatinib treatment; two months of lorlatinib treatment). Each arm was subsequently subdivided in 3 different groups according to the PD-1 administration (none, 15 days or one month – 5 injections each).

Not surprisingly, we observed that in both treatment arms (lorlatinib 1 and 2 months), CRISPR/Cas9-induced tumors showed almost complete regression at the end of both protocols. Also, either at 4 or 8 weeks after treatment suspension, the relapse rate was similar in both long-term protocols; not showing any advantage provided by the 2 months vs the 1 month long-term treatment protocol. This has suggested that naturally lorlatinib resistant cells may exist in the context of Ad-EA mice tumor microenvironment. Moreover, at the end of 2 months of lorlatinib treatment, we could observe that there was a wider range of responses to lorlatinib, which can either indicate that some tumors never completely respond to the treatment, maintaining a constant volume during treatment, or lorlatinib treatment has completely eliminated those sensitive clones and the naturally resistant clones have emerged. Even though lorlatinib is the most potent ALK inhibitor available in the clinical practice, and the last receiving FDA approval, Recondo G. and colleagues, have already described diverse biological mechanism that lead to lorlatinib resistance, such as epithelial-mesenchymal transition, compound mutations (L1196M/D1203N, F1174L/G1202R and C1156Y/G1269A), and novel bypass mechanism of resistance caused by NF2 loss-of-function mutation, which confers sensitivity to mTOR inhibitors [354]. Even though we did not analyze this matter, we cannot discard the possibility that 2 or even 1 month of lorlatinib treatment at low concentrations have selected lorlatinib resistant clones. One aspect that can support this hypothesis is the fact that, after treatment suspension, both lorlatinib arms had the same overall survival, indicating that the selection of lorlatinib resistant clone has happened before the 1 month treatment was completed.



In the groups treated with lorlatinib in combination with anti-PD-1, complete tumor regression was also reached. We also observed that both long-term lorlatinib treatments combined with 1 month of PD-1 administration, have shown a statistically significantly slower relapse rate at 4 weeks follow-up when compared with tumors treated with lorlatinib alone. These results confirmed previous observations and suggested that immune checkpoint therapy when combined with ALK inhibitors has a minor and transient effect that is lost in a long-term follow-up.

In order to optimize a mouse model for the study of the immunologic complexity inherent to ALK<sup>+</sup> NSCLC, two CRISPR/Cas9-induced immortalized mouse cell lines resembling human NSCLC cell lines were established. Both TECLA-1 and TECLA-2 express the mouse Eml4-Alk, are sensitive *in vitro* and *in vivo* to lorlatinib, express PD-L1 and generate tumors when injected into syngeneic BALB/c mice. These cell lines are an advantage for our purposes, not only because handling cell lines is easier, faster and cheaper, but also because we could control the tumor burden by injecting more or less cells.

However, when mice bearing subcutaneous tumors derived from TECLA-1 or TECLA-2 cell lines were enrolled in treatment protocols similar to what we previously have done, we verify that the cell lines behaved differently from what we expected and actually responded poorly to the treatment.

Even though TECLA-1 and TECLA-2 untreated tumors have similar change from baseline, TECLA-1 subcutaneous tumors have reached the 5mm diameter threshold faster than TECLA-2 (10 days vs 15 day; data not shown), and the same is observed *in vitro* (data not shown). Also, TECLA-1 has a fibroblast-like morphology and TECLA-2 presents an epithelial-like morphology (data not shown). Putting these facts together, we can postulate that TECLA-1 is more aggressive than TECLA-2. For this reason, we were not surprised to observe that TECLA-2 had a much slower tumor relapse rate than TECLA-1. But what really has puzzled us was the fact that subcutaneous tumors derived from TECLA-1, when treated with anti-PD-1 alone, grew faster than the untreated controls. However, the same was not observed in TECLA-2. Due the fact that the tumor volume did not decrease during follow-up, we have discarded the hypothesis of pseudorelapse as we postulated for Tg hEML4-ALK mice

when treated with crizotinib in combination with anti-PD-1. The TECLA-1-induced tumor progression as a result of PD-1 monotherapy remains to be clarified.

In both cell lines, we did not observe a statistically significant change in the relapse rate after treatment with lorlatinib in combination with anti-PD-1. This fact has suggested that mouse Alk-driven NSCLC cell lines are less immunogenic than Tg hEML4-ALK and Ad-EA mice, most likely because they have been subjected to two different selections (*in vivo* and *in vitro*). For that reason, we decided to include a more potent antigen by transducing TECLA-1 with the hEML4-ALK. The introduction of hEML4-ALK not only has reversed the outcome of anti-PD-1 treatment alone, but it also has prolonged the progression-free survival of the mice after treatment (both lorlatinib arms). And when both lorlatinib cohorts were compared, the addition of anti-PD-1 has clearly added a benefit. It seems that hTECLA-1 responds better to immune checkpoint monotherapy than TECLA-1 expressing only the mouse Alk, which means that strong antigens will respond better to immune checkpoint inhibitors. The hTECLA-1 was obtained by simply transducing the hEML4-ALK and no single cell clones were obtained, meaning that the bulk population was used for the *in vivo* experiments. In a normal viral transduction, we cannot control the number of viral copies that every single cell acquires. This means that naturally, in a bulk population as hTECLA-1, we will find subpopulations with different hEML4-ALK expression grades. We then hypothesized that subcutaneous tumors treated with the double combination would have been selected under immune pressure and the subpopulation that had survived would express less hALK than subcutaneous tumors treated with lorlatinib alone. However, when the tumors from both arms were analyzed by immunoblot, we verified that the hALK expression was lost in both arms, suggesting that a hEML4-ALK was an antigen strong enough to be eliminated by the spontaneous immune response that generates. To confirm this theory and discard any technical issue with the viral infection, we next injected subcutaneously hTECLA in immunocompromised (NSG) and immunocompetent (BALB/c) mice and analyzed the spontaneous immune response of BALB/c by comparing hALK expression in both immune environments. Not only tumors grew faster in NSG (where tumor cells are not

exposed to the immune pressure) but also only cells with weaker expression of ALK were selected in BALB/c immunocompetent mice.

When we knocked out the mALK from hTECLA-1 cell line (so no tumors cells could escape by losing hALK and keeping the signaling with mAlk), and boosted the immune system with an ALK-DNA-based vaccine combined with lorlatinib+PD-1, we observed that a strong immune response was induced in this graft mouse models, significantly reducing tumor relapse after treatment suspension. In this context, the ALK DNA-based vaccine turns ALK-driven NSCLC tumors more suitable for immune checkpoint therapy by increasing the number of cytotoxic CD8<sup>+</sup> T-cells in the tumor microenvironment <sup>[397]</sup>. It is known that not only the PD-L1 expression but also tumor-infiltrating lymphocytes (TILs) correlate with the efficacy of immune checkpoint inhibitors and ALK-driven NSCLC display a tumor microenvironment in which PD-L1 is expressed through ALK signaling and TILs are low. By increasing the absolute number of TIL in the tumor microenvironment through ALK-DNA-based vaccine <sup>[397]</sup>, anti-PD-1 has a preponderant effect in controlling the tumor relapse. Moreover, it has been described by our group that ALK-DNA-based vaccine has a maximum effect when the tumor burden is low <sup>[402]</sup>, explaining the fact that mice treated with triple combination did not develop metastasis in distant organs. The possible low numbers of tumor circulating cells that have escaped from the primary tumor were likely killed by the CD8<sup>+</sup> T-cell response elicited by the ALK DNA-vaccine.

Overall, these results suggest that the triple combination of lorlatinib, PD-1 blockade and ALK-DNA-based vaccine could work efficiently in the clinical setting, generating a strong and long-lasting immune response against ALK<sup>+</sup> in NSCLC.

## Part II

The discovery of ALK rearrangements in 5-7% of NSCLC patients in 2007 <sup>[64]</sup> brought a new hope for the treatment of these young patients. A tremendous effort was done by the scientific community in order to develop small molecules that would have the capacity to inhibit such a strong oncodriver. However, ALK inhibitors resistance came in as a pitfall difficult to solve. Several generations of ALK inhibitors (more specific and potent) were developed in consecutive years, however, what really took the scientific community by surprise was the fact that, even with the most potent ALK inhibitor (third-generation ALK inhibitor lorlatinib), ALK-driven cancer cells invariably develop resistance (throughout several resistance mechanism that can be either ALK-dependent or independent), leading to cancer proliferation and disease progression. It seems that the stronger the ALK inhibitor it is, the stronger and more complicate the mechanism of resistance tends to be. Besides the emergence of compound mutations causing resistance to lorlatinib, the spectrum of biologic mechanisms that drives resistance is enormous and sometimes, the same patient can harbor more than one mechanism of resistance. This represents a significant barrier to the successful treatment of ALK-driven patients. Therefore, the development of strategies to overcome/prevent/delay resistance is priority. These potential new approaches have the promise to improve the treatment of ALK-driven patients. One such therapeutic strategy is immunotherapy.

Immunotherapy aims to establish or enhance an effective immune response against tumor cells. Several strategies have been already developed, such as tumor vaccination, adoptive transfer of immune cells, and modification of the immune system to boost an already established immune response <sup>[389]</sup>. With the discovery of inhibitory pathways in immune cells, the so-called immune checkpoint, and the development of antibody-based blockades against these checkpoint molecules, such as anti-CTLA-4 and anti-PD-1/L1, cancer immunotherapy has entered in a new era <sup>[390]</sup>.

NSCLC patients with high PD-L1 expression have been experiencing good responses to immune checkpoint inhibitors against PD-1 with an objective response rate up to 20% [391-393]. It has also been observed that patients with heavy smoking history have better responses than those with light- or never-smokers records [394]. These differences may be due to the fact that smokers usually harbor higher mutational burden and thus have a higher number of expressed neo-antigens than non-smokers. Also, the tumor microenvironment in smokers is characterized by an increased frequency of active tumor-infiltrating CD8<sup>+</sup> T-cells as well as increased levels of anti-tumor cytokines such as IFN- $\gamma$  and granzyme, while the tumor microenvironment in non-smokers shows elevated immunosuppressive features such as a high number of FoxP3<sup>+</sup> regulatory T-cells, the accumulation of M2-like macrophages and less activated effector CD8<sup>+</sup> T-cells.

As mentioned before, ALK-driven NSCLC patients are non- or light-smokers which may represent a lower number of non-synonymous mutations than other subtypes of NSCLC [396]. Several clinical trials in which the effect of immune checkpoint inhibitors in these patients was evaluated, as well as our previous results discussed in Part I, have shown minimal responses [391-393]. Experimental evidences have demonstrated that ALK-driven NSCLC patients harbor an immunosuppressive tumor microenvironment with a low number of CD8<sup>+</sup> T-cell with exhausted phenotype [397], and also, PD-L1 expression in tumor cells is regulated through ALK signaling. This scenario raises questions regarding ALK immunogenicity. An immunologic desert as this here described might be the result of a strong immunoediting where the consequential tumor does not present tumor associated antigens or neo-antigens, and therefore invisible to the immune system. However, in the literature is possible to find several evidences that ALK generates *per se* an immune response. For instance, the presence of anti-NPM-ALK antibodies in ALCL patients has been extensively reported [400]; another example, two HLA-A2.1 restricted CD8<sup>+</sup> T-cell epitopes, p280-289 (SLAMDLLHV) and p375-389 (GVLLWEIFSL) from the ALK kinase domain, were identified and confirmed to be immunogenic in HLA-matched ALCL and neuroblastoma cell lines [401]. In principal, these peptides could be used for vaccination in ALK-driven tumors. In fact, our group has shown in 2008 that ALK-DNA-based

vaccination with a vector encoding the entire cytoplasmic domain of human ALK protects mice from local and systemic lymphoma growth in graft models. In this graft models, human NPM-ALK is transduced in lymphoma mouse cell lines and presented to naïve BALB/c mice. In this work conducted by Chiarle, our group has reported that the protection given by the ALK-DNA-based vaccine is potent and durable by eliciting and ALK-specific IFN- $\gamma$  response and CD8<sup>+</sup> T-cell-mediated cytotoxicity [402]. These results have confirmed the immunogenicity of the ALK protein. Nevertheless, this immunogenicity can be questioned due to the fact that most likely, the human ALK protein functioned as a neoantigen to the mouse immune system. Mouse and human ALK show 87% overall homology at the protein level, and more importantly, within the kinase domain they differ at only four amino acids. Also, human ALK contains one extra tyrosine residue, Tyr 1604, which has been implicated in tumor progression [115]. Even though minor, these differences at the protein level could act as neoantigens and justify the strong immune response elicited by the ALK-DNA-based vaccine in lymphoma graft models. Like human ALK, mouse Alk is indeed expressed in normal somatic cells, even though in very low amounts and in specific regions of the central nervous system. By being expressed, mouse-ALK-specific CD8<sup>+</sup> T-cells must have been selected in the thymus. The use of lymphoma grafts models potentially introduces other peptides that are not targeted by those mouse-ALK-specific CD8<sup>+</sup> T-cells, generating the expansion of other CD8<sup>+</sup> T-cells clones. In this case, this lymphoma mouse model would not be close to the human condition in which human ALK is expressed in low levels throughout life, generating human-ALK-specific CD8<sup>+</sup> T-cells that will target the ALK-driven tumor cells when the tumor develops. However, this issue was solved by our group in 2015 [397] when we described the efficacy of the ALK-DNA-based vaccine in lung cancer graft models and transgenic mouse model that express human EML4-ALK. In this transgenic mouse model, the human EML4-ALK fusion gene is under the SP-C promoter. SP-C protein is expressed in the mouse lung epithelium for the first time at the end of embryogenesis throughout the mouse life, which means that hEML4-ALK is expressed early on; however, lung tumors are only visible through MRI when mice are 12 weeks old. These results have suggested us that ALK protein can function as both neoantigen and tumor associated antigen. In both

cases, a strong ALK-specific CD8<sup>+</sup> T-cell response is elicited and capable of tumor reduction in graft and transgenic mouse models.

Some specific characteristics make ALK a potentially relevant tumor antigen. First, and as mentioned above, ALK is expressed by normal somatic cells in low amounts and in specific regions of the central nervous system. Therefore, activated anti-ALK-specific CD8<sup>+</sup> T-cells are unlikely to react against normal cells due to the low amount of ALK expression. Second, ALK is required for the transformation and maintenance of neoplastic cells and thus, the immune escape of tumor cells lacking ALK expression is unlikely, and finally, ALK-positive tumors, driven either by point mutations, ALK amplifications or chromosomal translocations, have the cytoplasmic portion of ALK in common, meaning that an ALK personalized immune response approach could cover several types of tumors.

Driven by all these premises, in the second part of my Ph.D. thesis, we aimed to identify the specific(s) ALK-peptide(s) responsible for the immune response generated through ALK-DNA-based vaccination. The identification of such peptide(s) would be a milestone for a more personalized medicine, as well as for our understanding of the immune reaction that is elicited.

For that, we have performed an *in vitro* screening using isolated splenocytes from mice immunized with the ALK-DNA-based vaccine, used in previous experiments. A set of 21 synthetic long peptides (SLP) were produced; each one 36 amino acids in length, covering the entire cytoplasmic portion of ALK (hALK<sub>1058-1620</sub>). Since MHC-I typically present peptides between 8-11 amino acids; each synthetic long peptide overlapped 15 amino acids with the previous and following peptide to ensure that every possible T-cell epitope was represented. We have identified 5 SLP (SLP2, SLP3, SLP7, SLP20 and SLP21) that elicited an IFN- $\gamma$ -induced reaction; four of each (SLP2, SLP3, SLP20 and SLP21) elicited a CD4 type of response and only one (SLP7) presented to be a specific CD8<sup>+</sup> T-cell epitope. Even though for the scope of this Ph.D. thesis only ALK-specific CD8<sup>+</sup> T-cells were further analyzed, it is important to mention that ALK-specific CD4<sup>+</sup> T-cells have been largely reported in the literature. The presence of IgG antibodies and CD8<sup>+</sup> memory T-cells against ALK in patients has suggested the involvement of CD4<sup>+</sup> T-cells in the ALK immunologic landscape [662-663].

Even though no further studies were performed regarding the nature of the CD4<sup>+</sup> T-cell immune response observed in our peptide screening, it is important to reference that our group has previously characterized the spontaneous humoral immune response in patients with ALK-rearranged NSCLC. We have developed an enzyme-linked immunosorbent assay (ELISA) to measure anti-ALK antibody levels and mapped specific peptide epitope sequences within the ALK cytoplasmic domain [662]. Across individual patients, anti-ALK antibodies recognized different epitopes in the ALK cytoplasmic domain, most of which clustered outside the tyrosine kinase domain, the same regions the four CD4<sup>+</sup> T-cell epitopes we have identified in our screening (SLP2, SLP3 and SLP20, SLP21) were located. This might suggest that these CD4<sup>+</sup> T-cell epitopes are responsible for a Th2-induced response. However, this hypothesis warrants further investigation.

Once identified the precise CD8<sup>+</sup> T-cell core epitope through MHC-I epitope-binding algorithms, we realized that the mouse ALK was significantly less immunogenic than the human ALK. For that reason, and aiming the establishment of a proper mouse model, we have genomically modified the mouse ALK in order to express the immunogenic peptide-7.

The generation of Edited-1 was a tremendous achievement for the scope of this Ph.D. thesis. Edited-1 represents the closest we can get to the human condition. The syngeneic mouse model we have developed turned possible the study of the immune value of ALK, and generated convincing results worth of clinical translation.

After the generation of Edited-1, and being sure that Edited-1 was, indeed, able to generate a spontaneous and measurable CD8<sup>+</sup> T-cell immune response in BALB/c background, we aimed a more comprehensive view of the effect of immune checkpoint inhibitors in the spontaneously established CD8<sup>+</sup>-specific immune response. For that, we have used a classical immune checkpoint inhibitors treatment approach by injecting Edited-1 subcutaneously into WT BALB/c mice and treating mice either with anti-PD-1, anti-CTLA-4 or both combined at days 3, 6 and 9 after tumor cells injection. As observed in previous experiments, anti-PD-1 treatment alone did not provide a significant advantage. A slight effect was observed around day 10 after tumor cells injections, but was immediately lost right after. However, when treated with anti-



CTLA-4 only one mouse developed subcutaneous tumor. All other mice reached a tumor volume pick around day 10 and by day 30 after tumor transplantation were found tumor-free. As it was mentioned before, T-cell activation is a process that requires more than one stimulatory signal. TCR binding to MHC-I provides specificity to T-cell activation; however, further costimulatory signals are required. The binding of CD80 or CD86 molecules on APC with CD28 molecules on the T-cells leads to a positive signal within T-cells. Sufficient levels of CD28:CD80/6 binding lead to T-cell proliferation, increased T-cell survival and differentiation. CTLA-4 is a CD28 homolog with much higher binding affinity to CD80/6 molecules. However, differently from CD28, CTLA-4:CD80/6 binding does not provide a stimulatory signal. Consequently, this competitive binding can prevent the costimulatory signal normally provided by CD28:CD80/6 binding [622, 624, 625]. The relative amount of CD28:CD80/6 binding vs CTLA-4: CD80/6 binding determines whether a T-cell undergo into activation or anergy. PD-1 is a member of the B7/CD28 family of costimulatory receptors. It regulates T-cell activation through the binding to its ligands PD-L1 and PD-L2. Like CTLA-4, PD-1 inhibits T-cell proliferation, IFN- $\gamma$ , TNF- $\alpha$  and IL-2 production, reducing T-cell survival [636]. If a T-cell experiences coincident TCR and PD-1 binding, PD-1 generates signals that prevent phosphorylation of key TCR signaling molecules which ends in early “exhausted” T-cells that have experienced high levels of stimulation or reduced CD4<sup>+</sup> T-cell help [618]. This exhaustion state that is known to occur during chronic infection and cancer is characterized by T-cell dysfunction that ultimately results in suboptimal control of infections and tumors. Both CTLA-4 and PD-1 binding have similar negative effects on T-cell activity, however, the timing of downregulation, the responsible signaling mechanism, and the anatomic location of immune inhibition of these two immune checkpoints are different. Unlike CTLA-4 (which is confined to T-cells), PD-1 is broadly expressed on activated T-cells, B-cells, and myeloid cells [636,637]. CTLA-4 functions during the priming phase of T-cell activation, whilst PD-1 functions during the effector phase, which is predominantly within peripheral tissues [636]. Putting together these facts, and analyzing here described, we can postulate that in normal conditions, when ALK-peptides are presented, CTLA-4 exerts a predominant effect in controlling T-cell activation. However, it is worth mention that CTLA-4

blockage has a wider spectrum of action in the immune regulation, which can explain the higher incidence of immune-mediated adverse events that patients treated with anti-CTLA-4 can experience.

However, when combined (anti-PD-1 + anti-CTLA-4), a larger number of mice developed subcutaneous tumors after treatment when compared to anti-CTLA-4 alone. Even though this issue was not addressed, we can hypothesize that this difference is due to the fact that both antibodies (anti-PD-1 and anti-CTLA-4) are Rat IgG and not mouse IgG, and therefore, can elicit an immune reaction against them in mouse background. In this particular group (combination of anti-PD-1 and anti-CTLA-4), double concentration (200µg of anti-PD-1 + 200µg of anti-CTLA-4) was used in each injection which might have increased the exposure of Rat epitopes. Having an immune reaction mounted against the antibodies could have affected the synergistic effect of this combination. However, further studies are needed to fully understand this issue.

Amazed by the results obtained in this classical approach of graft tumors, we then analyzed the effect of immune checkpoint inhibitors in an orthotopic model. WT BALB/c mice were injected intravenously with Edited-1 cells and around day 6 after tumor transplantation, tumor cells have niched in the lungs and formed tumor foci. The same therapeutic scheme was used as previous. However, the results obtained were far from the expected. All mice, from all treatment groups, have died due to respiratory failure around day 20 and 25 after tumor transplantation. Anti-CTLA-4 treatment, which in skin graft models has completely abrogated the tumor formation, had none effect in lung microenvironment. These results suggest that different organs establish different immune responses that might be a consequence of a more or less immunosuppressive microenvironment. Although these results were not further investigated, we can hypothesize that the lung microenvironment may be, *per se*, a more immunosuppressive (M2-like macrophages, Treg cells) organ in which only strong peptides will elicit an immune response in order to avoid exacerbated immune reactions that could hamper the vital function of the lung. Another hypothesis that we can postulate is the composition of the immune repertoire in both organs. One way to analyze this matter is through single cell RNA-sequencing and ultimately the comparison of both landscapes. And finally, would also be important to understand if

these particular results are or are not antigen-dependent. For that, several other peptides should be compared in the same conditions.

Even though these results are far from being understood, it is worth mention that historically, this type of therapeutic approaches has been performed in skin graft models, independently of the origin organ of the tumor that is scope of study, which might represent a serious concern; are we interpreting correctly the historically results obtained from this skin graft model?

Next, we hypothesized that increasing the number of CD8<sup>+</sup> T-cells in the lung tumor microenvironment through peptide-7-vaccination would turn the lung microenvironment into a more immune responsive environment and bring a significant benefit to the overall survival of the mice. Indeed, peptide-7-vaccine has slightly extended mice survival for 10 days, when compared with the remain groups. However, when the CD8<sup>+</sup> T-cell lung infiltrate was analyzed, we have noticed that, contrary to what we were expecting, peptide-7-vaccine did not substantially increase the overall number of ALK-specific-CD8<sup>+</sup> T-cells. However, when the exhausted markers were analyzed through flow cytometry (PD-1 expression), we were surprised to see that peptide-7-specific CD8<sup>+</sup> T-cells infiltrating the lung microenvironment in anti-CTLA-4 treated and peptide-7-vaccinated mice expressed lower levels of PD-1 when compared to untreated mice or anti-PD-1 treated mice. These results suggested that better priming (either with anti-CTLA-4 or peptide-vaccine) results in more active/cytotoxic rather than higher absolute numbers of ALK-specific CD8<sup>+</sup> T-cells infiltrating the tumor microenvironment.

Next, having reunited all conditions, we aimed the total lung tumor eradication that in ALK-rearranged tumor history has never been achieved.

Knowing from previous experiments that ALK-vaccine has a stronger effect in reduced tumor burden, we have combined the immunotherapeutic approaches with the potent third-generation-ALK inhibitor lorlatinib. Mice were subjected to 14 days of ALK inhibition either alone or in combination with immune checkpoint inhibitors, ALK-peptide-vaccine or triple combination. Remarkably, all vaccinated groups (independently of the combination) had a significantly extended overall survival. Untreated mice (control) presented a median survival of 19 days and not surprisingly,

lorlatinib alone and lorlatinib + PD-1 groups shown the same median survival (37 days). These results suggested that lorlatinib only extends the mice survival during lorlatinib treatment, and once suspended, mice rapidly die due to respiratory failure, and anti-PD-1 does not add any advantage. However, when mice were treated with lorlatinib in combination with anti-CTLA-4, the median survival was 42 days and 10% of the mice have survived more than 100 days after tumor transplantation. Once again, these results suggested a strong benefit of appropriate priming. Both lorlatinib + peptide-vaccine and lorlatinib + peptide-vaccine + PD-1 groups have reached 60 days of overall survival (23 days more than lorlatinib alone) and about 25% of the mice have survived more than 100 days after tumor transplantation. The addition of PD-1 in a vaccine context does not add any benefit. Surprisingly, the lorlatinib + peptide-vaccine + anti-CTLA-4 combination has not reached the median overall survival until the end of the experiment and 80% of the mice have survived longer than 100 days after tumor transplantation. These results put together suggested that anti-CTLA-4 potentiates the immune response elicited by the peptide-vaccine. Even though this seems to be the best combination for the treatment of ALK-driven NSCLC orthotopic mouse models, the pros and cons of the use of anti-CTLA-4 must be taken into account for the same reasons I have previously discussed.

Despite the incredible results observed in the therapeutic experiment, in which for the very first time in ALK-driven lung cancer mouse models we have cured a high percentage of mice, we observed that mice belong to untreated (control), lorlatinib alone, lorlatinib + anti-PD-1 and lorlatinib + anti-CTLA-4 groups experienced changed in their behavior during the experiment timeline. Around day 15/16 after tumor transplantation in untreated (control) mice and day 30/35 after tumor transplantation in lorlatinib groups, mice started to present motor disability, and in some cases even hemiparesis. They also presented an aggressive behavior accompanied by drastic involuntary movements. With this phenotype, we wondered whether the mice had developed brain metastasis. To answer this question, multiple brain sections were analyzed and shockingly we observed that almost all mice from non-vaccinated groups presented brain metastasis whilst in the vaccinated groups, none have developed brain metastasis. This outstanding result came as a clear hope for all ALK-driven NSCLC

patients. Brain metastasis is frequently associated with tumor progression, representing the end of the line for these young patients. The exact mechanism behind the complete abrogation of brain metastasis was not addressed in this thesis. However, we have clear evidences coming from previous published works that ALK-vaccine has a much stronger effect when the tumor burden is reduced. One can hypothesize that individual cells that would gain mobility and migrate to distant organs would be easily identified and eliminated by circulating ALK-specific-CD8<sup>+</sup> T-cells. However, this hypothesis needs further validation.

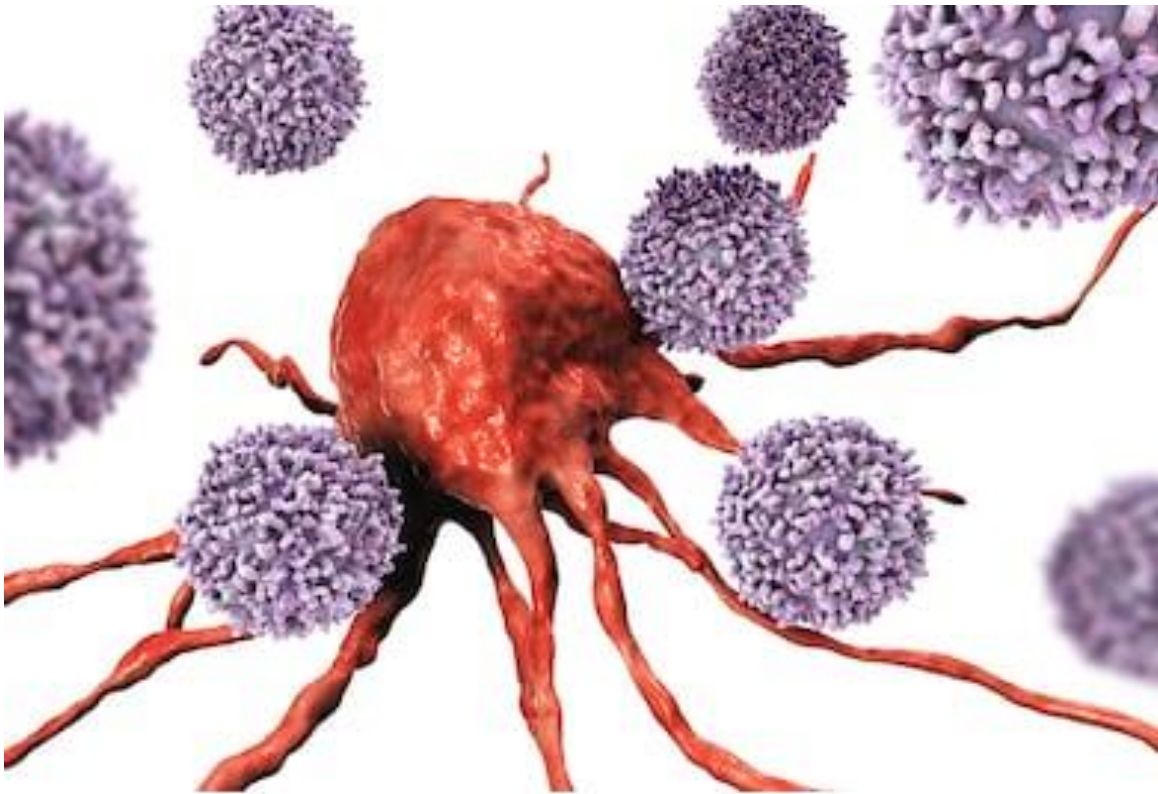
Finally, we tried to understand why still a high percentage of vaccinated mice did not respond to the treatment, relapsing and ultimately die from respiratory failure. Multiple *ex vivo* tumor cell lines were established and MHC-I expression was analyzed. Surprisingly, the vaccinated groups presented a significantly reduced MHC-I expression when compared to non-vaccinated groups, suggesting that the downregulation of MHC-I was the immune scape mechanism adopted by these cells. However, when asked either it was a reversible or irreversible event, we observed that upon IFN- $\gamma$  *in vitro* stimulation MHC-I expression is upregulated, confirming that MHC-I loss is a reversible event (probably regulated through an epigenetic event) and opening the possibility to other combined therapeutic strategies.

Lastly, the results here presented have a tremendous translational meaning, not only to ALK-driven NSCLC patients but to all ALK-driven malignancies.



---

## Chapter VI



*“If you wou’d not be forgotten  
As soon as you are dead and rotten  
Either write things worth reading  
Or do things worth the writing”*

Benjamin Franklin

## **6. Conclusion**





### 6) Conclusion

#### Part I

Regarding the Part I of my work, we have concluded that the mouse models confirmed preliminary observations in ALK-rearranged NSCLC, in which the addition of ICIs to an ALK inhibitor has limited effect. In this context, the addition of an ALK vaccine strongly potentiates the therapeutic activity of ALK TKIs and prevents metastatic dissemination of ALK<sup>+</sup> lung cancer cells.

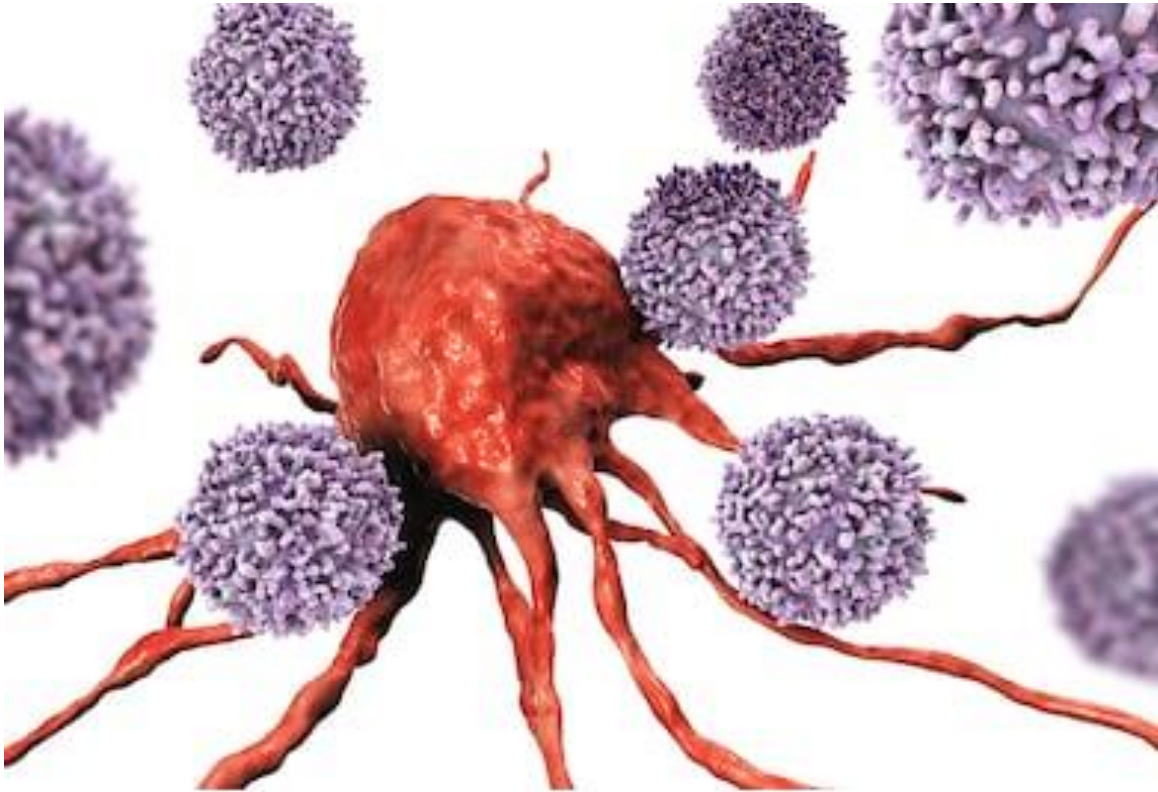
#### Part II

Regarding the Part II of my work, our orthotopic mouse model has confirmed that by increasing the number of ALK-specific-CD8<sup>+</sup> through vaccination, mice survival was greatly extended. Also, our data confirmed preliminary observations in preclinical ALK-rearranged NSCLC mouse models that the addition of a strong immune response, completely abrogate brain metastasis.



---

## Chapter VII



*“Forgive me if what has seemed little to you,  
to me is all”*

José Saramago,  
Noble prize in Literature 1998

## **7. References**



## 7) References

1. Palmer, R.H. and Vernersoon, E, *Anaplastic Lymphoma Kinase: Signalling in Development and Disease*, Biochem J, 2009. **420**: p. 345-361.
2. Hubbard, S.R. and J.H. Till, *Protein tyrosine kinase structure and function*. Annu Rev Biochem, 2000. **69**: p. 373-98.
3. Du, Z. and C.M. Lovly, *Mechanisms of receptor tyrosine kinase activation in cancer*. Mol Cancer, 2018. **17**(1): p. 58.
4. Manning, G., et al., *The protein kinase complement of the human genome*. Science, 2002. **298**(5600): p. 1912-34.
5. Li, E. and K. Hristova, *Receptor tyrosine kinase transmembrane domains: Function, dimer structure and dimerization energetics*. Cell Adh Migr, 2010. **4**(2): p. 249-54.
6. Robinson, D.R., Y.M. Wu, and S.F. Lin, *The protein tyrosine kinase family of the human genome*. Oncogene, 2000. **19**(49): p. 5548-57.
7. Vogelstein, B., et al., *Cancer genome landscapes*. Science, 2013. **339**(6127): p. 1546-58.
8. Hubbard, S.R., *Structural analysis of receptor tyrosine kinases*. Prog Biophys Mol Biol, 1999. **71**(3-4): p. 343-58.
9. Segaliny, A.I., et al., *Receptor tyrosine kinases: Characterisation, mechanism of action and therapeutic interests for bone cancers*. J Bone Oncol, 2015. **4**(1): p. 1-12.
10. Maruyama, I.N., *Mechanisms of activation of receptor tyrosine kinases: monomers or dimers*. Cells, 2014. **3**(2): p. 304-30.
11. Lemmon, M.A. and J. Schlessinger, *Cell signaling by receptor tyrosine kinases*. Cell, 2010. **141**(7): p. 1117-34.
12. Lemmon, M.A., J. Schlessinger, and K.M. Ferguson, *The EGFR family: not so prototypical receptor tyrosine kinases*. Cold Spring Harb Perspect Biol, 2014. **6**(4): p. a020768.
13. Kovacs, E., et al., *A structural perspective on the regulation of the epidermal growth factor receptor*. Annu Rev Biochem, 2015. **84**: p. 739-64.
14. Ullrich, A. and J. Schlessinger, *Signal transduction by receptors with tyrosine kinase activity*. Cell, 1990. **61**(2): p. 203-12.
15. Sorkin, A. and C.M. Waters, *Endocytosis of growth factor receptors*. Bioessays, 1993. **15**(6): p. 375-82.
16. Mori, S., et al., *Ligand-induced polyubiquitination of receptor tyrosine kinases*. Biochem Biophys Res Commun, 1995. **213**(1): p. 32-9.
17. Tonks, N.K. and B.G. Neel, *From form to function: signaling by protein tyrosine phosphatases*. Cell, 1996. **87**(3): p. 365-8.
18. Ostman, A. and F.D. Bohmer, *Regulation of receptor tyrosine kinase signaling by protein tyrosine phosphatases*. Trends Cell Biol, 2001. **11**(6): p. 258-66.
19. Schlessinger, J., *Cell signaling by receptor tyrosine kinases*. Cell, 2000. **103**(2): p. 211-25.
20. Lahiry, P., et al., *Kinase mutations in human disease: interpreting genotype-phenotype relationships*. Nat Rev Genet, 2010. **11**(1): p. 60-74.
21. Medves, S. and J.B. Demoulin, *Tyrosine kinase gene fusions in cancer: translating mechanisms into targeted therapies*. J Cell Mol Med, 2012. **16**(2): p. 237-48.
22. Wang, Z., et al., *Mechanistic insights into the activation of oncogenic forms of EGF receptor*. Nat Struct Mol Biol, 2011. **18**(12): p. 1388-93.
23. Sharma, S.V., et al., *Epidermal growth factor receptor mutations in lung cancer*. Nat Rev Cancer, 2007. **7**(3): p. 169-81.
24. Janne, P.A., J.A. Engelman, and B.E. Johnson, *Epidermal growth factor receptor mutations in non-small-cell lung cancer: implications for treatment and tumor biology*. J Clin Oncol, 2005. **23**(14): p. 3227-34.

## Chapter VII - References

---

25. Marchetti, A., et al., *EGFR mutations in non-small-cell lung cancer: analysis of a large series of cases and development of a rapid and sensitive method for diagnostic screening with potential implications on pharmacologic treatment.* J Clin Oncol, 2005. **23**(4): p. 857-65.
26. Red Brewer, M., et al., *Mechanism for activation of mutated epidermal growth factor receptors in lung cancer.* Proc Natl Acad Sci U S A, 2013. **110**(38): p. E3595-604.
27. Yun, C.H., et al., *Structures of lung cancer-derived EGFR mutants and inhibitor complexes: mechanism of activation and insights into differential inhibitor sensitivity.* Cancer Cell, 2007. **11**(3): p. 217-27.
28. Ou, S.I., et al., *HER2 Transmembrane Domain (TMD) Mutations (V659/G660) That Stabilize Homo- and Heterodimerization Are Rare Oncogenic Drivers in Lung Adenocarcinoma That Respond to Afatinib.* J Thorac Oncol, 2017. **12**(3): p. 446-457.
29. Bocharov, E.V., et al., *Alternative packing of EGFR transmembrane domain suggests that protein-lipid interactions underlie signal conduction across membrane.* Biochim Biophys Acta, 2016. **1858**(6): p. 1254-61.
30. Heinrich, M.C., et al., *Kinase mutations and imatinib response in patients with metastatic gastrointestinal stromal tumor.* J Clin Oncol, 2003. **21**(23): p. 4342-9.
31. Carraway, K.L., 3rd and C. Sweeney, *EGF receptor activation by heterologous mechanisms.* Cancer Cell, 2002. **1**(5): p. 405-6.
32. Albertson, D.G., *Gene amplification in cancer.* Trends Genet, 2006. **22**(8): p. 447-55.
33. Albertson, D.G., et al., *Chromosome aberrations in solid tumors.* Nat Genet, 2003. **34**(4): p. 369-76.
34. Lopez-Gines, C., et al., *New pattern of EGFR amplification in glioblastoma and the relationship of gene copy number with gene expression profile.* Mod Pathol, 2010. **23**(6): p. 856-65.
35. Hallberg, B. and R.H. Palmer, *The role of the ALK receptor in cancer biology.* Ann Oncol, 2016. **27 Suppl 3**: p. iii4-iii15.
36. Umapathy, G., et al., *Targeting anaplastic lymphoma kinase in neuroblastoma.* APMIS, 2019. **127**(5): p. 288-302.
37. Dutt, A., et al., *Inhibitor-sensitive FGFR1 amplification in human non-small cell lung cancer.* PLoS One, 2011. **6**(6): p. e20351.
38. Reis-Filho, J.S., et al., *FGFR1 emerges as a potential therapeutic target for lobular breast carcinomas.* Clin Cancer Res, 2006. **12**(22): p. 6652-62.
39. Helsten, T., et al., *The FGFR Landscape in Cancer: Analysis of 4,853 Tumors by Next-Generation Sequencing.* Clin Cancer Res, 2016. **22**(1): p. 259-67.
40. Fischbach, A., et al., *Fibroblast growth factor receptor (FGFR) gene amplifications are rare events in bladder cancer.* Histopathology, 2015. **66**(5): p. 639-49.
41. Kim, J.Y., et al., *Prognostic value of ERBB4 expression in patients with triple negative breast cancer.* BMC Cancer, 2016. **16**: p. 138.
42. Shi, J., et al., *Frequent gene amplification predicts poor prognosis in gastric cancer.* Int J Mol Sci, 2012. **13**(4): p. 4714-26.
43. Moreira, R.B., R.D. Peixoto, and M.R. de Sousa Cruz, *Clinical Response to Sorafenib in a Patient with Metastatic Colorectal Cancer and FLT3 Amplification.* Case Rep Oncol, 2015. **8**(1): p. 83-7.
44. Carvajal, R.D., et al., *KIT as a therapeutic target in metastatic melanoma.* JAMA, 2011. **305**(22): p. 2327-34.
45. Tabone, S., et al., *KIT overexpression and amplification in gastrointestinal stromal tumors (GISTs).* Biochim Biophys Acta, 2005. **1741**(1-2): p. 165-72.
46. Nobusawa, S., et al., *Amplification of the PDGFRA, KIT and KDR genes in glioblastoma: a population-based study.* Neuropathology, 2011. **31**(6): p. 583-8.

47. Sholl, L.M., et al., *Lung adenocarcinoma with EGFR amplification has distinct clinicopathologic and molecular features in never-smokers*. *Cancer Res*, 2009. **69**(21): p. 8341-8.
48. Sharma, G.G., et al., *Tumor Resistance against ALK Targeted Therapy-Where It Comes From and Where It Goes*. *Cancers (Basel)*, 2018. **10**(3).
49. Ludes-Meyers, J.H., et al., *Transcriptional activation of the human epidermal growth factor receptor promoter by human p53*. *Mol Cell Biol*, 1996. **16**(11): p. 6009-19.
50. Reznik, T.E., et al., *Transcription-dependent epidermal growth factor receptor activation by hepatocyte growth factor*. *Mol Cancer Res*, 2008. **6**(1): p. 139-50.
51. Hanawa, M., et al., *EGFR protein overexpression and gene amplification in squamous cell carcinomas of the esophagus*. *Int J Cancer*, 2006. **118**(5): p. 1173-80.
52. Maiti, G.P., et al., *Overexpression of EGFR in head and neck squamous cell carcinoma is associated with inactivation of SH3GL2 and CDC25A genes*. *PLoS One*, 2013. **8**(5): p. e63440.
53. Mudduluru, G., et al., *Regulation of Axl receptor tyrosine kinase expression by miR-34a and miR-199a/b in solid cancer*. *Oncogene*, 2011. **30**(25): p. 2888-99.
54. Stransky, N., et al., *The landscape of kinase fusions in cancer*. *Nat Commun*, 2014. **5**: p. 4846.
55. *Comprehensive molecular profiling of lung adenocarcinoma*. *Nature*, 2014. **511**(7511): p. 543-50.
56. Brennan, C.W., et al., *The somatic genomic landscape of glioblastoma*. *Cell*, 2013. **155**(2): p. 462-77.
57. Diamond, J., J.M. Goldman, and J.V. Melo, *BCR-ABL, ABL-BCR, BCR, and ABL genes are all expressed in individual granulocyte-macrophage colony-forming unit colonies derived from blood of patients with chronic myeloid leukemia*. *Blood*, 1995. **85**(8): p. 2171-5.
58. Melo, J.V., et al., *Expression of the ABL-BCR fusion gene in Philadelphia-positive acute lymphoblastic leukemia*. *Blood*, 1993. **81**(10): p. 2488-91.
59. Melo, J.V., et al., *The ABL-BCR fusion gene is expressed in chronic myeloid leukemia*. *Blood*, 1993. **81**(1): p. 158-65.
60. Druker, B.J., et al., *Efficacy and safety of a specific inhibitor of the BCR-ABL tyrosine kinase in chronic myeloid leukemia*. *N Engl J Med*, 2001. **344**(14): p. 1031-7.
61. O'Brien, S.G., et al., *Imatinib compared with interferon and low-dose cytarabine for newly diagnosed chronic-phase chronic myeloid leukemia*. *N Engl J Med*, 2003. **348**(11): p. 994-1004.
62. Morris, S.W., et al., *Fusion of a kinase gene, ALK, to a nucleolar protein gene, NPM, in non-Hodgkin's lymphoma*. *Science*, 1994. **263**(5151): p. 1281-4.
63. Kutok, J.L. and J.C. Aster, *Molecular biology of anaplastic lymphoma kinase-positive anaplastic large-cell lymphoma*. *J Clin Oncol*, 2002. **20**(17): p. 3691-702.
64. Soda, M., et al., *Identification of the transforming EML4-ALK fusion gene in non-small-cell lung cancer*. *Nature*, 2007. **448**(7153): p. 561-6.
65. Takeuchi, K., et al., *RET, ROS1 and ALK fusions in lung cancer*. *Nat Med*, 2012. **18**(3): p. 378-81.
66. Coffin, C.M., J.L. Hornick, and C.D. Fletcher, *Inflammatory myofibroblastic tumor: comparison of clinicopathologic, histologic, and immunohistochemical features including ALK expression in atypical and aggressive cases*. *Am J Surg Pathol*, 2007. **31**(4): p. 509-20.
67. Lovly, C.M., et al., *Inflammatory myofibroblastic tumors harbor multiple potentially actionable kinase fusions*. *Cancer Discov*, 2014. **4**(8): p. 889-95.
68. Lipson, D., et al., *Identification of new ALK and RET gene fusions from colorectal and lung cancer biopsies*. *Nat Med*, 2012. **18**(3): p. 382-4.
69. Lai, A.Z., et al., *Detection of an ALK Fusion in Colorectal Carcinoma by Hybrid Capture-Based Assay of Circulating Tumor DNA*. *Oncologist*, 2017. **22**(7): p. 774-779.
70. Chou, A., et al., *A detailed clinicopathologic study of ALK-translocated papillary thyroid carcinoma*. *Am J Surg Pathol*, 2015. **39**(5): p. 652-9.

## Chapter VII - References

71. Ren, H., et al., *Identification of anaplastic lymphoma kinase as a potential therapeutic target in ovarian cancer*. *Cancer Res*, 2012. **72**(13): p. 3312-23.
72. Konduri, K., et al., *EGFR Fusions as Novel Therapeutic Targets in Lung Cancer*. *Cancer Discov*, 2016. **6**(6): p. 601-11.
73. Chmielecki, J., et al., *Oncogenic alterations in ERBB2/HER2 represent potential therapeutic targets across tumors from diverse anatomic sites of origin*. *Oncologist*, 2015. **20**(1): p. 7-12.
74. Wiesner, T., et al., *Kinase fusions are frequent in Spitz tumours and spitzoid melanomas*. *Nat Commun*, 2014. **5**: p. 3116.
75. Huang, Q., et al., *PDGFRA rearrangement leading to hyper-eosinophilia, T-lymphoblastic lymphoma, myeloproliferative neoplasm and precursor B-cell acute lymphoblastic leukemia*. *Leukemia*, 2011. **25**(2): p. 371-5.
76. Bergethon, K., et al., *ROS1 rearrangements define a unique molecular class of lung cancers*. *J Clin Oncol*, 2012. **30**(8): p. 863-70.
77. Uguen, A. and M. De Braekeleer, *ROS1 fusions in cancer: a review*. *Future Oncol*, 2016. **12**(16): p. 1911-28.
78. Dacic, S., et al., *RET rearrangements in lung adenocarcinoma and radiation*. *J Thorac Oncol*, 2014. **9**(1): p. 118-20.
79. Nikiforov, Y.E., *RET/PTC rearrangement in thyroid tumors*. *Endocr Pathol*, 2002. **13**(1): p. 3-16.
80. Ito, T., et al., *In vitro irradiation is able to cause RET oncogene rearrangement*. *Cancer Res*, 1993. **53**(13): p. 2940-3.
81. Mizuno, T., et al., *Continued expression of a tissue specific activated oncogene in the early steps of radiation-induced human thyroid carcinogenesis*. *Oncogene*, 1997. **15**(12): p. 1455-60.
82. Mistry, A.R., et al., *DNA topoisomerase II in therapy-related acute promyelocytic leukemia*. *N Engl J Med*, 2005. **352**(15): p. 1529-38.
83. Tsai, A.G. and M.R. Lieber, *Mechanisms of chromosomal rearrangement in the human genome*. *BMC Genomics*, 2010. **11 Suppl 1**: p. S1.
84. Noh, K.W., et al., *Molecular breakdown: a comprehensive view of anaplastic lymphoma kinase (ALK)-rearranged non-small cell lung cancer*. *J Pathol*, 2017. **243**(3): p. 307-319.
85. Ju, Y.S., et al., *A transforming KIF5B and RET gene fusion in lung adenocarcinoma revealed from whole-genome and transcriptome sequencing*. *Genome Res*, 2012. **22**(3): p. 436-45.
86. Wu, Y.M., et al., *Identification of targetable FGFR gene fusions in diverse cancers*. *Cancer Discov*, 2013. **3**(6): p. 636-47.
87. Martelli, M.P., et al., *EML4-ALK rearrangement in non-small cell lung cancer and non-tumor lung tissues*. *Am J Pathol*, 2009. **174**(2): p. 661-70.
88. Corvi, R., et al., *RET/PCM-1: a novel fusion gene in papillary thyroid carcinoma*. *Oncogene*, 2000. **19**(37): p. 4236-42.
89. Chen, H.Y., D.C. Brady, and J. Villanueva, *Double Trouble: Kinase domain duplication as a new path to drug resistance*. *Pigment Cell Melanoma Res*, 2016. **29**(5): p. 493-5.
90. Gallant, J.N., et al., *EGFR Kinase Domain Duplication (EGFR-KDD) Is a Novel Oncogenic Driver in Lung Cancer That Is Clinically Responsive to Afatinib*. *Cancer Discov*, 2015. **5**(11): p. 1155-63.
91. Kondrashov, F.A., *Gene duplication as a mechanism of genomic adaptation to a changing environment*. *Proc Biol Sci*, 2012. **279**(1749): p. 5048-57.
92. L.M. Gay, D.P., J. Chung, S. Ramkissoon, S. Daniel, J.A. Elvin, E. Severson, T. Bivona, K.L. Reckamp, S.J. Klempner, S.I. Ou, A.B. Schrock, V.A. Miller, P.J. Stephens, J.S. Ross, S. Ganesan, C. Lovly, A. Mansfield, S.M. Ali, *Genomic profiling of 114,200 advanced cancers identifies recurrent kinase domain duplications (KDD) and oncogenic rearrangements (RE) across diverse tumor types*. *Annals of Oncology*, 2017. **28 (suppl\_5)**: v595-v604. [10.1093/annonc/mdx391](https://doi.org/10.1093/annonc/mdx391).



93. Walsh, J.H., et al., *Autocrine growth factors and solid tumor malignancy*. West J Med, 1991. **155**(2): p. 152-63.
94. Ciardiello, F. and G. Tortora, *A novel approach in the treatment of cancer: targeting the epidermal growth factor receptor*. Clin Cancer Res, 2001. **7**(10): p. 2958-70.
95. Kentsis, A., et al., *Autocrine activation of the MET receptor tyrosine kinase in acute myeloid leukemia*. Nat Med, 2012. **18**(7): p. 1118-22.
96. Yi, S. and M.S. Tsao, *Activation of hepatocyte growth factor-met autocrine loop enhances tumorigenicity in a human lung adenocarcinoma cell line*. Neoplasia, 2000. **2**(3): p. 226-34.
97. Krystal, G.W., S.J. Hines, and C.P. Organ, *Autocrine growth of small cell lung cancer mediated by coexpression of c-kit and stem cell factor*. Cancer Res, 1996. **56**(2): p. 370-6.
98. Esposito, I., et al., *The stem cell factor-c-kit system and mast cells in human pancreatic cancer*. Lab Invest, 2002. **82**(11): p. 1481-92.
99. Wiesner, C., et al., *C-kit and its ligand stem cell factor: potential contribution to prostate cancer bone metastasis*. Neoplasia, 2008. **10**(9): p. 996-1003.
100. Fujimoto, N., et al., *High expression of ErbB family members and their ligands in lung adenocarcinomas that are sensitive to inhibition of epidermal growth factor receptor*. Cancer Res, 2005. **65**(24): p. 11478-85.
101. Donzelli, S., et al., *MicroRNAs: Non-coding fine tuners of receptor tyrosine kinase signalling in cancer*. Semin Cell Dev Biol, 2016. **50**: p. 133-42.
102. Zhang, K.L., et al., *Blockage of a miR-21/EGFR regulatory feedback loop augments anti-EGFR therapy in glioblastomas*. Cancer Lett, 2014. **342**(1): p. 139-49.
103. Spill, F., et al., *Impact of the physical microenvironment on tumor progression and metastasis*. Curr Opin Biotechnol, 2016. **40**: p. 41-48.
104. Gattei, V., et al., *Expression of the RET receptor tyrosine kinase and GDNFR-alpha in normal and leukemic human hematopoietic cells and stromal cells of the bone marrow microenvironment*. Blood, 1997. **89**(8): p. 2925-37.
105. Voena, C., S. Peola, and R. Chiarle, *The anaplastic lymphoma kinase as an oncogene in solid tumors*. Front Biosci (Schol Ed), 2015. **7**: p. 269-82.
106. Iwahara, T., et al., *Molecular characterization of ALK, a receptor tyrosine kinase expressed specifically in the nervous system*. Oncogene, 1997. **14**(4): p. 439-49.
107. Morris, S.W., et al., *ALK, the chromosome 2 gene locus altered by the t(2;5) in non-Hodgkin's lymphoma, encodes a novel neural receptor tyrosine kinase that is highly related to leukocyte tyrosine kinase (LTK)*. Oncogene, 1997. **14**(18): p. 2175-88.
108. Palmer, R.H., et al., *Anaplastic lymphoma kinase: signalling in development and disease*. Biochem J, 2009. **420**(3): p. 345-61.
109. Loren, C.E., et al., *Identification and characterization of DAlk: a novel Drosophila melanogaster RTK which drives ERK activation in vivo*. Genes Cells, 2001. **6**(6): p. 531-44.
110. Stoica, G.E., et al., *Identification of anaplastic lymphoma kinase as a receptor for the growth factor pleiotrophin*. J Biol Chem, 2001. **276**(20): p. 16772-9.
111. Daly, N.L., et al., *Three-dimensional structure of a cysteine-rich repeat from the low-density lipoprotein receptor*. Proc Natl Acad Sci U S A, 1995. **92**(14): p. 6334-8.
112. Fass, D., et al., *Molecular basis of familial hypercholesterolaemia from structure of LDL receptor module*. Nature, 1997. **388**(6643): p. 691-3.
113. Beckmann, G. and P. Bork, *An adhesive domain detected in functionally diverse receptors*. Trends Biochem Sci, 1993. **18**(2): p. 40-1.
114. Loren, C.E., et al., *A crucial role for the Anaplastic lymphoma kinase receptor tyrosine kinase in gut development in Drosophila melanogaster*. EMBO Rep, 2003. **4**(8): p. 781-6.
115. Bai, R.Y., et al., *Nucleophosmin-anaplastic lymphoma kinase of large-cell anaplastic lymphoma is a constitutively active tyrosine kinase that utilizes phospholipase C-gamma to mediate its mitogenicity*. Mol Cell Biol, 1998. **18**(12): p. 6951-61.

116. Englund, C., et al., *Jeb signals through the Alk receptor tyrosine kinase to drive visceral muscle fusion*. *Nature*, 2003. **425**(6957): p. 512-6.
117. Lee, H.H., et al., *Jelly belly protein activates the receptor tyrosine kinase Alk to specify visceral muscle pioneers*. *Nature*, 2003. **425**(6957): p. 507-12.
118. Stute, C., et al., *Myoblast determination in the somatic and visceral mesoderm depends on Notch signalling as well as on milliways(mili(Alk)) as receptor for Jeb signalling*. *Development*, 2004. **131**(4): p. 743-54.
119. Klapper, R., et al., *The formation of syncytia within the visceral musculature of the Drosophila midgut is dependent on duf, sns and mbc*. *Mech Dev*, 2002. **110**(1-2): p. 85-96.
120. Martin, B.S., et al., *A distinct set of founders and fusion-competent myoblasts make visceral muscles in the Drosophila embryo*. *Development*, 2001. **128**(17): p. 3331-8.
121. Weiss, J.B., et al., *Jelly belly: a Drosophila LDL receptor repeat-containing signal required for mesoderm migration and differentiation*. *Cell*, 2001. **107**(3): p. 387-98.
122. Varshney, G.K. and R.H. Palmer, *The bHLH transcription factor Hand is regulated by Alk in the Drosophila embryonic gut*. *Biochem Biophys Res Commun*, 2006. **351**(4): p. 839-46.
123. Shirinian, M., et al., *Drosophila Anaplastic Lymphoma Kinase regulates Dpp signalling in the developing embryonic gut*. *Differentiation*, 2007. **75**(5): p. 418-26.
124. Bazigou, E., et al., *Anterograde Jelly belly and Alk receptor tyrosine kinase signaling mediates retinal axon targeting in Drosophila*. *Cell*, 2007. **128**(5): p. 961-75.
125. Liao, E.H., et al., *An SCF-like ubiquitin ligase complex that controls presynaptic differentiation*. *Nature*, 2004. **430**(6997): p. 345-50.
126. Reiner, D.J., et al., *C. elegans anaplastic lymphoma kinase ortholog SCD-2 controls dauer formation by modulating TGF-beta signaling*. *Curr Biol*, 2008. **18**(15): p. 1101-9.
127. Ishihara, T., et al., *HEN-1, a secretory protein with an LDL receptor motif, regulates sensory integration and learning in Caenorhabditis elegans*. *Cell*, 2002. **109**(5): p. 639-49.
128. Lopes, S.S., et al., *Leukocyte tyrosine kinase functions in pigment cell development*. *PLoS Genet*, 2008. **4**(3): p. e1000026.
129. Vernersson, E., et al., *Characterization of the expression of the ALK receptor tyrosine kinase in mice*. *Gene Expr Patterns*, 2006. **6**(5): p. 448-61.
130. Degoutin, J., et al., *ALK (Anaplastic Lymphoma Kinase) expression in DRG neurons and its involvement in neuron-Schwann cells interaction*. *Eur J Neurosci*, 2009. **29**(2): p. 275-86.
131. Pulford, K., et al., *Detection of anaplastic lymphoma kinase (ALK) and nucleolar protein nucleophosmin (NPM)-ALK proteins in normal and neoplastic cells with the monoclonal antibody ALK1*. *Blood*, 1997. **89**(4): p. 1394-404.
132. Morris, S.W., et al., *Fusion of a kinase gene, ALK, to a nucleolar protein gene, NPM, in non-Hodgkin's lymphoma*. *Science*, 1995. **267**(5196): p. 316-7.
133. Souttou, B., et al., *Activation of anaplastic lymphoma kinase receptor tyrosine kinase induces neuronal differentiation through the mitogen-activated protein kinase pathway*. *J Biol Chem*, 2001. **276**(12): p. 9526-31.
134. Degoutin, J., M. Vigny, and J.Y. Gouzi, *ALK activation induces Shc and FRS2 recruitment: Signaling and phenotypic outcomes in PC12 cells differentiation*. *FEBS Lett*, 2007. **581**(4): p. 727-34.
135. Moteji, A., et al., *ALK receptor tyrosine kinase promotes cell growth and neurite outgrowth*. *J Cell Sci*, 2004. **117**(Pt 15): p. 3319-29.
136. Pulford, K., S.W. Morris, and F. Turturro, *Anaplastic lymphoma kinase proteins in growth control and cancer*. *J Cell Physiol*, 2004. **199**(3): p. 330-58.
137. Bilsland, J.G., et al., *Behavioral and neurochemical alterations in mice deficient in anaplastic lymphoma kinase suggest therapeutic potential for psychiatric indications*. *Neuropsychopharmacology*, 2008. **33**(3): p. 685-700.
138. Lasek, A.W., et al., *An evolutionary conserved role for anaplastic lymphoma kinase in behavioral responses to ethanol*. *PLoS One*, 2011. **6**(7): p. e22636.

139. Mi, R., W. Chen, and A. Hoke, *Pleiotrophin is a neurotrophic factor for spinal motor neurons*. Proc Natl Acad Sci U S A, 2007. **104**(11): p. 4664-9.
140. Bernardis, A. and S.M. de la Monte, *The ltk receptor tyrosine kinase is expressed in pre-B lymphocytes and cerebral neurons and uses a non-AUG translational initiator*. EMBO J, 1990. **9**(7): p. 2279-87.
141. Yamada, S., et al., *Expression of a chimeric CSF1R-LTK mediates ligand-dependent neurite outgrowth*. Neuroreport, 2008. **19**(17): p. 1733-8.
142. Moog-Lutz, C., et al., *Activation and inhibition of anaplastic lymphoma kinase receptor tyrosine kinase by monoclonal antibodies and absence of agonist activity of pleiotrophin*. J Biol Chem, 2005. **280**(28): p. 26039-48.
143. Mathivet, T., P. Mazot, and M. Vigny, *In contrast to agonist monoclonal antibodies, both C-terminal truncated form and full length form of Pleiotrophin failed to activate vertebrate ALK (anaplastic lymphoma kinase)?* Cell Signal, 2007. **19**(12): p. 2434-43.
144. Hallberg, B. and R.H. Palmer, *Mechanistic insight into ALK receptor tyrosine kinase in human cancer biology*. Nat Rev Cancer, 2013. **13**(10): p. 685-700.
145. Murray, P.B., et al., *Heparin is an activating ligand of the orphan receptor tyrosine kinase ALK*. Sci Signal, 2015. **8**(360): p. ra6.
146. Reshetnyak, A.V., et al., *Augmentor alpha and beta (FAM150) are ligands of the receptor tyrosine kinases ALK and LTK: Hierarchy and specificity of ligand-receptor interactions*. Proc Natl Acad Sci U S A, 2015. **112**(52): p. 15862-7.
147. Lemke, G., *Adopting ALK and LTK*. Proc Natl Acad Sci U S A, 2015. **112**(52): p. 15783-4.
148. Knighton, D.R., et al., *Crystal structure of the catalytic subunit of cyclic adenosine monophosphate-dependent protein kinase*. Science, 1991. **253**(5018): p. 407-14.
149. Taylor, S.S. and A.P. Kornev, *Protein kinases: evolution of dynamic regulatory proteins*. Trends Biochem Sci, 2011. **36**(2): p. 65-77.
150. Taylor, S.S., et al., *Evolution of the eukaryotic protein kinases as dynamic molecular switches*. Philos Trans R Soc Lond B Biol Sci, 2012. **367**(1602): p. 2517-28.
151. Roskoski, R., Jr., *Anaplastic lymphoma kinase (ALK): structure, oncogenic activation, and pharmacological inhibition*. Pharmacol Res, 2013. **68**(1): p. 68-94.
152. Lee, C.C., et al., *Crystal structure of the ALK (anaplastic lymphoma kinase) catalytic domain*. Biochem J, 2010. **430**(3): p. 425-37.
153. Bossi, R.T., et al., *Crystal structures of anaplastic lymphoma kinase in complex with ATP competitive inhibitors*. Biochemistry, 2010. **49**(32): p. 6813-25.
154. Hanks, S.K., A.M. Quinn, and T. Hunter, *The protein kinase family: conserved features and deduced phylogeny of the catalytic domains*. Science, 1988. **241**(4861): p. 42-52.
155. Zhou, J. and J.A. Adams, *Participation of ADP dissociation in the rate-determining step in cAMP-dependent protein kinase*. Biochemistry, 1997. **36**(50): p. 15733-8.
156. Kornev, A.P. and S.S. Taylor, *Defining the conserved internal architecture of a protein kinase*. Biochim Biophys Acta, 2010. **1804**(3): p. 440-4.
157. Chiarle, R., et al., *The anaplastic lymphoma kinase in the pathogenesis of cancer*. Nat Rev Cancer, 2008. **8**(1): p. 11-23.
158. Vanhaesebroeck, B., L. Stephens, and P. Hawkins, *PI3K signalling: the path to discovery and understanding*. Nat Rev Mol Cell Biol, 2012. **13**(3): p. 195-203.
159. Marzec, M., et al., *Oncogenic tyrosine kinase NPM/ALK induces activation of the MEK/ERK signaling pathway independently of c-Raf*. Oncogene, 2007. **26**(6): p. 813-21.
160. Fujimoto, J., et al., *Characterization of the transforming activity of p80, a hyperphosphorylated protein in a Ki-1 lymphoma cell line with chromosomal translocation t(2;5)*. Proc Natl Acad Sci U S A, 1996. **93**(9): p. 4181-6.
161. Galkin, A.V., et al., *Identification of NVP-TAE684, a potent, selective, and efficacious inhibitor of NPM-ALK*. Proc Natl Acad Sci U S A, 2007. **104**(1): p. 270-5.

## Chapter VII - References

---

162. Takita, J., *The role of anaplastic lymphoma kinase in pediatric cancers*. *Cancer Sci*, 2017. **108**(10): p. 1913-1920.
163. Chen, Y., et al., *Oncogenic mutations of ALK kinase in neuroblastoma*. *Nature*, 2008. **455**(7215): p. 971-4.
164. Mosse, Y.P., et al., *Identification of ALK as a major familial neuroblastoma predisposition gene*. *Nature*, 2008. **455**(7215): p. 930-5.
165. Janoueix-Lerosey, I., et al., *Somatic and germline activating mutations of the ALK kinase receptor in neuroblastoma*. *Nature*, 2008. **455**(7215): p. 967-70.
166. George, R.E., et al., *Activating mutations in ALK provide a therapeutic target in neuroblastoma*. *Nature*, 2008. **455**(7215): p. 975-8.
167. Guan, J., et al., *Anaplastic lymphoma kinase L1198F and G1201E mutations identified in anaplastic thyroid cancer patients are not ligand-independent*. *Oncotarget*, 2017. **8**(7): p. 11566-11578.
168. Choi, Y.L., et al., *EML4-ALK mutations in lung cancer that confer resistance to ALK inhibitors*. *N Engl J Med*, 2010. **363**(18): p. 1734-9.
169. Sakamoto, H., et al., *CH5424802, a selective ALK inhibitor capable of blocking the resistant gatekeeper mutant*. *Cancer Cell*, 2011. **19**(5): p. 679-90.
170. Maris, J.M., et al., *Neuroblastoma*. *Lancet*, 2007. **369**(9579): p. 2106-20.
171. Bown, N., *Neuroblastoma tumour genetics: clinical and biological aspects*. *J Clin Pathol*, 2001. **54**(12): p. 897-910.
172. Maris, J.M., *Recent advances in neuroblastoma*. *N Engl J Med*, 2010. **362**(23): p. 2202-11.
173. Attiyeh, E.F., et al., *Chromosome 1p and 11q deletions and outcome in neuroblastoma*. *N Engl J Med*, 2005. **353**(21): p. 2243-53.
174. Brodeur, G.M., *Neuroblastoma: biological insights into a clinical enigma*. *Nat Rev Cancer*, 2003. **3**(3): p. 203-16.
175. Carpenter, E.L. and Y.P. Mosse, *Targeting ALK in neuroblastoma--preclinical and clinical advancements*. *Nat Rev Clin Oncol*, 2012. **9**(7): p. 391-9.
176. De Brouwer, S., et al., *Meta-analysis of neuroblastomas reveals a skewed ALK mutation spectrum in tumors with MYCN amplification*. *Clin Cancer Res*, 2010. **16**(17): p. 4353-62.
177. Ueda, T., et al., *ALK(R1275Q) perturbs extracellular matrix, enhances cell invasion and leads to the development of neuroblastoma in cooperation with MYCN*. *Oncogene*, 2016. **35**(34): p. 4447-58.
178. Berry, T., et al., *The ALK(F1174L) mutation potentiates the oncogenic activity of MYCN in neuroblastoma*. *Cancer Cell*, 2012. **22**(1): p. 117-30.
179. Dirks, W.G., et al., *Expression and functional analysis of the anaplastic lymphoma kinase (ALK) gene in tumor cell lines*. *Int J Cancer*, 2002. **100**(1): p. 49-56.
180. Cessna, M.H., et al., *Expression of ALK1 and p80 in inflammatory myofibroblastic tumor and its mesenchymal mimics: a study of 135 cases*. *Mod Pathol*, 2002. **15**(9): p. 931-8.
181. Miyake, I., et al., *Activation of anaplastic lymphoma kinase is responsible for hyperphosphorylation of ShcC in neuroblastoma cell lines*. *Oncogene*, 2002. **21**(38): p. 5823-34.
182. El Demellawy, D., et al., *Update on molecular findings in rhabdomyosarcoma*. *Pathology*, 2017. **49**(3): p. 238-246.
183. Powers, C., et al., *Pleiotrophin signaling through anaplastic lymphoma kinase is rate-limiting for glioblastoma growth*. *J Biol Chem*, 2002. **277**(16): p. 14153-8.
184. Grzelinski, M., et al., *Enhanced antitumorigenic effects in glioblastoma on double targeting of pleiotrophin and its receptor ALK*. *Neoplasia*, 2009. **11**(2): p. 145-56.
185. Perez-Pinera, P., et al., *Anaplastic lymphoma kinase is expressed in different subtypes of human breast cancer*. *Biochem Biophys Res Commun*, 2007. **358**(2): p. 399-403.
186. Riegel, A.T. and A. Wellstein, *The potential role of the heparin-binding growth factor pleiotrophin in breast cancer*. *Breast Cancer Res Treat*, 1994. **31**(2-3): p. 309-14.

187. Garver, R.I., Jr., et al., *Midkine and pleiotrophin expression in normal and malignant breast tissue*. *Cancer*, 1994. **74**(5): p. 1584-90.
188. Zhang, N., et al., *Human breast cancer growth inhibited in vivo by a dominant negative pleiotrophin mutant*. *J Biol Chem*, 1997. **272**(27): p. 16733-6.
189. Shiota, M., et al., *Hyperphosphorylation of a novel 80 kDa protein-tyrosine kinase similar to Ltk in a human Ki-1 lymphoma cell line, AMS3*. *Oncogene*, 1994. **9**(6): p. 1567-74.
190. Armstrong, F., et al., *Differential effects of X-ALK fusion proteins on proliferation, transformation, and invasion properties of NIH3T3 cells*. *Oncogene*, 2004. **23**(36): p. 6071-82.
191. Griffin, C.A., et al., *Recurrent involvement of 2p23 in inflammatory myofibroblastic tumors*. *Cancer Res*, 1999. **59**(12): p. 2776-80.
192. Rikova, K., et al., *Global survey of phosphotyrosine signaling identifies oncogenic kinases in lung cancer*. *Cell*, 2007. **131**(6): p. 1190-203.
193. Arber, D.A., L.H. Sun, and L.M. Weiss, *Detection of the t(2;5)(p23;q35) chromosomal translocation in large B-cell lymphomas other than anaplastic large cell lymphoma*. *Hum Pathol*, 1996. **27**(6): p. 590-4.
194. Jazii, F.R., et al., *Identification of squamous cell carcinoma associated proteins by proteomics and loss of beta tropomyosin expression in esophageal cancer*. *World J Gastroenterol*, 2006. **12**(44): p. 7104-12.
195. Stein, H., et al., *The expression of the Hodgkin's disease associated antigen Ki-1 in reactive and neoplastic lymphoid tissue: evidence that Reed-Sternberg cells and histiocytic malignancies are derived from activated lymphoid cells*. *Blood*, 1985. **66**(4): p. 848-58.
196. Stein, H., et al., *CD30(+) anaplastic large cell lymphoma: a review of its histopathologic, genetic, and clinical features*. *Blood*, 2000. **96**(12): p. 3681-95.
197. Amin, H.M. and R. Lai, *Pathobiology of ALK+ anaplastic large-cell lymphoma*. *Blood*, 2007. **110**(7): p. 2259-67.
198. Savage, K.J., et al., *ALK- anaplastic large-cell lymphoma is clinically and immunophenotypically different from both ALK+ ALCL and peripheral T-cell lymphoma, not otherwise specified: report from the International Peripheral T-Cell Lymphoma Project*. *Blood*, 2008. **111**(12): p. 5496-504.
199. Campo, E., et al., *The 2008 WHO classification of lymphoid neoplasms and beyond: evolving concepts and practical applications*. *Blood*, 2011. **117**(19): p. 5019-32.
200. Gascoyne, R.D., et al., *Prognostic significance of anaplastic lymphoma kinase (ALK) protein expression in adults with anaplastic large cell lymphoma*. *Blood*, 1999. **93**(11): p. 3913-21.
201. Shiota, M., et al., *Anaplastic large cell lymphomas expressing the novel chimeric protein p80NPM/ALK: a distinct clinicopathologic entity*. *Blood*, 1995. **86**(5): p. 1954-60.
202. Falini, B., et al., *ALK+ lymphoma: clinico-pathological findings and outcome*. *Blood*, 1999. **93**(8): p. 2697-706.
203. Brugieres, L., et al., *Relapses of childhood anaplastic large-cell lymphoma: treatment results in a series of 41 children--a report from the French Society of Pediatric Oncology*. *Ann Oncol*, 2000. **11**(1): p. 53-8.
204. Okuwaki, M., *The structure and functions of NPM1/Nucleophosmin/B23, a multifunctional nucleolar acidic protein*. *J Biochem*, 2008. **143**(4): p. 441-8.
205. Bischof, D., et al., *Role of the nucleophosmin (NPM) portion of the non-Hodgkin's lymphoma-associated NPM-anaplastic lymphoma kinase fusion protein in oncogenesis*. *Mol Cell Biol*, 1997. **17**(4): p. 2312-25.
206. Cools, J., et al., *Identification of novel fusion partners of ALK, the anaplastic lymphoma kinase, in anaplastic large-cell lymphoma and inflammatory myofibroblastic tumor*. *Genes Chromosomes Cancer*, 2002. **34**(4): p. 354-62.
207. Hernandez, L., et al., *TRK-fused gene (TFG) is a new partner of ALK in anaplastic large cell lymphoma producing two structurally different TFG-ALK translocations*. *Blood*, 1999. **94**(9): p. 3265-8.

## Chapter VII - References

---

208. Hernandez, L., et al., *Diversity of genomic breakpoints in TFG-ALK translocations in anaplastic large cell lymphomas: identification of a new TFG-ALK(XL) chimeric gene with transforming activity*. *Am J Pathol*, 2002. **160**(4): p. 1487-94.
209. Tort, F., et al., *Molecular characterization of a new ALK translocation involving moesin (MSN-ALK) in anaplastic large cell lymphoma*. *Lab Invest*, 2001. **81**(3): p. 419-26.
210. Lamant, L., et al., *A new fusion gene TPM3-ALK in anaplastic large cell lymphoma created by a (1;2)(q25;p23) translocation*. *Blood*, 1999. **93**(9): p. 3088-95.
211. Siebert, R., et al., *Complex variant translocation t(1;2) with TPM3-ALK fusion due to cryptic ALK gene rearrangement in anaplastic large-cell lymphoma*. *Blood*, 1999. **94**(10): p. 3614-7.
212. Meech, S.J., et al., *Unusual childhood extramedullary hematologic malignancy with natural killer cell properties that contains tropomyosin 4--anaplastic lymphoma kinase gene fusion*. *Blood*, 2001. **98**(4): p. 1209-16.
213. Ma, Z., et al., *Inv(2)(p23q35) in anaplastic large-cell lymphoma induces constitutive anaplastic lymphoma kinase (ALK) tyrosine kinase activation by fusion to ATIC, an enzyme involved in purine nucleotide biosynthesis*. *Blood*, 2000. **95**(6): p. 2144-9.
214. Trinei, M., et al., *A new variant anaplastic lymphoma kinase (ALK)-fusion protein (ATIC-ALK) in a case of ALK-positive anaplastic large cell lymphoma*. *Cancer Res*, 2000. **60**(4): p. 793-8.
215. Colleoni, G.W., et al., *ATIC-ALK: A novel variant ALK gene fusion in anaplastic large cell lymphoma resulting from the recurrent cryptic chromosomal inversion, inv(2)(p23q35)*. *Am J Pathol*, 2000. **156**(3): p. 781-9.
216. Lamant, L., et al., *Non-muscle myosin heavy chain (MYH9): a new partner fused to ALK in anaplastic large cell lymphoma*. *Genes Chromosomes Cancer*, 2003. **37**(4): p. 427-32.
217. Touriol, C., et al., *Further demonstration of the diversity of chromosomal changes involving 2p23 in ALK-positive lymphoma: 2 cases expressing ALK kinase fused to CLTCL (clathrin chain polypeptide-like)*. *Blood*, 2000. **95**(10): p. 3204-7.
218. Beardsley, G.P., et al., *Structure and functional relationships in human pur H*. *Adv Exp Med Biol*, 1998. **431**: p. 221-6.
219. Delsol, G., et al., *A new subtype of large B-cell lymphoma expressing the ALK kinase and lacking the 2; 5 translocation*. *Blood*, 1997. **89**(5): p. 1483-90.
220. Reichard, K.K., R.W. McKenna, and S.H. Kroft, *ALK-positive diffuse large B-cell lymphoma: report of four cases and review of the literature*. *Mod Pathol*, 2007. **20**(3): p. 310-9.
221. Momose, S., et al., *Hyperactivated STAT3 in ALK-positive diffuse large B-cell lymphoma with clathrin-ALK fusion*. *Hum Pathol*, 2009. **40**(1): p. 75-82.
222. Stachurski, D., et al., *Anaplastic lymphoma kinase-positive diffuse large B-cell lymphoma with a complex karyotype and cryptic 3' ALK gene insertion to chromosome 4 q22-24*. *Hum Pathol*, 2007. **38**(6): p. 940-5.
223. Lee, H.W., et al., *ALK-positive diffuse large B-cell lymphoma: report of three cases*. *Hematol Oncol*, 2008. **26**(2): p. 108-13.
224. Choung, H.S., et al., *[Cytomorphology and molecular characterization of CLTC-ALK rearrangement in 2 cases of ALK-positive diffuse large B-cell lymphoma with extensive bone marrow involvement]*. *Korean J Lab Med*, 2008. **28**(2): p. 89-94.
225. Onciu, M., et al., *ALK-positive plasmablastic B-cell lymphoma with expression of the NPM-ALK fusion transcript: report of 2 cases*. *Blood*, 2003. **102**(7): p. 2642-4.
226. Adam, P., et al., *A case of a diffuse large B-cell lymphoma of plasmablastic type associated with the t(2;5)(p23;q35) chromosome translocation*. *Am J Surg Pathol*, 2003. **27**(11): p. 1473-6.
227. Zamo, A., et al., *Anaplastic lymphoma kinase (ALK) activates Stat3 and protects hematopoietic cells from cell death*. *Oncogene*, 2002. **21**(7): p. 1038-47.
228. Zhang, Q., et al., *Multilevel dysregulation of STAT3 activation in anaplastic lymphoma kinase-positive T/null-cell lymphoma*. *J Immunol*, 2002. **168**(1): p. 466-74.

229. Gleason, B.C. and J.L. Hornick, *Inflammatory myofibroblastic tumours: where are we now?* J Clin Pathol, 2008. **61**(4): p. 428-37.
230. Umiker, W.O. and L. Iverson, *Postinflammatory tumors of the lung; report of four cases simulating xanthoma, fibroma, or plasma cell tumor.* J Thorac Surg, 1954. **28**(1): p. 55-63.
231. Coffin, C.M., et al., *Extrapulmonary inflammatory myofibroblastic tumor (inflammatory pseudotumor). A clinicopathologic and immunohistochemical study of 84 cases.* Am J Surg Pathol, 1995. **19**(8): p. 859-72.
232. Lawrence, B., et al., *TPM3-ALK and TPM4-ALK oncogenes in inflammatory myofibroblastic tumors.* Am J Pathol, 2000. **157**(2): p. 377-84.
233. Debiec-Rychter, M., et al., *ALK-AT1C fusion in urinary bladder inflammatory myofibroblastic tumor.* Genes Chromosomes Cancer, 2003. **38**(2): p. 187-90.
234. Patel, A.S., et al., *RANBP2 and CLTC are involved in ALK rearrangements in inflammatory myofibroblastic tumors.* Cancer Genet Cytogenet, 2007. **176**(2): p. 107-14.
235. Bridge, J.A., et al., *Fusion of the ALK gene to the clathrin heavy chain gene, CLTC, in inflammatory myofibroblastic tumor.* Am J Pathol, 2001. **159**(2): p. 411-5.
236. Debelenko, L.V., et al., *Identification of CARS-ALK fusion in primary and metastatic lesions of an inflammatory myofibroblastic tumor.* Lab Invest, 2003. **83**(9): p. 1255-65.
237. Ma, Z., et al., *Fusion of ALK to the Ran-binding protein 2 (RANBP2) gene in inflammatory myofibroblastic tumor.* Genes Chromosomes Cancer, 2003. **37**(1): p. 98-105.
238. Panagopoulos, I., et al., *Fusion of the SEC31L1 and ALK genes in an inflammatory myofibroblastic tumor.* Int J Cancer, 2006. **118**(5): p. 1181-6.
239. Coffin, C.M., et al., *ALK1 and p80 expression and chromosomal rearrangements involving 2p23 in inflammatory myofibroblastic tumor.* Mod Pathol, 2001. **14**(6): p. 569-76.
240. Cook, J.R., et al., *Anaplastic lymphoma kinase (ALK) expression in the inflammatory myofibroblastic tumor: a comparative immunohistochemical study.* Am J Surg Pathol, 2001. **25**(11): p. 1364-71.
241. Marino-Enriquez, A., et al., *Epithelioid inflammatory myofibroblastic sarcoma: An aggressive intra-abdominal variant of inflammatory myofibroblastic tumor with nuclear membrane or perinuclear ALK.* Am J Surg Pathol, 2011. **35**(1): p. 135-44.
242. Sanders, H.R., et al., *Exon scanning by reverse transcriptase-polymerase chain reaction for detection of known and novel EML4-ALK fusion variants in non-small cell lung cancer.* Cancer Genet, 2011. **204**(1): p. 45-52.
243. Li, Y., et al., *Evaluation of EML4-ALK fusion proteins in non-small cell lung cancer using small molecule inhibitors.* Neoplasia, 2011. **13**(1): p. 1-11.
244. Siegel, R.L., K.D. Miller, and A. Jemal, *Cancer statistics, 2019.* CA Cancer J Clin, 2019. **69**(1): p. 7-34.
245. Morgensztern, D., et al., *Trends in stage distribution for patients with non-small cell lung cancer: a National Cancer Database survey.* J Thorac Oncol, 2010. **5**(1): p. 29-33.
246. Goldstraw, P., et al., *The IASLC Lung Cancer Staging Project: Proposals for Revision of the TNM Stage Groupings in the Forthcoming (Eighth) Edition of the TNM Classification for Lung Cancer.* J Thorac Oncol, 2016. **11**(1): p. 39-51.
247. Travis, W.D., et al., *The 2015 World Health Organization Classification of Lung Tumors: Impact of Genetic, Clinical and Radiologic Advances Since the 2004 Classification.* J Thorac Oncol, 2015. **10**(9): p. 1243-1260.
248. Gazdar, A.F., P.A. Bunn, and J.D. Minna, *Small-cell lung cancer: what we know, what we need to know and the path forward.* Nat Rev Cancer, 2017. **17**(12): p. 765.
249. Herbst, R.S., D. Morgensztern, and C. Boshoff, *The biology and management of non-small cell lung cancer.* Nature, 2018. **553**(7689): p. 446-454.
250. Wynder, E.L. and E.A. Graham, *Tobacco smoking as a possible etiologic factor in bronchiogenic carcinoma; a study of 684 proved cases.* J Am Med Assoc, 1950. **143**(4): p. 329-36.

## Chapter VII - References

---

251. de Groot, P.M., et al., *The epidemiology of lung cancer*. *Transl Lung Cancer Res*, 2018. **7**(3): p. 220-233.
252. Hecht, S.S., *Tobacco smoke carcinogens and lung cancer*. *J Natl Cancer Inst*, 1999. **91**(14): p. 1194-210.
253. in *The Health Consequences of Smoking-50 Years of Progress: A Report of the Surgeon General* 2014: Atlanta (GA).
254. Asomaning, K., et al., *Second hand smoke, age of exposure and lung cancer risk*. *Lung Cancer*, 2008. **61**(1): p. 13-20.
255. Subramanian, J. and R. Govindan, *Lung cancer in never smokers: a review*. *J Clin Oncol*, 2007. **25**(5): p. 561-70.
256. Wakelee, H.A., et al., *Lung cancer incidence in never smokers*. *J Clin Oncol*, 2007. **25**(5): p. 472-8.
257. Parkin, D.M., et al., *Global cancer statistics, 2002*. *CA Cancer J Clin*, 2005. **55**(2): p. 74-108.
258. Samet, J.M., *Radiation and cancer risk: a continuing challenge for epidemiologists*. *Environ Health*, 2011. **10 Suppl 1**: p. S4.
259. Lubin, J.H., et al., *Lung cancer in radon-exposed miners and estimation of risk from indoor exposure*. *J Natl Cancer Inst*, 1995. **87**(11): p. 817-27.
260. Mossman, B.T., et al., *Asbestos: scientific developments and implications for public policy*. *Science*, 1990. **247**(4940): p. 294-301.
261. Pope, C.A., 3rd, et al., *Lung cancer, cardiopulmonary mortality, and long-term exposure to fine particulate air pollution*. *JAMA*, 2002. **287**(9): p. 1132-41.
262. Caron, O., et al., *Lung Adenocarcinoma as Part of the Li-Fraumeni Syndrome Spectrum: Preliminary Data of the LIFSCREEN Randomized Clinical Trial*. *JAMA Oncol*, 2017. **3**(12): p. 1736-1737.
263. Goodwin, S., J.D. McPherson, and W.R. McCombie, *Coming of age: ten years of next-generation sequencing technologies*. *Nat Rev Genet*, 2016. **17**(6): p. 333-51.
264. *Comprehensive genomic characterization of squamous cell lung cancers*. *Nature*, 2012. **489**(7417): p. 519-25.
265. Shames, D.S. and Wistuba, II, *The evolving genomic classification of lung cancer*. *J Pathol*, 2014. **232**(2): p. 121-33.
266. Jordan, E.J., et al., *Prospective Comprehensive Molecular Characterization of Lung Adenocarcinomas for Efficient Patient Matching to Approved and Emerging Therapies*. *Cancer Discov*, 2017. **7**(6): p. 596-609.
267. Barlesi, F., et al., *Routine molecular profiling of patients with advanced non-small-cell lung cancer: results of a 1-year nationwide programme of the French Cooperative Thoracic Intergroup (IFCT)*. *Lancet*, 2016. **387**(10026): p. 1415-1426.
268. Kris, M.G., et al., *Using multiplexed assays of oncogenic drivers in lung cancers to select targeted drugs*. *JAMA*, 2014. **311**(19): p. 1998-2006.
269. Koboldt, D.C., et al., *The next-generation sequencing revolution and its impact on genomics*. *Cell*, 2013. **155**(1): p. 27-38.
270. Han, B., et al., *EGFR mutation prevalence in Asia-Pacific and Russian patients with advanced NSCLC of adenocarcinoma and non-adenocarcinoma histology: The IGNITE study*. *Lung Cancer*, 2017. **113**: p. 37-44.
271. Li, S., et al., *Coexistence of EGFR with KRAS, or BRAF, or PIK3CA somatic mutations in lung cancer: a comprehensive mutation profiling from 5125 Chinese cohorts*. *Br J Cancer*, 2014. **110**(11): p. 2812-20.
272. Tseng, C.H., et al., *The Relationship Between Air Pollution and Lung Cancer in Nonsmokers in Taiwan*. *J Thorac Oncol*, 2019. **14**(5): p. 784-792.
273. Melloni, B.B., *Lung cancer in never-smokers: radon exposure and environmental tobacco smoke*. *Eur Respir J*, 2014. **44**(4): p. 850-2.



274. Sabir, S.R., et al., *EML4-ALK Variants: Biological and Molecular Properties, and the Implications for Patients*. *Cancers* (Basel), 2017. **9**(9).
275. Bayliss, R., et al., *Molecular mechanisms that underpin EML4-ALK driven cancers and their response to targeted drugs*. *Cell Mol Life Sci*, 2016. **73**(6): p. 1209-24.
276. Lin, J.J., et al., *Impact of EML4-ALK Variant on Resistance Mechanisms and Clinical Outcomes in ALK-Positive Lung Cancer*. *J Clin Oncol*, 2018. **36**(12): p. 1199-1206.
277. Heuckmann, J.M., et al., *Differential protein stability and ALK inhibitor sensitivity of EML4-ALK fusion variants*. *Clin Cancer Res*, 2012. **18**(17): p. 4682-90.
278. Choi, Y.L., et al., *Identification of novel isoforms of the EML4-ALK transforming gene in non-small cell lung cancer*. *Cancer Res*, 2008. **68**(13): p. 4971-6.
279. Richards, M.W., et al., *Microtubule association of EML proteins and the EML4-ALK variant 3 oncoprotein require an N-terminal trimerization domain*. *Biochem J*, 2015. **467**(3): p. 529-36.
280. Camidge, D.R., et al., *Updated Efficacy and Safety Data and Impact of the EML4-ALK Fusion Variant on the Efficacy of Alectinib in Untreated ALK-Positive Advanced Non-Small Cell Lung Cancer in the Global Phase III ALEX Study*. *J Thorac Oncol*, 2019. **14**(7): p. 1233-1243.
281. Shinmura, K., et al., *EML4-ALK fusion transcripts, but no NPM-, TPM3-, CLTC-, ATIC-, or TFG-ALK fusion transcripts, in non-small cell lung carcinomas*. *Lung Cancer*, 2008. **61**(2): p. 163-9.
282. Sagawa, R., et al., *ALK-Positive Squamous Cell Carcinoma Dramatically Responded to Alectinib*. *Case Rep Oncol Med*, 2018. **2018**: p. 4172721.
283. Boland, J.M., et al., *Pulmonary adenocarcinoma with signet ring cell features: a comprehensive study from 3 distinct patient cohorts*. *Am J Surg Pathol*, 2014. **38**(12): p. 1681-8.
284. Kerr, K.M. and F. Lopez-Rios, *Precision medicine in NSCLC and pathology: how does ALK fit in the pathway?* *Ann Oncol*, 2016. **27 Suppl 3**: p. iii16-iii24.
285. Wu, W., F. Haderk, and T.G. Bivona, *Non-Canonical Thinking for Targeting ALK-Fusion Onco-Proteins in Lung Cancer*. *Cancers* (Basel), 2017. **9**(12).
286. Shaw, A.T., et al., *Clinical features and outcome of patients with non-small-cell lung cancer who harbor EML4-ALK*. *J Clin Oncol*, 2009. **27**(26): p. 4247-53.
287. Pan, X., et al., *Frequent genomic alterations and better prognosis among young patients with non-small-cell lung cancer aged 40 years or younger*. *Clin Transl Oncol*, 2018. **20**(9): p. 1168-1174.
288. Suidan, A.M., et al., *Lung Cancer in Young Patients: Higher Rate of Driver Mutations and Brain Involvement, but Better Survival*. *J Glob Oncol*, 2019. **5**: p. 1-8.
289. Costa, D.B., et al., *Clinical Experience With Crizotinib in Patients With Advanced ALK-Rearranged Non-Small-Cell Lung Cancer and Brain Metastases*. *J Clin Oncol*, 2015. **33**(17): p. 1881-8.
290. Rangachari, D., et al., *Brain metastases in patients with EGFR-mutated or ALK-rearranged non-small-cell lung cancers*. *Lung Cancer*, 2015. **88**(1): p. 108-11.
291. Solomon, B.J., et al., *First-line crizotinib versus chemotherapy in ALK-positive lung cancer*. *N Engl J Med*, 2014. **371**(23): p. 2167-77.
292. Recondo, G., et al., *Making the first move in EGFR-driven or ALK-driven NSCLC: first-generation or next-generation TKI?* *Nat Rev Clin Oncol*, 2018. **15**(11): p. 694-708.
293. Solomon, B.J., et al., *Lorlatinib in patients with ALK-positive non-small-cell lung cancer: results from a global phase 2 study*. *Lancet Oncol*, 2018. **19**(12): p. 1654-1667.
294. Peters, S., et al., *Alectinib versus Crizotinib in Untreated ALK-Positive Non-Small-Cell Lung Cancer*. *N Engl J Med*, 2017. **377**(9): p. 829-838.
295. Soria, J.C., et al., *First-line ceritinib versus platinum-based chemotherapy in advanced ALK-rearranged non-small-cell lung cancer (ASCEND-4): a randomised, open-label, phase 3 study*. *Lancet*, 2017. **389**(10072): p. 917-929.
296. Camidge, D.R., et al., *Brigatinib versus Crizotinib in ALK-Positive Non-Small-Cell Lung Cancer*. *N Engl J Med*, 2018. **379**(21): p. 2027-2039.

297. Cui, J.J., et al., *Structure based drug design of crizotinib (PF-02341066), a potent and selective dual inhibitor of mesenchymal-epithelial transition factor (c-MET) kinase and anaplastic lymphoma kinase (ALK)*. J Med Chem, 2011. **54**(18): p. 6342-63.
298. Christensen, J.G., et al., *Cytoreductive antitumor activity of PF-2341066, a novel inhibitor of anaplastic lymphoma kinase and c-Met, in experimental models of anaplastic large-cell lymphoma*. Mol Cancer Ther, 2007. **6**(12 Pt 1): p. 3314-22.
299. Sun, Y., et al., *ALK inhibitor PF02341066 (crizotinib) increases sensitivity to radiation in non-small cell lung cancer expressing EML4-ALK*. Mol Cancer Ther, 2013. **12**(5): p. 696-704.
300. Solomon, B.J., et al., *Final Overall Survival Analysis From a Study Comparing First-Line Crizotinib Versus Chemotherapy in ALK-Mutation-Positive Non-Small-Cell Lung Cancer*. J Clin Oncol, 2018. **36**(22): p. 2251-2258.
301. Solomon, B.J., et al., *Intracranial Efficacy of Crizotinib Versus Chemotherapy in Patients With Advanced ALK-Positive Non-Small-Cell Lung Cancer: Results From PROFILE 1014*. J Clin Oncol, 2016. **34**(24): p. 2858-65.
302. Camidge, D.R., et al., *Activity and safety of crizotinib in patients with ALK-positive non-small-cell lung cancer: updated results from a phase 1 study*. Lancet Oncol, 2012. **13**(10): p. 1011-9.
303. Kwak, E.L., et al., *Anaplastic lymphoma kinase inhibition in non-small-cell lung cancer*. N Engl J Med, 2010. **363**(18): p. 1693-703.
304. Blackhall, F., et al., *Final results of the large-scale multinational trial PROFILE 1005: efficacy and safety of crizotinib in previously treated patients with advanced/metastatic ALK-positive non-small-cell lung cancer*. ESMO Open, 2017. **2**(3): p. e000219.
305. Shaw, A.T., et al., *Crizotinib versus chemotherapy in advanced ALK-positive lung cancer*. N Engl J Med, 2013. **368**(25): p. 2385-94.
306. Marsilje, T.H., et al., *Synthesis, structure-activity relationships, and in vivo efficacy of the novel potent and selective anaplastic lymphoma kinase (ALK) inhibitor 5-chloro-N2-(2-isopropoxy-5-methyl-4-(piperidin-4-yl)phenyl)-N4-(2-(isopropylsulfonyl)phenyl)pyrimidine-2,4-diamine (LDK378) currently in phase 1 and phase 2 clinical trials*. J Med Chem, 2013. **56**(14): p. 5675-90.
307. Fribolet, L., et al., *The ALK inhibitor ceritinib overcomes crizotinib resistance in non-small cell lung cancer*. Cancer Discov, 2014. **4**(6): p. 662-673.
308. Kim, D.W., et al., *Activity and safety of ceritinib in patients with ALK-rearranged non-small-cell lung cancer (ASCEND-1): updated results from the multicentre, open-label, phase 1 trial*. Lancet Oncol, 2016. **17**(4): p. 452-463.
309. Shaw, A.T., et al., *Ceritinib in ALK-rearranged non-small-cell lung cancer*. N Engl J Med, 2014. **370**(13): p. 1189-97.
310. Crino, L., et al., *Multicenter Phase II Study of Whole-Body and Intracranial Activity With Ceritinib in Patients With ALK-Rearranged Non-Small-Cell Lung Cancer Previously Treated With Chemotherapy and Crizotinib: Results From ASCEND-2*. J Clin Oncol, 2016. **34**(24): p. 2866-73.
311. Shaw, A.T., et al., *Ceritinib versus chemotherapy in patients with ALK-rearranged non-small-cell lung cancer previously given chemotherapy and crizotinib (ASCEND-5): a randomised, controlled, open-label, phase 3 trial*. Lancet Oncol, 2017. **18**(7): p. 874-886.
312. Tan, D.S., et al., *Comparative Efficacy of Ceritinib and Crizotinib as Initial ALK-Targeted Therapies in Previously Treated Advanced NSCLC: An Adjusted Comparison with External Controls*. J Thorac Oncol, 2016. **11**(9): p. 1550-7.
313. Novello, S., et al., *Alectinib versus chemotherapy in crizotinib-pretreated anaplastic lymphoma kinase (ALK)-positive non-small-cell lung cancer: results from the phase III ALUR study*. Ann Oncol, 2018. **29**(6): p. 1409-1416.
314. Katayama, R., et al., *P-glycoprotein Mediates Ceritinib Resistance in Anaplastic Lymphoma Kinase-rearranged Non-small Cell Lung Cancer*. EBioMedicine, 2016. **3**: p. 54-66.

315. Gainor, J.F., et al., *Alectinib salvages CNS relapses in ALK-positive lung cancer patients previously treated with crizotinib and ceritinib*. J Thorac Oncol, 2015. **10**(2): p. 232-6.
316. Gadgeel, S.M., et al., *Pooled Analysis of CNS Response to Alectinib in Two Studies of Pretreated Patients With ALK-Positive Non-Small-Cell Lung Cancer*. J Clin Oncol, 2016. **34**(34): p. 4079-4085.
317. Seto, T., et al., *CH5424802 (RO5424802) for patients with ALK-rearranged advanced non-small-cell lung cancer (AF-001JP study): a single-arm, open-label, phase 1-2 study*. Lancet Oncol, 2013. **14**(7): p. 590-8.
318. Tamura, T., et al., *Three-Year Follow-Up of an Alectinib Phase I/II Study in ALK-Positive Non-Small-Cell Lung Cancer: AF-001JP*. J Clin Oncol, 2017. **35**(14): p. 1515-1521.
319. Gadgeel, S.M., et al., *Safety and activity of alectinib against systemic disease and brain metastases in patients with crizotinib-resistant ALK-rearranged non-small-cell lung cancer (AF-002JG): results from the dose-finding portion of a phase 1/2 study*. Lancet Oncol, 2014. **15**(10): p. 1119-28.
320. Yang, J.C., et al., *Pooled Systemic Efficacy and Safety Data from the Pivotal Phase II Studies (NP28673 and NP28761) of Alectinib in ALK-positive Non-Small Cell Lung Cancer*. J Thorac Oncol, 2017. **12**(10): p. 1552-1560.
321. Hida, T., et al., *Alectinib versus crizotinib in patients with ALK-positive non-small-cell lung cancer (J-ALEX): an open-label, randomised phase 3 trial*. Lancet, 2017. **390**(10089): p. 29-39.
322. Zhang, S., et al., *The Potent ALK Inhibitor Brigatinib (AP26113) Overcomes Mechanisms of Resistance to First- and Second-Generation ALK Inhibitors in Preclinical Models*. Clin Cancer Res, 2016. **22**(22): p. 5527-5538.
323. L.A. Bazhenova, S.N.G., C.J. Langer, R. Salgia, K.A. Gold, R. Rosell, A.T. Shaw, G.J. Weiss, J. Haney, V.M. Rivera, D. Kerstein, R. Camidge, 1344P, *Brigatinib (BRG) in anaplastic lymphoma kinase (ALK)-positive non-small cell lung cancer (NSCLC): Long-term efficacy and safety results from a phase 1/2 trial*. Annals of Oncology, September 2017. **28**(suppl\_5).
324. Gettinger, S.N., et al., *Activity and safety of brigatinib in ALK-rearranged non-small-cell lung cancer and other malignancies: a single-arm, open-label, phase 1/2 trial*. Lancet Oncol, 2016. **17**(12): p. 1683-1696.
325. Kim, D.W., et al., *Brigatinib in Patients With Crizotinib-Refractory Anaplastic Lymphoma Kinase-Positive Non-Small-Cell Lung Cancer: A Randomized, Multicenter Phase II Trial*. J Clin Oncol, 2017. **35**(22): p. 2490-2498.
326. Zou, H.Y., et al., *PF-06463922, an ALK/ROS1 Inhibitor, Overcomes Resistance to First and Second Generation ALK Inhibitors in Preclinical Models*. Cancer Cell, 2015. **28**(1): p. 70-81.
327. Johnson, T.W., et al., *Discovery of (10R)-7-amino-12-fluoro-2,10,16-trimethyl-15-oxo-10,15,16,17-tetrahydro-2H-8,4-(m etheno)pyrazolo[4,3-h][2,5,11]-benzoxadiazacyclotetradecine-3-carbonitrile (PF-06463922), a macrocyclic inhibitor of anaplastic lymphoma kinase (ALK) and c-ros oncogene 1 (ROS1) with preclinical brain exposure and broad-spectrum potency against ALK-resistant mutations*. J Med Chem, 2014. **57**(11): p. 4720-44.
328. Akamine, T., et al., *Spotlight on lorlatinib and its potential in the treatment of NSCLC: the evidence to date*. Onco Targets Ther, 2018. **11**: p. 5093-5101.
329. Shaw, A.T., et al., *Lorlatinib in non-small-cell lung cancer with ALK or ROS1 rearrangement: an international, multicentre, open-label, single-arm first-in-man phase 1 trial*. Lancet Oncol, 2017. **18**(12): p. 1590-1599.
330. Shaw, A.T., et al., *ALK Resistance Mutations and Efficacy of Lorlatinib in Advanced Anaplastic Lymphoma Kinase-Positive Non-Small-Cell Lung Cancer*. J Clin Oncol, 2019. **37**(16): p. 1370-1379.
331. Wu, J., J. Savooji, and D. Liu, *Second- and third-generation ALK inhibitors for non-small cell lung cancer*. J Hematol Oncol, 2016. **9**: p. 19.

## Chapter VII - References

332. Zuccotto, F., et al., *Through the "gatekeeper door": exploiting the active kinase conformation*. J Med Chem, 2010. **53**(7): p. 2681-94.
333. Azam, M., et al., *Activation of tyrosine kinases by mutation of the gatekeeper threonine*. Nat Struct Mol Biol, 2008. **15**(10): p. 1109-18.
334. Lovly, C.M., et al., *Insights into ALK-driven cancers revealed through development of novel ALK tyrosine kinase inhibitors*. Cancer Res, 2011. **71**(14): p. 4920-31.
335. Sun, H.Y. and F.Q. Ji, *A molecular dynamics investigation on the crizotinib resistance mechanism of C1156Y mutation in ALK*. Biochem Biophys Res Commun, 2012. **423**(2): p. 319-24.
336. Cecon, M., et al., *Crizotinib-resistant NPM-ALK mutants confer differential sensitivity to unrelated Alk inhibitors*. Mol Cancer Res, 2013. **11**(2): p. 122-32.
337. Gambacorti Passerini, C., et al., *Crizotinib in advanced, chemoresistant anaplastic lymphoma kinase-positive lymphoma patients*. J Natl Cancer Inst, 2014. **106**(2): p. djt378.
338. Sasaki, T., et al., *The neuroblastoma-associated F1174L ALK mutation causes resistance to an ALK kinase inhibitor in ALK-translocated cancers*. Cancer Res, 2010. **70**(24): p. 10038-43.
339. Bresler, S.C., et al., *Differential inhibitor sensitivity of anaplastic lymphoma kinase variants found in neuroblastoma*. Sci Transl Med, 2011. **3**(108): p. 108ra114.
340. Ou, S.H., et al., *Identification of a novel HIP1-ALK fusion variant in Non-Small-Cell Lung Cancer (NSCLC) and discovery of ALK I1171 (I1171N/S) mutations in two ALK-rearranged NSCLC patients with resistance to Alectinib*. J Thorac Oncol, 2014. **9**(12): p. 1821-5.
341. Sasaki, T., et al., *A novel ALK secondary mutation and EGFR signaling cause resistance to ALK kinase inhibitors*. Cancer Res, 2011. **71**(18): p. 6051-60.
342. Katayama, R., et al., *Mechanisms of acquired crizotinib resistance in ALK-rearranged lung Cancers*. Sci Transl Med, 2012. **4**(120): p. 120ra17.
343. Doebele, R.C., et al., *Mechanisms of resistance to crizotinib in patients with ALK gene rearranged non-small cell lung cancer*. Clin Cancer Res, 2012. **18**(5): p. 1472-82.
344. Toyokawa, G., et al., *Identification of a Novel ALK G1123S Mutation in a Patient with ALK-rearranged Non-small-cell Lung Cancer Exhibiting Resistance to Ceritinib*. J Thorac Oncol, 2015. **10**(7): p. e55-7.
345. Sai-Hong Ignatius Ou, A.B.S., Kyle Gowen, Philip J. Stephens, Jeffrey S. Ross, Melissa Lynne Johnson, Christine Marie Lovly, Siraj Mahamed Ali, Vincent A. Miller, and Alice Tsang Shaw, *Association of ALK resistance mutations by EML4-ALK variant (v3 vs. non-v3) in ALK+ non-small cell lung cancer (NSCLC)*. Journal of Clinical Oncology, 2017. **35**(15\_suppl): p. 9010-9010.
346. Heuckmann, J.M., et al., *ALK mutations conferring differential resistance to structurally diverse ALK inhibitors*. Clin Cancer Res, 2011. **17**(23): p. 7394-401.
347. Michels, S.Y.F., et al., *ALK(G1269A) mutation as a potential mechanism of acquired resistance to crizotinib in an ALK-rearranged inflammatory myofibroblastic tumor*. NPJ Precis Oncol, 2017. **1**(1): p. 4.
348. Wang, H.Y., C.C. Ho, and J.Y. Shih, *Multiple Acquired Resistance Mutations of the ALK Tyrosine Kinase Domain after Sequential Use of ALK Inhibitors*. J Thorac Oncol, 2017. **12**(5): p. e49-e51.
349. Katayama, R., et al., *Two novel ALK mutations mediate acquired resistance to the next-generation ALK inhibitor alectinib*. Clin Cancer Res, 2014. **20**(22): p. 5686-96.
350. Cecon, M., et al., *Treatment Efficacy and Resistance Mechanisms Using the Second-Generation ALK Inhibitor AP26113 in Human NPM-ALK-Positive Anaplastic Large Cell Lymphoma*. Mol Cancer Res, 2015. **13**(4): p. 775-83.
351. Scott N. Gettinger, S.Z., J. Graeme Hodgson, Lyudmila Bazhenova, Sjaak Burgers, Dong-Wan Kim, Daniel Shao-Weng Tan, Han A. Koh, James C. M. Ho, Santiago Viteri Ramirez, Alice Tsang Shaw, Glen J. Weiss, Corey J. Langer, Rudolf M. Huber, Myung-Ju Ahn, William G Reichmann, David Kerstein, Victor M. Rivera, D. Ross Camidge,

- Activity of brigatinib (BRG) in crizotinib (CRZ) resistant patients (pts) according to ALK mutation status.* Journal of Clinical Oncology, 2017. **35**: p. 9065.
352. Gainor, J.F., et al., *Alectinib Dose Escalation Reinduces Central Nervous System Responses in Patients with Anaplastic Lymphoma Kinase-Positive Non-Small Cell Lung Cancer Relapsing on Standard Dose Alectinib.* J Thorac Oncol, 2016. **11**(2): p. 256-60.
  353. Yoda, S., et al., *Sequential ALK Inhibitors Can Select for Lorlatinib-Resistant Compound ALK Mutations in ALK-Positive Lung Cancer.* Cancer Discov, 2018. **8**(6): p. 714-729.
  354. Recondo, G., et al., *Diverse resistance mechanisms to the third-generation ALK inhibitor lorlatinib in ALK-rearranged lung cancer.* Clin Cancer Res, 2019.
  355. Tchekmedyian, N., et al., *Acquired ALK L1152R Mutation Confers Resistance to Ceritinib and Predicts Response to Alectinib.* J Thorac Oncol, 2016. **11**(7): p. e87-8.
  356. Ignatius Ou, S.H., et al., *Next-generation sequencing reveals a Novel NSCLC ALK F1174V mutation and confirms ALK G1202R mutation confers high-level resistance to alectinib (CH5424802/RO5424802) in ALK-rearranged NSCLC patients who progressed on crizotinib.* J Thorac Oncol, 2014. **9**(4): p. 549-53.
  357. Fontana, D., et al., *Activity of second-generation ALK inhibitors against crizotinib-resistant mutants in an NPM-ALK model compared to EML4-ALK.* Cancer Med, 2015. **4**(7): p. 953-65.
  358. Gainor, J.F., et al., *Molecular Mechanisms of Resistance to First- and Second-Generation ALK Inhibitors in ALK-Rearranged Lung Cancer.* Cancer Discov, 2016. **6**(10): p. 1118-1133.
  359. Shaw, A.T., et al., *Resensitization to Crizotinib by the Lorlatinib ALK Resistance Mutation L1198F.* N Engl J Med, 2016. **374**(1): p. 54-61.
  360. Okada, K., et al., *Prediction of ALK mutations mediating ALK-TKIs resistance and drug repurposing to overcome the resistance.* EBioMedicine, 2019. **41**: p. 105-119.
  361. Amin, A.D., et al., *Evidence Suggesting That Discontinuous Dosing of ALK Kinase Inhibitors May Prolong Control of ALK+ Tumors.* Cancer Res, 2015. **75**(14): p. 2916-27.
  362. Cecon, M., et al., *Excess of NPM-ALK oncogenic signaling promotes cellular apoptosis and drug dependency.* Oncogene, 2016. **35**(29): p. 3854-3865.
  363. Miyawaki, M., et al., *Overcoming EGFR Bypass Signal-Induced Acquired Resistance to ALK Tyrosine Kinase Inhibitors in ALK-Translocated Lung Cancer.* Mol Cancer Res, 2017. **15**(1): p. 106-114.
  364. Wilson, F.H., et al., *A functional landscape of resistance to ALK inhibition in lung cancer.* Cancer Cell, 2015. **27**(3): p. 397-408.
  365. Hrustanovic, G., et al., *RAS-MAPK dependence underlies a rational polytherapy strategy in EML4-ALK-positive lung cancer.* Nat Med, 2015. **21**(9): p. 1038-47.
  366. Tamura, T.e.a., *Updated Data of a Phase 1/2 Study (AF-001JP) of Alectinib, a CNS-Penetrant, Highly Selective ALK Inhibitor in ALK-rearranged Advanced NSCLC.* International Journal of Radiation Oncology, 2014. **90**(5).
  367. Laimer, D., et al., *PDGFR blockade is a rational and effective therapy for NPM-ALK-driven lymphomas.* Nat Med, 2012. **18**(11): p. 1699-704.
  368. Crystal, A.S., et al., *Patient-derived models of acquired resistance can identify effective drug combinations for cancer.* Science, 2014. **346**(6216): p. 1480-6.
  369. Lovly, C.M., et al., *Rationale for co-targeting IGF-1R and ALK in ALK fusion-positive lung cancer.* Nat Med, 2014. **20**(9): p. 1027-34.
  370. Redaelli, S., et al., *Lorlatinib Treatment Elicits Multiple On- and Off-Target Mechanisms of Resistance in ALK-Driven Cancer.* Cancer Res, 2018. **78**(24): p. 6866-6880.
  371. Dongre, A. and R.A. Weinberg, *New insights into the mechanisms of epithelial-mesenchymal transition and implications for cancer.* Nat Rev Mol Cell Biol, 2019. **20**(2): p. 69-84.
  372. Xu, J., S. Lamouille, and R. Derynck, *TGF-beta-induced epithelial to mesenchymal transition.* Cell Res, 2009. **19**(2): p. 156-72.

## Chapter VII - References

373. Wu, Y., et al., *Expression of Wnt3 activates Wnt/beta-catenin pathway and promotes EMT-like phenotype in trastuzumab-resistant HER2-overexpressing breast cancer cells*. *Mol Cancer Res*, 2012. **10**(12): p. 1597-606.
374. Natsuzaka, M., et al., *Interplay between Notch1 and Notch3 promotes EMT and tumor initiation in squamous cell carcinoma*. *Nat Commun*, 2017. **8**(1): p. 1758.
375. Avizienyte, E., et al., *Src-induced de-regulation of E-cadherin in colon cancer cells requires integrin signalling*. *Nat Cell Biol*, 2002. **4**(8): p. 632-8.
376. Ponzio, M.G., et al., *Met induces mammary tumors with diverse histologies and is associated with poor outcome and human basal breast cancer*. *Proc Natl Acad Sci U S A*, 2009. **106**(31): p. 12903-8.
377. Zhang, Z., et al., *Activation of the AXL kinase causes resistance to EGFR-targeted therapy in lung cancer*. *Nat Genet*, 2012. **44**(8): p. 852-60.
378. Webb, D.J., et al., *FAK-Src signalling through paxillin, ERK and MLCK regulates adhesion disassembly*. *Nat Cell Biol*, 2004. **6**(2): p. 154-61.
379. Fukuda, K., et al., *Epithelial-to-Mesenchymal Transition Is a Mechanism of ALK Inhibitor Resistance in Lung Cancer Independent of ALK Mutation Status*. *Cancer Res*, 2019. **79**(7): p. 1658-1670.
380. Oxnard, G.R., et al., *Assessment of Resistance Mechanisms and Clinical Implications in Patients With EGFR T790M-Positive Lung Cancer and Acquired Resistance to Osimertinib*. *JAMA Oncol*, 2018. **4**(11): p. 1527-1534.
381. Sequist, L.V., et al., *Genotypic and histological evolution of lung cancers acquiring resistance to EGFR inhibitors*. *Sci Transl Med*, 2011. **3**(75): p. 75ra26.
382. Piotrowska, Z., et al., *Landscape of Acquired Resistance to Osimertinib in EGFR-Mutant NSCLC and Clinical Validation of Combined EGFR and RET Inhibition with Osimertinib and BLU-667 for Acquired RET Fusion*. *Cancer Discov*, 2018. **8**(12): p. 1529-1539.
383. Park, S., J. Han, and J.M. Sun, *Histologic transformation of ALK-rearranged adenocarcinoma to squamous cell carcinoma after treatment with ALK inhibitor*. *Lung Cancer*, 2019. **127**: p. 66-68.
384. Hobeika, C., et al., *ALK-rearranged adenocarcinoma transformed to small-cell lung cancer: a new entity with specific prognosis and treatment? Per Med*, 2018. **15**(2): p. 111-115.
385. Cha, Y.J., et al., *A Case of ALK-Rearranged Adenocarcinoma with Small Cell Carcinoma-Like Transformation and Resistance to Crizotinib*. *J Thorac Oncol*, 2016. **11**(5): p. e55-e58.
386. Takegawa, N., et al., *Transformation of ALK rearrangement-positive adenocarcinoma to small-cell lung cancer in association with acquired resistance to alectinib*. *Ann Oncol*, 2016. **27**(5): p. 953-5.
387. Engelman, J.A., et al., *MET amplification leads to gefitinib resistance in lung cancer by activating ERBB3 signaling*. *Science*, 2007. **316**(5827): p. 1039-43.
388. Gouji, T., et al., *Crizotinib can overcome acquired resistance to CH5424802: is amplification of the MET gene a key factor? J Thorac Oncol*, 2014. **9**(3): p. e27-8.
389. Sharma, P., et al., *Novel cancer immunotherapy agents with survival benefit: recent successes and next steps*. *Nat Rev Cancer*, 2011. **11**(11): p. 805-12.
390. Sharma, P. and J.P. Allison, *The future of immune checkpoint therapy*. *Science*, 2015. **348**(6230): p. 56-61.
391. Brahmer, J., et al., *Nivolumab versus Docetaxel in Advanced Squamous-Cell Non-Small-Cell Lung Cancer*. *N Engl J Med*, 2015. **373**(2): p. 123-35.
392. Garon, E.B., et al., *Pembrolizumab for the treatment of non-small-cell lung cancer*. *N Engl J Med*, 2015. **372**(21): p. 2018-28.
393. Borghaei, H., et al., *Nivolumab versus Docetaxel in Advanced Nonsquamous Non-Small-Cell Lung Cancer*. *N Engl J Med*, 2015. **373**(17): p. 1627-39.
394. Rizvi, N.A., et al., *Cancer immunology. Mutational landscape determines sensitivity to PD-1 blockade in non-small cell lung cancer*. *Science*, 2015. **348**(6230): p. 124-8.

395. Kinoshita, T., et al., *Determination of poor prognostic immune features of tumour microenvironment in non-smoking patients with lung adenocarcinoma*. *Eur J Cancer*, 2017. **86**: p. 15-27.
396. Colli, L.M., et al., *Burden of Nonsynonymous Mutations among TCGA Cancers and Candidate Immune Checkpoint Inhibitor Responses*. *Cancer Res*, 2016. **76**(13): p. 3767-72.
397. Voena, C., et al., *Efficacy of a Cancer Vaccine against ALK-Rearranged Lung Tumors*. *Cancer Immunol Res*, 2015. **3**(12): p. 1333-1343.
398. Ott, P.A., et al., *An immunogenic personal neoantigen vaccine for patients with melanoma*. *Nature*, 2017. **547**(7662): p. 217-221.
399. Cai, A., et al., *Mutated BCR-ABL generates immunogenic T-cell epitopes in CML patients*. *Clin Cancer Res*, 2012. **18**(20): p. 5761-72.
400. Pulford, K., et al., *Immune response to the ALK oncogenic tyrosine kinase in patients with anaplastic large-cell lymphoma*. *Blood*, 2000. **96**(4): p. 1605-7.
401. Passoni, L., et al., *ALK as a novel lymphoma-associated tumor antigen: identification of 2 HLA-A2.1-restricted CD8+ T-cell epitopes*. *Blood*, 2002. **99**(6): p. 2100-6.
402. Chiarle, R., et al., *The anaplastic lymphoma kinase is an effective oncoantigen for lymphoma vaccination*. *Nat Med*, 2008. **14**(6): p. 676-80.
403. Hong, S., et al., *Upregulation of PD-L1 by EML4-ALK fusion protein mediates the immune escape in ALK positive NSCLC: Implication for optional anti-PD-1/PD-L1 immune therapy for ALK-TKIs sensitive and resistant NSCLC patients*. *Oncoimmunology*, 2016. **5**(3): p. e1094598.
404. Mittal, D., et al., *New insights into cancer immunoediting and its three component phases--elimination, equilibrium and escape*. *Curr Opin Immunol*, 2014. **27**: p. 16-25.
405. Shankaran, V., et al., *IFN $\gamma$  and lymphocytes prevent primary tumour development and shape tumour immunogenicity*. *Nature*, 2001. **410**(6832): p. 1107-11.
406. Dunn, G.P., C.M. Koebel, and R.D. Schreiber, *Interferons, immunity and cancer immunoediting*. *Nat Rev Immunol*, 2006. **6**(11): p. 836-48.
407. Burnet, M., *Cancer; a biological approach. I. The processes of control*. *Br Med J*, 1957. **1**(5022): p. 779-86.
408. Ward, J.P., M.M. Gubin, and R.D. Schreiber, *The Role of Neoantigens in Naturally Occurring and Therapeutically Induced Immune Responses to Cancer*. *Adv Immunol*, 2016. **130**: p. 25-74.
409. Smyth, M.J., D.I. Godfrey, and J.A. Trapani, *A fresh look at tumor immunosurveillance and immunotherapy*. *Nat Immunol*, 2001. **2**(4): p. 293-9.
410. Teng, M.W., et al., *From mice to humans: developments in cancer immunoediting*. *J Clin Invest*, 2015. **125**(9): p. 3338-46.
411. Diefenbach, A., et al., *Rae1 and H60 ligands of the NKG2D receptor stimulate tumour immunity*. *Nature*, 2001. **413**(6852): p. 165-71.
412. Smyth, M.J., et al., *Tumor necrosis factor-related apoptosis-inducing ligand (TRAIL) contributes to interferon gamma-dependent natural killer cell protection from tumor metastasis*. *J Exp Med*, 2001. **193**(6): p. 661-70.
413. Diamond, M.S., et al., *Type I interferon is selectively required by dendritic cells for immune rejection of tumors*. *J Exp Med*, 2011. **208**(10): p. 1989-2003.
414. Fuertes, M.B., et al., *Host type I IFN signals are required for antitumor CD8+ T cell responses through CD8 $\alpha$ + dendritic cells*. *J Exp Med*, 2011. **208**(10): p. 2005-16.
415. MacKie, R.M., R. Reid, and B. Junor, *Fatal melanoma transferred in a donated kidney 16 years after melanoma surgery*. *N Engl J Med*, 2003. **348**(6): p. 567-8.
416. Koebel, C.M., et al., *Adaptive immunity maintains occult cancer in an equilibrium state*. *Nature*, 2007. **450**(7171): p. 903-7.
417. Dunn, G.P., L.J. Old, and R.D. Schreiber, *The immunobiology of cancer immunosurveillance and immunoediting*. *Immunity*, 2004. **21**(2): p. 137-48.

## Chapter VII - References

---

418. Vesely, M.D., et al., *Natural innate and adaptive immunity to cancer*. *Annu Rev Immunol*, 2011. **29**: p. 235-71.
419. Yu, H., D. Pardoll, and R. Jove, *STATs in cancer inflammation and immunity: a leading role for STAT3*. *Nat Rev Cancer*, 2009. **9**(11): p. 798-809.
420. Coulie, P.G., et al., *Tumour antigens recognized by T lymphocytes: at the core of cancer immunotherapy*. *Nat Rev Cancer*, 2014. **14**(2): p. 135-46.
421. Heemskerck, B., P. Kvistborg, and T.N. Schumacher, *The cancer antigenome*. *EMBO J*, 2013. **32**(2): p. 194-203.
422. Ohminami, H., M. Yasukawa, and S. Fujita, *HLA class I-restricted lysis of leukemia cells by a CD8(+) cytotoxic T-lymphocyte clone specific for WT1 peptide*. *Blood*, 2000. **95**(1): p. 286-93.
423. Fisk, B., et al., *Identification of an immunodominant peptide of HER-2/neu protooncogene recognized by ovarian tumor-specific cytotoxic T lymphocyte lines*. *J Exp Med*, 1995. **181**(6): p. 2109-17.
424. Starr, T.K., S.C. Jameson, and K.A. Hogquist, *Positive and negative selection of T cells*. *Annu Rev Immunol*, 2003. **21**: p. 139-76.
425. Singer, A., S. Adoro, and J.H. Park, *Lineage fate and intense debate: myths, models and mechanisms of CD4- versus CD8-lineage choice*. *Nat Rev Immunol*, 2008. **8**(10): p. 788-801.
426. Klein, L., et al., *Positive and negative selection of the T cell repertoire: what thymocytes see (and don't see)*. *Nat Rev Immunol*, 2014. **14**(6): p. 377-91.
427. Takahama, Y., *Journey through the thymus: stromal guides for T-cell development and selection*. *Nat Rev Immunol*, 2006. **6**(2): p. 127-35.
428. Vasko, M.R. and H. Ono, *Adenosine analogs do not inhibit the potassium-stimulated release of substance P from rat spinal cord slices*. *Naunyn Schmiedeberg's Arch Pharmacol*, 1990. **342**(4): p. 441-6.
429. Kyewski, B. and L. Klein, *A central role for central tolerance*. *Annu Rev Immunol*, 2006. **24**: p. 571-606.
430. Anderson, G., P.J. Lane, and E.J. Jenkinson, *Generating intrathymic microenvironments to establish T-cell tolerance*. *Nat Rev Immunol*, 2007. **7**(12): p. 954-63.
431. Derbinski, J. and B. Kyewski, *How thymic antigen presenting cells sample the body's self-antigens*. *Curr Opin Immunol*, 2010. **22**(5): p. 592-600.
432. Sprent, J. and H. Kishimoto, *The thymus and negative selection*. *Immunol Rev*, 2002. **185**: p. 126-35.
433. Sakaguchi, S., et al., *Regulatory T cells and immune tolerance*. *Cell*, 2008. **133**(5): p. 775-87.
434. Ashton-Rickardt, P.G., et al., *Evidence for a differential avidity model of T cell selection in the thymus*. *Cell*, 1994. **76**(4): p. 651-63.
435. Sebzda, E., et al., *Positive and negative thymocyte selection induced by different concentrations of a single peptide*. *Science*, 1994. **263**(5153): p. 1615-8.
436. Takahama, Y., et al., *Positive selection of CD4+ T cells by TCR ligation without aggregation even in the absence of MHC*. *Nature*, 1994. **371**(6492): p. 67-70.
437. Hogquist, K.A., S.C. Jameson, and M.J. Bevan, *Strong agonist ligands for the T cell receptor do not mediate positive selection of functional CD8+ T cells*. *Immunity*, 1995. **3**(1): p. 79-86.
438. von Boehmer, H. and F. Melchers, *Checkpoints in lymphocyte development and autoimmune disease*. *Nat Immunol*, 2010. **11**(1): p. 14-20.
439. Stritesky, G.L., S.C. Jameson, and K.A. Hogquist, *Selection of self-reactive T cells in the thymus*. *Annu Rev Immunol*, 2012. **30**: p. 95-114.
440. Alam, S.M., et al., *T-cell-receptor affinity and thymocyte positive selection*. *Nature*, 1996. **381**(6583): p. 616-20.
441. Daniels, M.A., et al., *Thymic selection threshold defined by compartmentalization of Ras/MAPK signalling*. *Nature*, 2006. **444**(7120): p. 724-9.
442. Palmer, E. and D. Naeher, *Affinity threshold for thymic selection through a T-cell receptor-co-receptor zipper*. *Nat Rev Immunol*, 2009. **9**(3): p. 207-13.



443. Brown, J.H., et al., *Three-dimensional structure of the human class II histocompatibility antigen HLA-DR1*. *Nature*, 1993. **364**(6432): p. 33-9.
444. Bjorkman, P.J., et al., *The foreign antigen binding site and T cell recognition regions of class I histocompatibility antigens*. *Nature*, 1987. **329**(6139): p. 512-8.
445. Falk, K., et al., *Pool sequencing of natural HLA-DR, DQ, and DP ligands reveals detailed peptide motifs, constraints of processing, and general rules*. *Immunogenetics*, 1994. **39**(4): p. 230-42.
446. Falk, K., et al., *Allele-specific motifs revealed by sequencing of self-peptides eluted from MHC molecules*. *Nature*, 1991. **351**(6324): p. 290-6.
447. Madden, D.R., D.N. Garboczi, and D.C. Wiley, *The antigenic identity of peptide-MHC complexes: a comparison of the conformations of five viral peptides presented by HLA-A2*. *Cell*, 1993. **75**(4): p. 693-708.
448. Smith, K.J., et al., *Bound water structure and polymorphic amino acids act together to allow the binding of different peptides to MHC class I HLA-B53*. *Immunity*, 1996. **4**(3): p. 215-28.
449. Holland, C.J., D.K. Cole, and A. Godkin, *Re-Directing CD4(+) T Cell Responses with the Flanking Residues of MHC Class II-Bound Peptides: The Core is Not Enough*. *Front Immunol*, 2013. **4**: p. 172.
450. Walz, S., et al., *The antigenic landscape of multiple myeloma: mass spectrometry (re)defines targets for T-cell-based immunotherapy*. *Blood*, 2015. **126**(10): p. 1203-13.
451. Schmid, B.V., C. Kesmir, and R.J. de Boer, *Quantifying how MHC polymorphism prevents pathogens from adapting to the antigen presentation pathway*. *Epidemics*, 2010. **2**(3): p. 99-108.
452. Neefjes, J., et al., *Towards a systems understanding of MHC class I and MHC class II antigen presentation*. *Nat Rev Immunol*, 2011. **11**(12): p. 823-36.
453. Michalek, M.T., et al., *A role for the ubiquitin-dependent proteolytic pathway in MHC class I-restricted antigen presentation*. *Nature*, 1993. **363**(6429): p. 552-4.
454. Rock, K.L., et al., *Inhibitors of the proteasome block the degradation of most cell proteins and the generation of peptides presented on MHC class I molecules*. *Cell*, 1994. **78**(5): p. 761-71.
455. Reits, E., et al., *Peptide diffusion, protection, and degradation in nuclear and cytoplasmic compartments before antigen presentation by MHC class I*. *Immunity*, 2003. **18**(1): p. 97-108.
456. Cresswell, P., et al., *The nature of the MHC class I peptide loading complex*. *Immunol Rev*, 1999. **172**: p. 21-8.
457. Wearsch, P.A. and P. Cresswell, *Selective loading of high-affinity peptides onto major histocompatibility complex class I molecules by the tapasin-ERp57 heterodimer*. *Nat Immunol*, 2007. **8**(8): p. 873-81.
458. Garstka, M.A., et al., *The first step of peptide selection in antigen presentation by MHC class I molecules*. *Proc Natl Acad Sci U S A*, 2015. **112**(5): p. 1505-10.
459. Saveanu, L., et al., *Concerted peptide trimming by human ERAP1 and ERAP2 aminopeptidase complexes in the endoplasmic reticulum*. *Nat Immunol*, 2005. **6**(7): p. 689-97.
460. Serwold, T., et al., *ERAAP customizes peptides for MHC class I molecules in the endoplasmic reticulum*. *Nature*, 2002. **419**(6906): p. 480-3.
461. Morozov, G.I., et al., *Interaction of TAPBPR, a tapasin homolog, with MHC-I molecules promotes peptide editing*. *Proc Natl Acad Sci U S A*, 2016. **113**(8): p. E1006-15.
462. Hermann, C., et al., *TAPBPR alters MHC class I peptide presentation by functioning as a peptide exchange catalyst*. *Elife*, 2015. **4**.
463. Chang, S.C., et al., *The ER aminopeptidase, ERAP1, trims precursors to lengths of MHC class I peptides by a "molecular ruler" mechanism*. *Proc Natl Acad Sci U S A*, 2005. **102**(47): p. 17107-12.
464. York, I.A., et al., *The ER aminopeptidase ERAP1 enhances or limits antigen presentation by trimming epitopes to 8-9 residues*. *Nat Immunol*, 2002. **3**(12): p. 1177-84.

465. Nguyen, T.T., et al., *Structural basis for antigenic peptide precursor processing by the endoplasmic reticulum aminopeptidase ERA1P1*. *Nat Struct Mol Biol*, 2011. **18**(5): p. 604-13.
466. Roelse, J., et al., *Trimming of TAP-translocated peptides in the endoplasmic reticulum and in the cytosol during recycling*. *J Exp Med*, 1994. **180**(5): p. 1591-7.
467. Elliott, T., et al., *Peptide-induced conformational change of the class I heavy chain*. *Nature*, 1991. **351**(6325): p. 402-6.
468. Schumacher, T.N., et al., *Direct binding of peptide to empty MHC class I molecules on intact cells and in vitro*. *Cell*, 1990. **62**(3): p. 563-7.
469. Kelly, A., et al., *Assembly and function of the two ABC transporter proteins encoded in the human major histocompatibility complex*. *Nature*, 1992. **355**(6361): p. 641-4.
470. Neeffjes, J.J. and H.L. Ploegh, *Allele and locus-specific differences in cell surface expression and the association of HLA class I heavy chain with beta 2-microglobulin: differential effects of inhibition of glycosylation on class I subunit association*. *Eur J Immunol*, 1988. **18**(5): p. 801-10.
471. Rammensee, H., et al., *SYFPEITHI: database for MHC ligands and peptide motifs*. *Immunogenetics*, 1999. **50**(3-4): p. 213-9.
472. Yewdell, J.W., *DRiPs solidify: progress in understanding endogenous MHC class I antigen processing*. *Trends Immunol*, 2011. **32**(11): p. 548-58.
473. Rock, K.L., et al., *Re-examining class-I presentation and the DRiP hypothesis*. *Trends Immunol*, 2014. **35**(4): p. 144-52.
474. Monaco, J.J. and D. Nandi, *The genetics of proteasomes and antigen processing*. *Annu Rev Genet*, 1995. **29**: p. 729-54.
475. Gaczynska, M., K.L. Rock, and A.L. Goldberg, *Gamma-interferon and expression of MHC genes regulate peptide hydrolysis by proteasomes*. *Nature*, 1993. **365**(6443): p. 264-7.
476. Groettrup, M., et al., *A third interferon-gamma-induced subunit exchange in the 20S proteasome*. *Eur J Immunol*, 1996. **26**(4): p. 863-9.
477. Toes, R.E., et al., *Discrete cleavage motifs of constitutive and immunoproteasomes revealed by quantitative analysis of cleavage products*. *J Exp Med*, 2001. **194**(1): p. 1-12.
478. Kincaid, E.Z., et al., *Specialized proteasome subunits have an essential role in the thymic selection of CD8(+) T cells*. *Nat Immunol*, 2016. **17**(8): p. 938-45.
479. Ossendorp, F., et al., *A single residue exchange within a viral CTL epitope alters proteasome-mediated degradation resulting in lack of antigen presentation*. *Immunity*, 1996. **5**(2): p. 115-24.
480. Tomaru, U., et al., *Exclusive expression of proteasome subunit {beta}5t in the human thymic cortex*. *Blood*, 2009. **113**(21): p. 5186-91.
481. Yewdell, J.W., E. Reits, and J. Neeffjes, *Making sense of mass destruction: quantitating MHC class I antigen presentation*. *Nat Rev Immunol*, 2003. **3**(12): p. 952-61.
482. Meyer, V.S., et al., *Identification of natural MHC class II presented phosphopeptides and tumor-derived MHC class I phospholigands*. *J Proteome Res*, 2009. **8**(7): p. 3666-74.
483. Haurum, J.S., et al., *Presentation of cytosolic glycosylated peptides by human class I major histocompatibility complex molecules in vivo*. *J Exp Med*, 1999. **190**(1): p. 145-50.
484. Petersen, J., A.W. Purcell, and J. Rossjohn, *Post-translationally modified T cell epitopes: immune recognition and immunotherapy*. *J Mol Med (Berl)*, 2009. **87**(11): p. 1045-51.
485. Gromme, M., et al., *The rational design of TAP inhibitors using peptide substrate modifications and peptidomimetics*. *Eur J Immunol*, 1997. **27**(4): p. 898-904.
486. Andersen, M.H., et al., *Phosphorylated peptides can be transported by TAP molecules, presented by class I MHC molecules, and recognized by phosphopeptide-specific CTL*. *J Immunol*, 1999. **163**(7): p. 3812-8.
487. Mohammed, F., et al., *Phosphorylation-dependent interaction between antigenic peptides and MHC class I: a molecular basis for the presentation of transformed self*. *Nat Immunol*, 2008. **9**(11): p. 1236-43.

488. Zarling, A.L., et al., *Phosphorylated peptides are naturally processed and presented by major histocompatibility complex class I molecules in vivo*. J Exp Med, 2000. **192**(12): p. 1755-62.
489. Unanue, E.R., V. Turk, and J. Neefjes, *Variations in MHC Class II Antigen Processing and Presentation in Health and Disease*. Annu Rev Immunol, 2016. **34**: p. 265-97.
490. Jones, E.Y., *MHC class I and class II structures*. Curr Opin Immunol, 1997. **9**(1): p. 75-9.
491. Stern, L.J., et al., *Crystal structure of the human class II MHC protein HLA-DR1 complexed with an influenza virus peptide*. Nature, 1994. **368**(6468): p. 215-21.
492. Suri, A., S.B. Lovitch, and E.R. Unanue, *The wide diversity and complexity of peptides bound to class II MHC molecules*. Curr Opin Immunol, 2006. **18**(1): p. 70-7.
493. Cresswell, P. and P.A. Roche, *Invariant chain-MHC class II complexes: always odd and never invariant*. Immunol Cell Biol, 2014. **92**(6): p. 471-2.
494. Neefjes, J., *CIIV, MIIC and other compartments for MHC class II loading*. Eur J Immunol, 1999. **29**(5): p. 1421-5.
495. Ghosh, P., et al., *The structure of an intermediate in class II MHC maturation: CLIP bound to HLA-DR3*. Nature, 1995. **378**(6556): p. 457-62.
496. Denzin, L.K. and P. Cresswell, *HLA-DM induces CLIP dissociation from MHC class II alpha beta dimers and facilitates peptide loading*. Cell, 1995. **82**(1): p. 155-65.
497. Pos, W., et al., *Crystal structure of the HLA-DM-HLA-DR1 complex defines mechanisms for rapid peptide selection*. Cell, 2012. **151**(7): p. 1557-68.
498. Wubbolts, R., et al., *Direct vesicular transport of MHC class II molecules from lysosomal structures to the cell surface*. J Cell Biol, 1996. **135**(3): p. 611-22.
499. Boes, M., et al., *T-cell engagement of dendritic cells rapidly rearranges MHC class II transport*. Nature, 2002. **418**(6901): p. 983-8.
500. Kleijmeer, M., et al., *Reorganization of multivesicular bodies regulates MHC class II antigen presentation by dendritic cells*. J Cell Biol, 2001. **155**(1): p. 53-63.
501. Nielsen, M., et al., *NetMHCIIpan-2.0 - Improved pan-specific HLA-DR predictions using a novel concurrent alignment and weight optimization training procedure*. Immunome Res, 2010. **6**: p. 9.
502. Paul, P., et al., *A Genome-wide multidimensional RNAi screen reveals pathways controlling MHC class II antigen presentation*. Cell, 2011. **145**(2): p. 268-83.
503. Cella, M., et al., *Inflammatory stimuli induce accumulation of MHC class II complexes on dendritic cells*. Nature, 1997. **388**(6644): p. 782-7.
504. Pierre, P., et al., *Developmental regulation of MHC class II transport in mouse dendritic cells*. Nature, 1997. **388**(6644): p. 787-92.
505. Steinman, R.M., *Decisions about dendritic cells: past, present, and future*. Annu Rev Immunol, 2012. **30**: p. 1-22.
506. Lanzavecchia, A. and F. Sallusto, *The instructive role of dendritic cells on T cell responses: lineages, plasticity and kinetics*. Curr Opin Immunol, 2001. **13**(3): p. 291-8.
507. Steinman, R., *Cancer therapeutics: time to swim downstream?* Oncologist, 2011. **16**(10): p. 1479-80.
508. Zitvogel, L., et al., *Cancer and the gut microbiota: an unexpected link*. Sci Transl Med, 2015. **7**(271): p. 271ps1.
509. Chen, D.S. and I. Mellman, *Oncology meets immunology: the cancer-immunity cycle*. Immunity, 2013. **39**(1): p. 1-10.
510. Lowe, S.W., E. Cepero, and G. Evan, *Intrinsic tumour suppression*. Nature, 2004. **432**(7015): p. 307-15.
511. Kuilman, T., et al., *Oncogene-induced senescence relayed by an interleukin-dependent inflammatory network*. Cell, 2008. **133**(6): p. 1019-31.
512. Kang, T.W., et al., *Senescence surveillance of pre-malignant hepatocytes limits liver cancer development*. Nature, 2011. **479**(7374): p. 547-51.

## Chapter VII - References

---

513. Naito, Y., et al., *CD8+ T cells infiltrated within cancer cell nests as a prognostic factor in human colorectal cancer*. *Cancer Res*, 1998. **58**(16): p. 3491-4.
514. Braumuller, H., et al., *T-helper-1-cell cytokines drive cancer into senescence*. *Nature*, 2013. **494**(7437): p. 361-5.
515. Snyder, A., et al., *Genetic basis for clinical response to CTLA-4 blockade in melanoma*. *N Engl J Med*, 2014. **371**(23): p. 2189-2199.
516. Verdegaal, E.M., et al., *Neoantigen landscape dynamics during human melanoma-T cell interactions*. *Nature*, 2016. **536**(7614): p. 91-5.
517. Anagnostou, V., et al., *Evolution of Neoantigen Landscape during Immune Checkpoint Blockade in Non-Small Cell Lung Cancer*. *Cancer Discov*, 2017. **7**(3): p. 264-276.
518. Klemm, F. and J.A. Joyce, *Microenvironmental regulation of therapeutic response in cancer*. *Trends Cell Biol*, 2015. **25**(4): p. 198-213.
519. Juntila, M.R. and F.J. de Sauvage, *Influence of tumour micro-environment heterogeneity on therapeutic response*. *Nature*, 2013. **501**(7467): p. 346-54.
520. Bjorkman, P.J., et al., *Structure of the human class I histocompatibility antigen, HLA-A2*. *Nature*, 1987. **329**(6139): p. 506-12.
521. Hershberg, R.M., et al., *Highly polarized HLA class II antigen processing and presentation by human intestinal epithelial cells*. *J Clin Invest*, 1998. **102**(4): p. 792-803.
522. Wu, Z., et al., *HLA-DMB expression by thyrocytes: indication of the antigen-processing and possible presenting capability of thyroid cells*. *Clin Exp Immunol*, 1999. **116**(1): p. 62-9.
523. Monach, P.A., et al., *A unique tumor antigen produced by a single amino acid substitution*. *Immunity*, 1995. **2**(1): p. 45-59.
524. Muranski, P., et al., *Tumor-specific Th17-polarized cells eradicate large established melanoma*. *Blood*, 2008. **112**(2): p. 362-73.
525. Degenhardt, Y., et al., *Distinct MHC gene expression patterns during progression of melanoma*. *Genes Chromosomes Cancer*, 2010. **49**(2): p. 144-54.
526. Donia, M., et al., *Aberrant Expression of MHC Class II in Melanoma Attracts Inflammatory Tumor-Specific CD4+ T- Cells, Which Dampen CD8+ T-cell Antitumor Reactivity*. *Cancer Res*, 2015. **75**(18): p. 3747-59.
527. Cabrera, T., F. Ruiz-Cabello, and F. Garrido, *Biological implications of HLA-DR expression in tumours*. *Scand J Immunol*, 1995. **41**(4): p. 398-406.
528. Ekkirala, C.R., et al., *Class II transactivator-induced MHC class II expression in pancreatic cancer cells leads to tumor rejection and a specific antitumor memory response*. *Pancreas*, 2014. **43**(7): p. 1066-72.
529. Surmann, E.M., et al., *Association of high CD4-positive T cell infiltration with mutations in HLA class II-regulatory genes in microsatellite-unstable colorectal cancer*. *Cancer Immunol Immunother*, 2015. **64**(3): p. 357-66.
530. Arnold, P.Y., et al., *The majority of immunogenic epitopes generate CD4+ T cells that are dependent on MHC class II-bound peptide-flanking residues*. *J Immunol*, 2002. **169**(2): p. 739-49.
531. Linnemann, C., et al., *High-throughput epitope discovery reveals frequent recognition of neoantigens by CD4+ T cells in human melanoma*. *Nat Med*, 2015. **21**(1): p. 81-5.
532. Giorda, E., et al., *The antigen processing machinery of class I human leukocyte antigens: linked patterns of gene expression in neoplastic cells*. *Cancer Res*, 2003. **63**(14): p. 4119-27.
533. Lundegaard, C., et al., *NetMHC-3.0: accurate web accessible predictions of human, mouse and monkey MHC class I affinities for peptides of length 8-11*. *Nucleic Acids Res*, 2008. **36**(Web Server issue): p. W509-12.
534. Gubin, M.M., et al., *Checkpoint blockade cancer immunotherapy targets tumour-specific mutant antigens*. *Nature*, 2014. **515**(7528): p. 577-81.
535. Matsushita, H., et al., *Cancer exome analysis reveals a T-cell-dependent mechanism of cancer immunoediting*. *Nature*, 2012. **482**(7385): p. 400-4.

536. van Rooij, N., et al., *Tumor exome analysis reveals neoantigen-specific T-cell reactivity in an ipilimumab-responsive melanoma*. J Clin Oncol, 2013. **31**(32): p. e439-42.
537. Yadav, M., et al., *Predicting immunogenic tumour mutations by combining mass spectrometry and exome sequencing*. Nature, 2014. **515**(7528): p. 572-6.
538. Engels, B., et al., *Relapse or eradication of cancer is predicted by peptide-major histocompatibility complex affinity*. Cancer Cell, 2013. **23**(4): p. 516-26.
539. Sanchez-Perez, L., et al., *Potent selection of antigen loss variants of B16 melanoma following inflammatory killing of melanocytes in vivo*. Cancer Res, 2005. **65**(5): p. 2009-17.
540. Zhong, S., et al., *T-cell receptor affinity and avidity defines antitumor response and autoimmunity in T-cell immunotherapy*. Proc Natl Acad Sci U S A, 2013. **110**(17): p. 6973-8.
541. Woller, N., et al., *Viral Infection of Tumors Overcomes Resistance to PD-1-immunotherapy by Broadening Neoantigenome-directed T-cell Responses*. Mol Ther, 2015. **23**(10): p. 1630-40.
542. Duan, F., et al., *Genomic and bioinformatic profiling of mutational neoepitopes reveals new rules to predict anticancer immunogenicity*. J Exp Med, 2014. **211**(11): p. 2231-48.
543. Galon, J., et al., *Type, density, and location of immune cells within human colorectal tumors predict clinical outcome*. Science, 2006. **313**(5795): p. 1960-4.
544. Schneider, C., et al., *Adaptive immunity suppresses formation and progression of diethylnitrosamine-induced liver cancer*. Gut, 2012. **61**(12): p. 1733-43.
545. DuPage, M., et al., *Expression of tumour-specific antigens underlies cancer immunoediting*. Nature, 2012. **482**(7385): p. 405-9.
546. Khong, H.T. and N.P. Restifo, *Natural selection of tumor variants in the generation of "tumor escape" phenotypes*. Nat Immunol, 2002. **3**(11): p. 999-1005.
547. Garrido, F., T. Cabrera, and N. Aptsiauri, *"Hard" and "soft" lesions underlying the HLA class I alterations in cancer cells: implications for immunotherapy*. Int J Cancer, 2010. **127**(2): p. 249-56.
548. Hanson, H.L., et al., *CD4-directed peptide vaccination augments an antitumor response, but efficacy is limited by the number of CD8+ T cell precursors*. J Immunol, 2004. **172**(7): p. 4215-24.
549. Nishimura, T., et al., *Distinct role of antigen-specific T helper type 1 (Th1) and Th2 cells in tumor eradication in vivo*. J Exp Med, 1999. **190**(5): p. 617-27.
550. Mattes, J., et al., *Immunotherapy of cytotoxic T cell-resistant tumors by T helper 2 cells: an eotaxin and STAT6-dependent process*. J Exp Med, 2003. **197**(3): p. 387-93.
551. Knutson, K.L. and M.L. Disis, *Tumor antigen-specific T helper cells in cancer immunity and immunotherapy*. Cancer Immunol Immunother, 2005. **54**(8): p. 721-8.
552. LaCasse, C.J., et al., *Th-1 lymphocytes induce dendritic cell tumor killing activity by an IFN-gamma-dependent mechanism*. J Immunol, 2011. **187**(12): p. 6310-7.
553. Preusser, M., et al., *Cancer immune cycle: a video introduction to the interaction between cancer and the immune system*. ESMO Open, 2016. **1**(3): p. e000056.
554. Schirmacher, V., et al., *Tumour-specific CTL response requiring interactions of four different cell types and recognition of MHC class I and class II restricted tumour antigens*. Immunol Cell Biol, 1993. **71** ( Pt 4): p. 311-26.
555. Marzo, A.L., et al., *T-cell receptor transgenic analysis of tumor-specific CD8 and CD4 responses in the eradication of solid tumors*. Cancer Res, 1999. **59**(5): p. 1071-9.
556. Church, S.E., et al., *Tumor-specific CD4+ T cells maintain effector and memory tumor-specific CD8+ T cells*. Eur J Immunol, 2014. **44**(1): p. 69-79.
557. Bos, R. and L.A. Sherman, *CD4+ T-cell help in the tumor milieu is required for recruitment and cytolytic function of CD8+ T lymphocytes*. Cancer Res, 2010. **70**(21): p. 8368-77.
558. Bos, R., et al., *Functional differences between low- and high-affinity CD8(+) T cells in the tumor environment*. Oncoimmunology, 2012. **1**(8): p. 1239-1247.

## Chapter VII - References

559. Wong, S.B., R. Bos, and L.A. Sherman, *Tumor-specific CD4<sup>+</sup> T cells render the tumor environment permissive for infiltration by low-avidity CD8<sup>+</sup> T cells.* J Immunol, 2008. **180**(5): p. 3122-31.
560. Surman, D.R., et al., *Cutting edge: CD4<sup>+</sup> T cell control of CD8<sup>+</sup> T cell reactivity to a model tumor antigen.* J Immunol, 2000. **164**(2): p. 562-5.
561. Nesbeth, Y.C., et al., *CD4<sup>+</sup> T cells elicit host immune responses to MHC class II-negative ovarian cancer through CCL5 secretion and CD40-mediated licensing of dendritic cells.* J Immunol, 2010. **184**(10): p. 5654-62.
562. Baxevasis, C.N., et al., *Tumor-specific CD4<sup>+</sup> T lymphocytes from cancer patients are required for optimal induction of cytotoxic T cells against the autologous tumor.* J Immunol, 2000. **164**(7): p. 3902-12.
563. Ghorashian, S., et al., *CD8 T cell tolerance to a tumor-associated self-antigen is reversed by CD4 T cells engineered to express the same T cell receptor.* J Immunol, 2015. **194**(3): p. 1080-9.
564. Gerner, M.Y., K.A. Casey, and M.F. Mescher, *Defective MHC class II presentation by dendritic cells limits CD4 T cell help for antitumor CD8 T cell responses.* J Immunol, 2008. **181**(1): p. 155-64.
565. Schietinger, A., et al., *Bystander killing of cancer requires the cooperation of CD4(+) and CD8(+) T cells during the effector phase.* J Exp Med, 2010. **207**(11): p. 2469-77.
566. Kwong, L.N., et al., *Modeling Genomic Instability and Selection Pressure in a Mouse Model of Melanoma.* Cell Rep, 2017. **19**(7): p. 1304-1312.
567. Brunkow, M.E., et al., *Disruption of a new forkhead/winged-helix protein, scurfy, results in the fatal lymphoproliferative disorder of the scurfy mouse.* Nat Genet, 2001. **27**(1): p. 68-73.
568. Shimizu, J., et al., *Stimulation of CD25(+)CD4(+) regulatory T cells through GITR breaks immunological self-tolerance.* Nat Immunol, 2002. **3**(2): p. 135-42.
569. Adeegbe, D.O. and H. Nishikawa, *Natural and induced T regulatory cells in cancer.* Front Immunol, 2013. **4**: p. 190.
570. Chen, W., et al., *Conversion of peripheral CD4<sup>+</sup>CD25<sup>-</sup> naive T cells to CD4<sup>+</sup>CD25<sup>+</sup> regulatory T cells by TGF-beta induction of transcription factor Foxp3.* J Exp Med, 2003. **198**(12): p. 1875-86.
571. Mucida, D., et al., *Reciprocal TH17 and regulatory T cell differentiation mediated by retinoic acid.* Science, 2007. **317**(5835): p. 256-60.
572. Liu, W., et al., *CD127 expression inversely correlates with FoxP3 and suppressive function of human CD4<sup>+</sup> T reg cells.* J Exp Med, 2006. **203**(7): p. 1701-11.
573. Ohue, Y. and H. Nishikawa, *Regulatory T (Treg) cells in cancer: Can Treg cells be a new therapeutic target?* Cancer Sci, 2019. **110**(7): p. 2080-2089.
574. Nolz, J.C., *Molecular mechanisms of CD8(+) T cell trafficking and localization.* Cell Mol Life Sci, 2015. **72**(13): p. 2461-73.
575. Kim, P.S. and R. Ahmed, *Features of responding T cells in cancer and chronic infection.* Curr Opin Immunol, 2010. **22**(2): p. 223-30.
576. Kmiecik, J., et al., *Elevated CD3<sup>+</sup> and CD8<sup>+</sup> tumor-infiltrating immune cells correlate with prolonged survival in glioblastoma patients despite integrated immunosuppressive mechanisms in the tumor microenvironment and at the systemic level.* J Neuroimmunol, 2013. **264**(1-2): p. 71-83.
577. Piersma, S.J., et al., *High number of intraepithelial CD8<sup>+</sup> tumor-infiltrating lymphocytes is associated with the absence of lymph node metastases in patients with large early-stage cervical cancer.* Cancer Res, 2007. **67**(1): p. 354-61.
578. Rodriguez, J.A., *HLA-mediated tumor escape mechanisms that may impair immunotherapy clinical outcomes via T-cell activation.* Oncol Lett, 2017. **14**(4): p. 4415-4427.
579. Jiang, Y., Y. Li, and B. Zhu, *T-cell exhaustion in the tumor microenvironment.* Cell Death Dis, 2015. **6**: p. e1792.

580. Curiel, T.J., et al., *Specific recruitment of regulatory T cells in ovarian carcinoma fosters immune privilege and predicts reduced survival*. *Nat Med*, 2004. **10**(9): p. 942-9.
581. Andersen, M.H., et al., *Cytotoxic T cells*. *J Invest Dermatol*, 2006. **126**(1): p. 32-41.
582. Bandola-Simon, J. and P.A. Roche, *Dysfunction of antigen processing and presentation by dendritic cells in cancer*. *Mol Immunol*, 2019. **113**: p. 31-37.
583. Bai, X.F., et al., *On the site and mode of antigen presentation for the initiation of clonal expansion of CD8 T cells specific for a natural tumor antigen*. *Cancer Res*, 2001. **61**(18): p. 6860-7.
584. Marzo, A.L., et al., *Tumor antigens are constitutively presented in the draining lymph nodes*. *J Immunol*, 1999. **162**(10): p. 5838-45.
585. Thompson, E.D., et al., *Tumor masses support naive T cell infiltration, activation, and differentiation into effectors*. *J Exp Med*, 2010. **207**(8): p. 1791-804.
586. Wolkers, M.C., et al., *Redundancy of direct priming and cross-priming in tumor-specific CD8+ T cell responses*. *J Immunol*, 2001. **167**(7): p. 3577-84.
587. Sarkar, S., et al., *Functional and genomic profiling of effector CD8 T cell subsets with distinct memory fates*. *J Exp Med*, 2008. **205**(3): p. 625-40.
588. Shipkova, M. and E. Wieland, *Surface markers of lymphocyte activation and markers of cell proliferation*. *Clin Chim Acta*, 2012. **413**(17-18): p. 1338-49.
589. Kalia, V., et al., *Prolonged interleukin-2Ralpha expression on virus-specific CD8+ T cells favors terminal-effector differentiation in vivo*. *Immunity*, 2010. **32**(1): p. 91-103.
590. Pipkin, M.E., et al., *Interleukin-2 and inflammation induce distinct transcriptional programs that promote the differentiation of effector cytolytic T cells*. *Immunity*, 2010. **32**(1): p. 79-90.
591. Rosenberg, S.A., et al., *Use of tumor-infiltrating lymphocytes and interleukin-2 in the immunotherapy of patients with metastatic melanoma. A preliminary report*. *N Engl J Med*, 1988. **319**(25): p. 1676-80.
592. Dudley, M.E., et al., *Cancer regression and autoimmunity in patients after clonal repopulation with antitumor lymphocytes*. *Science*, 2002. **298**(5594): p. 850-4.
593. Dudley, M.E., et al., *Adoptive cell therapy for patients with metastatic melanoma: evaluation of intensive myeloablative chemoradiation preparative regimens*. *J Clin Oncol*, 2008. **26**(32): p. 5233-9.
594. Palmer, D.C., et al., *Vaccine-stimulated, adoptively transferred CD8+ T cells traffic indiscriminately and ubiquitously while mediating specific tumor destruction*. *J Immunol*, 2004. **173**(12): p. 7209-16.
595. Williams, M.A. and M.J. Bevan, *Effector and memory CTL differentiation*. *Annu Rev Immunol*, 2007. **25**: p. 171-92.
596. Brignone, C., et al., *First-line chemoimmunotherapy in metastatic breast carcinoma: combination of paclitaxel and IMP321 (LAG-3Ig) enhances immune responses and antitumor activity*. *J Transl Med*, 2010. **8**: p. 71.
597. Mami-Chouaib, F., et al., *Resident memory T cells, critical components in tumor immunology*. *J Immunother Cancer*, 2018. **6**(1): p. 87.
598. Slaney, C.Y., M.H. Kershaw, and P.K. Darcy, *Trafficking of T cells into tumors*. *Cancer Res*, 2014. **74**(24): p. 7168-74.
599. Cham, C.M., et al., *Glucose deprivation inhibits multiple key gene expression events and effector functions in CD8+ T cells*. *Eur J Immunol*, 2008. **38**(9): p. 2438-50.
600. Masopust, D. and J.M. Schenkel, *The integration of T cell migration, differentiation and function*. *Nat Rev Immunol*, 2013. **13**(5): p. 309-20.
601. Harlin, H., et al., *Chemokine expression in melanoma metastases associated with CD8+ T-cell recruitment*. *Cancer Res*, 2009. **69**(7): p. 3077-85.
602. Masopust, D. and L.J. Picker, *Hidden memories: frontline memory T cells and early pathogen interception*. *J Immunol*, 2012. **188**(12): p. 5811-7.

## Chapter VII - References

---

603. Kaech, S.M., et al., *Molecular and functional profiling of memory CD8 T cell differentiation*. Cell, 2002. **111**(6): p. 837-51.
604. Murali-Krishna, K., et al., *Counting antigen-specific CD8 T cells: a reevaluation of bystander activation during viral infection*. Immunity, 1998. **8**(2): p. 177-87.
605. Wherry, E.J. and R. Ahmed, *Memory CD8 T-cell differentiation during viral infection*. J Virol, 2004. **78**(11): p. 5535-45.
606. Arbones, M.L., et al., *Lymphocyte homing and leukocyte rolling and migration are impaired in L-selectin-deficient mice*. Immunity, 1994. **1**(4): p. 247-60.
607. Forster, R., et al., *CCR7 coordinates the primary immune response by establishing functional microenvironments in secondary lymphoid organs*. Cell, 1999. **99**(1): p. 23-33.
608. Sallusto, F., et al., *Two subsets of memory T lymphocytes with distinct homing potentials and effector functions*. Nature, 1999. **401**(6754): p. 708-12.
609. Bachmann, M.F., et al., *Functional properties and lineage relationship of CD8+ T cell subsets identified by expression of IL-7 receptor alpha and CD62L*. J Immunol, 2005. **175**(7): p. 4686-96.
610. Masopust, D., et al., *Preferential localization of effector memory cells in nonlymphoid tissue*. Science, 2001. **291**(5512): p. 2413-7.
611. Sallusto, F., J. Geginat, and A. Lanzavecchia, *Central memory and effector memory T cell subsets: function, generation, and maintenance*. Annu Rev Immunol, 2004. **22**: p. 745-63.
612. Klebanoff, C.A., L. Gattinoni, and N.P. Restifo, *CD8+ T-cell memory in tumor immunology and immunotherapy*. Immunol Rev, 2006. **211**: p. 214-24.
613. Beckhove, P., et al., *Specifically activated memory T cell subsets from cancer patients recognize and reject xenotransplanted autologous tumors*. J Clin Invest, 2004. **114**(1): p. 67-76.
614. Feuerer, M., et al., *Enrichment of memory T cells and other profound immunological changes in the bone marrow from untreated breast cancer patients*. Int J Cancer, 2001. **92**(1): p. 96-105.
615. Pages, F., et al., *Effector memory T cells, early metastasis, and survival in colorectal cancer*. N Engl J Med, 2005. **353**(25): p. 2654-66.
616. Chapuis, A.G., et al., *Transferred melanoma-specific CD8+ T cells persist, mediate tumor regression, and acquire central memory phenotype*. Proc Natl Acad Sci U S A, 2012. **109**(12): p. 4592-7.
617. Wang, L.X., et al., *Memory T cells originate from adoptively transferred effectors and reconstituting host cells after sequential lymphodepletion and adoptive immunotherapy*. J Immunol, 2004. **172**(6): p. 3462-8.
618. Wherry, E.J., *T cell exhaustion*. Nat Immunol, 2011. **12**(6): p. 492-9.
619. Wherry, E.J., et al., *Viral persistence alters CD8 T-cell immunodominance and tissue distribution and results in distinct stages of functional impairment*. J Virol, 2003. **77**(8): p. 4911-27.
620. Blackburn, S.D., et al., *Coregulation of CD8+ T cell exhaustion by multiple inhibitory receptors during chronic viral infection*. Nat Immunol, 2009. **10**(1): p. 29-37.
621. Fuertes Marraco, S.A., et al., *Inhibitory Receptors Beyond T Cell Exhaustion*. Front Immunol, 2015. **6**: p. 310.
622. Chambers, C.A., et al., *CTLA-4-mediated inhibition in regulation of T cell responses: mechanisms and manipulation in tumor immunotherapy*. Annu Rev Immunol, 2001. **19**: p. 565-94.
623. Collins, A.V., et al., *The interaction properties of costimulatory molecules revisited*. Immunity, 2002. **17**(2): p. 201-10.
624. Egen, J.G., M.S. Kuhns, and J.P. Allison, *CTLA-4: new insights into its biological function and use in tumor immunotherapy*. Nat Immunol, 2002. **3**(7): p. 611-8.
625. Parry, R.V., et al., *CTLA-4 and PD-1 receptors inhibit T-cell activation by distinct mechanisms*. Mol Cell Biol, 2005. **25**(21): p. 9543-53.



626. Cha, E. and E.J. Small, *Is there a role for immune checkpoint blockade with ipilimumab in prostate cancer?* Cancer Med, 2013. **2**(2): p. 243-52.
627. Krummel, M.F. and J.P. Allison, *CD28 and CTLA-4 have opposing effects on the response of T cells to stimulation.* J Exp Med, 1995. **182**(2): p. 459-65.
628. Fallarino, F., P.E. Fields, and T.F. Gajewski, *B7-1 engagement of cytotoxic T lymphocyte antigen 4 inhibits T cell activation in the absence of CD28.* J Exp Med, 1998. **188**(1): p. 205-10.
629. Masteller, E.L., et al., *Structural analysis of CTLA-4 function in vivo.* J Immunol, 2000. **164**(10): p. 5319-27.
630. Schneider, H., et al., *Reversal of the TCR stop signal by CTLA-4.* Science, 2006. **313**(5795): p. 1972-5.
631. Linsley, P.S., et al., *Intracellular trafficking of CTLA-4 and focal localization towards sites of TCR engagement.* Immunity, 1996. **4**(6): p. 535-43.
632. Krummel, M.F. and J.P. Allison, *CTLA-4 engagement inhibits IL-2 accumulation and cell cycle progression upon activation of resting T cells.* J Exp Med, 1996. **183**(6): p. 2533-40.
633. Piccirillo, C.A. and E.M. Shevach, *Naturally-occurring CD4+CD25+ immunoregulatory T cells: central players in the arena of peripheral tolerance.* Semin Immunol, 2004. **16**(2): p. 81-8.
634. Takahashi, T., et al., *Immunologic self-tolerance maintained by CD25(+)CD4(+) regulatory T cells constitutively expressing cytotoxic T lymphocyte-associated antigen 4.* J Exp Med, 2000. **192**(2): p. 303-10.
635. Wing, K., et al., *CTLA-4 control over Foxp3+ regulatory T cell function.* Science, 2008. **322**(5899): p. 271-5.
636. Qureshi, O.S., et al., *Trans-endocytosis of CD80 and CD86: a molecular basis for the cell-extrinsic function of CTLA-4.* Science, 2011. **332**(6029): p. 600-3.
637. Keir, M.E., et al., *PD-1 and its ligands in tolerance and immunity.* Annu Rev Immunol, 2008. **26**: p. 677-704.
638. Fife, B.T. and J.A. Bluestone, *Control of peripheral T-cell tolerance and autoimmunity via the CTLA-4 and PD-1 pathways.* Immunol Rev, 2008. **224**: p. 166-82.
639. Chen, D.S., B.A. Irving, and F.S. Hodi, *Molecular pathways: next-generation immunotherapy--inhibiting programmed death-ligand 1 and programmed death-1.* Clin Cancer Res, 2012. **18**(24): p. 6580-7.
640. Latchman, Y.E., et al., *PD-L1-deficient mice show that PD-L1 on T cells, antigen-presenting cells, and host tissues negatively regulates T cells.* Proc Natl Acad Sci U S A, 2004. **101**(29): p. 10691-6.
641. Chen, L., *Co-inhibitory molecules of the B7-CD28 family in the control of T-cell immunity.* Nat Rev Immunol, 2004. **4**(5): p. 336-47.
642. Taube, J.M., et al., *Association of PD-1, PD-1 ligands, and other features of the tumor immune microenvironment with response to anti-PD-1 therapy.* Clin Cancer Res, 2014. **20**(19): p. 5064-74.
643. Hino, R., et al., *Tumor cell expression of programmed cell death-1 ligand 1 is a prognostic factor for malignant melanoma.* Cancer, 2010. **116**(7): p. 1757-66.
644. Zou, W. and L. Chen, *Inhibitory B7-family molecules in the tumour microenvironment.* Nat Rev Immunol, 2008. **8**(6): p. 467-77.
645. Rozali, E.N., et al., *Programmed death ligand 2 in cancer-induced immune suppression.* Clin Dev Immunol, 2012. **2012**: p. 656340.
646. Youngnak, P., et al., *Differential binding properties of B7-H1 and B7-DC to programmed death-1.* Biochem Biophys Res Commun, 2003. **307**(3): p. 672-7.
647. Akbari, O., et al., *PD-L1 and PD-L2 modulate airway inflammation and iNKT-cell-dependent airway hyperreactivity in opposing directions.* Mucosal Immunol, 2010. **3**(1): p. 81-91.
648. Huber, S., et al., *Alternatively activated macrophages inhibit T-cell proliferation by Stat6-dependent expression of PD-L2.* Blood, 2010. **116**(17): p. 3311-20.

## Chapter VII - References

649. Butte, M.J., et al., *Programmed death-1 ligand 1 interacts specifically with the B7-1 costimulatory molecule to inhibit T cell responses*. *Immunity*, 2007. **27**(1): p. 111-22.
650. Francisco, L.M., et al., *PD-L1 regulates the development, maintenance, and function of induced regulatory T cells*. *J Exp Med*, 2009. **206**(13): p. 3015-29.
651. Wang, C., et al., *In vitro characterization of the anti-PD-1 antibody nivolumab, BMS-936558, and in vivo toxicology in non-human primates*. *Cancer Immunol Res*, 2014. **2**(9): p. 846-56.
652. Ott, P.A., F.S. Hodi, and C. Robert, *CTLA-4 and PD-1/PD-L1 blockade: new immunotherapeutic modalities with durable clinical benefit in melanoma patients*. *Clin Cancer Res*, 2013. **19**(19): p. 5300-9.
653. Cheng, W., et al., *Unwrapping the genomic characteristics of urothelial bladder cancer and successes with immune checkpoint blockade therapy*. *Oncogenesis*, 2018. **7**(1): p. 2.
654. Nayak, L., et al., *PD-1 blockade with nivolumab in relapsed/refractory primary central nervous system and testicular lymphoma*. *Blood*, 2017. **129**(23): p. 3071-3073.
655. Seidemann, K., et al., *Short-pulse B-non-Hodgkin lymphoma-type chemotherapy is efficacious treatment for pediatric anaplastic large cell lymphoma: a report of the Berlin-Frankfurt-Munster Group Trial NHL-BFM 90*. *Blood*, 2001. **97**(12): p. 3699-706.
656. Brugieres, L., et al., *Impact of the methotrexate administration dose on the need for intrathecal treatment in children and adolescents with anaplastic large-cell lymphoma: results of a randomized trial of the EICNHL Group*. *J Clin Oncol*, 2009. **27**(6): p. 897-903.
657. Stadler, S., et al., *Immune Response against ALK in Children with ALK-Positive Anaplastic Large Cell Lymphoma*. *Cancers (Basel)*, 2018. **10**(4).
658. Ait-Tahar, K., et al., *B and CTL responses to the ALK protein in patients with ALK-positive ALCL*. *Int J Cancer*, 2006. **118**(3): p. 688-95.
659. Mussolin, L., et al., *Kinetics of humoral response to ALK and its relationship with minimal residual disease in pediatric ALCL*. *Leukemia*, 2009. **23**(2): p. 400-2.
660. Ait-Tahar, K., et al., *Correlation of the autoantibody response to the ALK oncoantigen in pediatric anaplastic lymphoma kinase-positive anaplastic large cell lymphoma with tumor dissemination and relapse risk*. *Blood*, 2010. **115**(16): p. 3314-9.
661. Damm-Welk, C., et al., *Anti-ALK Antibodies in Patients with ALK-Positive Malignancies Not Expressing NPM-ALK*. *J Cancer*, 2016. **7**(11): p. 1383-7.
662. Awad, M.M., et al., *Epitope mapping of spontaneous autoantibodies to anaplastic lymphoma kinase (ALK) in non-small cell lung cancer*. *Oncotarget*, 2017. **8**(54): p. 92265-92274.
663. Passoni, L., et al., *In vivo T-cell immune response against anaplastic lymphoma kinase in patients with anaplastic large cell lymphomas*. *Haematologica*, 2006. **91**(1): p. 48-55.
664. V, K.S., et al., *Analysis of nucleophosmin-anaplastic lymphoma kinase (NPM-ALK)-reactive CD8(+) T cell responses in children with NPM-ALK(+) anaplastic large cell lymphoma*. *Clin Exp Immunol*, 2016. **186**(1): p. 96-105.
665. Janssen, E.M., et al., *CD4+ T cells are required for secondary expansion and memory in CD8+ T lymphocytes*. *Nature*, 2003. **421**(6925): p. 852-6.
666. Crotty, S., *A brief history of T cell help to B cells*. *Nat Rev Immunol*, 2015. **15**(3): p. 185-9.
667. Ait-Tahar, K., M.C. Barnardo, and K. Pulford, *CD4 T-helper responses to the anaplastic lymphoma kinase (ALK) protein in patients with ALK-positive anaplastic large-cell lymphoma*. *Cancer Res*, 2007. **67**(5): p. 1898-901.
668. Kasprzycka, M., et al., *Nucleophosmin/anaplastic lymphoma kinase (NPM/ALK) oncoprotein induces the T regulatory cell phenotype by activating STAT3*. *Proc Natl Acad Sci U S A*, 2006. **103**(26): p. 9964-9.
669. Thibodeau, J., et al., *Interleukin-10-induced MARCH1 mediates intracellular sequestration of MHC class II in monocytes*. *Eur J Immunol*, 2008. **38**(5): p. 1225-30.
670. Chattopadhyay, G. and E.M. Shevach, *Antigen-specific induced T regulatory cells impair dendritic cell function via an IL-10/MARCH1-dependent mechanism*. *J Immunol*, 2013. **191**(12): p. 5875-84.

671. Tze, L.E., et al., *CD83 increases MHC II and CD86 on dendritic cells by opposing IL-10-driven MARCH1-mediated ubiquitination and degradation*. J Exp Med, 2011. **208**(1): p. 149-65.
672. Marzec, M., et al., *Oncogenic kinase NPM/ALK induces through STAT3 expression of immunosuppressive protein CD274 (PD-L1, B7-H1)*. Proc Natl Acad Sci U S A, 2008. **105**(52): p. 20852-7.
673. Busch, S.E., et al., *Lung Cancer Subtypes Generate Unique Immune Responses*. J Immunol, 2016. **197**(11): p. 4493-4503.
674. Koh, J., et al., *EML4-ALK enhances programmed cell death-ligand 1 expression in pulmonary adenocarcinoma via hypoxia-inducible factor (HIF)-1alpha and STAT3*. Oncoimmunology, 2016. **5**(3): p. e1108514.
675. Nagahashi, M., et al., *Common driver mutations and smoking history affect tumor mutation burden in lung adenocarcinoma*. J Surg Res, 2018. **230**: p. 181-185.
676. Gainor, J.F., et al., *EGFR Mutations and ALK Rearrangements Are Associated with Low Response Rates to PD-1 Pathway Blockade in Non-Small Cell Lung Cancer: A Retrospective Analysis*. Clin Cancer Res, 2016. **22**(18): p. 4585-93.
677. Gibbons, D.L., L.A. Byers, and J.M. Kurie, *Smoking, p53 mutation, and lung cancer*. Mol Cancer Res, 2014. **12**(1): p. 3-13.
678. Gainor JF, R.H., Jimenez Aguilar E, Mooradian M, Lydon CA, Anderson D, et al., *Response and durability of anti-PD-(L)1 therapy in never- or light-smokers with non-small cell lung cancer (NSCLC) and high PD-L1 expression*. J Clin Oncol., 2018. **36**(15\_suppl):9011. .
679. Zhou, P., et al., *In vivo discovery of immunotherapy targets in the tumour microenvironment*. Nature, 2014. **506**(7486): p. 52-7.
680. Vladimer, G.I., et al., *Global survey of the immunomodulatory potential of common drugs*. Nat Chem Biol, 2017. **13**(6): p. 681-690.
681. Spigel, D.R., et al., *Phase 1/2 Study of the Safety and Tolerability of Nivolumab Plus Crizotinib for the First-Line Treatment of Anaplastic Lymphoma Kinase Translocation - Positive Advanced Non-Small Cell Lung Cancer (CheckMate 370)*. J Thorac Oncol, 2018. **13**(5): p. 682-688.
682. Felip, E.D.B., F. G.; Maur, M.; Loong, H. H. F.; Shaw, A. T.; Vansteenkiste, J. F.; John, T.; Liu, G.; Lolkema, M. P.; Scott, J. W.; Yu, R.; Selvaggi, G.; Mishra, K.; Lau, Y.-Y. Y.; Tan, D. S.-W., *Ceritinib plus nivolumab (NIVO) in patients (pts) with anaplastic lymphoma kinase positive (ALK+) advanced non-small cell lung cancer (NSCLC)*. J Clin Oncol, 2017. **35**, 2502–2502.
683. Shaw, A.T.L., S.-H.; Ramalingam, S. S.; Bauer, T. M.; Boyer, M. J.; Carcereny Costa, E.; Felip, E.; Han, J.-Y.; Hida, T.; Hughes, B. G. M.; Kim, S.-W.; Nishio, M.; Seto, T.; Ezhel, P.; Chakrabarti, D.; Wang, J.; Chang, A.; Fumagalli, L.; Solomon, B. J., *Avelumab (anti-PD-L1) in combination with crizotinib or lorlatinib in patients with previously treated advanced NSCLC: Phase 1b results from JAVELIN Lung 101*. J Clin Oncol 2018. **36**, 9008–9008.
684. Kim, D.-W.G., S. M.; Gettinger, S. N.; Riely, G. J.; Oxnard, G. R.; Mekhail, T.; Schmid, P.; Dowlati, A.; Heist, R. S.; Wozniak, A. J.; Hernandez, G.; Sarkar, I.; Mitry, E.; Foster, P.; O'Hear, C.; Spahn, J.; Ou, S.-H. I, *Safety and clinical activity results from a phase 1b study of alectinib plus atezolizumab in ALK + advanced NSCLC (aNSCLC)*. J Clin Oncol, 2018. **36**, 9009–9009, doi:10.1200/JCO.2018.36.15\_suppl.9009.
685. Peters, S.C., D. R.; Shaw, A. T.; Gadgeel, S.; Ahn, J. S.; Kim, D.-W.; Ou, S.-H. I.; Pérol, M.; Dziadziuszko, R.; Rosell, R.; Zeaiter, A.; Mitry, E.; Golding, S.; Balas, B.; Noe, J.; Morcos, P. N.; Mok, T., *Alectinib versus Crizotinib in Untreated ALK -Positive Non-Small-Cell Lung Cancer*. N Engl J Med, 2017. **NEJMoa1704795**, doi:10.1056/NEJMoa1704795.
686. Vizcarrondo, F.R.P., S. P.; Pennell, N. A.; Pakkala, S.; West, H.; Kratzke, R.; Tarazi, J.; Wilner, K.; Polli, A.; Tan, W.; Liu, Y.; Valota, O.; Piperdi, B.; Reckamp, K. L. , *Phase 1b study of crizotinib in combination with pembrolizumab in patients (pts) with untreated ALK-*

## Chapter VII - References

---

- positive (+) advanced non-small cell lung cancer (NSCLC). *Ann Oncol* 2016. **27**, doi:10.1093/annonc/mdw383.91.
687. Blasco, R.B., et al., *Simple and rapid in vivo generation of chromosomal rearrangements using CRISPR/Cas9 technology*. *Cell Rep*, 2014. **9**(4): p. 1219-27.
688. Riccardo, F., et al., *Characterization of a genetic mouse model of lung cancer: a promise to identify Non-Small Cell Lung Cancer therapeutic targets and biomarkers*. *BMC Genomics*, 2014. **15 Suppl 3**: p. S1.
689. Ferrara, R., et al., *Pseudoprogression in Non-Small Cell Lung Cancer upon Immunotherapy: Few Drops in the Ocean?* *J Thorac Oncol*, 2019. **14**(3): p. 328-331.
690. Wang, Z.L., et al., *PD-L2 expression is correlated with the molecular and clinical features of glioma, and acts as an unfavorable prognostic factor*. *Oncoimmunology*, 2019. **8**(2): p. e1541535.

# Wiskott–Aldrich syndrome protein (WASP) is a tumor suppressor in T cell lymphoma

Matteo Menotti<sup>1,13</sup>, Chiara Ambrogio<sup>2,15</sup>, Taek-Chin Cheong<sup>3,15</sup>, Chiara Pighi<sup>1,3</sup>, Ines Mota<sup>1</sup>, Seth H. Cassel<sup>4,5,6,7</sup>, Mara Compagno<sup>1,3</sup>, Qi Wang<sup>3</sup>, Riccardo Dall'Olio<sup>1</sup>, Valerio G. Minero<sup>1</sup>, Teresa Poggio<sup>1</sup>, Geeta Geeta Sharma<sup>8</sup>, Enrico Patrucco<sup>1</sup>, Cristina Mastini<sup>1</sup>, Ramesh Choudhari<sup>11,14</sup>, Achille Pich<sup>1</sup>, Alberto Zamo<sup>9</sup>, Roberto Piva<sup>1</sup>, Silvia Giliani<sup>10</sup>, Luca Mologni<sup>8</sup>, Clayton K. Collings<sup>4,5</sup>, Cigall Kadoch<sup>4,5</sup>, Carlo Gambacorti-Passerini<sup>8</sup>, Luigi D. Notarangelo<sup>11</sup>, Ines M. Anton<sup>12</sup>, Claudia Voena<sup>1\*</sup> and Roberto Chiarle<sup>1,3\*</sup>

**In T lymphocytes, the Wiskott–Aldrich Syndrome protein (WASP) and WASP-interacting-protein (WIP) regulate T cell antigen receptor (TCR) signaling, but their role in lymphoma is largely unknown. Here we show that the expression of WASP and WIP is frequently low or absent in anaplastic large cell lymphoma (ALCL) compared to other T cell lymphomas. In anaplastic lymphoma kinase-positive (ALK+) ALCL, WASP and WIP expression is regulated by ALK oncogenic activity via its downstream mediators STAT3 and C/EBP- $\beta$ . ALK+ lymphomas were accelerated in WASP- and WIP-deficient mice. In the absence of WASP, active GTP-bound CDC42 was increased and the genetic deletion of one CDC42 allele was sufficient to impair lymphoma growth. WASP-deficient lymphoma showed increased mitogen-activated protein kinase (MAPK) pathway activation that could be exploited as a therapeutic vulnerability. Our findings demonstrate that WASP and WIP are tumor suppressors in T cell lymphoma and suggest that MAP-kinase kinase (MEK) inhibitors combined with ALK inhibitors could achieve a more potent therapeutic effect in ALK+ ALCL.**

Loss-of-function mutations in the *WAS* gene, which encodes WASP, causes Wiskott–Aldrich syndrome (WAS), a rare X-linked primary immunodeficiency of variable severity characterized by microthrombocytopenia, eczema, autoimmunity, recurrent infections and a predisposition to lymphoma development<sup>1</sup>. As WASP is selectively expressed in hematopoietic cells, the phenotype in patients with WAS is associated with defects in hematopoiesis and the immune system. WASP abundance in cells is regulated by WIP. WIP, encoded by the gene *WIPF1*, binds to the WH1 domain of WASP and protects WASP from degradation<sup>2–5</sup>. The main regulator of WASP activation is the Rho family GTPase cell division cycle 42 (CDC42). In its GTP-bound state, CDC42 binds the GTPase-binding domain of WASP to release the verprolin homology domain–cofilin homology domain–acidic region autoinhibitory domain and to permit the binding to the actin-related protein–2/3 (ARP2/3) complex and actin nucleation<sup>4,6,7</sup>. Additional mediators, such as PIP2, and hematopoietic-specific kinases, such as BTK, LTK, FYN and NCK1, contribute to the activation of WASP<sup>7,8</sup>.

T lymphocytes from patients with WAS and WASP- and WIP-deficient mice show a number of defects, including defective proliferation in response to T cell receptor (TCR) stimulation, disturbed formation of surface projections, defective cytokine polarization

and secretion, disrupted assembly of filamentous actin at the immunological synapse and impaired TCR-mediated signaling<sup>7–10</sup>. Other cells of the adaptive immune system, such as B cells, as well as cells of the innate immune system, such as macrophages and dendritic cells, also have functional defects that have yet to be completely characterized<sup>7,11</sup>. Importantly, WASP-dependent actin nucleation is essential for the formation of the immunological synapses in T cells and several other WASP-mediated phenotypes<sup>4,7</sup>.

Increasing evidence supports the concept that TCR-mediated signaling is also critical for the pathology of T cell lymphoma. Mutations in genes involved in TCR signaling, such as *KRAS*, *RHOA*, *VAV1*, *CD28*, *FYN*, *LCK* and *PLCG1*, are frequently found in T cell lymphomas that retain TCR expression, such as peripheral T cell lymphoma (PTCL-NOS) and angioimmunoblastic T cell lymphoma (AITL)<sup>12</sup>. By contrast, in ALCL, TCR signaling is typically lost and is bypassed by oncogenic tyrosine kinase signaling, most often secondary to aberrant activation of ALK, ROS1 or TYK2<sup>13–16</sup>. Recent discoveries have highlighted, among several pathways downstream of TCR signaling, the pathogenetic role of Rho GTPases, such as RAC1, CDC42 and RHOA, in T cell lymphoma<sup>12</sup>. Inactivating or dominant negative mutations in *RHOA* are the

<sup>1</sup>Department of Molecular Biotechnology and Health Sciences, University of Torino, Torino, Italy. <sup>2</sup>Department of Medical Oncology, Dana-Farber Cancer Institute, Boston, MA, USA. <sup>3</sup>Department of Pathology, Boston Children's Hospital and Harvard Medical School, Boston, MA, USA. <sup>4</sup>Department of Pediatric Oncology, Dana-Farber Cancer Institute and Harvard Medical School, Boston, MA, USA. <sup>5</sup>The Broad Institute of MIT and Harvard, Cambridge, MA, USA. <sup>6</sup>Biomedical and Biological Sciences Program, Harvard Medical School, Boston, MA, USA. <sup>7</sup>Medical Scientist Training Program, Harvard Medical School, Boston, MA, USA. <sup>8</sup>School of Medicine and Surgery, University of Milan-Bicocca, Monza, Italy. <sup>9</sup>Department of Oncology, University of Torino, Torino, Italy. <sup>10</sup>Nocivelli Institute for Molecular Medicine, Department of Molecular and Translational Medicine, University of Brescia, Brescia, Italy. <sup>11</sup>Laboratory of Clinical Immunology and Microbiology, National Institute of Allergy and Infectious Diseases, National Institutes of Health, Bethesda, MD, USA. <sup>12</sup>Department of Molecular and Cellular Biology, Centro Nacional de Biotecnología (CNB-CSIC), Madrid, Spain. <sup>13</sup>Present address: Cell Signalling Group, Cancer Research UK Manchester Institute, University of Manchester, Manchester, UK. <sup>14</sup>Present address: Center of Emphasis in Cancer, Paul L. Foster School of Medicine, Department of Biomedical Sciences, Texas Tech University Health Sciences Center, El Paso, TX, USA. <sup>15</sup>These authors contributed equally: Chiara Ambrogio, Taek-Chin Cheong. \*e-mail: [claudia.voena@unito.it](mailto:claudia.voena@unito.it); [roberto.chiarle@childrens.harvard.edu](mailto:roberto.chiarle@childrens.harvard.edu)

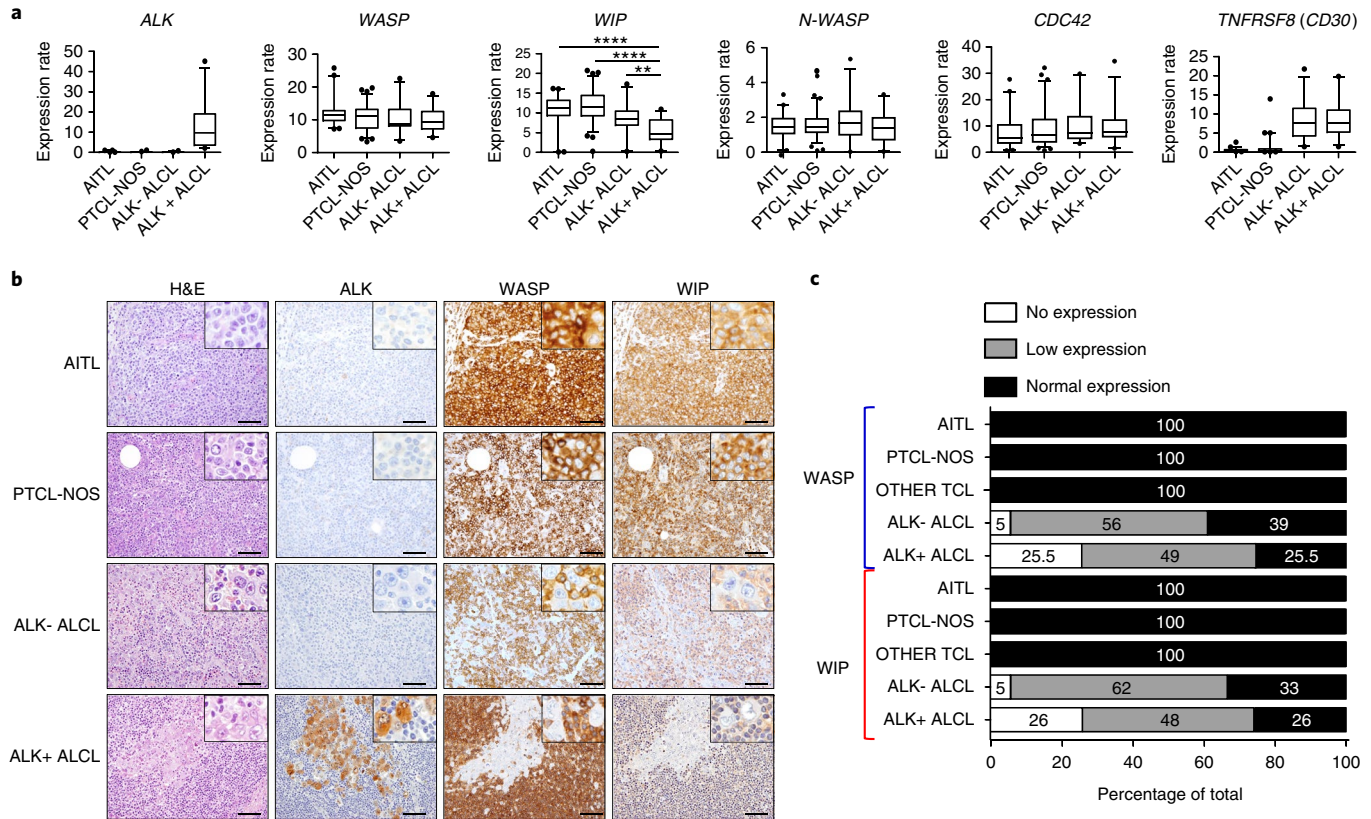


**Fig. 1 | Wasp and Wip are selectively down-regulated in ALCL.** **a**, Gene-expression profiling analysis of *ALK*, *WASP*, *WIP*, *N-WASP*, *CDC42* and *TNFRSF8* (*CD30*) on different cases of human T cell lymphomas: AITL,  $n = 40$ ; PTCL-NOS,  $n = 74$ ; ALK- ALCL,  $n = 24$ ; ALK+ ALCL,  $n = 30$ . The boxes represent the first and third quartiles and the line represents the median. The whiskers represent the upper and lower limits of the range (ALK+ ALCL versus AITL,  $***P = 5.85 \times 10^{-6}$ ; ALK+ ALCL versus PTCL-NOS,  $****P = 6.08 \times 10^{-12}$ ; ALK+ ALCL versus ALK- ALCL,  $**P = 0.0075$ ; significance was determined by unpaired, two-tailed Student's *t*-test). *TNFRSF8* (*CD30*) is strongly expressed in ALK- and ALK+ ALCL but not in other TCL subtypes. **b**, Representative H&E staining and immunohistochemistry stainings performed with the indicated antibody on human T cell lymphoma subtypes. The number of human T cell lymphoma samples analyzed is reported in Fig. 1c. *WASP* antibody was validated in formalin-fixed samples with inducible *WASP* expression (Supplementary Fig. 7f). *WIP* antibody cross reacts with mouse *WIP* and was validated on *WIP* knockout cells (Supplementary Fig. 1b). Scale bar, 100  $\mu$ m. Insets: high-magnification images. **c**, *WASP* and *WIP* expression in human T cell lymphoma subtypes. AITL,  $n = 20$ ; PTCL-NOS,  $n = 20$ ; ALK- ALCL,  $n = 29$ ; ALK+ ALCL,  $n = 43$  for *WASP* and  $n = 31$  for *WIP*; other TCL are natural killer (NK)/T cell lymphoma, nasal-type,  $n = 3$  and hepatosplenic  $\gamma\delta$  T cell lymphoma,  $n = 3$ . The number of patient samples is indicated for each lymphoma subtype. *WASP* and *WIP* expressions were quantified by immunostaining. Normal expression, expression equal to surrounding reactive T cells; low expression, decreased expression compared to surrounding reactive T cells; and no expression, absence of expression in lymphoma cells.

most common recurrent genetic event in AITL and are also present in PTCL-NOS<sup>17–19</sup>. *RAC1* and *CDC42* genes are not recurrently mutated in lymphoma, yet they are activated by mutations of upstream GTP-exchange factors (GEFs), such as *VAV1* and *VAV3*. *VAV1* is frequently activated by mutations and translocations in PTCL<sup>20</sup>, whereas oncogenic *ALK* constitutively activates *VAV1* and *VAV3* in ALCL, thereby increasing *RAC1* and *CDC42* activity and promoting lymphoma survival<sup>21–23</sup>. Taken together, these studies indicate there is a critical role of downstream mediators of TCR signaling and Rho GTPases in T cell lymphoma. In this context, in contrast to the well-characterized function of *WASP* and *WIP* in normal TCR signaling, their role in T cell lymphoma is largely unknown.

We investigated *WASP* and *WIP* expression in a series of T cell lymphomas and found that *WASP* and *WIP* expression are selectively low or absent in ALCL but retained in lymphomas with conserved TCR signaling, such as PTCL-NOS and AITL. *WASP* or *WIP* deficiency significantly accelerated the development of ALK-driven lymphoma in mice by increasing active *CDC42* and enhancing MAPK signaling. Reduction of *CDC42* abundance by deletion of one copy of *Cdc42* abrogated the acceleration of lymphomagenesis in *WASP*-deficient mice. Therapeutically, the forced re-expression

of *WASP* impaired lymphoma growth, and MAPK inhibitors potentiated the effect of the ALK inhibitor crizotinib and exposed an enhanced vulnerability in ALK-driven lymphoma. Overall, these results indicate that *WASP* is a tumor suppressor in ALCL and high-light specific therapeutic susceptibilities.

## Results

**Selective low expression of *WASP* and *WIP* in ALCL.** To investigate the potential role of *WASP* and *WIP* in the ontogeny of T cell lymphomas, we analyzed *WASP* and *WIP* mRNA expression in a series of human T cell lymphomas, including AITL, PTCL-NOS, ALK+ and ALK-negative (ALK-) ALCL, which altogether account for more than 90% of T cell lymphomas<sup>24</sup>. *ALK* expression was confined to ALK+ ALCL, *TNFRSF8* (*CD30*) expression was enriched in ALCL; *WASP*, *CDC42* and *WASL* (*N-WASP*) mRNA expression was similar in various subtypes of T cell lymphoma, whereas *WIP* mRNA was significantly lower in ALCL and lowest in ALK+ ALCL (Fig. 1a). Considering that *WIP* regulates *WASP* stability, we investigated the expression of *WASP* and *WIP* proteins by immunohistochemistry in a series of T lymphomas. We found that expression of *WASP* and *WIP* was frequently low or negative in ALCL, but it was always retained in

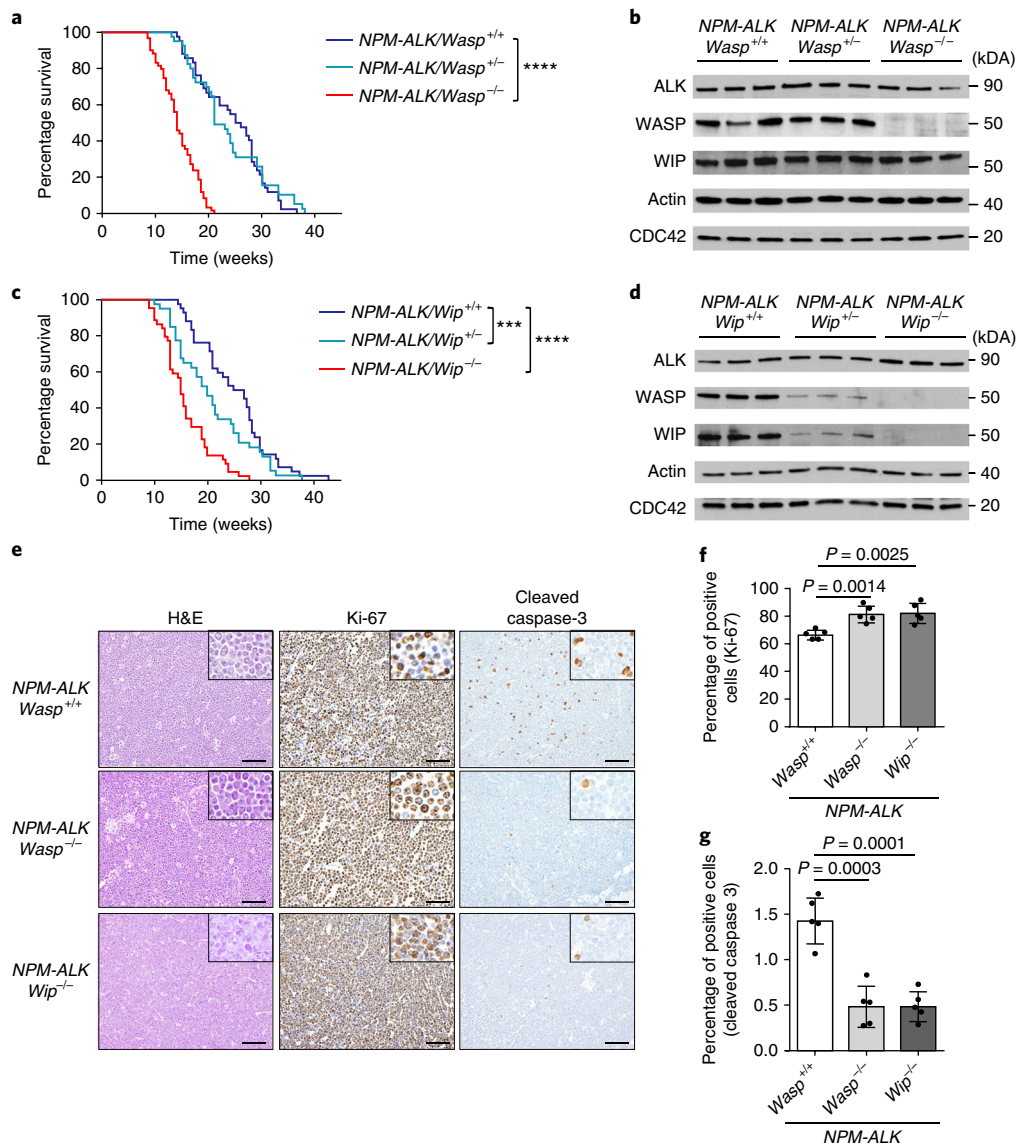


**Fig. 2 | WASP is an oncosuppressor in ALK+ T cell lymphoma. a**, Kaplan-Meier analysis of overall survival of *NPM-ALK* transgenic mice crossed with WASP-deficient mice (blue, *NPM-ALK/Wasp*<sup>+/+</sup>, n = 35; light blue, *NPM-ALK/Wasp*<sup>+/-</sup>, n = 37; red, *NPM-ALK/Wasp*<sup>-/-</sup>, n = 30). The number of mice for each genotype is indicated. *NPM-ALK/Wasp*<sup>+/+</sup> versus *NPM-ALK/Wasp*<sup>-/-</sup>, \*\*\*\*P < 0.0001; significance was determined by log-rank (Mantel-Cox) test. **b**, Western blot analysis from n = 3 independent primary lymphomas isolated from *NPM-ALK* transgenic mice crossed with WASP-deficient mice. The blot is representative of at least two independent experiments with similar results. Actin was used as a loading control. Uncropped blots are available in Supplementary Fig. 11. **c**, Kaplan-Meier analysis of overall survival of *NPM-ALK* transgenic mice crossed with WIP-deficient mice (blue, *NPM-ALK/Wip*<sup>+/+</sup>, n = 26; light blue, *NPM-ALK/Wip*<sup>+/-</sup>, n = 32; red, *NPM-ALK/Wip*<sup>-/-</sup>, n = 30). The number of mice for each genotype is indicated. *NPM-ALK/Wip*<sup>+/+</sup> versus *NPM-ALK/Wip*<sup>-/-</sup>, \*\*\*\*P = 0.0044; *NPM-ALK/Wip*<sup>+/+</sup> versus *NPM-ALK/Wip*<sup>+/-</sup>, \*\*\*\*P < 0.0001; significance was determined by log-rank (Mantel-Cox) test. **d**, Western blot analysis from n = 3 independent primary lymphomas isolated from *NPM-ALK* transgenic mice crossed with WIP-deficient mice. The blot is representative of at least two independent experiments with similar results. Actin was used as a loading control. Uncropped blots are available in Supplementary Fig. 11. **e**, Representative H&E stain (left) and immunohistochemistry for Ki-67 (middle) and cleaved Caspase 3 (right), performed on *NPM-ALK* lymphoma with the indicated genotypes (n = 5 mice for each genotype). Scale bar, 100 μm. Insets: high-magnification images. **f**, **g**, Quantification of Ki-67 (**f**) and cleaved caspase 3 (**g**) positive cells in *NPM-ALK* lymphoma with the indicated genotypes (n = 5 mice for each genotype). Data are shown as means ± s.d.; significance was determined by an unpaired, two-tailed Student's t-test.

AITL and PTCL-NOS as well as in other rare T cell lymphoma, such as natural killer (NK)/T cell lymphoma and γδ hepatosplenic T cell lymphoma (Fig. 1b,c and Supplementary Fig. 1a,b). Taken together, these data showed that WASP and WIP expression is selectively decreased in ALCL as compared to other T cell lymphomas.

**WASP or WIP deficiencies accelerate T cell lymphoma development.** WASP-deficient mice do not develop lymphoma spontaneously and have normal T thymic cell maturation, but they exhibit

defective T cell activation<sup>9</sup>. To directly address the biological role of WASP and WIP in ALCL, we crossed *NPM-ALK* transgenic mice with *Wasp*<sup>-/-</sup> mice. The *NPM-ALK* fusion protein is the canonical and most frequent driver oncogene in ALCL, and *NPM-ALK* transgenic mice develop T cell lymphoma with high penetrance<sup>25</sup>. *NPM-ALK/Wasp*<sup>-/-</sup> females and *NPM-ALK/Wasp*<sup>-/-</sup> males showed similar phenotypes and are collectively referred to as *NPM-ALK/Wasp*<sup>-/-</sup> mice. As expected, *NPM-ALK/Wasp*<sup>-/-</sup> mice had a complete lack of WASP (Supplementary Fig. 1c). The number of T cells and the pattern of

thymic T cell development were comparable in *NPM-ALK* and *NPM-ALK/Wasp<sup>-/-</sup>* mice (Supplementary Fig. 1d,e). Remarkably, WASP deficiency significantly accelerated the onset of lymphomas and hastened mortality (Fig. 2a,b). *NPM-ALK/Wasp<sup>+/-</sup>* female mice had protein abundance comparable to *NPM-ALK/Wasp<sup>+/+</sup>* mice and did not show any acceleration in lymphomagenesis (Fig. 2a,b).

Mice with WIP deficiency have impaired T and B cell activation as a result of defects in the subcortical actin filament network. WASP is almost undetectable in *Wip<sup>-/-</sup>* mice because WASP stability depends on binding to WIP<sup>2</sup>. Recently, patients with disruptive mutations in *WIP* have been identified. These patients lack expression of both WIP and WASP and present with a clinical phenotype similar to patients with WAS<sup>26,27</sup>. Therefore, we reasoned that if the amount of WASP protein is critical for the kinetics of NPM-ALK-driven lymphoma, WIP deficiency should accelerate lymphomagenesis in a manner similar to WASP deficiency. Indeed, *NPM-ALK/Wip<sup>-/-</sup>* mice phenocopied *NPM-ALK/Wasp<sup>-/-</sup>* mice with regard to the onset of lymphoma. In contrast to *NPM-ALK/Wasp<sup>+/-</sup>* mice, *NPM-ALK/Wip<sup>+/-</sup>* mice had a phenotype intermediate between *NPM-ALK/Wip<sup>-/-</sup>* and *NPM-ALK/Wip<sup>+/+</sup>* mice (Fig. 2c). When we analyzed the protein levels, as expected, *NPM-ALK/Wip<sup>-/-</sup>* lymphomas had undetectable levels of both WIP and WASP<sup>3</sup>, whereas *NPM-ALK/Wip<sup>+/-</sup>* lymphomas expressed intermediate levels of both WIP and WASP (Fig. 2d). Immunostains for cleaved caspase 3 and Ki-67 protein demonstrated that the accelerated lymphomagenesis in *NPM-ALK/Wasp<sup>-/-</sup>* or *NPM-ALK/Wip<sup>-/-</sup>* mice was associated with reduced apoptosis and increased proliferation of lymphoma cells (Fig. 2e–g). The similarity of the survival phenotype between WASP and WIP-deficient mice (Fig. 2a–c) is consistent with the near complete absence of WASP in WIP-deficient mice (Fig. 2d) and is in keeping with the known role of WIP in WASP stability<sup>3</sup>. Heterozygous *Wip<sup>+/-</sup>* mice had intermediate levels of WASP and WIP expression as well as an intermediate survival phenotype, indicating that relative levels of WASP can contribute to the kinetics of lymphoma development. Overall, these data suggest that WASP deficiency probably bears responsibility for the phenotype in WIP-deficient mice. These results mirror the findings in human patients with WAS, in whom a complete absence of the protein is associated with a more profound phenotype, including a higher risk of lymphoma development, compared to patients that retain partial expression of WASP and present with milder phenotypes and a lower incidence of lymphoid malignancies<sup>10,28</sup>.

Oncogenic activity of NPM-ALK in lymphocytes controls actin polymerization via a direct activation of VAV1 and VAV3, which are GEFs for RAC1 and CDC42<sup>21,22</sup>. Lymphocytes transformed by NPM-ALK are large and irregular (hence the term ‘anaplastic’ that collectively defines ALK-rearranged lymphoma), hypermotile and have accentuated cellular polarization due to polar assembly of actin filaments<sup>21,23</sup>. Lymphomas that developed in *NPM-ALK/Wasp<sup>-/-</sup>* or *NPM-ALK/Wip<sup>-/-</sup>* mice had a significantly smaller mean cellular diameter than *NPM-ALK* lymphoma cells (Supplementary Fig. 2a,b). *NPM-ALK/Wasp<sup>-/-</sup>* or *NPM-ALK/Wip<sup>-/-</sup>* lymphoma cells also showed markedly decreased actin polarization (Supplementary Fig. 2a,c), consistent with defects of actin nucleation and assembly associated with complete loss of WASP or WIP. In reverse experiments, doxycycline-inducible overexpression of WASP and WIP in human ALCL resulted in increased mean cellular diameter and actin polymerization (Supplementary Fig. 2d,e).

**CDC42 mediates accelerated lymphoma development in WASP-deficient cells.** To elucidate the mechanisms of accelerated lymphomagenesis in the absence of WASP, we characterized the expression profiles of *NPM-ALK-Wasp<sup>-/-</sup>* lymphomas (Supplementary Fig. 3a). Gene set enrichment analysis demonstrated that serum response factor pathway, known to be activated by Rho family GTPase signaling<sup>29</sup>, as well as other GTPase signatures, were significantly

enriched in *NPM-ALK/Wasp<sup>-/-</sup>* lymphoma compared to *NPM-ALK/Wasp<sup>+/+</sup>* lymphoma (Supplementary Fig. 3b–d). Since WASP is a critical substrate of GTP-bound CDC42, we reasoned that WASP deficiency could affect CDC42 activity in lymphoma cells, resulting in an increased GTPase signature. To explore this possibility, we assessed the abundance of active GTP-bound CDC42 in *NPM-ALK/Wasp<sup>-/-</sup>* lymphoma. We analyzed *NPM-ALK/Wasp<sup>-/-</sup>* and *NPM-ALK/Wasp<sup>+/+</sup>* lymphomas by CDC42-specific GTPase assay. *NPM-ALK/Wasp<sup>-/-</sup>* lymphomas had significantly higher levels of GTP-bound CDC42 than *NPM-ALK/Wasp<sup>+/+</sup>* lymphomas (Fig. 3a), indicating that the amount of active CDC42 is increased in cells that lack WASP. In addition to increased CDC42 activation, *NPM-ALK/Wasp<sup>-/-</sup>* lymphomas also showed increased activation of the MAPK pathway as assessed by ERK1/2 phosphorylation (Fig. 3b).

To assess directly whether CDC42 abundance was critical for lymphoma acceleration in WASP-deficient cells, we crossed *NPM-ALK/Wasp<sup>-/-</sup>* mice with a conditional *Cdc42<sup>lox</sup>* allele; deletion of *Cdc42* in T cells was accomplished by further crossing with *CD4-Cre* mice<sup>23</sup>. The deletion of one *Cdc42* allele was associated with decreased protein abundance (Fig. 3c) and was sufficient to delay lymphoma development in *NPM-ALK/Wasp<sup>-/-</sup>* mice (Fig. 3d). Remarkably, lymphoma development and survival of *NPM-ALK/Wasp<sup>-/-</sup>/Cdc42<sup>+/+</sup>/CD4-Cre* mice was similar to *NPM-ALK/Wasp<sup>+/+</sup>* mice. *NPM-ALK/Wasp<sup>-/-</sup>* mice with a complete knockout of *Cdc42* (*NPM-ALK/Wasp<sup>-/-</sup>/Cdc42<sup>0/0</sup>/CD4-Cre* mice) died prematurely because of multiorgan failure due to an inflammatory infiltrate, and so the development of lymphoma could not be assessed. Apoptosis was uniformly higher and proliferation consistently lower in *NPM-ALK/Wasp<sup>-/-</sup>/Cdc42<sup>+/+</sup>/CD4-Cre* lymphomas than in *NPM-ALK/Wasp<sup>-/-</sup>* lymphomas but was comparable to *NPM-ALK/Wasp<sup>+/+</sup>* lymphomas (Fig. 3e–g). We conclude that the accelerated lymphomagenesis in *NPM-ALK/Wasp<sup>-/-</sup>* mice depends on the abundance of CDC42.

To further characterize the role of CDC42 in *NPM-ALK/Wasp<sup>-/-</sup>* lymphomas, we immortalized lymphoma cell lines of different genotypes and induced *Cdc42* deletion with a tamoxifen-inducible Cre-recombinase. As expected, deletion of one *Cdc42* allele reduced CDC42 protein abundance by approximately 50%, whereas biallelic deletion abrogated CDC42 expression (Fig. 4a). Deletion of one *Cdc42* allele significantly impaired the growth of *NPM-ALK/Wasp<sup>-/-</sup>* lymphoma cells but not of *NPM-ALK/Wasp<sup>+/+</sup>* lymphoma cells (Fig. 4b), mirroring the results obtained in mice (Fig. 3d) and confirming that CDC42 abundance is critical for *Wasp<sup>-/-</sup>* lymphoma. Consistently, deletion of one *Cdc42* allele produced an increase in apoptosis in *NPM-ALK/Wasp<sup>-/-</sup>* lymphomas but not in *NPM-ALK/Wasp<sup>+/+</sup>* lymphoma cells (Fig. 4c). Consistent with our previous findings<sup>23</sup>, in *NPM-ALK/Wasp<sup>+/+</sup>* lymphoma only the biallelic deletion of *Cdc42* induced impairment of lymphoma growth and apoptosis (Fig. 4c). Altogether, these data demonstrate that WASP-deficient cells are exquisitely sensitive to the cellular abundance of CDC42.

**Oncogenic ALK activity promotes WASP and WIP downregulation via STAT3 and C/EBP- $\beta$ .** To investigate WASP- and WIP-dependent mechanisms of ALK+ ALCL lymphoma progression, we measured WASP and WIP expression in ALK cell lines and confirmed that in several cell lines they were lower than in normal T cells or other lymphoma types (Fig. 5a and Supplementary Fig. 4a). By contrast, N-WASP was not decreased in ALCL (Supplementary Fig. 5a). *WIP* mRNA was lower in ALK+ ALCL cell lines than in other T cell lines or in T cells from normal donors, whereas *WASP* mRNA was more variable (Fig. 5b). Overall, these patterns of gene expression in ALCL cell lines recapitulate the findings in primary ALCL from patients (Fig. 1).

As it is known that ALK oncogenic activity controls protein expression by transcriptional regulation or epigenetic silencing<sup>30,31</sup>, we tested whether WASP and WIP expression were directly controlled



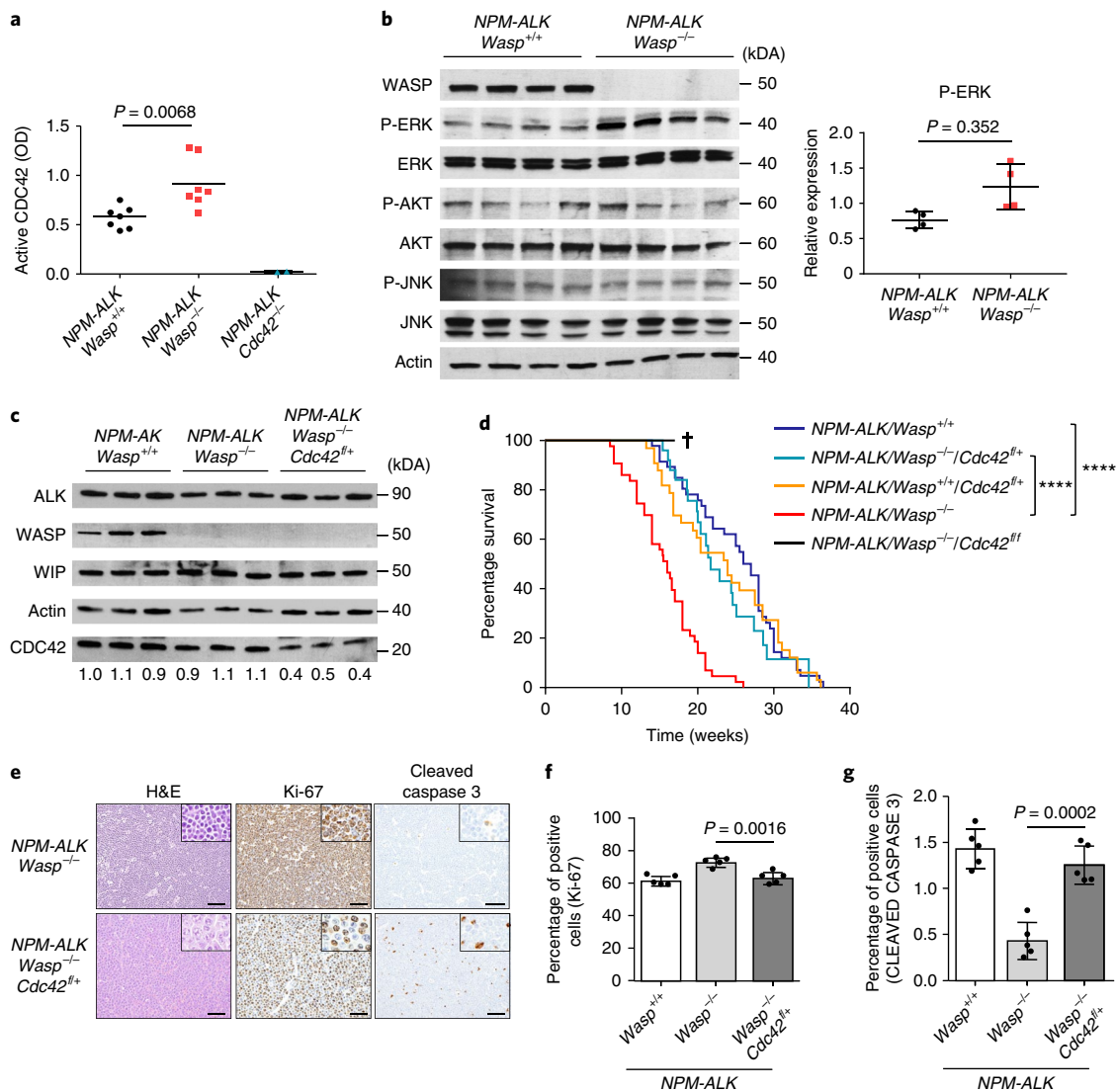


**Fig. 3 | CDC42 and ERK hyperactivation in WASP-deficient lymphoma.** **a**, Quantification of active GTP-bound CDC42 using CDC42 G-LISA assay kit on cell lines derived from *NPM-ALK* lymphoma with the indicated genotypes (*NPM-ALK/Wasp*<sup>+/+</sup> and *NPM-ALK/Wasp*<sup>-/-</sup>, *n* = 7). *Cdc42* knockout cell lines (*NPM-ALK/Cdc42*<sup>fl/fl</sup>/*CD4-Cre* cell lines, *n* = 2) were used as a control for the assay. Data are shown as means. Significance was determined by an unpaired, two-tailed Student's *t*-test. **b**, Western blot performed with the indicated antibodies on lymphoma cell lines obtained from *NPM-ALK* transgenic mice with the indicated genotypes (left); quantification of phosphorylated ERK (P-ERK) in lymphoma cell lines (right) (*n* = 4 biologically independent samples). Data are shown as means  $\pm$  s.d.; significance was determined by an unpaired, two-tailed Student's *t*-test. Actin was used as a loading control. Uncropped blots are available in Supplementary Fig. 11. **c**, Western blot analysis for WASP, WIP and CDC42 expression on the indicated lymphoma cell lines. Densitometric values of the CDC42 bands normalized to actin are indicated. The blot is representative of at least two independent experiments with similar results. Actin was used as a loading control. Uncropped blots are available in Supplementary Fig. 11. **d**, Kaplan-Meier survival curves of *NPM-ALK* transgenic mice crossed with *Wasp*<sup>+/+</sup> or *Wasp*<sup>-/-</sup> mice with *Cdc42* haploinsufficiency (blue, *NPM-ALK/Wasp*<sup>+/+</sup>, *n* = 35 mice; light blue, *NPM-ALK/Wasp*<sup>-/-</sup>/*Cdc42*<sup>fl/fl</sup>/*CD4-Cre*, *n* = 24; red, *NPM-ALK/Wasp*<sup>-/-</sup>, *n* = 30; black, *NPM-ALK/Wasp*<sup>-/-</sup>/*Cdc42*<sup>fl/fl</sup>/*CD4-Cre*, *n* = 8; orange, *NPM-ALK/Wasp*<sup>+/+</sup>/*Cdc42*<sup>fl/fl</sup>/*CD4-Cre*, *n* = 34). The number of mice for each genotype is indicated. \*\*\*\**P* < 0.0001; significance was determined by log-rank (Mantel-Cox) test. **e**, Representative H&E stain (left) and immunohistochemistry for Ki-67 (middle) and cleaved caspase 3 (right), performed on *NPM-ALK* lymphoma with the indicated genotypes (*n* = 4 mice for each genotype). Scale bar, 100  $\mu$ m. Insets: high-magnification images. **f, g**, Quantification of Ki-67 (**f**) and cleaved caspase 3 (**g**) positive cells in *NPM-ALK* lymphoma with the indicated genotypes (*n* = 5 mice for each genotype). Data are shown as means  $\pm$  s.d.; significance was determined by an unpaired, two-tailed Student's *t*-test.

by ALK activity. Knocking-down *ALK* expression with an inducible shRNA system<sup>32</sup>, led to increased *WASP* and *WIP* mRNA and protein expression (Fig. 5c,d). Consistently, inhibition of ALK activity by the ALK inhibitors crizotinib and alectinib resulted in increased *WASP* and *WIP* mRNA expression (Fig. 5e). Conversely, doxycycline-inducible expression of oncogenic ALK in ALK-negative lymphoma cells down-regulated the expression of both *WASP* and *WIP* (Supplementary Fig. 5b). Treatment of cells with azacitidine, which

is known to restore expression of genes, such as *LAT* and *ZAP70*, that are repressed by ALK through methylation<sup>30,31</sup>, did not change *WASP* and *WIP* expression (Supplementary Fig. 5c,d). Oncogenic ALK activates several downstream pathways, with *STAT3* and *C/EBP- $\beta$*  representing key downstream effectors<sup>16</sup>. Knock-down of either *STAT3* or *C/EBP- $\beta$*  resulted in an increased *WASP* and *WIP* mRNA and protein levels (Fig. 5f and Supplementary Fig. 5e-g). Taken together, these data indicate that ALK oncogenic activity

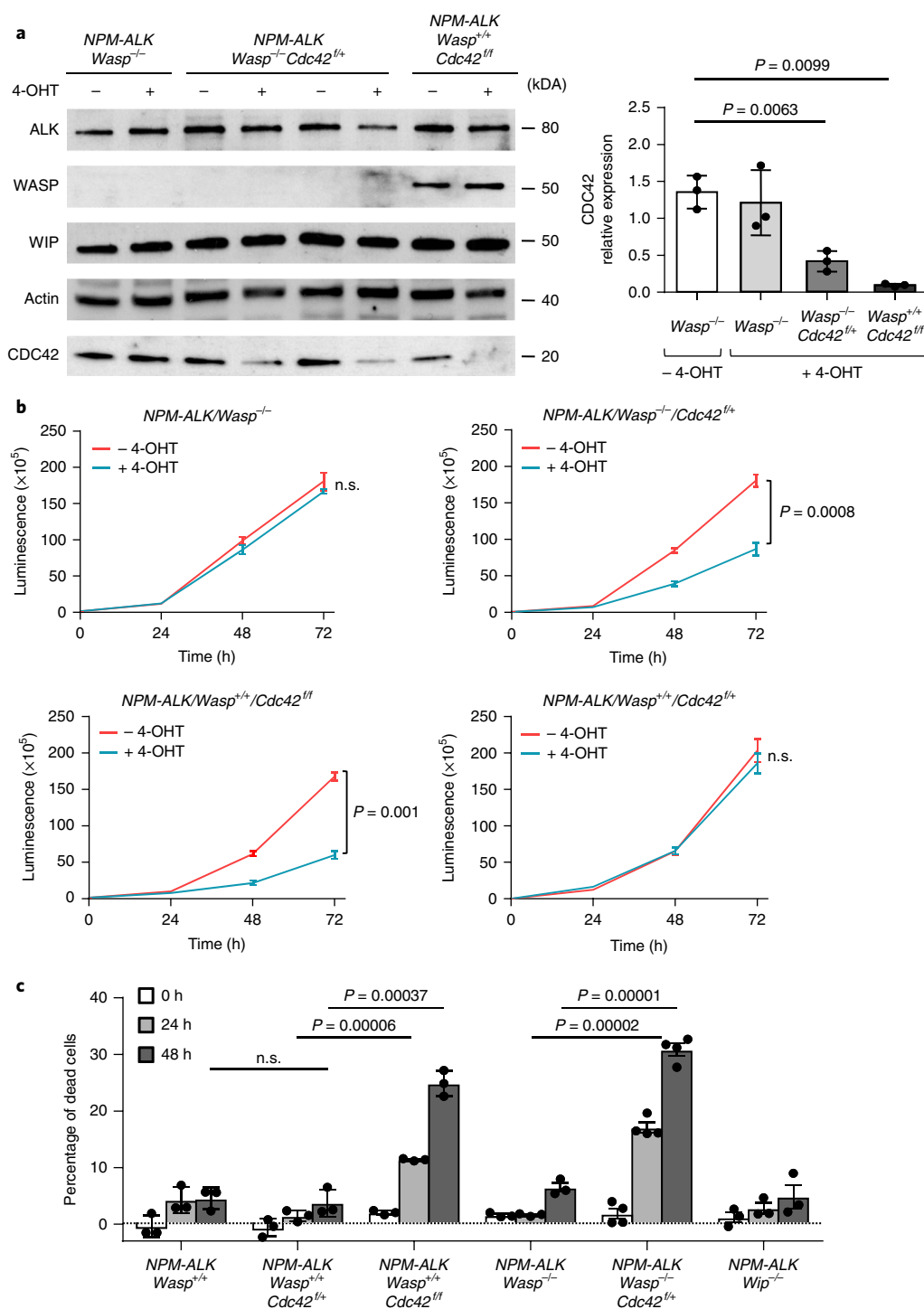


**Fig. 4 | CDC42 is essential for the survival of WASP-deficient lymphoma cells. a**, Western blot analysis for ALK, WASP, WIP and CDC42 on lymphoma cell lines obtained from *NPM-ALK* transgenic mice with the indicated genotypes, transduced with *Cre*<sup>ERT2</sup> and treated with 10 nM 4-hydroxytamoxifen (4-OHT) for 4 h (left). The blot is representative of three independent experiments with similar results. Actin was used as a loading control. Uncropped blots are available in Supplementary Fig. 11. Mean protein expression of CDC42 in mouse cell lines that were treated with 4-OHT or were not treated (right). Data are shown as means ± s.d. from three independent experiments with similar results; significance was determined by an unpaired, two-tailed Student's *t*-test. **b**, Cell growth assay performed on lymphoma cell lines obtained from *NPM-ALK* transgenic mice with the indicated genotypes, transduced with *Cre*<sup>ERT2</sup> and treated with 4-OHT. Measurements were taken at the indicated time points (*n* = 3 biologically independent samples). Data are shown as means ± s.e.m.; significance was determined by unpaired, two-tailed Student's *t*-test; n.s., not significant. **c**, Apoptosis analysis performed on lymphoma cell lines obtained from *NPM-ALK* transgenic mice with the indicated genotypes that were treated as in **a**. Measurements were taken at the indicated time points by TMRM staining and flow cytometry analysis. The percentage of dead cells was calculated above background (*n* = 3 independent experiments). Data are shown as means ± s.d.; significance was determined by unpaired, two-tailed Student's *t*-test.

impairs WASP and WIP expression by a transcriptional repression mediated by STAT3 and C/EBP- $\beta$ . To investigate if STAT3 and C/EBP- $\beta$  might directly regulate expression of *WAS* and *WIPF1* genes, we performed chromatin immunoprecipitation and sequencing (ChIP-seq) on ALCL cell lines treated with crizotinib. As expected, 3h of treatment with crizotinib blocked ALK phosphorylation that in turn resulted in a marked de-phosphorylation of STAT3 without affecting total STAT3 levels (Supplementary Fig. 6a). When ALK was active, STAT3 bound genome-wide, whereas in the presence of crizotinib STAT3 binding was almost completely abrogated throughout the genome (Fig. 5g and Supplementary Fig. 6c), including at loci proximal to both the *WAS* and *WIPF1* genes (Fig. 5h,i). In contrast, C/EBP- $\beta$  bound to *WAS* and *WIPF1* genes but its binding was not affected by ALK blockade (Fig. 5h,i and Supplementary Fig. 6b,c). Remarkably, STAT3 and C/EBP- $\beta$  binding sites co-localized with H3K4me3 and H3K27Ac marks indicating that they could functionally contribute to WASP and WIP expression (Supplementary Fig. 6d). Thus, our results are consistent with a model by which STAT3 and C/EBP- $\beta$  regulate WASP and WIP expression where STAT3 regulation directly depends on an ALK-mediated activation.

**WASP and WIP abundance control lymphoma growth.** As absence of WASP accelerates lymphoma growth in mouse models, we reasoned that decreased WASP and WIP expression could contribute also to the biology of human ALK+ ALCL. To test this hypothesis, we forcibly re-expressed WASP and WIP in ALCL cells by using a doxycycline-inducible lentiviral vector. Transduction with WASP vector alone did not increase WASP expression (data not shown), whereas transduction with WIP lentivirus induced a moderate increase in endogenous WASP (Supplementary Fig. 7a), confirming that the levels of WASP in ALCL are regulated by WIP as they are in normal T cells. When ALCL cells were co-transduced with both WASP and WIP lentiviruses, WASP expression was comparable to normal T cells (Fig. 6a). On WASP and WIP induction, the GTP-bound form of CDC42 markedly decreased in ALCL cells, thus confirming that the WASP expression level regulates the abundance of active CDC42 also in human ALCL cell lines (Fig. 6b). Next, we found that ALCL cell lines with induced WASP and WIP expression had impaired growth in vitro (Supplementary Fig. 7b–d) associated with an increased fraction of cells arrested in G1 phase of the cell cycle (Supplementary Fig. 7e). Consistently, the growth of ALCL mouse xenografts was significantly reduced when WASP and WIP expression was induced in vivo (Fig. 6c). Induced expression of WASP in ALCL xenografts was associated with a significant

increase in apoptosis and a decrease in proliferation (Fig. 6d,e and Supplementary Fig. 7f). Furthermore, the activation of the MAPK pathway, as measured by phosphorylated ERK1/2 levels, decreased upon WASP and WIP induction, concomitant with an increase in cleaved caspase 3 (Supplementary Fig. 4b). Thus, the low expression of WASP and WIP contributes the pathogenesis of ALCL, and the restoration of their expression impairs lymphoma growth by decreasing the amount of active CDC42 and MAPK signaling.

**MAPK activation is a therapeutic vulnerability in WASP-deficient lymphoma.** Finally, we reasoned that increased MAPK signaling in ALCL cells expressing low levels of WASP could represent a therapeutic vulnerability. To test this concept, we treated lymphoma cells with trametinib, a MEK inhibitor approved for melanoma treatment and currently in trial for lymphoma (NCT00687622). Lymphomas from *NPM-ALK/Wasp<sup>-/-</sup>* mice were more sensitive than wild-type lymphoma to trametinib (Fig. 6f) as well as to additional MEK inhibitors (selumetinib, MEK162 and PD0325901) (Supplementary Fig. 8a). Consistently, human ALCL with low WASP expression (SU-DHL1 and JB6) were also more sensitive than ALCL with higher WASP expression (TS and L82) (Supplementary Fig. 8b). Considering that ALK inhibitors have potent clinical activity in ALK+ ALCL<sup>16,33</sup>, we also investigated whether MEK inhibition could potentiate ALK inhibitors in a combination therapy, as has been recently suggested for ALK-rearranged lung cancer<sup>34</sup>. In vitro, *NPM-ALK* lymphoma lines were sensitive to crizotinib, and the combination with trametinib further potentiated crizotinib activity (Supplementary Fig. 8c). In vivo, trametinib alone did not have an effect against *NPM-ALK* lymphoma, as expected from similar experiment in ALK+ lung cancer<sup>34</sup>. In contrast, the combination of trametinib with crizotinib was more potent than crizotinib alone for the treatment of *NPM-ALK/Wasp<sup>-/-</sup>* but not wild-type lymphoma (Fig. 6g), supporting the concept that the MAPK pathway is a therapeutic vulnerability in WASP-deficient lymphoma.

**Lymphocytes from patients with WAS show increased CDC42 activity and MAPK signaling.** Patients with WAS have a variety of mutations in the *WAS* gene that result in a variably reduced abundance or function WASP<sup>7</sup>. As in human ALCL and mouse models, the reduced or absent expression of WASP increases the abundance of active CDC42, and so we reasoned that lymphocytes from patients with absent or very low WASP expression should display higher CDC42 activation than control lymphocytes. We characterized Epstein–Barr virus (EBV)-immortalized B lymphocytes from three patients with WAS with defined WAS mutations (Supplementary

**Fig. 5 | Oncogenic ALK down-regulates WASP and WIP expression through STAT3 and C/EBP $\beta$ .** **a**, Western blot performed on human ALK+ ALCL cell lines and ALK- T lymphoma lines or normal T cells blotted with the indicated antibodies. The blot is representative of two independent experiments with similar results. Actin was used as a loading control. Uncropped blots are available in Supplementary Fig. 11. **b**, Quantitative real-time PCR (qRT-PCR) expression analysis of *WASP* and *WIP* mRNA in human ALK+ ALCL cell lines and ALK- T lymphoma lines or normal T cells ( $n=3$  independent experiments). Data are shown as means  $\pm$  s.d. **c**, qRT-PCR expression analysis of *WASP* and *WIP* mRNA on two representative ALK+ ALCL human cell lines (TS and SU-DHL1) transduced with a doxycycline-dependent ALK shRNA or control shRNA ( $n=3$  independent experiments). Data are shown as means  $\pm$  s.d.; significance was determined by an unpaired, two-tailed Student's *t*-test. **d**, Western blot analysis on the same cells as in **c** collected at 96 h. Densitometric values of the bands are indicated. One representative experiment out of three performed is shown. Actin was used as a loading control. Uncropped blots are available in Supplementary Fig. 11. **e**, qRT-PCR expression analysis of *WASP* and *WIP* mRNA on three representative ALK+ ALCL human cell lines (TS, JB6 and Karpas-299) treated with two different ALK inhibitors, alectinib (30 nM) and crizotinib (100 nM) for 12 h (JB6 and Karpas-299) or 24 h (TS) ( $n=3$  independent experiments). Data are shown as means  $\pm$  s.d.; significance was determined by an unpaired, two-tailed Student's *t*-test. **f**, qRT-PCR expression analysis of *WASP* and *WIP* mRNA on the ALK+ TS cell line in which the expression of STAT3 has been knocked down by the specific shRNA. The corresponding western blot of the shRNA knockdown is shown on the left. Two independent shRNA have been used for each knockdown assay (indicated with numbers 1 and 2). A scrambled shRNA has been used as control ( $n=3$  independent experiments). Data are shown as means  $\pm$  s.d.; significance was determined by an unpaired, two-tailed Student's *t*-test. The blot is representative of three independent experiments with similar results. Actin was used as a loading control. Uncropped blots are available in Supplementary Fig. 11. **g**, Heatmaps (left) and metaplots (right) of global STAT3 peaks obtained by ChIP-seq in SU-DHL1 cells treated for 3 h with crizotinib (300 nM). **h,i**, STAT3 or C/EBP- $\beta$  ChIP-seq tracks at *WAS* (**h**) and *WIPF1* (**i**) genes on two representative ALK+ ALCL human cell lines (JB6 and SU-DHL1) treated for 3 h with crizotinib (300 nM). The experiment was performed once on two independent cell lines with similar results.

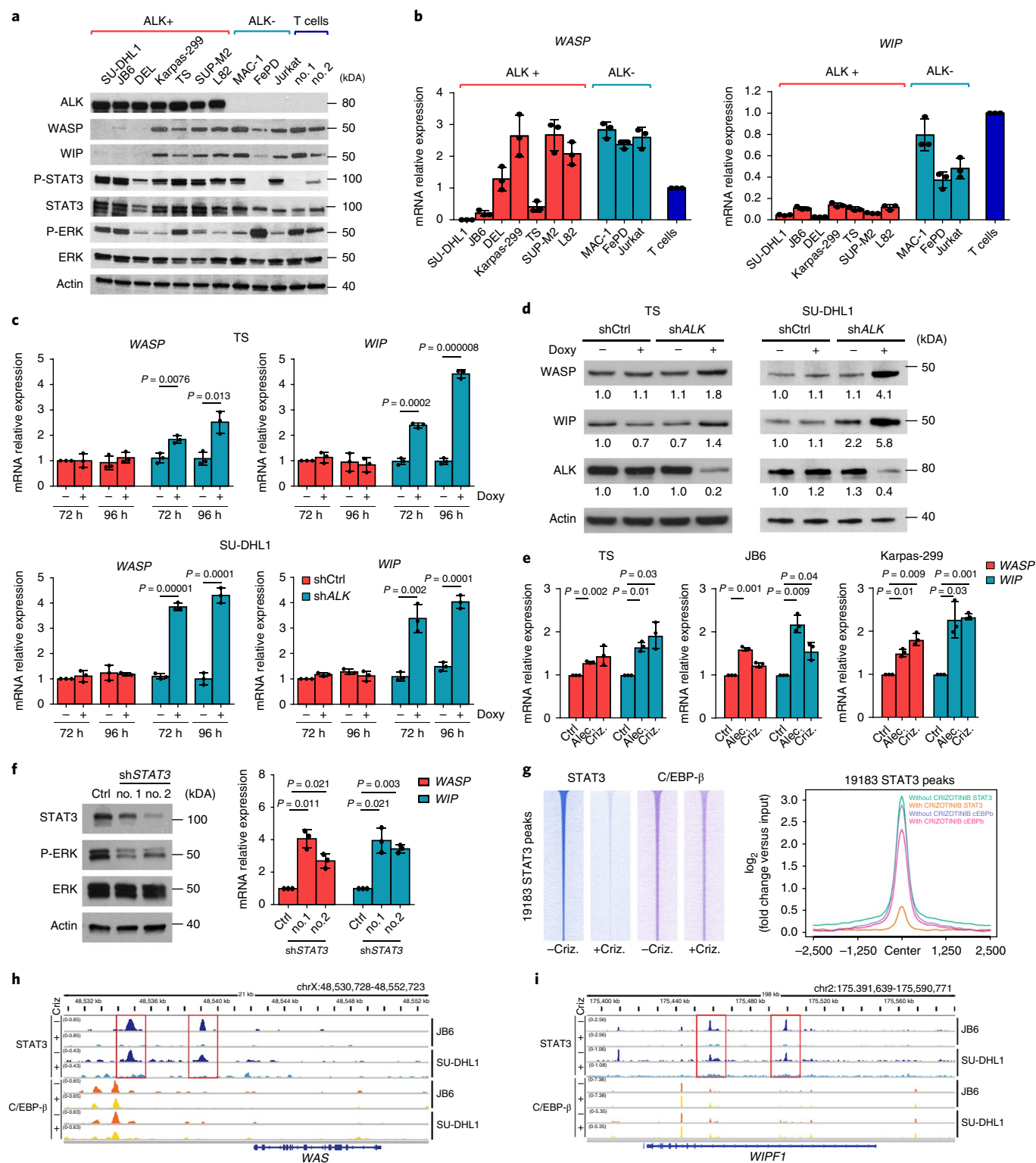
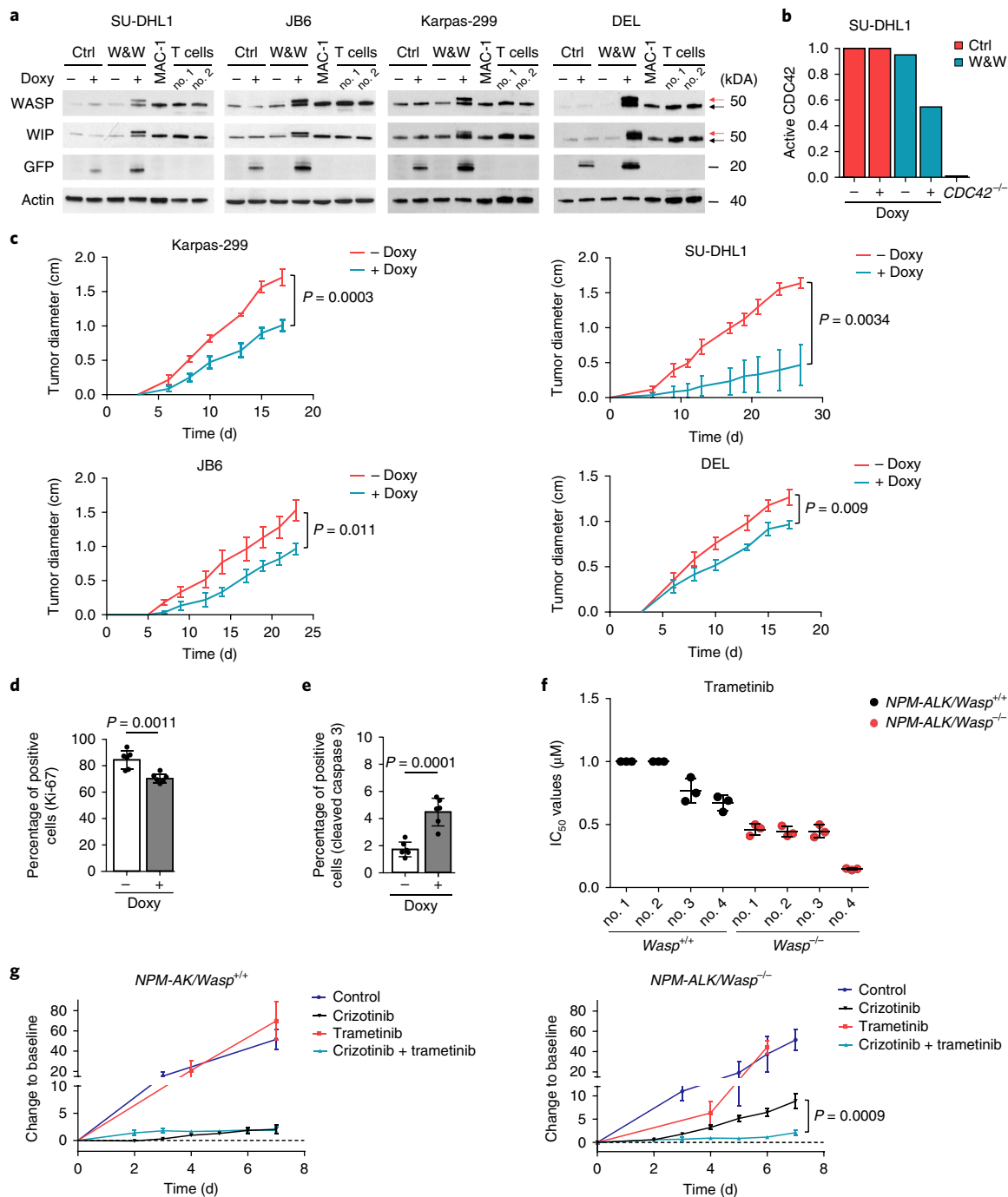


Fig. 9a) and low or absent WASP expression (Supplementary Fig. 9b). Indeed, lymphocytes from patients with WAS showed higher levels of CDC42 activation than control cells (Supplementary Fig. 9c), in keeping with observations in *NPM-ALK* lymphoma cells. In addition, WAS lymphocytes showed decreased phosphorylation of STAT3 and AKT, consistent with defective cytokine production in WASP-deficient lymphocytes<sup>35</sup>, but they showed higher levels of ERK and S6 phosphorylation, consistent with increased activation of the MAPK pathway (Supplementary Fig. 9b). These

data show that lymphocytes from patients with WAS with absent WASP expression have higher activity of CDC42 and MAPK signaling, suggesting the possibility that the predisposition of patients with WAS to lymphoma could be associated to an intrinsic aberrant signaling in their lymphocytes.

### Discussion

WASP and WIP are essential regulators of the cytoskeleton in hematopoietic cells. Proper cytoskeletal regulation is fundamental for a



**Fig. 6 | MAPK pathway is a therapeutic vulnerability in WASP-deficient cells.** **a**, Western blot analysis of ALK+ ALCL cell lines (SU-DHL1, JB6, Karpas-299 and DEL) transduced with doxycycline (doxy)-inducible lentivirus co-expressing WASP and WIP (W&W) or a control reporter GFP (Ctrl). Black arrows: endogenous WASP and WIP; red arrows: Flag-tagged WASP and WIP. The MAC-1 cell line and normal T cells were used as controls. The blot is representative of at least two independent experiments with similar results. Actin was used as a loading control. Uncropped blots are available in Supplementary Fig. 11. **b**, Quantification of active GTP-bound CDC42 on the SU-DHL1 cell line after induction of WASP and WIP expression using CDC42 activation assay kit. CDC42 knockout (*CDC42<sup>-/-</sup>*) cells were used as a negative control of the assay. One representative of two independent experiments in triplicates is shown. **c**, Growth of xenografted tumors in Nod scid gamma (NSG) mice injected with ALK+ ALCL cells (Karpas-299, SU-DHL1, JB6 and DEL) transduced with doxycycline-inducible WASP and WIP vectors. Mice were treated with normal (red line) or doxycycline-treated (light blue line) water ( $n = 6$  independent tumors). Data are shown as means  $\pm$  s.e.m.; significance was determined by an unpaired, two-tailed Student's  $t$ -test. Doxycycline treatment started at day 0 when cells were injected sub cutis. **d,e**, Quantification of Ki-67 (**d**) and cleaved Caspase 3 (**e**) positive cells in ALK+ ALCL xenograft lymphoma as in **c** ( $n = 6$  tumors). Data are shown as means  $\pm$  s.e.m.; significance was determined by an unpaired, two-tailed Student's  $t$ -test. **f**, Sensitivity to trametinib of mouse *NPM-ALK* lymphoma cells with the indicated genotypes treated for 72 h with trametinib. Shown are absolute half-maximal inhibitory concentration ( $IC_{50}$ ) values ( $\mu$ M,  $n = 3$  biologically independent samples). Data are shown as means  $\pm$  s.d. **g**, Growth of WASP wild type or knockout *NPM-ALK* lymphoma cells grafted in NSG mice treated with trametinib alone ( $1.5 \text{ mg kg}^{-1}$ ) or crizotinib ( $30 \text{ mg kg}^{-1}$ ) alone or in combination with trametinib ( $1.5 \text{ mg kg}^{-1}$ ). Values shown are the changes in tumor volume from baseline ( $n = 5$  independent tumors). Data are shown as means  $\pm$  s.e.m.; significance was determined by an unpaired, two-tailed Student's  $t$ -test.

variety of functions in lymphocytes and other hematopoietic cells, including lymphocyte proliferation and homeostasis<sup>7</sup>. Patients with WAS have a variable degree of immunodeficiency and an overall increased risk of developing hematologic malignancies, mostly lymphomas, that are thought to develop because of the immunodeficiency state<sup>10</sup>. In this work, we provide evidence that WASP is an oncosuppressor in T lymphocytes, and we identify ALCL as a specific subtype of T cell lymphoma in which WASP and WIP expression is selectively downregulated and contributes to lymphoma pathogenesis. An interesting expansion of this work would be to study WASP and WIP expression in B cell lymphoma or other hematologic malignancies. Furthermore, we provide evidence that the levels of the Rho GTPase CDC42 are essential for the tumor-suppressor functions of WASP. The acceleration of lymphoma development in *Wasp*<sup>-/-</sup> mice was dependent on the abundance of CDC42 in lymphoma cells; *Wasp*<sup>-/-</sup> lymphomas had significantly higher amount of active GTP-bound CDC42 and a reduction of about half CDC42 protein was sufficient to revert the phenotype in vitro and in vivo (Fig. 3d and Fig. 4b,c). Similar WASP-dependent regulation of active CDC42 was found in human ALCL (Fig. 6b) as well as in immortalized B lymphocytes from patients with WAS (Supplementary Fig. 9c), demonstrating that active CDC42 accumulates in normal and tumor lymphocytes in the absence of WASP.

Considering the known role of WASP and WIP in T cell activation, we evaluated the possibility that the accelerated lymphoma development observed in WASP- and WIP-deficient mice could be associated to a defective immunosurveillance. However, several findings suggest that defective immunosurveillance is not sufficient to explain the accelerated lymphomagenesis in WASP- and WIP-deficient mice. First, in contrast to other classical immunodeficient strains such as Nod scid mice, *Wasp*<sup>-/-</sup> and *Wip*<sup>-/-</sup> mice do not develop spontaneous lymphomas or other tumors<sup>2,9</sup>, thus implying that the level of immunodeficiency is probably mild in these mice. Second, T cell functional defects are more pronounced in *Wip*<sup>-/-</sup> mice than in *Wasp*<sup>-/-</sup> mice<sup>2</sup>, yet the acceleration of lymphomagenesis is comparable in the two genetic backgrounds. Third, *Wasp*<sup>-/-</sup>/*Cdc42*<sup>fl/fl</sup>/*CD4-Cre* T cells had defective T cell proliferation (Supplementary Fig. 10a) and defective MAPK pathway activation (Supplementary Fig. 10b) similar to *Wasp*<sup>-/-</sup> T cells, yet the loss of one copy of *Cdc42* is sufficient to revert the lymphoma acceleration observed in *Wasp*<sup>-/-</sup> mice (Fig. 3d). Fourth, if the immunodeficiency of *Wasp*<sup>-/-</sup> mice would be a major contribution to the accelerated lymphomagenesis, *Wasp*<sup>-/-</sup> lymphoma should have incurred into a limited immunoeediting and have growth significantly impaired when transplanted into immunocompetent mice. In contrast, wild-type and *Wasp*<sup>-/-</sup> lymphoma grew equally in immunocompetent mice (Supplementary Fig. 10c). Finally, experiments in human ALCL clearly show that the cellular levels of WASP and WIP intrinsically contribute to lymphoma growth in vitro and in vivo.

We showed that WASP and WIP expression are selectively decreased in ALCL, a subtype of T cell lymphoma that can be driven by translocations involving the *ALK* gene in ALK+ ALCL or by translocations involving other tyrosine kinases or phosphatases in ALK- ALCL<sup>14,15</sup>. Interestingly, aberrant STAT3 activation is frequent in both ALK+ and ALK- ALCL where STAT3 phosphorylation is directly controlled by ALK or other oncogenic tyrosine kinases, such as ROS1 and TYK2<sup>14,36</sup>. We showed that ALK oncogenic activity mediates downregulation of WASP and WIP through a STAT3 and C/EBP- $\beta$  dependent transcriptional repression. ChIP-seq experiments showed that abrogation of STAT3 activation by ALK inhibitors resulted in a profound genome-wide loss of STAT3 binding as well as that at *WAS* and *WIPF1* genes (Fig. 5g-i and Supplementary Fig. 6b,c). Therefore, WASP and WIP downregulation could represent a common feature of T cell lymphomas where the activity of STAT3 predominates, typically those induced by deregulated tyrosine kinases such as ALCL. In contrast, AITL

and PTCL are more dependent on a tonic TCR signaling that relies on the maintenance of cytoskeletal signaling functions in which WASP and WIP are essential. However, TCR ligation induces WASP degradation that in turn modifies assembly of F-actin. Thus, reduced levels of WASP after TCR engagement could also play a role in downstream signaling in normal T cells<sup>37</sup>.

Other mechanisms may contribute to the downregulation of WASP or WIP in ALCL. For example, a recent study showed that NPM-ALK directly phosphorylates Tyr102 of WASP; this phosphorylation impairs the binding of WASP to WIP and increases proteasome-dependent WASP degradation<sup>38</sup>, overall confirming that ALK downregulates WASP expression by multiple mechanisms. In contrast to our findings, however, this study concluded that WASP contributes to the oncogenic activity of ALK. This discrepancy probably originates from a different approach that focused on abrogating the residual WASP expression by shRNA rather than investigating the overall low levels of WASP in ALCL.

Whereas *WAS* and *WIPF1* mutations in ALCL have not been systematically studied, interestingly somatic loss of function (*WAS*<sup>G229E</sup>) or frame-shift mutations (*WAS*<sup>G333fs</sup> and *WAS*<sup>P329fs</sup>) leading to premature WASP truncation similar to patients with WAS have been detected in 4.6% of PTCL-NOS<sup>19</sup>, raising the intriguing possibility that a fraction of other T cell lymphomas rely on somatic inactivation of WASP. In an ongoing effort to characterize *WAS* and *WIPF1* genes in ALCL, we performed whole-exome sequencing in six cases of ALK+ ALCL. No somatic mutations of the *WAS*, *WIPF1* and *CDC42* genes were found, but deletions of chromosome X in the region containing the *WAS* gene was detected in two out of six cases, suggesting that gene deletion could be an additional mechanisms for WASP inactivation in ALCL. Furthermore, we found one case with a mutation of the intersectin 2 (*ITSN2*) gene and two cases with mutations of the Myosin Heavy Chain 8 (*MYH8*) genes (Supplementary Table 1). *ITSN2* is a GEF for CDC42 and regulates its activation<sup>39</sup> and interacts directly with WASP<sup>40</sup>. *MYH8* is associated with the PAK and GTPase pathways. Interestingly, this gene was recently found also mutated in ALK- ALCL<sup>14</sup>. These are limited observations that need to be expanded in larger series of cases but could underlie additional potential mechanisms that alter the CDC42-WASP axis in T cell lymphoma.

Taken together, it is tempting to propose that T cell lymphomas can be divided into two main categories. In T cell lymphomas that retain TCR signaling dependence, such as PTCL-NOS and AITL, WASP and WIP functions are maintained, at least initially, as they are key molecules for the immunological synapse and TCR signaling; once a lymphoma is established, inactivating mutations of WASP could be further selected by providing additional growth advantage. On the other hand, in T cell lymphomas that lost TCR signaling and depend on aberrant tyrosine kinase activity, such as ALCL, WASP and WIP are lost or downregulated as they act as tumor suppressors; their downregulation provides a biological advantage by increased active CDC42 and MAPK signaling. In these lymphomas, the hyperactivated MAPK pathway could represent an actionable therapeutic vulnerability when combined with the inhibition of ALK, which is the driver oncogene in ALK+ ALCL. Thus, inhibition of both ALK and MEK inhibitors could represent a more powerful therapeutic strategy in ALK+ ALCL, possibly for those patients who respond poorly to crizotinib<sup>33</sup>. A similar concept has been recently suggested for ALK+ lung cancers<sup>34</sup>.

In conclusion, by combining genetic and functional assays we have demonstrated an unexpected role for WASP and WIP as oncosuppressor proteins in lymphomas. Mechanistically, we have shown that the levels of CDC42 activation are increased in the absence of a binding to WASP, leading to increased proliferation and survival of lymphoma cells. The activation of CDC42 and MAPK pathway provides a therapeutic vulnerability in lymphoma with low WASP expression.

## Online content

Any methods, additional references, Nature Research reporting summaries, source data, statements of data availability and associated accession codes are available at <https://doi.org/10.1038/s41591-018-0262-9>.

Received: 3 December 2017; Accepted: 25 September 2018;  
Published online: 3 December 2018

## References

1. Sullivan, K. E., Mullen, C. A., Blaese, R. M. & Winkelstein, J. A. A multi-institutional survey of the Wiskott–Aldrich syndrome. *J. Pediatr.* **125**, 876–885 (1994).
2. Anton, I. M. et al. WIP deficiency reveals a differential role for WIP and the actin cytoskeleton in T and B cell activation. *Immunity* **16**, 193–204 (2002).
3. de la Fuente, M. A. et al. WIP is a chaperone for Wiskott–Aldrich syndrome protein (WASP). *Proc. Natl Acad. Sci. USA* **104**, 926–931 (2007).
4. Ramesh, N. & Geha, R. Recent advances in the biology of WASP and WIP. *Immunol. Res.* **44**, 99–111 (2009).
5. Ramesh, N., Anton, I. M., Hartwig, J. H. & Geha, R. S. WIP, a protein associated with wiskott-aldrich syndrome protein, induces actin polymerization and redistribution in lymphoid cells. *Proc. Natl Acad. Sci. USA* **94**, 14671–14676 (1997).
6. Abdul-Manan, N. et al. Structure of Cdc42 in complex with the GTPase-binding domain of the 'Wiskott–Aldrich syndrome' protein. *Nature* **399**, 379–383 (1999).
7. Thrasher, A. J. & Burns, S. O. WASP: a key immunological multitasker. *Nat. Rev. Immunol.* **10**, 182–192 (2010).
8. Massaad, M. J., Ramesh, N. & Geha, R. S. Wiskott–Aldrich syndrome: a comprehensive review. *Ann. N. Y. Acad. Sci.* **1285**, 26–43 (2013).
9. Snapper, S. B. et al. Wiskott–Aldrich syndrome protein-deficient mice reveal a role for WASP in T but not B cell activation. *Immunity* **9**, 81–91 (1998).
10. Ochs, H. D. & Thrasher, A. J. The Wiskott–Aldrich syndrome. *J. Allergy Clin. Immunol.* **117**, 725–738 (2006). quiz 739.
11. Recher, M. et al. B cell-intrinsic deficiency of the Wiskott–Aldrich syndrome protein (WASP) causes severe abnormalities of the peripheral B-cell compartment in mice. *Blood* **119**, 2819–2828 (2012).
12. Boddicker, R. L., Razioldo, G. L. & Feldman, A. L. Genetic alterations affecting GTPases and T-cell receptor signaling in peripheral T-cell lymphomas. *Small GTPases* **29**, 1–7 (2016).
13. Scarfo, I. et al. Identification of a new subclass of ALK-negative ALCL expressing aberrant levels of ERBB4 transcripts. *Blood* **127**, 221–232 (2016).
14. Crescenzo, R. et al. Convergent mutations and kinase fusions lead to oncogenic STAT3 activation in anaplastic large cell lymphoma. *Cancer Cell* **27**, 516–532 (2015).
15. Parrilla Castellar, E. R. et al. ALK-negative anaplastic large cell lymphoma is a genetically heterogeneous disease with widely disparate clinical outcomes. *Blood* **124**, 1473–1480 (2014).
16. Werner, M. T., Zhao, C., Zhang, Q. & Wasik, M. A. Nucleophosmin-anaplastic lymphoma kinase: the ultimate oncogene and therapeutic target. *Blood* **129**, 823–831 (2017).
17. Yoo, H. Y. et al. A recurrent inactivating mutation in RHOA GTPase in angioimmunoblastic T cell lymphoma. *Nat. Genet.* **46**, 371–375 (2014).
18. Sakata-Yanagimoto, M. et al. Somatic RHOA mutation in angioimmunoblastic T cell lymphoma. *Nat. Genet.* **46**, 171–175 (2014).
19. Palomero, T. et al. Recurrent mutations in epigenetic regulators, RHOA and FYN kinase in peripheral T cell lymphomas. *Nat. Genet.* **46**, 166–170 (2014).
20. Abate, F. et al. Activating mutations and translocations in the guanine exchange factor VAV1 in peripheral T-cell lymphomas. *Proc. Natl Acad. Sci. USA* **114**, 764–769 (2017).
21. Ambrogio, C. et al. The anaplastic lymphoma kinase controls cell shape and growth of anaplastic large cell lymphoma through Cdc42 activation. *Cancer Res.* **68**, 8899–8907 (2008).
22. Colomba, A. et al. Activation of Rac1 and the exchange factor Vav3 are involved in NPM-ALK signaling in anaplastic large cell lymphomas. *Oncogene* **27**, 2728–2736 (2008).
23. Choudhari, R. et al. Redundant and nonredundant roles for Cdc42 and Rac1 in lymphomas developed in NPM-ALK transgenic mice. *Blood* **127**, 1297–1306 (2016).
24. Swerdlow, S. H. et al. The 2016 revision of the World Health Organization classification of lymphoid neoplasms. *Blood* **127**, 2375–2390 (2016).
25. Chiarle, R. et al. NPM-ALK transgenic mice spontaneously develop T-cell lymphomas and plasma cell tumors. *Blood* **101**, 1919–1927 (2003).
26. Lanzi, G. et al. A novel primary human immunodeficiency due to deficiency in the WASP-interacting protein WIP. *J. Exp. Med.* **209**, 29–34 (2012).
27. Al-Mousa, H. et al. Hematopoietic stem cell transplantation corrects WIP deficiency. *J. Allergy Clin. Immunol.* **139**, 1039–1040 e1034 (2017).
28. Notarangelo, L. D., Notarangelo, L. D. & Ochs, H. D. WASP and the phenotypic range associated with deficiency. *Curr. Opin. Allergy. Clin. Immunol.* **5**, 485–490 (2005).
29. Hill, C. S., Wynne, J. & Treisman, R. The Rho family GTPases RhoA, Rac1, and CDC42Hs regulate transcriptional activation by SRF. *Cell* **81**, 1159–1170 (1995).
30. Ambrogio, C. et al. NPM-ALK oncogenic tyrosine kinase controls T-cell identity by transcriptional regulation and epigenetic silencing in lymphoma cells. *Cancer Res.* **69**, 8611–8619 (2009).
31. Hassler, M. R. et al. Insights into the pathogenesis of anaplastic large-cell lymphoma through genome-wide DNA methylation profiling. *Cell Rep.* **17**, 596–608 (2016).
32. Piva, R. et al. Ablation of oncogenic ALK is a viable therapeutic approach for anaplastic large-cell lymphomas. *Blood* **107**, 689–697 (2006).
33. Gambacorti Passerini, C. et al. Crizotinib in advanced, chemoresistant anaplastic lymphoma kinase-positive lymphoma patients. *J. Natl Cancer. Inst.* **106**, djt378 (2014).
34. Hrustanovic, G. et al. RAS-MAPK dependence underlies a rational polytherapy strategy in EML4-ALK-positive lung cancer. *Nat. Med.* **21**, 1038–1047 (2015).
35. Rivers, E. & Thrasher, A. J. Wiskott–Aldrich syndrome protein: emerging mechanisms in immunity. *Eur. J. Immunol.* **47**, 1857–1866 (2017).
36. Chiarle, R. et al. Stat3 is required for ALK-mediated lymphomagenesis and provides a possible therapeutic target. *Nat. Med.* **11**, 623–629 (2005).
37. Watanabe, Y. et al. T-cell receptor ligation causes Wiskott–Aldrich syndrome protein degradation and F-actin assembly downregulation. *J. Allergy Clin. Immunol.* **132**, 648–655 e641 (2013).
38. Murga-Zamalloa, C. A. et al. NPM-ALK phosphorylates WASP Y102 and contributes to oncogenesis of anaplastic large cell lymphoma. *Oncogene* **36**, 2085–2094 (2017).
39. Zhang, J. et al. Intersectin 2 controls actin cap formation and meiotic division in mouse oocytes through the Cdc42 pathway. *FASEB J* **31**, 4277–4285 (2017).
40. McGavin, M. K. et al. The intersectin 2 adaptor links Wiskott Aldrich Syndrome protein (WASP)-mediated actin polymerization to T cell antigen receptor endocytosis. *J. Exp. Med.* **194**, 1777–1787 (2001).

## Acknowledgements

We thank M.S. Scalzo and D. Corino for technical assistance, and B. Castella for providing purified human T cells. The work has been supported by grant no. FP7 ERC-2009-StG (Proposal No. 242965—'Lunely') (R.C.) grant no. R01 CA196703-01 (R.C.); AIRC grant no. MFAG (C.A. and M.C.); National Research Foundation of Korea (NRF) fellowship 2016R1A6A3A03006840 (T.-C.C.); Bando Giovani Ricercatori grant no. 2009-GR 1603126 (M.C.); MINECO/FEDER grant no. SAF2015–70368-R and Fundación Ramón Areces (I.M.A.); the Division of Intramural Research, National Institute of Allergy and Infectious Diseases, National Institutes of Health (L.D.N.); and award no. T32GM007753 from the National Institute of General Medical Sciences (S.H.C.) (the content is solely the responsibility of the authors and does not necessarily represent the official views of the National Institute of General Medical Sciences or the National Institutes of Health); and in part by awards from the National Institutes of Health DP2 New Innovator award no. 1DP2CA195762-01 (C.K.); the American Cancer Society Research Scholar award no. RSG-14-051-01-DMC and the Pew-Stewart Scholars in Cancer Research Grant (C.K.); and the European Union Horizon 2020 Marie Skłodowska-Curie Innovative Training Network Grant award no. 675712 for the European Research Initiative for ALK-Related Malignancies (G.G.S., I.M., C.G.P. and R.C.).

## Author contributions

M.M., C.A., T.-C.C., C.P., I.M., S.H.C., M.C., R.D., T.P., E.P., C.M. and C.V. performed experiments. M.M., V.M., C.V. and R. Choudhari performed mice experiments. Q.W. and C.K.C. performed bioinformatics analysis. A.P. analyzed data. R.P. provided gene expression data on lymphoma samples. C.K. provided reagents for ChIP-seq. S.G. and L.G.N. provided WAS patient samples and analyzed data. G.G.S., L.M. and C.G.-P. provided sequencing data on patients with ALCL. A.Z. provided lymphoma cases. I.M.A. contributed mouse strains and analyzed data. C.V. and R. Chiarle conceived and analyzed the experiments. M.M., C.V. and R. Chiarle wrote the manuscript.

## Competing Interests

The authors declare no competing interests.

## Additional information

**Supplementary information** is available for this paper at <https://doi.org/10.1038/s41591-018-0262-9>.

**Reprints and permissions information** is available at [www.nature.com/reprints](http://www.nature.com/reprints).

**Correspondence and requests for materials** should be addressed to C.V. or R.C.

**Publisher's note:** Springer Nature remains neutral with regard to jurisdictional claims in published maps and institutional affiliations.

© This is a U.S. government work and not under copyright protection in the U.S.; foreign copyright protection may apply 2018

## Methods

**Transgenic mice and tumor xenografts.** *CD4-NPM-ALK* transgenic mice<sup>25</sup>, *CD4-Cre*<sup>26</sup>, *Cdc42<sup>fl/fl</sup>*, *Wasp<sup>-/-</sup>* and *Wip<sup>-/-</sup>* (ref. <sup>2</sup>) were previously described. *CD4-NPM-ALK*, *Wasp<sup>-/-</sup>* and *Wip<sup>-/-</sup>* mice were bred in C57BL/6 background. NSG immunocompromised mice were purchased from Charles River Laboratories. For subcutaneous xenografts, human ALCL cell lines transduced with inducible lentiviral vectors expressing WASP and WIP complementary DNA were injected in both flanks of NSG mice;  $5 \times 10^6$  cells were resuspended in 150  $\mu$ l PBS and injected. Injected mice were administered drinking water containing doxycycline (1 mg ml<sup>-1</sup>) (Sigma) to express WASP and WIP cDNA. Tumor growth was measured with a caliper every two days. Mice were euthanized at humane endpoint, and tumors were resected with a scalpel and snapped frozen or paraffin fixed in buffer neutral formalin for further experiments.

Mice were treated with trametinib (1.5 mg kg<sup>-1</sup>) or crizotinib (30 mg kg<sup>-1</sup>) or a combination of the two inhibitors by oral gavage once a day for a week. Tumor growth was measured with a caliper every two days. Both drugs were dissolved in 0.5% methylcellulose + 0.05% Tween-80. Mice were euthanized at humane endpoint.

Lymphoma cell lines obtained from *NPM-ALK* transgenic mice were injected subcutaneously in both flanks of syngeneic C57BL/6 or NSG mice, and  $10 \times 10^6$  cells were resuspended in 150  $\mu$ l PBS and injected. Tumor growth was followed as described above.

Mice were handled and treated in accordance with European Community guidelines under the mouse protocol approved by the Italian Ministry of Research (no. 254/2017-PR).

**Cell lines and reagents.** Human ALK+ ALCL cell lines (TS, SU-DHL1, Jb6, Karpas-299, DEL, SUP-M2 and L82) and ALK– cell lines (MAC-1, FePD and Jurkat) ALCL cell lines were obtained from DSMZ (German collection of Microorganisms and Cell Cultures). Cell lines were maintained in RPMI 1640 (Lonza) with 10% fetal bovine serum (FBS), 2% penicillin, streptomycin (5 mg ml<sup>-1</sup>), (Gibco) and 1% glutamine (Gibco). Cell lines were grown at 37°C in a humidified atmosphere with 5% CO<sub>2</sub>. ALCL cell lines transduced with doxycycline-inducible shRNA to knock down ALK expression were previously described<sup>12</sup>.

HEK-293T and 293 Phoenix packaging cells were obtained from DSMZ and cultured in DMEM, 10% FBS, 2% penicillin, streptomycin 5 mg ml<sup>-1</sup> and 1% glutamine.

ALK+ Ki-JK and ALK– T cell lymphoma lines were kindly provided by D. Weinstock (Dana-Farber Cancer Institute). DL-40 (ALK-negative ALCL) were maintained in IMDM + 20% FBS; Ki-JK, OCI-Ly13.2 (T cell lymphoma) and OCI-Ly12 (PTCL-NOS) were maintained in RPMI + 10% FBS; MAC2A (ALK-negative ALCL) was maintained in RPMI + 20% FBS; and DERYL2 (hepatosplenic T cell lymphoma) was maintained in RPMI + 20% FBS + 100 U/ml human IL-2. ALK+ COST cell line was kindly provided by L. Lamant (Centre de Recherche en Cancérologie de Toulouse).

Immortalized EBV-transformed B lymphoblastoid cell lines were obtained from healthy controls and patients with WAS (enrolled in clinical protocol 04-09-113R) as previously described<sup>42</sup> and cultured in RPMI 1640 medium (Thermo Fisher Scientific) supplemented with 10% FBS, 2% penicillin, streptomycin 5 mg ml<sup>-1</sup> (Gibco) and 1% glutamine (Gibco).

Murine lymphoma cell lines were obtained from transgenic mice with the corresponding genotype. Briefly, at the humane endpoint mice were euthanized and tumoral thymuses were resected. Single-cell suspensions were prepared from fresh tumoral thymuses with mechanical disaggregation and were isolated by using 40- $\mu$ m nylon cell strainer (BD Biosystems). Cells were grown in RPMI and cultured for at least 4 weeks before proceeding with further experiments.

**Virus preparation and cell transduction.** Lentiviruses were produced using the third-generation production system. Briefly, 293T cell lines were cultured in DMEM with 10% FBS. Cells at 70% confluency were co-transfected with pVSVG, pCMVR8.74, pRSV-Rev and a lentiviral vector expressing the construct of interest. Medium was replenished 12 or 18 h after transfection, and the supernatant was collected after 24 and 48 h. Collected supernatants were filtered through a 0.22- $\mu$ m filter, concentrated by ultracentrifugation ( $\times 50,000g$  for 2 h) and resuspended in 500  $\mu$ l of sterile PBS. For infection,  $5 \times 10^4$  cells were infected with the prepared lentivirus along with polybrene (8  $\mu$ g ml<sup>-1</sup>), and cells with viral particles were spun down at 2,500 r.p.m. for 90 min and then incubated at 37°C overnight.

STAT3- and C/EBP $\beta$ -specific shRNAs and inducible ALK shRNA have been previously described<sup>43,44</sup>. Human Flag-WASP and Flag-WIP cDNA were obtained from A. Galy (Institut Gustave Roussy) and from Addgene, respectively. For the doxycycline-inducible system (Tet-ON), WASP and WIP cDNA were cloned into a modified pCCL vector as previously described<sup>45</sup>. SU-DHL1, Jb6, DEL and Karpas-299 cell lines were co-infected with pCCL and rTA plasmids. For cell-sorting enrichment, cells were induced with 1  $\mu$ g ml doxycycline for 12 h and sorted for GFP expression on a MoFlo High-Performance Cell Sorter (DAKO Cytomation).

Retroviruses were generated by transfection of pWZL Blast vector expressing CRE-ERT2 in 293 Phoenix packaging cells. Transfected cells were incubated at 37°C for 12 or 18 h, and supernatants containing viral particles were collected at 24

and 48 h. 300  $\mu$ l retroviral supernatants were used to transduce  $5 \times 10^4$  lymphoma cells as previously described<sup>23</sup>. CRE-ERT2-transduced cells were selected using blasticidin (Calbiochem) at 25  $\mu$ g ml<sup>-1</sup> for 6 days.

**Cell lysis and immunoblotting.** Total cellular protein was extracted with GST-FISH buffer (10 mM MgCl<sub>2</sub>, 150 mM NaCl, 1% NP40, 2% glycerol, 1 mM EDTA, 25 mM HEPES pH 7.5), added with 1 mM phenylmethylsulfonyl fluoride, 10 mM NaF, 1 mM Na<sub>3</sub>VO<sub>4</sub> and protease inhibitors (Roche). Total cell lysate was cleared by centrifugation (13,000 r.p.m.) at 4°C in a microcentrifuge for 10 min and quantified using the Bio-Rad protein assay method. Protein samples were normalized based on protein concentration, denatured by addition of Laemmli buffer and boiled for 10 min. Thirty to fifty micrograms of proteins were run on sodium dodecyl sulfate-polyacrylamide gel electrophoresis under reducing conditions and transferred to nitrocellulose (GE Healthcare). Membranes were incubated with specific antibodies, detected with peroxidase-conjugated secondary antibodies (GE Healthcare) and enhanced using chemiluminescent reagent (Amersham).

The following primary antibodies were used: anti-ALK (Invitrogen, Catalog no. 35-4300), anti-human WASP (Epitomics, Clone:EP2541Y, Catalog no. 2422-1), anti-murine WASP (Cell Signaling Technology, Catalog no. 4860), anti-N-WASP (Cell Signaling Technology, Clone:30D10, Catalog no. 4848), anti-WIP (Santa Cruz Biotechnology, Clone:H-224, Catalog no. sc-25533), anti-phospho-STAT3 (Tyr705) (Cell Signaling Technology, Catalog no. 9131), anti-STAT3 (Cell Signaling Technology, Clone:79D7, Catalog no. 4904), anti-phospho-ERK (Thr202/Tyr204) (Cell Signaling Technology, Catalog no. 9101), anti-ERK (Cell Signaling Technology, Catalog no. 9102), anti-phospho-AKT (Ser473) (Cell Signaling Technology, Clone:D9E, Catalog no. 4060), anti-AKT (Cell Signaling Technology, Clone:11E7, Catalog no. 4685), anti-phospho-JNK (Thr183/Tyr185) (Cell Signaling Technology Clone:G9, Catalog no. 9255), anti-JNK (Cell Signaling Technology, Catalog no. 9252), anti-CDC42 (BD Transduction Laboratory, Catalog no. 610929), anti-C/EBP $\beta$  (Santa Cruz Biotechnology, Clone:C-19, Catalog no. sc-150), anti-Cleaved Caspase 3 (Asp175) (Cell Signaling Technology, Catalog no. 9661), anti-phospho S6 (Ser235/236) (Cell Signaling Technology, Clone:D57.2.2.E, Catalog no. 4858) and anti-S6 (Cell Signaling Technology, Clone:54D2, Catalog no. 2317), HSP90 (Santa Cruz Biotechnology, Clone:H114, Catalog no. sc-7947), anti-ZAP70 (Millipore, Clone:2F3.2, Catalog no. 05-253) anti-GFP (Invitrogen, Catalog no. A-11122), anti-Actin (Sigma-Aldrich, Catalog no. A2066).

**Histology, immunohistochemistry and immunofluorescence.** For histology, tissue samples were formalin-fixed and paraffin embedded, cut into 4- $\mu$ m-thick sections and stained with H&E.

For immunohistochemistry, formalin-fixed sections were de-waxed in xylene and dehydrated by passage through graded alcohols to water; sections were microwaved in citrate buffer pH 6 for 15 min and then transferred to PBS. Endogenous peroxidase was blocked using 1.6% hydrogen peroxide in PBS for 10 min followed by washing in distilled water. Normal serum diluted to 10% in 1% bovine serum albumin (BSA) was used to block nonspecific staining.

The slides were then incubated for 1 h with the following primary antibodies: anti-WASP (Epitomics), anti-WIP (Clone:H-224, Santa Cruz Biotechnology), anti-ALK (Clone: 18-0266, Zymed); anti-cleaved caspase 3 (Cell Signaling Technology), anti-murine Ki-67 (AbCam, Clone:SP6, Catalog no. ab16667) and anti-human Ki-67 (DAKO, Clone:MIB-1, Catalog no. M7240). After washing, sections were incubated with biotinylated secondary goat antibody to rabbit IgG and visualized with the EnVision system (Dako).

For immunofluorescence, cells were plated on glass coverslips pretreated with fibronectine (10  $\mu$ g ml<sup>-1</sup> PBS) at 37°C for 1 h and incubated overnight in fresh medium. Samples were fixed in 4% paraformaldehyde at room temperature for 10 min and permeabilized with 0.3% Triton X-100 for 5 min. Coverslips were incubated with 3% BSA for 1 h at room temperature and then stained with phycoerythrin-conjugated phalloidin (1/500, Sigma) and HOECHST (300 ng ml<sup>-1</sup>, Sigma). Coverslips were mounted on microscope slides using anti-fading solution and viewed using a Leica photomicroscope. Images were acquired at room temperature by means of H&C PL APO  $\times 100/1.40$  OIL (Leica, Heidelberg, Germany) and analyzed by DM LM Leica software. Cell dimension has been measured using ImageJ software.

The slides were reviewed by experienced hematopathologists, and quantification of the levels of WASP and WIP expression was performed selectively in multiple areas where lymphoma cells were clearly enriched. This selection was achieved by comparing the areas on serial sections stained with the following markers: ALK for ALK+ ALCL, CD30 for ALK– ALCL, CD10 for AITL. When a marker was not available (such as loss of a particular T cell antigen) for PTCL-NOS, NK/T cell lymphoma and hepatosplenic  $\gamma\delta$  T cell lymphoma, the selection of the areas with enriched lymphoma cells was based on morphologic criteria, such as a cluster of atypical cells or invasion of specific structures such as vessels in NK/T cell lymphoma or sinusoids in hepatosplenic  $\gamma\delta$  T cell lymphoma. The quantification of WASP and WIP expression levels was achieved by comparison with an internal control constituted by normal B and T lymphocytes.

**qRT-PCR analysis.** Total RNA was extracted from cells using TRIzol solution (Invitrogen), followed by cDNA preparation from 1  $\mu$ g of total RNA. cDNA



products were quantified by real-time PCR using SYBR Green Supermix (Bio-rad) on Bio-Rad iCycler iQ Real-Time PCR Detection System. Normalization was performed against the housekeeping human acidic ribosomal protein (*HuPO*) or Actin according to the formula  $2^{-\Delta\Delta C_t}$ , where the  $\Delta C_t = \frac{1}{2} C_t$  (threshold cycle) gene of interest  $- C_t$  internal control, as indicated by the manufacturer.

WASP-specific primers: forward 5'-GAAACGCTCAGGGAAGAAGA-3', reverse 5'-CTGCCCTGGAGAACGACTC-3';  
WIP-specific primers: forward 5'-ACAGGATAATGATTCTGGAGG-3', reverse 5'-CTGGAGAAGGCACAGGAAAC-3';  
HuPO-specific primers: forward 5'-GCTTCTGGAGGGTGTC-3', reverse 5'-GCTTCTGGAGGGTGTC-3';  
Actin-specific primers: forward 5'-ACGAGCCCCCTGAAAC-3', reverse 5'-CAGGTCCAGACGACGAGGATGTC-3';  
LAT-specific primers forward 5'-ACAGTGTGGCGAGCTACG-3', reverse 5'-CGTTCAGTAATCATCAATGG-3'

**DNA demethylation.** ALK+ ALCL cell lines (TS, SU-DHL1 and JB6) were plated in a six-well plate ( $5 \times 10^5$  cells per ml), treated with  $5 \mu\text{M}$  of the methyltransferase inhibitor 5-aza-2-deoxycytidine (Sigma). Cells were washed twice in PBS and collected at 0, 48, 72, 96 and 144 h after the treatment. Cells were collected for western blot and qRT-PCR assays.

ZAP70 and LAT were used as positive controls for western blot and qRT-PCR, respectively, as previously reported<sup>30</sup>.

**Chromatin immunoprecipitation.** JB6 and SU-DHL1 cells were fixed in 1% formaldehyde (Sigma-Aldrich, F8775) for 10 min at  $37^\circ\text{C}$ . Subsequently, glycine was added to 125 mM and incubated at  $37^\circ\text{C}$  for 5 min at  $37^\circ\text{C}$ . Next, cells were pelleted and washed twice with cold PBS. Pellets were stored at  $-80^\circ\text{C}$  until use.

Nuclei from 10M cells per ChIP-seq were extracted, and chromatin was sonicated with a Covaris sonicator. Immunoprecipitation reactions were performed overnight with anti-STAT3 (Cell Signaling Technology, Clone:124H6, Catalog no. 9139) or anti-C/EBP- $\beta$  (Abcam, Clone:E299, Catalog no. ab32358) antibodies. The next morning, antibodies and chromatin were captured using Protein G Dynabeads (Thermo Fisher). Material was washed, eluted and treated with RNase A (Roche 11 119 915 011) for 30 min at  $37^\circ\text{C}$  and Proteinase K (Life Technologies 100005393) for 3 h at  $65^\circ\text{C}$ . DNA was extracted using SPRI beads (Beckman Coulter Agencourt AMP Xpure).

H3K4me3, H3K27ac and H3K27me3 profiles on Jurkat<sup>46-48</sup> and GM12878<sup>49</sup> cell lines were obtained from public databases, including ENCODE.

**Library preparation and sequencing.** Library preparation of ChIP-seq DNA was performed using the Ultra II Library Prep Kit (NEB E7103L) and Multiplex Oligos for Illumina (NEB E7335L) and sequenced on an Illumina Nextseq 500 (75 base pairs single end).

**ChIP-seq data processing.** ChIP-seq samples were sequenced with the Illumina NextSeq technology, and output data were demultiplexed and converted to FASTQ format using the *bcl2fastq* software tool. Read quality was assessed by FASTQC, and ChIP-seq reads were aligned to the hg19 genome with Bowtie2 v2.29 in the  $-k 1$  reporting mode<sup>50</sup>. Output BAM files were converted into BigWig track files using the 'callpeak' function of MACS2 v2.1.1 with the '-B -SPMR' option followed by the use of the BEDTools<sup>51</sup> 'sort' function and the UCSC utility 'bedgraphToBigWig'<sup>52</sup>, and the tracks were visualized in IGV v2.4.3. Narrow peaks were called with the MACS2 v2.1.1 software using input as controls and a  $q$  value cutoff of 0.001<sup>53</sup>. Metaplots and heatmaps were generated using *ngsplot* v2.61<sup>54</sup>.

**Gene-expression profiling.** Total RNA was extracted from primary *NPM-ALK/Wasp*<sup>+/+</sup> or *NPM-ALK/Wasp*<sup>-/-</sup> lymphoma using TRIzol reagent (Invitrogen) and purified using the RNeasy total RNA Isolation Kit (Qiagen). GeneChip Mouse Gene 1.0ST Array from Affymetry was used for profiling.

**Apoptosis assay and cell cycle analysis.** Cre-ERT2-transduced murine cells were grown in six-well plates after treatment with  $10 \text{ nM}$  4-hydroxytamoxifen (4OHT; Sigma) for 4 h. At 0, 24 and 48 h after the treatment, cells were stained with 200 nM tetramethylrodamine methyl-ester (TMRM) for 15 min in dark and washed twice in PBS, and the percentage of apoptotic cells was measured by flow cytometry (BD FACSCALIBUR) using the CellQuest Program.

For cell cycle analysis, the DNA content was determined with propidium iodide staining. SU-DHL1 and Karpas-299 cell lines either expressing WASP- and WIP-inducible vector or the GFP control were treated for 168 h with doxycycline ( $1 \mu\text{g ml}^{-1}$ ), cells were washed with PBS, resuspended in citric acid buffer (0.05 M Na<sub>2</sub>HPO<sub>4</sub>, 25 mM sodium citrate and 0.1% Triton X-100 (pH 7.3)), treated with RNase ( $0.25 \text{ mg ml}^{-1}$ ) and then stained with propidium iodide ( $50 \mu\text{g ml}^{-1}$ ) for 15 min at  $37^\circ\text{C}$  in the dark. The G<sub>1</sub> and S/G<sub>2</sub>-M cell fractions were calculated for the nonapoptotic cell population only.

**Cell viability assay.** Cell viability assay on human ALK+ ALCL cell lines was performed using CellTiter-Glo (Promega), according to manufacturer's instruction.

Briefly, cells were seeded into white walled 96-well plates (three wells per sample) in the presence or absence of treatment (doxycycline, 4-hydroxytamoxifen or trametinib). CellTiter-Glo reagent was added to each well, and luminescence output data were taken at 0, 24, 48 and 72 h by GloMax-Multi Detection System (Promega). Trametinib was purchased from Selleckem, diluted in DMSO and used at the indicated concentrations.

**Drug-sensitivity assay.** Drug-sensitivity assays were performed as previously described<sup>55</sup>. Briefly, cells ( $2 \times 10^3$ ) were seeded in 96-well plates in RPMI complete medium. The following day, cells were treated with selumetinib (Selleckchem, Catalog no. S1008), trametinib (Selleckchem Catalog no. S2673), crizotinib (kindly provided by Pfizer), MEK162 (Selleckchem Catalog no. S7007) or PD0325901 (Selleckchem Catalog no. S1036) using a ten-point dose titration scheme from 1 nM to  $10 \mu\text{M}$  or from 1 nM to  $1 \mu\text{M}$ . After 72 h, cell viability was assessed using colorimetric MTS assay (CellTiter 96 AQueous Non-Radioactive Cell Proliferation Assay (MTS) Powder, Promega). Absolute inhibitory concentration values were calculated using four-parameter logistic curve fitting. All experimental points were a result of three to six replicates and all experiments were repeated at least three times. The data was graphically displayed using GraphPad Prism 7 for Windows (GraphPad Software). Each point (mean  $\pm$  s.d.) represents growth of treated cells compared to untreated cells. The curves were fitted using a nonlinear regression model with a sigmoidal dose response.

**Measurement of GTP-bound CDC42.** To measure the amount of GTP-bound CDC42, cells were plated at the same concentration in six-well plates and incubated in RPMI medium overnight. Cells were collected and lysed as previously described. CDC42 activity was determined using CDC42 G-LISA assay kit in accordance with the manufacturer's instructions (Cytoskeleton Inc.). Briefly, cells were collected and washed three times in ice-cold PBS on cold centrifuge, and protein lysates were transferred to ice-cold 1.5-ml centrifuge tubes and clarified by centrifuging at 10,000 r.p.m. for 2 min and then were immediately snapped frozen in liquid nitrogen. Protein concentrations were determined using the Precision Red Advance Protein Assay (Cytoskeleton), and  $1.0 \text{ mg ml}^{-1}$  protein was used for the GTPase activation assay. Fifty microlitres of protein lysate were added to a precoated 96-well plate, and then the plate was washed and antigen-presenting buffer was added, which was followed by primary and secondary antibodies. The reaction was detected using horseradish peroxidase detection reagent followed by the stop buffer. The plate was read immediately by measuring absorbance at 490 nm on a microplate spectrophotometer.

Human ALCL cell lines, stably transfected with Tet-ON WASP & WIP and the empty control Tet-ON GFP plasmid, were treated with doxycycline ( $1 \mu\text{g ml}^{-1}$ ). After 48 h, cells were lysed, and GTP-bound CDC42 was immunoprecipitated using CDC42 Activation Assay Kit (NewEast Biosciences). Quantification was performed by densitometric analysis of the western blot bands.

**Flow cytometry.** Six-week-old mice were euthanized, and thymuses were resected and used for flow cytometry analysis. Single-cell suspensions were prepared from fresh pretumoral thymuses with mechanic disaggregation and isolated by using  $40\text{-}\mu\text{m}$  nylon cell strainers (BD Biosystems). Cells were resuspended in PBS and stained with PE-anti-mouse CD4 (clone GK1.5; Miltenyi Biotec) and PerCP-anti-mouse CD8a (clone 53-6.7; BioLegend) for 15 min, and then were washed and resuspended in PBS. Cells were then acquired in a FACSCalibur flow cytometer (BD Bioscience) and analyzed using the FlowJo software.

For co-culture assays, SU-DHL1 and JB6 cell lines either expressing WASP and WIP inducible vector or the GFP control were mixed 1:1 with parental cells, the percentage of GFP positive cells was followed over time for 40 days by flow cytometry.

**T cell purification, ex vivo activation and proliferation analysis.** Untouched T cells were isolated from spleens of WASP- and WIP-deficient mice and wild-type mice by immunomagnetic depletion of B cells, monocytes/macrophages, natural killer cells, dendritic cells, erythrocytes and granulocytes.

Briefly, spleens were collected, placed on ice, washed in PBS to remove residual blood, cut into small pieces, crushed and physically dissociated using a Falcon cell strainer and subjected to hypotonic lysis of erythrocytes. Cells were resuspended in isolation buffer (PBS supplemented with 0.1% BSA and 2 mM EDTA). All non-T cells were depleted with a mixture of rat monoclonal IgG antibodies against non-T cells ('Antibody mix': anti mouse CD45R, CD11b, Ter-119 and CD16/CD32; Invitrogen) combined with Mouse Depletion Dynabeads ( $4.5 \mu\text{m}$  diameter beads coated with a polyclonal sheep anti-rat IgG antibody; Invitrogen) following the manufacturer's instructions.

Isolated mouse T cells, bead- and antibody-free, were activated by adding Dynabeads Mouse T-Activator CD3/CD28 (polyclonal activation; Invitrogen).

For T cell proliferation analysis, purified and activated T cells ( $1 \times 10^6$  cells) were plated in a six-well plate and cultured at  $37^\circ\text{C}$  in RPMI 1640 medium supplemented with 15% FBS, 2% penicillin, streptomycin  $5 \text{ mg ml}^{-1}$  and 50 mM 2-mercaptoethanol for 48 h. Cells were then collected for CellTiter-Glo analysis (Promega) following the manufacturer's instructions.

For western blot analysis, cells were collected after 15 min of incubation with the cocktail of CD3/CD28 beads, centrifuged and washed with cold PBS for protein extraction.

**Statistical analysis.** Statistical analysis was performed with GraphPad PRISM 7.0 software. *P* values were calculated by using the unpaired, two-tailed Student's *t*-test with Welch's correction as indicated in each figure legend. Kaplan–Meier analysis for survival curve was performed with GraphPad Prism 7, and *P* values were determined with a log-rank (Mantel–Cox) test.

**Reporting Summary.** Further information on research design is available in the Nature Research Reporting Summary linked to this article.

### Data availability

The Gene Expression Omnibus repository accession number for the gene expression profiling data from wild type and *Wasp*<sup>-/-</sup> mice is [GSE102889](#) (token: gzelisgodjkdxtq); and for ChIP-seq data, the accession number is [GSE117164](#) (token: chupqsgklxivtox). Gene-expression profiling data for human T cell lymphoma have been deposited with Gene Expression Omnibus repository accession number [GSE65823](#) (ref. <sup>13</sup>).

### References

41. Wu, X. et al. Cdc42 controls progenitor cell differentiation and beta-catenin turnover in skin. *Genes Dev.* **20**, 571–585 (2006).
42. Facchetti, F. et al. Defective actin polymerization in EBV-transformed B-cell lines from patients with the Wiskott–Aldrich syndrome. *J. Pathol.* **185**, 99–107 (1998).
43. Martinengo, C. et al. ALK-dependent control of hypoxia inducible factors mediates tumor growth and metastasis. *Cancer Res.* **74**, 6094–106 (2014).
44. Piva, R. et al. Functional validation of the anaplastic lymphoma kinase signature identifies CEBPB and BCL2A1 as critical target genes. *J. Clin. Invest.* **116**, 3171–3182 (2006).
45. Ceccon, M. et al. Excess of NPM-ALK oncogenic signaling promotes cellular apoptosis and drug dependency. *Oncogene* **35**, 3854–3865 (2016).
46. Orlando, D. A. et al. Quantitative ChIP-seq normalization reveals global modulation of the epigenome. *Cell reports* **9**, 1163–1170 (2014).
47. Mansour, M. R. et al. Oncogene regulation. An oncogenic super-enhancer formed through somatic mutation of a noncoding intergenic element. *Science* **346**, 1373–1377 (2014).
48. Manser, M. et al. ELF-MF exposure affects the robustness of epigenetic programming during granulopoiesis. *Sci. Rep.* **7**, 43345 (2017).
49. Thurman, R. E. et al. The accessible chromatin landscape of the human genome. *Nature* **489**, 75–82 (2012).
50. Langmead, B. & Salzberg, S. L. Fast gapped-read alignment with Bowtie 2. *Nat. Methods* **9**, 357–359 (2012).
51. Quinlan, A. R. & Hall, I. M. BEDTools: a flexible suite of utilities for comparing genomic features. *Bioinformatics* **26**, 841–842 (2010).
52. Kuhn, R. M., Haussler, D. & Kent, W. J. The UCSC genome browser and associated tools. *Brief. Bioinform.* **14**, 144–161 (2013).
53. Zhang, Y. et al. Model-based analysis of ChIP-seq (MACS). *Genome. Biol.* **9**, R137 (2008).
54. Shen, L., Shao, N., Liu, X. & Nestler, E. ngs.plot: quick mining and visualization of next-generation sequencing data by integrating genomic databases. *BMC Genomics* **15**, 284 (2014).
55. Ambrogio, C. et al. Kras dimerization impacts MEK inhibitor sensitivity and oncogenic activity of mutant KRAS. *Cell* **172**, 857–868 e815 (2018).

## Life Sciences Reporting Summary

Nature Research wishes to improve the reproducibility of the work that we publish. This form is intended for publication with all accepted life science papers and provides structure for consistency and transparency in reporting. Every life science submission will use this form; some list items might not apply to an individual manuscript, but all fields must be completed for clarity.

For further information on the points included in this form, see [Reporting Life Sciences Research](#). For further information on Nature Research policies, including our [data availability policy](#), see [Authors & Referees](#) and the [Editorial Policy Checklist](#).

Please do not complete any field with "not applicable" or n/a. Refer to the help text for what text to use if an item is not relevant to your study. For final submission: please carefully check your responses for accuracy; you will not be able to make changes later.

### ► Experimental design

#### 1. Sample size

Describe how sample size was determined.

In the transgenic mice experiment more than 30 mice for each genotype has been used. This large number of mice was achieved in several years of breeding. The only exception was the NPM-ALK, WASP<sup>-/-</sup> CDC42f/f, CD4-CRE genotype that showed short lifespan and therefore was not useful to determine lymphoma incidence. No sample size calculation was predetermined. All mice were bred to perform various experiments required by the project and survival curves were then calculated by collecting the total number of mice for each genotype.

#### 2. Data exclusions

Describe any data exclusions.

Each mouse was evaluated by autopsy for lymphoma. Mice that died for other causes without evidence of lymphoma were excluded from survival curves. No exclusion criteria were pre-established.

#### 3. Replication

Describe the measures taken to verify the reproducibility of the experimental findings.

All experiments have been repeated in technical and/or biological triplicates as indicated in the Figure legends. All attempts at replication were successful.

#### 4. Randomization

Describe how samples/organisms/participants were allocated into experimental groups.

All mice were randomly allocated in each group. For WASP deficient mice, because WASP is on the X chromosome, WASP<sup>-/-</sup> females and WASP<sup>-/-</sup> males were equally distributed between experimental groups.

#### 5. Blinding

Describe whether the investigators were blinded to group allocation during data collection and/or analysis.

No blinded group allocation was used during the experiment procedures. Blinding was not relevant to this study as each experiment was associated with proper controls. For xenografts experiments with human lymphoma, for ethical reason the minimum number of mice to provide statistical values was determined based on previous experimental data and published articles.

Note: all in vivo studies must report how sample size was determined and whether blinding and randomization were used.

## 6. Statistical parameters

For all figures and tables that use statistical methods, confirm that the following items are present in relevant figure legends (or in the Methods section if additional space is needed).

n/a Confirmed

- The exact sample size ( $n$ ) for each experimental group/condition, given as a discrete number and unit of measurement (animals, litters, cultures, etc.)
- A description of how samples were collected, noting whether measurements were taken from distinct samples or whether the same sample was measured repeatedly
- A statement indicating how many times each experiment was replicated
- The statistical test(s) used and whether they are one- or two-sided  
*Only common tests should be described solely by name; describe more complex techniques in the Methods section.*
- A description of any assumptions or corrections, such as an adjustment for multiple comparisons
- Test values indicating whether an effect is present  
*Provide confidence intervals or give results of significance tests (e.g.  $P$  values) as exact values whenever appropriate and with effect sizes noted.*
- A clear description of statistics including central tendency (e.g. median, mean) and variation (e.g. standard deviation, interquartile range)
- Clearly defined error bars in all relevant figure captions (with explicit mention of central tendency and variation)

*See the web collection on [statistics for biologists](#) for further resources and guidance.*

## ► Software

Policy information about [availability of computer code](#)

### 7. Software

Describe the software used to analyze the data in this study.

ImageJ v. 1.50i; iCycler iQ Software v. 3.1; CellQues Pro v6.0; FlowJo v10.5; GloMax Microplate Luminometer Software v1.9.3; GraphPad Prism v6.05; Leica Application Suite X; Demultiplexing: bcl2fastq; Quality Control: FASTQC; Read Alignment: Bowtie2 version 2.29; Peak Calling: MACS2 version 2.1.1; Track Generation: MACS2 version 2.1.1 “callpeak” function with “-B --SPMR” option, BEDTools “sort” function, the UCSC utility “bedgraphToBigWig”; Track Visualization: IGV version 2.4.3; Metaplot and Heatmap Generation: ngsplot version 2.6.1

For manuscripts utilizing custom algorithms or software that are central to the paper but not yet described in the published literature, software must be made available to editors and reviewers upon request. We strongly encourage code deposition in a community repository (e.g. GitHub). *Nature Methods* [guidance for providing algorithms and software for publication](#) provides further information on this topic.

## ► Materials and reagents

Policy information about [availability of materials](#)

### 8. Materials availability

Indicate whether there are restrictions on availability of unique materials or if these materials are only available for distribution by a third party.

Mouse models and primary derived cells lines of all genotypes are available for distribution without restrictions.

## 9. Antibodies

Describe the antibodies used and how they were validated for use in the system under study (i.e. assay and species).

We validated anti-Wasp and anti-Wip antibodies used in the study by internal controls such as comparing WT to knock-out or knock-down cells in WB blot and immunohistochemistry. Flow cytometry antibodies were validated by using corresponding negative cells for each stains.

For WB and immunohistochemistry, the antibodies were purchased by qualified vendors that provided a validation on the manufacturer's website.

The following antibodies were used:

anti-ALK 1:2000(Invitrogen, Catalog#:35-4300), anti-human WASP 1:2000 (Epitomics, Clone:EP2541Y, Catalog#:2422-1), anti-murine WASP 1:2000 (Cell Signaling Technology, Catalog#:4860), anti-N-WASP 1:1000 (Cell Signaling Technology, Clone:30D10, Catalog#:4848), anti-WIP 1:2000 (Santa Cruz Biotechnology, Clone:H-224, Catalog#:sc-25533), anti-phospho-STAT3 (Tyr705) 1:2000 (Cell Signaling Technology, Catalog#:9131), anti-STAT3 1:2000 (Cell Signaling Technology, Clone:79D7, Catalog#:4904), antiphospho-ERK (Thr202/Tyr204) 1:2000 (Cell Signaling Technology, Catalog#:9101), anti-ERK 1:2000 (Cell Signaling Technology, Catalog#:9102), anti-phospho-AKT (Ser473) 1:1000 (Cell Signaling Technology, Clone:D9E, Catalog#:4060), anti-AKT 1:2000 (Cell Signaling Technology, Clone:11E7, Catalog#:4685), anti-phospho-JNK (Thr183/Tyr185) 1:1000 (Cell Signaling Technology, Catalog#:9255), anti-JNK 1:2000 (Cell Signaling Technology, Catalog#:610929), anti-C/EBP $\beta$  1:1000 (Santa Cruz Biotechnology,Clone:C-19, Catalog#:sc-150), anti-Cleaved Caspase-3 (Asp175) 1:1000 (Cell Signaling Technology,Catalog#:9661), anti-phospho S6 1:1000 (Cell Signaling Technology, clone D57.2.2E, Catalog#:4858), anti-S6 1:1000 (Cell Signaling Technology, clone 54D2, Catalog#:2317), anti-HSP90 1:2000 (Santa Cruz Biotechnology, #H114), anti-ZAP70 1:1000 (Millipore, Clone:2F3.2, Catalog#:05-253), anti-GFP 1:2000 (Invitrogen, Catalog #:A-11122), anti-Actin 1:4000 (Sigma-Aldrich, Catalog#:A2066)

## 10. Eukaryotic cell lines

a. State the source of each eukaryotic cell line used.

Human ALK+ ALCL cell lines (SU-DHL1, Karpas-299, DEL, SUP-M2 and L82) and ALK- cell lines (MAC-1 and Jurkat) ALCL cell lines were obtained from DSMZ (German collection of Microorganisms and Cell Cultures).

HEK-293T and 293 Phoenix packaging cells were obtained from DSMZ.

ALK-positive Ki-JK cell line and ALK negative T cell lymphoma lines (DL-40, OCI-Ly13.2, OCI-Ly12, MAC2A and DERL2) were kindly provided by Dr. David Weinstock (Dana-Farber Cancer Institute, Boston, USA).

ALK-positive COST cell line was kindly provided by Dr. Laurence Lamant (Centre de Recherche en Cancérologie de Toulouse, France).

ALK-positive (TS and JB6) and ALK-negative FePD cell lines were kindly provided by Dr. Giorgio Inghirami (Department of Pathology and Laboratory Medicine, Weill Cornell Medicine, New York, NY, USA)

b. Describe the method of cell line authentication used.

Stock of cells lines were immediately generated after purchase. For experiments, cell lines were never kept for more than 3 consecutive months in culture, if needed for longer time a new stock was used. For some cells lines we also further authenticated them by sequencing of the mutations present in the p53 gene which are unique for each NPM-ALK cell line.

c. Report whether the cell lines were tested for mycoplasma contamination.

Cell lines were tested for mycoplasma monthly. If cells resulted positive for contamination, they were treated with mycoplasma removal agents until three consecutive PCR tests were negative.

d. If any of the cell lines used are listed in the database of commonly misidentified cell lines maintained by [ICLAC](#), provide a scientific rationale for their use.

No commonly misidentified cell lines has been used

## ► Animals and human research participants

Policy information about [studies involving animals](#); when reporting animal research, follow the [ARRIVE guidelines](#)

### 11. Description of research animals

Provide all relevant details on animals and/or animal-derived materials used in the study.

All the animals in the studies are mice, all the transgenic mice were maintained in C57BL/6 background; male and female mice were randomly selected. Primary lymphoma cell lines with different genotypes were immortalized from mice spontaneously without any type of genetic manipulation.

Pre-tumoral thymuses were collected from 4-6 weeks old mice; tumoral thymuses were collected from 12-16 weeks old mice.

For xenograft experiments NSG immunocompromised mice were used. Mice of 8  $\pm$  2 weeks of age and randomly sorted by sex were used.

## 12. Description of human research participants

Describe the covariate-relevant population characteristics of the human research participants.

This study did not involve human research

## SEPSIS

# Comment on “ALK is a therapeutic target for lethal sepsis”

Rafael B. Blasco<sup>1\*</sup>, Enrico Patrucco<sup>2\*</sup>, Ines Mota<sup>2</sup>, Wei-Tien Tai<sup>1</sup>, Roberto Chiarle<sup>1,2†</sup>

Physiologically relevant ALK (anaplastic lymphoma kinase) expression was not detected in human and mouse monocytes and macrophages, suggesting that the effects of bioactive compounds on stimulator of interferon genes (STING) activation may not depend on ALK.

Sepsis is a life-threatening condition associated with high lethality. The pathogenesis of sepsis is complex and requires the activation of the innate immune system by microbial pathogens. Part of this activation relies on the recognition of bacteria-derived cyclic dinucleotides (CDN) by the stimulator of interferon genes (STING) transmembrane protein that in turn binds TANK-binding kinase 1 to regulate the transcription of inflammatory genes triggered by the interferon regulatory factor 3. To discover actionable targets for the treatment of sepsis, Zeng *et al.* (1) recently screened a library of kinase inhibitors for STING-modulating properties and found that some inhibitors, including LDK378 [a U.S. Food and Drug Administration (FDA)-approved anaplastic lymphoma kinase (ALK) inhibitor also called ceritinib], AP26113 (an FDA-approved ALK inhibitor also called brigatinib), and AZD3463 [a preclinical ALK/insulin-like factor receptor 1 (IGF-1R) inhibitor] can efficiently block STING-mediated interferon- $\beta$  release in cells stimulated with CDN. Understandably, they then focused on demonstrating ALK expression in monocytes and macrophages, which are important cells that mediate sepsis.

Surprisingly, they showed abundant expression of ALK in both human and murine monocytes and macrophages. These findings were puzzling as the current knowledge is that ALK is a tyrosine kinase receptor expressed during embryonic development by neurons and muscles, whereas in adults its expression is restricted to different areas of the brain (2–6). In contrast to normal cells, ALK can be readily detected in tumors such as neuroblastoma, ALK-rearranged anaplastic large cell lymphoma (ALCL), non-small cell lung cancer (NSCLC), or inflammatory fibroblastic tumor (4, 5). In clinical practice, ALK antibodies are considered highly specific for the detection of the oncogenic ALK because tumor cells express ALK more highly than ALK-negative normal cells. Detection of ALK expression in tumors is a critical point for the clinical decision on the use of ALK inhibitors in lung cancer patients, to the extent that the FDA has specifically approved an immunohistochemistry-based test to detect ALK-rearranged NSCLC (7).

We therefore decided to reexamine ALK expression in normal cells, particularly monocytes and macrophages. According to common databases such as the Genotype-Tissue Expression (GTEx) Project ([www.gtexportal.org/home/gene/ALK](http://www.gtexportal.org/home/gene/ALK)) or to the Expression Atlas ([www.ebi.ac.uk/gxa](http://www.ebi.ac.uk/gxa)), ALK expression is overall low and largely

confined to few areas in the brain or in the testis. Importantly, tissues rich in monocytes and macrophages such as peripheral blood, spleen, and lung have undetectable ALK expression (Fig. 1A). To directly characterize ALK expression in monocytes and macrophages, we performed Western blot assays with the rabbit monoclonal antibody SP8 from Abcam on the same mouse cell lines largely used in Zeng *et al.* (1), which are immortalized bone marrow-derived macrophages (iBMDMs) and murine macrophage-like RAW264.7 cells. We used three different protein extraction buffers, all yielding comparable results for ALK expression. The SP8 antibody specifically detected ALK in 293T cells transfected with a plasmid encoding for the mouse full-length *Alk* receptor as well as the EML4-ALK fusion protein generated by CRISPR-Cas9 from the endogenous mouse *Alk* gene in lung cancer cells (8)(Fig. 1B). Surprisingly, this antibody did not detect any band corresponding to the mouse ALK receptor in iBMDMs or RAW264 cells (Fig. 1B). We then blotted the same lysates with the F-12 antibody used by Zeng *et al.* (1). This antibody was raised against an epitope mapping between amino acids 117 to 145 within the N-terminal extracellular domain of human ALK and recognized the transfected mouse ALK but not the EML4-ALK fusion that contains only the cytoplasmic portion of ALK. Strikingly, it failed to recognize any band consistent with ALK in iBMDMs or RAW264 (Fig. 1B).

Next, we tested human peripheral blood mononuclear cells (PBMCs) and the human THP-1 cell line also used by Zeng *et al.* (1) to seek for ALK expression in human monocytes and macrophages. We used the FDA-approved D5F3 antibody for ALK detection (7) and neuroblastoma cells that express the endogenous human ALK as controls. As expected, the D5F3 antibody specifically recognized the ALK protein in neuroblastoma lines with a pattern consisted in two bands of 220 to 230 kDa and 130 to 140 kDa as previously reported, where the lower band corresponds to a cleavage product of the ALK receptor (9). In contrast, no bands with such pattern were seen in PBMCs or THP-1 cells even after long exposure of the membrane (Fig. 1C). When the same cell lysates were probed with the F-12 antibody used by Zeng *et al.* (1), the antibody correctly detected the 220- to 230-kDa full-length ALK in neuroblastoma cells, but not the 130- to 140-kDa cleaved ALK protein that lacks amino acids 117 to 145. Unexpectedly, this antibody also recognized a band of approximately 190 to 200 kDa that was detected across all human cells (Fig. 1C). However, this band is different from the pattern of ALK expression in neuroblastoma and was also seen in negative controls such as the ALK-negative Burkitt lymphoma cell lines Raji and Ramos (Fig. 1C). In addition, expression data from the Cancer Cell Line Encyclopedia (CCLE) (<https://portals.broadinstitute.org/ccle>) did not show detectable ALK mRNA in THP-1 cells (Fig. 2).

<sup>1</sup>Department of Pathology, Children’s Hospital Boston and Harvard Medical School, Boston, MA 02115 USA. <sup>2</sup>Department of Molecular Biotechnology and Health Sciences, University of Torino, Torino 10126 Italy.

\*These authors contributed equally to this work.

†Corresponding author. Email: roberto.chiarle@childrens.harvard.edu

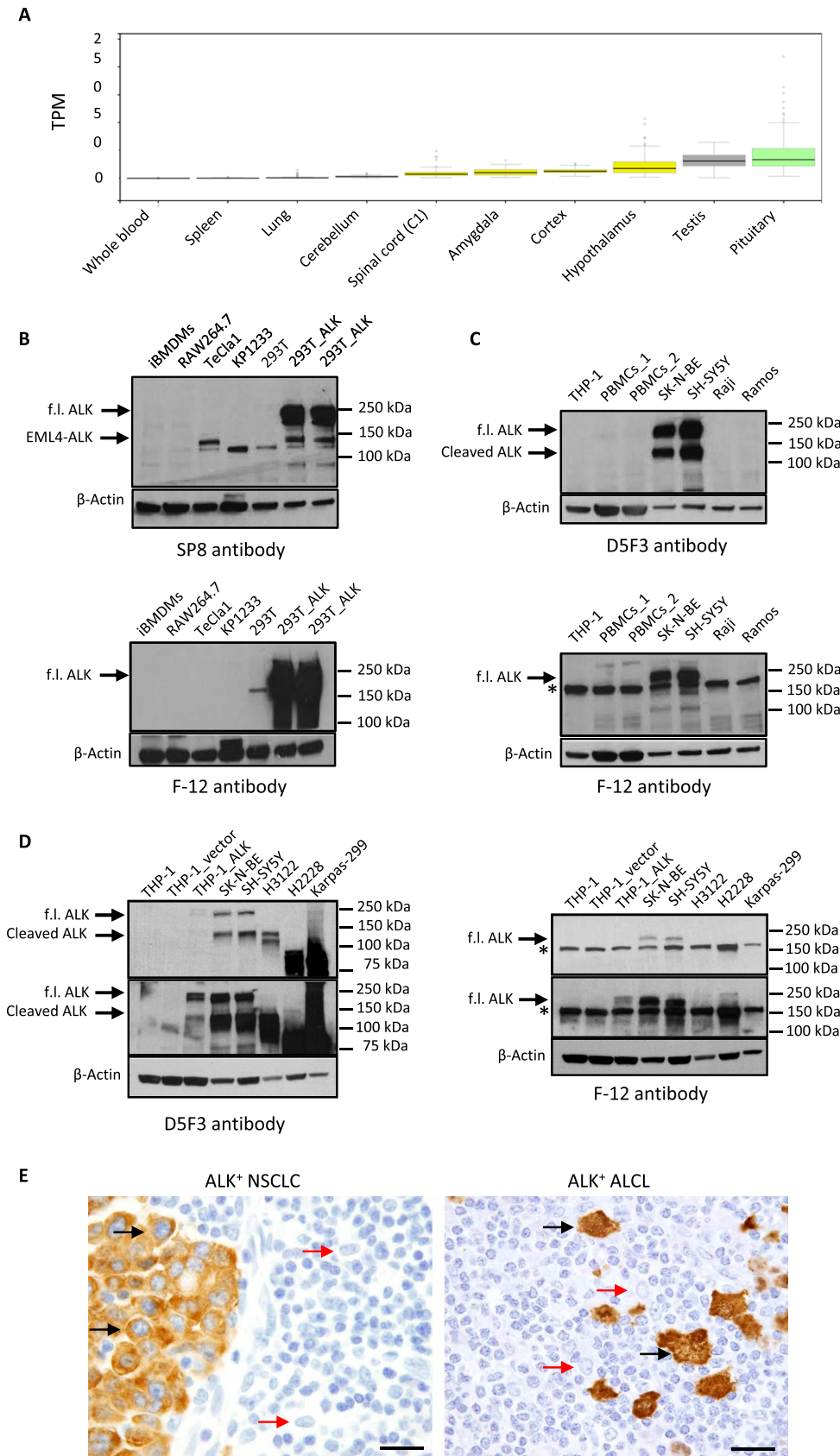


**Fig. 1. Undetectable ALK expression in monocytes and macrophages.** (A) ALK mRNA expression in tissues according to the GTEx project. TPM, transcripts per million. (B) ALK expression in murine cell lines [top: SP8 anti-ALK antibody (1:1000); bottom: F-12 anti-ALK antibody (1:100)]. 293T cells transfected with mouse *Alk* (293T\_ALK) and EML4-ALK-expressing TeCla1 cells (positive controls). Untransfected 293T and KP1233 murine KRAS<sup>G12D</sup>-driven NSCLC cells (negative controls). Arrows indicate the full-length (f.l.) ALK or the EML4-ALK fusion. (C) ALK expression in human cell lines [top: D5F3 anti-ALK antibody (1:1000); bottom: F-12 anti-ALK antibody (1:100)]. Human neuroblastoma cell lines SK-N-BE and SH-SY5Y (positive controls). Human B-lymphoma Raji and Ramos cell lines (negative controls). Arrows indicate the full-length ALK or the cleaved ALK. Asterisk indicates the nonspecific band detected by the F-12 antibody. (D) ALK expression in human cell lines [left: D5F3 anti-ALK (1:1000); right: F-12 anti-ALK antibody (1:100)]. THP-1 cells transduced with human ALK receptor (THP-1\_ALK) (positive control). THP-1 cells transduced with empty retroviral vector (THP-1\_vector) (negative control). H3122 and H2228 NSCLC cell lines carry the *EML4-ALK* (ex13-ex20) and the *EML4-ALK* (ex6-ex20) rearrangements that generate fusion proteins of 130 and 90 kDa, respectively. Karpas-299 is an *NPM-ALK*-rearranged cell line that generates a fusion protein of 80 kDa. Arrows indicate the full-length ALK or the cleaved ALK. Asterisk indicates the nonspecific band detected by the F-12 antibody. Top panels: Short exposure. Bottom panels: Long exposure. (E) Immunohistochemistry performed on an ALK-rearranged NSCLC case (D5F3 anti-ALK antibody) and on an ALCL case (4C5B8 anti-ALK antibody). Tumor cells shown by black arrows; macrophages shown by red arrows. Scale bar, 50  $\mu$ m.

Downloaded from <http://stm.sciencemag.org/> by guest on July 6, 2020



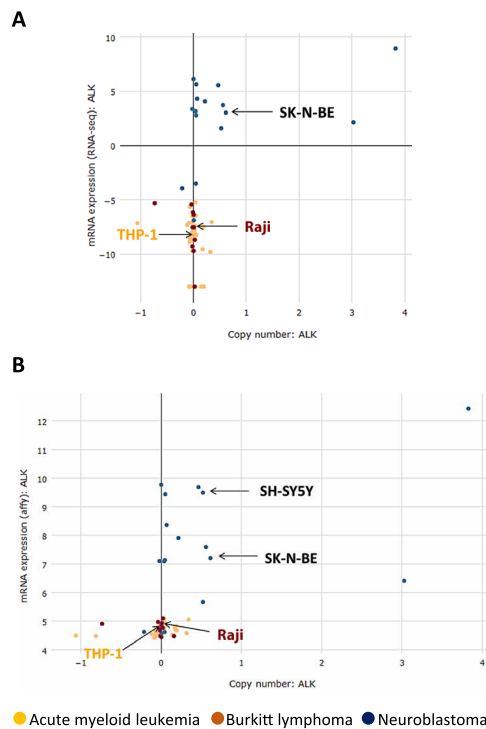


**Fig. 2. Undetectable ALK mRNA expression in Raji and THP-1 cell lines.** ALK mRNA expression in different tumor cell lines according to two different datasets in CCLE (<https://portals.broadinstitute.org/ccle>). (A) RNA sequencing (RNA-seq) data. (B) Gene expression profiling data. Raji, THP-1, and the ALK-positive neuroblastoma cell lines SH-SY5Y and SK-N-BE are indicated by arrows.

To exclude an unexpected expression or cleavage of ALK in macrophages, we transduced human THP-1 cells with a retroviral vector encoding human ALK. Both the D5F3 and F-12 antibody recognized a band in ALK-transduced THP-1 cells, but not in THP-1 cells transduced with an empty vector, with a pattern similar to neuroblastoma cells. Again, the F-12 antibody recognized a lower band in all cell lines, including ALK-rearranged NSCLC and ALCL, that carry ALK fusions with different molecular weights (Fig. 1D). We concluded that the 190- to 200-kDa band detected by the F-12 antibody in all human cells is nonspecific. Last, immunohistochemistry failed to detect ALK expression in normal macrophages surrounding ALK-rearranged NSCLC and ALCL (Fig. 1E).

Notably, Zeng *et al.* (1) performed both the library compound screening and all the experiments with LDK378 or AP26113 with an inhibitor concentration of 10  $\mu$ M. However, drug concentration is critical for selective ALK inhibition. For example, LDK378 is selective for ALK with a median inhibitory concentration ( $IC_{50}$ ) of 200 pM but at higher concentrations inhibits other tyrosine kinases such as IGF-1R ( $IC_{50}$  of 8 nM), with broad inhibition of several tyrosine kinases at concentrations above 100 nM (10). Likewise, AP26113 has an  $IC_{50}$  of 370 pM for ALK and of 24.9 nM for IGF-1R (11). Therefore, when used at 10  $\mu$ M [such as in the experiments performed by Zeng *et al.* (1)], it is likely that these compounds block multiple tyrosine kinases.

Together, our findings indicate that mouse and human monocytes and macrophages do not express detectable amounts of the

ALK receptor. Thus, the interesting findings that LDK378 blocks CDN-induced STING activation in vitro, as well as polymicrobial sepsis or lipopolysaccharide-induced endotoxemia in vivo, may be explained by the activity of this compound against other kinase(s) different than ALK.

## SUPPLEMENTARY MATERIALS

[www.sciencetranslationalmedicine.org/cgi/content/full/10/471/ear4321/DC1](http://www.sciencetranslationalmedicine.org/cgi/content/full/10/471/ear4321/DC1)  
Materials and Methods

## REFERENCES AND NOTES

- L. Zeng, R. Kang, S. Zhu, X. Wang, L. Cao, H. Wang, T. R. Billiar, J. Jiang, D. Tang, ALK is a therapeutic target for lethal sepsis. *Sci. Transl. Med.* **9**, eaan5689 (2017).
- T. Iwahara, J. Fujimoto, D. Wen, R. Cupples, N. Bucay, T. Arakawa, S. Mori, B. Ratzkin, T. Yamamoto, Molecular characterization of ALK, a receptor tyrosine kinase expressed specifically in the nervous system. *Oncogene* **14**, 439–449 (1997).
- S. W. Morris, C. Naevae, P. Mathew, P. L. James, M. N. Kirstein, X. Cui, D. P. Witte, **ALK**, the chromosome 2 gene locus altered by the t(2;5) in non-Hodgkin's lymphoma, encodes a novel neural receptor tyrosine kinase that is highly related to leukocyte tyrosine kinase (LTK). *Oncogene* **14**, 2175–2188 (1997).
- R. Chiarle, C. Voena, C. Ambrogio, R. Piva, G. Inghirami, The anaplastic lymphoma kinase in the pathogenesis of cancer. *Nat. Rev. Cancer* **8**, 11–23 (2008).
- B. Hallberg, R. H. Palmer, Mechanistic insight into ALK receptor tyrosine kinase in human cancer biology. *Nat. Rev. Cancer* **13**, 685–700 (2013).
- E. Vernersson, N. K. S. Khoo, M. L. Henriksson, G. Roos, R. H. Palmer, B. Hallberg, Characterization of the expression of the ALK receptor tyrosine kinase in mice. *Gene Expr. Patterns* **6**, 448–461 (2006).
- E. Conde, S. Hernandez, M. Prieto, R. Martinez, F. Lopez-Rios, Profile of Ventana ALK (D5F3) companion diagnostic assay for non-small-cell lung carcinomas. *Expert Rev. Mol. Diagn.* **16**, 707–713 (2016).
- R. B. Blasco, E. Karaca, C. Ambrogio, T. C. Cheong, E. Karayol, V. G. Minero, C. Voena, R. Chiarle, Simple and rapid in vivo generation of chromosomal rearrangements using CRISPR/Cas9 technology. *Cell Rep.* **9**, 1219–1227 (2014).
- C. Moog-Lutz, J. Degoutin, J. Y. Gouzi, Y. Frobort, N. B. D. Carvalho, J. Bureau, C. Créminon, M. Vigny, Activation and inhibition of anaplastic lymphoma kinase receptor tyrosine kinase by monoclonal antibodies and absence of agonist activity of pleiotrophin. *J. Biol. Chem.* **280**, 26039–26048 (2005).
- T. H. Marsilje, W. Pei, B. Chen, W. Lu, T. Uno, Y. Jin, T. Jiang, S. Kim, N. Li, M. Warmuth, Y. Sarkisova, F. Sun, A. Steffy, A. C. Pferdekammer, A. G. Li, S. B. Joseph, Y. Kim, B. Liu, T. Tuntland, X. Cui, N. S. Gray, R. Steensma, Y. Wan, J. Jiang, G. Chopiuk, J. Li, W. P. Gordon, W. Richmond, K. Johnson, J. Chang, T. Groessel, Y.-Q. He, A. Phimister, A. Aycinena, C. C. Lee, B. Bursulaya, D. S. Karanewsky, H. M. Seidel, J. L. Harris, P.-Y. Michellys, Synthesis, structure–activity relationships, and in vivo efficacy of the novel potent and selective anaplastic lymphoma kinase (ALK) inhibitor 5-chloro-N2-(2-isopropoxy-5-methyl-4-(piperidin-4-yl)phenyl)-N4-(2-(isopropylsulfonyl)phenyl)pyrimidine-2,4-diamine (LDK378) currently in phase 1 and phase 2 clinical trials. *J. Med. Chem.* **56**, 5675–5690 (2013).
- W.-S. Huang, S. Liu, D. Zou, M. Thomas, Y. Wang, T. Zhou, J. Romero, A. Kohlmann, F. Li, J. Qi, L. Cai, T. A. Dwight, Y. Xu, R. Xu, R. Dodd, A. Toms, L. Parillon, X. Lu, R. Anjum, S. Zhang, F. Wang, J. Keats, S. D. Wardwell, Y. Ning, Q. Xu, L. E. Moran, Q. K. Mohemmad, H. G. Jang, T. Clackson, N. I. Narasimhan, V. M. Rivera, X. Zhu, D. Dalgarno, W. C. Shakespeare, Discovery of brigatinib (AP26113), a phosphine oxide-containing, potent, orally active inhibitor of anaplastic lymphoma kinase. *J. Med. Chem.* **59**, 4948–4964 (2016).

**Acknowledgments:** We would like to thank C. Ambrogio for the helpful discussion and critical reading of the manuscript. We would like to thank K. Fitzgerald (Medical School, University of Massachusetts) for the THP-1, RAW264.7, and iBMDMs cell lines and T. Jacks (MIT) for the KP1233 cell line. **Funding:** The work was supported by the R01 CA196703, D2017-026 V Foundation, and Translational Research Program (TRP) grants to R.C.

Submitted 19 December 2017

Accepted 9 November 2018

Published 12 December 2018

10.1126/scitranslmed.aar4321

**Citation:** R. B. Blasco, E. Patrucco, I. Mota, W.-T. Tai, R. Chiarle, Comment on "ALK is a therapeutic target for lethal sepsis". *Sci. Transl. Med.* **10**, ear4321 (2018).

# Science Translational Medicine

## Comment on "ALK is a therapeutic target for lethal sepsis"

Rafael B. Blasco, Enrico Patrucco, Ines Mota, Wei-Tien Tai and Roberto Chiarle

*Sci Transl Med* **10**, eaar4321.  
DOI: 10.1126/scitranslmed.aar4321

ARTICLE TOOLS	<a href="http://stm.sciencemag.org/content/10/471/eaar4321">http://stm.sciencemag.org/content/10/471/eaar4321</a>
SUPPLEMENTARY MATERIALS	<a href="http://stm.sciencemag.org/content/suppl/2018/12/10/10.471.eaar4321.DC1">http://stm.sciencemag.org/content/suppl/2018/12/10/10.471.eaar4321.DC1</a>
RELATED CONTENT	<a href="http://stm.sciencemag.org/content/scitransmed/9/412/eaan5689.full">http://stm.sciencemag.org/content/scitransmed/9/412/eaan5689.full</a> <a href="http://stm.sciencemag.org/content/scitransmed/10/471/eaas9817.full">http://stm.sciencemag.org/content/scitransmed/10/471/eaas9817.full</a>
REFERENCES	This article cites 11 articles, 2 of which you can access for free <a href="http://stm.sciencemag.org/content/10/471/eaar4321#BIBL">http://stm.sciencemag.org/content/10/471/eaar4321#BIBL</a>
PERMISSIONS	<a href="http://www.sciencemag.org/help/reprints-and-permissions">http://www.sciencemag.org/help/reprints-and-permissions</a>

Use of this article is subject to the [Terms of Service](#)



---

*Science Translational Medicine* (ISSN 1946-6242) is published by the American Association for the Advancement of Science, 1200 New York Avenue NW, Washington, DC 20005. The title *Science Translational Medicine* is a registered trademark of AAAS.

Copyright © 2018 The Authors, some rights reserved; exclusive licensee American Association for the Advancement of Science. No claim to original U.S. Government Works

Review

# Tumor Resistance against ALK Targeted Therapy—Where It Comes From and Where It Goes

Geeta Geeta Sharma <sup>1,†</sup> , Ines Mota <sup>2,†</sup>, Luca Mologni <sup>1,3</sup> , Enrico Patrucco <sup>2</sup>, Carlo Gambacorti-Passerini <sup>1,3,4,†</sup> and Roberto Chiarle <sup>2,5,†,\*</sup>

<sup>1</sup> Department of Medicine and Surgery, University of Milano-Bicocca, Monza 20900, Italy; geeta.geeta@unimib.it (G.G.S.); luca.mologni@unimib.it (L.M.); carlo.gambacorti@unimib.it (C.G.-P.)

<sup>2</sup> Department of Molecular Biotechnology and Health Sciences, University of Turin, Turin 10124, Italy; ines.mota05@gmail.com (I.M.); enrico.patrucco@unito.it (E.P.)

<sup>3</sup> Galkem Srl, Monza 20900, Italy

<sup>4</sup> Hematology and Clinical Research Unit, San Gerardo Hospital, Monza 20900, Italy

<sup>5</sup> Department of Pathology, Boston Children's Hospital, Harvard Medical School, Boston, MA 02115, USA

\* Correspondence: roberto.chiarle@childrens.harvard.edu

† These authors contributed equally to this work.

Received: 1 February 2018; Accepted: 26 February 2018; Published: 28 February 2018

**Abstract:** Anaplastic lymphoma kinase (ALK) is a validated molecular target in several ALK-rearranged malignancies, particularly in non-small-cell lung cancer (NSCLC), which has generated considerable interest and effort in developing ALK tyrosine kinase inhibitors (TKI). Crizotinib was the first ALK inhibitor to receive FDA approval for ALK-positive NSCLC patients treatment. However, the clinical benefit observed in targeting ALK in NSCLC is almost universally limited by the emergence of drug resistance with a median of occurrence of approximately 10 months after the initiation of therapy. Thus, to overcome crizotinib resistance, second/third-generation ALK inhibitors have been developed and received, or are close to receiving, FDA approval. However, even when treated with these new inhibitors tumors became resistant, both in vitro and in clinical settings. The elucidation of the diverse mechanisms through which resistance to ALK TKI emerges, has informed the design of novel therapeutic strategies to improve patients disease outcome. This review summarizes the currently available knowledge regarding ALK physiologic function/structure and neoplastic transforming role, as well as an update on ALK inhibitors and resistance mechanisms along with possible therapeutic strategies that may overcome the development of resistance.

**Keywords:** anaplastic large-cell lymphoma (ALCL); anaplastic lymphoma kinase (ALK); ALK inhibitors; non-small-cell lung cancer (NSCLC); resistance to ALK inhibitors; targeted therapies; tyrosine kinase (TK)

## 1. Introduction

Over the last decade, the development of drugs that selectively target driver oncogenes has played an important role to establish novel treatment guidelines in the field of oncology. Unlike traditional chemo and radio-therapies that kill all rapidly dividing cells, targeted therapies are more selective and specific towards their target, exploiting the biology that drives the growth of tumor cells such as genetic deletions, chromosomal rearrangements and point mutations. Furthermore, targeted therapies have significantly impacted outcomes in terms of prolonged survival and a better quality of life for cancer patients.

Imatinib, a small molecule tyrosine kinase inhibitor (TKI) developed to treat chronic myeloid leukemia (CML) patients bearing t(9;22)(q34;q11), was the first breakthrough in the journey of target

therapies [1]. Five years follow-up studies have shown that patients treated with imatinib achieved molecular responses and overall survival not different from the general population [2].

Another tyrosine kinase extensively explored as a target for TKI treatment is the anaplastic lymphoma kinase (ALK). ALK was first described in 1994 as the NPM-ALK fusion protein that is expressed in the majority of anaplastic large-cell lymphomas (ALCL), approximately 55% of adult patients and more than 90% of pediatric patients [3]. There are several reasons why ALK is an ideal target of personalized medicine, including that ALK-transformed cells are in general strongly dependent on ALK tyrosine kinase activity for survival and proliferation and ALK expression is limited in non-tumoral cells, being detected in limited areas of the brain [4]. Therefore, its blockage is catastrophic for cancer cells but irrelevant for normal tissues. Since its discovery, more than 20 different ALK fusion partner genes have been reported across multiple malignancies [5,6]. Perhaps the most widely recognized is the echinoderm microtubule-associated protein-like 4 (EML4)-ALK fusion, identified in 5–6% of non-small-cell lung cancer (NSCLC) patients in 2007 [7]. Even though the relative proportion of NSCLC bearing ALK rearrangements is significantly lower than ALCL or inflammatory myofibroblastic tumors (IMT), ALK-positive NSCLC represent overall the largest cohort of ALK-rearranged patients due to the fact that lung cancer has a high incidence worldwide. The identification of ALK rearrangements in lung cancer patients has sparked the development of a series of ALK TKI from different companies. To date, four ALK inhibitors (crizotinib, ceritinib, alectinib and brigatinib) have received approval by the FDA for treatment of ALK-rearranged NSCLC, while others such as lorlatinib have shown promising results in early clinical trials [8]. The use of these new therapies has improved the quality of life and increased the survival of patients, as demonstrated in their respective clinical trials, with remarkable responses in NSCLC patients carrying ALK-rearrangements [9–16]. As with any targeted therapy, ALK-driven NSCLC tumor cells inevitably acquire drug resistance, leading to clinical relapse. At the present time, ALK inhibitors have not yet been approved for use in other ALK-driven cancers than NSCLC; however, some studies have reported remarkable responses, and less frequent relapses, to ALK inhibitors in patients with ALK-positive ALCL and IMT. The apparently higher sensitivity to ALK inhibitors of ALCL and IMT tumors likely reflects a stronger dependency on ALK signaling and/or a lower level of tumor heterogeneity than in ALK-rearranged NSCLC [17–19]. Yet, our current knowledge regarding ALK inhibitors resistance originates mostly from ALK-positive NSCLC patients.

While much information has been gathered since the discovery of the first ALK TKI crizotinib to the latest third generation inhibitors regarding the clinical activity of TKIs, there is still limited understanding how acquired resistance develops and undermines the effects of ALK TKIs. This review will summarize the current knowledge about the activity of different ALK inhibitors and their inherent resistance mechanisms that have been reported. We will also discuss potential future therapeutic approaches that can be used to tackle TKI resistance and improve patient outcome.

## 2. Anaplastic Lymphoma Kinase-Physiological Expression and Functional Role

The ALK gene is located on chromosomal region 2p23 and encodes a highly conserved receptor tyrosine kinase (RTK), which is a member of the insulin receptor superfamily, and is most closely related to leukocyte tyrosine kinase (LTK) [20–22]. The ALK receptor is composed of an extracellular domain, a single-pass transmembrane region, and an intracellular kinase domain [20]. The extracellular domain contains a glycine-rich region, two MAM segments (meprin, A5 protein, and receptor protein tyrosine phosphatase  $\mu$ ) and one LDLa domain (low density lipoprotein class A). The intracellular portion comprises a juxtamembrane segment, a protein kinase domain and a carboxyterminal tail [6,23,24].

The specific role of ALK in human development and physiology is still poorly understood but several studies on different animal models have partially clarified the ALK functions in development. In *Drosophila melanogaster*, ALK signaling is involved in the differentiation of mesenchymal cells, in the development of the visual system [25], the maturation of the neuromuscular junction [26] and in the regulation of body size, learning and memory [27]. In this context, ALK is activated by its ligand

Jelly Belly (Jeb) leading to the downstream signaling of the Ras-MAPK pathway [28]. The mammal ALK receptor is unable to bind the Jeb ligand [29], which indicate an evolutionary divergence between mammals and *D. melanogaster* ALK proteins. In *Caenorhabditis elegans*, SCD-2 (the nematode homolog of ALK), is required for the integration of sensory inputs and the development of neuromuscular junctions [30]. In zebrafish, LTK and ALK show a significant structural homology (such as the presence of MAM domains) and contribute to neural crest nervous system embryogenesis [31].

ALK expression patterns throughout the nervous system during mouse embryogenesis suggest important roles in the central nervous system (CNS) development and function in mammals [6,20,32,33]. Iwahara et al. have described that the intensity of ALK mRNA and protein expression in mice diminishes in all tissues after birth, reaching a minimum after three weeks of age and maintained at low levels during the adult life of the animal [20]. Bilsland et al. [34] and Lasek et al. [35], reported that ALK deficient mice are viable and fertile without obvious alterations. Remarkably, the loss of ALK signaling results in a decrease in newborn neurons and in impaired regeneration of myelinated axons [5] and an increased number of progenitor cells within the hippocampus (a defect that can be associated with their behavioral changes) [34]. In 1997, Morris et al. [36] reported that ALK mRNA is expressed in adult human brain, small intestine, testis, prostate, and colon but not in normal human lymphoid cells, spleen, thymus, ovary, heart, placenta, lung, liver, skeletal muscle, kidney, or pancreas.

Several proteins, such as pleiotrophin (PTN), midkine (MK), osteoblast-specific factor-1 (OSF-1), heparin affinity regulatory peptide (HARP) and heparin-binding neurotrophic factor (HBNF), have been historically reported to be the activating ligands of mammalian ALK [4]. However, recent studies have shown that augmentor  $\alpha$  and  $\beta$  (FAM150) are validated ligands of ALK [3,37,38]. Although our knowledge of the mechanism of activation of mammalian ALK protein-tyrosine kinase is incomplete, Lemmon and Schlessinger have described the mechanism of activation of several receptor protein-tyrosine kinases, providing us a hypothetical scheme for ALK activation [21]. Upon ligand binding in the extracellular domain, the receptor protein-tyrosine kinase is activated by inducing receptor dimerization or oligomerization. A possible mechanism for ligand and dimer-induced activation of ALK involves the phosphorylation of one or more of the juxtamembrane tyrosine residues (Tyr 1078, 1092, 1096 and 1131), which in turn would be followed by consecutive phosphorylations until the active form of ALK is established [21].

### 3. ALK Gene Alterations in Cancers

The deregulation of tyrosine kinase (TK) activity is one of the major mechanisms of human carcinogenesis and can occur through several mechanisms such as chromosomal translocations, gene amplification or deregulation and point mutation. The abnormal TK activation leads to constitutive activation of several downstream signaling pathways that contribute to the development of neoplastic phenotypes. Tyrosine kinase translocations are found in up to 3% of all human tumors [39].

Usually, translocations comprising transmembrane tyrosine kinase receptors take place between exons that encode the juxtamembrane region or the transmembrane domain. In both cases, these phenomena give rise to the elimination of the extracellular region and, consequently, the ligand-binding regulation, resulting in the constitutive and uncontrolled activation of the fusion typically through an obligatory dimerization dictated by the partner gene [40]. ALK breakpoints are almost invariably located between exons 19 and 20 of ALK. Each translocation creates a fusion protein in which the ALK TK-domain at the 3'-end is connected with distinct proteins portion of different partners at the 5'-end of the fusion, capable of providing constitutive dimerization [41]. ALK rearrangement was first described in 1994, in the anaplastic large cell lymphoma (ALCL) cell lines, with ALK being one of the fused partner in a recurrent chromosomal translocation t(2;5)(p23;q35) together with the nucleophosmin (NPM) gene located on chromosome 5 [36]. This rearrangement produces a fusion gene called NPM-ALK resulting in the expression of an oncogenic fusion protein, NPM-ALK. NPM mediates receptor dimerization of the NPM-ALK protein in a ligand-independent fashion which leads to the constitutive activation of ALK kinase, and ultimately, to the activation of a number of its downstream

signaling pathways [20,23,42]. These include JAK/STAT and PI3K/AKT pathways that mediate cell survival and the Ras/Raf/MEK/ERK1/2 pathway which plays a role in cell division and cell proliferation (Figure 1A) [4,6].

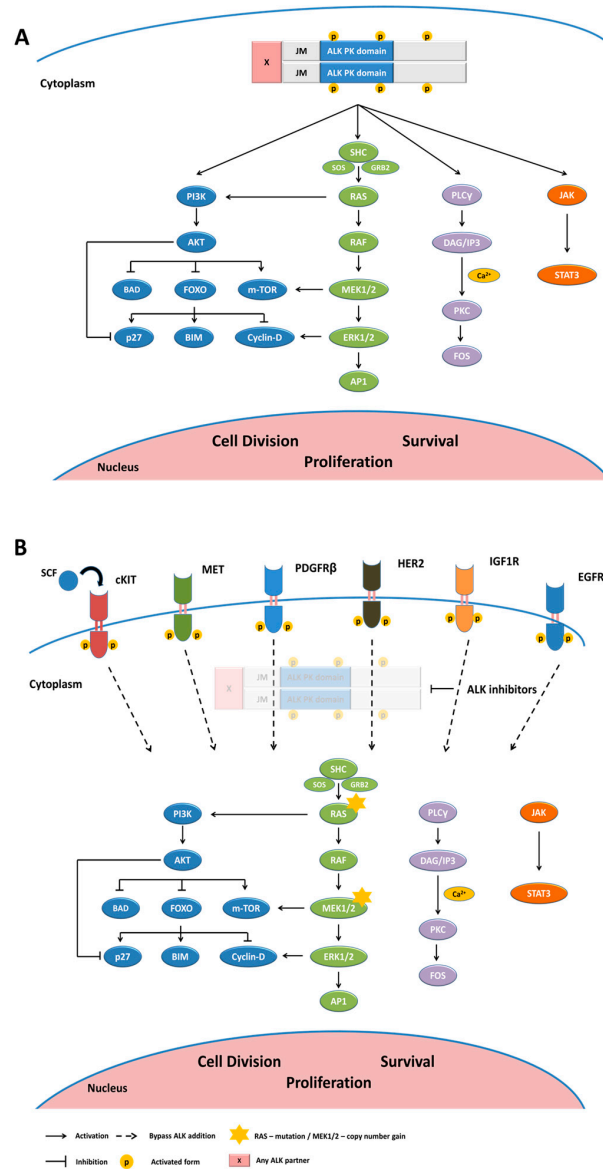


**Figure 1.** ALK downstream pathways and bypass signaling (A) Anaplastic lymphoma kinase (ALK) mediates signaling via the PI3K/AKT, RAS/MAPK, phospholipase C $\gamma$  (PLC $\gamma$ ) and Janus kinase (JAK)-signal transducer and activator of transcription (STAT); (B) ALK-independent resistance mechanism. Activation of bypass signaling pathways when ALK is inhibited with TKIs: EGFR activation, without EGFR mutations or amplifications; HER2 activation; c-KIT gene amplification in the presence of stem cell factor (SCF); MET activation bypassing ALK inhibitors without anti-MET activity; regulation via transcriptional of PDGFR $\beta$  and IGF1R activation. Mutations in KRAS and copy number gain of wild-type KRAS; JM, Juxtamembrane.

Inflammatory myofibroblastic tumor (IMT) was the first non-hematological tumor found to harbor ALK rearrangements in about 50% of cases [43] (Table 1). Non-small-cell lung cancer (NSCLC) was the second non-hematological tumor in which oncogenic ALK fusion were detected. In 2007, Simultaneously, Soda et al. and Rikova et al. reported the identification of the EML4-ALK fusion

protein in a small cohort of Japanese patients with NSCLC [44]. The novel EML4-ALK fusion protein is the result of an inversion within chromosome 2p that fuses portions of the echinoderm microtubule-associated protein-like 4 (EML4) gene and ALK gene [7]. Since the first report, ALK fusions have been detected in 3% to 7% of NSCLC and associated with a non-smoker history, younger age and adenocarcinoma histology [45]. Many other studies have identified several additional ALK fusion proteins (Table 1) which occur less frequently than EML4-ALK. Moreover, a number of breakpoints variants may be seen for a given fusion protein. EML4-ALK has over 10 distinct variants [46]. Also, it has been reported by Heuckamnn et al. that different ALK fusion genes and EML4-ALK variants exhibited differential sensitivity to crizotinib [47].

**Table 1.** ALK rearrangements in human malignancies.

Cancer Type	ALK Fusion Partner (Chromosomal Localization)	Frequency %	References
ALCL	NPM1 (5q35.1) TPM3 (1q21.3) ATIC (2q35) TFG (3q12.2) TRAF1 (9q33.2) CLTC (17q23.1) RNF213 (17q25.3) TPM4 (19p13.1) MYH9 (22q12.3) MSN (Xq12)	~55% (in adults)	[36,48–57]
Additional rare rearrangements			
Breast cancer	EML4 (2p21)	N.D.	[58]
Colorectal cancer	EML4 (2p21) WDCP (2p23.3)	<1%	[58–61]
DLBCL	RANBP2 (2q13) EML4 (2p21) SEC31A (4q21.22) SQSTM1 (5q35) NPM1 (5q35.1)	<1%	[62–68]
Esophageal cancer	TPM4 (19p13.1)	N.D.	[69,70]
IMT	TPM3 (1q21.3) RANBP2 (2q13) ATIC (2q35) SEC31A (4q21.22) CARS (11p15.4) PPFIBP1 (12p11) CLTC (17q23.1) TPM4 (19p13.1)	Up to 50%	[43,49,71–80]
NSCLC	EML4 (2p21) TPR (1q31.1) CRIM1 (2p22.2) STRN (2p22.1) TFG (3q12.2) HIP1 (7q11.23) PTPN3 (9q31) KIF5B (10p11.22) KLC1 (14q32.3) CLTC (17q23.1)	3–7%	[7,44,81–84]
Ovarian cancer	FN1 (2q35)	N.D.	[85]
RCC	VCL (10q22.2) TPM3 (1q21.2) EML4 (2p21) STRN (2p22.2)	<1%	[86–89]
RMC	VCL (10q22.2)	N.D.	[90]

Abbreviations (alphabetic order): ALK, anaplastic lymphoma kinase; ALCL, anaplastic large-cell lymphoma; ATIC, 5-Aminoimidazole-4-Carboxamide Ribonucleotide Formyltransferase/IMP Cyclohydrolase; CARS, cysteinyl-tRNA synthetase; CLTC, clatherin heavy chain; CRIM1, cysteine rich transmembrane BMP regulator 1; DLBCL, diffuse large B-cell lymphoma; EML4, echinoderm microtubule-associated protein-like 4; FN1, fibronectin 1; HIP1, huntingtin interacting protein 1; IMT, inflammatory myofibroblastic tumor; KIF5B, kinesin family member 5B; KLC1, kinesin light chain 1; MSN, moesin; MYH9, myosin heavy chain 9; N.D., not described; NPM1, nucleophosmin; NSCLC, non-small-cell lung cancer; PPFIBP1, PPFIA binding protein 1; PTPN3, protein tyrosine phosphatase, non-receptor type 3; RANBP2, RAN binding protein 2; RCC, renal cell carcinoma; RMC, renal medullary carcinoma; RNF213, ring finger protein 213; SEC31A, SEC31 Homolog A; SQSTM1, sequestosome 1; STRN, Striatin; TFG, TRK-fused gene; TPM3, tropomyosin 3; TPM4, tropomyosin 4; TPR, translocated promoter region, nuclear basket protein; TRAF1, TNF receptor associated factor 1; VCL, vinculin; WDCP, WD repeat and coiled coil containing.

With the advent of next-generation sequencing (NSG)-based diagnostics, more than 20 different ALK fusion partners genes have been described in other type of cancer (i.e., colorectal cancer, breast cancer, esophageal cancer, ovarian cancer, renal cell cancer, anaplastic thyroid carcinoma, and diffuse large B-cell lymphoma) even though in low frequencies (Table 1). Armstrong et al. [91] have shown that the level of ALK fusion protein expression and the degree of signaling depend on the partner gene. Using NIH3T3 cells, they were able to demonstrate different effects of ALK fusion proteins on cell proliferation and invasion depending on the exact fusion. In the years following this study, the same group has demonstrated that TPM3-ALK fusion protein expression specifically induces changes in cell morphology and cytoskeleton organization, and it confers higher metastatic capacities than other ALK fusion proteins [92].

Additional molecular mechanisms can affect ALK signaling in human cancer other than chromosomal translocations/inversions: ALK up-regulation/amplification and ALK gene mutations [93]. ALK up-regulation has been described in tumors that occasionally harbor ALK-chromosomal translocations, such as NSCLC, rhabdomyosarcoma, breast and ovarian cancer and also reported in neoplasms usually not associated with ALK fusions, such as melanoma, retinoblastoma, Ewing's sarcoma and neuronal tumors (i.e., glioblastoma, astrocytoma) [4] (Table 1). ALK amplification has also been reported in neuroblastoma almost invariably together with amplification of the adjacent gene MYCN, with possible synergic effects in driving cell growth and survival [94]. ALK TK activation mechanisms in neuroblastoma are not limited to ALK amplification. Mutations in the ALK gene are documented in 4–8% of sporadic neuroblastomas and account for the majority of hereditary cases; ALK variants contribute to the acquisition of neoplastic phenotype and are associated with overall poor-prognosis [94,95]. As observed in ALK rearrangements, ALK point mutations have been described in number of cancers (i.e., anaplastic thyroid cancer [ATC], IMT and NSCLC), although less frequently than in neuroblastoma (Table 1).

Several studies have permitted the classification of ALK mutations into three different groups: (1) ligand-independent activation mutations; (2) ligand-dependent activating mutations; and (3) kinase-inactivating mutations (known as kinase dead) [96,97]. Ligand-independent mutations (e.g., F1174I, F1174S and F1174L) generate constitutively activated ALK and induce uncontrolled cell proliferation and cell survival [95]; ligand-dependent mutations (e.g., D1091N, T1151M and A1234T) may contribute to pathogenesis [97]. Kinase-inactivating mutations (e.g., I1250T) are very rare and may contribute to the neoplastic phenotype by interfering with the remaining wild-type ALK copy [4].

## 4. ALK Inhibitors

### 4.1. Crizotinib: A First-Generation ALK Inhibitor

Substantial evidence linking aberrations in ALK to various tumors and the success of TKIs such as imatinib and gefitinib led to the discovery and accelerated approval of first ALK inhibitor, crizotinib (PF-02341066 Xalkori). Crizotinib is an orally available drug which was originally discovered as a c-Met kinase inhibitor [98]. The compound binds the ATP pocket of MET kinase in a DFG-in conformation, forming classical hydrogen bonds (Hb) with hinge region residues [99]; in addition, its phenyl ring forms a  $\pi$ - $\pi$  interaction with the activation loop (A-loop). Ironically, the drug was found to have off-target effects on other kinases including ALK. The crystal structure of crizotinib bound to ALK revealed a similar binding mode, with conserved Hb to the hinge region (Figure 2A), but lacking the  $\pi$  stacking to A-loop, which may explain lower activity against ALK compared to MET. Given the pathogenic role of ALK in different malignancies, crizotinib was then pursued as an ALK inhibitor [100]. Following a number of successful in vitro studies [98] showing the efficacy of crizotinib in ALK inhibition, crizotinib entered into early phase I study (PROFILE 1001) presenting a sustained response in locally advanced or metastatic NSCLC patients carrying the EML4-ALK fusion gene [101]. Subsequently, crizotinib was evaluated in a phase II study (PROFILE 1005) with the final results published recently [102].



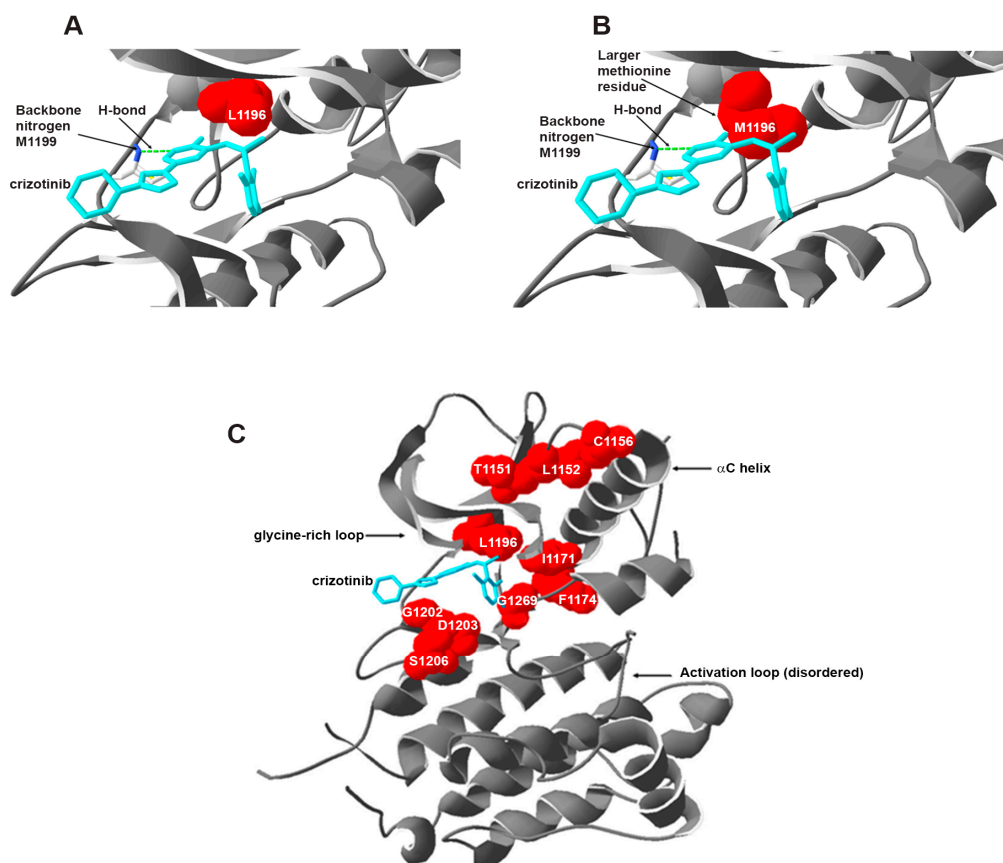


**Figure 2.** Crystal structure of ALK in complex with crizotinib (PDB: 2XP2). (A) Close view of crizotinib bound in the active site of wild-type ALK. The gatekeeper residue L1196 is shown as red surface. Crizotinib is shown as cyan sticks. The green dashed line indicates the hydrogen bonding to the backbone nitrogen of M1199 (indicated in sticks). Secondary structures are represented with grey ribbon; (B) The native L1196 from panel A was mutated in silico to M1196, to show steric clash with crizotinib; (C) Overall architecture of ALK bound to crizotinib. Key residues associated with resistance to crizotinib are shown as red surface and labeled. Some important regulatory regions of the kinase are indicated by arrows.

The objective response rates (ORR) were 54% and 41% in the central and local-testing ALK-detection sub-groups, respectively. Phase II results support the clinical benefits of using crizotinib in ALK-positive NSCLC that had progressed on previous chemotherapy regimens. Two phase III studies, PROFILE 1007 [9] and PROFILE 1014 [10], provided further proof in favor of the use of crizotinib over standard second-line chemotherapy and over first-line chemotherapy, respectively in advanced ALK-positive NSCLC.

Crizotinib was found to be generally well tolerated in the patients with mostly mild treatment-related adverse events (TRAEs). The most commonly reported TRAEs in ALK-positive NSCLC patients include vision disorder, nausea, diarrhea and vomiting of grade 1 and 2. However, elevated transaminases and neutropenia associated with crizotinib treatment of grade 3 or 4 have also been observed in the patients. Other not so common TRAEs of crizotinib in patients that have been observed over the years, include interstitial lung disease (ILD), bradycardia, QTc prolongation, renal cysts and decreased total testosterone in males. Most of the TRAEs were reversible with crizotinib discontinuation or drug holiday period [102]. Altogether these results led to the approval of crizotinib by FDA for the treatment of locally advanced or metastatic ALK-positive NSCLC in 2011. Additionally, significant therapeutic responses have also been reported in ALCL [103,104], neuroblastoma [105],

and IMT [18] patients. There are ongoing clinical trials that are evaluating long-term efficacy and safety profile of crizotinib in patients carrying ALK gene abnormalities.

#### 4.2. Second Generation ALK Inhibitors

Even though there are diverse mechanisms through which resistance against ALK inhibition has been shown to develop, crizotinib-resistant tumors still continue to be ALK-dependent for their growth in many cases. Around 30% of crizotinib-resistant NSCLC patients develop secondary resistance mutations in the ALK TK domain [46]. Therefore, more potent, selective and structurally different next-generation ALK inhibitors have been developed or are in the pipeline to overcome crizotinib resistance. Although they are not functionally or structurally related to crizotinib (except lorlatinib, see below) they are usually referred as second-generation inhibitors, as they were all developed to tackle crizotinib-resistance mutants. Eight novel ALK inhibitors have entered the clinic, including ceritinib, alectinib, and brigatinib, that have demonstrated potent and durable activity in ALK-positive NSCLC.

##### 4.2.1. Ceritinib (LDK378; Zykadia; Novartis)

Ceritinib is an ATP-competitive, selective oral ALK inhibitor that was found to be 20 fold more potent than crizotinib in enzymatic assays [106,107]. It was developed starting from the original first-generation, non-clinical compound NVP-TAE684 [108] with a few significant structural changes, in order to increase kinase selectivity and reduce the formation of reactive metabolites that impaired NVP-TAE684 clinical development due to toxicity [106]. The new compound (LDK378) was shown to form reactive adducts in negligible amount compared to its parent compound, while maintaining low nanomolar anti-ALK activity. Ceritinib also showed activity against insulin-like growth factor 1 receptor (IGF-R1), insulin receptor (IR) and ROS1 but with a 5–11 fold higher IC<sub>50</sub> as compared to its IC<sub>50</sub> for ALK. Ceritinib inhibited *in vitro* and *in vivo* the growth of ALK-positive cells carrying crizotinib-resistant mutations, L1196M, G1269A, I1171T, and S1206Y but failed to inhibit the growth of G1202R and F1174V/C mutants [107]. Structural data can explain why ceritinib retains potency against some crizotinib-resistant mutants: for instance, while mutation of Gly1269 to Ala causes steric clash with the halogenated phenyl ring of crizotinib, it is not predicted to have any impact on ceritinib binding. Similarly, ceritinib interacts equally well with Leu1196 as with Met1196 [107]. Phase I study, conducted on ALK+ NSCLC patients that had been previously treated with cytotoxic chemotherapy or crizotinib, showed an ORR of 58% in patients who received ceritinib at a daily dose of 750 mg [11]. Based on the pre-clinical studies and ASCEND-1 data, ceritinib received an accelerated approval from FDA for the treatment of ALK-positive metastatic NSCLC patients with disease progression or intolerance to crizotinib. Subsequently, ceritinib demonstrated higher anti-tumor efficacy in ALK-rearranged NSCLC patients previously treated with chemotherapy and crizotinib as well as in crizotinib naïve patients during ASCEND-2 [109] and ASCEND-3 [110] clinical trials. Results from the ASCEND-4, a randomized, open-label, phase 3 study, were published recently [111]. The study evaluated the efficacy and safety of ceritinib in comparison to platinum-based chemotherapy as a first line treatment in advanced ALK-rearranged NSCLC. The median progression-free survival of ceritinib-treated group was 16.6 months as compared to 8.1 months in the chemotherapy-treated group. Most of the adverse events related to ceritinib treatment reported in the study were of grade 1 or 2 gastrointestinal (GI) toxicity (diarrhea, nausea, vomiting) and grade 3 or 4 hepatotoxicity (increased alanine and aspartate aminotransferases). 80% of the patients needed dose reduction or interruption to manage these adverse events [111]. Ceritinib is approved at 750 mg per day in a fasted state for expanded use in first-line ALK-positive metastatic NSCLC [112]. Since most of the serious adverse events (SAE) to ceritinib treatment are GI toxicity related, a multicenter, randomized open-label study ASCEND-8 evaluated the safety profile of ceritinib at lower doses (450 mg or 600 mg) taken daily with a low-fat meal compared to 750 mg daily in fasted patients with ALK-positive NSCLC [113]. Results from the study show that a lower dose of ceritinib (450 mg) taken with food reduced the number of GI

toxicity related AE. Most of the GI toxicities in the 450 mg dose arm were mostly grade 1, and no grade 3 or 4 GI toxicities were reported in that arm. Additionally, the number of patients requiring dose adjustment or drug interruption in the 450 mg ceritinib arm were the lowest compared to the 600 mg with food ceritinib and 700 mg fasted ceritinib treatment arm [113]. These results indicate that a lower dosage of 450 mg ceritinib taken with food maintains the same exposure as the currently approved dose of 750 mg fasted but with less severe and frequent GI toxicity profile.

#### 4.2.2. Alectinib (CH5424802; Chugai-Roche)

Alectinib is another second generation ALK inhibitor, highly selective and potent against the ALK tyrosine kinase protein [114]. It binds the ATP binding site of ALK, forming a canonical Hb with M1199. In addition, alectinib interacts via solvent water molecules with several other surrounding residues from the  $\alpha$ C-helix (K1150, E1167), the catalytic loop (R1253) and the DFG motif (G1269, D1270). The compound is thus embedded in a stabilizing global Hb network which can probably compensate for any single mutation at the binding site. Moreover, alectinib establishes a  $\pi$  interaction with L1196, which is maintained when Leu is mutated to Met, accounting for its high activity against the crizotinib-resistant gatekeeper L1196M mutant [115]. A phase II study in Japan reported an ORR of 93.5% with alectinib treatment in ALK+ NSCLC patients who had not been treated with an ALK inhibitor [116]. Apart from its excellent activity against ALK, alectinib also showed remarkable activity in patients with CNS metastases [117]. Alectinib received a breakthrough therapy designation (BTD) by the FDA for ALK-positive NSCLC patients who progressed on crizotinib while it was approved in Japan in 2014 for the treatment of ALK-rearranged NSCLC patients. Alectinib also showed substantial efficacy against crizotinib-resistant and/or ALK secondary mutations including the gatekeeper L1196M in vitro and in vivo [115,118] however, it was less effective against the G1202R [118]. Additionally, other ALK resistance mutations (V1180L, I1171T, F1174V) have been observed that arise against alectinib treatment [119]. Two phase II studies, the North American study (NCT01871805) and global study (NCT01801111), evaluated the safety and efficacy of alectinib in 87 and 138 ALK+ NSCLC patients who had progressed on crizotinib, respectively [14]. The patients received alectinib at a dose of 600 mg BID. ORR of 48% and 50% were reported recently from the North American and global study respectively. Most common side effects reported in the studies were constipation, fatigue, myalgia and peripheral edema. Grade 3 or higher AEs were observed in 26% of patients that included increased blood creatine phosphokinase and neutropenia [120]. In the global phase II study, the CNS ORR with baseline measurable CNS lesions was 57% while in the North American study the intracranial response was reported to be 75%. These two studies have demonstrated that alectinib is effective and well tolerated in ALK+ NSCLC patients refractory to crizotinib. Results from a randomized phase III trial comparing alectinib with crizotinib in treatment naïve ALK+ NSCLC has been published recently. Peters S et al. have showed that alectinib was more efficacious and less toxic as a primary treatment for the patients [15].

#### 4.2.3. Brigatinib (AP26113; Ariad)

Brigatinib, another orally available potent next-generation-ALK/ROS1/EGFR inhibitor had displayed activity against the tyrosine kinases as well as some of their mutant forms in cellular and pre-clinical models [121]. Brigatinib is a close analogue of NVP-TAE684, with the original sulfonyl group replaced by a phosphine-oxide moiety. According to structure-activity relationship (SAR) data, this group confers favorable Absorption, Distribution, Metabolism, and Excretion (ADME) properties to the molecule and higher selectivity versus IGF1R and IR [121]. Similar to other ALK inhibitors, brigatinib forms Hb to the hinge region residue L1198 as well as the gatekeeper L1196. Preclinical data showed that brigatinib has pan-ALK inhibitory profile (i.e., blocks all crizotinib-resistant mutants) in cellular models at clinically achievable levels [122], although it still suffers a significant loss of activity against the G1202R mutant [123,124]. A phase I/II study to evaluate the safety and activity of brigatinib was recently reported [125]. Phase I study aimed to establish the recommended phase

II dose of brigatinib in patients with advanced malignancies other than leukemia. Based on phase I results, three regimens were tested in the phase II: 180 mg daily, 90 mg daily and 180 mg daily with a 7-day lead-in at 90 mg daily. The phase II expansion study was divided into five histologically and molecularly defined cohorts based on prior chemotherapy and/or tyrosine kinase inhibitor treatments as well as the cancer types and CNS involvement. Crizotinib pre-treated ALK-rearranged NSCLC patient cohort had a confirmed objective response of 62% with a median progression-free survival of 13.2 months upon brigatinib treatment. Kim et al. have published results from the ongoing phase II, randomized, open-label, multicenter international study (ALK in Lung Cancer Trial of brigatinib; ALTA, ClinicalTrials.gov identifier: NCT02094573) that evaluated the efficacy and safety of two different brigatinib dosage regimens (90 mg daily and 180 mg daily) in crizotinib-treated ALK+ locally advanced or metastatic NSCLC patients [16]. After a median follow-up of 8 months, investigator-assessed ORR was 45% and 54% in the 90 mg daily and 180 mg daily dosage groups, respectively. A confirmed partial response in a patient with the G1202R mutation was also reported from the 180 mg daily group. In the phase II study, most common treatment-emergent adverse events (TEAE) included GI symptoms, headache and cough that were of low grade. AEs of grade >3 were hypertension, increased blood creatine phosphokinase, pneumonia and increased lipase. Pulmonary AEs (dyspnea, hypoxia, cough, pneumonia, and pneumonitis) with an early onset, usually within 24–48 h of treatment initiation, were observed in phase I/II study as well as in the phase II study [16,125]. In the ALTA study, all the pulmonary AEs occurred only at 90 mg brigatinib dose while no such events occurred after escalation to 180 mg dose [119]. On 28 April, 2017, the FDA granted an accelerated approval to brigatinib for the treatment of ALK+ metastatic NSCLC patients [126]. A phase III trial, ALTA-1L (NCT02737501) is ongoing to compare the efficacy and safety of brigatinib with those of crizotinib as a first-line treatment in patients with ALK+ metastatic NSCLC.

#### 4.3. Other ALK TKI Under Development

Apart from the above mentioned inhibitors, there are other tyrosine kinase inhibitors that are under development (pre-clinical or clinical). Table 2 lists currently available details regarding these small molecule inhibitors. Given the developing resistance against the second-generation inhibitors, these new inhibitors are anticipated to be more potent against ALK-driven tumor cells, have improved intracranial penetrance as well the ability to overcome the existing drug resistance. One example is lorlatinib (PF-06463922), a potent and brain-penetrant third generation TKI developed by Pfizer through cyclization and further modification of their first-generation compound, crizotinib, with the aim to improve brain penetration and inhibition of drug-resistant ALK mutants [127]. Indeed, lorlatinib showed good brain exposure and broad activity against resistant mutations. The compound interacts with the P-loop (L1122, G1123, and V1130) and with the conserved K1150. Lorlatinib inhibited wild-type and mutant ALK at a sub-nanomolar concentrations in cell-line models. It also exhibited high potency against all known clinically acquired ALK mutations, including the highly resistant G1202R mutant [128]. Zou HY et al. have demonstrated in in vivo experiments, that lorlatinib lead to regression of EML4-ALK-driven brain metastases ensuring a prolonged mouse survival [128]. In a phase I study, 42% (11/26) ALK-positive NSCLC patients who had been previously treated and progressed on first- and second-generation ALK TKIs, responded to lorlatinib. Also, lorlatinib showed both systemic and intracranial activity. These results suggest that lorlatinib may be an effective therapeutic approach for patients with ALK-driven NSCLC who have become resistant to the currently available TKIs, including second-generation ALK TKIs [8].

**Table 2.** FDA Approved and new ALK inhibitors under development.

Inhibitor	Targeted Kinase/s	Activity against Mutant Forms	Clinical Evidence	Brain Penetrance	References
Crizotinib * (Xalkori–Pfizer)	ALKc-MET sROS1	EML4-ALK <sup>L1198F</sup>	Phase I Phase II Phase III s(Complete)	No	[9,10,101,102]
Ceritinib * s(Zykadia–Novartis)	ALK IGR-1R INSR STK22D	EML4-ALK <sup>I1171T/N, L1196M, S1206C/Y, G1269A/S</sup>	Phase I Phase II Phase III (NCT02393625)	Yes	[11,109–111]
Alectinib * (Alecensa–Roche)	ALK LTK GAK	EML4-ALK <sup>L1152P/R, C1156Y/T, L1196M, F1174C/Y, S1206C/Y</sup> DCTN1-ALK <sup>G1269/S</sup>	Phase I Phase II Phase III (NCT02075840)	Yes	[14,116,117,127, 129,130]
Brigatinib * (AP26113–Ariad)	ALK ROS1	EML4-ALK <sup>I1151Tins, C1156Y/T, L1196M, L1152P/R, F1174C/L/V, G1269A/S1</sup> EML4-ALK <sup>G1202R</sup>	Phase I Phase II Phase III (NCT02094573)	Yes	[16,121,123– 125,131–133]
PF-06463922 (Lorlatinib–Pfizer)	ALK ROS1	ROS1 <sup>G2032R</sup> ROS1 <sup>L2026M</sup> EML4-ALK <sup>L1196M, G1269A, S1206Y, C1156Y, F1174L, L1152R, I1151Tins</sup>	Phase I Phase II (NCT01970865) Phase III (NCT03052608)	Yes (NCT02927340)	[8,127,134–136]
RDX-101 (Entrectinib–Ignyta)	ALK ROS1 TrkA TrkB TrkC	EML4-ALK <sup>C1156Y, L1196M</sup>	Phase I (ALKA-372-001 and STARTRK-1; NCT02097810)	Yes	[137,138]
ASP3026 (Astellas Pharma)	ALK ACK ROS1	EML4-ALK <sup>L1196M</sup> NPM-ALK <sup>L231N</sup> NPM-ALK <sup>L256Q</sup>	Phase I (NCT01284192)	N.D.	[139–141]
X-376 and X-396 (Xcovery)	ALK MET	EML4-ALK <sup>L1196M, C1156Y</sup>	Phase I/II (X-396) (NCT01625234)	Yes	[142,143]
CEP-28122 (Teva)	ALK FAK	N.D.	Phase I (NCT01922752)	N.D.	[144]
TSR-011 (Tesaro)	ALK TrkA TrkB TrkC	N.D.	Phase I/IIa (NCT02048488)	N.D.	[145]

Abbreviations (alphabetic order): FAK, focal adhesion kinase; MET, proto-oncogene, receptor tyrosine kinase; N.D., not described; ROS1, ROS proto-oncogene 1, receptor tyrosine kinase; TrkA, tyrosine kinase receptor A; TrkB, tyrosine kinase receptor B; TrkC, tyrosine kinase receptor C. \*; FDA approved. <sup>1</sup> Brigatinib was reported to have activity against the G1202R mutation [124,125,146], however, G1202R mutation has also been detected in biopsy specimens from ALK-positive NSCLC patients who relapsed on brigatinib [129].

In the phase I, dose escalation study, commonly observed AEs were hypercholesterolemia, hypertriglyceridemia, peripheral neuropathy, and peripheral edema in 72%, 39%, 39%, and 39% patients, respectively. GI symptoms (constipation and nausea) were less frequent and predominantly grade 1. The authors also reported mild neurocognitive side-effects (difficulty multitasking, slowing of speech, and short-term memory deficits) and mood side-effects that were reversible with dose interruption or dose reduction. However, how lorlatinib affects the lipid metabolism and causes hypercholesterolemia, hypertriglyceridemia, AEs unique to lorlatinib treatment, is still not known [8]. A phase III study comparing lorlatinib with crizotinib as monotherapy in terms of prolonging progression-free survival and overall survival in treatment naïve advanced ALK-positive NSCLC patients is currently ongoing (NCT03052608). Even though lorlatinib is a potent inhibitor, the L1198F resistant mutation was reported in one ALK+ NSCLC patient after receiving lorlatinib treatment for 8 months [147]. The patient had been treated with two prior TKIs; crizotinib and ceritinib and became refractory to both of them. Surprisingly, the L1198F lorlatinib resistant tumor regained sensitivity to crizotinib [147].

## 5. ALK TKI Resistance Mechanisms

Resistance to targeted therapies can be either primary or acquired. Primary resistance to a targeted therapy implies an intrinsic lack of response to the treatment from the beginning while acquired resistance denotes disease progression after an initial response (partial or complete) to the therapy [120]. Though mechanisms of intrinsic resistance are poorly understood, acquired resistance mechanisms broadly fall under two categories; ALK-dependent or ALK-independent mechanisms of resistance.

### 5.1. ALK-Dependent Resistance Mechanisms

#### 5.1.1. Secondary Mutations in the ALK Tyrosine Kinase Domain

In general, secondary mutations within the target kinase cause drug resistance by re-activation of the kinase and its downstream signaling pathways despite the presence of the TKI. These resistance mutations often occur around the surface lining the drug binding site (Figure 2C), although a number of mutations have been described that lie far from the active site. Depending on their location, mutations can directly hamper TKI binding to the target kinase, alter the conformation of the kinase, and/or modify the ATP-binding affinity of the kinase.

#### Resistance against Crizotinib

Despite the remarkable responses that have been observed in patients with ALK rearrangements, resistance to crizotinib eventually develops and rather quickly, making durable response unachievable, particularly in NSCLC. One of the important mechanisms of acquired resistance to crizotinib is the selection of point mutations within the drug target that alter drug sensitivity (Table 3). The first case of resistance against crizotinib was reported in an EML4-ALK-positive NSCLC patient [148]. The tumor resumed growth after an initial partial response over a period of 5 months. Deep sequencing analysis of the patient sample revealed a L1196M mutation and a C1156Y substitution at a relatively high frequency. The L1196 residue is a conserved gatekeeper residue located close to the ATP pocket and crizotinib binding site. In this secondary mutation, a smaller residue (leucine) is replaced by a larger residue (methionine) (Figure 2A,B). In contrast to a larger residue, a smaller one does not block the access of the inhibitor to the adjacent hydrophobic pocket [149]. Methionine substitution, in addition, has been reported to increase the enzyme activity by strengthening the hydrophobic R-spine which then promotes the formation of the active protein conformation [150]. L1196M mutant EML4-ALK protein was found to have higher phosphorylation levels [142]. These results show that the L1196M substitution confers drug resistance by increasing the protein kinase activity. On the other hand, the C1156Y mutation creates a displacement of crizotinib along with some conformational changes in the binding site of the drug that eventually decreases crizotinib affinity and leads to drug resistance [151]. Interestingly, a different gatekeeper mutation (L1196Q) was identified in crizotinib-resistant ALCL cells *in vitro* [152]. The same paper described an I1171N mutant that was resistant to all tested inhibitors; this mutation was later identified in an ALCL patient progressing on crizotinib [17]. Sasaki and colleagues described another case of crizotinib resistance in an IMT patient [153]. These investigators found the F1174L mutation in the RANBP2-ALK kinase domain in the relapsed tumor lesions. The F1174L mutation had earlier been detected in neuroblastoma [95]. The 1174 residue is found at the carboxyterminal end of the  $\alpha$ C-helix and has been shown to reduce ALK sensitivity to crizotinib by increasing ATP binding affinity in neuroblastoma cell lines and *in vivo* models [154]. Another mutant variant at the same position, F1174V, was also found in an ALK+ NSCLC patient resistant to crizotinib [155]. Secondary mutation L1152R with an EGFR and c-Met hyperactivation was reported in a cell line established from the NSCLC patient who relapsed after 3 months of crizotinib treatment [156]. The L1152R mutation affected crizotinib-mediated inhibition of downstream AKT and ERK phosphorylation in the resistant cells. As the L1152R mutation does not seem to be in direct contact with the ATP-binding pocket [157], how L1152R mediates ALK inhibitor

resistance is still unclear. A number of other secondary mutations such as S1206Y, G1202R, 1151Tins, G1269A were also found in crizotinib-refractory NSCLC patients (Figure 2C) [158,159]. Both, G1202R and S1206Y, are located at the solvent front of the kinase domain and presumably interfere with inhibitor binding due to steric hindrance and conformational changes of the kinase. While the insertion of a threonine residue at 1151 position is speculated to lead to a change in the affinity of ALK for ATP [157]. The Gly1269 residue is situated at the end of the ATP-binding pocket of ALK and its substitution with the larger Ala residue leads to a decrease in the binding of crizotinib to ALK due to steric hindrance [159]. Another ALK mutation found commonly in neuroblastoma is R1275Q [94], which has been shown to increase the ATP-binding affinity in the mutated ALK in vitro [154].

**Table 3.** Mutational profile of ALK that induce TKI resistance.

TKI	Sensitive Mutants	Resistant Mutants	Disease	Evidence (In Vitro/ In Vivo/Clinical)	Reference
Crizotinib	L1198F	I1151Tins	NSCLC	Clinical	[158]
		L1152R	NSCLC	Clinical	[156]
		C1156Y	NSCLC	Clinical	[148]
		I1171T/N	NSCLC	Clinical	[160]
		F1174L	IMT	Clinical	[156]
		L1196M	NSCLC	Clinical	[148]
		L1196Q	NSCLC	Clinical	[161]
		L1198P	EML4-ALK BaF3 cells	In vitro	[162]
		G1202R	NSCLC	Clinical	[158]
		D1203N	NSCLC	Clinical	[161]
		S1206Y	NSCLC	Clinical	[158]
		G1269A	NSCLC, IMT	Clinical	[159,163]
Ceritinib	G1269A, I1171T, S1206Y, L1196M	R1275Q	Neuroblastoma	In vitro	[94]
		L1152P/R	NSCLC	In vitro	[107]
		D1203	NSCLC	Clinical	[164]
		G1202R	NSCLC	Clinical	[107]
		F1174C/V	NSCLC	Clinical	[107]
		L1198F	NSCLC	In vitro	[165]
		C1156Y/T	NSCLC	In vitro	[107]
Alectinib	G1269A, S1206Y, L1152R, F1174L, 1151Tins	I1171T	NSCLC	Clinical	[119]
		V1180L	NSCLC	In vitro	[155]
		G1202R	NSCLC	Clinical	[155]
Brigatinib	G1269A, S1206Y, L1152R, F1174C, 1151Tins, I1171T, D1203N, E1210K, F1245C	F1174V+L1198F	ALCL	In vitro	[166]
		G1202R	NSCLC	Clinical	[167]
		S1206C/F	NSCLC	Clinical	[167]
Lorlatinib	L1196M, G1202R, G1269A	L1198F	NSCLC	Clinical	[147]

### Resistance to Second-Generation ALK TKIs

Even though the second generation of ALK inhibitors is proven to be more potent and highly selective with tolerable adverse events, the biggest setback still stays in the form of acquired resistance against them. For example, while ceritinib was able to overcome some of the secondary ALK resistance mutations that arise after crizotinib treatment, G1202R, F1174C/V mutations were reported to be selected by ceritinib. Structural analysis revealed that G1202R substitution causes a significant loss in ceritinib binding due to steric hindrance [107]. Other secondary mutations such as C1156Y, 1152Tins, and L1152R, G1123S have also been documented to be associated with resistance against ceritinib [160,168].

On the other hand, alectinib was shown to be effective against crizotinib or ceritinib resistant mutations, but leads to the acquisition of I1171T and V1180L resistant mutations in vitro and in a patient upon alectinib treatment. Interestingly, these two mutations could be overcome with ceritinib treatment which supports the idea of using two different inhibitors/combinatorial therapy. Again, the G1202R emerged as a highly intractable mutant [169]. Indeed, this mutation was reported to be resistant to all clinically available inhibitors, thereby representing the biggest current clinical challenge [123]. Point mutations L1122V, F1174V+L1198F, S1206C, and L1198F have been shown to confer resistance against brigatinib in ALCL cell lines [166]. Except for the S1206C mutation, most of the brigatinib

resistance could be overcome by switching back to crizotinib, other ALK TKIs or using alternative inhibitors such as heat shock protein 90 (HSP90) inhibitors [166].

Emergence of compound mutations upon sequential TKI treatment appears to be the next hurdle. Given the structural differences among the available ALK TKIs, it is perhaps not surprising that each ALK TKI appears to be associated with a specific profile of secondary ALK resistance mutations (Table 3). One such example of the compound mutations is the presence of a double mutation, C1156Y and L1198F in an advanced ALK+ NSCLC patient treated sequentially with crizotinib, ceritinib and lorlatinib [147]. Even though C1156Y mutation is sensitive to lorlatinib, the addition of L1198F disrupts binding of the drug with the kinase and leads to lorlatinib resistance. But interestingly, *in vitro* studies showed that L1198F mutation paradoxically leads to re-sensitization to the less potent and selective inhibitor crizotinib. Based on these findings, the patient was retreated with crizotinib and had a durable response [170]. Other examples of the compound mutation phenomenon include detection of C1156Y and I1171N double mutation after progression on crizotinib, ceritinib, and alectinib sequential treatment and presence of E1210K with D1203N mutation after sequential crizotinib and brigatinib treatment [129]. Given the number of different ALK TKIs that are being approved and their implementation in clinic for sequential TKI treatment, we are bound to see an increase in the number and variety of compound mutations (Table 3).

### 5.1.2. Amplification of ALK

Another ALK-dependent resistance mechanism is the amplification of *ALK* gene which occurs less frequently than secondary mutations, but is a recognized cause of acquired resistance to crizotinib. Katayama et al. reported high-level of wild type EML4-*ALK* gene amplification in 1 of the 15 patients that progressed on crizotinib [158]. The authors did not find any additional secondary mutations in the sample. Doebele et al. also documented an increase in the copy number of rearranged *ALK* gene per cells in 2 out of 12 patients' samples from post-crizotinib treatment [159]. Copy number gain (CNG) in the rearranged *ALK* gene was accompanied by the resistant mutation G1269A in 1 of these 2 samples. Based on the present clinical evidence it is difficult to say under which circumstances/factors, amplification of *ALK* gene is sufficient enough to render the tumor cells resistant. Genomic amplification of *ALK* locus has also been described to mediate ALK TKI resistance in ALCL cell lines [166,171]. Ceccon et al. observed that the brigatinib resistant ALCL cells had overexpressed NPM-*ALK* due to the *ALK* amplification [166]. Interestingly, the resistant cells were dependent/addicted to the TKI for their growth and proliferation [172]. Remarkably, drug withdrawal lead to apoptotic death of these drug-addicted TKI resistant cells mediated by the activation of the DNA damage response pathway due to an unbalanced NPM-*ALK* signaling [172].

## 5.2. ALK-Independent Resistance Mechanisms

### 5.2.1. Activation of Bypass Signaling Pathways

One important category of ALK-independent resistance mechanism is the activation of bypass signaling pathways through genetic alterations, autocrine signaling, or dysregulation of feedback signaling which leads to the survival and growth of tumor cells even when the target driven gene is inhibited with the TKI.

One such example is the epidermal growth factor receptor (EGFR) activation [156,158,173]. Studies conducted in ALK-rearranged lung cancer cell lines have shown an increment of EGFR phosphorylation in crizotinib-resistant cell lines which did not present secondary ALK mutation/up-regulation, when compared with parental crizotinib-sensitive cells, leading to a persistent activation of downstream ERK and AKT signaling. However, those cells did not present any EGFR mutations or amplification, telling that EGFR activity may result from receptor or ligand up-regulation [156,173]. Gene expression profiling of crizotinib-resistant versus crizotinib-naïve NSCLC tumor samples using RNA sequencing followed by single-sample gene set enrichment analysis (ssGSEA) has identified EGFR and HER2



(members of the HER receptor family) signatures as two of the most enriched gene expression marks in resistant tumors [174].

In ALK-positive lung adenocarcinoma cell lines and mouse xenograft models, the RAS–MEK pathway was found to be the critical downstream effector of EML4–ALK. In a recent study, using next generation sequencing analysis in a patient-derived ALK-translocated lung cancer cell line after ceritinib treatment, a MAP2K1-K57N activating mutation was found as the primary genetic alteration which was leading to MEK activation. More importantly, a separate study verified that ALK/MEK dual blockade may be effective not only in overcoming but also in delaying ALK TKI resistance [175,176]. In addition, c-KIT gene amplification in the presence of stem cell factor (SCF) has also been reported to impart some degree of resistance against crizotinib in patient samples [158]. A combination of crizotinib and imatinib (c-KIT/ABL inhibitor) treatment was able to overcome the resistance in c-KIT overexpressing crizotinib-resistant H3122 cells [158].

Laimer et al. [117] have shown in a mouse model of NPM-ALK-triggered lymphomagenesis, that the activator protein 1 family members JUN and JUNB promote lymphoma development and tumor dissemination via transcriptional regulation of platelet-derived growth factor receptor- $\beta$  (PDGFR $\beta$ ). When PDGFR $\beta$  is inhibited therapeutically, the survival of NPM-ALK transgenic mice is prolonged. Also, its inhibition leads to an increased efficacy of an ALK-specific inhibitor in transplanted NPM-ALK tumors. Remarkably, a patient with refractory late-stage ALK-rearranged ALCL treated with PDGFR $\alpha$  and PDGFR $\beta$  inhibitors had a rapid and complete remission [177].

Doebele et al. reported mutation in *KRAS* gene in 2 of the 11 NSCLC patients who relapsed on crizotinib [159]. One patient had a KRASG12C mutation which was detected in both, pre- and post-crizotinib biopsy samples. The second patient had a G12V substitution in *KRAS* gene only in the post-crizotinib biopsy sample. Interestingly, when the author introduced the G12V substitution in H3122 cells to evaluate its effect on resistance, they did not see a significant difference in IC50 values between parental and mutant cells [159]. Additionally, re-activation of MAPK signaling pathway due to a copy number gain (CNG) of wild-type *KRAS* gene or reduced levels of MAPK phosphatase DUSP6 was also reported to impart resistance against ALK TKIs in mouse models [175]. Using an upfront dual ALK and MEK-inhibitor therapy the authors were able to suppress the development of resistance in vitro. Other examples of bypass mechanisms clinically implicated in ALK TKI resistance include PIK3CA mutations (one of 27 samples (3.7%), post-alectinib; a case post-ceritinib) [129,176], IGF1R activation (four of five samples (80%), post-crizotinib [178]; and SRC activation [176]) (Figure 1B).

### 5.2.2. Other Mechanisms

In case of NSCLC, change in morphology has also been shown to contribute towards TKI resistance. Epithelial-to-mesenchymal transition (EMT) is one such morphological change in which epithelial cells lose their polarity and cell-to-cell junction and become more fibroblastic as well as more motile and invasive. EMT has been reported to confer resistance against first and second generation ALK TKIs in NSCLC cell lines [179] as well tumor samples [129]. However, how exactly and to what extent EMT contributes to this resistance still needs to be uncovered. Another recently identified mechanism of resistance against ALK TKIs is the histological transformation from a NSCLC entity to Small Cell Lung Cancer (SCLC). Several reports have been published reporting the transformation in NSCLC patients after progression on crizotinib [180,181], alectinib [182–184] and also on ceritinib [185]. In all of these reported cases, the SCLC tumor cells retained the ALK expression. None of the investigators were able to firmly demonstrate if the SCLC transformation appeared as a novel resistance mechanism or the SCLC cells could have co-existed but not discovered during the initial diagnoses. Even though the transformation mechanism is not yet completely understood, loss of retinoblastoma (*RB*) gene seems to be important for this type of transformation. Mutations in *TP53* and *PTEN* genes have also been found in a patient presenting with the SCLC transformation [185].

## 6. Other Therapeutic Strategies to Overcome ALK-Related Resistance

### 6.1. ALK TKIs Combined with Other Inhibitors Targeting Different Kinases

The majority of studies performed on ALK TKI resistance has focused on the development of next-generation ALK inhibitors, which can overcome at least some of resistant mutants. Around 30% of crizotinib resistance in ALK-positive NSCLC is related to secondary ALK mutations and/or amplifications, which maintain their sensitivity to next-generation ALK inhibitors. However, nearly to 40% of the resistant cases to second-generation inhibitors is no longer ALK-dependent. Activation of bypass signaling has emerged as other potential strategy to combat ALK TKI resistance. Combination strategies that target both ALK and a second kinase may be needed to overcome the different bypass pathways that mediate ALK resistance.

As mentioned above, MEK reactivation is a key example of resistance mechanism involving other TKs. Crystal et al. in a patient-derived ALK-rearranged lung cancer cell line post-ceritinib harboring MAP2K1<sup>K57N</sup> activation mutation of MEK, have shown that the MEK inhibitor selumetinib was a potent hit when combined with ceritinib [176]. Confirming these results, a separated study lead by Hrustanovic et al. demonstrated that the dual blockage of ALK/MEK may be effective not only in overcoming but also in delaying ALK TKI resistance [175]. Based on these findings, a large variety of combination therapies of ALK and MEK inhibitors may be a potential therapeutic strategy.

Current clinical trials are testing the efficacy of ALK TKI in combination with other target agents. Alectinib combined with bevacizumab (angiogenesis agent targeting vascular endothelial growth factor-VEGF) is being tested in patients with ALK-rearranged NSCLC with at least one target lesion in CNS (NCT02521051) and combinations of ceritinib with either LEE011 (CDK4/6 inhibitor) or everolimus (mTOR inhibitor) are in early-phase testing in NSCLC (NCT02292550 and NCT02321501, respectively). Other potential combinations include ALK TKI with EGFR inhibitor, cKIT inhibitor and SRC inhibitor. The selection of the appropriate combination should be individualized based on the resistance mechanism identified and toxicities of combinations may be a major limitation. MET activation is a very well-known bypass signaling pathway in EGFR-mutant NSCLC but in ALK-rearranged NSCLC does not cause resistance to the first-generation TKI crizotinib, which is also a potent MET inhibitor [186,187]. However, some of the next-generation ALK TKIs do not have activity against MET and indeed, MET has been reported as a bypass signaling mechanism in a patient who has failed second-generation ALK inhibitors. This patient subsequently responded to crizotinib [188]. Similarly, the fact that each ALK TKI is associated with a unique spectrum of ALK resistance mutations, suggests that combinations of ALK TKIs could also be beneficial and enable more durable responses than those achieved in monotherapies.

### 6.2. ALK Inhibitors Combined with Immunotherapy

#### 6.2.1. Immune Checkpoint Inhibitors

Immunotherapy with immune checkpoints inhibitors, specifically PD-1 and PD-L1, has demonstrated good responses in advanced NSCLC, ranging from 15 to 20%, with some patients exhibiting durable responses after discontinuing therapy [189–194]. In 2015, two immune checkpoints inhibitors received FDA approval for second-line therapy of NSCLC, namely nivolumab and pembrolizumab both targeting the programmed cell death-1 (PD-1). In 2016, another checkpoint inhibitor (atezolizumab, a programmed cell death-ligand 1 [PD-L1]) received its approval from FDA for first-line NSCLC treatment in patients with high PD-L1 expressing tumors [189,195–198]. Some clinical trials are investigating the efficacy and safety of an ALK TKI combined with immunotherapy in lung cancer, namely, crizotinib with nivolumab or ipilimumab (NCT01998126) or pembrolizumab (NCT02511184); alectinib with atezolizumab (NCT02013219); ceritinib combined with nivolumab (NCT02393625) and lorlatinib with avelumab (NCT02584634). Yet, there are still limited preclinical data to support this combination strategy. Although those immune checkpoints inhibitors have demonstrated durable

responses after disruption of the therapy, only 20% of the patients benefit this effect and it has been associated with high expression levels of PD-L1, high mutational load and smoking history [189,191]. Patients bearing ALK-rearrangements tend to be never-smokers and with a low tumor mutational load [199] and to respond poorly to PD-1 blockade [200]. Thus, the potential benefit of the addition of immunotherapy to ALK TKI treatment is still unclear.

### 6.2.2. Vaccine Therapy

The administration of immunogenic tumor-associated antigens or cells in conjunction with an immune-adjuvant that elicits specific antitumor immune response, boost the immune system against tumor cells [201]. These therapeutic vaccines identify specific tumor-associated antigen and elicit the immune system against them. ALK has unique biological characteristics that are attractive for a tumor antigen. First, ALK is not expressed in obviously detectable levels by non-tumoral cells with the exception of specific regions of the central nervous system and the testis, both immunologically privileged sites. Many evidences support that ALK is spontaneously recognized as a tumor antigen in human patients [202]. Circulating antibodies against NPM-ALK and EML4-ALK proteins were found in ALK-positive ACLC and NSCLC, respectively [203,204]. In 2008 we have demonstrated in vivo the efficacy of a DNA-based vaccine encoding portions of the cytoplasmic domain of ALK. This combination enhanced the survival of mice challenged with ALK-positive lymphomas [205]. More recently, our group has shown that ALK vaccination induce a strong and specific immune response either prophylactically or therapeutically against ALK+ lung tumors in preclinical models. The ALK vaccine in combination with ALK TKI treatment significantly delayed tumor relapse after TKI suspension [206]. Many of the vaccine trials in NSCLC showed an immune response after vaccination, usually in form of an increase of target specific cytotoxic T-cells. Unfortunately, this has not translated into significant survival advantage in the phase III trials to date. In terms of toxicity, most of these vaccine-based therapies show less toxicity when compared to traditional chemotherapies or other immune therapies. While vaccine therapy trials in NSCLC have so far failed to show significant clinical benefit, the demonstration of enhanced immune response in these trials suggests that an ALK-directed vaccine therapy could have more degree of clinical efficacy in combination with checkpoint inhibitors.

## 7. Conclusions

ALK represents a validated therapeutic target in numerous malignancies such as NSCLC, ALCL, IMT and neuroblastoma. Since its discovery as a fusion oncogene, four ALK inhibitors have been approved and will become standard of cure for NSCLC patients harboring ALK-rearrangements. More ALK inhibitors are in clinical development and some have already shown strong efficacy in cohorts of patients with ALK-positive tumors. Notwithstanding these remarkable responses, ALK TKIs effect is transient and never achieves a complete cure. Patients invariably relapse due to acquired resistance, which represents a significant barrier to the successful treatment of ALK-positive patients. Therefore, the development of strategies to overcome/prevent/delay resistance is a priority. With the current knowledge of the complex and heterogeneous mechanisms process behind ALK resistance, multiple next-generation ALK inhibitors and combinatorial treatment approaches can be envisioned. These potential new therapeutic strategies have the promise to improve the treatment of an increasing portion of patients ALK-positive cancers.

**Acknowledgments:** Geeta Geeta Sharma, Ines Mota, Luca Mologni, Carlo Gambacorti-Passerini and Roberto Chiarle are in receipt of a European Union Horizon 2020 Marie Skłodowska-Curie Innovative Training Network (ITN-ETN) Grant, Award No.: 675712 and in the European Research Initiative for ALK-Related Malignancies (ERIA). The work has been supported by grant R01 CA196703-01 to Roberto Chiarle.

**Conflicts of Interest:** The authors declare no conflict of interest.

## References

1. Druker, B.J.; Talpaz, M.; Resta, D.J.; Peng, B.; Buchdunger, E.; Ford, J.M.; Lydon, N.B.; Kantarjian, H.; Capdeville, R.; Ohno-Jones, S.; et al. Efficacy and safety of a specific inhibitor of the BCR-ABL tyrosine kinase in chronic myeloid leukemia. *N. Engl. J. Med.* **2001**, *344*, 1031–1037. [[CrossRef](#)] [[PubMed](#)]
2. Druker, B.J.; Guilhot, F.; O'Brien, S.G.; Gathmann, I.; Kantarjian, H.; Gattermann, N.; Deininger, M.W.; Silver, R.T.; Goldman, J.M.; Stone, R.M.; et al. Five-year follow-up of patients receiving imatinib for chronic myeloid leukemia. *N. Engl. J. Med.* **2006**, *355*, 2408–2417. [[CrossRef](#)] [[PubMed](#)]
3. Murray, P.B.; Lax, I.; Reshetnyak, A.; Ligon, G.F.; Lillquist, J.S.; Natoli, E.J., Jr.; Shi, X.; Folta-Stogniew, E.; Gunel, M.; Alvarado, D.; et al. Heparin is an activating ligand of the orphan receptor tyrosine kinase ALK. *Sci. Signal.* **2015**, *8*, ra6. [[CrossRef](#)] [[PubMed](#)]
4. Chiarle, R.; Voena, C.; Ambrogio, C.; Piva, R.; Inghirami, G. The anaplastic lymphoma kinase in the pathogenesis of cancer. *Nat. Rev. Cancer* **2008**, *8*, 11–23. [[CrossRef](#)] [[PubMed](#)]
5. Mi, R.; Chen, W.; Hoke, A. Pleiotrophin is a neurotrophic factor for spinal motor neurons. *Proc. Natl. Acad. Sci. USA* **2007**, *104*, 4664–4669. [[CrossRef](#)] [[PubMed](#)]
6. Hallberg, B.; Palmer, R.H. Mechanistic insight into ALK receptor tyrosine kinase in human cancer biology. *Nat. Rev. Cancer* **2013**, *13*, 685–700. [[CrossRef](#)] [[PubMed](#)]
7. Soda, M.; Choi, Y.L.; Enomoto, M.; Takada, S.; Yamashita, Y.; Ishikawa, S.; Fujiwara, S.; Watanabe, H.; Kurashina, K.; Hatanaka, H.; et al. Identification of the transforming EML4-ALK fusion gene in non-small-cell lung cancer. *Nature* **2007**, *448*, 561–566. [[CrossRef](#)] [[PubMed](#)]
8. Shaw, A.T.; Felip, E.; Bauer, T.M.; Besse, B.; Navarro, A.; Postel-Vinay, S.; Gainor, J.F.; Johnson, M.; Dietrich, J.; James, L.P.; et al. Lorlatinib in non-small-cell lung cancer with ALK or ros1 rearrangement: An international, multicentre, open-label, single-arm first-in-man phase 1 trial. *Lancet Oncol.* **2017**, *18*, 1590–1599. [[CrossRef](#)]
9. Shaw, A.T.; Kim, D.W.; Nakagawa, K.; Seto, T.; Crino, L.; Ahn, M.J.; De Pas, T.; Besse, B.; Solomon, B.J.; Blackhall, F.; et al. Crizotinib versus chemotherapy in advanced ALK-positive lung cancer. *N. Engl. J. Med.* **2013**, *368*, 2385–2394. [[CrossRef](#)] [[PubMed](#)]
10. Solomon, B.J.; Mok, T.; Kim, D.W.; Wu, Y.L.; Nakagawa, K.; Mekhail, T.; Felip, E.; Cappuzzo, F.; Paolini, J.; Usari, T.; et al. First-line crizotinib versus chemotherapy in ALK-positive lung cancer. *N. Engl. J. Med.* **2014**, *371*, 2167–2177. [[CrossRef](#)] [[PubMed](#)]
11. Shaw, A.T.; Kim, D.W.; Mehra, R.; Tan, D.S.; Felip, E.; Chow, L.Q.; Camidge, D.R.; Vansteenkiste, J.; Sharma, S.; De Pas, T.; et al. Ceritinib in ALK-rearranged non-small-cell lung cancer. *N. Engl. J. Med.* **2014**, *370*, 1189–1197. [[CrossRef](#)] [[PubMed](#)]
12. Kim, D.W.; Mehra, R.; Tan, D.S.; Felip, E.; Chow, L.Q.; Camidge, D.R.; Vansteenkiste, J.; Sharma, S.; De Pas, T.; Riely, G.J.; et al. Activity and safety of ceritinib in patients with ALK-rearranged non-small-cell lung cancer (ascend-1): Updated results from the multicentre, open-label, phase 1 trial. *Lancet Oncol.* **2016**, *17*, 452–463. [[CrossRef](#)]
13. Ou, S.H.; Ahn, J.S.; De Petris, L.; Govindan, R.; Yang, J.C.; Hughes, B.; Lena, H.; Moro-Sibilot, D.; Bearz, A.; Ramirez, S.V.; et al. Alectinib in crizotinib-refractory ALK-rearranged non-small-cell lung cancer: A phase ii global study. *J. Clin. Oncol.* **2016**, *34*, 661–668. [[CrossRef](#)] [[PubMed](#)]
14. Shaw, A.T.; Gandhi, L.; Gadgeel, S.; Riely, G.J.; Cetnar, J.; West, H.; Camidge, D.R.; Socinski, M.A.; Chiappori, A.; Mekhail, T.; et al. Alectinib in ALK-positive, crizotinib-resistant, non-small-cell lung cancer: A single-group, multicentre, phase 2 trial. *Lancet Oncol.* **2016**, *17*, 234–242. [[CrossRef](#)]
15. Peters, S.; Camidge, D.R.; Shaw, A.T.; Gadgeel, S.; Ahn, J.S.; Kim, D.W.; Ou, S.I.; Perol, M.; Dziadziuszko, R.; Rosell, R.; et al. Alectinib versus crizotinib in untreated ALK-positive non-small-cell lung cancer. *N. Engl. J. Med.* **2017**, *377*, 829–838. [[CrossRef](#)] [[PubMed](#)]
16. Kim, D.W.; Tiseo, M.; Ahn, M.J.; Reckamp, K.L.; Hansen, K.H.; Kim, S.W.; Huber, R.M.; West, H.L.; Groen, H.J.M.; Hochmair, M.J.; et al. Brigatinib in patients with crizotinib-refractory anaplastic lymphoma kinase-positive non-small-cell lung cancer: A randomized, multicenter phase II trial. *J. Clin. Oncol.* **2017**, *35*, 2490–2498. [[CrossRef](#)] [[PubMed](#)]
17. Gambacorti Passerini, C.; Farina, F.; Stasia, A.; Redaelli, S.; Ceccon, M.; Mologni, L.; Messa, C.; Guerra, L.; Giudici, G.; Sala, E.; et al. Crizotinib in advanced, chemoresistant anaplastic lymphoma kinase-positive lymphoma patients. *J. Natl. Cancer Inst.* **2014**, *106*, djt378. [[CrossRef](#)] [[PubMed](#)]

18. Butrynski, J.E.; D'Adamo, D.R.; Hornick, J.L.; Dal Cin, P.; Antonescu, C.R.; Jhanwar, S.C.; Ladanyi, M.; Capelletti, M.; Rodig, S.J.; Ramaiya, N.; et al. Crizotinib in ALK-rearranged inflammatory myofibroblastic tumor. *N. Engl. J. Med.* **2010**, *363*, 1727–1733. [[CrossRef](#)] [[PubMed](#)]
19. Richly, H.; Kim, T.M.; Schuler, M.; Kim, D.W.; Harrison, S.J.; Shaw, A.T.; Boral, A.L.; Yovine, A.; Solomon, B. Ceritinib in patients with advanced anaplastic lymphoma kinase-rearranged anaplastic large-cell lymphoma. *Blood* **2015**, *126*, 1257–1258. [[CrossRef](#)] [[PubMed](#)]
20. Iwahara, T.; Fujimoto, J.; Wen, D.; Cupples, R.; Bucay, N.; Arakawa, T.; Mori, S.; Ratzkin, B.; Yamamoto, T. Molecular characterization of ALK, a receptor tyrosine kinase expressed specifically in the nervous system. *Oncogene* **1997**, *14*, 439–449. [[CrossRef](#)] [[PubMed](#)]
21. Lemmon, M.A.; Schlessinger, J. Cell signaling by receptor tyrosine kinases. *Cell* **2010**, *141*, 1117–1134. [[CrossRef](#)] [[PubMed](#)]
22. Palmer, R.H.; Vernersson, E.; Grabbe, C.; Hallberg, B. Anaplastic lymphoma kinase: Signalling in development and disease. *Biochem. J.* **2009**, *420*, 345–361. [[CrossRef](#)] [[PubMed](#)]
23. Morris, S.W.; Naeve, C.; Mathew, P.; James, P.L.; Kirstein, M.N.; Cui, X.; Witte, D.P. ALK, the chromosome 2 gene locus altered by the t(2;5) in non-hodgkin's lymphoma, encodes a novel neural receptor tyrosine kinase that is highly related to leukocyte tyrosine kinase (LTK). *Oncogene* **1997**, *14*, 2175–2188. [[CrossRef](#)] [[PubMed](#)]
24. Loren, C.E.; Englund, C.; Grabbe, C.; Hallberg, B.; Hunter, T.; Palmer, R.H. A crucial role for the anaplastic lymphoma kinase receptor tyrosine kinase in gut development in drosophila melanogaster. *EMBO Rep.* **2003**, *4*, 781–786. [[CrossRef](#)] [[PubMed](#)]
25. Bazigou, E.; Apitz, H.; Johansson, J.; Loren, C.E.; Hirst, E.M.; Chen, P.L.; Palmer, R.H.; Salecker, I. Anterograde jelly belly and ALK receptor tyrosine kinase signaling mediates retinal axon targeting in drosophila. *Cell* **2007**, *128*, 961–975. [[CrossRef](#)] [[PubMed](#)]
26. Rohrbough, J.; Broadie, K. Anterograde jelly belly ligand to ALK receptor signaling at developing synapses is regulated by mind the gap. *Development* **2010**, *137*, 3523–3533. [[CrossRef](#)] [[PubMed](#)]
27. Gouzi, J.Y.; Moressis, A.; Walker, J.A.; Apostolopoulou, A.A.; Palmer, R.H.; Bernardis, A.; Skoulakis, E.M. The receptor tyrosine kinase ALK controls neurofibromin functions in drosophila growth and learning. *PLoS Genet.* **2011**, *7*, e1002281. [[CrossRef](#)] [[PubMed](#)]
28. Lee, H.H.; Norris, A.; Weiss, J.B.; Frasch, M. Jelly belly protein activates the receptor tyrosine kinase ALK to specify visceral muscle pioneers. *Nature* **2003**, *425*, 507–512. [[CrossRef](#)] [[PubMed](#)]
29. Yang, H.L.; Eriksson, T.; Vernersson, E.; Vigny, M.; Hallberg, B.; Palmer, R.H. The ligand jelly belly (JEB) activates the drosophila ALKRTK to drive PC12 cell differentiation, but is unable to activate the mouse ALKRTK. *J. Exp. Zool. Part B Mol. Dev. Evolut.* **2007**, *308*, 269–282. [[CrossRef](#)] [[PubMed](#)]
30. Reiner, D.J.; Ailion, M.; Thomas, J.H.; Meyer, B.J. *C. elegans* anaplastic lymphoma kinase ortholog scd-2 controls dauer formation by modulating TGF- $\beta$  signaling. *Curr. Biol. CB* **2008**, *18*, 1101–1109. [[CrossRef](#)] [[PubMed](#)]
31. Yao, S.; Cheng, M.; Zhang, Q.; Wasik, M.; Kelsh, R.; Winkler, C. Anaplastic lymphoma kinase is required for neurogenesis in the developing central nervous system of zebrafish. *PLoS ONE* **2013**, *8*, e63757. [[CrossRef](#)] [[PubMed](#)]
32. Hurley, S.P.; Clary, D.O.; Copie, V.; Lefcort, F. Anaplastic lymphoma kinase is dynamically expressed on subsets of motor neurons and in the peripheral nervous system. *J. Comp. Neurol.* **2006**, *495*, 202–212. [[CrossRef](#)] [[PubMed](#)]
33. Vernersson, E.; Khoo, N.K.; Henriksson, M.L.; Roos, G.; Palmer, R.H.; Hallberg, B. Characterization of the expression of the ALK receptor tyrosine kinase in mice. *Gene Express. Patterns GEP* **2006**, *6*, 448–461. [[CrossRef](#)] [[PubMed](#)]
34. Bilsland, J.G.; Wheeldon, A.; Mead, A.; Znamenskiy, P.; Almond, S.; Waters, K.A.; Thakur, M.; Beaumont, V.; Bonnert, T.P.; Heavens, R.; et al. Behavioral and neurochemical alterations in mice deficient in anaplastic lymphoma kinase suggest therapeutic potential for psychiatric indications. *Neuropsychopharmacology* **2008**, *33*, 685–700. [[CrossRef](#)] [[PubMed](#)]
35. Lasek, A.W.; Lim, J.; Kliethermes, C.L.; Berger, K.H.; Joslyn, G.; Brush, G.; Xue, L.; Robertson, M.; Moore, M.S.; Vranizan, K.; et al. An evolutionary conserved role for anaplastic lymphoma kinase in behavioral responses to ethanol. *PLoS ONE* **2011**, *6*, e22636. [[CrossRef](#)] [[PubMed](#)]

36. Morris, S.W.; Kirstein, M.N.; Valentine, M.B.; Dittmer, K.G.; Shapiro, D.N.; Saltman, D.L.; Look, A.T. Fusion of a kinase gene, ALK, to a nucleolar protein gene, nrm, in non-hodgkin's lymphoma. *Science* **1994**, *263*, 1281–1284. [[CrossRef](#)] [[PubMed](#)]
37. Reshetnyak, A.V.; Murray, P.B.; Shi, X.; Mo, E.S.; Mohanty, J.; Tome, F.; Bai, H.; Gunel, M.; Lax, I.; Schlessinger, J. Augmentor alpha and  $\beta$  (FAM150) are ligands of the receptor tyrosine kinases ALK and LTK: Hierarchy and specificity of ligand-receptor interactions. *Proc. Natl. Acad. Sci. USA* **2015**, *112*, 15862–15867. [[CrossRef](#)] [[PubMed](#)]
38. Lemke, G. Adopting ALK and LTK. *Proc. Natl. Acad. Sci. USA* **2015**, *112*, 15783–15784. [[CrossRef](#)] [[PubMed](#)]
39. Shaw, A.T.; Hsu, P.P.; Awad, M.M.; Engelman, J.A. Tyrosine kinase gene rearrangements in epithelial malignancies. *Nat. Rev. Cancer* **2013**, *13*, 772–787. [[CrossRef](#)] [[PubMed](#)]
40. Toffalini, F.; Demoulin, J.B. New insights into the mechanisms of hematopoietic cell transformation by activated receptor tyrosine kinases. *Blood* **2010**, *116*, 2429–2437. [[CrossRef](#)] [[PubMed](#)]
41. Ladanyi, M.; Cavalchire, G. Molecular variant of the nrm-ALK rearrangement of KI-1 lymphoma involving a cryptic ALK splice site. *Genes Chromosom. Cancer* **1996**, *15*, 173–177. [[CrossRef](#)]
42. Lamant, L.; Pulford, K.; Bischof, D.; Morris, S.W.; Mason, D.Y.; Delsol, G.; Mariame, B. Expression of the ALK tyrosine kinase gene in neuroblastoma. *Am. J. Pathol.* **2000**, *156*, 1711–1721. [[CrossRef](#)]
43. Lovly, C.M.; Gupta, A.; Lipson, D.; Otto, G.; Brennan, T.; Chung, C.T.; Borinstein, S.C.; Ross, J.S.; Stephens, P.J.; Miller, V.A.; et al. Inflammatory myofibroblastic tumors harbor multiple potentially actionable kinase fusions. *Cancer Discov.* **2014**, *4*, 889–895. [[CrossRef](#)] [[PubMed](#)]
44. Rikova, K.; Guo, A.; Zeng, Q.; Possemato, A.; Yu, J.; Haack, H.; Nardone, J.; Lee, K.; Reeves, C.; Li, Y.; et al. Global survey of phosphotyrosine signaling identifies oncogenic kinases in lung cancer. *Cell* **2007**, *131*, 1190–1203. [[CrossRef](#)] [[PubMed](#)]
45. Shaw, A.T.; Yeap, B.Y.; Mino-Kenudson, M.; Digumarthy, S.R.; Costa, D.B.; Heist, R.S.; Solomon, B.; Stubbs, H.; Admane, S.; McDermott, U.; et al. Clinical features and outcome of patients with non-small-cell lung cancer who harbor EML4-ALK. *J. Clin. Oncol.* **2009**, *27*, 4247–4253. [[CrossRef](#)] [[PubMed](#)]
46. Shaw, A.T.; Engelman, J.A. ALK in lung cancer: Past, present, and future. *J. Clin. Oncol.* **2013**, *31*, 1105–1111. [[CrossRef](#)] [[PubMed](#)]
47. Heuckmann, J.M.; Balke-Want, H.; Malchers, F.; Peifer, M.; Sos, M.L.; Koker, M.; Meder, L.; Lovly, C.M.; Heukamp, L.C.; Pao, W.; et al. Differential protein stability and ALK inhibitor sensitivity of EML4-ALK fusion variants. *Clin. Cancer Res.* **2012**, *18*, 4682–4690. [[CrossRef](#)] [[PubMed](#)]
48. Lamant, L.; Dastugue, N.; Pulford, K.; Delsol, G.; Mariame, B. A new fusion gene TPM3-ALK in anaplastic large cell lymphoma created by a (1;2)(q25;p23) translocation. *Blood* **1999**, *93*, 3088–3095. [[PubMed](#)]
49. Cools, J.; Wlodarska, I.; Somers, R.; Mentens, N.; Peddeutour, F.; Maes, B.; De Wolf-Peeters, C.; Pauwels, P.; Hagemeijer, A.; Marynen, P. Identification of novel fusion partners of ALK, the anaplastic lymphoma kinase, in anaplastic large-cell lymphoma and inflammatory myofibroblastic tumor. *Genes Chromosom. Cancer* **2002**, *34*, 354–362. [[CrossRef](#)] [[PubMed](#)]
50. Lamant, L.; Gascoyne, R.D.; Duplantier, M.M.; Armstrong, F.; Raghav, A.; Chhanabhai, M.; Rajcan-Separovic, E.; Raghav, J.; Delsol, G.; Espinos, E. Non-muscle myosin heavy chain (MYH9): A new partner fused to ALK in anaplastic large cell lymphoma. *Genes Chromosom. Cancer* **2003**, *37*, 427–432. [[CrossRef](#)] [[PubMed](#)]
51. Meech, S.J.; McGavran, L.; Odom, L.F.; Liang, X.; Meltesen, L.; Gump, J.; Wei, Q.; Carlsen, S.; Hunger, S.P. Unusual childhood extramedullary hematologic malignancy with natural killer cell properties that contains tropomyosin 4—Anaplastic lymphoma kinase gene fusion. *Blood* **2001**, *98*, 1209–1216. [[CrossRef](#)] [[PubMed](#)]
52. Tort, F.; Pinyol, M.; Pulford, K.; Roncador, G.; Hernandez, L.; Nayach, I.; Kluin-Nelemans, H.C.; Kluin, P.; Touriol, C.; Delsol, G.; et al. Molecular characterization of a new ALK translocation involving moesin (MSN-ALK) in anaplastic large cell lymphoma. *Lab. Invest.* **2001**, *81*, 419–426. [[CrossRef](#)] [[PubMed](#)]
53. Tort, F.; Campo, E.; Pohlman, B.; Hsi, E. Heterogeneity of genomic breakpoints in MSN-ALK translocations in anaplastic large cell lymphoma. *Hum. Pathol.* **2004**, *35*, 1038–1041. [[CrossRef](#)] [[PubMed](#)]
54. Colleoni, G.W.; Bridge, J.A.; Garicochea, B.; Liu, J.; Filippa, D.A.; Ladanyi, M. Atic-ALK: A novel variant ALK gene fusion in anaplastic large cell lymphoma resulting from the recurrent cryptic chromosomal inversion, inv(2)(p23q35). *Am. J. Pathol.* **2000**, *156*, 781–789. [[CrossRef](#)]

55. Touriol, C.; Greenland, C.; Lamant, L.; Pulford, K.; Bernard, F.; Rousset, T.; Mason, D.Y.; Delsol, G. Further demonstration of the diversity of chromosomal changes involving 2p23 in ALK-positive lymphoma: 2 cases expressing ALK kinase fused to CLTCL (clathrin chain polypeptide-like). *Blood* **2000**, *95*, 3204–3207. [[PubMed](#)]
56. Abate, F.; Todaro, M.; van der Krogt, J.A.; Boi, M.; Landra, I.; Machiorlatti, R.; Tabbo, F.; Messina, K.; Abele, C.; Barreca, A.; et al. A novel patient-derived tumorgraft model with TRAF1-ALK anaplastic large-cell lymphoma translocation. *Leukemia* **2015**, *29*, 1390–1401. [[CrossRef](#)] [[PubMed](#)]
57. Hernandez, L.; Bea, S.; Bellosillo, B.; Pinyol, M.; Falini, B.; Carbone, A.; Ott, G.; Rosenwald, A.; Fernandez, A.; Pulford, K.; et al. Diversity of genomic breakpoints in TFG-ALK translocations in anaplastic large cell lymphomas: Identification of a new TFG-ALK(XL) chimeric gene with transforming activity. *Am. J. Pathol.* **2002**, *160*, 1487–1494. [[CrossRef](#)]
58. Lin, E.; Li, L.; Guan, Y.; Soriano, R.; Rivers, C.S.; Mohan, S.; Pandita, A.; Tang, J.; Modrusan, Z. Exon array profiling detects EML4-ALK fusion in breast, colorectal, and non-small cell lung cancers. *Mol. Cancer Res. MCR* **2009**, *7*, 1466–1476. [[CrossRef](#)] [[PubMed](#)]
59. Medico, E.; Russo, M.; Picco, G.; Cancelliere, C.; Valtorta, E.; Corti, G.; Buscarino, M.; Isella, C.; Lamba, S.; Martinoglio, B.; et al. The molecular landscape of colorectal cancer cell lines unveils clinically actionable kinase targets. *Nat. Commun.* **2015**, *6*, 7002. [[CrossRef](#)] [[PubMed](#)]
60. Lipson, D.; Capelletti, M.; Yelensky, R.; Otto, G.; Parker, A.; Jarosz, M.; Curran, J.A.; Balasubramanian, S.; Bloom, T.; Brennan, K.W.; et al. Identification of new ALK and ret gene fusions from colorectal and lung cancer biopsies. *Nat. Med.* **2012**, *18*, 382–384. [[CrossRef](#)] [[PubMed](#)]
61. Aisner, D.L.; Nguyen, T.T.; Paskulin, D.D.; Le, A.T.; Haney, J.; Schulte, N.; Chionh, F.; Hardingham, J.; Mariadason, J.; Tebbutt, N.; et al. ROS1 and ALK fusions in colorectal cancer, with evidence of intratumoral heterogeneity for molecular drivers. *Mol. Cancer Res. MCR* **2014**, *12*, 111–118. [[CrossRef](#)] [[PubMed](#)]
62. Lee, S.E.; Kang, S.Y.; Takeuchi, K.; Ko, Y.H. Identification of RANBP2-ALK fusion in ALK positive diffuse large B-cell lymphoma. *Hematol. Oncol.* **2014**, *32*, 221–224. [[CrossRef](#)] [[PubMed](#)]
63. Adam, P.; Katzenberger, T.; Seeberger, H.; Gattenlohner, S.; Wolf, J.; Steinlein, C.; Schmid, M.; Muller-Hermelink, H.K.; Ott, G. A case of a diffuse large B-cell lymphoma of plasmablastic type associated with the t(2;5)(p23;q35) chromosome translocation. *Am. J. Surg. Pathol.* **2003**, *27*, 1473–1476. [[CrossRef](#)] [[PubMed](#)]
64. Sakamoto, K.; Nakasone, H.; Togashi, Y.; Sakata, S.; Tsuyama, N.; Baba, S.; Dobashi, A.; Asaka, R.; Tsai, C.C.; Chuang, S.S.; et al. ALK-positive large B-cell lymphoma: Identification of EML4-ALK and a review of the literature focusing on the ALK immunohistochemical staining pattern. *Int. J. Hematol.* **2016**, *103*, 399–408. [[CrossRef](#)] [[PubMed](#)]
65. D’Amore, E.S.; Visco, C.; Menin, A.; Famengo, B.; Bonvini, P.; Lazzari, E. Stat3 pathway is activated in ALK-positive large B-cell lymphoma carrying sqstm1-ALK rearrangement and provides a possible therapeutic target. *Am. J. Surg. Pathol.* **2013**, *37*, 780–786. [[CrossRef](#)] [[PubMed](#)]
66. Onciu, M.; Behm, F.G.; Raimondi, S.C.; Moore, S.; Harwood, E.L.; Pui, C.H.; Sandlund, J.T. ALK-positive anaplastic large cell lymphoma with leukemic peripheral blood involvement is a clinicopathologic entity with an unfavorable prognosis. Report of three cases and review of the literature. *Am. J. Clin. Pathol.* **2003**, *120*, 617–625. [[CrossRef](#)] [[PubMed](#)]
67. De Paepe, P.; Baens, M.; van Krieken, H.; Verhasselt, B.; Stul, M.; Simons, A.; Poppe, B.; Laureys, G.; Brons, P.; Vandenberghe, P.; et al. ALK activation by the cltc-ALK fusion is a recurrent event in large B-cell lymphoma. *Blood* **2003**, *102*, 2638–2641. [[CrossRef](#)] [[PubMed](#)]
68. Van Roosbroeck, K.; Cools, J.; Dierickx, D.; Thomas, J.; Vandenberghe, P.; Stul, M.; Delabie, J.; De Wolf-Peters, C.; Marynen, P.; Wlodarska, I. ALK-positive large B-cell lymphomas with cryptic sec31a-ALK and npm1-ALK fusions. *Haematologica* **2010**, *95*, 509–513. [[CrossRef](#)] [[PubMed](#)]
69. Du, X.L.; Hu, H.; Lin, D.C.; Xia, S.H.; Shen, X.M.; Zhang, Y.; Luo, M.L.; Feng, Y.B.; Cai, Y.; Xu, X.; et al. Proteomic profiling of proteins dysregulated in chinese esophageal squamous cell carcinoma. *J. Mol. Med. (Berl.)* **2007**, *85*, 863–875. [[CrossRef](#)] [[PubMed](#)]
70. Jazii, F.R.; Najafi, Z.; Malekzadeh, R.; Conrads, T.P.; Ziaee, A.A.; Abnet, C.; Yazdznbod, M.; Karkhane, A.A.; Salekdeh, G.H. Identification of squamous cell carcinoma associated proteins by proteomics and loss of  $\beta$  tropomyosin expression in esophageal cancer. *World J. Gastroenterol.* **2006**, *12*, 7104–7112. [[CrossRef](#)] [[PubMed](#)]

71. Takeuchi, K.; Soda, M.; Togashi, Y.; Sugawara, E.; Hatano, S.; Asaka, R.; Okumura, S.; Nakagawa, K.; Mano, H.; Ishikawa, Y. Pulmonary inflammatory myofibroblastic tumor expressing a novel fusion, PPFIBP1-ALK: Reappraisal of anti-ALK immunohistochemistry as a tool for novel ALK fusion identification. *Clin. Cancer Res.* **2011**, *17*, 3341–3348. [[CrossRef](#)] [[PubMed](#)]
72. Bridge, J.A.; Kanamori, M.; Ma, Z.; Pickering, D.; Hill, D.A.; Lydiatt, W.; Lui, M.Y.; Colleoni, G.W.; Antonescu, C.R.; Ladanyi, M.; et al. Fusion of the ALK gene to the clathrin heavy chain gene, CLTC, in inflammatory myofibroblastic tumor. *Am. J. Pathol.* **2001**, *159*, 411–415. [[CrossRef](#)]
73. Debelenko, L.V.; Arthur, D.C.; Pack, S.D.; Helman, L.J.; Schrupp, D.S.; Tsokos, M. Identification of cars-ALK fusion in primary and metastatic lesions of an inflammatory myofibroblastic tumor. *Lab. Investig.* **2003**, *83*, 1255–1265. [[CrossRef](#)] [[PubMed](#)]
74. Panagopoulos, I.; Nilsson, T.; Domanski, H.A.; Isaksson, M.; Lindblom, P.; Mertens, F.; Mandahl, N. Fusion of the sec3111 and ALK genes in an inflammatory myofibroblastic tumor. *Int. J. Cancer* **2006**, *118*, 1181–1186. [[CrossRef](#)] [[PubMed](#)]
75. Lawrence, B.; Perez-Atayde, A.; Hibbard, M.K.; Rubin, B.P.; Dal Cin, P.; Pinkus, J.L.; Pinkus, G.S.; Xiao, S.; Yi, E.S.; Fletcher, C.D.; et al. TPM3-ALK and TPM4-ALK oncogenes in inflammatory myofibroblastic tumors. *Am. J. Pathol.* **2000**, *157*, 377–384. [[CrossRef](#)]
76. Debiec-Rychter, M.; Marynen, P.; Hagemeyer, A.; Pauwels, P. ALK-atic fusion in urinary bladder inflammatory myofibroblastic tumor. *Genes Chromosom. Cancer* **2003**, *38*, 187–190. [[CrossRef](#)] [[PubMed](#)]
77. Ma, Z.; Hill, D.A.; Collins, M.H.; Morris, S.W.; Sumegi, J.; Zhou, M.; Zuppan, C.; Bridge, J.A. Fusion of ALK to the ran-binding protein 2 (RANBP2) gene in inflammatory myofibroblastic tumor. *Genes Chromosom. Cancer* **2003**, *37*, 98–105. [[CrossRef](#)] [[PubMed](#)]
78. Li, J.; Yin, W.H.; Takeuchi, K.; Guan, H.; Huang, Y.H.; Chan, J.K. Inflammatory myofibroblastic tumor with RANBP2 and ALK gene rearrangement: A report of two cases and literature review. *Diagn. Pathol.* **2013**, *8*, 147. [[CrossRef](#)] [[PubMed](#)]
79. Chen, S.T.; Lee, J.C. An inflammatory myofibroblastic tumor in liver with ALK and RANBP2 gene rearrangement: Combination of distinct morphologic, immunohistochemical, and genetic features. *Hum. Pathol.* **2008**, *39*, 1854–1858. [[CrossRef](#)] [[PubMed](#)]
80. Patel, A.S.; Murphy, K.M.; Hawkins, A.L.; Cohen, J.S.; Long, P.P.; Perlman, E.J.; Griffin, C.A. RANBP2 and cltc are involved in ALK rearrangements in inflammatory myofibroblastic tumors. *Cancer Genet. Cytogenet.* **2007**, *176*, 107–114. [[CrossRef](#)] [[PubMed](#)]
81. Jung, Y.; Kim, P.; Keum, J.; Kim, S.N.; Choi, Y.S.; Do, I.G.; Lee, J.; Choi, S.J.; Kim, S.; Lee, J.E.; et al. Discovery of ALK-PTPN3 gene fusion from human non-small cell lung carcinoma cell line using next generation rna sequencing. *Genes Chromosom. Cancer* **2012**, *51*, 590–597. [[CrossRef](#)] [[PubMed](#)]
82. Togashi, Y.; Soda, M.; Sakata, S.; Sugawara, E.; Hatano, S.; Asaka, R.; Nakajima, T.; Mano, H.; Takeuchi, K. KLC1-ALK: A novel fusion in lung cancer identified using a formalin-fixed paraffin-embedded tissue only. *PLoS ONE* **2012**, *7*, e31323. [[CrossRef](#)] [[PubMed](#)]
83. Takeuchi, K.; Choi, Y.L.; Togashi, Y.; Soda, M.; Hatano, S.; Inamura, K.; Takada, S.; Ueno, T.; Yamashita, Y.; Satoh, Y.; et al. KIF5B-ALK, a novel fusion oncokinas identified by an immunohistochemistry-based diagnostic system for ALK-positive lung cancer. *Clin. Cancer Res.* **2009**, *15*, 3143–3149. [[CrossRef](#)] [[PubMed](#)]
84. Choi, Y.L.; Lira, M.E.; Hong, M.; Kim, R.N.; Choi, S.J.; Song, J.Y.; Pandey, K.; Mann, D.L.; Stahl, J.A.; Peckham, H.E.; et al. A novel fusion of tpr and ALK in lung adenocarcinoma. *J. Thorac. Oncol.* **2014**, *9*, 563–566. [[CrossRef](#)] [[PubMed](#)]
85. Ren, H.; Tan, Z.P.; Zhu, X.; Crosby, K.; Haack, H.; Ren, J.M.; Beausoleil, S.; Moritz, A.; Innocenti, G.; Rush, J.; et al. Identification of anaplastic lymphoma kinase as a potential therapeutic target in ovarian cancer. *Cancer Res.* **2012**, *72*, 3312–3323. [[CrossRef](#)] [[PubMed](#)]
86. Kusano, H.; Togashi, Y.; Akiba, J.; Moriya, F.; Baba, K.; Matsuzaki, N.; Yuba, Y.; Shiraishi, Y.; Kanamaru, H.; Kuroda, N.; et al. Two cases of renal cell carcinoma harboring a novel STRN-ALK fusion gene. *Am. J. Surg. Pathol.* **2016**, *40*, 761–769. [[CrossRef](#)] [[PubMed](#)]
87. Sugawara, E.; Togashi, Y.; Kuroda, N.; Sakata, S.; Hatano, S.; Asaka, R.; Yuasa, T.; Yonese, J.; Kitagawa, M.; Mano, H.; et al. Identification of anaplastic lymphoma kinase fusions in renal cancer: Large-scale immunohistochemical screening by the intercalated antibody-enhanced polymer method. *Cancer* **2012**, *118*, 4427–4436. [[CrossRef](#)] [[PubMed](#)]



88. Debelenko, L.V.; Raimondi, S.C.; Daw, N.; Shivakumar, B.R.; Huang, D.; Nelson, M.; Bridge, J.A. Renal cell carcinoma with novel VCL-ALK fusion: New representative of ALK-associated tumor spectrum. *Mod. Pathol.* **2011**, *24*, 430–442. [[CrossRef](#)] [[PubMed](#)]
89. Sukov, W.R.; Hodge, J.C.; Lohse, C.M.; Akre, M.K.; Leibovich, B.C.; Thompson, R.H.; Chevillat, J.C. ALK alterations in adult renal cell carcinoma: Frequency, clinicopathologic features and outcome in a large series of consecutively treated patients. *Mod. Pathol.* **2012**, *25*, 1516–1525. [[CrossRef](#)] [[PubMed](#)]
90. Marino-Enriquez, A.; Ou, W.B.; Weldon, C.B.; Fletcher, J.A.; Perez-Atayde, A.R. ALK rearrangement in sickle cell trait-associated renal medullary carcinoma. *Genes Chromosom. Cancer* **2011**, *50*, 146–153. [[CrossRef](#)] [[PubMed](#)]
91. Armstrong, F.; Duplantier, M.M.; Trempat, P.; Hieblot, C.; Lamant, L.; Espinos, E.; Racaud-Sultan, C.; Allouche, M.; Campo, E.; Delsol, G.; et al. Differential effects of X-ALK fusion proteins on proliferation, transformation, and invasion properties of NIH3T3 cells. *Oncogene* **2004**, *23*, 6071–6082. [[CrossRef](#)] [[PubMed](#)]
92. Armstrong, F.; Lamant, L.; Hieblot, C.; Delsol, G.; Touriol, C. TPM3-ALK expression induces changes in cytoskeleton organisation and confers higher metastatic capacities than other ALK fusion proteins. *Eur. J. Cancer* **2007**, *43*, 640–646. [[CrossRef](#)] [[PubMed](#)]
93. Marino-Enriquez, A.; Dal Cin, P. ALK as a paradigm of oncogenic promiscuity: Different mechanisms of activation and different fusion partners drive tumors of different lineages. *Cancer Genet.* **2013**, *206*, 357–373. [[CrossRef](#)] [[PubMed](#)]
94. De Brouwer, S.; De Preter, K.; Kumps, C.; Zabrocki, P.; Porcu, M.; Westerhout, E.M.; Lakeman, A.; Vandesompele, J.; Hoebeeck, J.; Van Maerken, T.; et al. Meta-analysis of neuroblastomas reveals a skewed ALK mutation spectrum in tumors with mycn amplification. *Clin. Cancer Res.* **2010**, *16*, 4353–4362. [[CrossRef](#)] [[PubMed](#)]
95. Chen, Y.; Takita, J.; Choi, Y.L.; Kato, M.; Ohira, M.; Sanada, M.; Wang, L.; Soda, M.; Kikuchi, A.; Igarashi, T.; et al. Oncogenic mutations of ALK kinase in neuroblastoma. *Nature* **2008**, *455*, 971–974. [[CrossRef](#)] [[PubMed](#)]
96. Schonherr, C.; Ruuth, K.; Eriksson, T.; Yamazaki, Y.; Ottmann, C.; Combaret, V.; Vigny, M.; Kamaraj, S.; Palmer, R.H.; Hallberg, B. The neuroblastoma ALK(I1250T) mutation is a kinase-dead RTK in vitro and in vivo. *Transl. Oncol.* **2011**, *4*, 258–265. [[CrossRef](#)] [[PubMed](#)]
97. Chand, D.; Yamazaki, Y.; Ruuth, K.; Schonherr, C.; Martinsson, T.; Kogner, P.; Attiyeh, E.F.; Maris, J.; Morozova, O.; Marra, M.A.; et al. Cell culture and drosophila model systems define three classes of anaplastic lymphoma kinase mutations in neuroblastoma. *Dis. Models Mech.* **2013**, *6*, 373–382. [[CrossRef](#)] [[PubMed](#)]
98. Zou, H.Y.; Li, Q.; Lee, J.H.; Arango, M.E.; McDonnell, S.R.; Yamazaki, S.; Koudriakova, T.B.; Alton, G.; Cui, J.J.; Kung, P.P.; et al. An orally available small-molecule inhibitor of c-Met, PF-2341066, exhibits cytoreductive antitumor efficacy through antiproliferative and antiangiogenic mechanisms. *Cancer Res.* **2007**, *67*, 4408–4417. [[CrossRef](#)] [[PubMed](#)]
99. Cui, J.J.; Tran-Dube, M.; Shen, H.; Nambu, M.; Kung, P.P.; Pairish, M.; Jia, L.; Meng, J.; Funk, L.; Botrous, I.; et al. Structure based drug design of crizotinib (PF-02341066), a potent and selective dual inhibitor of mesenchymal-epithelial transition factor (c-Met) kinase and anaplastic lymphoma kinase (ALK). *J. Med. Chem.* **2011**, *54*, 6342–6363. [[CrossRef](#)] [[PubMed](#)]
100. Christensen, J.G.; Zou, H.Y.; Arango, M.E.; Li, Q.; Lee, J.H.; McDonnell, S.R.; Yamazaki, S.; Alton, G.R.; Mroczkowski, B.; Los, G. Cytoreductive antitumor activity of PF-2341066, a novel inhibitor of anaplastic lymphoma kinase and c-Met, in experimental models of anaplastic large-cell lymphoma. *Mol. Cancer Ther.* **2007**, *6*, 3314–3322. [[CrossRef](#)] [[PubMed](#)]
101. Kwak, E.L.; Bang, Y.J.; Camidge, D.R.; Shaw, A.T.; Solomon, B.; Maki, R.G.; Ou, S.H.; Dezube, B.J.; Janne, P.A.; Costa, D.B.; et al. Anaplastic lymphoma kinase inhibition in non-small-cell lung cancer. *N. Engl. J. Med.* **2010**, *363*, 1693–1703. [[CrossRef](#)] [[PubMed](#)]
102. Blackhall, F.; Ross Camidge, D.; Shaw, A.T.; Soria, J.C.; Solomon, B.J.; Mok, T.; Hirsh, V.; Janne, P.A.; Shi, Y.; Yang, P.C.; et al. Final results of the large-scale multinational trial profile 1005: Efficacy and safety of crizotinib in previously treated patients with advanced/metastatic ALK-positive non-small-cell lung cancer. *ESMO Open* **2017**, *2*, e000219. [[CrossRef](#)] [[PubMed](#)]
103. Gambacorti-Passerini, C.; Messa, C.; Pogliani, E.M. Crizotinib in anaplastic large-cell lymphoma. *N. Engl. J. Med.* **2011**, *364*, 775–776. [[CrossRef](#)] [[PubMed](#)]

104. Gambacorti-Passerini, C.; Orlov, S.; Zhang, L.; Braiteh, F.; Huang, H.; Esaki, T.; Horibe, K.; Ahn, J.S.; Beck, J.T.; Edenfield, W.J.; et al. Long-term effects of crizotinib in ALK-positive tumors (excluding NSCLC): A phase 1b open-label study. *Am. J. Hematol.* **2018**. [[CrossRef](#)] [[PubMed](#)]
105. Mosse, Y.P.; Lim, M.S.; Voss, S.D.; Wilner, K.; Ruffner, K.; Laliberte, J.; Rolland, D.; Balis, F.M.; Maris, J.M.; Weigel, B.J.; et al. Safety and activity of crizotinib for paediatric patients with refractory solid tumours or anaplastic large-cell lymphoma: A children's oncology group phase 1 consortium study. *Lancet Oncol.* **2013**, *14*, 472–480. [[CrossRef](#)]
106. Marsilje, T.H.; Pei, W.; Chen, B.; Lu, W.; Uno, T.; Jin, Y.; Jiang, T.; Kim, S.; Li, N.; Warmuth, M.; et al. Synthesis, structure-activity relationships, and in vivo efficacy of the novel potent and selective anaplastic lymphoma kinase (ALK) inhibitor 5-chloro-n2-(2-isopropoxy-5-methyl-4-(piperidin-4-yl)phenyl)-n4-(2-(isopropylsulfonyl)phenyl)pyrimidine-2,4-diamine (LDK378) currently in phase 1 and phase 2 clinical trials. *J. Med. Chem.* **2013**, *56*, 5675–5690. [[PubMed](#)]
107. Friboulet, L.; Li, N.; Katayama, R.; Lee, C.C.; Gainor, J.F.; Crystal, A.S.; Michellys, P.Y.; Awad, M.M.; Yanagitani, N.; Kim, S.; et al. The ALK inhibitor ceritinib overcomes crizotinib resistance in non-small cell lung cancer. *Cancer Discov.* **2014**, *4*, 662–673. [[CrossRef](#)] [[PubMed](#)]
108. Galkin, A.V.; Melnick, J.S.; Kim, S.; Hood, T.L.; Li, N.; Li, L.; Xia, G.; Steensma, R.; Chopiuk, G.; Jiang, J.; et al. Identification of NVP-TAE684, a potent, selective, and efficacious inhibitor of nrm-ALK. *Proc. Natl. Acad. Sci. USA* **2007**, *104*, 270–275. [[CrossRef](#)] [[PubMed](#)]
109. Mok, T.; Spigel, D.; Felip, E.; de Marinis, F.; Ahn, M.J.; Groen, H.J.M.; Wakelee, H.A.; Hida, T.; Crino, L.; Nishio, M.; et al. Ascend-2: A single-arm, open-label, multicenter phase II study of ceritinib in adult patients (PTS) with ALK-rearranged (ALK plus) non-small cell lung cancer (NSCLC) previously treated with chemotherapy and crizotinib (CRZ). *J. Clin. Oncol.* **2015**, *33*. [[CrossRef](#)]
110. Felip, E.; Orlov, S.; Park, K.; Yu, C.J.; Tsai, C.M.; Nishio, M.; Dols, M.C.; McKeage, M.J.; Su, W.C.; Mok, T.; et al. Ascend-3: A single-arm, open-label, multicenter phase ii study of ceritinib in ALKi-naive adult patients (PTS) with ALK-rearranged (ALK plus) non-small cell lung cancer (NSCLC). *J. Clin. Oncol.* **2015**, *33*. [[CrossRef](#)]
111. Soria, J.C.; Tan, D.S.W.; Chiari, R.; Wu, Y.L.; Paz-Ares, L.; Wolf, J.; Geater, S.L.; Orlov, S.; Cortinovis, D.; Yu, C.J.; et al. First-line ceritinib versus platinum-based chemotherapy in advanced ALK-rearranged non-small-cell lung cancer (ascend-4): A randomised, open-label, phase 3 study. *Lancet* **2017**, *389*, 917–929. [[CrossRef](#)]
112. Novartis. Novartis Receives FDA Approval for Expanded Use of Zykadia® in First-Line ALK-Positive Metastatic Non-Small Cell Lung Cancer (NSCLC). Available online: <https://www.novartis.com/news/media-releases/novartis-receives-fda-approval-expanded-use-zykadiar-first-line-ALK-positive> (accessed on 12 December 2017).
113. Cho, B.C.; Kim, D.W.; Bearz, A.; Laurie, S.A.; McKeage, M.; Borra, G.; Park, K.; Kim, S.W.; Ghosn, M.; Ardizzoni, A.; et al. Ascend-8: A randomized phase 1 study of ceritinib, 450 mg or 600 mg, taken with a low-fat meal versus 750 mg in fasted state in patients with anaplastic lymphoma kinase (ALK)-rearranged metastatic non-small cell lung cancer (NSCLC). *J. Thorac. Oncol.* **2017**, *12*, 1357–1367. [[CrossRef](#)] [[PubMed](#)]
114. Kinoshita, K.; Asoh, K.; Furuichi, N.; Ito, T.; Kawada, H.; Hara, S.; Ohwada, J.; Miyagi, T.; Kobayashi, T.; Takanashi, K.; et al. Design and synthesis of a highly selective, orally active and potent anaplastic lymphoma kinase inhibitor (ch5424802). *Bioorg. Med. Chem.* **2012**, *20*, 1271–1280. [[CrossRef](#)] [[PubMed](#)]
115. Sakamoto, H.; Tsukaguchi, T.; Hiroshima, S.; Kodama, T.; Kobayashi, T.; Fukami, T.A.; Oikawa, N.; Tsukuda, T.; Ishii, N.; Aoki, Y. Ch5424802, a selective ALK inhibitor capable of blocking the resistant gatekeeper mutant. *Cancer Cell* **2011**, *19*, 679–690. [[CrossRef](#)] [[PubMed](#)]
116. Seto, T.; Kiura, K.; Nishio, M.; Nakagawa, K.; Maemondo, M.; Inoue, A.; Hida, T.; Yamamoto, N.; Yoshioka, H.; Harada, M.; et al. Ch5424802 (RO5424802) for patients with ALK-rearranged advanced non-small-cell lung cancer (AF-001jp study): A single-arm, open-label, phase 1-2 study. *Lancet Oncol.* **2013**, *14*, 590–598. [[CrossRef](#)]
117. Tamura, T.; Seto, T.; Nakagawa, K.; Maemondo, M.; Inoue, A.; Hida, T.; Yoshioka, H.; Harada, M.; Ohe, Y.; Nogami, N.; et al. Updated data of a phase 1/2 study (AF-001jp) of alectinib, a CNS-penetrant, highly selective ALK inhibitor in ALK-rearranged advanced NSCLC. *Int. J. Radiat. Oncol.* **2014**, *90*, S6. [[CrossRef](#)]
118. Kodama, T.; Tsukaguchi, T.; Yoshida, M.; Kondoh, O.; Sakamoto, H. Selective ALK inhibitor alectinib with potent antitumor activity in models of crizotinib resistance. *Cancer Lett.* **2014**, *351*, 215–221. [[CrossRef](#)] [[PubMed](#)]

119. Katayama, R.; Friboulet, L.; Koike, S.; Lockerman, E.L.; Khan, T.M.; Gainor, J.F.; Iafrate, A.J.; Takeuchi, K.; Taiji, M.; Okuno, Y.; et al. Two novel ALK mutations mediate acquired resistance to the next-generation ALK inhibitor alectinib. *Clin. Cancer Res.* **2014**, *20*, 5686–5696. [[CrossRef](#)] [[PubMed](#)]
120. Wu, J.; Savooji, J.; Liu, D. Second- and third-generation ALK inhibitors for non-small cell lung cancer. *J. Hematol. Oncol.* **2016**, *9*, 19. [[CrossRef](#)] [[PubMed](#)]
121. Huang, W.S.; Liu, S.; Zou, D.; Thomas, M.; Wang, Y.; Zhou, T.; Romero, J.; Kohlmann, A.; Li, F.; Qi, J.; et al. Discovery of brigatinib (ap26113), a phosphine oxide-containing, potent, orally active inhibitor of anaplastic lymphoma kinase. *J. Med. Chem.* **2016**, *59*, 4948–4964. [[CrossRef](#)] [[PubMed](#)]
122. Zhang, S.; Anjum, R.; Squillace, R.; Nadworny, S.; Zhou, T.; Keats, J.; Ning, Y.; Wardwell, S.D.; Miller, D.; Song, Y.; et al. The potent ALK inhibitor ap26113 can overcome mechanisms of resistance to first- and second-generation ALK TKIs in preclinical models. *Clin. Cancer Res.* **2015**. [[CrossRef](#)]
123. Fontana, D.; Ceccon, M.; Gambacorti-Passerini, C.; Mologni, L. Activity of second-generation ALK inhibitors against crizotinib-resistant mutants in an npm-ALK model compared to EML4-ALK. *Cancer Med.* **2015**, *4*, 953–965. [[CrossRef](#)] [[PubMed](#)]
124. Zhang, S.; Anjum, R.; Squillace, R.; Nadworny, S.; Zhou, T.; Keats, J.; Ning, Y.; Wardwell, S.D.; Miller, D.; Song, Y.; et al. The potent ALK inhibitor brigatinib (ap26113) overcomes mechanisms of resistance to first- and second-generation ALK inhibitors in preclinical models. *Clin. Cancer Res.* **2016**, *22*, 5527–5538. [[CrossRef](#)] [[PubMed](#)]
125. Gettinger, S.N.; Bazhenova, L.A.; Langer, C.J.; Salgia, R.; Gold, K.A.; Rosell, R.; Shaw, A.T.; Weiss, G.J.; Tugnait, M.; Narasimhan, N.I.; et al. Activity and safety of brigatinib in ALK-rearranged non-small-cell lung cancer and other malignancies: A single-arm, open-label, phase 1/2 trial. *Lancet Oncol.* **2016**, *17*, 1683–1696. [[CrossRef](#)]
126. Staff, N. FDA grants brigatinib accelerated approval for metastatic non-small cell lung cancer. In *FDA Grants Brigatinib Accelerated Approval for Metastatic Non-Small Cell Lung Cancer*; National Cancer Institute: Rockville, MD, USA, 2017; Volume 2017.
127. Johnson, T.W.; Richardson, P.F.; Bailey, S.; Brooun, A.; Burke, B.J.; Collins, M.R.; Cui, J.J.; Deal, J.G.; Deng, Y.L.; Dinh, D.; et al. Discovery of (10R)-7-Amino-12-fluoro-2,10,16-trimethyl-15-oxo-10,15,16,17-tetrahydro-2H-8,4-(metheno)pyrazolo[4,3-h][2,5,11]-benzoxadiazacyclotetradecine-3-carbonitrile (PF-06463922), a macrocyclic inhibitor of anaplastic lymphoma kinase (ALK) and c-ros oncogene 1 (ros1) with preclinical brain exposure and broad-spectrum potency against ALK-resistant mutations. *J. Med. Chem.* **2014**, *57*, 4720–4744. [[PubMed](#)]
128. Zou, H.Y.; Friboulet, L.; Kodack, D.P.; Engstrom, L.D.; Li, Q.; West, M.; Tang, R.W.; Wang, H.; Tsaparikos, K.; Wang, J.; et al. PF-06463922, an ALK/ROS1 inhibitor, overcomes resistance to first and second generation ALK inhibitors in preclinical models. *Cancer Cell* **2015**, *28*, 70–81. [[CrossRef](#)] [[PubMed](#)]
129. Gainor, J.F.; Dardaei, L.; Yoda, S.; Friboulet, L.; Leshchiner, I.; Katayama, R.; Dagogo-Jack, I.; Gadgeel, S.; Schultz, K.; Singh, M.; et al. Molecular mechanisms of resistance to first- and second-generation ALK inhibitors in ALK-rearranged lung cancer. *Cancer Discov.* **2016**, *6*, 1118–1133. [[CrossRef](#)] [[PubMed](#)]
130. Lin, J.J.; Kennedy, E.; Sequist, L.V.; Brastianos, P.K.; Goodwin, K.E.; Stevens, S.; Wanat, A.C.; Stober, L.L.; Digumarthy, S.R.; Engelman, J.A.; et al. Clinical activity of alectinib in advanced ret-rearranged non-small cell lung cancer. *J. Thorac. Oncol.* **2016**, *11*, 2027–2032. [[CrossRef](#)] [[PubMed](#)]
131. Zhang, S.; Wang, F.; Keats, J.; Ning, Y.; Wardwell, S.D.; Moran, L.; Mohemmad, Q.K.; Anjum, R.; Wang, Y.; Zhu, X.; et al. Ap26113, a potent ALK inhibitor, overcomes mutations in EML4ALK that confer resistance to PF-02341066 (PF1066). *Cancer Res.* **2014**. [[CrossRef](#)]
132. Squillace, R.M.; Anjum, R.; Miller, D.; Vodala, S.; Moran, L.; Wang, F.; Clackson, T.; Garner, A.P.; Rivera, V.M. Ap26113 possesses pan-inhibitory activity versus crizotinib-resistant ALK mutants and oncogenic ROS1 fusions. *Cancer Res.* **2014**. [[CrossRef](#)]
133. Kim, D.W.; Tiseo, M.; Ahn, M.J.; Reckamp, K.L.; Holmskov Hansen, K.; Kim, S.W.; Huber, R.M.; West, H.J.; Groen, H.J.; Hochmair, M.J.; et al. Brigatinib (BRG) in patients (PTS) with crizotinib (CRZ)-refractory ALK+ non-small cell lung cancer (NSCLC): First report of efficacy and safety from a pivotal randomized phase (PH) 2 trial ( $\alpha$ ). *Clin. Oncol.* **2016**, *34*. [[CrossRef](#)]

134. Zou, H.Y.; Li, Q.; Engstrom, L.D.; West, M.; Appleman, V.; Wong, K.A.; McTigue, M.; Deng, Y.L.; Liu, W.; Brooun, A.; et al. PF-06463922 is a potent and selective next-generation ROS1/ALK inhibitor capable of blocking crizotinib-resistant ROS1 mutations. *Proc. Natl. Acad. Sci. USA* **2015**, *112*, 3493–3498. [[CrossRef](#)] [[PubMed](#)]
135. Shaw, A.T.; Ou, S.H.; Felip, E.; Bauer, T.M.; Besse, B.; Gadgeel, S.M.; Camidge, D.R.; Lin, C.C.; Seto, T.; Soo, R.A.; et al. Efficacy and safety of lorlatinib in patients (PTS) with ALK+ non-small cell lung cancer (NSCLC) with one or more prior ALK tyrosine kinase inhibitor (TKI): A phase I/II study. *J. Clin. Oncol.* **2017**. [[CrossRef](#)]
136. Solomon, B.; Shaw, A.; Ou, S.; Besse, B.; Felip, E.; Bauer, T.; Soo, R.; Bearz, A.; Lin, C.; Clancy, J.; et al. Oa 05.06 phase 2 study of lorlatinib in patients with advanced ALK+/ROS1+ non-small- cell lung cancer. *J. Thorac. Oncol.* **2017**, *12*, S1756. [[CrossRef](#)]
137. Ardini, E.; Menichincheri, M.; Banfi, P.; Bosotti, R.; De Ponti, C.; Pulci, R.; Ballinari, D.; Ciomei, M.; Texido, G.; Degrassi, A.; et al. Entrectinib, a PAN-TRK, ROS1, and ALK inhibitor with activity in multiple molecularly defined cancer indications. *Mol. Cancer Ther.* **2016**, *15*, 628–639. [[CrossRef](#)] [[PubMed](#)]
138. Drilon, A.; Siena, S.; Ou, S.I.; Patel, M.; Ahn, M.J.; Lee, J.; Bauer, T.M.; Farago, A.F.; Wheler, J.J.; Liu, S.V.; et al. Safety and antitumor activity of the multitargeted PAN-TRK, ROS1, and ALK inhibitor entrectinib: Combined results from two phase I trials (ALKa-372-001 and startrk-1). *Cancer Discov.* **2017**, *7*, 400–409. [[CrossRef](#)] [[PubMed](#)]
139. Mori, M.; Ueno, Y.; Konagai, S.; Fushiki, H.; Shimada, I.; Kondoh, Y.; Saito, R.; Mori, K.; Shindou, N.; Soga, T.; et al. The selective anaplastic lymphoma receptor tyrosine kinase inhibitor asp3026 induces tumor regression and prolongs survival in non-small cell lung cancer model mice. *Mol. Cancer Ther.* **2014**, *13*, 329–340. [[CrossRef](#)] [[PubMed](#)]
140. George, S.K.; Vishwamitra, D.; Manshoury, R.; Shi, P.; Amin, H.M. The ALK inhibitor asp3026 eradicates NPM-ALK(+) T-cell anaplastic large-cell lymphoma in vitro and in a systemic xenograft lymphoma model. *Oncotarget* **2014**, *5*, 5750–5763. [[CrossRef](#)] [[PubMed](#)]
141. Li, T.; LoRusso, P.; Maitland, M.L.; Ou, S.H.; Bahceci, E.; Ball, H.A.; Park, J.W.; Yuen, G.; Tolcher, A. First-in-human, open-label dose-escalation and dose-expansion study of the safety, pharmacokinetics, and antitumor effects of an oral ALK inhibitor asp3026 in patients with advanced solid tumors. *J. Hematol. Oncol.* **2016**, *9*, 23. [[CrossRef](#)] [[PubMed](#)]
142. Lovly, C.M.; Heuckmann, J.M.; de Stanchina, E.; Chen, H.; Thomas, R.K.; Liang, C.; Pao, W. Insights into ALK-driven cancers revealed through development of novel ALK tyrosine kinase inhibitors. *Cancer Res.* **2011**, *71*, 4920–4931. [[CrossRef](#)] [[PubMed](#)]
143. Reckamp, K.L.; Infante, J.R.; Blumenschein, G.R.; Wakelee, H.; Carter, C.A.; Gockerman, J.P.; Lovly, C.; Dukart, G.; Harrow, K.; Liang, C.; et al. Phase I/II trial of x-396, a novel anaplastic lymphoma kinase (ALK) inhibitor, in patients with ALK+ non-small cell lung cancer (NSCLC). *J. Thorac. Oncol.* **2016**, *11*, S36–S37. [[CrossRef](#)]
144. Cheng, M.; Quail, M.R.; Gingrich, D.E.; Ott, G.R.; Lu, L.; Wan, W.; Albom, M.S.; Angeles, T.S.; Aimone, L.D.; Cristofani, F.; et al. Cep-28122, a highly potent and selective orally active inhibitor of anaplastic lymphoma kinase with antitumor activity in experimental models of human cancers. *Mol. Cancer Ther.* **2012**, *11*, 670–679. [[CrossRef](#)] [[PubMed](#)]
145. Arkenau, H.T.; Sachdev, J.C.; Mita, M.M.; Dziadziuszko, R.; Lin, C.C.; Yang, J.C.; Infante, J.R.; Anthony, S.P.; Voskoboinik, M.; Su, W.C.; et al. Phase (PH) 1/2a study of TSR-011, a potent inhibitor of ALK and TRK, in advanced solid tumors including crizotinib-resistant ALK positive non-small cell lung cancer. *J. Clin. Oncol.* **2015**. [[CrossRef](#)]
146. Gettinger, S.N.; Zhang, S.; Hodgson, J.G.; Bazhenova, L.; Burgers, S.; Kim, D.W.; Tan, D.S.; Koh, H.A.; Ho, J.C.; Viteri Ramirez, S.; et al. Activity of brigatinib (BRG) in crizotinib (CRZ) resistant patients (PTS) according to ALK mutation status. *J. Clin. Oncol.* **2016**, *34*. [[CrossRef](#)]
147. Gainor, J.F.; Chi, A.S.; Logan, J.; Hu, R.; Oh, K.S.; Brastianos, P.K.; Shih, H.A.; Shaw, A.T. Alectinib dose escalation reinduces central nervous system responses in patients with anaplastic lymphoma kinase-positive non-small cell lung cancer relapsing on standard dose alectinib. *J. Thorac. Oncol.* **2016**, *11*, 256–260. [[CrossRef](#)] [[PubMed](#)]

148. Choi, Y.L.; Soda, M.; Yamashita, Y.; Ueno, T.; Takashima, J.; Nakajima, T.; Yatabe, Y.; Takeuchi, K.; Hamada, T.; Haruta, H.; et al. EML4-ALK mutations in lung cancer that confer resistance to ALK inhibitors. *N. Engl. J. Med.* **2010**, *363*, 1734–1739. [[CrossRef](#)] [[PubMed](#)]
149. Zuccotto, F.; Ardini, E.; Casale, E.; Angiolini, M. Through the “gatekeeper door”: Exploiting the active kinase conformation. *J. Med. Chem.* **2010**, *53*, 2681–2694. [[CrossRef](#)] [[PubMed](#)]
150. Azam, M.; Seeliger, M.A.; Gray, N.S.; Kuriyan, J.; Daley, G.Q. Activation of tyrosine kinases by mutation of the gatekeeper threonine. *Nat. Struct. Mol. Biol.* **2008**, *15*, 1109–1118. [[CrossRef](#)] [[PubMed](#)]
151. Sun, H.Y.; Ji, F.Q. A molecular dynamics investigation on the crizotinib resistance mechanism of C1156Y mutation in ALK. *Biochem. Biophys. Res. Commun.* **2012**, *423*, 319–324. [[CrossRef](#)] [[PubMed](#)]
152. Ceccon, M.; Mologni, L.; Bisson, W.; Scapozza, L.; Gambacorti-Passerini, C. Crizotinib-resistant npm-ALK mutants confer differential sensitivity to unrelated ALK inhibitors. *Mol. Cancer Res. MCR* **2013**, *11*, 122–132. [[CrossRef](#)] [[PubMed](#)]
153. Sasaki, T.; Okuda, K.; Zheng, W.; Butrynski, J.; Capelletti, M.; Wang, L.; Gray, N.S.; Wilner, K.; Christensen, J.G.; Demetri, G.; et al. The neuroblastoma-associated f1174l ALK mutation causes resistance to an ALK kinase inhibitor in ALK-translocated cancers. *Cancer Res.* **2010**, *70*, 10038–10043. [[CrossRef](#)] [[PubMed](#)]
154. Bresler, S.C.; Wood, A.C.; Haglund, E.A.; Courtright, J.; Belcastro, L.T.; Plegaria, J.S.; Cole, K.; Toporovskaya, Y.; Zhao, H.; Carpenter, E.L.; et al. Differential inhibitor sensitivity of anaplastic lymphoma kinase variants found in neuroblastoma. *Sci. Transl. Med.* **2011**, *3*, 108ra114. [[CrossRef](#)] [[PubMed](#)]
155. Ou, S.H.; Klempner, S.J.; Greenbowe, J.R.; Azada, M.; Schrock, A.B.; Ali, S.M.; Ross, J.S.; Stephens, P.J.; Miller, V.A. Identification of a novel hip1-ALK fusion variant in non-small-cell lung cancer (NSCLC) and discovery of ALKI1171 (I1171N/S) mutations in two ALK-rearranged NSCLC patients with resistance to alectinib. *J. Thorac. Oncol.* **2014**, *9*, 1821–1825. [[CrossRef](#)] [[PubMed](#)]
156. Sasaki, T.; Koivunen, J.; Ogino, A.; Yanagita, M.; Nikiforow, S.; Zheng, W.; Lathan, C.; Marcoux, J.P.; Du, J.; Okuda, K.; et al. A novel ALK secondary mutation and egfr signaling cause resistance to ALK kinase inhibitors. *Cancer Res.* **2011**, *71*, 6051–6060. [[CrossRef](#)] [[PubMed](#)]
157. Bossi, R.T.; Saccardo, M.B.; Ardini, E.; Menichincheri, M.; Rusconi, L.; Magnaghi, P.; Orsini, P.; Avanzi, N.; Borgia, A.L.; Nesi, M.; et al. Crystal structures of anaplastic lymphoma kinase in complex with atp competitive inhibitors. *Biochemistry* **2010**, *49*, 6813–6825. [[CrossRef](#)] [[PubMed](#)]
158. Katayama, R.; Shaw, A.T.; Khan, T.M.; Mino-Kenudson, M.; Solomon, B.J.; Halmos, B.; Jessop, N.A.; Wain, J.C.; Yeo, A.T.; Benes, C.; et al. Mechanisms of acquired crizotinib resistance in ALK-rearranged lung cancers. *Sci. Transl. Med.* **2012**, *4*, 120ra117. [[CrossRef](#)] [[PubMed](#)]
159. Doebele, R.C.; Pilling, A.B.; Aisner, D.L.; Kutateladze, T.G.; Le, A.T.; Weickhardt, A.J.; Kondo, K.L.; Linderman, D.J.; Heasley, L.E.; Franklin, W.A.; et al. Mechanisms of resistance to crizotinib in patients with ALK gene rearranged non-small cell lung cancer. *Clin. Cancer Res.* **2012**, *18*, 1472–1482. [[CrossRef](#)] [[PubMed](#)]
160. Toyokawa, G.; Inamasu, E.; Shimamatsu, S.; Yoshida, T.; Nosaki, K.; Hirai, F.; Yamaguchi, M.; Seto, T.; Takenoyama, M.; Ichinose, Y. Identification of a novel ALKG1123S mutation in a patient with ALK-rearranged non-small-cell lung cancer exhibiting resistance to ceritinib. *J. Thorac. Oncol.* **2015**, *10*, e55–e57. [[CrossRef](#)] [[PubMed](#)]
161. Ou, S.-H.I.; Schrock, A.B.; Gowen, K.; Stephens, P.J.; Ross, J.S.; Johnson, M.L.; Lovly, C.M.; Ali, S.M.; Miller, V.A.; Shaw, A.T. Association of ALK resistance mutations by EML4-ALK variant (V3 vs. Non-V3) in ALK+ non-small cell lung cancer (NSCLC). *J. Clin. Oncol.* **2017**, *35*, 9010. [[CrossRef](#)]
162. Heuckmann, J.M.; Holzel, M.; Sos, M.L.; Heynck, S.; Balke-Want, H.; Koker, M.; Peifer, M.; Weiss, J.; Lovly, C.M.; Grutter, C.; et al. ALK mutations conferring differential resistance to structurally diverse ALK inhibitors. *Clin. Cancer Res.* **2011**, *17*, 7394–7401. [[CrossRef](#)] [[PubMed](#)]
163. Michels, S.Y.F.; Scheel, A.H.; Wündisch, T.; Heuckmann, J.M.; Menon, R.; Puesken, M.; Kobe, C.; Pasternack, H.; Heydt, C.; Scheffler, M.; et al. ALKG1269A mutation as a potential mechanism of acquired resistance to crizotinib in an ALK-rearranged inflammatory myofibroblastic tumor. *Precis. Oncol.* **2017**, *1*, 4. [[CrossRef](#)]
164. Wang, H.Y.; Ho, C.C.; Shih, J.Y. Multiple acquired resistance mutations of the ALK tyrosine kinase domain after sequential use of ALK inhibitors. *J. Thorac. Oncol.* **2017**, *12*, e49–e51. [[CrossRef](#)] [[PubMed](#)]

165. Katayama, R.; Sakashita, T.; Yanagitani, N.; Ninomiya, H.; Horiike, A.; Friboulet, L.; Gainor, J.F.; Motoi, N.; Dobashi, A.; Sakata, S.; et al. P-glycoprotein mediates ceritinib resistance in anaplastic lymphoma kinase-rearranged non-small cell lung cancer. *eBioMedicine* **2016**, *3*, 54–66. [[CrossRef](#)] [[PubMed](#)]
166. Ceccon, M.; Mologni, L.; Giudici, G.; Piazza, R.; Pirola, A.; Fontana, D.; Gambacorti-Passerini, C. Treatment efficacy and resistance mechanisms using the second-generation ALK inhibitor ap26113 in human npm-ALK-positive anaplastic large cell lymphoma. *Mol. Cancer Res. MCR* **2015**, *13*, 775–783. [[CrossRef](#)] [[PubMed](#)]
167. Bazhenova, L.; Hodgson, J.G.; Langer, C.J.; Simon, G.R.; Gettinger, S.N.; Ou, S.-H.I.; Reckamp, K.L.; West, H.J.; Chiappori, A.; Koh, H.A.; et al. Activity of brigatinib (BRG) in crizotinib (CRZ)-resistant ALK+ NSCLC patients (PTS) according to ALK plasma mutation status. *J. Clin. Oncol.* **2017**, *35*, 9065.
168. Tchekmedyian, N.; Ali, S.M.; Miller, V.A.; Haura, E.B. Acquired ALK I1152r mutation confers resistance to ceritinib and predicts response to alectinib. *J. Thorac. Oncol.* **2016**, *11*, e87–e88. [[CrossRef](#)] [[PubMed](#)]
169. Ignatius Ou, S.H.; Azada, M.; Hsiang, D.J.; Herman, J.M.; Kain, T.S.; Siwak-Tapp, C.; Casey, C.; He, J.; Ali, S.M.; Klempner, S.J.; et al. Next-generation sequencing reveals a novel NSCLCALK f1174v mutation and confirms ALKG1202R mutation confers high-level resistance to alectinib (ch5424802/ro5424802) in ALK-rearranged NSCLC patients who progressed on crizotinib. *J. Thorac. Oncol.* **2014**, *9*, 549–553. [[PubMed](#)]
170. Shaw, A.T.; Engelman, J.A. Crizotinib resensitization by compound mutation. *N. Engl. J. Med.* **2016**, *374*, 1790–1791. [[CrossRef](#)] [[PubMed](#)]
171. Amin, A.D.; Rajan, S.S.; Liang, W.S.; Pongtornpipat, P.; Groysman, M.J.; Tapia, E.O.; Peters, T.L.; Cuyugan, L.; Adkins, J.; Rimsza, L.M.; et al. Evidence suggesting that discontinuous dosing of ALK kinase inhibitors may prolong control of ALK+ tumors. *Cancer Res.* **2015**, *75*, 2916–2927. [[CrossRef](#)] [[PubMed](#)]
172. Ceccon, M.; Merlo, M.E.B.; Mologni, L.; Poggio, T.; Varesio, L.M.; Menotti, M.; Bombelli, S.; Rigolio, R.; Manazza, A.D.; Di Giacomo, F.; et al. Excess of NPM-ALK oncogenic signaling promotes cellular apoptosis and drug dependency. *Oncogene* **2016**, *35*, 3854–3865. [[CrossRef](#)] [[PubMed](#)]
173. Miyawaki, M.; Yasuda, H.; Tani, T.; Hamamoto, J.; Arai, D.; Ishioka, K.; Ohgino, K.; Nukaga, S.; Hirano, T.; Kawada, I.; et al. Overcoming EGFR bypass signal-induced acquired resistance to ALK tyrosine kinase inhibitors in ALK-translocated lung cancer. *Mol. Cancer Res. MCR* **2017**, *15*, 106–114. [[CrossRef](#)] [[PubMed](#)]
174. Wilson, F.H.; Johannessen, C.M.; Piccioni, F.; Tamayo, P.; Kim, J.W.; Van Allen, E.M.; Corsello, S.M.; Capelletti, M.; Calles, A.; Butaney, M.; et al. A functional landscape of resistance to ALK inhibition in lung cancer. *Cancer Cell* **2015**, *27*, 397–408. [[CrossRef](#)] [[PubMed](#)]
175. Hrustanovic, G.; Olivias, V.; Pazarentzos, E.; Tulpule, A.; Asthana, S.; Blakely, C.M.; Okimoto, R.A.; Lin, L.; Neel, D.S.; Sabnis, A.; et al. RAS-MAPK dependence underlies a rational polytherapy strategy in EML4-ALK-positive lung cancer. *Nat. Med.* **2015**, *21*, 1038–1047. [[CrossRef](#)] [[PubMed](#)]
176. Crystal, A.S.; Shaw, A.T.; Sequist, L.V.; Friboulet, L.; Niederst, M.J.; Lockerman, E.L.; Frias, R.L.; Gainor, J.F.; Amzallag, A.; Greninger, P.; et al. Patient-derived models of acquired resistance can identify effective drug combinations for cancer. *Science* **2014**, *346*, 1480–1486. [[CrossRef](#)] [[PubMed](#)]
177. Laimer, D.; Dolznig, H.; Kollmann, K.; Vesely, P.W.; Schlederer, M.; Merkel, O.; Schiefer, A.I.; Hassler, M.R.; Heider, S.; Amenitsch, L.; et al. Pdgfr blockade is a rational and effective therapy for NPM-ALK-driven lymphomas. *Nat. Med.* **2012**, *18*, 1699–1704. [[CrossRef](#)] [[PubMed](#)]
178. Lovly, C.M.; McDonald, N.T.; Chen, H.; Ortiz-Cuaran, S.; Heukamp, L.C.; Yan, Y.; Florin, A.; Ozretic, L.; Lim, D.; Wang, L.; et al. Rationale for co-targeting IGF-1R and ALK in ALK fusion-positive lung cancer. *Nat. Med.* **2014**, *20*, 1027–1034. [[CrossRef](#)] [[PubMed](#)]
179. Kim, H.R.; Kim, W.S.; Choi, Y.J.; Choi, C.M.; Rho, J.K.; Lee, J.C. Epithelial-mesenchymal transition leads to crizotinib resistance in H2228 lung cancer cells with EML4-ALK translocation. *Mol. Oncol.* **2013**, *7*, 1093–1102. [[CrossRef](#)] [[PubMed](#)]
180. Cha, Y.J.; Cho, B.C.; Kim, H.R.; Lee, H.J.; Shim, H.S. A case of ALK-rearranged adenocarcinoma with small cell carcinoma-like transformation and resistance to crizotinib. *J. Thorac. Oncol.* **2016**, *11*, e55–e58. [[CrossRef](#)] [[PubMed](#)]
181. Zhu, Y.C.; Liao, X.H.; Wang, W.X.; Xu, C.W.; Zhuang, W.; Zhong, L.H.; Du, K.Q.; Chen, Y.P.; Chen, G.; Fang, M.Y. Patients harboring ALK rearrangement adenocarcinoma after acquired resistance to crizotinib and transformation to small-cell lung cancer: A case report. *OncoTargets Ther.* **2017**, *10*, 3187–3192. [[CrossRef](#)] [[PubMed](#)]

182. Miyamoto, S.; Ikushima, S.; Ono, R.; Awano, N.; Kondo, K.; Furuhashi, Y.; Fukumoto, K.; Kumasaka, T. Transformation to small-cell lung cancer as a mechanism of acquired resistance to crizotinib and alectinib. *Jpn. J. Clin. Oncol.* **2016**, *46*, 170–173. [[CrossRef](#)] [[PubMed](#)]
183. Fujita, S.; Masago, K.; Katakami, N.; Yatabe, Y. Transformation to sclc after treatment with the ALK inhibitor alectinib. *J. Thorac. Oncol.* **2016**, *11*, e67–e72. [[CrossRef](#)] [[PubMed](#)]
184. Takegawa, N.; Hayashi, H.; Iizuka, N.; Takahama, T.; Ueda, H.; Tanaka, K.; Takeda, M.; Nakagawa, K. Transformation of ALK rearrangement-positive adenocarcinoma to small-cell lung cancer in association with acquired resistance to alectinib. *Ann. Oncol.* **2016**, *27*, 953–955. [[CrossRef](#)] [[PubMed](#)]
185. Levacq, D.; D’Haene, N.; de Wind, R.; Rimmelman, M.; Berghmans, T. Histological transformation of ALK rearranged adenocarcinoma into small cell lung cancer: A new mechanism of resistance to ALK inhibitors. *Lung Cancer* **2016**, *102*, 38–41. [[CrossRef](#)] [[PubMed](#)]
186. Engelman, J.A.; Zejnullahu, K.; Mitsudomi, T.; Song, Y.; Hyland, C.; Park, J.O.; Lindeman, N.; Gale, C.M.; Zhao, X.; Christensen, J.; et al. Met amplification leads to gefitinib resistance in lung cancer by activating ERBB3 signaling. *Science* **2007**, *316*, 1039–1043. [[CrossRef](#)] [[PubMed](#)]
187. Sequist, L.V.; Waltman, B.A.; Dias-Santagata, D.; Digumarthy, S.; Turke, A.B.; Fidias, P.; Bergethon, K.; Shaw, A.T.; Gettinger, S.; Cosper, A.K.; et al. Genotypic and histological evolution of lung cancers acquiring resistance to egfr inhibitors. *Sci. Transl. Med.* **2011**, *3*, 75ra26. [[CrossRef](#)] [[PubMed](#)]
188. Gouji, T.; Takashi, S.; Mitsuhiro, T.; Yukito, I. Crizotinib can overcome acquired resistance to ch5424802: Is amplification of the met gene a key factor? *J. Thorac. Oncol.* **2014**, *9*, e27–e28. [[CrossRef](#)] [[PubMed](#)]
189. Brahmer, J.; Reckamp, K.L.; Baas, P.; Crino, L.; Eberhardt, W.E.; Poddubskaya, E.; Antonia, S.; Pluzanski, A.; Vokes, E.E.; Holgado, E.; et al. Nivolumab versus docetaxel in advanced squamous-cell non-small-cell lung cancer. *N. Engl. J. Med.* **2015**, *373*, 123–135. [[CrossRef](#)] [[PubMed](#)]
190. Huang, M.; Lou, Y.; Pellissier, J.; Burke, T.; Liu, F.X.; Xu, R.; Velcheti, V. Cost-effectiveness of pembrolizumab versus docetaxel for the treatment of previously treated PD-L1 positive advanced NSCLC patients in the united states. *J. Med. Econ.* **2017**, *20*, 140–150. [[CrossRef](#)] [[PubMed](#)]
191. Rizvi, N.A.; Hellmann, M.D.; Brahmer, J.R.; Juergens, R.A.; Borghaei, H.; Gettinger, S.; Chow, L.Q.; Gerber, D.E.; Laurie, S.A.; Goldman, J.W.; et al. Nivolumab in combination with platinum-based doublet chemotherapy for first-line treatment of advanced non-small-cell lung cancer. *J. Clin. Oncol.* **2016**, *34*, 2969–2979. [[CrossRef](#)] [[PubMed](#)]
192. Reck, M.; Rodriguez-Abreu, D.; Robinson, A.G.; Hui, R.; Czoszi, T.; Fulop, A.; Gottfried, M.; Peled, N.; Tafreshi, A.; Cuffe, S.; et al. Pembrolizumab versus chemotherapy for PD-L1-positive non-small-cell lung cancer. *N. Engl. J. Med.* **2016**, *375*, 1823–1833. [[CrossRef](#)] [[PubMed](#)]
193. Brahmer, J.R.; Rodriguez-Abreu, D.; Robinson, A.G.; Hui, R.; Czoszi, T.; Fulop, A.; Gottfried, M.; Peled, N.; Tafreshi, A.; Cuffe, S.; et al. Health-related quality-of-life results for pembrolizumab versus chemotherapy in advanced, PD-L1-positive NSCLC (keynote-024): A multicentre, international, randomised, open-label phase 3 trial. *Lancet Oncol.* **2017**, *18*, 1600–1609. [[CrossRef](#)]
194. Rizvi, N.A.; Hellmann, M.D.; Snyder, A.; Kvistborg, P.; Makarov, V.; Havel, J.J.; Lee, W.; Yuan, J.; Wong, P.; Ho, T.S.; et al. Cancer immunology. Mutational landscape determines sensitivity to PD-1 blockade in non-small cell lung cancer. *Science* **2015**, *348*, 124–128. [[CrossRef](#)] [[PubMed](#)]
195. Rizvi, N.A.; Mazieres, J.; Planchard, D.; Stinchcombe, T.E.; Dy, G.K.; Antonia, S.J.; Horn, L.; Lena, H.; Minenza, E.; Mennecier, B.; et al. Activity and safety of nivolumab, an anti-PD-1 immune checkpoint inhibitor, for patients with advanced, refractory squamous non-small-cell lung cancer (checkmate 063): A phase 2, single-arm trial. *Lancet Oncol.* **2015**, *16*, 257–265. [[CrossRef](#)]
196. Garon, E.B.; Rizvi, N.A.; Hui, R.; Leighl, N.; Balmanoukian, A.S.; Eder, J.P.; Patnaik, A.; Aggarwal, C.; Gubens, M.; Horn, L.; et al. Pembrolizumab for the treatment of non-small-cell lung cancer. *N. Engl. J. Med.* **2015**, *372*, 2018–2028. [[CrossRef](#)] [[PubMed](#)]
197. Herbst, R.S.; Soria, J.C.; Kowanetz, M.; Fine, G.D.; Hamid, O.; Gordon, M.S.; Sosman, J.A.; McDermott, D.F.; Powderly, J.D.; Gettinger, S.N.; et al. Predictive correlates of response to the anti-PD-L1 antibody mpdl3280a in cancer patients. *Nature* **2014**, *515*, 563–567. [[CrossRef](#)] [[PubMed](#)]
198. Liu, B.; Song, Y.; Liu, D. Recent development in clinical applications of PD-1 and PD-L1 antibodies for cancer immunotherapy. *J. Hematol. Oncol.* **2017**, *10*, 174. [[CrossRef](#)] [[PubMed](#)]

199. Govindan, R.; Ding, L.; Griffith, M.; Subramanian, J.; Dees, N.D.; Kanchi, K.L.; Maher, C.A.; Fulton, R.; Fulton, L.; Wallis, J.; et al. Genomic landscape of non-small cell lung cancer in smokers and never-smokers. *Cell* **2012**, *150*, 1121–1134. [[CrossRef](#)] [[PubMed](#)]
200. Gainor, J.F.; Shaw, A.T.; Sequist, L.V.; Fu, X.; Azzoli, C.G.; Piotrowska, Z.; Huynh, T.G.; Zhao, L.; Fulton, L.; Schultz, K.R.; et al. Egfr mutations and ALK rearrangements are associated with low response rates to PD-1 pathway blockade in non-small cell lung cancer: A retrospective analysis. *Clin. Cancer Res.* **2016**, *22*, 4585–4593. [[CrossRef](#)] [[PubMed](#)]
201. Ott, P.A.; Hu, Z.; Keskin, D.B.; Shukla, S.A.; Sun, J.; Bozym, D.J.; Zhang, W.; Luoma, A.; Giobbie-Hurder, A.; Peter, L.; et al. An immunogenic personal neoantigen vaccine for patients with melanoma. *Nature* **2017**, *547*, 217–221. [[CrossRef](#)] [[PubMed](#)]
202. Mastini, C.; Martinengo, C.; Inghirami, G.; Chiarle, R. Anaplastic lymphoma kinase: An oncogene for tumor vaccination. *J. Mol. Med.* **2009**, *87*, 669–677. [[CrossRef](#)] [[PubMed](#)]
203. Pulford, K.; Falini, B.; Banham, A.H.; Codrington, D.; Robertson, H.; Hatton, C.; Mason, D.Y. Immune response to the ALK oncogenic tyrosine kinase in patients with anaplastic large-cell lymphoma. *Blood* **2000**, *96*, 1605–1607. [[PubMed](#)]
204. Awad, M.M.; Mastini, C.; Blasco, R.B.; Mologni, L.; Voena, C.; Mussolin, L.; Mach, S.L.; Adeni, A.E.; Lydon, C.A.; Sholl, L.M.; et al. Epitope mapping of spontaneous autoantibodies to anaplastic lymphoma kinase (ALK) in non-small cell lung cancer. *Oncotarget* **2017**, *8*, 92265–92274. [[CrossRef](#)] [[PubMed](#)]
205. Chiarle, R.; Martinengo, C.; Mastini, C.; Ambrogio, C.; D’Escamard, V.; Forni, G.; Inghirami, G. The anaplastic lymphoma kinase is an effective oncoantigen for lymphoma vaccination. *Nat. Med.* **2008**, *14*, 676–680. [[CrossRef](#)] [[PubMed](#)]
206. Voena, C.; Menotti, M.; Mastini, C.; Di Giacomo, F.; Longo, D.L.; Castella, B.; Merlo, M.E.B.; Ambrogio, C.; Wang, Q.; Minero, V.G.; et al. Efficacy of a cancer vaccine against ALK-rearranged lung tumors. *Cancer Immunol. Res.* **2015**, *3*, 1333–1343. [[CrossRef](#)] [[PubMed](#)]



© 2018 by the authors. Licensee MDPI, Basel, Switzerland. This article is an open access article distributed under the terms and conditions of the Creative Commons Attribution (CC BY) license (<http://creativecommons.org/licenses/by/4.0/>).